Oklahoma Geological Survey
Charles J. Mankin, *Director*

Circular 104
ISSN 0078-4397

Pennsylvanian and Permian Geology and Petroleum in the Southern Midcontinent, 1998 Symposium

KENNETH S. JOHNSON, *Editor*

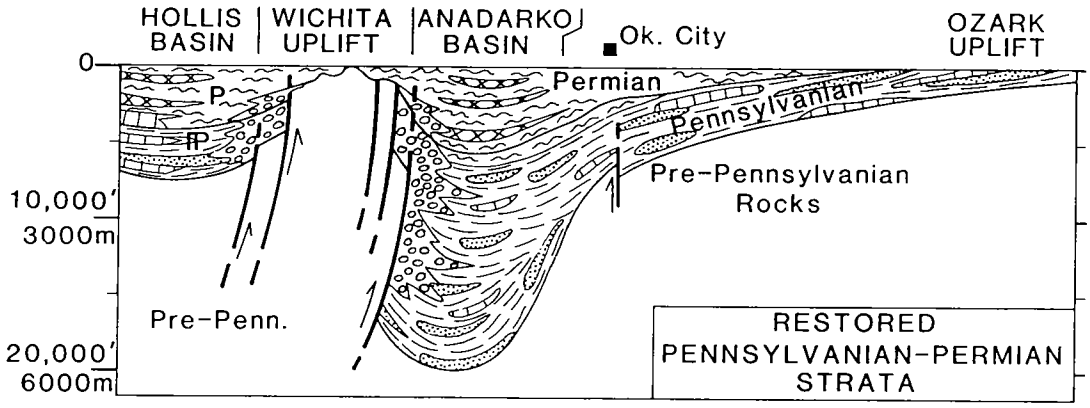

Proceedings of a symposium held April 7–8, 1998, in Norman, Oklahoma.

Co-sponsored by:

Oklahoma Geological Survey

and

National Petroleum Technology Office,
U.S. Department of Energy

The University of Oklahoma
Norman

2001

OKLAHOMA GEOLOGICAL SURVEY

CHARLES J. MANKIN, *Director*
KENNETH S. JOHNSON, *Associate Director*

SURVEY STAFF

JAMES H. ANDERSON, *Cartographic Technician III*
RICHARD D. ANDREWS, *Geologist III*
LARRY T. AUSTIN, *Core and Sample Library Assistant*
BETTY D. BELLIS, *Word-Processing Operator II/Technical Typist*
MITZI G. BLACKMON, *Clerk-Typist I*
JERLENE A. BRIGHT, *Technical Project Specialist*
RAYMON L. BROWN, *Geophysicist III*
RUTH E. BROWN, *Assistant to the Director*
JOCK A. CAMPBELL, *Geologist IV*
BRIAN J. CARDOTT, *Geologist IV*
JAMES R. CHAPLIN, *Geologist IV*
JANISE L. COLEMAN, *Office Assistant IV*
CHRISTIE L. COOPER, *Editor*
TAMMIE K. CREEL, *Secretary II*
CHARLES R. DYER III, *Drilling Technician*
WALTER C. ESRY, *Manager, Core and Sample Library*
ROBERT O. FAY, *Geologist IV*
AMIE R. FRIEND, *Research Specialist I*
T. WAYNE FURR, *Manager of Cartography*
PATRONALIA M. HANLEY, *Chemist*
PRISCILLA A. JOHNSON, *Office Assistant IV*
MICHAEL A. KELLEY, *Computer Specialist*
JAMES W. KING, *Research Specialist I*
JAMES E. LAWSON, JR., *Chief Geophysicist*
LAURIE A. LOLLIS, *Cartographic Technician II*
KENNETH V. LUZA, *Geologist IV*
MICHAEL J. MERCER, *Manager, Log Library*
RICHARD G. MURRAY, *Copy Center Operator*
SUE M. PALMER, *Office Assistant II*
DAVID O. PENNINGTON, *Operations Assistant II*
CONNIE G. SMITH, *Promotion and Information Specialist*
PAUL E. SMITH, *Supervisor, Offset Press Copy Center*
THOMAS M. STANLEY, *Geologist II*
LLOYD N. START, *Assistant Drilling Technician*
JOYCE A. STIEHLER, *Chief Clerk*
MICHELLE J. SUMMERS, *Technical Project Coordinator*
NEIL H. SUNESON, *Geologist IV*
JANE L. WEBER, *Coordinator, Departmental Computer Systems*
STEPHEN J. WEBER, *Chief Chemist*

Cover Picture

Schematic cross section showing restored thickness of Pennsylvanian and Permian strata in Oklahoma at the end of Permian time (from p. 4 of this volume).

This publication, printed by the Oklahoma Geological Survey, is issued by the Oklahoma Geological Survey as authorized by Title 70, Oklahoma Statutes, 1981, Sections 231–238. 1,050 copies have been prepared for distribution at a cost of $12,021 to the taxpayers of the State of Oklahoma. Copies have been deposited with the Publications Clearinghouse of the Oklahoma Department of Libraries.

PREFACE

The transfer of technical information will aid in the search for, and production of, our oil and gas resources. To facilitate this technology transfer, the Oklahoma Geological Survey (OGS) and the U.S. Department of Energy, National Petroleum Technology Office (DOE–NPTO), in Tulsa, cosponsored a symposium dealing with the search for, and production of, oil and gas resources from reservoirs of Pennsylvanian and Permian age in the southern Midcontinent. The symposium was held on April 7–8, 1998, in Norman, Oklahoma. This volume contains the proceedings of that symposium.

Research reported upon at the symposium focused on the reservoirs, geologic events, and petroleum of rocks deposited during the Pennsylvanian and Permian Periods. Clastic and carbonate reservoirs of this age are major sources of oil and gas in the southern Midcontinent, and they have great potential for additional recovery using advanced technologies. The research reports on geology, depositional settings, diagenetic history, sequence stratigraphy, reservoir characterization, exploration, petroleum production, and enhanced oil recovery. In describing these petroleum reservoirs of Pennsylvanian and Permian age, the researchers have increased our understanding of how the geologic history of an area can affect reservoir heterogeneity and our ability to efficiently recover the hydrocarbons they contain. We hope that the symposium and these proceedings will bring such research to the attention of the geoscience and energy-research community, and will help foster exchange of information and increased research interest by industry, university, and government workers.

Twenty-two talks and posters presented at the symposium are printed here as full papers or extended abstracts. An additional eight talks and posters are presented as abstracts at the end of the volume. About 215 persons attended the symposium. Stratigraphic nomenclature and age determinations used by the various authors in this volume do not necessarily agree with those of the OGS.

This is the eleventh symposium in as many years dealing with topics of major interest to geologists and others involved in petroleum-resource development in Oklahoma and adjacent states. These symposia are intended to foster the exchange of information that will improve our ability to find and recover our nation's oil and gas resources. Earlier symposia covered: Anadarko Basin (published as OGS Circular 90); Late Cambrian–Ordovician Geology of the Southern Midcontinent (OGS Circular 92); Source Rocks in the Southern Midcontinent (OGS Circular 93); Petroleum-Reservoir Geology in the Southern Midcontinent (OGS Circular 95); Structural Styles in the Southern Midcontinent (OGS Circular 97); Fluvial-Dominated Deltaic Reservoirs in the Southern Midcontinent (OGS Circular 98); Simpson and Viola Groups in the Southern Midcontinent (OGS Circular 99); Ames Structure in Northwest Oklahoma and Similar Features—Origin and Petroleum Production (OGS Circular 100); Platform Carbonates in the Southern Midcontinent (OGS Circular 101); and Marine Clastics in the Southern Midcontinent (OGS Circular 103).

Persons involved in the organization and planning of this symposium include: Kenneth Johnson and Charles Mankin of the OGS; and Tom Wesson and Herb Tiedemann of DOE–NPTO. Other personnel who contributed include Michelle Summers and Tammie Creel, registration co-chairs; LeRoy Hemish, poster-session chair; Connie Smith, publicity chair; and Judy Schmidt, exhibits coordinator. Technical editing of this volume was done by Thomas W. Henry, Westminster, Colorado; layout and production was done by Sandra Rush, Denver, Colorado. Appreciation is expressed to each of them and to the many authors who worked toward a highly successful symposium.

KENNETH S. JOHNSON
General Chairman

CONTENTS

Geology and Petroleum Reservoirs in Pennsylvanian and Permian Rocks of Oklahoma

Kenneth S. Johnson
Oklahoma Geological Survey
Norman, Oklahoma

Robert A. Northcutt
Independent Geologist
Oklahoma City, Oklahoma

G. Carlyle Hinshaw
Independent Geologist
Norman, Oklahoma

Kathy E. Hines
Geo Information Systems
Norman, Oklahoma

ABSTRACT.—Pennsylvanian and Permian rocks in Oklahoma comprise a thick sedimentary sequence that underlies most parts of the State, and they are important sources of oil and gas throughout most of their distribution. Pennsylvanian strata are marine and nonmarine shales, sandstones, conglomerates, and limestones that thicken markedly into the major structural and depositional basins. The total thickness of Pennsylvanian strata in the various basins is as follows: at least 15,000 ft in the Anadarko, Ardmore, Marietta, and Arkoma/Ouachita basins; and about 4,000 ft in the Hollis/Hardeman basin. Permian strata are dominated by redbeds and evaporites but also include Lower Permian marine carbonates and shales that underlie most of the western half of the State. The maximum thickness of Permian strata is about 7,000 ft in the Anadarko basin and 4,000 ft in the Hollis/Hardeman basin.

Production data for leases producing from Pennsylvanian and Permian reservoirs since 1979 can be retrieved from the Natural Resources Information System (NRIS) data files by the geologic names of the producing intervals. Of the more than 700 geologic names for producing intervals in the NRIS files, about 600 are units of Pennsylvanian (including Springeran) or Permian age. Using these data, we prepared a series of five maps and related production data for the following geologic intervals: Springeran, Lower Pennsylvanian (Morrowan and Atokan), Middle Pennsylvanian (Desmoinesian), Upper Pennsylvanian (Missourian and Virgilian), and Permian. Cumulative production from all five intervals from 1979 through 1997 was about 1.64 billion barrels of oil and condensate, and about 29.8 trillion cubic feet of natural gas and casing-head gas.

INTRODUCTION

Oklahoma is one of the leading petroleum-producing states in the nation, and a significant part of its production is from reservoirs of Pennsylvanian and Permian age. In 1998, Oklahoma ranked fifth in crude-oil production, third in natural-gas production, and second in number of wells drilled for petroleum. Unfortunately, production from Pennsylvanian and Permian reservoirs commonly is commingled with production from other reservoirs in many major oil and gas fields, so precise data on yields of individual reservoirs are not available.

This paper discusses the general geology of Pennsylvanian and Permian strata in Oklahoma, and then presents the plays (types of traps) that have yielded the greatest amounts of oil and gas from these strata. An understanding of these major petroleum-producing

Johnson, K. S.; Northcutt, R. A.; Hinshaw, G. C.; and Hines, K. E., 2001, Geology and petroleum reservoirs in Pennsylvanian and Permian rocks of Oklahoma, *in* Johnson, K. S. (ed.), Pennsylvanian and Permian geology and petroleum in the southern Midcontinent, 1998 symposium: Oklahoma Geological Survey Circular 104, p. 1–19.

plays should improve our search for new oil and gas fields or reservoirs and should also improve our techniques of recovery from established fields.

Production data for leases were retrieved from the Natural Resources Information System (NRIS) by Geo Information Systems (GIS), a research department of The University of Oklahoma, by the geologic names of the producing intervals. Oklahoma petroleum production is recorded by lease, *not by well*, by the Oklahoma Tax Commission. Liquid production (crude oil and condensate) and gas production (associated and non-associated) are able to be identified as "pure," where all lease production is from a single producing interval, i.e., Springeran, Lower Pennsylvanian, etc., or "commingled," where lease production is from two or more producing intervals. These data are public records and are marketed in several forms by commercial and governmental organizations. GIS provides the data six months in arrears, updated each six months. The database begins in 1979, with oil, condensate, associated gas, and non-associated gas recorded monthly. It is possible, through the mapping capabilities of SAS (an integrated system of software), to post a location map at almost any scale for one or several (or all) producing intervals by product or products. Also, individuals or companies can acquire the raw data and construct their own analyses.

GENERAL GEOLOGIC SETTING

Oklahoma is a geologically complex region with a number of major depositional and structural basins, separated by orogenic uplifts and mountain ranges created during the Pennsylvanian (Fig. 1).

Upper Cambrian through Mississippian rocks in Oklahoma are represented by marine sediments that were deposited in a broad epicontinental sea—the Oklahoma basin—that extended across almost all parts of the southern Midcontinent (Fig. 2). The Oklahoma basin was a shelf-like area that received a sequence of remarkably thick and extensive sediments now represented by marine carbonates interbedded with thinner marine shales and sandstones. These strata are readily correlated throughout the basin. The sedimentary units thicken into protobasins (Anadarko, Ardmore, Arkoma, and others), which were accentuated later during Pennsylvanian orogenies, and they also were deposited upon and across the present-day major uplifts, from which they were subsequently stripped during Pennsylvanian uplift and erosion. The southern Oklahoma aulacogen was the depositional center for the Oklahoma basin. General discussions on pre-Pennsylvanian geology are presented by Johnson and others (1988) and Johnson and Cardott (1992).

Late Paleozoic geologic development in Oklahoma centered on orogenic activity during the Pennsylvanian Period. Sharply uplifted crustal blocks subdivided the broad, shallow-marine Oklahoma basin into a series of well-defined marine basins. Orogenic activity was limited to folding, faulting, and uplift and was not accompanied by igneous activity or metamorphism. Pennsylvanian orogenic pulses caused (or contributed to): (1) folding and thrusting of the Ouachita fold belt; (2) raising of the Wichita, Criner, Arbuckle, and Nemaha uplifts; (3) pronounced down-warping of the Anadarko, Ardmore, Arkoma, and Marietta basins; and (4) moderate subsidence of the Hugoton embayment and the Hollis basin (Fig. 1).

Pennsylvanian strata of Oklahoma consist of sequences of marine and nonmarine shale, sandstone,

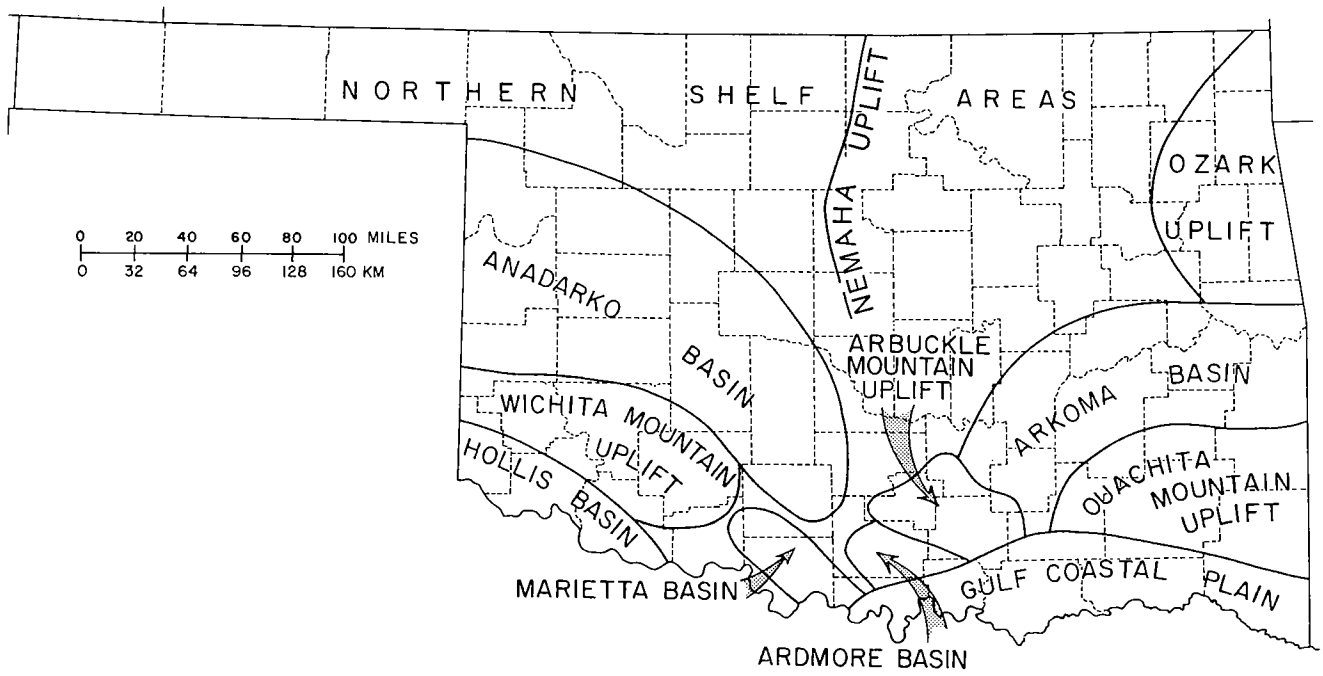

Figure 1. Major geologic provinces of Oklahoma. From Johnson (1971).

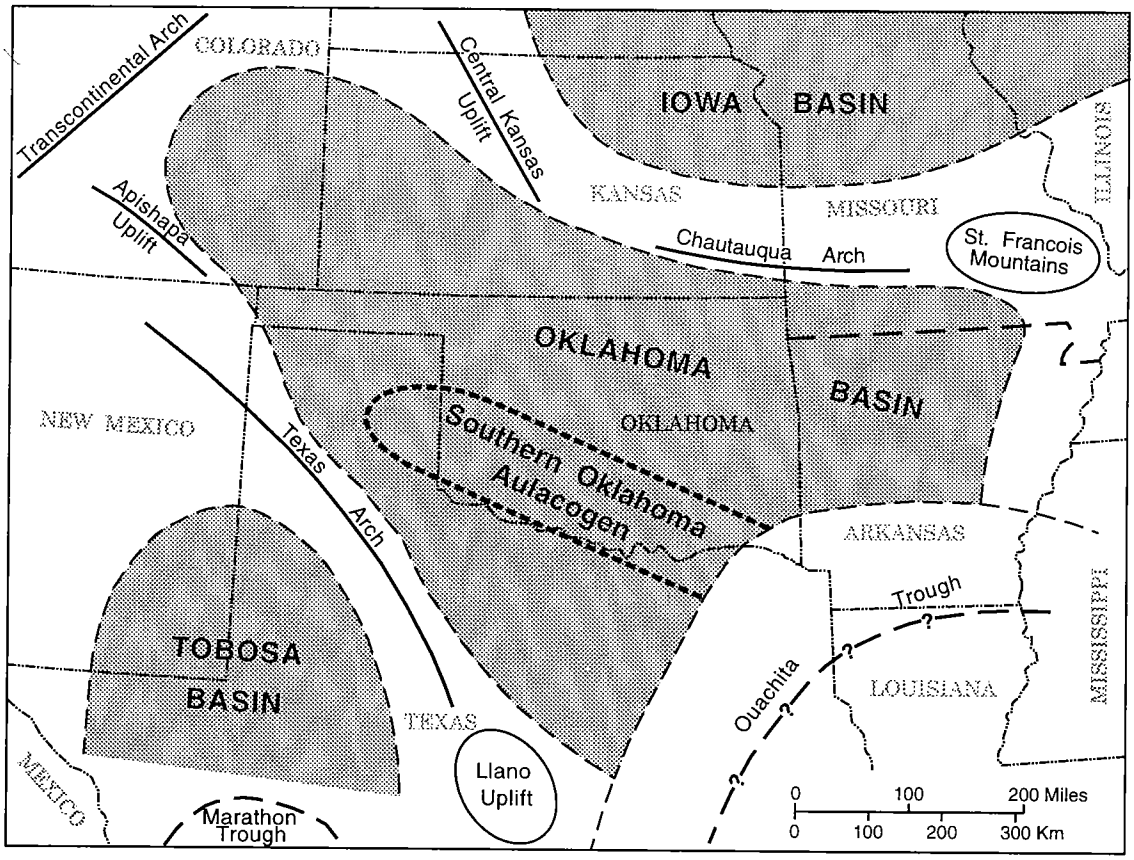

Figure 2. Map of southwestern United States, showing approximate boundary of the Oklahoma basin and other major features that existed in early and middle Paleozoic time. After Johnson and others (1988).

conglomerate, and limestone that thicken markedly into the rapidly subsiding basins. Thick wedges of terrigenous clastic sediments were shed from nearby uplifts, and thinner carbonate sequences were deposited on shallow-water shelf areas distal to the uplifts. Successively younger Pennsylvanian units commonly overlap older units at the margins of the basins and across some of the uplifts. Thin coal beds are abundant in Desmoinesian strata, mainly in the Arkoma basin and on the Cherokee platform. Total thickness of Pennsylvanian strata in the various basins is 10,000–15,000 ft in the Anadarko, Ardmore, Arkoma, and Marietta basins and about 4,000 ft in the Hollis basin. In most of the shelf or platform areas, Pennsylvanian strata typically are 1,500–4,000 ft thick.

In the Ouachita trough, deep-water flysch sedimentation continued through Morrowan and Atokan time, although the depocenter shifted northward in Atokan time to the southern part of the Arkoma basin. The trough was then destroyed during the Ouachita orogeny (Desmoinesian), with northward thrusting and complex folding of Ouachita-facies rocks to form the present-day Ouachita Mountains.

Permian strata are limited to the western half of Oklahoma. Clastics were eroded from the Ouachitas (reduced to low mountains by this time) on the east, the ancestral Rocky Mountains on the west, and the Wichita uplift in southwestern Oklahoma. Sediments accumulated mainly in the Anadarko basin, and also in the Hollis basin and the Panhandle region. Early Permian (Wolfcampian) carbonates and shales, both gray and redbeds, are overlain by a major evaporite and redbed sequence of Leonardian, Guadalupian, and Ochoan age. Evaporites (salt and gypsum/anhydrite) thicken into the basins that continued to subside more than the adjacent uplifts and arches. Permian strata are as much as 7,000 ft thick in the Anadarko basin, 4,000 ft thick in the Hollis basin, and 1,000–3,000 ft thick in nearby shelf or platform areas.

A schematic representation of the restored thickness and distribution of Pennsylvanian and Permian strata, restored to the end of Permian time, is given in Figure 3. Pennsylvanian and Permian strata are the most widespread of outcropping bedrock units in Oklahoma. Pennsylvanian rocks crop out in about 25% of the State, and Permian outcrops comprise about 45% (Fig. 4). A generalized chart showing correlation of Pennsylvanian and Permian strata in Oklahoma is presented in Figure 5.

General discussions of Pennsylvanian and Permian geology are presented by McKee and others (1967, 1975), Ham and Wilson (1967), Rascoe and Adler (1983), Johnson and others (1988), and Johnson (1996). Much of the geologic discussion that follows is taken from the work by various authors in the report by Johnson and others (1988).

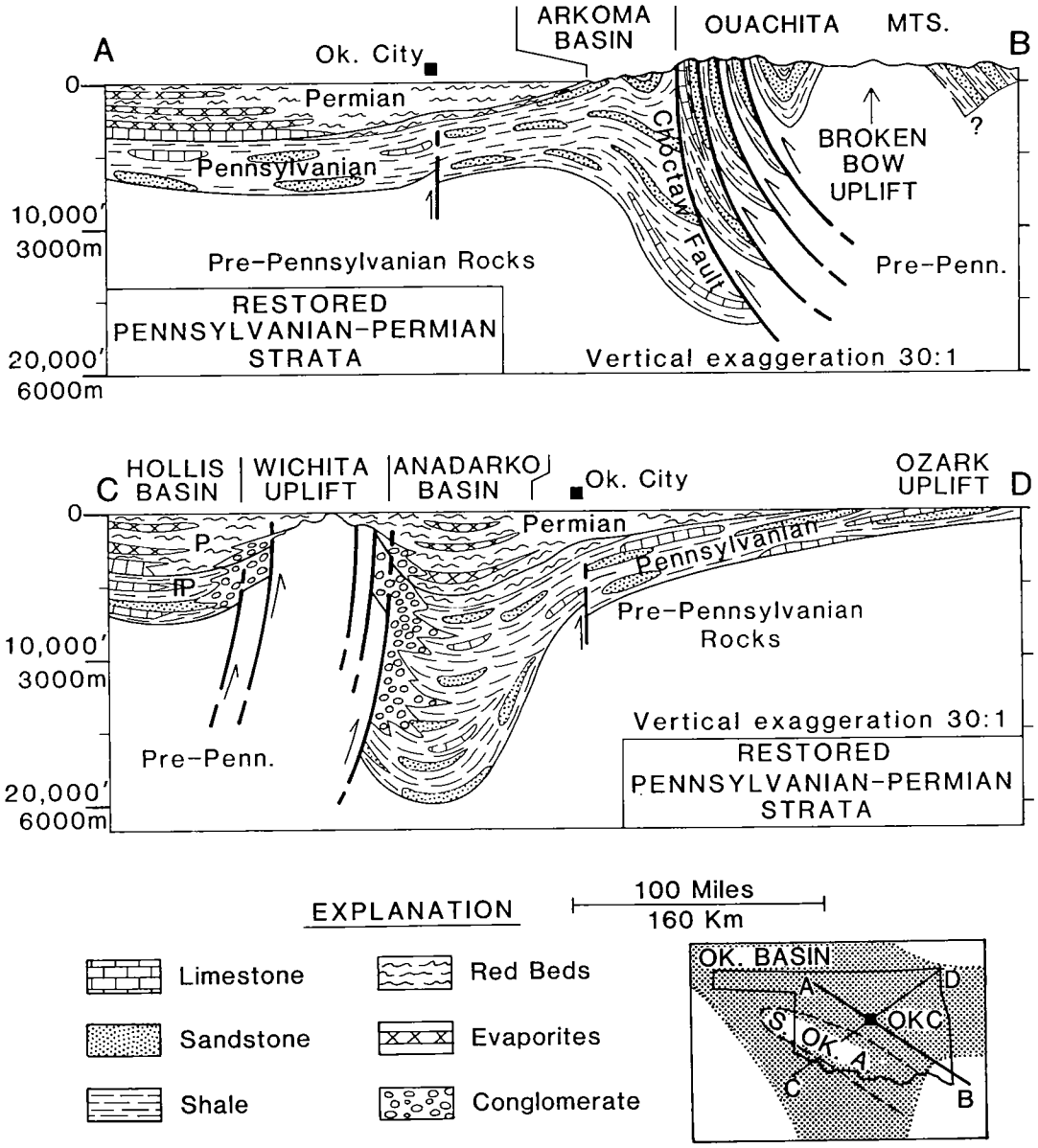

Figure 3. Schematic cross sections showing restored thickness of Pennsylvanian and Permian strata in Oklahoma at the end of Permian time. From Johnson and Cardott (1992).

PENNSYLVANIAN GEOLOGY AND RESERVOIRS

Springeran

Springeran Series

Although the top of the Mississippian System is well marked by a pre-Pennsylvanian unconformity in most parts of the southern Midcontinent, the Mississippian–Pennsylvanian boundary occurs within the thick sequence of shales and sands of the Springer Formation and equivalent strata, where sedimentation was uninterrupted in the deep parts of the Anadarko and Ardmore basins. These Springer clastic rocks in Oklahoma commonly are assigned a "Springeran" age—an age that spans a period between the Late Mississippian Chester Epoch and the Early Pennsylvanian Morrowan Epoch. We will follow that concept here because we cannot separate out the Pennsylvanian part of the Springeran. Also, we will present data on all Springeran production as Pennsylvanian in age.

Deposition of the Springeran sandstones in the Anadarko–Ardmore basins marked a change from the dominantly carbonate and shale deposition of the Late Mississippian to the clastic environments of the Early Pennsylvanian. Rapid subsidence of the Anadarko–Ardmore basins and the adjacent shelf areas in Late Mississippian and Early Pennsylvanian time caused transgression of the Springeran seas over the shelf areas of Chester carbonates and deposition of shallow-marine and shoreline sands of the Springer. Intervals of Springer sands in the Anadarko and Ardmore basins are as much as 250 ft thick in some areas, with discrete

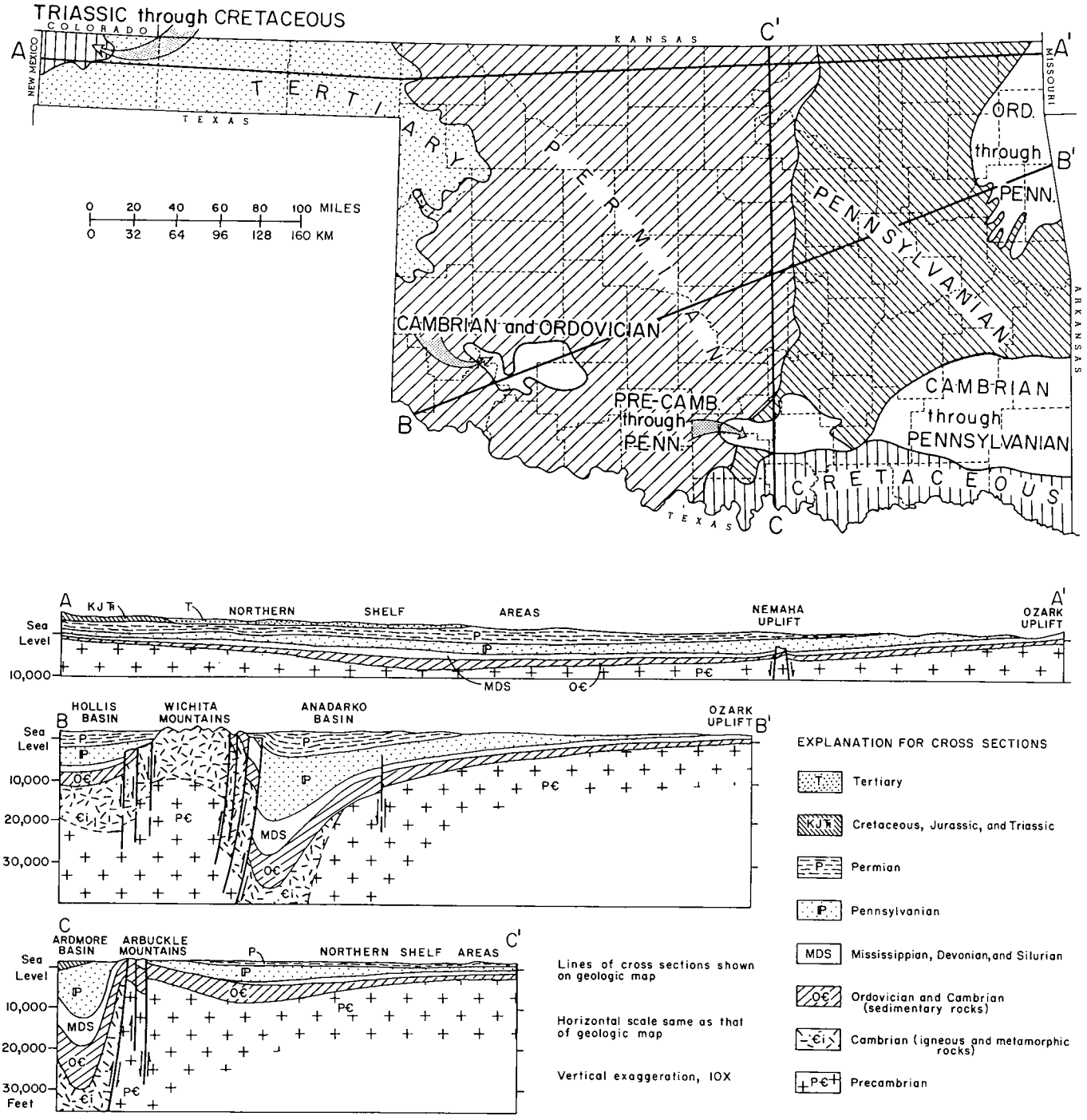

Figure 4. Generalized geologic map and geologic cross sections of Oklahoma. Cross sections follow lines A–A′, B–B′, and C–C′ on map. From Johnson (1971).

marine sand bars attaining a thickness of 50 ft or more for several miles (Brown and Northcutt, 1993).

Springeran Production

Springer sands were first named after leases in the fields of southern Oklahoma where they produced oil and/or gas. Correlation of the individual sands was not attempted between fields, so some of the names of the Springer producing intervals shown in Table 1 may, in fact, be equivalent.

The production map for the Springeran (Fig. 6) shows oil and gas production from Springeran reservoirs, mainly marine sands, in the Anadarko and Ardmore basins and in the frontal-fault belt of the Wichita uplift. Springeran production is found in both stratigraphic and structural traps. Stratigraphic traps dominate in the Anadarko and Ardmore basins, and structural traps are prevalent in the faulted and folded belts of southern Oklahoma and in the faulted frontal area of the Wichita uplift.

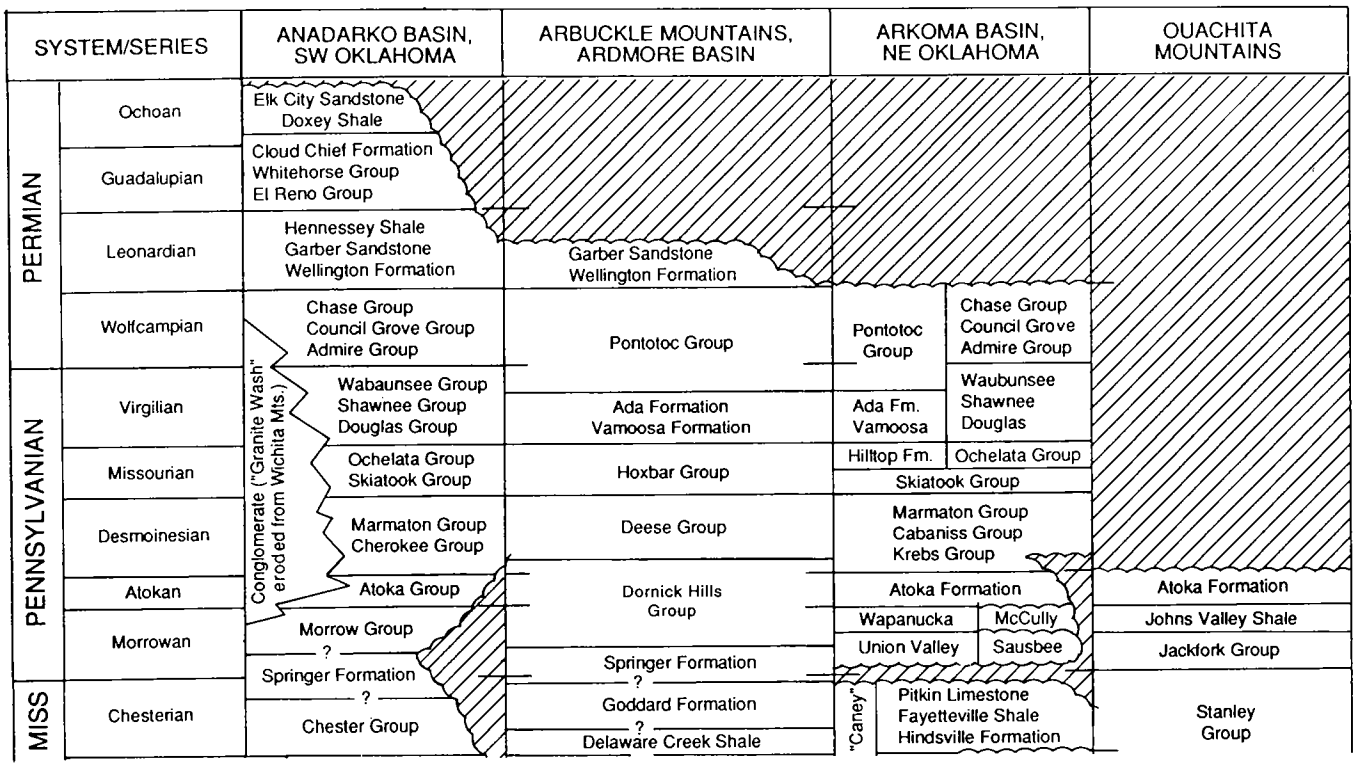

Figure 5. Generalized correlation of Pennsylvanian and Permian rock units in Oklahoma. Modified from Johnson and Cardott (1992).

Table 1.—Names Used for Springeran Reservoir Rocks that Produce Petroleum in Oklahoma

SPRINGERAN	
Springeran Series	
Springer Group	
Springer	Parks
Overbrook	Britt
Woods	Flattop
Rod Club	Hutson
Velma	Sims
Cunningham	Goodwin
Markham	Spiers
Aldridge	Inscore
Humphreys	Boatwright
Horton	Anderson

Cumulative production (pure and commingled) (1/1/79 through 12/31/97)
Oil: 200,007,026 bbl
Gas: 3,560,472,946 mcf

Graphs of annual production for the period 1979 through 1997 from Springeran reservoirs for pure and commingled leases show liquid production (crude oil and condensate) in Figure 7 and gas production (associated and non-associated) in Figure 8. Cumulative lease production from Springeran reservoirs (pure and commingled) for the period 1979–1997 was 200,007,026 barrels (bbl) of oil and 3,560,472,946 thousand cubic feet (mcf) of gas.

Lower Pennsylvanian

Morrowan Series

In most parts of the Anadarko basin and the Hugoton embayment, Morrowan sediments were deposited on a surface of eroded Mississippian rocks. Along and adjacent to the axis of the Anadarko basin, Morrowan beds overlie lithologically similar strata of Springeran age. The lower part of the Morrowan Series consists of shallow-marine shales, sandstones, and limestones. These sediments, deposited in the transgressing Morrowan sea, onlap the surface of eroded Mississippian rocks and are markedly diachronous from the Anadarko basin, where they are older, onto the shelf areas to the north and northeast, where they are younger. A basal sandstone unit is a sporadic but prominent member of this transgressive sequence. Thickening of this sandstone unit appears to mark the positions of ancient shorelines, which formed during still-stands of the Morrowan seas. Carbonate cement is a common constituent of these basal sandstones; it was probably introduced into the marginal-marine environment by streams that flowed across the carbonate terrain of exposed Mississippian rocks and emptied into the Morrowan seas (Adams, 1964).

These transgressive lower Morrowan beds are overlain by a sequence that consists principally of shales

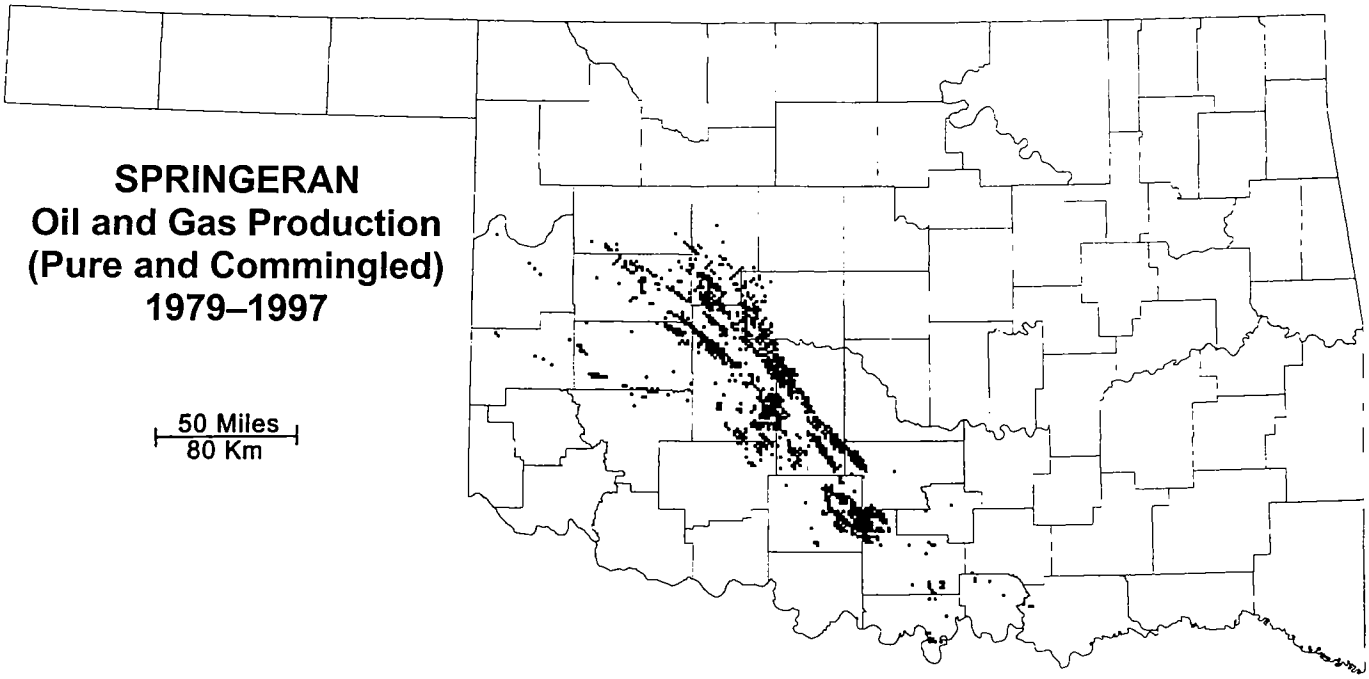

Figure 6. Map of oil and gas lease production from Springeran reservoirs in Oklahoma, 1979–1997. Map was generated by Geo Information Systems from the Natural Resources Information System (NRIS) data files.

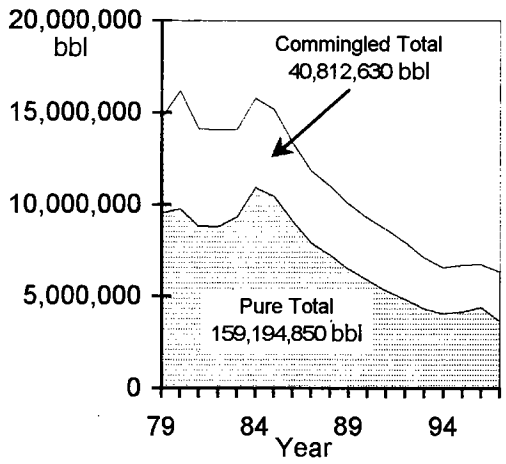

Figure 7. Graph of annual pure and commingled liquid (oil and condensate) production from leases producing from Springeran reservoirs in Oklahoma, 1979–1997. Total cumulative lease liquid production from Springeran reservoirs is 200,007,026 barrels (bbl).

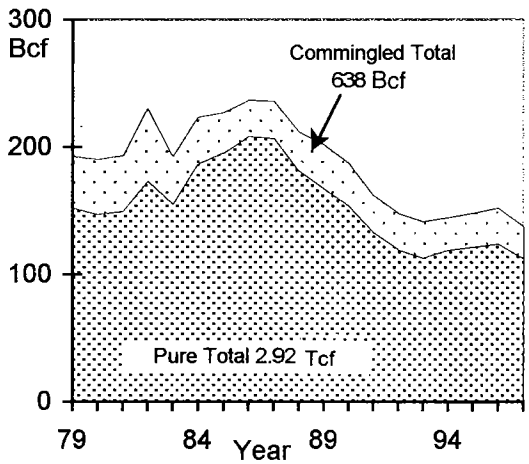

Figure 8. Graph of annual pure and commingled gas (associated and non-associated) production from leases producing from Springeran reservoirs in Oklahoma, 1979–1997. Total cumulative lease gas production from Springeran reservoirs is 3,560,472,946 thousand cubic feet (mcf). Abbreviations: Bcf—billion cubic feet; Tcf—trillion cubic feet.

with lenticular, discontinuous sandstones and minor conglomerates, coals, and thin, dark limestones. This upper Morrowan section is the product of a prograding deltaic phase with the following environmental facies (Swanson, 1979): (1) point-bar and stream-mouth-bar sandstones and conglomerates, (2) prodelta shales, (3) back-swamp–marsh shales, and (4) meander-channel–fill sandstones and shales. Shelby (1979) and Evans (1979) have described and mapped upper Morrowan fan-delta chert conglomerates in the Texas Panhandle and western Oklahoma. The Wichita–Amarillo uplift was the source area for these clastics, which were derived by the weathering of cherty limestones and dolomites of Mississippian age. The presence of these chert conglomerates in the upper part of the Morrowan Series dates the initiation of the Wichita–Amarillo uplift.

In the Ardmore and Marietta basins of southern Oklahoma, local uplifts in the Arbuckle Mountains,

Criner Hills, and Wichita uplift had an impact on Morrowan sedimentation. Thick shales are interbedded with limestones, sandstones, and conglomerates, and the entire sequence is referred to as the Lower Dornick Hills Group. Only the Primrose sand, the basal sand, is normally identified as a named member.

In the Arkoma basin, the early Morrowan sea transgressed north from the Ouachita trough onto the Arkoma shelf, across the truncated Mississippian surface. The depositional pattern throughout the Morrowan is one of marked lateral changes in facies and thickness. The dominant source direction on the Arkoma shelf was from the northeast, primarily from the Illinois basin.

The Morrowan carbonate facies in the southern Ozarks of northeastern Oklahoma extends southward for about 10 mi in the subsurface of the Arkoma basin, south of the southern limit of the present outcrop area in Oklahoma. Farther south, the percentage of limestone in the Morrowan interval below the Wapanucka Limestone distinctly decreases, and the percentage of shale and sandstone increases. In the central and southern parts of the Arkoma basin, the typical Morrowan sequence begins with the Pennsylvanian Caney, which cannot be subdivided in most places from the underlying Mississippian Caney. Most subsurface workers therefore use the base of the overlying Cromwell Sandstone as a marker for the base of the Pennsylvanian.

In the Ouachita Trough to the south, turbidite deposition continued during Morrowan time with deposition of the Jackfork Sandstone and the Johns Valley Shale. Transport directions recorded for the Jackfork Sandstone on the outcrop in both Arkansas and Oklahoma are to the west, parallel to the basin axis. Owen and Carozzi (1986) presented evidence that part of the source for the upper Jackfork sandstones was to the southeast of Arkansas, from the orogenic belt southwest of the Black Warrior basin. The Johns Valley is well known for its great variety of erratic limestone boulders that possibly originated from fault scarps on the shelf margin to the north (Shideler, 1970).

Discussion of Morrowan petroleum reservoirs and production is deferred to the end of the next section on the "Atokan Series."

Atokan Series

Atokan rocks in the Anadarko basin and the Hugoton embayment consist of a cyclic sequence of thin marine limestones and shales. These sediments compose the so-called "thirteen-finger limestone" of the Atoka Group. This rock unit is generally 60–100 ft thick, and the cyclic arrangement of these Atokan limestones and shales resembles the lower Desmoinesian section, which conformably overlies the Atokan.

Along the northern margin of the Wichita–Amarillo uplift, Atokan limestones and shales grade abruptly into the massive clastic deposits, which consist of granite, limestone, and dolomite fragments. In this "granite-wash" sequence, the boundaries of the Atokan Series are uncertain; however, the Atokan appears to thicken into this clastic facies, so that a maximum thickness of several hundred feet is possible.

In the Anadarko basin, the contact of the Atokan Series with the underlying Morrowan Series ranges from gradational to disconformable. On the northern shelf of the Anadarko basin, Atokan sediments locally overstep the limit of the Morrowan Series and unconformably onlap rocks of Mississippian age. Along the southern margin of the Anadarko basin, pre-Atokan rocks underwent intense folding and faulting as a result of the Wichita orogeny of late Morrowan–early Atokan time. Consequently, Atokan rocks are commonly absent on local positive structures. Erosion of the carbonate and igneous terrain of the emerging Wichita–Amarillo uplift continued during Atokan time.

In southern Oklahoma, the Wichita–Criner orogeny intensified in Atokan time, with further uplift and deposition along the northeast margin of the Criner Hills axis. The dominant lithologies are limestone- and chert-pebble conglomerates interbedded irregularly with shales. The limestone-pebble conglomerates did not extend northeastward across the Ardmore basin, suggesting that the pebbles were not carried that far. However, in the northern part of the basin there is a regional unconformity at or near the base of the unnamed shale that overlies the Bostwick in the southern Ardmore basin. This shale can be correlated across the entire basin.

In the Arkoma basin, the Atokan series is mainly represented by the Atoka Formation and by the upper part of the Wapanucka Formation. A regional unconformity separates the Atoka Formation from underlying strata of Morrowan age in all areas except along the southern part of the Arkoma shelf and in the basin to the south. The sea was displaced from the shelf on the north, primarily by a southward tilting of the Morrow surface (as an aspect of the subsidence of the Ouachita trough), and extensive subaerial erosion resulted. Progressively older strata were eroded northward on this inclined surface.

Beginning approximately with the deposition of the middle Atoka, the southern margin of the Arkoma shelf was subjected to flexural bending, caused by continued basin closure that resulted in the development of large east-trending normal faults. Development of these syndepositional faults was not synchronous, and it appears that the southernmost syndepositional faults became active earliest and that active faulting migrated northward with time (Houseknecht, 1986). The middle Atoka makes up the major part of the thickness of the formation in the southern part of the basin; it consists predominantly of shale with a few thick sandstone units. It is best developed in the southern part of the basin and displays marked increases in thickness on the downthrown sides of east-trending, syndepositional normal faults.

In the Ouachita trough, deep-water flysch sedimentation continued through Atokan time, although the depocenter shifted northward to the southern part of the Arkoma basin. Atokan strata are the youngest Paleozoic units preserved in the Ouachita Mountains. The

trough was then destroyed during the Ouachita orogeny (Desmoinesian), with northward thrusting and complex folding of Ouachita-facies rocks to form the present-day Ouachita Mountains.

Morrowan and Atokan Production

Names of Lower Pennsylvanian (Atokan and Morrowan) producing intervals are listed in Table 2. Most of the Atokan names are used only in the Arkoma basin and are named only in local areas. Most of the Atokan producing intervals are just designated as "Atoka." Gilcrease and Dutcher are names used in east-central Oklahoma and the western part of the Arkoma basin. In southern Oklahoma, the Atoka is called the Upper Dornick Hills, and Morrowan strata are named the Lower Dornick Hills Group. Only the Primrose sand, the basal sand, is normally identified as a named member. In the Anadarko basin and shelf area of northwestern Oklahoma, individual Morrow Group sands have been named locally. Generally, throughout the basin and shelf area, the term "Morrow" has been applied to the various producing intervals without any attempt to name individual sands, because of the difficulty in correlation of the sands.

Table 2.—Names Used for Lower Pennsylvanian Reservoir Rocks that Produce Petroleum in Oklahoma

LOWER PENNSYLVANIAN	
Atokan Series	
Atoka Group	
Upper Dornick Hills	Red Oak
Atoka	Panola
Carpenter Atoka	Diamond
Alma	Brazil
Gilcrease	Bullard
Dutcher	Cecil
Gose	Shay
Dirty Creek	Pope Chapel
Dunn	Panola
Smallwood	Spiro
Fanshawe	Bostwick
Morris	Thirteen Finger Lime
Morrowan Series	
Morrow Group	
Lower Dornick Hills	Kelly
Morrow	Pierce
Mouser	Bradstreet
Stuart Morrow	Mocane
Fields	Laverne
Hamilton	Keyes
Purdy	Wapanucka
Purvis	Chicochoc Chert
Puryear	Jack Fork
Sturgis	Union Valley
Bowles	Cromwell
Lips	Jefferson
Hollis	Primrose

Cumulative production (pure and commingled) (1/1/79 through 12/31/97)
Oil: 209,957,428 bbl
Gas: 9,035,256,535 mcf

The production map for the Lower Pennsylvanian (Fig. 9) shows oil and gas lease production from Atokan and Morrowan reservoirs. The Morrowan rocks, mainly marine sands in the Anadarko and Ardmore basins, produce from stratigraphic traps and local structural traps. Stratigraphic traps dominate in the prograding deltaic deposits of the upper Morrowan on the shelf area of the Anadarko basin of northwestern and Panhandle areas of Oklahoma. The Wapanucka Limestone, a platform carbonate in the Arkoma basin of eastern Oklahoma, produces gas from structural traps along the frontal-fault zone of the Ouachita Mountains uplift. The Cromwell, a marine sand, produces oil and gas from combination structural/stratigraphic traps in east-central Oklahoma.

Atokan reservoirs produce gas from structural traps in and adjacent to the Arkoma basin of eastern Oklahoma. West of the Arkoma basin, oil and gas are produced from Gilcrease and Dutcher (Atokan) sandstones in combination structural–stratigraphic traps. Atokan reservoirs also produce gas in the Anadarko basin from stratigraphic and structural traps along the frontal zone of the Wichita uplift.

Graphs of annual production (1979 through 1997) from Lower Pennsylvanian reservoirs for pure and commingled leases show liquid production (crude oil and condensate) in Figure 10 and gas production (associated and non-associated) in Figure 11. Cumulative lease production from Lower Pennsylvanian reservoirs (pure and commingled) for the period 1979–1997 is 209,957,428 bbl of oil and 9,035,256,535 mcf of gas.

Middle Pennsylvanian

Desmoinesian Series

In the Anadarko basin and the Hugoton embayment, the Desmoinesian Series consists mostly of cyclic marine limestones and shales; "granite wash" constitutes the Desmoinesian section in a belt adjacent to the Wichita–Amarillo uplift. The lower part of the cyclic marine section is the Cherokee Group, which consists of numerous thin limestones interbedded with shales; on the northern shelf area in Oklahoma, lenticular point-bar and channel-fill sandstones occur in the Cherokee Group. In northwestern Oklahoma and the Panhandle, the proportion of limestones to shales is roughly equal. Eastward, the increase in limestones in the Cherokee Group is gradual until along the Nemaha uplift the ratio of limestone to shale is approximately 10:1.

The Marmaton Group conformably overlies the Cherokee Group. In the Hugoton embayment, the Marmaton consists of four prominent limestone formations (Ft. Scott, Pawnee, Altamont, and Lenapah, in ascending order); in the Anadarko basin, the Marmaton is composed of the Big Limestone (above) and the Oswego Limestone (below). Thickness of the

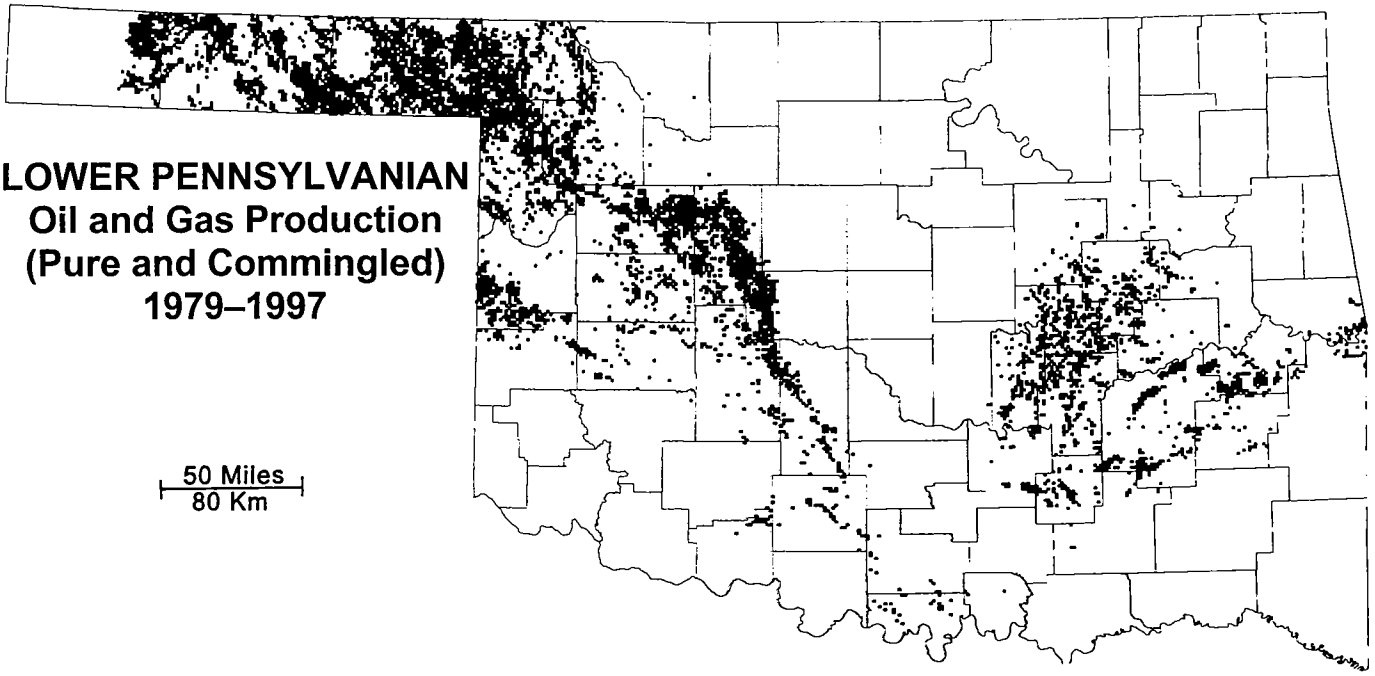

Figure 9. Map of oil and gas lease production from Lower Pennsylvanian (Morrowan and Atokan) reservoirs in Oklahoma, 1979–1997. Map was generated by Geo Information Systems from the Natural Resources Information System (NRIS) data files.

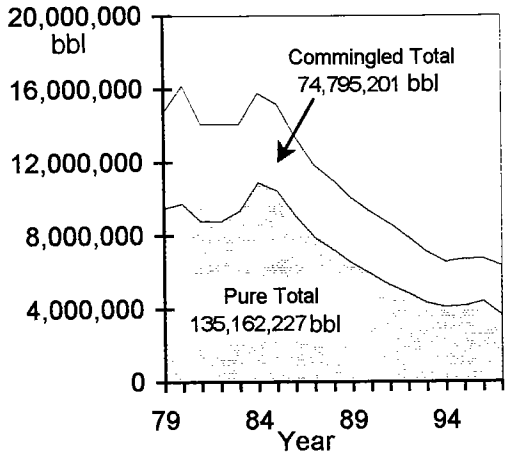

Figure 10. Graph of annual pure and commingled liquid (oil and condensate) production from leases producing from Lower Pennsylvanian (Atokan and Morrowan) reservoirs in Oklahoma, 1979–1997. Total cumulative lease liquid production (1979–1997) from Lower Pennsylvanian reservoirs is 209,957,428 barrels (bbl).

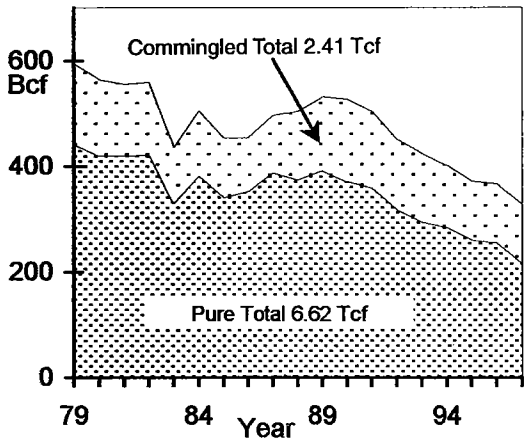

Figure 11. Graph of annual pure and commingled gas (associated and unassociated) production from leases producing from Lower Pennsylvanian reservoirs in Oklahoma, 1979–1997. Total cumulative lease gas production (1979–1997) from Lower Pennsylvanian reservoirs is 9,035,256,535 thousand cubic feet (mcf). Abbreviations: Bcf—billion cubic feet; Tcf—trillion cubic feet.

Desmoinesian Series ranges from less than 250 ft on the north, to more than 5,000 ft along the foredeep of the Anadarko basin.

Desmoinesian rocks conformably overlie the Atokan Series in the Anadarko basin and the Hugoton embayment; over this region these strata are very similar, so that the Atokan–Desmoinesian boundary is difficult to determine. Missourian sediments are mildly disconformable on Desmoinesian strata. Desmoinesian sediments overstep the limits of the Atokan Series on the northeastern margin of the Anadarko basin and onlap pre-Pennsylvanian rocks across the Nemaha uplift.

By the early Desmoinesian, the uplift along the Criner Hills in southern Oklahoma had ceased and generally quiescent conditions prevailed across the

Ardmore basin. Sandstones are mostly fine grained and well sorted, and probably came from the erosion of previous Springer sandstones, or alternatively from a metamorphic-source rock in the Red River–Muenster arch, southwest of the southern Oklahoma aulacogen. Desmoinesian facies are complex; most of the thin limestone layers of the Frensley, in particular, are discontinuous laterally and in part represent deposition between prodelta lobes. The Caddo anticline and Berwyn syncline continued to rise and sink in the early Desmoinesian, as indicated by both the high-energy carbonate facies and thinner shale sequences on the Caddo anticline and the lower-energy carbonates and thicker shale sequences in the Berwyn syncline (Tennant, 1981).

In the Ardmore basin, the first indication of uplift on the Ouachita foldbelt to the southeast is the occurrence—in the southernmost exposure of the Pumpkin Creek Limestone in the Ardmore basin (on Pumpkin Creek)—of common chert granules and a few chert pebbles greater than 0.5 in. in diameter. The chert granules decrease in abundance northward along the outcrop, and chert pebbles have not been observed north of Pumpkin Creek. Overlying strata also show a source from the southeast, based upon cross-bed directions, thickness trends, and distribution of chert pebbles derived from the Ouachitas.

The Desmoinesian Series in the Arkoma basin and adjacent area to the northwest consists of the Krebs, Cabaniss, and Marmaton Groups (Fig. 5). Only the Krebs is preserved across the present-day basin, and the Cabaniss and Marmaton Groups crop out along the northwest margin of the basin in Oklahoma. The source area for most of the Krebs Group strata is from the shelf area in the north (Visher, 1968). These units show marked thickening southward into the subsiding foreland basin. The depositional pattern was nonmarine to deltaic, with rapid deposition of sands, muds, and thin coals. The Boggy Formation, including the Bartlesville–Bluejacket, reached a thickness of 2,000 ft in the Arkoma basin, compared to a thickness of less than 500 ft on the shelf 45 mi to the north.

Uplift, folding, and erosion of the foreland basin occurred following deposition of the Krebs Group. Boggy and pre-Boggy rocks of the Krebs Group are more complexly folded and faulted than are post-Boggy strata, and there is a conspicuous difference in strike between the two. The Krebs is the only part of the Desmoinesian that was deposited during major subsidence of the Arkoma foreland basin before initial folding of the area. The Krebs is 7,000 ft thick in the basin, compared to about 800 ft thick on the shelf 50 mi to the north. During deposition of the remainder of the Desmoinesian Cabaniss and Marmaton Groups, the successor basin (termed the Arkoma seaway by Bennison, 1984) continued to receive terrigenous sediments, including some chert-pebble conglomerates, from the erosion of the rocks of the Ouachita foldbelt.

The Ouachita Mountains continued to be the primary source of terrigenous sediments in central Oklahoma throughout the remainder of the Pennsylvanian and into the Permian.

Desmoinesian Production

Names of Middle Pennsylvanian (Desmoinesian) producing intervals are listed in Table 3. The number of names for producing intervals in the Desmoinesian

Table 3.—Names Used for Middle Pennsylvanian Reservoir Rocks that Produce Petroleum in Oklahoma

MIDDLE PENNSYLVANIAN
Desmoinesian Series
Marmaton Group

Desmoines	Norris
Deese	Pharoah
Granite Wash	Big Lime
Holdenville	Wewoka
Cleveland	Culberson
Jones	Lone Grove
Dillard	Weiser
Homer	Pawnee
Wayside	Peru
Whiting	Cashion
Boyd	Dykeman
Glover	Oswego
Hewitt	Wetumka
Charlson	Wheeler
Kistler	Rue

Cabaniss Group

Cherokee	Tatums
Calvin	Pooler
Fusulinid	Eason
Johnson	Graham
Arnold	Hart
Prue	Skinner
Lagonda	Chelsea
Perrymen	Allen
Gibson	Olympic
Squirrel	Berry
Wanette	Chicken Farm
Fulton	Ashalintubbi
Senora	Carpenter
Verdigris	Morris
Tussy	Williams
Edwards	Thurman
Mona	

Krebs Group

Cherokee	Boggy
Red Fork	Osborne
Earlsboro	Hefner
Burbank	Booch
Inola	Tucker
Bartlesville	Burgess
Bluejacket	Hartshorne
Glenn	

Cumulative production (pure and commingled)
(1/1/79 through 12/31/97)
Oil: 872,228,104 bbl
Gas: 13,019,273,083 mcf

is large, mainly because of the widespread area of deposition and many facies changes. Most of these intervals have both marine and non-marine (deltaic) components.

The oil and gas lease production map for the Middle Pennsylvanian (Fig. 12) shows the extensive area of Desmoinesian production in Oklahoma. The dominance of the fluvial-deltaic areas in northern Oklahoma extends southward into the Anadarko basin in western Oklahoma. The Desmoinesian rocks in the Arkoma basin and southern Oklahoma generally produce from marine clastics. In the Anadarko basin and shelf areas, the platform carbonates, principally the Oswego limestone of the Marmaton Group, are also productive. Stratigraphic traps dominate in the Middle Pennsylvanian production; however, many have structural components in areas of local structure.

Graphs of annual production for the period 1979 through 1997 from Middle Pennsylvanian reservoirs for pure and commingled leases show liquid production (crude oil and condensate) in Figure 13 and gas production (associated and non-associated) in Figure 14. Cumulative lease production from Middle Pennsylvanian reservoirs (pure and commingled) for the period 1979–1997 is 872,228,104 bbl of oil and 13,019,273,083 mcf of gas.

Upper Pennsylvanian

Missourian Series

The Missourian Series in the Hugoton embayment and the northern shelf of the Anadarko basin is predominantly carbonate strata with shale interbeds. In the Anadarko basin, the Missourian Series consists of shale and sandstones with minor carbonate units. Along the western margin of the Hugoton embayment the Missourian carbonate-shale section is replaced by a clastic sequence of shales, siltstones, and sandstones, commonly red in color. On the northern flank of the Wichita–Amarillo uplift, the Missourian Series is composed of arkosic and carbonate "wash" sediments that were eroded from the uplift.

The major positive tectonic elements active during Missourian time were: (1) the Arbuckle uplift to the south, from which conglomeratic debris was eroded; (2) the Wichita–Amarillo uplift to the southwest, which was a source area of coarse detritus; and (3) the Apishapa uplift to the west-southwest, from which mostly fine-grained clastics were eroded.

Southward across Kansas, toward the Anadarko basin, carbonates of the early Missourian thicken at the expense of the shales and form locally thick, linear carbonate banks. Farther south, these massive carbonates are replaced abruptly by shales and fine-grained sandstones, with several regionally extensive limestone marker beds. Work in recent years indicates that the Missourian clastic section of the Anadarko basin is composed of a number of clastic wedges of limited areal extent.

The depositional history of the Hoxbar Group in the Ardmore basin is poorly understood, and source directions have not been established. It is predominantly a marine sequence with several named limestone units, but one local coal layer (about 3 ft thick) occurs just below the Daube Limestone. Some of the scattered limestone and chert-pebble conglomerates may have come from the uplifting Hunton arch on the shelf to the north.

Discussion of Missourian petroleum reservoirs and production is deferred to the end of the next section on the "Virgilian Series."

Virgilian Series

The Virgilian Series consists of limestones with shale interbeds in the Hugoton embayment and adjacent shelf area. In central Oklahoma, the Virgilian Series consists of continental to shallow-marine shales, siltstones, and mudstones; to the west, in the Anadarko basin, the Virgilian is represented by prodelta shales and delta-plain sandstones. The shelf carbonates of the Hugoton embayment grade westward into red shales, siltstones, and some sandstones in southeastern Colorado and northwestern New Mexico. These clastic sediments were probably derived from the Apishapa and Sierra Grande uplifts, and they represent mixed marine and continental deposits. The Apishapa uplift was almost completely covered by Virgilian sediment. The Wichita–Amarillo uplift remained a positive feature during Virgilian time, and coarse detritus was deposited along its northern margin.

In the early part of the Virgilian, shales and sandstones of the Douglas Group and the equivalent Vamoosa Formation were widely deposited over the Hugoton embayment and the Anadarko basin. These sediments represent fluvial-deltaic environments, indicating that basin filling was nearly complete. Later in Virgilian time, wedges of clastic material derived from the Ouachita source area to the east-southeast accumulated along the eastern margin of the Anadarko basin and prograded westward. These clastic wedges were deposited during the regressive phases of cyclic sedimentation in response to the lowering of sea level. The transgressive phases, in response to rises in sea level, were marked by deposition of limestones over the Hugoton embayment and the adjacent shelf area. These limestones are characterized by shelf-edge carbonate banks that are as much as 300 ft thick and consist mainly of fossil hash and oolites. In this manner, a constructional shelf was established along the eastern margin of the Anadarko basin in Virgilian time.

In southern Oklahoma, the Virgilian Arbuckle orogeny produced uplift and sharp folding of the Arbuckle anticline, and simultaneously produced sharp folding, compression, and faulting of the Ardmore basin, Criner Hills axis, and Marietta basin. The Collings Ranch Conglomerate, preserved in the central Arbuckle Mountains, was deposited in middle Virgilian time, followed in the late Virgilian by the deposition of great alluvial fans of limestone-cobble conglomerates (Vanoss Conglomerate) around the north, west, and south margins of the Arbuckle anticline. In the Ardmore basin, these limestone-cobble conglomerates were deposited across most of the area and rest unconformably on the

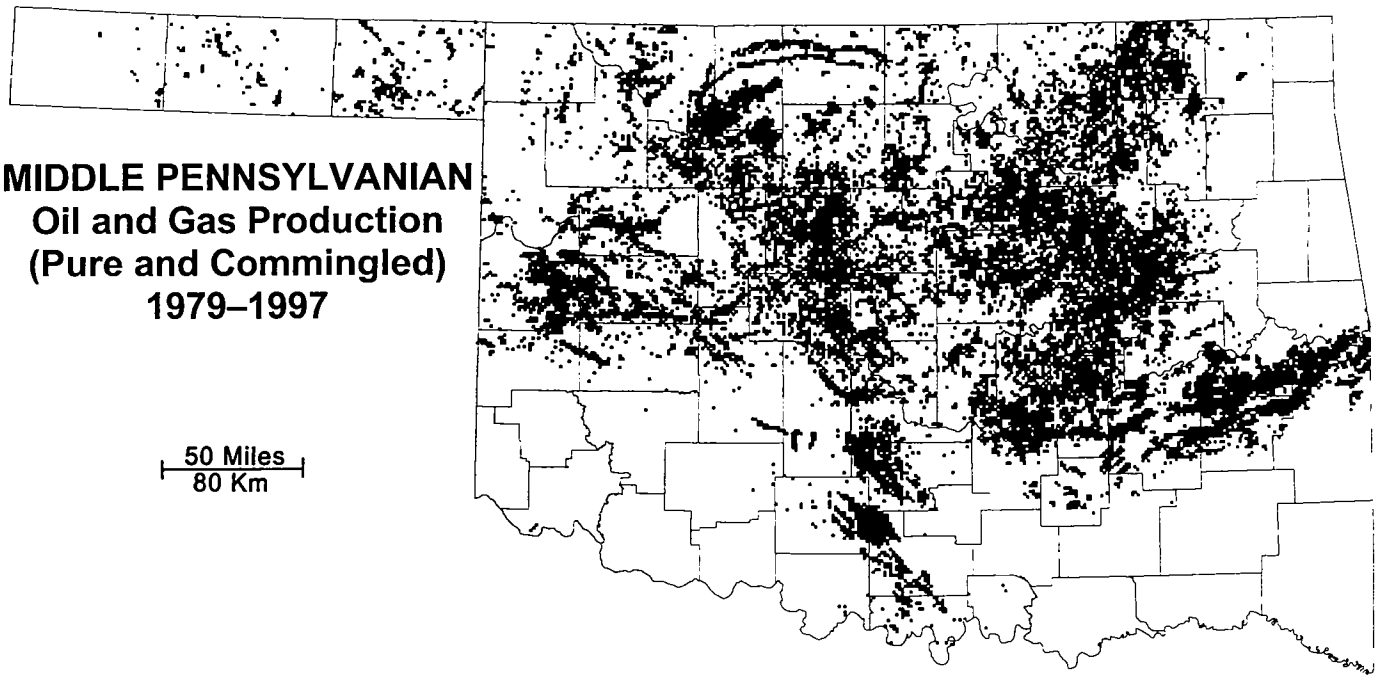

Figure 12. Map of oil and gas lease production from Middle Pennsylvanian (Desmoinesian) reservoirs in Oklahoma, 1979–1997. Map was generated by Geo Information Systems from the Natural Resources Information System (NRIS) data files.

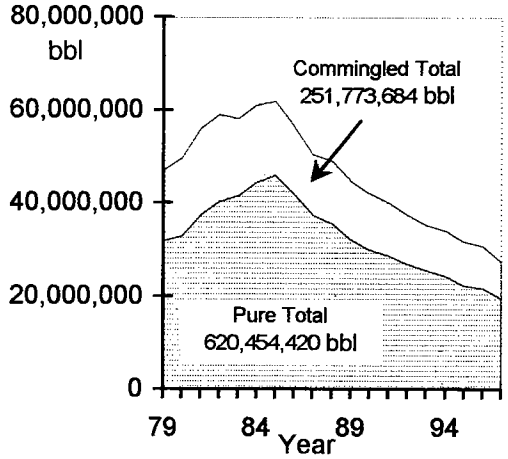

Figure 13. Graph of annual pure and commingled liquid (oil and condensate) production from leases producing from Middle Pennsylvanian reservoirs in Oklahoma, 1979–1997. Total cumulative lease liquid production (1979–1997) from Middle Pennsylvanian reservoirs is 872,228,104 barrels (bbl).

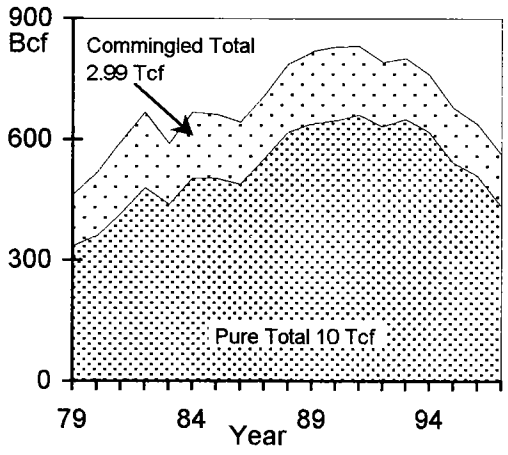

Figure 14. Graph of annual pure and commingled gas (associated and non-associated) production from leases producing from Middle Pennsylvanian reservoirs in Oklahoma, 1979–1997. Total cumulative lease gas production (1979–1997) from Middle Pennsylvanian reservoirs is 13,019,273,083 thousand cubic feet (mcf). Abbreviations: Bcf—billion cubic feet; Tcf—trillion cubic feet.

steeply truncated margins of all of the Mississippian and Pennsylvanian formations (Ham, 1969).

Missourian and Virgilian Production

Names of Upper Pennsylvanian (Missourian and Virgilian) producing intervals are listed in Table 4, and the areas of Upper Pennsylvanian production are shown in Figure 15. Most of these intervals have both marine and non-marine (deltaic) components. Deltaic deposition was common in north-central Oklahoma, whereas shallow-marine clastic deposition extended to northwestern Oklahoma and into the Anadarko and Ardmore basins. The limited production from carbonate reservoirs is located in central Oklahoma and the Panhandle. Stratigraphic traps account for most of the production from the Upper Pennsylvanian reservoirs; however, local structures are also productive from these intervals.

Table 4.—Names Used for Upper Pennsylvanian Reservoir Rocks that Produce Petroleum in Oklahoma

UPPER PENNSYLVANIAN

Virgilian Series

Wabaunsee Group

Granite Wash-Penn	Vertz
Cisco	Garber
Campbell	Cooper
Ragan	Ruel Blake
Sams	Newkirk
Crews	Cache Creek

Shawnee Group

Pawhuska	Elgin
Topeka	Hoover
Thomas	Armstrong
Blaydes	Sears
Deer Creek	Swastika
Garner	Zypsie
Megargle	Carmichael
Coline	Rowe
Griffin	Oread
Gunsight	Endicott

Douglas Group

Douglas	Stalnaker
Lovell	Perry
Wynona	Niles
Haskell	Henderson
Tonkawa	Hervey

Missourian Series

Ochelata Group

Missouri	Daube
Granite Wash-Missouri	County Line
Hoxbar	Hoxbar Oolitic
Lansing	Kansas City
Loco	

Skiatook Group

Yule	Osage-Layton
Anadarche	Musselem
Oolitic	Bayou
Belle City	Burns
Dewey	Burns-Brundidge
Wade	Edwards
Hedlund	Randolph
Tuley	Layton
Medrano	Checkerboard
Hogshooter	Sasakwa
Healdton	Confederate
Marchand	Chubbee
Cottage Grove	Hewit

Cumulative production (pure and commingled) (1/1/79 through 12/31/97)

Oil: 286,975,776 bbl
Gas: 2,605,154,393 mcf

Graphs of annual production for the period 1979 through 1997 from Upper Pennsylvanian reservoirs for pure and commingled leases show liquid production (crude oil and condensate) in Figure 16 and gas production (associated and non-associated) in Figure 17. Cumulative lease production from Upper Pennsylvanian reservoirs (pure and commingled) for the period 1979–1997 is 286,975,776 bbl of oil and 2,605,154,393 mcf of gas.

PERMIAN GEOLOGY AND RESERVOIRS

Permian

Wolfcampian Series

In Permian time, a fairly well-defined seaway extended north–south from west Texas across the western half of the southern Midcontinent. Coarse clastics were eroded from the Ouachita lowlands on the east, the ancestral Rocky Mountains (Sierra Grande and Apishapa uplifts) on the west, and Amarillo–Wichita uplift in the center.

Tectonic elements present in the Anadarko basin–Hugoton embayment region during the Late Pennsylvanian persisted into the Early Permian; however, the influence of these features diminished greatly during the Permian. The Wichita uplift, a significant positive element during the Pennsylvanian, probably was expressed topographically as an archipelago in the Early Permian. There, a terrain of Paleozoic limestone and Precambrian granite was eroded, and clasts of these rocks are present in Wolfcampian sediments on the flanks of the uplift. The Anadarko basin continued to subside in the Early Permian, but far more slowly than in the Pennsylvanian. As a result of continued subsidence, Wolfcampian sediments lie comformably upon Virgilian strata within the basin, and regional lithofacies patterns of the Wolfcampian and Virgilian Series are quite similar.

In a northeast–southwest belt across the Midcontinent, Wolfcampian rocks consist mainly of cyclic, shallow-marine limestones and shales. These sediments make up the Admire, Council Grove, and Chase Groups. These units and many of their constituent limestone formations can be recognized over Kansas, western Oklahoma, and the Oklahoma Panhandle. Mostly fine-grained, clastic redbed sediments border this belt of limestones and shales on the east and west; these strata represent mixed marine and continental environments, and they are indicative of marine regression from the region. In south-central Oklahoma, clastic sediments considered Wolfcampian in age (and referred to the upper part of the Pontotoc Group) covered all but the highest peaks of the Wichita uplift.

Discussion of all Permian petroleum reservoirs and production is deferred to the end of the section on the "Ochoan Series."

Leonardian Series

Leonardian time was marked by continued subsidence of the Anadarko basin and the Hugoton embayment, and by continued regression of the sea from the

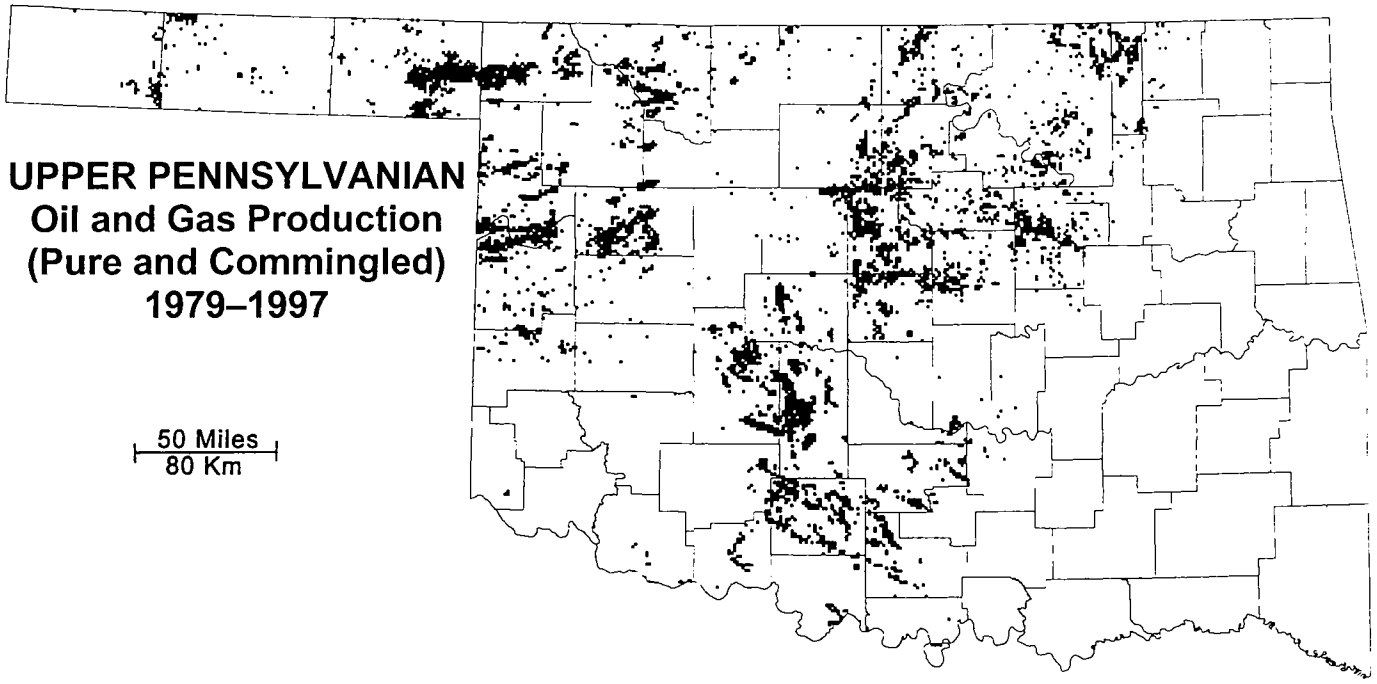

Figure 15. Map of oil and gas lease production from Upper Pennsylvanian (Missourian and Virgilian) reservoirs in Oklahoma, 1979–1997. Map was generated by Geo Information Systems from the Natural Resources Information System (NRIS) data files.

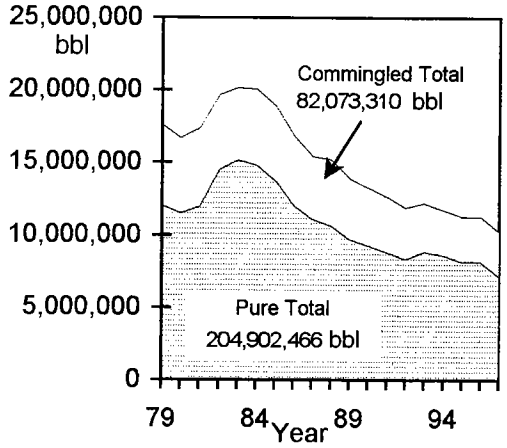

Figure 16. Graph of annual pure and commingled liquid (oil and condensate) production from leases producing from Upper Pennsylvanian reservoirs in Oklahoma, 1979–1997. Total cumulative lease liquid production (1979–1997) from Upper Pennsylvanian reservoirs is 286,975,776 barrels (bbl).

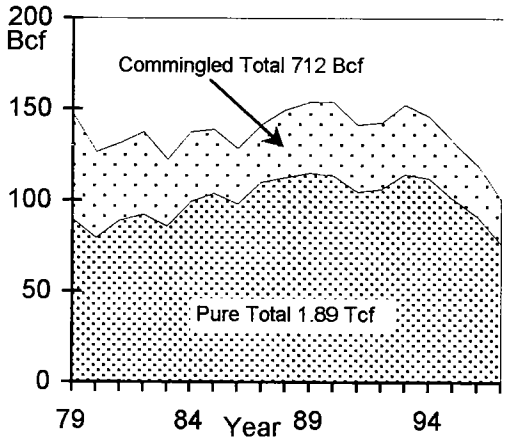

Figure 17. Graph of annual pure and commingled gas (associated and non-associated) production from leases producing from Upper Pennsylvanian reservoirs in Oklahoma, 1979–1997. Total cumulative lease gas production (1979–1997) from Upper Pennsylvanian reservoirs is 2,605,154,393 thousand cubic feet (mcf). Abbreviations: Bcf—billion cubic feet; Tcf—trillion cubic feet.

region. As a result, the dominant lithologies of the Leonardian Series are redbeds and evaporites deposited in continental and shallowing marine environments; cyclic patterns of sedimentation suggest that eustatic fluctuations of sea level continued in Leonardian time.

Strata now cropping out on the east side of the Anadarko basin are the Wellington and Garber Formations and the Hennessey Group. These redbed clastic units, deposited near the eastern shore of the basin, were derived by erosion of lowland areas that extended across eastern Oklahoma and adjacent areas. The Garber and Wellington outcrops comprise a complex system of interbedded alluvial and deltaic sandstones and shales that are thickest and coarsest in central and south-central Oklahoma. These strata, and shales of

the overlying Hennessey, grade westward into two thick evaporite units, the Wellington and Cimarron evaporites, which consist of interbedded halite, shale, and anhydrite.

The Wichita uplift continued to have a modest influence on sedimentation in the Anadarko basin. Clastic debris was shed northward onto the south flank of the basin where it interfingered with the evaporites.

Guadalupian Series

In Guadalupian time, the Anadarko basin continued to subside, and it received as much as 1,500 ft of redbeds and evaporites along its depocenter. The Wichita uplift subsided at a somewhat slower rate than the basin, and all but the highest mountain peaks were probably buried by fine clastics. Sands entered the basin from east, north, and northwest, and graded into shale, salt, and gypsum toward the central and southwest parts of the basin. The Wichita Mountains were essentially buried, and the sources for clastics deposited in the southern and eastern parts of the basin were the lowland areas of eastern Oklahoma and the deeply eroded Ouachita belt of southeastern Oklahoma and northeastern Texas.

Ochoan Series

Ochoan rocks are mainly redbed sandstones and shales, but they contain some anhydrite and dolomite in the western part of the Anadarko basin. Little is known about Ochoan paleogeography in and around the Anadarko basin, but it likely was similar to that of the late Guadalupian. Outcropping Ochoan strata typically contain chaotic structures, collapse features, and other evidence of disturbed bedding due to dissolution of underlying Guadalupian halite beds along the flanks of the Anadarko basin. Such collapse features also occur in some of the Guadalupian and post-Permian strata.

Permian Production

Names of Permian producing intervals are listed in Table 5. Most of these intervals are producing from shallow platform carbonates, although marine clastics are also productive.

The oil and gas lease production map for the Permian (Fig. 18) shows the four main areas of Permian production. Platform carbonates produce from structural and stratigraphic traps, sometimes combination traps, in north-central Oklahoma and on the Wichita uplift in southwest Oklahoma. The large area of Permian production in the Oklahoma Panhandle is part of the Guymon–Hugoton gas field, one of the world's largest gas fields and a very large stratigraphic trap in a platform carbonate. Permian marine clastics produce from structural traps in southern Oklahoma.

Graphs of annual production for the period 1979 through 1997 from Permian reservoirs for pure and commingled leases show liquid production (crude oil and condensate) in Figure 19 and gas production (associated and non-associated) in Figure 20. Cumulative lease production from Upper Pennsylvanian reservoirs (pure and commingled) for the period 1979–1997 is 68,396,513 bbl of oil and 1,577,393,162 mcf of gas.

Table 5.—Names Used for Permian Reservoir Rocks that Produce Petroleum in Oklahoma

PERMIAN	
Leonardian Series	
Granite Wash-Permian	Ramsey
Sumner	Fortuna
Nichols	
Wolfcampian Series	
Wolfcampian	Pontotoc
Chase Group	
Herington	Winfield
Panhandle Dolomite	Frensley
Brown Dolomite	Fort Riley
Kisner	Florence
Nolan	Hoy
Krider	Wreford
Crystaline	White Dolomite
Council Grove Group	
Crouse	Neva
Olson	Red Eagle
Noble-Olson	Foraker
Admire Group	
Admire	Belveal

Cumulative production (pure and commingled) (1/1/79 through 12/31/97)
Oil: 68,396,513 bbl
Gas: 1,577,393,162 mcf

SUMMARY

Reservoirs in Pennsylvanian and Permian rocks of Oklahoma yield large amounts of oil and gas throughout the State. The first commercial production of oil in Oklahoma was discovered in 1897, and it came from a Pennsylvanian reservoir—the Bartlesville sand. The geologic history of reservoir development and petroleum entrapment in these rocks encompasses many depositional, diagenetic, orogenic, and tectonic environments. Discovery of new reservoirs and the application of new methods to develop old reservoirs in the Pennsylvanian and Permian rocks continue today.

Graphs combining the oil and gas production for all five geologic intervals in the Pennsylvanian and Permian annual production of liquids (Fig. 21) and gas (Fig. 22) are shown for the period from 1979 through 1997. Total production of liquids (crude oil and condensate) from Pennsylvanian and Permian reservoirs for both pure and commingled leases for 1979–1997 was 1,637,564,847 barrels (about 1.64 million bbl). Total production of gas (casing-head and natural gas) from Pennsylvanian and Permian reservoirs for

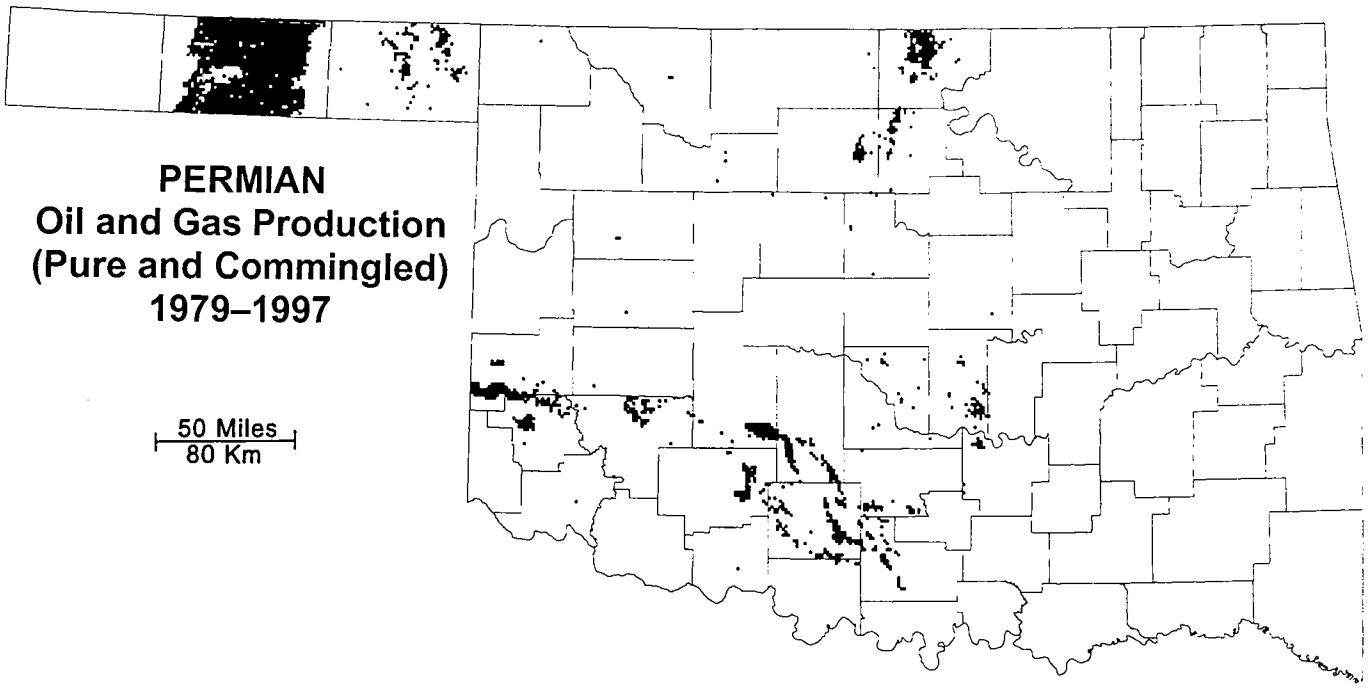

Figure 18. Map of oil and gas lease production from Permian reservoirs in Oklahoma, 1979–1997. Map was generated by Geo Information Systems from the Natural Resources Information System (NRIS) data files.

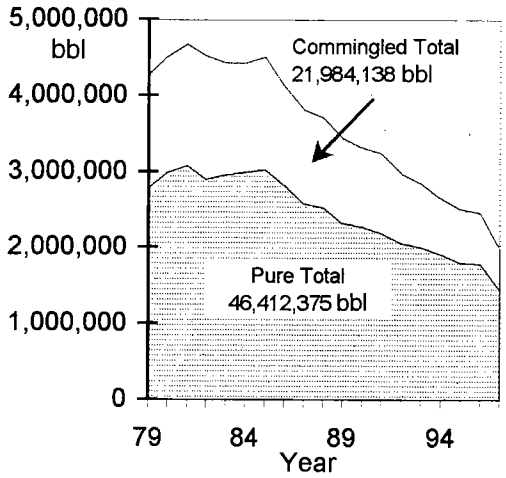

Figure 19. Graph of annual pure and commingled liquid (oil and condensate) production from leases producing from Permian reservoirs in Oklahoma, 1979–1997. Total cumulative lease liquid production (1979–1997) from Permian reservoirs is 68,396,513 barrels (bbl).

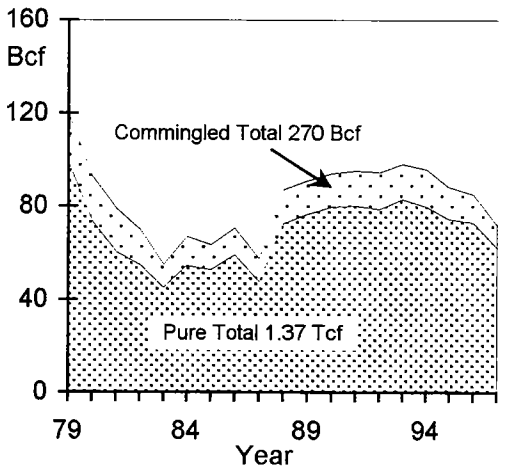

Figure 20. Graph of annual pure and commingled gas (associated and non-associated) production from leases producing from Permian reservoirs in Oklahoma, 1979–1997. Total cumulative lease gas production (1979–1997) from Permian reservoirs is 1,577,393,162 thousand cubic feet (mcf). Abbreviations: Bcf—billion cubic feet; Tcf—trillion cubic feet.

both pure and commingled leases for 1979–1997 was 29,797,550,119 thousand cubic feet (about 29.8 trillion cubic feet) of gas.

REFERENCES CITED

Adams, W. L., 1964, Diagenetic aspects of lower Morrowan Pennsylvanian sandstones, northwestern Oklahoma: American Association of Petroleum Geologists Bulletin, v. 48, p. 1568–1580.

Bennison, A. P., 1984, Shelf to trough correlations of Late Desmoinesian and Missourian carbonate banks and related strata, northeast Oklahoma, *in* Hyne, N. J. (ed.), Limestones of the Mid-Continent: Tulsa Geological Society Special Publication 2, p. 93–126.

Brown, R. W.; and Northcutt, R. A., 1993, Springer marine sandstone—Anadarko basin, *in* Bebout, D. G.; White, W. A.; Hentz, T. F.; and Grasmick, M. K. (eds.), Atlas of major Midcontinent gas reservoirs: Bureau of Economic Geology, University of Texas at Austin, p. 53–54.

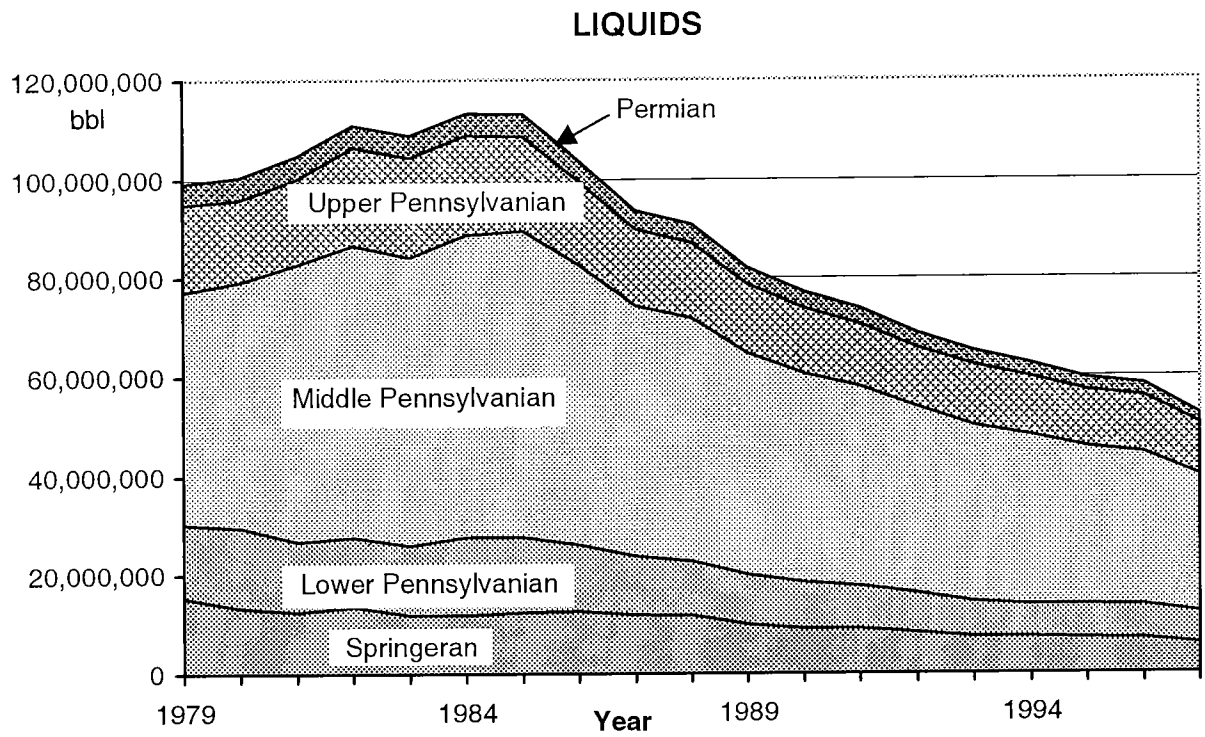

Figure 21. Graph of annual pure and commingled liquid (crude oil and condensate) production in barrels (bbl) from leases producing from all Pennsylvanian and Permian reservoirs in Oklahoma, 1979–1997. Total cumulative lease liquid production (1979–1997) from all Pennsylvanian and Permian reservoirs was 1,637,564,847 bbl.

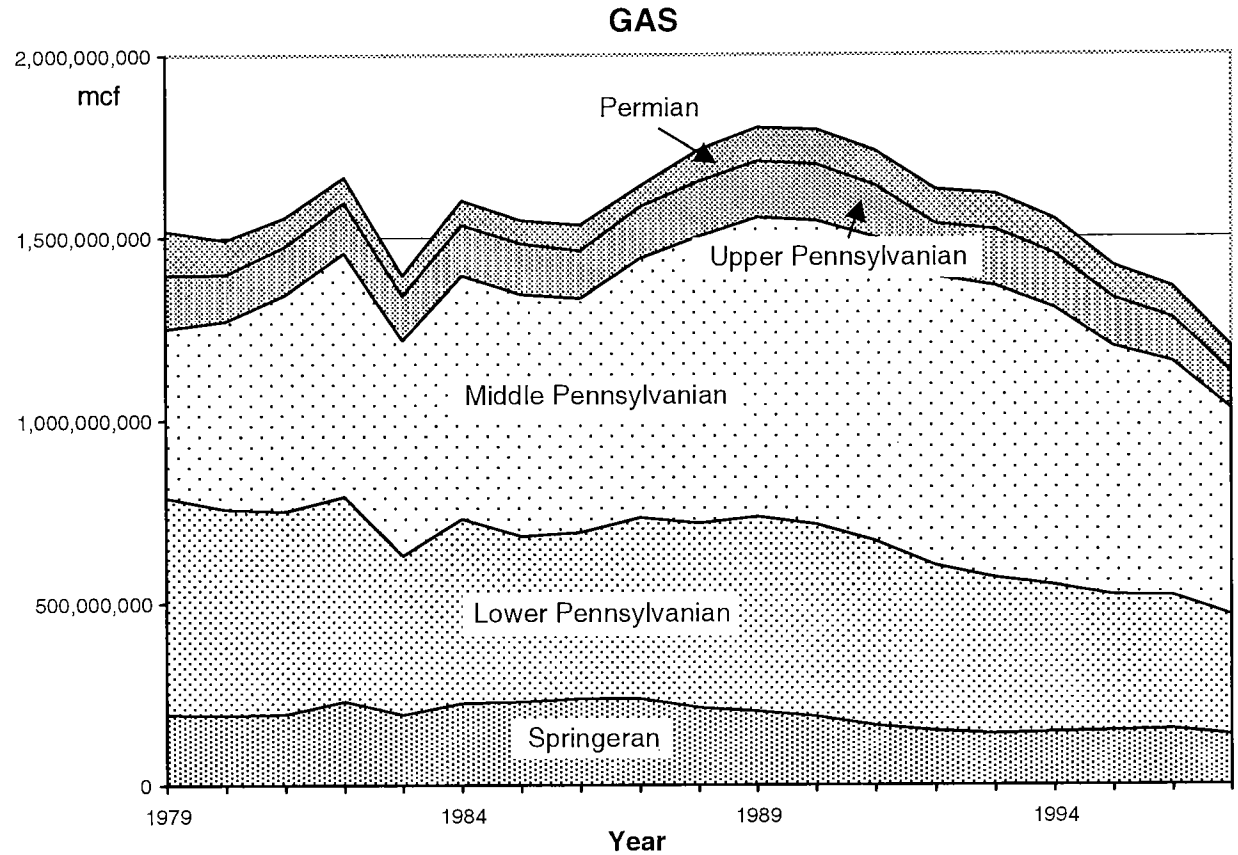

Figure 22. Graph of annual pure and commingled gas (associated and non-associated) production from leases producing from all Pennsylvanian and Permian reservoirs in Oklahoma, 1979–1997. Total cumulative lease gas production (1979–1997) from all Pennsylvanian and Permian reservoirs was 29,797,550,119 thousand cubic feet (mcf).

Evans, J. L., 1979, Major structural and stratigraphic features of the Anadarko basin, *in* Hyne, N. J. (ed.), Pennsylvanian sandstones of the Mid-Continent: Tulsa Geological Society Special Publication 1, p. 97–113.

Ham, W. E., 1969, Regional geology of the Arbuckle Mountains, Oklahoma: Oklahoma Geological Survey Guidebook 17, 52 p.

Ham, W. E.; and Wilson, J. L., 1967, Paleozoic epeirogeny and orogeny in the central United States: American Journal of Science, v. 265, p. 332–407.

Houseknecht, D. W., 1986, Evolution from passive margin to foreland basin: the Atoka Formation of the Arkoma basin, south-central U.S.A., *in* Allen, P. A.; and Homewood, P. (eds.), Foreland basins: Blackwell Scientific Publications, Oxford, International Association of Sedimentologists Special Publication 8, p. 327–345.

Johnson, K. S. (ed.), 1996, Deltaic reservoirs in the southern Midcontinent, 1993 symposium: Oklahoma Geological Survey Circular 98, 295 p.

Johnson, K. S.; and Cardott, B. J., 1992, Geologic framework and hydrocarbon source rocks of Oklahoma, *in* Johnson, K. S.; and Cardott, B. J. (eds.), Source rocks in the southern Midcontinent, 1990 symposium: Oklahoma Geological Survey Circular 93, p. 21–37.

Johnson, K. S.; Amsden, T. W.; Denison, R. E.; Dutton, S. P.; Goldstein, A. G.; Rascoe, B., Jr.; Sutherland, P. K.; and Thompson, C. M., 1988, Southern Midcontinent region, *in* Sloss, L. L. (ed.), Sedimentary cover—North American craton, U.S.: Geological Society of America, The Geology of North America, v. D-2, p. 307–359. [Reprinted in 1989 as Oklahoma Geological Survey Special Publication 89–2, 53 p.]

McKee, E. D., and 16 others, 1967, Paleotectonic maps of the Permian System: U.S. Geological Survey Miscellaneous Geologic Investigations Map I-450, scale 1:5,000,000.

McKee, E. D., and 17 others, 1975, Paleotectonic investigations of the Pennsylvanian System in the United States: U.S. Geological Survey Professional Paper 853, part I, 349 p.; part II, 192 p.; part III, 17 plates.

Owen, M. R.; and Carozzi, A. V., 1986, Southern provenance of upper Jackfork Sandstone, southern Ouachita Mountains: cathodoluminescence petrology: Geological Society of America Bulletin, v. 97, p. 110–115.

Rascoe, B., Jr., and Adler, F. J., 1983, Permo-Carboniferous hydrocarbon accumulations, Mid-Continent, U.S.A.: American Association of Petroleum Geologists Bulletin, v. 67, p. 979–1001.

Shelby, J. M., 1979, Upper Morrow fan-delta deposits of Anadarko basin [abstract]: American Association of Petroleum Geologists Bulletin, v. 63, p. 2119.

Shideler, G. L., 1970, Provenance of Johns Valley boulders in late Paleozoic facies, southeastern Oklahoma and southwestern Arkansas: American Association of Petroleum Geologists Bulletin, v. 54, p. 789–806.

Swanson, D. C., 1979, Deltaic deposits in the Pennsylvanian upper Morrow Formation of the Anadarko basin, *in* Hyne, N. J. (ed.), Pennsylvanian sandstones of the Mid-Continent: Tulsa Geological Society Special Publication 1, p. 115–168.

Tennant, S. H., 1981, Lithostratigraphy and depositional environments of the upper Dornick Hills Group (Lower Pennsylvanian) in the northern part of the Ardmore basin, Oklahoma: University of Oklahoma unpublished M.S. thesis, 291 p.

Visher, G. S., 1968, Depositional framework of the Bluejacket–Bartlesville Sandstone, *in* Visher, G. S. (ed.), Geology of the Bluejacket–Bartlesville Sandstone, Oklahoma: Oklahoma City Geological Society Guidebook, p. 32–44.

Major Pennsylvanian Fluvial-Deltaic Light-Oil Reservoir Systems in Oklahoma

Jock A. Campbell
Oklahoma Geological Survey
Norman, Oklahoma

Robert A. Northcutt
Independent Geologist
Oklahoma City, Oklahoma

Richard D. Andrews
Oklahoma Geological Survey
Norman, Oklahoma

Roy M. Knapp
University of Oklahoma
Norman, Oklahoma

ABSTRACT.—The Oklahoma Geological Survey (OGS) identified and studied the major Pennsylvanian fluvial-dominated deltaic light-oil reservoir systems in Oklahoma during 1993–1997. They were mapped on a new map of geologic provinces based primarily on Pennsylvanian structure as a base. Eight play-based publications and workshops were developed from those studies of 11 depositional systems. Twenty-one geologic-reservoir case histories were also developed, nine of which also underwent reservoir-engineering studies.

Although each reservoir system is unique in terms of geographic distribution, variations in thickness, and details of facies relations, there are also numerous similarities because of the generally fine-grained sandstones deposited in fluvial-deltaic and floodplain environments on a stable shelf.

In the 21 reservoirs studied, there was commonly a lack of good reservoir management practiced. The application of the two elementary approaches to reservoir management would have improved oil recovery in every case. These are: (1) geologic description as a guide to exploitation and development, and (2) the disposal of produced water in the structurally lowest position as a first step to pressure maintenance.

BACKGROUND

Studies by the Texas Bureau of Economic Geology (Fisher and Galloway, 1983; Tyler and others, 1984) indicated that fluvial and fluvial-dominated deltaic oil reservoirs have consistently low- to average-oil recovery efficiencies, largely due to reservoir heterogeneities. Inasmuch as fluvial-deltaic light-oil reservoirs are far more common than those of fluvial origin, the U.S. Department of Energy determined to fund studies that potentially could improve oil recovery from this class of oil reservoirs, designated DOE Class I (U.S. Department of Energy, 1991).

In December 1997, the Oklahoma Geological Survey (OGS) completed a 5-year study of fluvial-dominated deltaic (FDD) light-oil reservoirs in Oklahoma, with cooperative funding from the U.S. Department of Energy (DOE) under their Class I petroleum reservoirs program (Cooperative agreement no. DE-FC22-93BC 14956). The investigative team also included personnel from Geo Information Systems and the School of Petroleum and Geological Engineering, both of The University of Oklahoma.

PURPOSE

The purpose of the program was to identify and transfer technologies (including geologic mapping techniques) that could sustain and perhaps improve production from FDD reservoirs in and beyond Oklahoma. The immediate objectives of the FDD project were:

Campbell, J. A.; Northcutt, R. A.; Andrews, R. D.; and Knapp, R. M., 2001, Major Pennsylvanian fluvial-deltaic light-oil reservoir systems in Oklahoma, *in* Johnson, K. S. (ed.), Pennsylvanian and Permian geology and petroleum in the southern Midcontinent, 1998 symposium: Oklahoma Geological Survey Circular 104, p. 21–32.

- Identify all light-oil FDD reservoirs in Oklahoma.
- Group those reservoirs into geologic plays (a play can be defined as a genetic rock system that has similar exploration and development characteristics).
- Collect, organize, and analyze available data on these reservoirs.
- Conduct characterization and simulation studies on selected reservoirs in each play.
- Implement a technology-transfer program directed toward the oil operators of FDD reservoirs and other interested parties.

The latter consisted of workshops conducted over a 2½-year period and continues through the workshop publications and the OGS NRIS (Natural Resources Information System of Oklahoma) computer facility in Norman, Oklahoma. That facility is jointly funded through the Petroleum Technology Transfer Council (PTTC). In addition, the workshops are being repeated for the benefit of those who were unable to attend previously under the joint auspices of the Oklahoma City Geological Society, the Tulsa Geological Society, the PTTC, and the OGS. The 11 plays were presented at 13 workshops between June 1995 and November 1997. They were prepared as eight publications and workshop titles (Table 1). Four workshops were presented more than one time. Total attendance at the original 13 workshops was nearly 1,100 persons, including about 590 operators of Oklahoma oil and gas leases. Other attendees were mostly geologists, geophysicists, engineers, and petroleum landsmen.

INTRODUCTION

A geologic provinces map (Fig. 1; Northcutt and Campbell, 1995, 1996a, 1996b) based on structure developed primarily during Pennsylvanian time, was developed in order to improve understanding of the regional setting of depositional systems.

All of the 11 FDD light-oil reservoirs studied are of Pennsylvanian age (Fig. 2). They are located primarily in the Cherokee platform province (Fig. 1), which extends northward into Kansas. The more extensive reservoir systems extend locally into the Arkoma basin, Nemaha uplift, Anadarko shelf, and/or the Anadarko basin areas of Oklahoma, Kansas, and the Texas Panhandle. One play, the Morrow Formation, extends also into southeastern Colorado.

The 11 plays are important in Oklahoma because

Table 1.—Fluvial-Dominated Deltaic (FDD) Plays and Accompanying Reservoir Studies

OGS Special Publication	Play	Field	County	Reservoir	No. of prod. wells	Township and range
SP 97-3	Tonkawa	Blackwell*	Kay	Tonkawa	56	27&28N–1W
SP 96-1	Layton and Osage-Layton	Lake Blackwell E*	Payne	Osage-Layton	12	19N–1E
		Coyle S	Payne	Layton	13	17N–1E
SP 97-5	Cleveland and Peru	Pleasant Mound*	Lincoln	Cleveland	35	16N–6E
		Hogshooter	Washington	Peru	12	26N–13E
SP 96-2	Skinner and Prue	Perry SE	Noble	Skinner	39	21N–1E&1W
		Salt Fork N*	Grant	Skinner	20	25N–3&4W
		Guthrie SW	Logan	L. Skinner	10	16N–2&3W
		Long Branch*	Payne	Prue	16	18N–4E
SP 97-1	Red Fork	Carmen N*	Alfalfa	Red Fork	14	24&25N–12W
		Otoe City S	Noble	Red Fork	28	22N–1E
		Long Branch	Payne	Red Fork	11	18N–4E
SP 97-6	Bartlesville	Paradise*	Payne	Bartlesville	12	17&18N–1E
		Russell NW	Logan	Bartlesville	34	18N–2&3W
		Ohio-Osage	Osage	Bartlesville	15	21N–9E
SP 95-3	Booch	Holdenville	Hughes	Booch	64	6N–8E
		Seminole	Seminole	Booch	90	9&10N–7E
		Greasy Creek*	Hughes	Booch	15	8&9N–11E
SP 95-1	Morrow	Canton SW	Dewey	L. Morrow	34	18N–14W
		Balko S	Beaver	U. Morrow	48	2N–23ECM
		Rice NE*	Texas	U. Morrow	30	3N–10ECM
					608+	

NOTE: All publications are of the Oklahoma Geological Survey. Number of Special Publications is 8; number of play studies is 11; number of reservoir studies is 21; number of reservoir simulation studies is 9 (indicated by *). +Arithmetic mean of producing wells is 29.

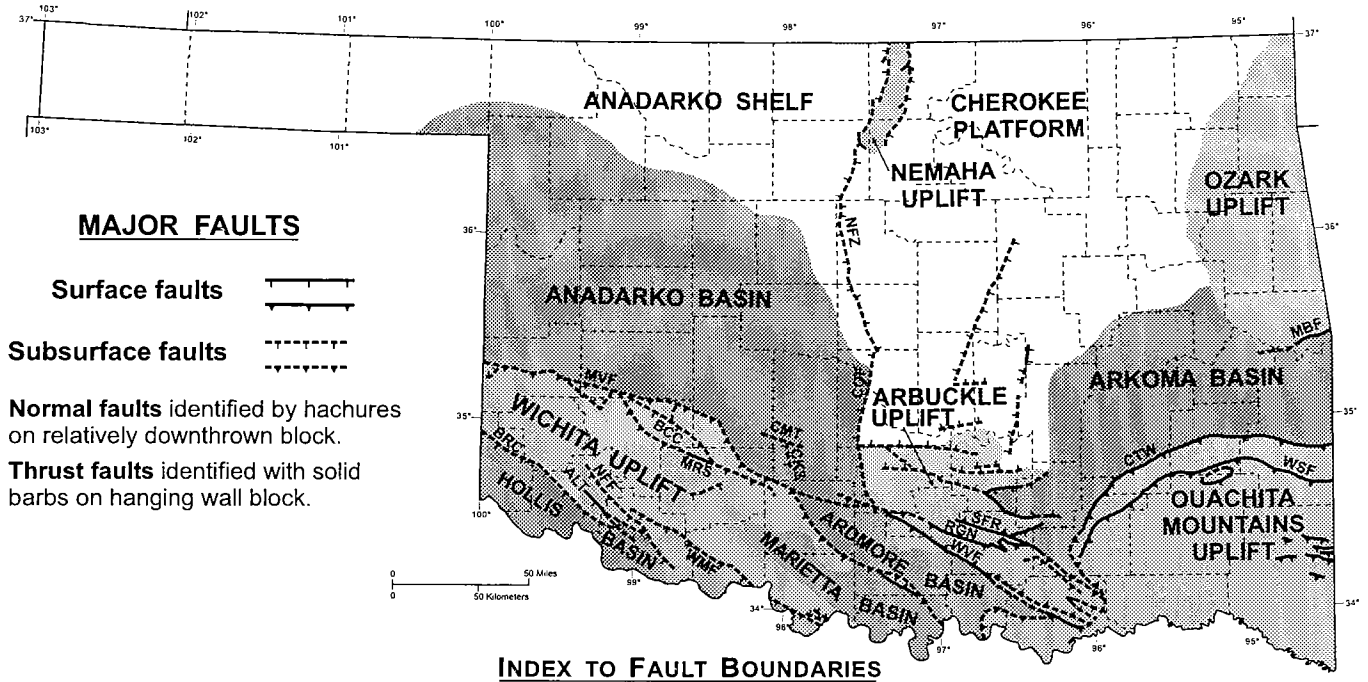

INDEX TO FAULT BOUNDARIES

ALT	Altus Fault	COF	Central Oklahoma Fault Zone	NFF	North Fork Fault
BCC	Blue Creek Canyon Fault	MRS	Meers Fault	RGN	Reagan Fault
BRC	Burch Fault	MVF	Mountain View Fault	SFR	Sulphur Fault
CMT	Cement Fault	MBF	Mulberry Fault	WVF	Washita Valley Fault
CKS	Chickasha Fault	NFZ	Nemaha Fault Zone	WMF	Waurika-Muenster Fault
CTW	Choctaw Fault			WSF	Windingstair Fault

Figure 1. Geologic provinces of Oklahoma. Adapted from Northcutt and Campbell (1995).

they constitute about 15% of the State's current (1995) oil production. Historically, they probably have produced about 15–20% of the State's total oil production. The first commercial oil well in Oklahoma, drilled in 1897, was completed in the Bartlesville sand, an FDD reservoir. The reservoirs in these plays are those in which reservoir complexity and compartmentalization are prevalent—a fact that has commonly not been recognized in reservoir management. There are also some reservoirs in which pressure was lost due to completion methods inherent to the cable-tool drilling method.

A number of siliciclastic intervals underwent preliminary review, primarily by Northcutt. Most of them were not selected for further study because they did not meet the criteria of unstructured, FDD light-oil reservoirs or that FDD was evidently too small a part of the subject interval. Eighteen stratigraphic intervals were identified initially as potential FDD light-oil plays, and 11 of those are addressed in the subject studies (Table 1). The remaining seven stratigraphic intervals were not undertaken as studies because they were determined not to be FDD, the reservoirs were prone to natural gas rather than oil, or the oil plays were too small to warrant a workshop. The smallest play undertaken was the Peru sand, which produces oil from 15 reservoirs. The intervals reviewed, but not developed into workshops, are summarized in Table 2.

Among the intervals not addressed in our studies is the Gypsy sandstone (also known as the Endicott sand and Wynona Sandstone) in the Vamoosa Formation (Virgilian). The formation produces very little oil and gas. It was deposited primarily in a flood-plain environment; as such, it exhibits common fluvial-channel sandstone bodies. The Gypsy sandstone has undergone extensive geologic, geophysical, and reservoir-engineering studies (including field experiments) at two field sites in Pawnee County, Oklahoma, by BP Exploration and the Center for Reservoir Characterization at The University of Oklahoma (Doyle and Sweet, 1995). Studies of the Gypsy sandstone are potentially valuable to all of us who are interested in fluvial deposits as petroleum reservoirs.

SYNTHESIS

The major contributions of these studies are twofold: First, regional distribution of sandstone within the studied intervals have not previously been mapped in their entirety in the public domain. Second, the reservoir case histories provide examples of application of FDD and related-facies mapping to actual reservoirs and how oil recovery from them can be (or could have been) improved. It is the *knowledge* of reservoir architecture coupled with informed oil-field practice that will ultimately result in improved recovery of oil from this class (and all classes) of reservoirs.

Plays are based on informal subsurface nomenclature, because that is the basis on which operators and

STRATIGRAPHIC COLUMN
FLUVIAL-DOMINATED DELTAIC RESERVOIRS IN OKLAHOMA

SYSTEM	SERIES	GROUP	FORMATION OR MEMBER[a] FORMAL (SURFACE)	INFORMAL (SUBSURFACE)
PENNSYLVANIAN	VIRGIL	Wabaunsee		
		SHAWNEE	Elgin Sandstone	Hoover sand (Carmichael sand)
			Wynona Sandstone	Endicott sand
		DOUGLAS	Cheshewalla Sandstone	**Tonkawa sand**
			Tonganoxie Ss. (Kansas)	Stalnaker sand (Kansas)
	MISSOURI	OCHELATA	Cottage Grove Sandstone	**Osage–Layton sand** (Layton & Musselem sands)
			_____	Wade sand[b]
			_____	Medrano sand[b]
		SKIATOOK	Dodds Creek Sandstone	**Layton sand**
			_____	Marchand sand[b]
			Seminole Fm.	(Seminole & Cleveland sands)
	DESMOINES	MARMATON	Tulsa Sandstone	**u. Cleveland sand** (Jones)
			Jenks Sandstone	**l. Cleveland sand** (Dillard)
			Walter Johnson Ss.	Wayside sand
			Englevale Sandstone	**Peru sand**
		CABANISS	Lagonda Sandstone	**Prue sand** (Squirrel & Perryman sands)
			Calvin Sandstone	Calvin sandstone
			Oowala Sandstone	Skinner sand u: Senora, Allen, etc.
			Chelsea Sandstone	m: Allen, Olympic, etc.
				l: Hart, Senora, etc.
		KREBS	Taft Sandstone	**Red Fork sand** (Burbank, Earlsboro, Osborn, Dora & Chicken Farm sands)
			Bluejacket Sandstone	**Bartlesville sand** (Glenn & Salt sands)
			Warner Sandstone	**Booch sand**
			Hartshorne Fm.	Hartshorne sandstone
	ATOKA		_____	Gilcrease sand
			_____	Dutcher sand
			_____	Spiro sand
	MORROW		Kearny Fm. (Kansas)	Morrow formation[b] u: Purdy, Sturgis, Bowles, Kelly and Lips
				l: Mocane-Laverne and Keyes sands

Cherokee group (former)

[a] Bold print indicates fluvial systems investigated in FDD light-oil studies. Names in parentheses are names applied locally in the subsurface.

[b] Reservoirs systems occur only in southern and western Oklahoma.

Figure 2. Stratigraphic column of Pennsylvanian petroleum-reservoir sandstones in northern and central Oklahoma. Bold print indicates systems investigated in FDD light-oil studies.

many technical and nontechnical people know the subject matter. Furthermore, informal nomenclature is the basis for the historical records of drilling and production. However, every play also describes the formal stratigraphy and shows how the informal nomenclature relates to it.

In the course of detailed study of the play materials, we came to realize that many parts of the sedimentary systems were deposited in flood-plain rather than in deltaic environments—that fact could not have been determined prior to detailed studies. A characteristic common to all of the studied intervals, however, is that of incised fluvial channels; those are particularly well developed in the Morrow, Bartlesville, Red Fork, Skinner, Prue, and Cleveland sands.

Reservoir Studies

A high level of reservoir heterogeneity occurs commonly in fluvial and in fluvial-dominated deltaic reservoirs, contrasted to those originating in marine depositional environments. Alpay (1972) and Fisher and Galloway (1983) pointed out that there are three levels of reservoir heterogeneity. They are: (1) microscopic (grain and pore-level heterogeneities), (2) macroscopic (generally well-to-well variations), and (3) megascopic variations. These are commonly facies changes and may occur also at the well-to-well scale, depending on well spacing and geologic variables. Our reservoir studies focus on facies mapping and associated well-log interpretation—i.e., items 2 and 3 (above). The reservoirs studied range from 10 to 90 (arithmetic mean = 29) producing wells (Table 1).

Our criteria for selecting reservoirs in each of the plays were, by necessity, nongeologic. Of primary importance was a "clean" production history, i.e., that single-formation production histories were available or interpretable, so that production from the studied reservoir was factual. Second, we needed a suite of modern wireline logs in most wells (item 1, below).

Small companies or one to several individuals operated virtually all of the reservoirs studied. Therefore, they are representative of the "evolved" oil industry in Oklahoma and adjacent states. Our message to improve oil recovery is:

1. Run a suite of logs that includes at least the standard induction-electrical survey, a gamma ray, and a porosity tool (preferably density-neutron).
2. Study the logs (or have a qualified geologist do so), recognize the depositional environments, and build subsurface maps accordingly, as shown in the play workshop publications (Table 1).
3. Map the different facies separately, if possible.
4. Continue development of the reservoir with facies distribution in mind (plan ahead).
5. Maintain reservoir pressure as soon as possible.

Regional Studies

The presence of sandstone-bearing facies and the major transition from fluvial-deltaic to marine facies are of major interest for exploration and development geology. Each of these regional subsurface geologic maps required the review of hundreds, even thousands, of well logs that are provided for each play. Two or more regional stratigraphic cross sections provided examples of the variation in thickness and facies distribution of the studied intervals. Although the areas studied are typically densely drilled, the maps presented in the play-workshop publications will be modified and refined with the knowledge of continued drilling to the necessary depths.

Other maps presented with each play are regional structure, oil fields that have production from the subject interval, and productive wells or oil and gas leases with production from the subject interval.

Table 2.—Pennsylvanian Sandstone Intervals Reviewed, but Not Developed into Light-Oil Plays in the Fluvial-Dominated Deltaic Series

Interval[a]	Depositional environment(s)	Reason for not developing play	Reviewer	References[b]
Hoover sand	Fluvial-dominated deltaic	Natural gas play	Andrews	Khaiwka, 1968
Endicott sand	Fluvial-dominated deltaic	Natural gas play	Andrews; Northcutt	Khaiwka, 1968; Busch, 1974
Wade sand	Marine and tide-dominated deltaic	Little, if any, FDD	Campbell; Northcutt	Lange, 1984
Medrano sand	Deep marine fans and submarine canyon-fill	Not FDD	Campbell	Lange, 1984; Galloway and others, 1977
Marchand sand	Tide-dominated setting: includes tidal-channels, accretion bars, and possible estuarine	Not FDD	Campbell; Northcutt	White and others, 1999; Baker, 1979
Atokan sandstones: Gilcrease sand, Dutcher sand	Marine shore-face and near-shore	Not FDD	Northcutt	Houseknecht, 1987; Zachry and Sutherland, 1984

[a]Refer to Figure 1 for stratigraphic position.

[b]Only the most definitive references are included here, following investigation by reviewer.

MORROW PLAY

The Morrow Formation occurs in the Anadarko basin and shelf areas of western Oklahoma and adjacent Texas, Kansas, and Colorado (Fig. 3). The major reservoir studied is the upper Morrow Purdy sand in the Northeast Rice field. This coarse- to very coarse grained, arkosic sandstone was deposited in a west- and south-trending, fluvial-channel system in Texas County, Oklahoma. Production from the lower Morrow occurs farther to the east, with reservoir facies consisting of fine- to medium-grained sandstone. Coarse-grained to conglomeratic sandstones also occur locally.

BOOCH PLAY

The Booch sand (Warner Sandstone) occurs in the lower part of the McAlester Formation (lower Desmoinesian). The play is located on the Cherokee platform and in the northwestern part of the Arkoma basin (Fig. 4). The main reservoir case history is that of the Greasy Creek field, Hughes County. It is a stratigraphic/structural trap in a distributary-channel sandstone.

BARTLESVILLE PLAY

The Bartlesville sand (Bluejacket Sandstone) occurs in the lower part of the Boggy Formation (Desmoinesian). The play is widespread on the Cherokee platform and extends into the Arkoma basin to the south (Fig. 5). One of three reservoir studies presented here is in the Ohio-Osage field, Osage County. The sandstone was probably deposited in a south-trending, incised fluvial channel, and entrapment is stratigraphic.

RED FORK PLAY

The Red Fork sand (Taft Sandstone) occurs in the upper part of the Boggy Formation. Lower Red Fork fluvial and deltaic sandstones are located widely on the Cherokee platform and extend westward into the Anadarko basin, but the upper Red Fork play occurs only in the Anadarko basin. The geographic area of the entire Red Fork play is shown in Figure 6. The main reservoir case history is that of the North Carmen field in Alfalfa County. It is a stratigraphic trap in point-bar and channel-margin sandstones of the lower Red Fork in a west-trending channel.

SKINNER AND PRUE PLAYS

The Skinner sand (Chelsea and Oowala Sandstones) occurs in the lower part of the Senora Formation (Desmoinesian). The play also is located widely on the Cherokee platform and extends to the Anadarko basin to the west (Fig. 7). The major reservoir case history is that of the lower and upper Skinner sand in the North Salt Fork field in Grant County. Oil and gas are trapped stratigraphically in meandering, fluvial, channel-fill sandstones.

The Prue sand (Lagonda Sandstone) occurs in the upper part of the Senora Formation. The Prue and associated strata are confined mostly to the Cherokee platform; a few depositional trends extend west of the Nemaha fault zone into the Anadarko basin province (Fig. 8). Fluvial elements of the lower Prue sand occur in the Long Branch field in Payne County. Trapping is primarily stratigraphic, and the sandstone typically has a relatively high calculated water saturation of 40–50%.

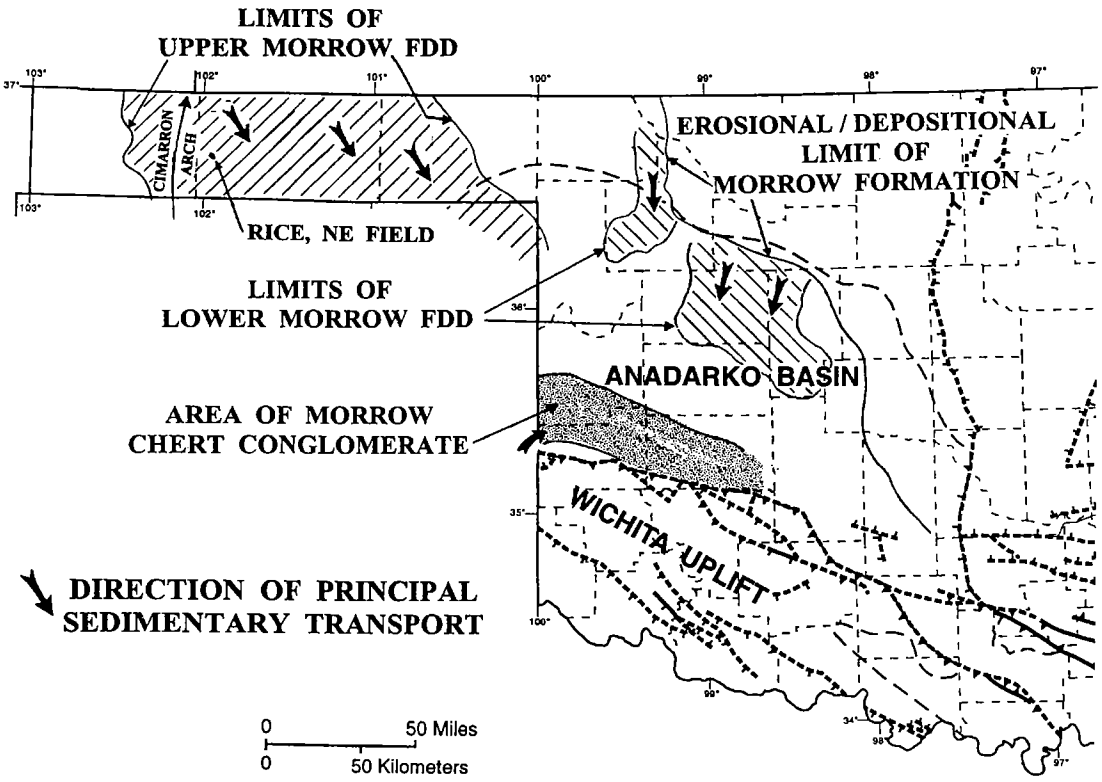

Figure 3. Regional distribution of Morrow fluvial sandstone and other strata in the subsurface of western Oklahoma. Chert conglomerate adapted from Al-Shaieb and others (1993).

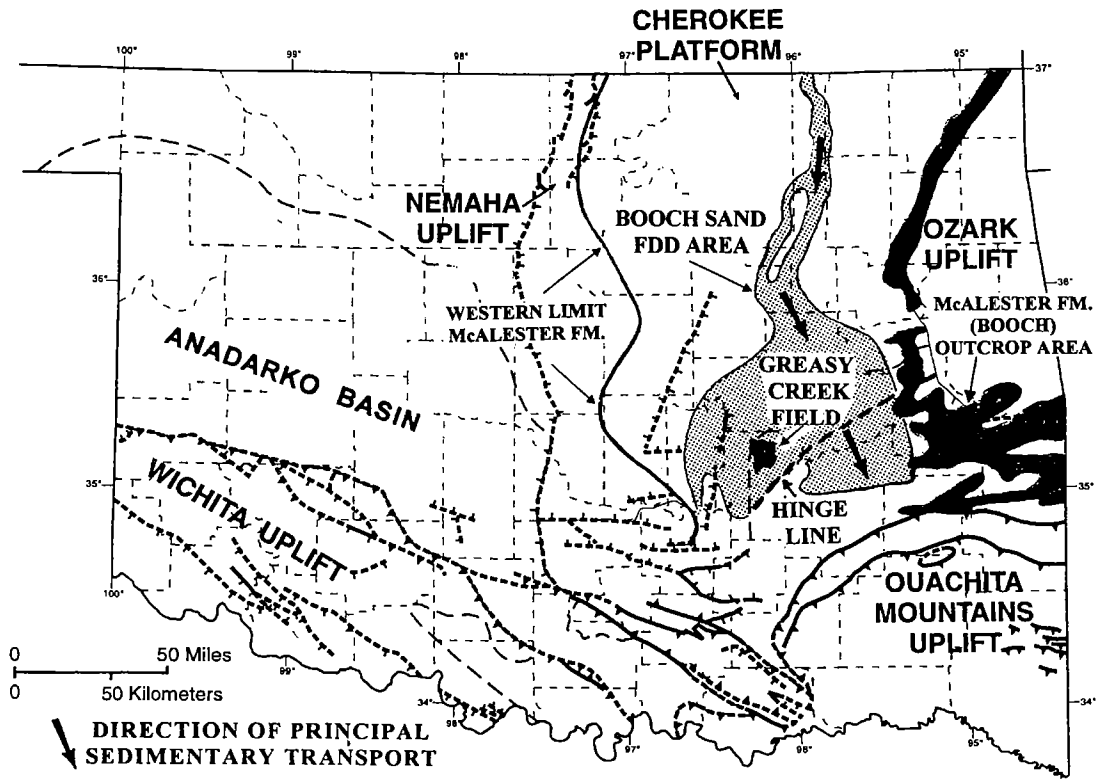

Figure 4. Regional distribution of Booch sand in the subsurface and outcrop of the McAlester Formation in Oklahoma. Modified in part from Busch (1959) and J. E. O'Brien (unpublished data, including mapping of Booch sand in northern part of Cherokee platform, Oklahoma). Outcrop from Miser and others (1954).

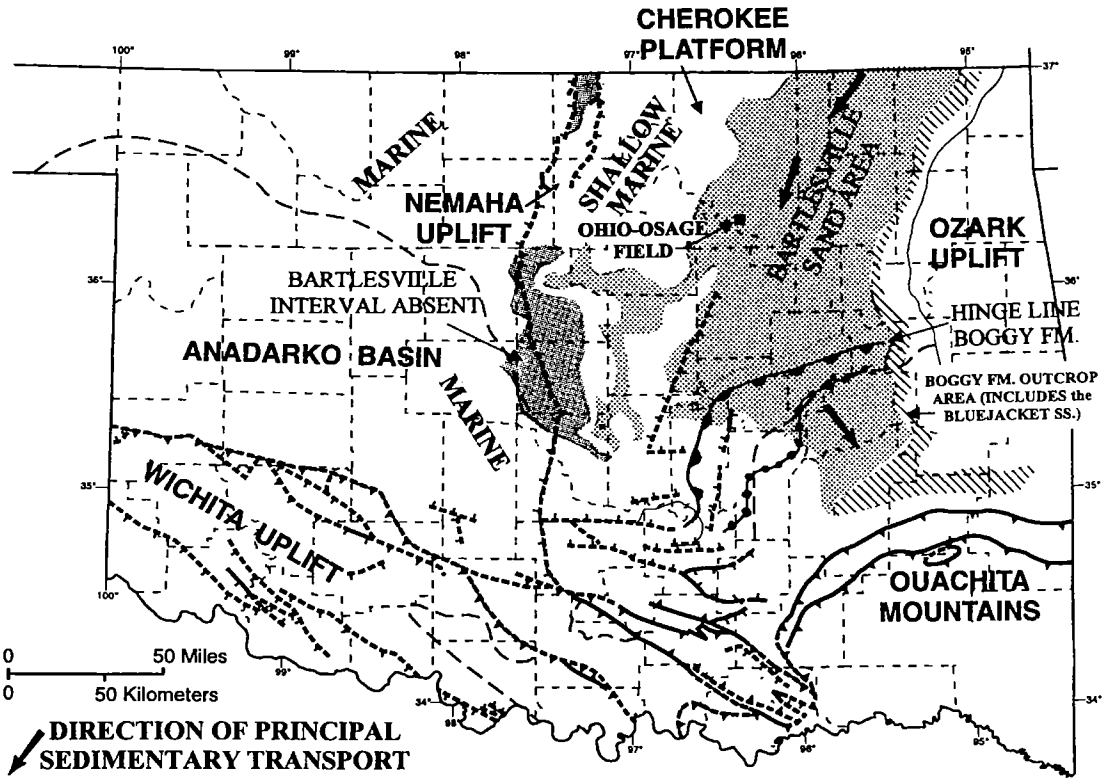

Figure 5. Regional distribution of Bartlesville sand in the subsurface and outcrop of the Bluejacket Sandstone. Outcrop from Miser and others (1954).

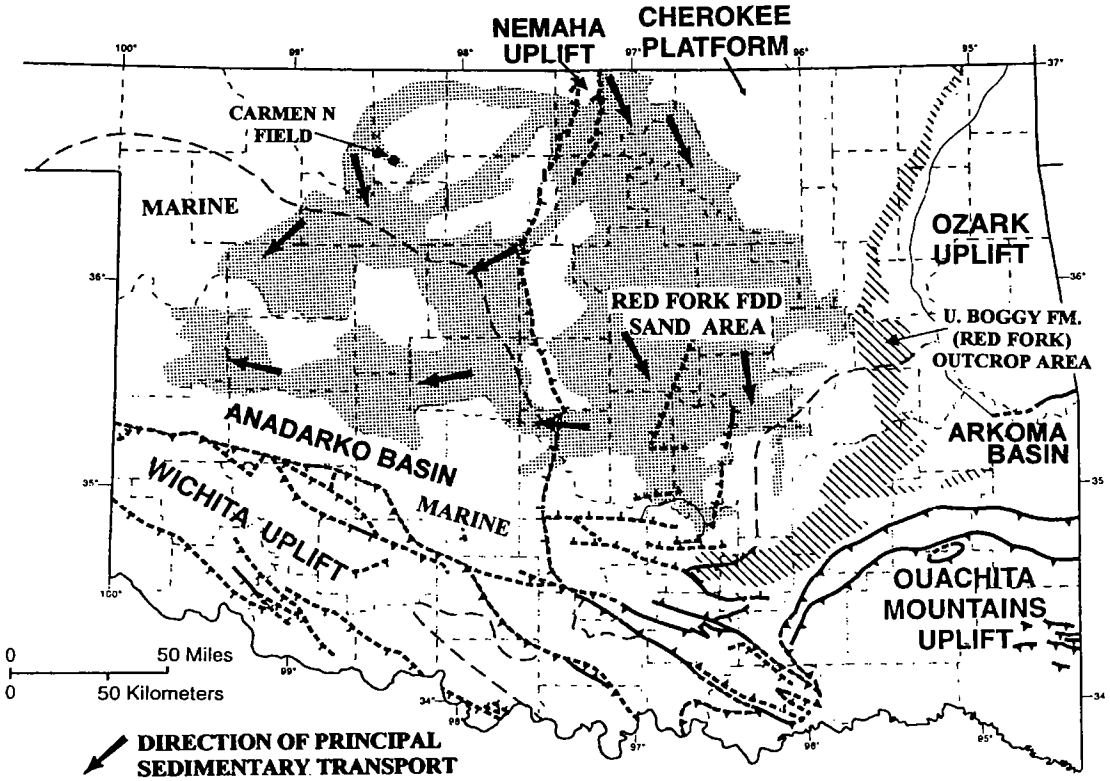

Figure 6. Regional distribution of Red Fork sand in the subsurface and outcrop of the upper part of the Boggy Formation in Oklahoma. Outcrop from Miser and others (1954).

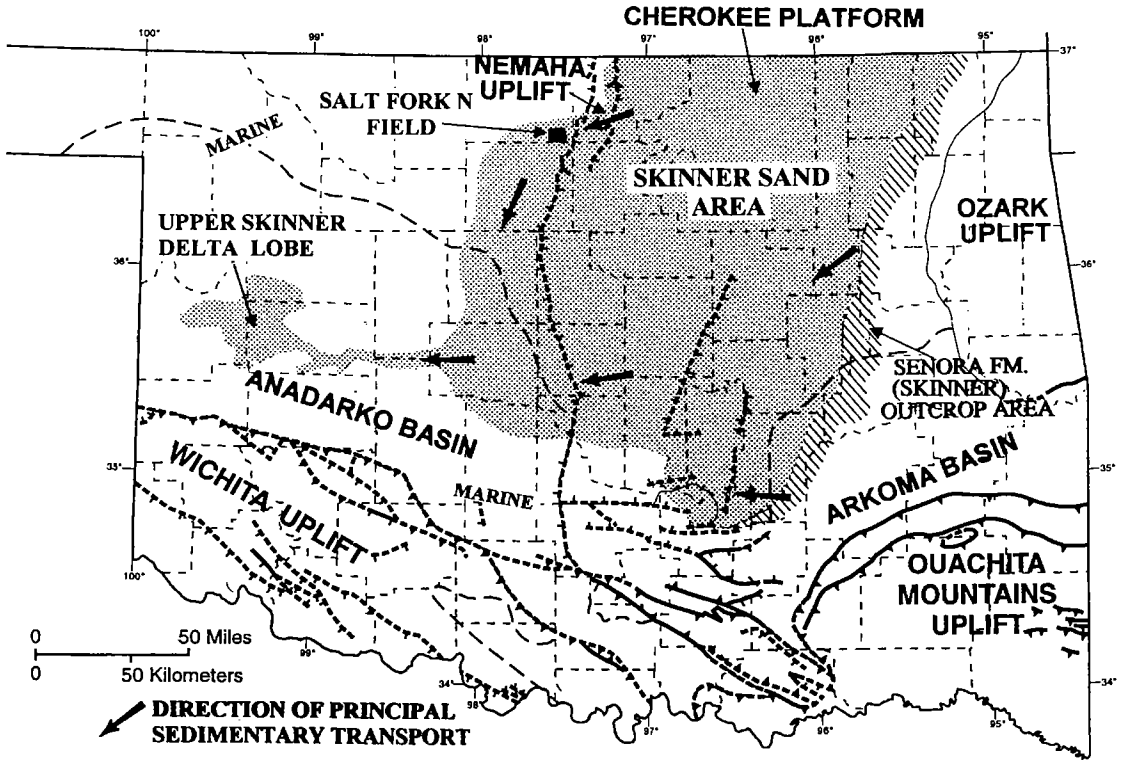

Figure 7. Regional distribution of Skinner sand in the subsurface and outcrop of the Senora Formation in Oklahoma. Outcrop from Miser and others (1954).

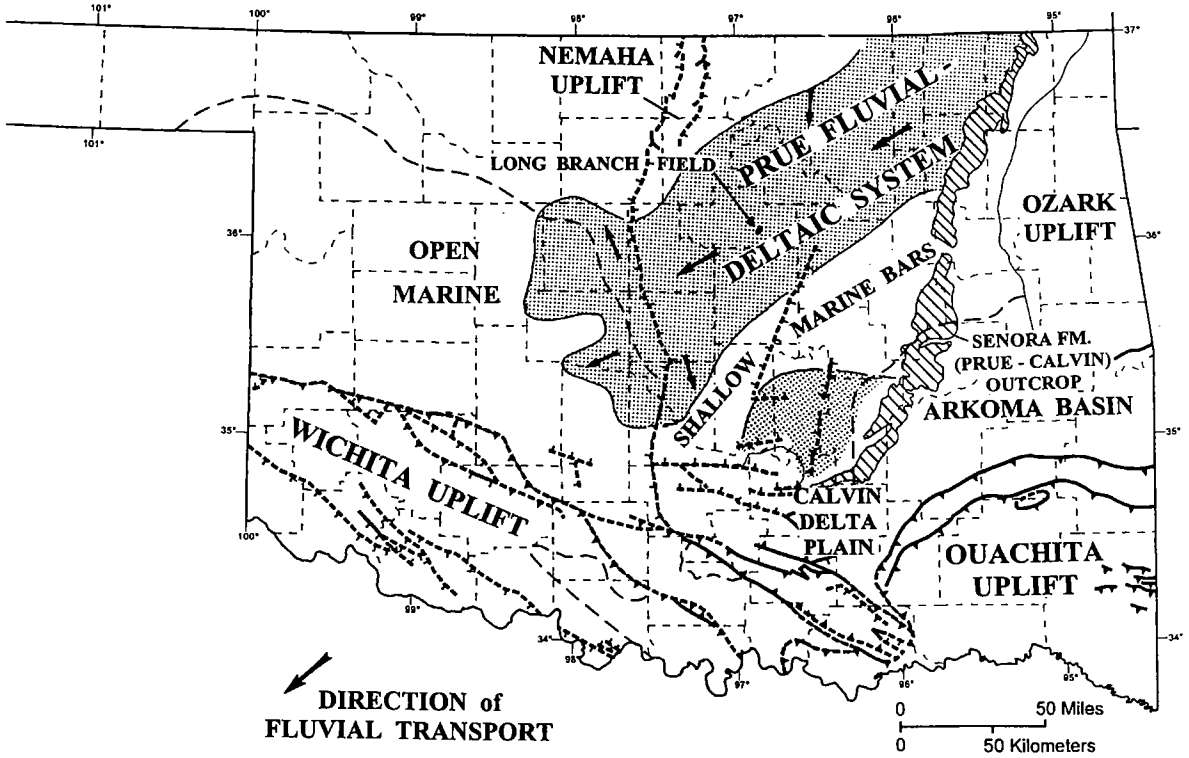

Figure 8. Regional distribution of Prue sand and Calvin Sandstone in the subsurface and outcrop of the Senora Formation in Oklahoma. Outcrop from Miser and others (1954).

CLEVELAND AND PERU PLAYS

The Peru sand (Englevale Sandstone) occurs in the Labette Shale (upper Desmoinesian). The formation has limited geographic distribution, and the play is located in Osage, Washington, and Nowata Counties in Oklahoma, and in adjacent Kansas (Fig. 9). The representative reservoir is in the Hogshooter field in Washington County, a stratigraphic trap with obscure structural ramifications.

The Cleveland sand is an informal subsurface name applied to sandstones in the upper part of the Holdenville Formation (uppermost Desmoinesian), and locally to sandstones in the Seminole Formation (lowermost Missourian). The play is located on much of the Cherokee platform, and extends westward into the Anadarko basin locally (Fig. 9). The play is represented by the reservoir case history in the Pleasant Mound field, Lincoln County. Hydrocarbons in the Cleveland sand are stratigraphically trapped in distributary-channel and delta-front sandstones related to a locally prograding delta.

LAYTON AND OSAGE-LAYTON PLAY

The Layton ("true Layton") sand (Dodds Creek Sandstone) occurs in the upper part of the Coffeyville Formation, and the Osage-Layton sand (Cottage Grove Sandstone) occurs in the upper part of the Chanute Formation. They are early Missourian in age. The two plays are located mainly on the Cherokee platform (Figs. 10, 11); however, the Osage-Layton play is geographically larger, and extends westward on to the shelf of the Anadarko basin (Fig. 11). The Layton sand reservoir in the South Coyle field is a stratigraphic trap. A case-history study of Osage-Layton sand in the East Lake Blackwell field (Payne County) identifies four fluvial- and crevasse-splay sandstones that form stratigraphic traps on a west-plunging structural nose. The two formations are presented in the same geologic play because of duplicate application of the informal subsurface name, "Layton" sand.

TONKAWA PLAY

The Tonkawa sand (Stalnaker sand in Kansas) is equivalent to the Cheshewalla Sandstone in the Vamoosa Formation (Oklahoma) and the Tonganoxie Sandstone in the Stranger Formation (Kansas), both of which are early Virgilian in age. The play is located in Oklahoma and Kansas, on the western part of the Cherokee platform, Nemaha uplift, and adjacent shelf of the Anadarko basin (Fig. 12). Petroleum production occurs on and adjacent to structure in the FDD play. Geologic mapping of the Tonkawa reservoir in the northern part of the Blackwell field (Kay County) indicates that structurally and stratigraphically trapped oil has been by-passed.

The Tonkawa FDD light-oil play (Fig. 12) is relatively small, and required only half-a-day for presentation. Recognizing the developing and geologically related Tonkawa marine sandstone gas play to the west, the Oklahoma Geological Survey (OGS), with Geo Information Systems (GIS) and the Petroleum Technology Transfer Council (PTTC), funded the preparation of that play (Hinshaw and Rottmann, 1997). It has been presented with the Tonkawa FDD play, and the two plays are available from the OGS. Tonkawa sand reservoirs studied are in the Blackwell field in Kay County (FDD) and in the Waynoka NE field (marine), in Woods County.

CONCLUSIONS

Regional studies that are parts of the FDD-play series represent the first availability of the mapped regional distribution of these hydrocarbon-bearing strata in the public domain. Figures 3–12 represent that mapping at a smaller scale than those originally published.

Studies of 21 reservoirs indicate that detailed geologic mapping, particularly of depositional facies, will result in better understanding of reservoir architecture. Such mapping will improve development drilling and secondary recovery design through recognition of probable reservoir compartments and delineation of depositional trends. Facies analysis from well logs also will benefit operators by identifying preferred directions of natural permeability and by improved understanding of barriers to flow in reservoir rocks. This relatively inexpensive procedure can be expected to improve ultimate recovery.

In the 21 reservoir studies conducted, we found a common lack of reservoir-management practice during primary and secondary recovery, with a few outstanding exceptions. The examples we found of excellent reservoir management practice were the Rice NE Morrow reservoir, the Carmen, North Red Fork reservoir, and the Long Branch, Prue, and Red Fork reservoirs. What we propose is not "rocket science"; substantially more oil would have been recovered had the cardinal rule of reservoir engineering been followed: *maintain reservoir pressure*. In all cases, produced brine was being disposed of *somehow* and *somewhere*; had that brine alone been injected into a structurally low reservoir well, *some* reservoir pressure would have been maintained. Whereas there is a level of sophistication in the reservoir simulation studies using BOAST 3 or ECLIPSE mathematical strategies, these are only tools that help to determine the optimum strategies for reservoir development following geologic description. The geologic concepts and engineering principles and practice have been with us for decades. It must be realized, however, that neither geologic description nor reservoir simulation are able to identify *all* heterogeneities in a reservoir; even so, geologic description alone found definite or probable developable oil that was evidently not previously recognized in the following reservoirs:

- Blackwell Tonkawa
- East Lake Blackwell Osage-Layton
- Pleasant Mound Cleveland
- Ohio-Osage Bartlesville
- Greasy Creek Booch

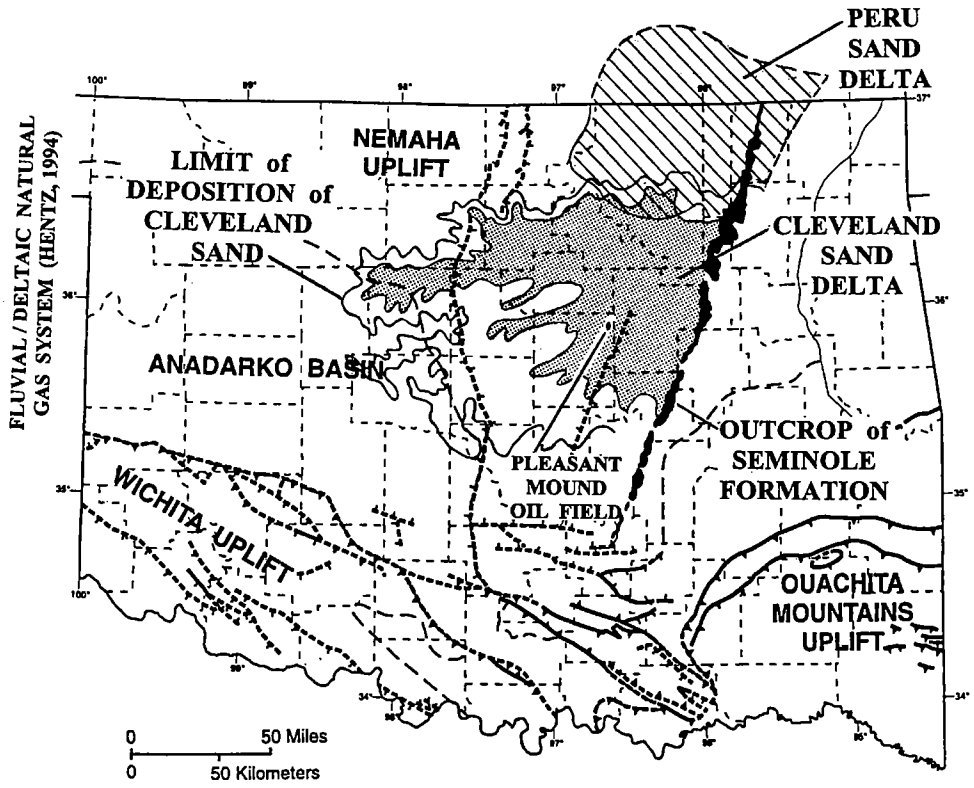

Figure 9. Regional distribution of the Cleveland sand and the Peru sand in the subsurface and outcrop of Seminole Formation in Oklahoma. Adapted in part from Cole (1970) and Berg (1973). Outcrop from Miser and others (1954).

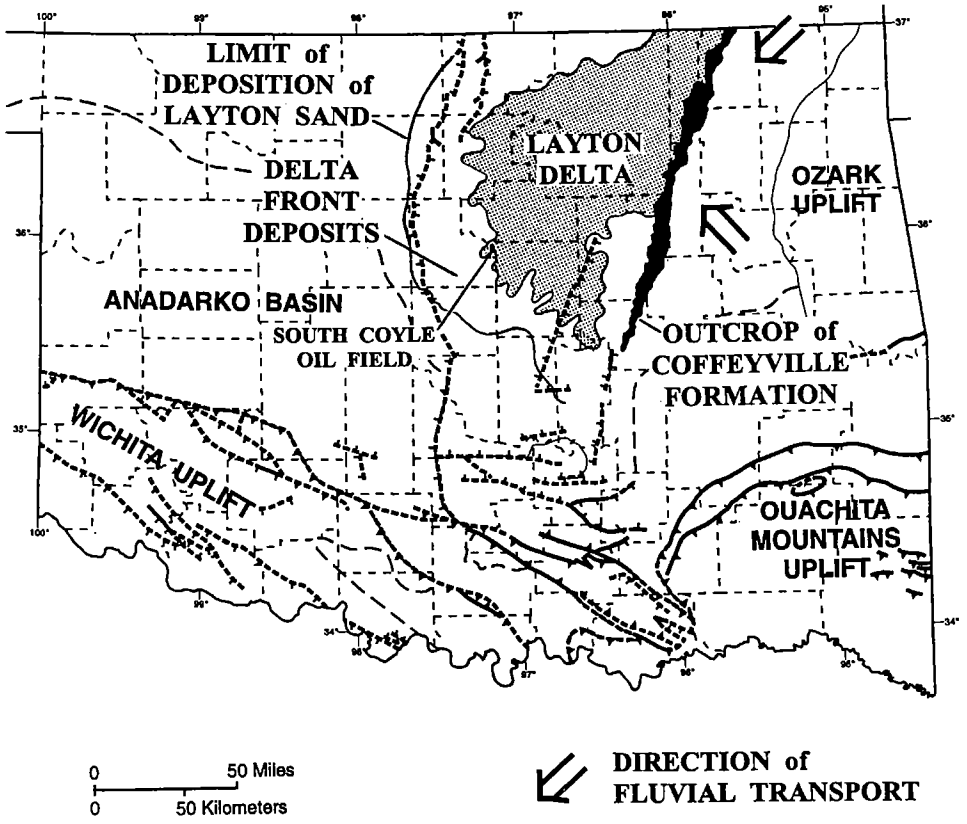

Figure 10. Regional distribution and generalized depositional environments of Layton sand in the subsurface and outcrop of Coffeyville Formation in Oklahoma. Outcrop from Miser and others (1954).

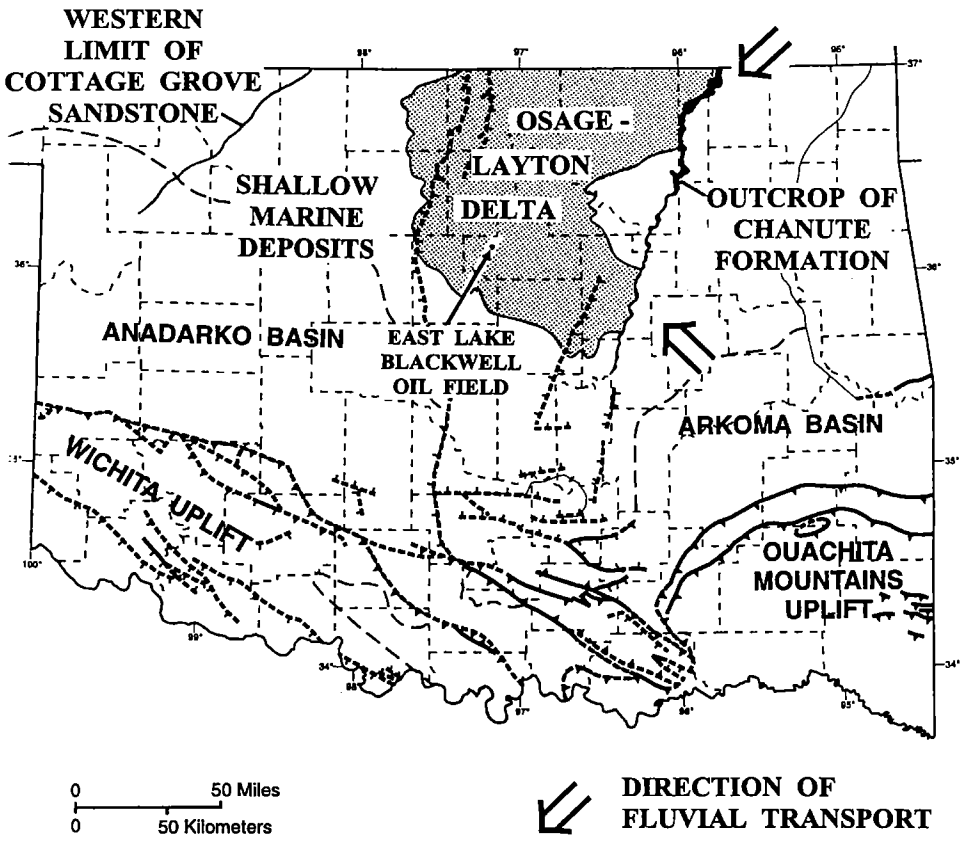

Figure 11. Regional distribution of Osage-Layton sand (Cottage Grove Sandstone) fluvial-deltaic system in the subsurface and outcrop of the Chanute Formation in Oklahoma. Outcrop from Miser and others (1954).

REFERENCES CITED

Al-Shaieb, Zuhair; Puckette, James; Ely, Patrick; and Abdalla, Azhari, 1993, The upper Morrowan fan-delta chert conglomerate in Cheyenne and Reydon fields: completely sealed gas-bearing pressure compartments, *in* Johnson, K. S.; and Campbell, J. A. (eds.), Petroleum-reservoir geology in the southern Midcontinent, 1991 symposium: Oklahoma Geological Survey Circular 95, p. 26–39.

Alpay, O. A., 1972, A practical approach to defining reservoir heterogeneity: Journal of Petroleum Technology, v. 24, p. 841–848.

Baker, R. K., 1979, The depositional environment of the Pennsylvanian upper Marchand sandstones, northern Caddo County, Oklahoma, *in* Hyne, N. J. (ed.), Pennsylvanian sandstones of the Mid-Continent: Tulsa Geological Society Special Publication 1, p. 195–219.

Berg, O. R., 1973, Quantitative study of the Marmaton Group, west flank of the Nemaha ridge, north-central Oklahoma: Shale Shaker, v. 23, no. 7, p. 152–161, 164–168.

Busch, D. A., 1959, Prospecting for stratigraphic traps: American Association of Petroleum Geologists Bulletin, v. 43, p. 2829–2843.

Busch, D. A., 1974, Deltas, *in* Stratigraphic traps in sandstones—exploration techniques: American Association of Petroleum Geologists Memoir 21, p. 108–144.

Cole, J. G., 1970, Marmaton Group, east flank of the Nemaha ridge: Shale Shaker, v. 21, no. 3, p. 52–67.

Doyle, J. D.; and Sweet, M. L., 1995, Three-dimensional distribution of lithofacies, bounding surfaces, porosity, and permeability in a fluvial sandstone—Gypsy sandstone of northern Oklahoma: American Association of Petroleum Geologists Bulletin, v. 79, p. 70–96.

Feldman, H. R.; Gibling, M. R.; Archer, A. W.; Wightman, W. G.; and Lanier, W. P., 1995, Stratigraphic architecture of the Tonganoxie paleovalley (lower Virgilian) in northeastern Kansas: American Association of Petroleum Geologists Bulletin, v. 79, p. 1019–1043.

Fisher, W. L.; and Galloway, W. E., 1983, Potential for additional oil recovery in Texas: University of Texas at Austin, Bureau of Economic Geology, Geological Circular 83-2, 20 p.

Galloway, W. E.; Marshall, S. Y.; and Whipple, A. P., 1977, Seismic stratigraphic model of depositional platform margin, eastern Anadarko basin, Oklahoma: American Association of Petroleum Geologists Bulletin, v. 61, p. 1437–1447.

Hentz, T. F., 1994, Sequence stratigraphy of the Upper Pennsylvanian Cleveland Formation: a major tight-gas sandstone, western Anadarko basin, Texas Panhandle: American Association of Petroleum Geologists Bulletin, v. 78, p. 569–595.

Hinshaw, Carlyle; and Rottmann, Kurt, 1997, The marine Tonkawa sands: natural gas and associated liquids pro-

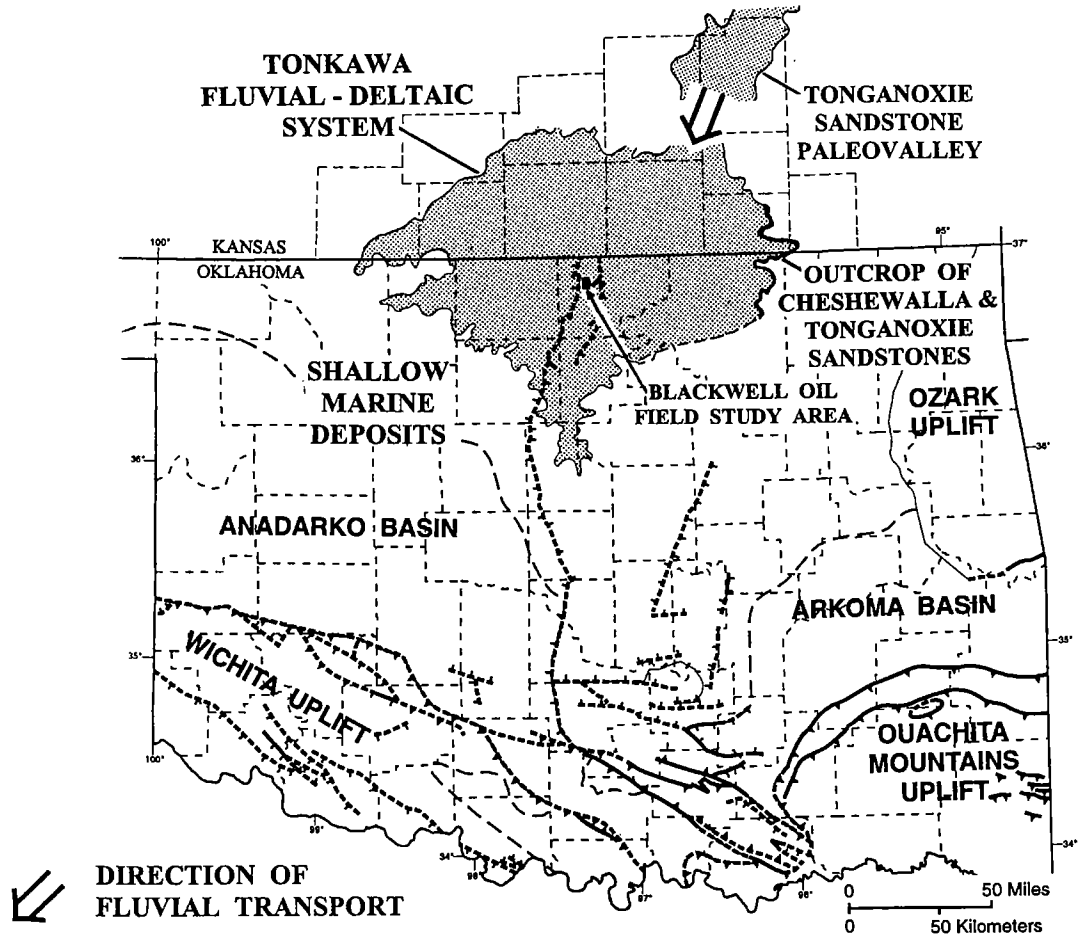

Figure 12. Regional distribution of the Tonkawa fluvial-deltaic system in the subsurface of north-central Oklahoma and adjacent Kansas and outcrop of the Cheshewalla Sandstone in Oklahoma and the Tonganoxie Sandstone in Kansas. Modified in part from Winchell (1957) and Feldman and others (1995). Outcrop of the Cheshewalla Sandstone (lower part of the Vamoosa Group) from Miser and others (1954).

duction in the Anadarko basin: Oklahoma Geological Survey Open-File Report 3-97, unpaginated.

Houseknecht, D. W., 1987, Evolution from passive margin to foreland basin: the Atoka Formation of the Arkoma basin, south-central U.S.A., *in* Allen, P. A., and others (eds.), Foreland basins: International Association of Sedimentologists Special Publication 8, p. 327–345.

Khaiwka, M. H., 1968, Geometry and depositional environments of Pennsylvanian reservoir sandstones, northwest Oklahoma: University of Oklahoma unpublished Ph.D. dissertation, 126 p.

Lange, E. B., Jr., 1984, Middle Hoxbar (Missourian) from shelf to basin in the northeastern Anadarko basin, *in* Hyne, N. J. (ed.), Limestones of the Midcontinent: Tulsa Geological Society Special Publication 2, p. 273–306.

Miser, H. D.; Oakes, M. C.; Ham, W. E.; Huffman, G. G.; Branson, C. C.; Chase, G. W.; McKinley, M. E.; Warren, J. H.; Harris, R. L.; Ford, D. H.; and Fishburn, D. J., 1954, Geologic map of Oklahoma: U.S. Geological Survey and Oklahoma Geological Survey, 1 sheet, scale 1:100,000.

Northcutt, R. A.; and Campbell, J. A., 1995, Geologic provinces of Oklahoma: Oklahoma Geological Survey Open-File Report 5-95, scale 1:750,000.

_____ 1996a, Geologic provinces of Oklahoma, *in* Swindler, D. L.; and Williams, C. P. (compilers), Transactions of the 1995 American Association of Petroleum Geologists Mid-Continent Section Meeting: Tulsa Geological Society, p. 128–134.

_____ 1996b, Geologic provinces of Oklahoma: Shale Shaker, v. 46, no. 5, p. 99–103.

Tyler, Noel; Galloway, W. E.; Garrett, C. M.; and Ewing, T. E., 1984, Oil accumulation, production characteristics, and targets for additional recovery in major oil reservoirs of Texas: University of Texas at Austin, Bureau of Economic Geology, Geological Circular 84-2, 31 p.

U.S. Department of Energy, Office of Fossil Energy, 1991, Opportunities to improve oil productivity in unstructured deltaic reservoirs: U.S. Department of Energy Report DOE/BC –91/6/SP DE 91002237, 154 p.

White, Howard; Kirkland, Rodney; Glassman, Ed; and Schnerk, George, 1999, Revisiting Pennsylvanian reservoir architecture—Chitwood, Norge, and Northeast Verden fields, Caddo and Grady Counties, Oklahoma, *in* Merriam, D. F. (ed.), Transactions of the 1999 American Association of Petroleum Geologists Midcontinent Section Meeting: Kansas Geological Survey Open-File Report 99-28, p. 212–219.

Winchell, R. L., 1957, Relationship of the Lansing Group and the Tonganoxie ("Stalnaker") Sandstone in south-central Kansas: Kansas Geological Survey Bulletin 127, pt. 4, p. 123–152.

Characteristics of Incised Paleovalley Fluvial- and Tidal-Sandstone Reservoirs, Morrow Stateline Trend, Colorado, Kansas, and Oklahoma

Roderick W. Tillman
Consulting Geologist/Stratigrapher
Tulsa, Oklahoma

ABSTRACT.—Recent work on middle and upper Morrow (Pennsylvanian) deposits in the Colorado-Kansas Stateline Trend and Oklahoma Panhandle indicates that these deposits are primarily paleovalley-fill deposits. They differ from deltaic deposits with which they have been confused. Paleovalley-fill reservoirs differ from deltaic deposits depositionally, geometrically, and in the characteristics and distribution of flow-unit properties. Because there are significant differences in the distribution of reservoir seals and internal heterogeneity characteristics in valley-fill reservoirs, compared to deltaic and river-channel (fluvial) reservoirs, different patterns of production will occur within individual fields and pools that produce from these distinctly different geologic environments. In recent years a number of characteristics have been recognized that allow paleovalleys to be differentiated from deltaic deposits.

Several widely quoted papers published between 1979 and 1993 attribute most of the middle and upper Morrow channel deposits in Southwest Colorado and the Oklahoma Panhandle to deltaic deposition. This widely accepted opinion has significantly impeded exploration and development of middle and upper Morrow sandstones.

INTRODUCTION

Detailed sedimentologic and petrophysical analyses of cores from producing Morrow Sandstone fields in the Stateline Trend (Figs. 1, 2) indicate that reservoir-production properties vary in both predictable and locally somewhat random ways among the paleovalley-fill producing facies. The producing facies are primarily fluvial and tidal (estuarine) sandstones. Overbank and fine-grained levee deposits, typical of deltas, are commonly absent at the margins of valley-fill reservoirs.

The suite of sedimentary structures observable in cores allows differentiation between fluvial and tidal deposits in fields such as the Southwest Stockholm Field in Kansas, Moore-Johnson and Arapahoe Fields in southeast Colorado, and Tracy Field in the Oklahoma Panhandle. Careful calibration of logs in wells that contain Morrow cores can aid significantly in developing criteria for differentiating fluvial- and tidal-sandstone facies in non-cored wells. Prospecting and locating step-out wells may be aided significantly by applying core-calibrated, log-facies models.

Because of their relatively small size (0.5–4 mi wide), poorly understood origins, and difficult to predict occurrences, valley-fill reservoirs have not always been attractive targets for drilling. However, in the last few years with the advent of three-dimensional (3D) seismic and denser well control, valley-fill reservoirs along the Stateline Trend and in the Oklahoma Panhandle continue to be prospective.

UPPER MORROW HISTORICAL INTERPRETATIONS

Prior to the 1980s, very few models for estuarine and tidal deposits were considered when shoreline deposits were encountered in exploration or production. Donald Swanson in his several papers on the Morrow (1979, 1987, 1993) advocated deltaic origins for all of what he termed upper Morrow reservoirs in the Oklahoma and Texas Panhandles. He indicated that what he termed *stream-mouth bars* and what had been called "bar-finger sandstones" by Fisk (1951) were important elongate reservoirs in the Morrow (Fig. 3). He stated that the irregular surfaces at the base of many Morrow reservoirs were due to two causes: (1) "sinking down" of sands into the underlying muds and "post-depositional structural movement" (Fisk, 1979, p. 158). He suggested that the sandstones graded downward into the muds underlying the Morrow reservoirs, and he interpreted the muds to be delta-front deposits. These characteristics may have been applicable in some of the areas of the Texas Panhandle but subsequently have been questioned by many recent workers in Oklahoma, Colorado, and Kansas.

Tillman, R. W., 2001, Characteristics of incised paleovalley fluvial- and tidal-sandstone reservoirs, Morrow Stateline Trend, Colorado, Kansas, and Oklahoma, *in* Johnson, K. S. (ed.), Pennsylvanian and Permian geology and petroleum in the southern Midcontinent, 1998 symposium: Oklahoma Geological Survey Circular 104, p. 33–40.

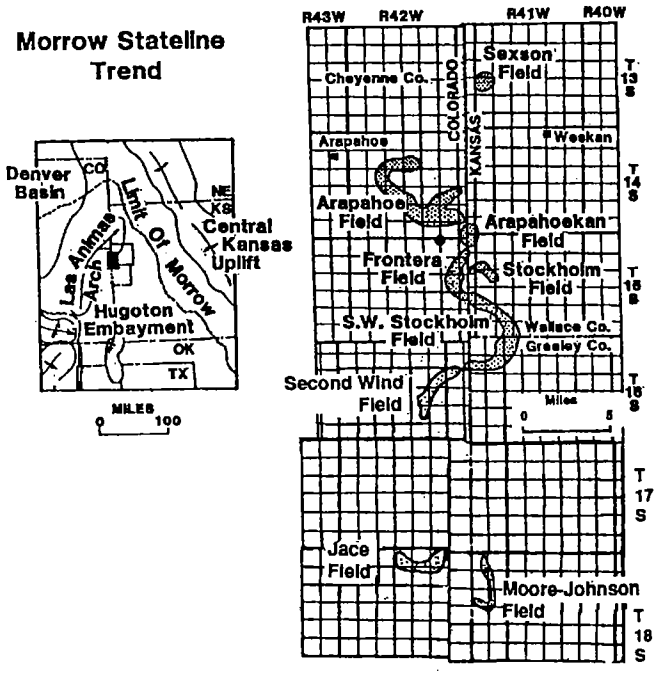

Figure 1. Location of the more than 25-mi-long "Stateline Trend" Morrow sandstone fields that produce from paleovalley-fill–sandstone reservoirs. Fields located in Kansas are in Greeley and Wallace Counties. Fields that produce in Colorado are in Kiowa and Cheyenne Counties. Morrow Oklahoma Panhandle fields lie immediately south of map. (Modified from Shumard and Avis, 1990.)

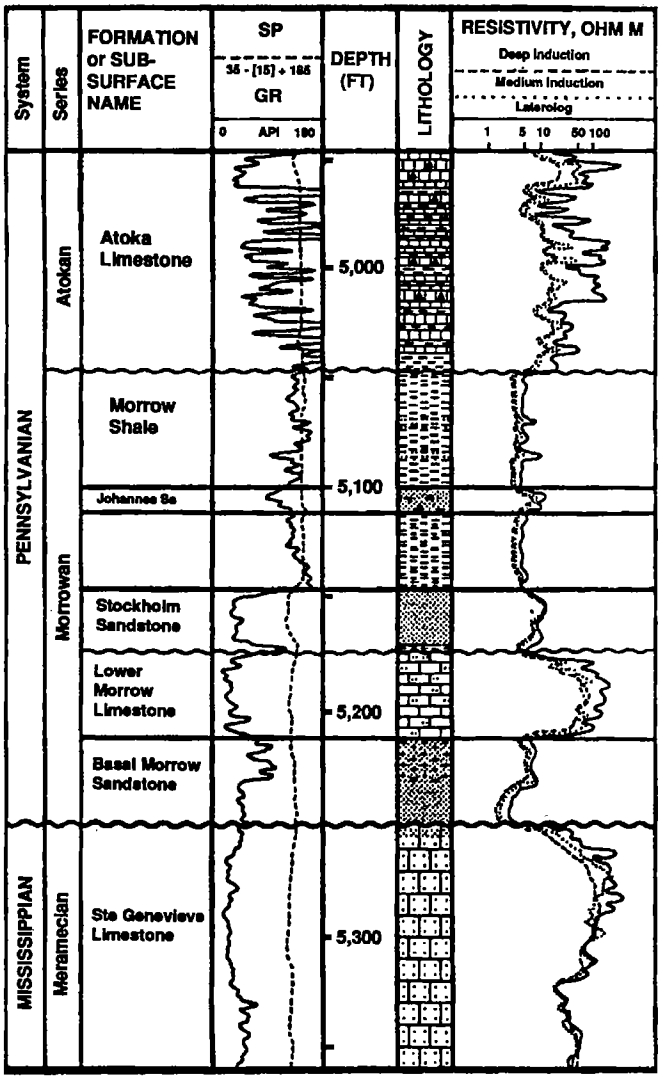

Figure 2. Typical log from the Stateline Trend area; the log is that of the Texas Oil & Gas No. 4 Evans, NW¼NE¼SE¼ sec. 11, T. 16 S., R. 43 W., Greeley Co., Kansas. Note that three potentially productive sandstones are present in the Morrow interval in the Southwest Stockholm Field. The basal Morrow sandstone and the lower Morrow limestone are nonproductive. The middle of the three Morrow sandstones is the major producer in the Southwest Stockholm Field. The contact between the Morrow and the Mississippian limestones is a regional unconformity that in most areas forms the bottom of the valley that is filled with numerous lithologies including sandstone, limestone, and shale. (Modified from Shumard and Avis, 1990.)

Many of the upper Morrow sandstone reservoirs in the Oklahoma Panhandle and along the Colorado-Kansas Stateline Trend are now considered to be paleovalley-fill sandstones deposited in *lowstand* (LST) or early in *transgressive sequence tracts* (TSTs). Numerous cores, which include the bases of upper Morrow sandstones, indicate that they are cut into offshore marine shales or carbonates and that, for the most part, gradational contacts with "prodelta muds" are not encountered. The bases of the sandstones are sharp, not gradational. In deltaic deposits, the lateral facies are commonly *friable* fine-grained deposits. Morrow sandstones are now commonly known to have lateral boundaries that were eroded into *indurated* deposits. Rather than being contemporaneous, as is common in deltaic deposition, the deposits lateral to the paleovalley-fill sandstones are older—sometimes significantly older—than the deposits that fill the paleovalleys. The stream-mouth bars of Swanson (Fig. 3) are probably mostly backfills of incised paleovalleys cut by rivers.

Attributing the cause of irregular bases of sandstones to "sinking down" and post-depositional structural movement can be contradicted by carefully constructing cross sections that include units immediately below the sandstones. These cross sections will show that intervals bounded by correlatable markers immediately below the base of the paleovalleys can be observed to maintain a uniform thickness under and lateral to the valleys. If the sandstones were "sinking" into the underlying fine-grained deposits, they would be thinner under the paleovalley. This is generally not the case.

Pre-, post-, and syndepositional-fault movement may be associated with paleovalleys. Pre-depositional movement in some areas has created lows into which the rivers that cut the paleovalleys flowed. The faulting may also cause localized areas of fracturing, which can be more easily be eroded. Syndepositional fault move-

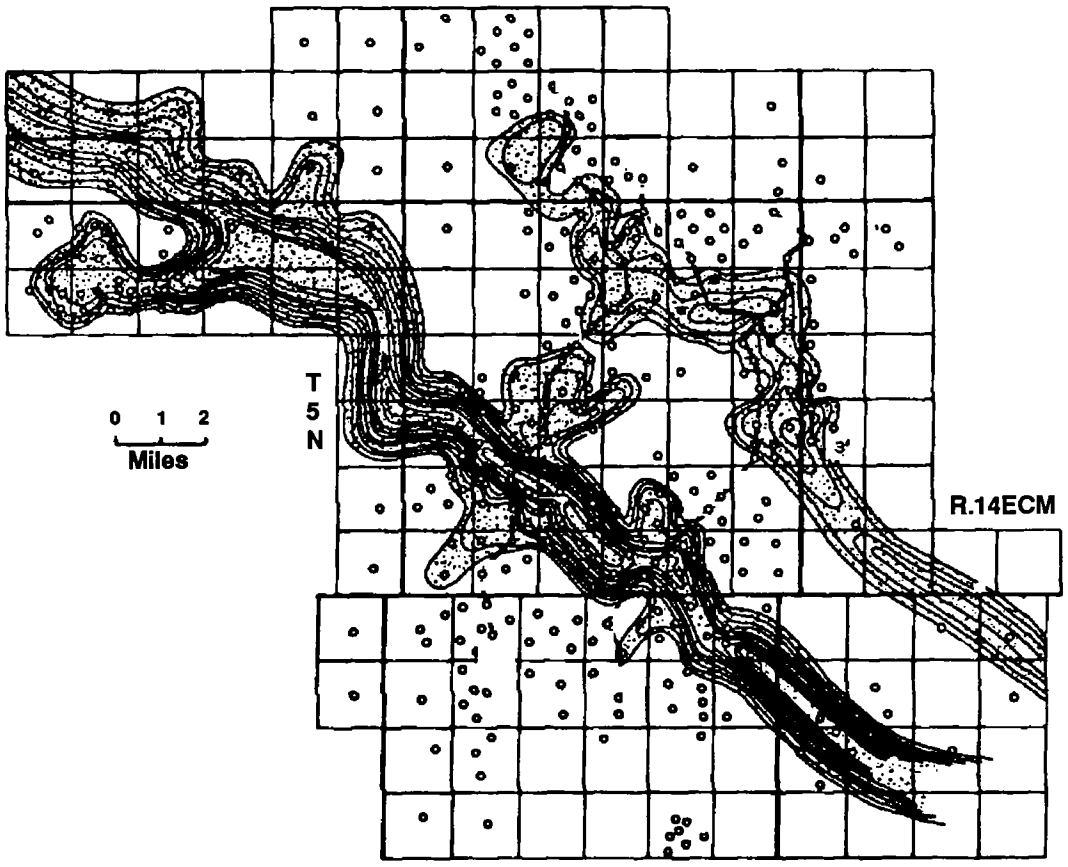

Figure 3. Isolith map of upper Morrow sandstone in the Hough area, Texas County, Oklahoma. Interpreted by Swanson (1979) as a *stream mouth deposit.* The elongate nature of the deposits that exhibit gentle curves and apparent tributaries are interpreted by this author as incised paleovalley sandstones. (From Swanson, 1979.)

ment may increase accommodation space significantly in portions of paleovalleys (Tillman, 1998). Post-depositional fault movement will preserve the same thickness in the units immediately underlying the sandstones, however offset.

Swanson identified a number of features that he placed in back-swamp/marsh environments (carbonaceous material, clay pebbles, roots, burrows, and slumps); however, he did indicate that these might in part be "meander channel-fill claystones" (1979, p. 122). Recent work indicates that all these features may also be observed in tidal point bars and their associated fine-grained, tidal-channel–fill sediments.

James Coleman (1976, personal communication), formerly at Louisiana State University, implied that distributary channels associated with deltas were most commonly conduits by which sediment moved from fluvial channels to distributary-mouth bars and subsequently farther down the slope. In other words, they were not generally areas of localized, thick sand deposits as suggested in the delta model proposed for the Morrow by Swanson (1979, 1987, 1993).

Sequence models presented by Ross and Ross (1988) indicate that the Morrowan deposition was a time of sea-level lowstand with short intervals of minor sea-level rise and fall (Fig. 4). Evidence in the northern part of the Anadarko basin supports that model. The likelihood of having extensive shoreline deltas form during a lowstand seems remote. Instead, during transgression following lowstand, bay-head deltas may form in estuaries and flooded valleys.

The evidence strongly favors a paleovalley interpretation of most of the middle and upper Morrow reservoirs in the Oklahoma Panhandle and along the Stateline Trend.

STATELINE TREND RESERVOIRS

Valley-fill heterogeneous reservoirs in the Morrowan (Pennsylvanian) age Stateline Trend along the Kansas-Colorado border and the Oklahoma Panhandle (Figs. 1, 2) produce from valley-fill reservoirs and are internally complex, contain geographically and vertically limited reservoirs, and can only be effectively drained if the detailed internal architecture of the reservoirs is understood. Development of detailed geologic models utilizing core interpretations for fluvially and tidally deposited valley-fill sandstone reservoirs enhance prospecting results and reservoir simulation and improve planning for secondary recovery and possible tertiary production. Only by recognizing the location and degree of impermeability of barriers to flow at the margins of

and within the valley-fill reservoirs can prospecting for and development of valley-fill reservoirs be successful.

The valleys in which the reservoirs occur in the Stateline Trend were cut by rivers during drops in sea level and remained as conduits (narrow, open valleys trending perpendicular to or at a high angles to the regional shoreline). At a later time, as sea level rose, the valleys were filled from the landward side by rivers, from the seaward side by tidal or shoreline processes, or alternately from both the landward and seaward sides at the same time. Several periods of deposition and erosion occur in most of the valleys. Mapping the results of erosion of earlier-deposited paleovalley-fill sandstones is important in isolating flow units (Fig. 5). Deposition of the paleovalley-fills occurs primarily during transgression in a LST.

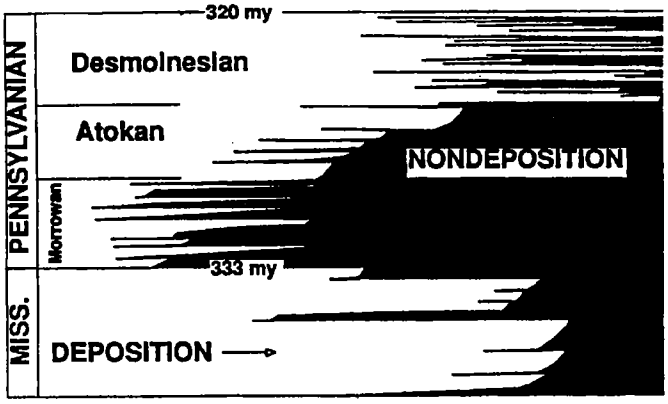

Figure 4. Coastal-onlap curve as an indication of eustatic sea-level changes during the Carboniferous. The Morrowan was deposited during the lowest lowstand of the Mississippian–Pennsylvanian (Carboniferous). (Modified from Ross and Ross, 1988.) Abbreviation: my—million years.

One of the most commonly referred to valley-fill models for the Morrow sandstone reservoirs (Wheeler and others, 1990) infers that the basal-most valley fill should be fluvial sandstones. However, in some Morrow Stateline Trend paleovalleys, the basal-most sandstones are tidal in origin. The topography on which the sandstones are deposited may be in part controlling which facies occur at the base of the reservoirs.

Valley-fill deposits occur *below* the regional transgression surface of erosion (TSE) rather than above it as do many deltaic deposits (Fig. 6). Because of this relationship, cross sections of valley-fill deposits should also be hung on markers (flooding surfaces?) *immediately above* the top of the valley.

SOUTHEAST TRACY FIELD CORE

A core from the Cities Service Buzzard D-2 well in Texas County, Oklahoma, is a typical tidal- to tidally influenced, paleovalley-fill reservoir. Numerous thin units, such as observed in the Buzzard D-2 core, are typical of many tidally deposited or tidally influenced

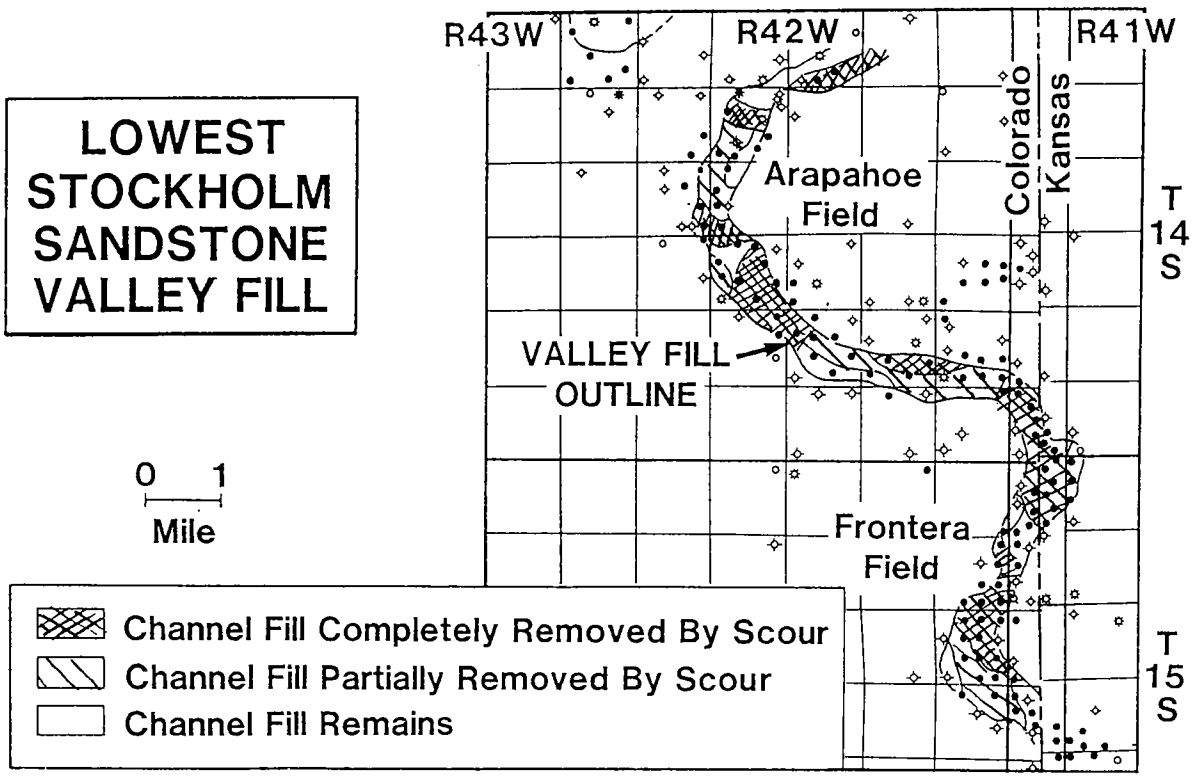

Figure 5. Paleovalley-fill map of lowest producing reservoirs in Arapahoe Field showing meandering nature of valley. Note that erosion has removed part or all of the reservoir sandstones in many areas of the valley. (Modified from Blakeney and others, 1990.)

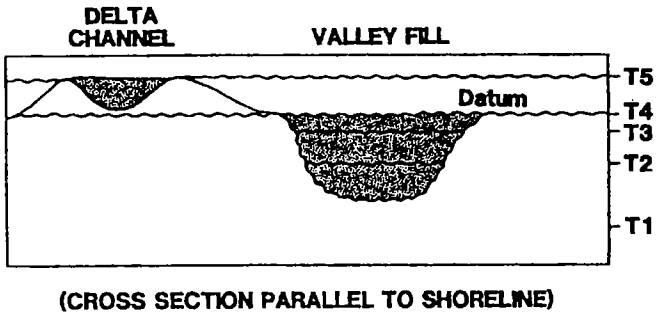

Figure 6. Datum-reference diagram. Paleovalley-fill reservoirs always occur below regional datums (flooding surfaces), whereas deltaic reservoirs occur mostly above regional datums. The paleovalley fill and the delta deposit were both deposited following "Time 4"; however, their relationship to the datum is significantly different. Abbreviation: T—time.

reservoirs (Fig. 7; Tables 1, 2). Several units in the core show no evidence of tidal influence and are designated as fluvial sandstones.

Andrews (1999) also described this core. He interpreted it as an "incised fluvial channel"; however, he recognized clay drapes and clasts, carbonaceous laminae, and carbonaceous shale, all of which are common in tidal and tidally influenced environments. The clay and finely disseminated carbonaceous material can both settle out of suspension during periods of slack tides.

Environmental interpretations of the facies and subfacies present in the Buzzard D-2 core are presented in Table 1, and the details of the core are shown as Figure 7. Detailed descriptions of units representative of each of the facies and subfacies present in the core are given in Table 2.

SOUTHWEST STOCKHOLM FIELD

Detailed geologic analysis of cores such as those from Southwest Stockholm Field combined with cross sections and isopach and structure maps yield details of reservoir heterogeneity. Reservoir-production properties of fluvial and tidal (estuarine) sandstones may be quite different (Arapahoe Field, Krystinik and Blakeney, 1990), but, in some fields (e.g., Southwest Stockholm), little difference exists in many producing wells among porosities and permeabilities in the two major valley-fill producing facies (Fig. 8). Within the approximately 150-ft-thick valley-fill vertical sequence at Southwest Stockholm Field (Fig. 9), just one of the three sandstones yields significant production. Also, within Southwest Stockholm, topographic highs on the valley bottom, covering an area as large as one half of a section, reduce the depositional thickness of the reservoir sandstones. Impermeable limestones and shales commonly form lateral barriers to flow at valley margins and locally within the valleys (Tillman and Pittman, 1993). Erosion of portions of potentially productive sandstones within the valleys also was found to be important in isolating reservoirs (flow units), especially in the Arapahoe Field (Fig. 5; Blakeney and others, 1990).

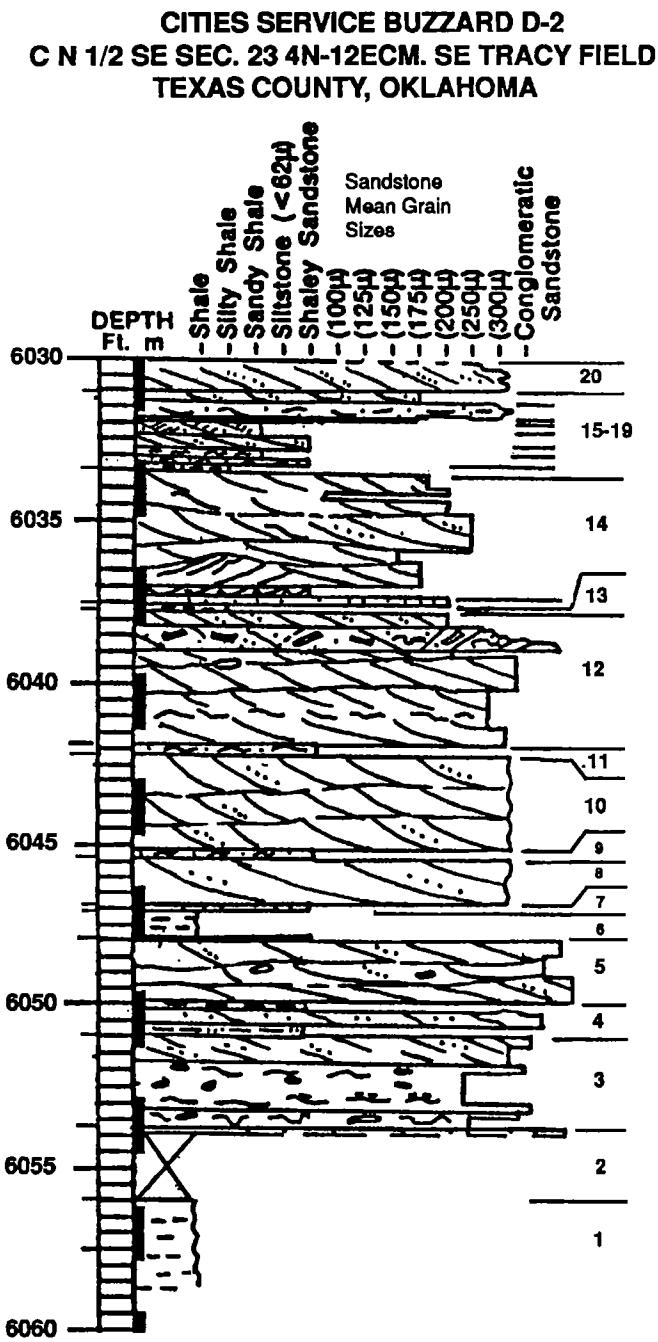

Figure 7. Stratigraphic section of core from the Cities Service Buzzard D-2 well, located in the C., N½SE¼ sec. 12, T. 4 N., R. 12 ECM., Texas County, Oklahoma, in the SE Tracy Field. Facies from 6,038.25 to 6,105 ft are given in Table 1 and correspond to unit numbers shown on the right side of the figure. Paleovalley-fill facies in this core range from fluvial, to tidally influenced fluvial, to tidal. Gross lithologies and grain-size depicted on column, with sand-sized material ranging from 100 μ to 200 μ.

Flow Units

Tidally deposited (estuarine) sandstones are generally finer grained and more clay prone than the fluvial sandstones, and, consequently, may have poorer reser-

Table 1.—Description of Core and Interpretation of Depositional Environments from Cities Service Buzzard D-2 Well

Location: C N½SE¼ sec. 23, T. 4 N., R. 12 ECM., Texas County, Oklahoma

Unit number	Cored interval (ft)	Thickness (ft)	Environmental interpretation	Probability[a]
20	6,030.0–6,030.9	0.9	Fluvial-channel sandstone	80%
19	6,030.9–6,031.35	0.45	Tidally influenced, fluvial-channel sandstone	80%
18	6,031.35–6,031.75	0.4	Tidal-channel sandstone	90%
17	6,031.75–6,031.9	0.15	Tidal-creek sandstone	85%
16D	**6,031.9–6,032.2**	**0.3**	**Tidal-creek deposit**	**75%**
16C	6,032.2–6,032.35	0.15	Tidal-creek–accretion-bar sandstone	75%
16B	**6,032.35–6,032.7**	**0.35**	**Tidal-creek–accretion-bar sandstone, slightly slumped**	**80%**
16A	6,032.7–6,033.25	0.5	Tidal-creek mudstone to siltstone	90%
15	**6,033.25–6,033.4**	**0.15**	**Tidal mudstone**	**95%**
14C	**6,033.4–6,036.9**	**2.5**	**Tidally influenced fluvial-channel sandstone**	**75%**
14B	6,036.9–6,037.1	0.2	Tidal sandstone	90%
14A	6,037.1–6,037.45	0.35	Tidally influenced, fluvial-channel sandstone	75%
13	6,037.45–6,037.55	0.1	Tidal mudstone	75%
12C	**6,037.55–6,038.25**	**0.7**	**Fluvial-channel sandstone**	**90%**
12B	6,038.25–6,038.85	0.6	Tidally influenced, fluvial-channel sandstone	75%
12A	6,038.85–6,041.7	2.85	Fluvial-channel sandstone	90%
11	6,041.7–6,042.3	0.6	Tidally influenced, fluvial-channel sandstone	90%
10	6,042.3–6,045.2	1.9	Fluvial-channel sandstone	90%
9	6,045.2–6,045.4	0.2	Tidally influenced, fluvial-channel sandsone	75%
8	6,045.4–6,046.9	1.5	Tidally influenced, fluvial-channel sandstone	90%
7B	6,046.9–6,047.1	0.2	Tidal-channel sandstone[b]	75%
6	6047.1–6047.95	0.85	Core not preserved or recovered	75%
5	6,047.95–6,050.05	2.1	Tidal-"delta" sandstone/open-bay deposit	70%
4	6,050.05–6,051.0	0.95	Fluvially influenced, tidal-channel sandstone	70%
3C	6,051.0–6,051.7	0.7	Tidal-creek sandstone	75%
3B	**6,051.7–6,053.25**	**1.55**	**Tidal-channel sandstone**	**80%**
3A	6,053.25–6,053.8	0.55	Tidal-channel sandstone	80%
2B	6,053.8–6,054.0	0.1	Tidal-creek sandstone	75%
2A	6,054.0–6,056.2	2.2	Tidal-channel sandstone[b]	—
1	6,056.2–6,107.01	48.8	Marine shale	95%

Notes: Core described by R. W. Tillman, 05/11/2000, from cored interval 6,030–6,060 ft.
Core to log corrections: 6,030–6,046.9 ft, log depth 1 ft shallower; 6,046.9–6,053.9 ft, log depth 2 ft shallower.
Units shown in boldface type are described in more detail in Table 2.

[a] "Probability" of correct interpretation is based on observed rock characteristics.
[b] Some of core in interval not preserved or recovered.

voir properties. In the Southwest Stockholm Field, fluvial deposits have average porosities of 15.4% (range of 2.8% to 21.6%) and average permeabilities of 784 millidarcies (md) with a range of 0.03–5,500 md. Tidal-channel sandstones have average porosities of 10% (range from 3.1% to 18.4%) and permeabilities of 129 md (range of 0.12 to 470 md). Note the significant differences in the *mean* values for the two types of deposits.

Tidal sandstones in the Southwest Stockholm Field interfinger with fluvial sandstones. Where interfingering of facies occurs, vertical permeability is diminished, and flow units may be fragmented. As previously stated, tidally deposited (estuarine) sandstones are generally both finer grained and more clay rich than fluvial sandstones. Consequently, they may have poorer reservoir properties. However, as observed in Figure 8, many of the tidally deposited sandstones have the same permeabilities and porosities as fluvial sandstones. Traditionally, only the fluvial-facies rocks have been perforated in Morrow sandstones in the Stateline Trend. This perforation scheme may be leaving producible oil behind pipe in the reservoirs.

Porosity Origin and Distribution

All sandstones *deposited* by the same processes are assigned to the same lithofacies and subfacies (Tables 1, 2). Secondary (post-burial) events, however, also af-

Table 2.—Description of Core and Interpretation of Depositional Environments from Selected Units from Cities Service Buzzard D-2 Well

Unit or subunit	Thickness (ft)	Core depth (ft) (Log depth) (ft)[a]	Description	Environment of deposition	Probability[b]
16D	0.3	6,031.9–6,032.2 (6,030.9–6,031.2)	Silty sandstone (grain size: 100–125 μ, 175 μ maximum; sorting, moderately well). 90% climbing ripples, micro-faulted. 10% silty-shale drapes between climbing-ripple sets.	Tidal-creek deposit	75%
16B	0.35	6,032.35–6,032.7 (6,031.35–6,031.7)	Sandstone (grain size: 100 μ, 150 μ maximum; sorting: moderately well). Trace of glauconite. Upper 0.1 ft mildly deformed (slumped). Carbonaceous (30%). Finely rippled, carbonaceous laminae inter-laminated with sand. 5% brown shale rip-up clasts.	Tidal-creek–accretion-bar sandstone (slightly slumped)	80%
15	0.15	6033.25–6,033.4 (6,032.25–6,032.4)	Shale, dark gray, fissile, silty and sandy (grain size: 150 μ, maximum 300 μ) as streaks and thin beds. Mildly deformed. Traces of glauconite and carbonaceous grains. Abundant elongate grains (1,000 μ, shards).	Tidal mudstone	95%
14C	2.5	6,033.4–6,036.9 (6,032.4–6,036.9)	Sandstone (grain size: 75, 150, 175, 200 μ, maximum 125, 250, 500, 750 μ; sorting: variable—well, moderate, moderately poor, and poor). Trough cross-stratified (massive appearing). Trace of carbonaceous grains. 5% wisps of discontinuous, carbonaceous laminae in fine intervals. Siltstone clasts near top. Trace of glauconite near top.	Tidally influenced, fluvial-channel sandstone	75%
12C	0.7	6,037.55–6,038.25 (6,036.55–6,037.25)	Sandstone (grain size: 200 μ, maximum 500 μ; sorting: poor). Trough cross-stratified, massive appearing. Contrast in grain size between beds within subunit. Trace of carbonaceous grains.	Fluvial-channel sandstone	90%
3B	1.55	6,051.7–6,053.25 (6,049.7–6,051.25)	Sandstone (grain size: 250–400 μ, maximum 1,000 μ; sorting: very poor). Massive (slumped) to low-angle planar cross-stratified. 15% 0.25–1 in. long elongate, brown, rounded, carbonaceous, variously oriented, clasts scattered throughout sandstone. Trace of shale drapes. 5% discontinuous coaly lenses, 2% small (1–3 mm) coaly clasts.	Tidal-channel sandstone	80%

Note: Abbreviated descriptions of units or subunits are shown in boldface type in Table 1.
1,000 μ = 1 mm.

[a]Corrections between core/log depths: 6,030–6,046.9 ft, log depth 1 ft shallower; 6,046.9–6,053.9 ft, log depth 2 ft shallower.
[b]"Probability" of correct interpetation is based on observed rock characteristics.

fected the production characteristics of the reservoirs. The post-depositional events that affected the reservoirs were significantly different in several of the seven recognized depositional lithofacies. Where millimeter-thick shale lenses were deposited within tidally deposited sands, pressure solution of quartz in contact with the clay reduced porosity. Thin, millimeter-thick clay drapes, common in tidal-channel–accretion point-bar sandstones, may significantly reduce vertical permeabilities but have much less effect on horizontal permeabilities.

Up to half of the porosity in the Southwest Stockholm Field may be leached (secondary) porosity (Tillman and Pittman, 1993). Leaching by secondary processes may hamper log-facies recognition, and the results of the post-burial (secondary) processes should be considered when calculating net pay. Understanding the differences in heterogeneity characteristics between fluvial and tidal (estuarine) valley-fills, such as those in the Stateline Trend, allows proper economic evaluation and more efficient reservoir management of these kinds of reservoirs.

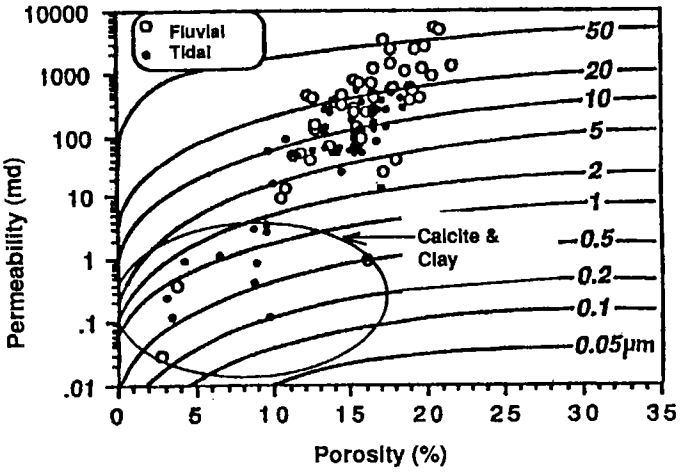

Figure 8. Plot of permeability versus porosity for tidal and fluvial sandstones from cored wells in the Southwest Stockholm Field. Samples in circled area are degraded by excessive amounts of clay and/or calcite cement. Note that many of the tidal sandstones (outside the circled area) have similar porosities and permeabilities to the fluvial samples. Porosity distribution is strongly influenced by diagenetic processes. The curved lines are graphic solutions to Winland's equation. (Modified from Tillman and Pittman, 1993.)

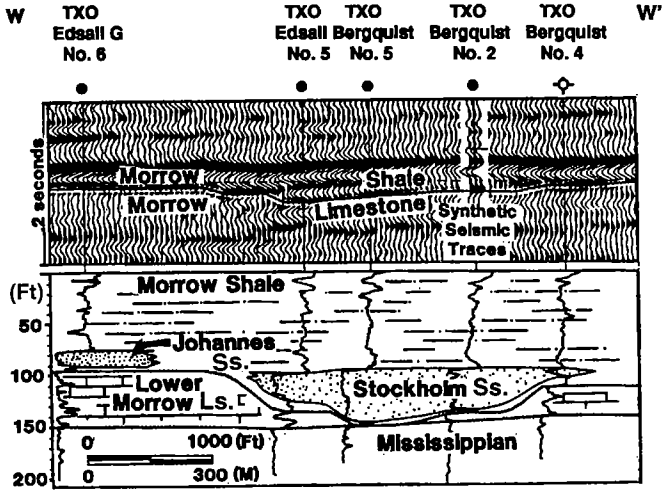

Figure 9. Stratigraphic and seismic cross sections through two laterally separated Morrow sandstone paleovalley-fill reservoirs in the Southwest Stockholm Field, Kansas. A synthetic seismic profile was calculated for the TXO Bergquist No. 2 well. Note that the Morrow sandstone fills are in an erosional "channel" that bottoms in limestone. The flow direction in the "channel" was out of the diagram. (Modified from Brown and others, 1990).

REFERENCES CITED

Andrews, R. D., 1999, Morrow gas play in the Anadarko basin and shelf of Oklahoma: Oklahoma Geological Survey Special Publication 99-4, 133 p.

Blakeney, B. A.; Krystinik, L. F.; and Downey, A. A., 1990, Reservoir heterogeneity in Morrow Valley fills, Stateline Trend: implications for reservoir management and field expansion, *in* Sonnenberg, S. A.; Shannon, L.; Rader, T. K.; von Drehle, W. F.; and Martin, G. W. (eds.), Morrow sandstones of southeast Colorado and adjacent areas: Rocky Mountain Association of Geologists, Denver, p. 131–142.

Brown, L. G.; Miller, W. A.; Handley-Goff, E. M.; and Veal, S., 1990, Southwest Stockholm Field, *in* Sonnenberg, S. A.; Shannon, L. T.; Rader, K.; von Drehle, W. F.; and Martin, G. W. (eds.), Morrow sandstones of southeast Colorado and adjacent areas: Rocky Mountain Association of Geologists, Denver, p. 117–130.

Krystinik, L. F.; and Blakeney, B. A., 1990, Sedimentology of the upper Morrow Formation in eastern Colorado and western Kansas, *in* Sonnenberg, S. A.; Shannon, L.; Rader, T. K.; von Drehle, W. F.; and Martin, G. W. (eds.), Morrow sandstones of southeast Colorado and adjacent areas: Rocky Mountain Association of Geologists, Denver, p. 37–50.

Ross, C. A.; and Ross, J. R., 1988, Late Paleozoic transgressive deposition, *in* Wilgus, D. K.; Hasting, B. S.; Kendall, C. G. St.C.; Postmentier, H.; Ross, C. A.; and Van Wagoner, J. C. (eds.), Sea level changes: an integrated approach: Society of Economic Paleontologists and Mineralogists, Society for Sedimentary Geology Special Publication 42, p. 227–247.

Shumard, C. B.; and Avis, L. E., 1990, Key Morrow predictive exploration model: Southwest Stockholm field: Oil and Gas Journal, v. 88, p. 87–94.

Swanson, D. C., 1979, Deltaic deposits in the Pennsylvanian upper Morrow Formation in the Anadarko basin, *in* Hyne, N. J. (ed.), Pennsylvanian sandstones of the Mid-Continent: Tulsa Geological Society Publication 1, p. 115–168.

_____ 1987, Deltaic deposits in the Pennsylvanian upper Morrow Formation in the Anadarko basin, Pennsylvanian sandstones of the Mid-Continent, *in* Reservoir II Sandstones, Treatise of Petroleum Geology Reprint Series No. 4: American Association of Petroleum Geologists, Tulsa, Oklahoma, p. 73–126.

_____ 1993, The importance of fluvial processes and related reservoir deposits: Journal of Petroleum Technology, v. 45, p. 368–377.

Tillman, R. W., 1998, Compartmentalization in tidal valley-fill sandstone reservoirs, Sun Ranch field, Wyoming, *in* Slatt, R. (ed.), Compartmentalized reservoirs in Rocky Mountain basins: Rocky Mountain Association of Geologists, Denver, p. 131–149.

Tillman, R. W.; and Pittman, E. D., 1993, Reservoir heterogeneity in valley-fill sandstone reservoirs Southwest Stockholm field, Kansas, *in* Linville, B. (ed.), Reservoir characterization III: PennWell Books, Tulsa, Oklahoma, p. 51–106.

Wheeler, D. M.; Scott, A. J.; Coringrato, V. J.; and Devine, P. E. 1990, Stratigraphy and depositional history of the Morrow Formation, southeast Colorado and southwest Kansas, *in* Sonnenberg, S. A.; Shannon, L. T.; Rader, K.; von Drehle, W. F.; and Martin, G. W. (eds.), Morrow sandstones of southeast Colorado and adjacent areas: Rocky Mountain Association of Geologists, Denver, p. 9–35.

Geochemical Characterization of Selected Oils and Source Rocks from the Chester Formation, Springer Formation, and Morrow Group of the Anadarko Basin

H. D. Wang and R. Paul Philp
University of Oklahoma
Norman, Oklahoma

ABSTRACT.—Selected source rock and crude oil samples from the Upper Mississippian to Pennsylvanian Chester, Springer, and Morrow sequences of the Anadarko basin, Oklahoma, have been characterized using various organic geochemical techniques. The Upper Devonian Woodford Shale also has been investigated and used as a reference for comparison with the other formations examined in this study. The samples were characterized by techniques including stable carbon isotope ($\delta^{13}C$), gas chromatography (GC), gas chromatography and mass spectrometry (GCMS and GCMSMS), and pyrolysis gas chromatography and mass spectrometry (PYGCMS). The distributions and concentrations (both relative and absolute) for the biomarkers were determined for the source rocks, and crude oils were evaluated in terms of maturity, migration, and weathering. The biomarker characteristics were combined with other geochemical and geologic information to interpret sources, depositional environments, maturity, migration, and weathering of the source rocks and associated crude oils.

INTRODUCTION

General Description of the Anadarko Basin

The Anadarko basin ranges from the west central portion of Oklahoma into the Oklahoma Panhandle, and the northern Texas Panhandle (Fig. 1). The basin is bounded on the south by the Wichita–Amarillo uplift, on the east by the Nemaha ridge, on the west by the Cimarron arch, and on the north by the Hugoton embayment (Johnson, 1989). The Anadarko basin is the deepest sedimentary and structural basin in the cratonic interior of the North American Continent. Paleozoic sedimentary rocks, as much as 40,000 ft in thickness, are present along the basin's axis, which is near the southern margin of this asymmetrical basin. Even in the shallower northern portion of the basin, the sedimentary sequence still ranges from 10,000 to 25,000 ft in thickness (Kennedy and others, 1982).

It is widely believed that the Upper Devonian Woodford Shale is a major source rock in the Anadarko basin (Kennedy and others, 1982; Johnson and others, 1988; Rascoe and Hyne, 1988). However, the volume of the Woodford Shale is limited (the average thickness of the Woodford Shale in the Anadarko basin is about 200 ft). The variable geochemical features of crude oils produced in the Anadarko basin cannot all be correlated with the geochemical features of the Woodford Shale extracts. This paper will investigate some of the geochemical characteristics of selected Pennsylvanian oils and source rocks, particularly those from the Springer and Morrow sequences, and discuss similarities and differences between these samples and those related to the Woodford Shale, as well as present a brief discussion about certain geochemical features of the Chester Formation.

Papers presented at a previous Oklahoma Geological Survey (OGS) symposium on the Anadarko basin (Johnson, 1989) provide valuable background information covering many topics about the geology of the basin (Amsden, 1989; Burruss and Hatch, 1989; Cardott, 1989; Davis and Northcutt, 1989; Jorgensen, 1989; Keighin and Flores, 1989; Pitman and Burruss, 1989; Rice and others, 1989; Schmoker, 1989). Gilbert (1992) described the origin and evolutionary history of the Anadarko basin and discussed some of the ambiguous and confusing interpretations about the origin and evolutionary history of the basin. Previous geochemical studies on the Anadarko basin include a number of maturity related investigations of the Woodford Shale (Cardott and Lambert, 1985; Schmoker, 1986; Cardott, 1989; Pawlewicz, 1989; Hussain and Bloom, 1991). Lewan (1983) conducted hydrous pyrolysis experiments on the Woodford Shale to study the effects of maturity, and similar maturity studies have been conducted on the Upper Morrow Formation (Tsiris, 1983; Walker 1986). Schmoker (1986) developed a thermal-maturity

Wang, H. D.; and Philp, R. P., 2001, Geochemical characterization of selected oils and source rocks from the Chester Formation, Springer Formation, and Morrow Group of the Anadarko basin, *in* Johnson, K. S. (ed.), Pennsylvanian and Permian geology and petroleum in the southern Midcontinent, 1998 symposium: Oklahoma Geological Survey Circular 104, p. 41–57.

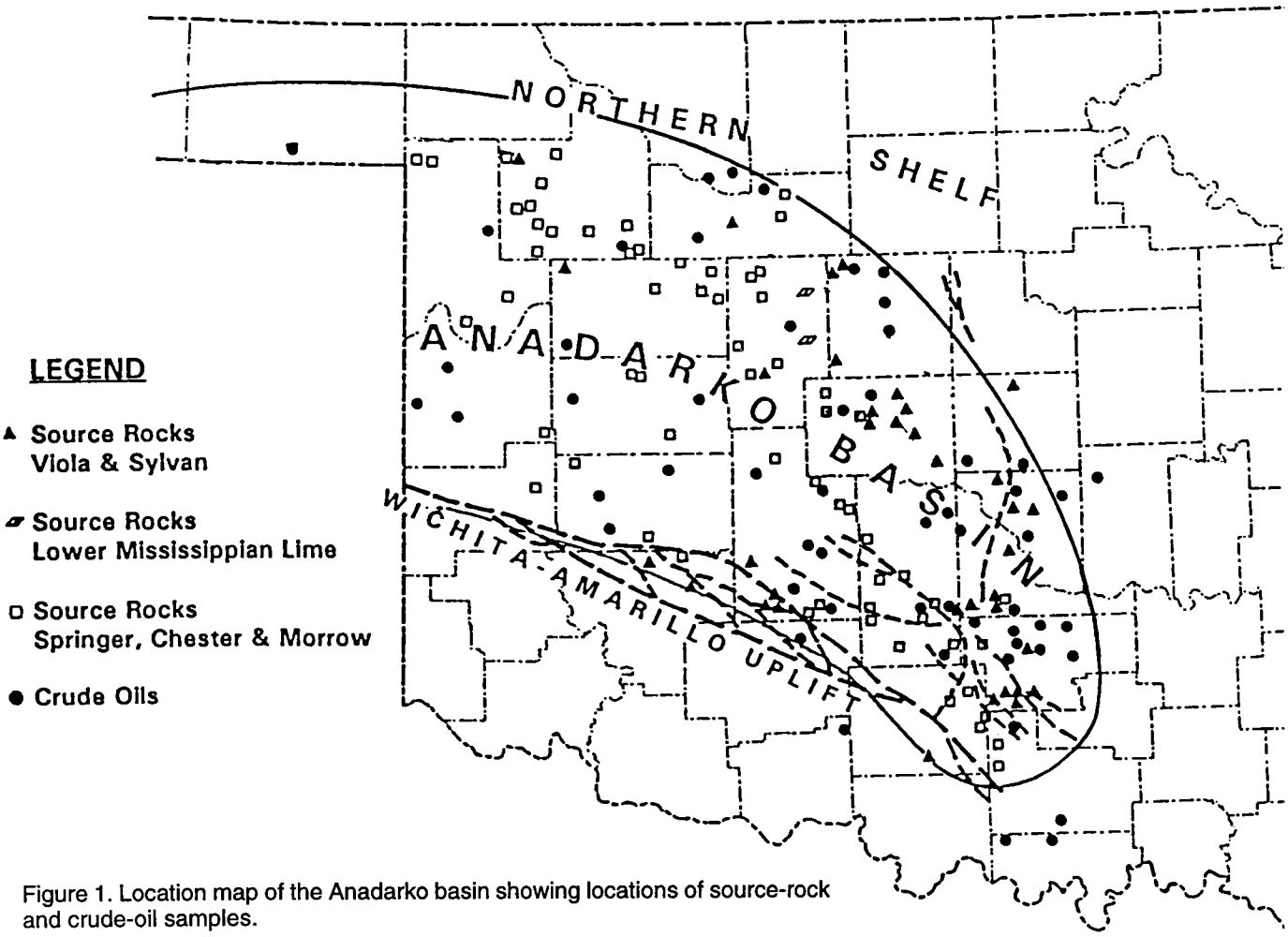

Figure 1. Location map of the Anadarko basin showing locations of source-rock and crude-oil samples.

model for the Anadarko basin based on a modified time-temperature–index (TTI) method (Lopatin, 1971), in which the relationship of TTI to burial depths and thermal-maturity levels of formations was proposed. Engel and others (1988) conducted an organic geochemical correlation of Oklahoma crude oils using R- and Q-mode factor analyses. Burruss and Hatch (1989) reported geochemical analyses of 96 crude oils and condensates produced in the Anadarko basin and demonstrated the presence of three major oil types based on the age of the reservoirs. Philp and others (1989) conducted a geochemical investigation of some oils, source rocks, and tar sands in the Anadarko and Ardmore basins. Jones (1986) and Jones and Philp (1990) conducted geochemical studies on source rocks and oils in the Pauls Valley area of the Anadarko basin. Hester and others (1990) introduced log-derived total-organic-carbon (TOC) contour maps of the Woodford Shale in the northwestern Anadarko basin. Values of TOC per unit surface area were estimated and mapped.

Chester and Springer Formations and Morrow Group

The Middle Mississippian Chester Formation, which was deposited in a normal marine environment, consist mainly of shale with some limestone and basin-marginal sandstones in the lower part of the section and mainly limestone with some shale in the upper part. Many apparent lithologic changes in Chester rocks did not result from facies variations during deposition but commonly reflect post-Mississippian uplift and erosion. The upper limestone units of the Chester Formation were removed in the northwestern Anadarko basin, leaving only the lower shaley units at the basin margins (Johnson and others, 1988). The thickness of the Chester unit varies from 200 to 1,300 ft; however, neither the shale nor the limestone of the Chester Formation is very rich in organic matter.

The Upper Mississippian Springer Formation consists of black shale and sandstone, and the lithofacies and the depositional environment of the Springer are very similar to that of the Morrow Group sediments so that it is commonly difficult to distinguish the two. The Springer Formation exists only in and near the deep Anadarko basin. At the northern part of the Anadarko basin, the Springer Formation was probably eroded together with the upper part of the Chester Formation (Johnson and others, 1988). The post-Mississippian erosion brought the Springer rock to the surface or near enough to the surface so that biodegradation of organic matter is a common feature of the Springer source rock. The average thickness of the Springer Formation is

about 500 ft, and more than 60% of it is shale and mudstone. The black shale in the Springer Formation is fairly rich in organic matter with an average TOC value of 1.65%.

The Morrow Group was deposited in a shallow-marine to shoreline and deltaic environment during the Early to Middle Pennsylvanian (Tsiris, 1983; Keighin and Flores, 1989). The lithofacies of the Lower Morrow is mainly black shale with interbedded sandstone and thin layers of limestone that were presumably in a transgressive sea. In the Middle Morrow, the dominant facies are marine shales and carbonates, with fewer sandstone layers than the Lower Morrow. The Upper Morrow was deposited during the subsequent regression, which resulted in the deposition of thin layers of coal and lagoonal shale, with black shale being the dominant lithofacies. Recycled organic materials with a small portion of indigenous woody-herbaceous organic matter are important components of the Upper Morrow shale. The Morrow Group is very thick because of rapid subsidence during the Pennsylvanian. The average thickness of the Morrow Group is about 1,500 ft, and more than 60% of this section is shale and mudstone. The black shale in the Morrow Group is fairly rich in organic matter (average TOC = 1.04%).

The Morrow Group is represented by a thick layer of conglomerate named the Granite Wash in the deep Anadarko basin near the Wichita–Amarillo uplift. The Granite Wash was formed from the erosion of the Wichita–Amarillo uplift due to rapid uplifting and subsidence along the southern margin of the Anadarko basin (Kennedy and others, 1982). Composition of the Granite Wash is mainly igneous-rock detritus. The Granite Wash was not investigated in this study.

The Chesterian to Morrowan was a transition time in the evolutionary history of the Anadarko basin. The collision of the continental margins along the Ouachita trough became progressively more intense and changed the stress field of the paleo-Anadarko basin from extension to compression. The subsidence rate increased up to the late Morrowan, when folding and faulting generated the Wichita–Amarillo uplift, the Arbuckle uplift, and other uplifts that separated the present Anadarko basin from the remainder of the Oklahoma basin. The Anadarko basin then became a foreland basin, whereas earlier it had been a cratonic basin.

EXPERIMENTAL

Sample Collection and Selection

Core samples were obtained from the Core and Sample Library of the Oklahoma Geological Survey. Cutting samples were obtained from the Shawnee Sample Cutting Library and the Ardmore Sample and Cut Library. Crude oil samples were obtained from the collection of the Organic Geochemical Laboratory of the School of Geology and Geophysics at The University of Oklahoma, the collection of M. H. Engel (The University of Oklahoma), and the collection of Mobil Dallas Research Laboratory (Dallas, Texas). The oil samples were collected to cover reservoir formations ranging in geologic age from Ordovician to Permian. The physical properties of the crude oils varied from very light, clear condensates to very heavy, black oils.

Screening Analysis

The majority of rock samples were treated with hydrochloric acid (HCl) to remove inorganic carbon and analyzed using a LECO CR-12 Carbon Determinator to obtain TOC values. The rock samples were also characterized using a RUSKA PYRAN Level I-FID System, which is a Rock-Eval–type instrument. The rock or kerogen samples were heated in a helium flow of 60 ml/min from 30°C to 600°C at a rate of 30°C/min, and then held at 600°C for 5 min. The components eluting between 30°C and 330°C were taken as S_1, and the components eluting between 330°C and 600°C were taken as S_2. The maximum eluting temperature (T_{MAX}) values were calculated from the relationship between retention time and programmed temperature. Hydrogen index (HI) values were calculated using S_2 and TOC values.

The major analytical techniques, such as gas chromatography (GC) and gas chromatography mass spectrometry (GCMS), and isotope ratio mass spectrometry, have been described in previous publications and will not be discussed again in this paper.

RESULTS AND DISCUSSION

Screening Analysis

The 36 Springer Formation shale samples analyzed had an average TOC value of 1.60% (one large TOC value from one bituminous sample was excluded from this calculation), which characterizes it as a fair to good shale source rock. For the 36 Morrow Group shale samples analyzed, the average TOC value was 1.04% (one large TOC value from a bituminous sample was again excluded from the calculation), which may be considered fair to good for a shale source rock. The average TOC values of the Chester Formation and the Lower Mississippian Limestone were generally less than 1.0%.

A kerogen-typing plot using hydrogen index (HI) versus T_{MAX} is shown in Figure 2, and plots of present burial depth versus T_{MAX} for the Springer Formation and the Morrow Group are shown in Figures 3 and 4. The plots support the geologic interpretation that the major Anadarko basin was a tectonically quiet basin, with the linear relationship between the burial depth and the maturity level of the source rocks basically valid (Schmoker, 1986; Walker, 1986). Plots of Rock-Eval pyrolysis S_2 values versus TOC values for the two formations (the Springer Formation and the Morrow Group) are shown in Figures 5 and 6, and a similar plot for the Woodford Shale is given for comparative purposes (Fig. 7).

The S_2-TOC plots provide a better method for the interpretation of TOC and pyrolysis data (Langford and Blanc-Valleron, 1990) because the S3 is not required. The slope of the regression line represents the true hydrogen index, and errors caused by rock matrix effect

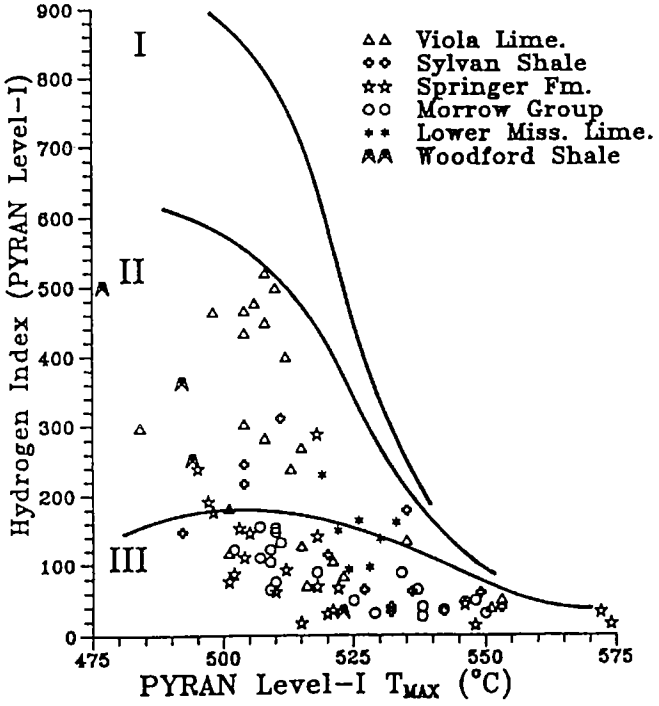

Figure 2. Plot of kerogen typing by hydrogen index (HI) versus T_{MAX} PYRAN Level-I pyrolysis (in °C).

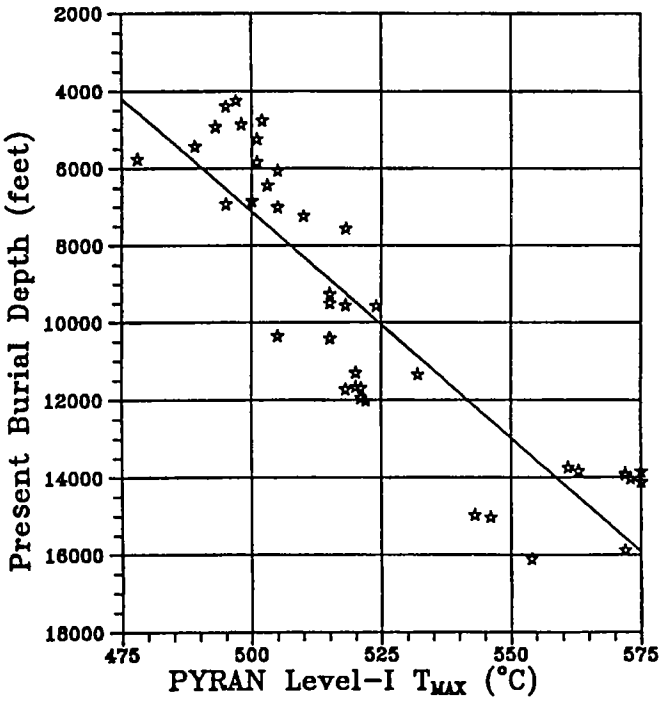

Figure 3. Plot of T_{MAX} (in °C) versus present burial depth (in feet) for the Springer Formation.

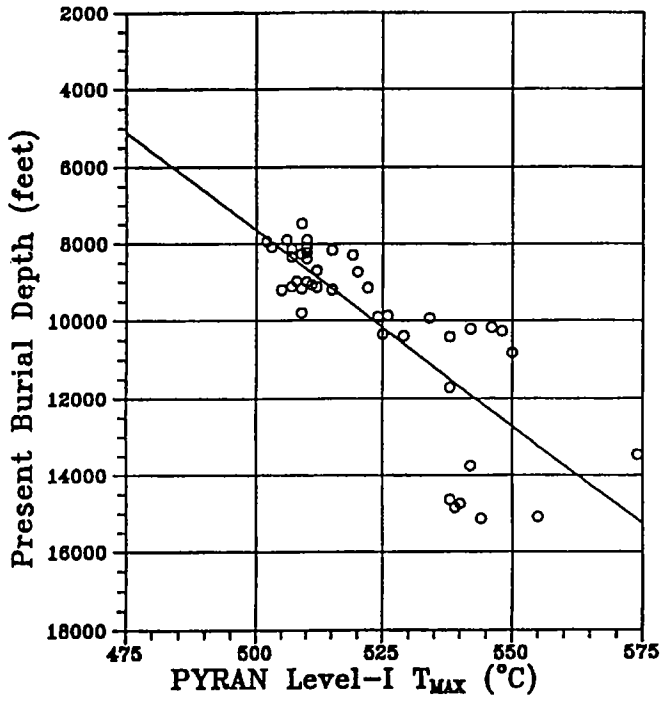

Figure 4. Plot of T_{MAX} (in °C) versus present burial depth (in feet) for the Morrow Group.

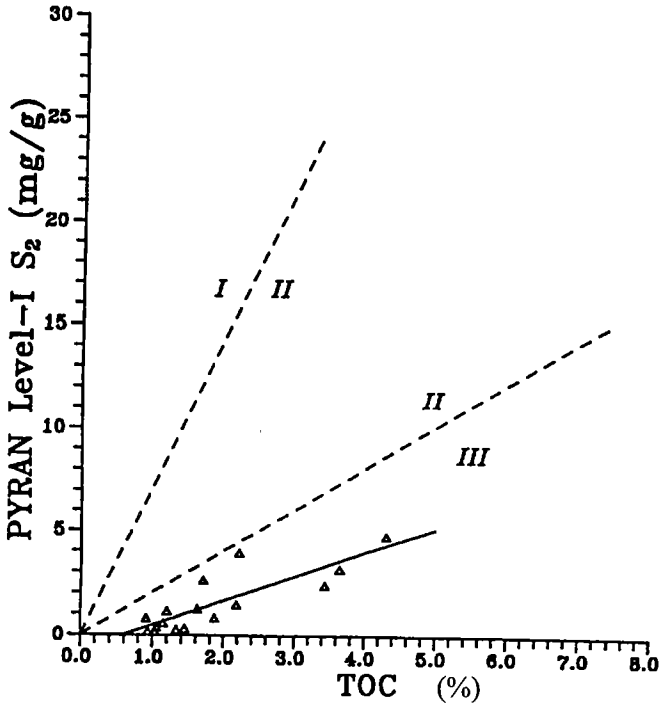

Figure 5. Plot of S2 PYRAN LEVEL-I (in mg/g) versus total organic carbon (TOC) (in %) for the Springer Formation. Numerals I, II, and III refer to standard kerogen types; the plot is divided into the regions for these three kerogen types based on literature data and information previously published. The Springer Formation samples are represented by the triangles; the solid line is the line of best fit through those points (Y = 1.16X – 0.68, with an X-intercept of 0.59).

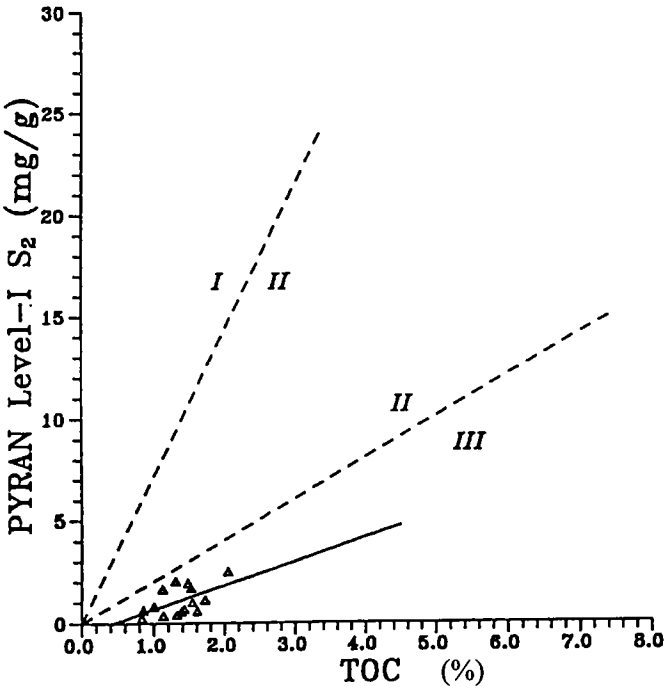

Figure 6. Plot of S2 PYRAN LEVEL-I (in mg/g) versus total organic carbon (TOC) (in %) for the Morrow Group. Numerals I, II, and III refer to standard kerogen types; the plot is divided into the regions for these three kerogen types based on literature data and information previously published. The samples from the Morrow Group are represented by the triangles, and the solid line is the line of best fit through those points (Y = 1.16X – 0.50, with an X-intercept of 0.43).

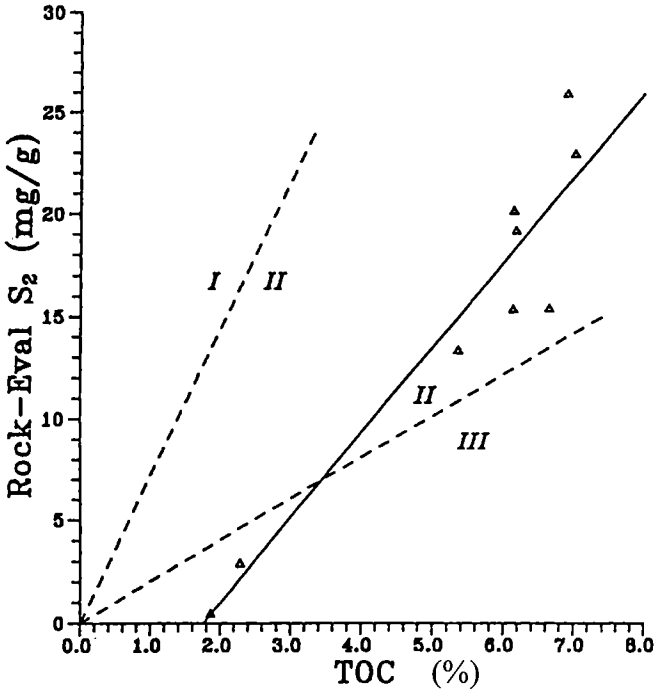

Figure 7. Plot of S2 PYRAN LEVEL-I (in mg/g) versus total organic carbon (TOC) (in %) for the Woodford Shale. Numerals I, II, and III refer to standard kerogen types; the plot is divided into the regions for these three kerogen types based on literature data and information previously published. The Woodford Shale samples are represented by the triangles, and the solid line is the line of best fit through those points (Y = 4.15X – 7.32) with an X-intercept of 1.76).

and the variation of richness of the source rocks are eliminated (Peters, 1986). The maturity trend is along the regression line from the upper-right corner to the lower-left corner of the plot. The types of organic matter are the same for all samples (which may have different maturity levels or are different in richness) in this line. A greater slope indicates higher kerogen rank. For example, the slopes of the Springer Formation and Morrow Group are low (1.16–1.81), indicating that these source rocks are mainly Type-III kerogens. On the other hand, the slope of the Woodford Shale is much higher (4.15–5.11). Those higher values indicate that these two source rocks are mainly Type-II kerogens. Langford and Blanc-Valleron, (1990), have suggested that the boundary (the slope of a S2-TOC plot) between Type-I and Type-II kerogens is about 7.0, whereas the boundary between Type-II and Type-III kerogens is about 2.0. These boundaries were plotted as dashed lines in Figures 5–7. Scattered data indicate type or facies variations that can be seen on the plots of the Springer Formation and the Morrow Group.

The S_2-TOC plots can be used to interpret rock-matrix–adsorption effect. Theoretically, a regression line in a S_2-TOC plot should pass through the origin point of the plot, because even very small amounts of organic matter yield hydrocarbons (as S_2) during pyrolysis. However, typical S_2-TOC lines always have positive intercepts on the X-axis. These positive intercepts indicate that the rock matrix adsorbs a threshold amount of organic matter. The Woodford source rock has the greatest adsorption effect (the X-intercept is 1.76; Fig. 7) because it is a shale. The Springer Formation and Morrow Group have smaller intercepts than that of the Woodford, indicating that these three shale formations are more calcareous than the Woodford Shale, which can be shown from the data of carbonate contents (Figs. 5–7).

Stable Carbon-Isotope Analysis

Saturate and aromatic fractions of selected source rocks and crude oils were characterized by stable-carbon isotopic mass spectrometry, and a plot of the carbon-isotope values of aromatic versus saturate fractions of the source rocks is shown in Figure 8, a relationship first used to differentiate marine and nonmarine oils (waxy versus non-waxy in the plot) by Sofer (1984). The data points that fall in the upper-left part of the plot are interpreted to be from nonmarine sources, and the data points that fall in the lower-right part of the plot are interpreted to be from marine sources. However, statistical studies have shown that there are many exceptions to the broad generalization (Peters and others, 1986).

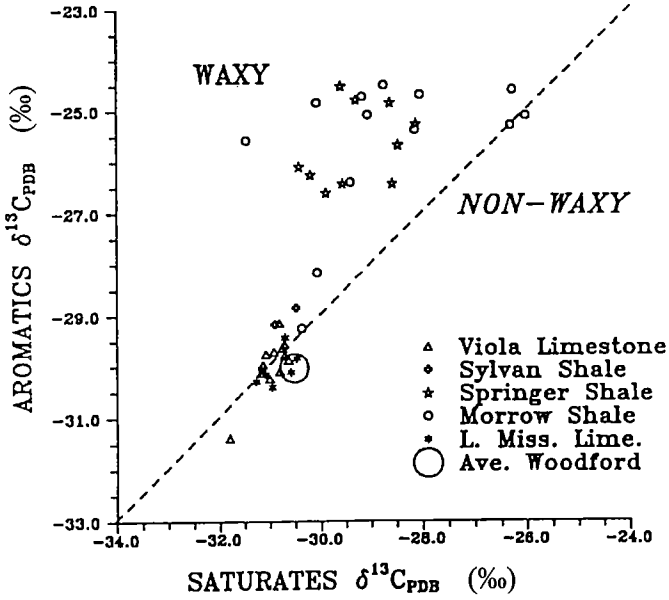

Figure 8. Plot of the $\delta^{13}C$ stable carbon-isotope (^{13}C) values for the saturate and aromatic fractions for the source-rock extracts examined in this study. These values are measured relative to the Pee Dee Belemnite (PDB) standard.

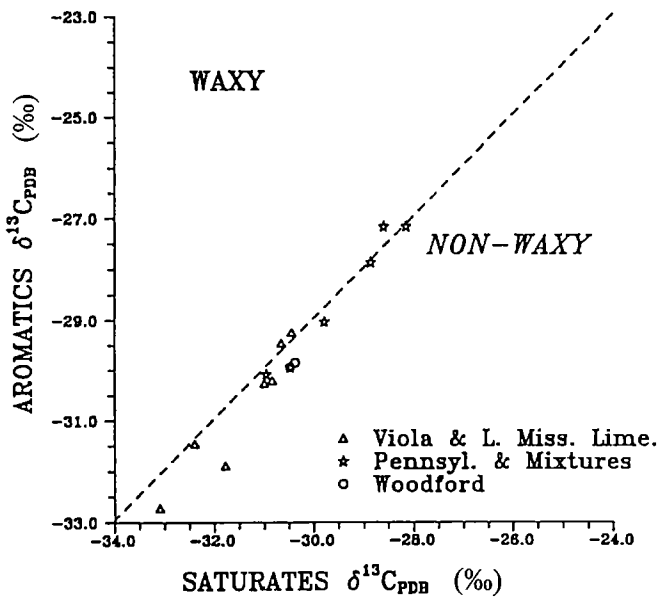

Figure 9. Plot of the $\delta^{13}C$ stable carbon-isotope (^{13}C) values for the saturate and aromatic fractions for the crude-oil extracts examined in this study. These values are measured relative to the Pee Dee Belemnite (PDB) standard.

It has been suggested that this approach can be used for oil–source-rock correlation (Schoell, 1983; Moldowan and others, 1985). The data points for the Springer and Morrow source rocks fall on the waxy region and are ^{13}C enriched, which may be due to the generation of gas, which is very ^{13}C depleted, such that the remaining hydrocarbons left in the source rock become ^{13}C enriched. The data points of the Springer and Morrow source rocks are scattered, and the effects of facies variation in the two formations may cause this scattering and the effects of recycled organic matter in the Morrow source rocks (Tsiris, 1983; Walker, 1986).

A similar $\delta^{13}C$ plot of aromatic versus saturate fractions of the crude oils is provided in Figure 9. A comparison of the data in Figures 8 and 9 illustrates a positive correlation between the Viola and Lower Mississippian source rocks and the crude oils. The oils are more depleted in ^{13}C than the source rocks, which may be due to migration effects (Sofer, 1984). The oil samples labeled "Pennsyl. and Mixtures" in Figure 9 are those oils that could be correlated with the Pennsylvanian source rocks by biomarker data or considered as mixtures of multi-sources. The correlation is not obvious, which may mean that carbon isotope data alone cannot fully distinguish these oils from others and that biomarker data must be used to achieve more definitive correlation.

Gas Chromatography

The saturate fractions of source rocks and crude oils were analyzed by gas chromatography to obtain the distribution of normal alkanes and acyclic isoprenoids.

Springer and Morrow Shales

Selected gas chromatograms of the saturate fractions from Springer shale and Morrow shale extracts are shown in Figures 10 and 11, respectively. The ratios of pristine/phytane (Pr/Ph) for all the samples are significantly higher than those for the Viola and Lower Mississippian Limestones but do not exceed a value of 3.0 or fall below a value of 1, possibly indicating an origin from a low-wax, marine source rock (McKirdy and others, 1983) and possibly some terrestrial input. Maturity can also cause an increase in Pr/Ph ratios (Alexander and others, 1981) and, thus, for samples with large burial depths (e.g., Spr-29 and Mor-33 in Figs. 10 and 11, respectively), the maturity factor should be considered. Most of CPI values for both formations are close to or greater than 1.0. A few Morrow Group samples have CPI values slightly less than 1.0, which may due to the influence of carbonate layers interbedded with the shales.

A bimodal distribution of the normal alkanes is very common in Morrow source rocks but less common in Springer source rocks. The relatively high concentration of higher molecular-weight, normal alkanes (C_{21} to C_{30}) is due to the contribution of higher plants to the organic matter (Tissot and Welte, 1984). This explanation supports the geologic interpretation that the Morrow Group was deposited in nearshore and deltaic environments, which received terrestrial input during deposition. A few samples in the Springer formation do not have bimodal distribution of normal alkanes (e.g., Spr-15 in Fig. 10), which may indicate that they received less input from higher plants.

Several Springer Formation samples exhibit a unique distribution of normal alkanes, as shown in the

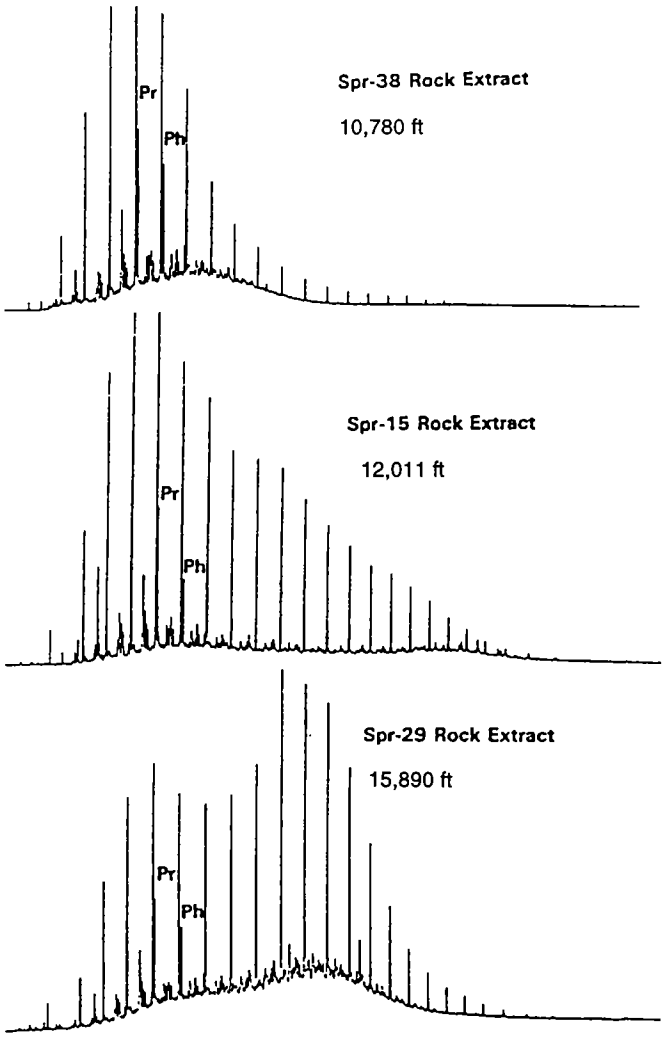

Figure 10. Gas chromatograms of three Springer source-rock saturate fractions. Depth of samples in feet. Abbreviations: Pr—pristane; Ph—phytane.

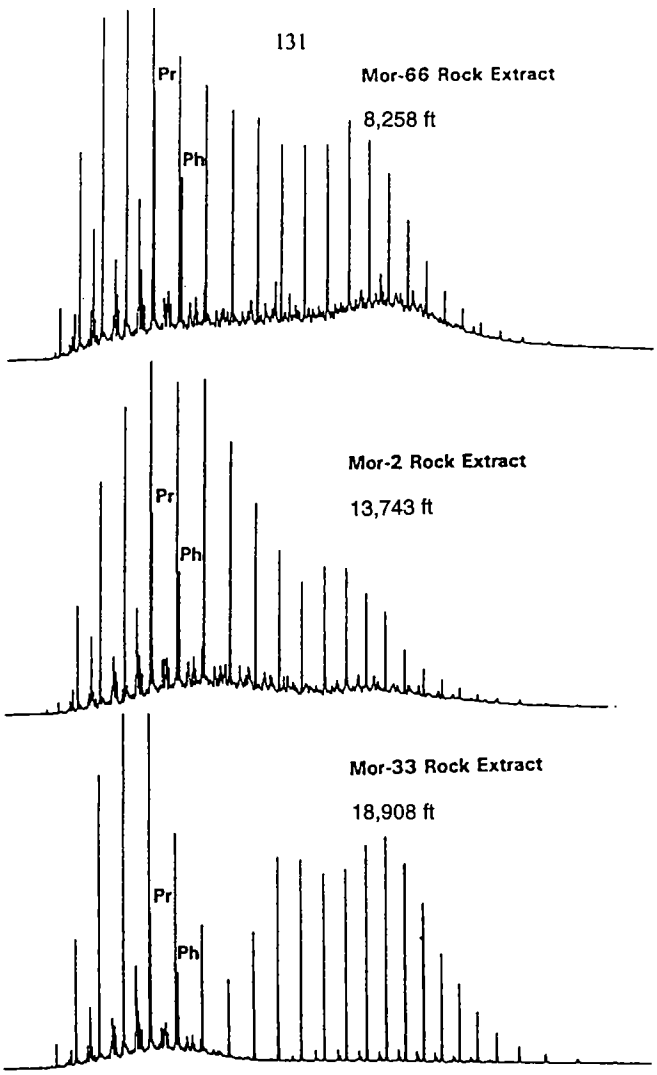

Figure 11. Gas chromatograms of three Morrow source-rocks saturate fractions. Depth of samples in feet. Abbreviations: Pr—pristane; Ph—phytane.

chromatogram of sample Spr-38 in the upper part of Figure 10. Spr-38 has a very low concentration of C_{20+} higher molecular-weight, normal alkanes. Similar distribution of normal alkanes can be found in samples Spr-13, Spr-28, and Spr-62. This type of distribution may be interpreted as a combination of several factors: (1) maturity, which decreases the relative concentration of higher molecular-weight, normal alkanes; (2) source, where the input of precursors of higher molecular-weight, normal alkanes was low; (3) migration in that the source rock itself is not organic rich but has received a contribution of migrated hydrocarbons, which are dominated with lower molecular-weight, normal alkanes; and (4) weathering, which will be discussed in more detail below.

Details of the distributions of hydrocarbons in the saturate fraction from samples of the Woodford Shale have been well documented in the literature (Jones, 1986; Philp and others, 1989; Burruss and Hatch, 1989; Jones and Philp 1990) and will not be discussed in detail in this paper. Major features of these chromatograms include Pr/Ph ratios greater than 1.0 and unimodal distribution of normal alkanes with a relatively low concentration of C_{20+} n-alkanes.

Crude Oils

Chromatograms of the saturate fractions of crude oils that can be correlated with the source rocks studied in this study are shown in Figure 12 (names of the reservoirs are given on the chromatograms). Oil sample E-1 is a typical Pennsylvanian oil (Burruss and Hatch, 1989) and is characterized by a Pr/Ph ratio >1.0, CPI slightly greater than 1.0, and relatively abundant C_{20+} n-alkanes. The bimodal distribution—evident in the chromatograms of Morrow and Springer source rocks—is not evident in the chromatogram of the E-1 oil. GCMS data provide additional support for the correla-

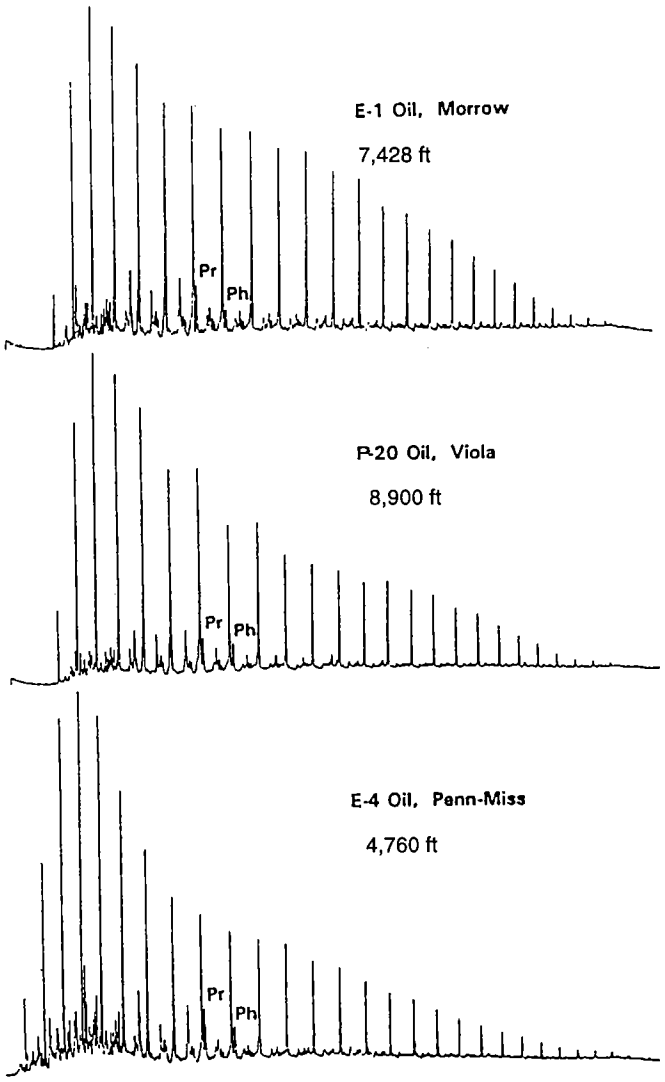

Figure 12. Gas chromatograms of the saturate fractions from three crude oils produced from the Morrow Group, Viola Formation and Pennsylvanian–Mississippian sequence. Depth of samples in feet. Abbreviations: Pr—pristane; Ph—phytane.

tion between this oil and Morrow (and/or Springer) source rocks.

On the other hand, it should be noted that in many cases oils generally contain contributions from more than one source rock. Oil E-1 probably received major contributions from Morrow and/or Springer source rocks and also received minor contributions from other formations, making it more difficult to make a precise correlation between this oil and Morrow and/or Springer source rocks.

Comparisons between the chromatograms of the oils and source rocks provide a preliminary correlation between the oils and source rocks, but these correlations are not definitive. Carbon-isotope values and biomarker distributions described below were obtained in an effort to confirm these correlations.

Gas Chromatography–Mass Spectrometry

Chester, Springer, and Morrow Sequences

As discussed above, the lithologic features of the Springer and Morrow shales are very similar, so that it is commonly difficult to distinguish the two formations. The geochemical features of the Chester Formation are also similar to those of the Springer and Morrow source rocks, also making it difficult to geochemically distinguish the samples.

Terpanes and Steranes

A partial m/z 123 chromatogram of the sesquiterpanes in Morrow source rock is shown in Figure 13, and tentative identifications for some of the C_{15} and C_{16} sesquiterpanes are given in Table 1. The distribution of the sesquiterpanes in the Morrow, Chester, and Springer Formation extracts are similar to the Lower Mississippian source rock, except that the relative concentrations of compounds, other than drimanes, are higher than those in the Lower Mississippian source rock. By comparing Figures 13 and 14, it can be seen that the relative concentrations of peaks no. 3 [4α(H)-eudesmane], 5, 8, and 9 are higher, relative to other sesquiterpanes, in the Morrow source rock than in the Lower Mississippian source rocks. These compounds, particularly 4α(H)-eudesmane, have been proposed as indicators of higher plants (Noble, 1986; Peters and Moldowan, 1993). The increase in relative concentration of the sesquiterpanes from the Viola source rock to the Lower Mississippian source rock and from the Lower Mississippian source rock to the Chester, Springer, and Morrow source rocks may indicate the increasing contribution of higher plants in the Anadarko basin from the Ordovician to the Pennsylvanian.

Table 1.—Identification of Bicyclic Sesquiterpanes in the Partial m/z 123 Chromatogram

Peak nos.	Compounds	
1	C_{15} Sesquiterpane	
2	C_{15} Sesquiterpane	
3	C_{15} 4β(H)-Eudesmane	
4	C_{15} Sesquiterpane	(15S)*
5	C_{15} 8β(H)-Drimane	
6	C_{15} Sesquiterpane	
7	C_{15} 8α(H)-Drimane	
8	C_{16} Sesquiterpane	
9	C_{16} Sesquiterpane	
10	C_{16} 8β(H)-Homodrimane	(16S)*
11	C_{16} Sesquiterpane	
12	C_{16} 8α(H)-Homodrimane	

*Abbreviations used in the text, figures, and tables.

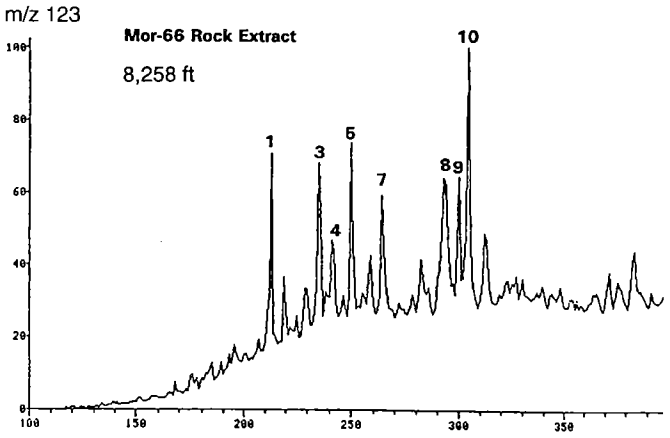

Figure 13. Typical distribution of sesquiterpanes in a Morrow source-rock extract (8,258 ft) as obtained by the gas chromatography and mass spectrometry (GCMS) and single-ion monitoring analysis of the ion at m/z 123 of the saturate fraction. Peak identities are given in Table 1.

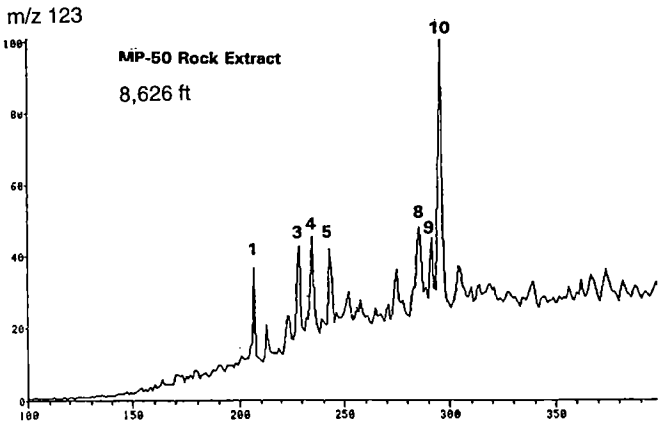

Figure 14. Typical distribution of sesquiterpanes in a Lower Mississipian source-rock extract (8,626 ft) as obtained by the gas chromatography and mass spectrometry (GCMS) and single-ion monitoring analysis of the ion at m/z 123 of the saturate fraction. Peak identities are given in Table 1.

A typical m/z 217 chromatogram for the Morrow source rock is shown in Figure 15, and tentative identifications of the steranes are given in Table 2. The distribution of C_{27+} regular and diasteranes in Morrow (and similarly in the Chester and Springer Formations) source rock feature a high concentration of C_{29} regular steranes relative to the C_{27} and C_{28} isomers, and high ratio of $\beta\beta/\alpha\alpha$ isomers. Another feature of the Morrow, Chester, and Springer source rock extracts is the very high concentration of diasteranes contrasted to the regular steranes. The relative concentration of C_{27} diasteranes is especially high contrasted to that of C_{27} regular steranes. High ratios of diasteranes to regular steranes are believed to result from conversion of sterols to diasterenes during diagenesis catalyzed by acidic sites on clays (Rubinstein and others, 1975; Sieskind and others, 1979), although acidic clay catalysis may not be the only reason for these high ratios. Relatively high concentrations of diasteranes appear to be characteristic of Paleozoic source rocks and may be source related in this situation. The Morrow, Chester, and Springer source-rock extracts contain relatively high concentrations of C_{30} regular steranes contrasted to that of the Viola and Lower Mississippian source rocks, but the absolute concentration of these C_{30} regular steranes is low. The existence of C_{30} regular steranes confirms the marine origin of these source rocks (Peters and others, 1986).

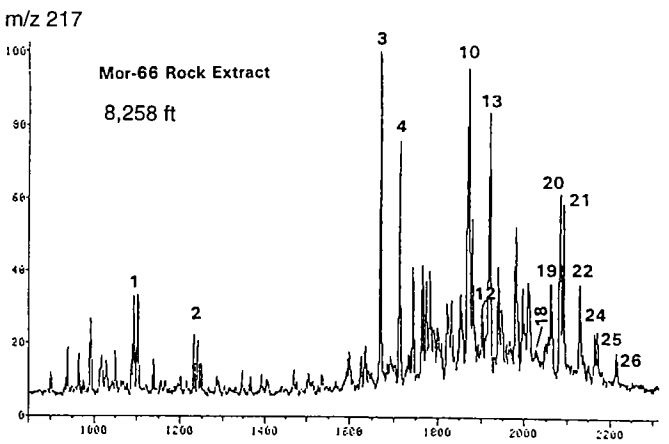

Figure 15. Typical distribution of steranes in a Morrow source-rock extract (8,258 ft) as obtained by the gas chromatography and mass spectrometry (GCMS) and single-ion monitoring analysis of the ion at m/z 217 of the saturate fraction. Peak identities are given in Table 2.

A representative m/z 231 chromatogram of the Morrow source rock is plotted together with a partial m/z 217 chromatogram in Figure 16. The distribution of 3α-methyl and 2α-methyl steranes in Morrow (and similarly in the Chester and Springer Formations) source rock is similar to that of the Viola source rock, but the absolute concentration of these methyl steranes is relatively low contrasted to that of the Viola source rock. The peaks marked with question marks in Figure 16 are probably 4-methyl steranes, which do not exist (or in very low concentration) in the Viola, Sylvan, Woodford, and Lower Mississippian source rocks. Because of the low concentration of these methyl steranes, the identification of 4-methyl steranes could not be confirmed by GCMSMS analyses monitoring daughter ions at m/z 98 and 231.

Special Biomarker Feature of the Morrow, Chester, and Springer Sequences—17α(H)-Diahopanes

A typical partial m/z 191 chromatogram of the Morrow source rock is shown in Figure 17, with tentative identifications of the di- and triterpanes being given in Table 3. The distribution of terpanes in Morrow, Chester, and Springer source rocks features relatively low concentrations of tricyclic terpanes contrasted to the pentacyclic hopanes, a high Ts/Tm ratio, and relatively low concentrations of the C_{31+} homohopanes contrasted to the C_{30} hopane.

Table 2.—Identification of Steranes in the Partial m/z 217 Chromatogram

Peak nos.	Compounds	
1	C_{21} Pregnane	(Preg)*
2	C_{22} Homopregnane	
3	C_{27} 13β(H),17α(H)-Diacholestane (20S)	(27Dia)*
4	C_{27} 13β(H),17α(H)-Diacholestane (20R)	
5	C_{27} 13α(H),17β(H)-Diacholestane (20S)	
6	C_{27} 13α(H),17β(H)-Diacholestane (20R)	
7	C_{28} 24-Methyl-13β(H),17α(H)-Diacholestane (20S)	
8	C_{28} 24-Methyl-13β(H),17α(H)-Diacholestane (20R)	
9	C_{28} 24-Methyl-13α(H),17β(H)-Diacholestane (20S)†	
	C_{27} 14α(H),17α(H)-Cholestane (20S)	
10	C_{28} 24-Methyl-13β(H),17α(H)-Diacholestane (20R)†	
	C_{27} 14β(H),17β(H)-Cholestane (20R)	
11	C_{27} 14β(H),17β(H)-Cholestane (20S)†	
	C_{28} 24-Methyl-13α(H),17β(H)-Diacholestane (20R)	
12	C_{27} 14α(H),17α(H)-Cholestane (20R)	(27R)*
13	C_{29} 24-Ethyl-13β(H),17α(H)-Diacholestane (20R)	
14	C_{29} 24-Ethyl-13α(H),17β(H)-Diacholestane (20S)	
15	C_{28} 24-Methyl-14α(H),17α(H)-Cholestane (20S)	
16	C_{29} 24-Ethyl-13α(H),17β(H)-Diacholestane (20R)†	
	C_{28} 24-Methyl-14β(H),17β(H)-Cholestane (20R)	
17	C_{28} 24-Methyl-14β(H),17β(H)-Cholestane (20S)	
18	C_{28} 24-Methyl-14α(H),17α(H)-Cholestane (20R)	(28R)*
19	C_{29} 24-Ethyl-14α(H),17α(H)-Cholestane (20R)	(29S)*
20	C_{29} 24-Ethyl-14β(H),17β(H)-Cholestane (20R)	(29ββR)*
21	C_{29} 24-Ethyl-14β(H),17β(H)-Cholestane (20R)	(29ββS)*
22	C_{29} 24-Ethyl-14α(H),17α(H)-Cholestane (20R)	(29R)*
23	C_{30} 24-Propyl-14α(H),17α(H)-Cholestane (20R)	(30S)*
24	C_{30} 24-Propyl-14β(H),17β(H)-Cholestane (20R)	(30ββR)*
25	C_{30} 24-Propyl-14β(H),17β(H)-Cholestane (20R)	(30ββS)*
26	C_{30} 24-Propyl-14α(H),17α(H)-Cholestane (20R)	(30R)*

*Abbreviations used in the text, figures, and tables.

†The two compounds identified elute together on the chromatogram and actually appear as one peak.

The most characteristic feature of the Morrow, Chester, and Springer source rocks is the relatively high concentrations of 18α(H)-neohopanes and 17α(H)-diahopanes. These rearranged hopanes were originally detected by Philp and others (1984) and referred to as "compound X" until they were identified by Moldowan and others (1991) using X-ray crystallography and advanced NMR methods. 18α(H)-neohopane (29Ts) has the same structure as Ts 18α(H)-22,29,30-trisnorhopane with an extra C_2H_5 group at carbon number 21 of the hopane skeleton (peak No. 17, Fig. 17).

The 17α(H)-diahopanes have the same structure as regular hopanes, except that the CH_3 (carbon number 27) group at carbon number 14 of the hopane skeleton is rearranged to carbon number 15. The 17α(H)-diahopanes are present as a pseudohomologue from C_{29} to C_{34} (peak No. 18 in Fig. 17 is the C_{30} member). It has been proposed that diahopanes, like diasteranes, were formed during diagenesis by clay catalysis or by partial oxidation in a suboxic environment. The origin of the rearranged hopane series may be related to the same common bacterial hopane precursors (Summons and others, 1988a,b; Peters and Moldowan, 1993). The ratio of the C_{30} diasterane over the 18α(H)–neohopane (C_{29}Ts) has been proposed to be dependant on the depositional environment. A higher ratio indicates shale deposited from oxic–suboxic conditions, whereas low ratios indicate more anoxic conditions (Peters and Moldowan, 1993).

Figure 18 is a partial GCMSMS chromatogram monitoring the daughter ion at m/z 191 from the parent ions 370 to 468 (corresponding to C_{27} to C_{34} hopanes) and illustrating the occurrence

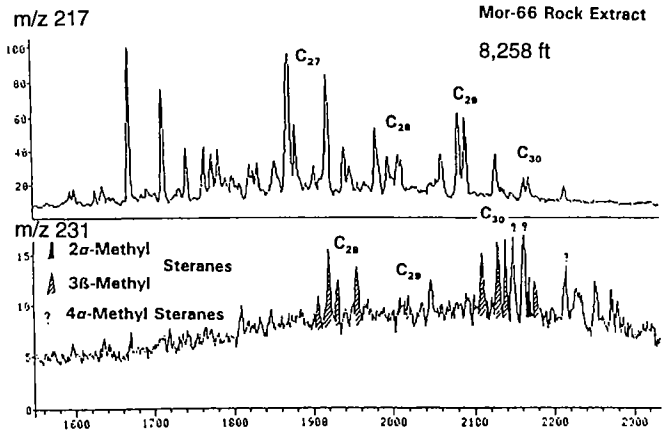

Figure 16 *(left).* Typical distribution of steranes (upper chromatogram) and methylsteranes in a Morrow source-rock extract (8,258 ft) as obtained by the gas chromatography and mass spectrometry (GCMS) and single-ion monitoring analysis of the ions at m/z 217 and 231, respectively, of the saturate fraction. The labels C_{27} (etc.) refer to the groups of isomer homologies with that number of carbon atoms. Individual isomers are not identified in this particular chromatogram.

Table 3.—Identification of Di- and Triterpanes in the Partial m/z 191 Chromatogram

Peak nos.	Compounds	
1	C_{20} Tricyclic Terpane	
2	C_{21} Tricyclic Terpane	
3	C_{23} Tricyclic Terpane	(23T)*
4	C_{24} Tricyclic Terpane	
5	C_{25} Tricyclic Terpane	
6	C_{24} Tetracyclic Terpane	(24T)*
7	C_{26} Tricyclic Terpane	
8	C_{28} Tricyclic Terpanes	
9	C_{29} Tricyclic Terpanes	
10	C_{27} 18α(H)-22,29,30-Trisnorhopane	(Ts)*
11	C_{27} 17α(H)-22,29,30-Trisnorhopane	(Tm)*
12	C_{27} 17β(H)-22,29,30-Trisnorhopane	(17β))*
13	C_{30} Tricyclic Terpanes	
14	C_{28} 28,30-Bisnorhopane	
15	C_{31} Tricyclic Terpanes	
16	C_{29} 17α(H), 21β(H)-30-Norhopane	(29H)*
17	C_{29} 18α(H)-30-Norneohopane	(29Ts)*
18	C_{30}17α(H)-Diahopane	
19	C_{29} 17β(H), 21α(H)-30-Normoretane	(29M)*
20	C_{30} 17α(H), 21β(H)-Hopane	(30H)*
21	C_{30} 17β(H), 21α(H)-Moretane	(30M)*
22	C_{31} 17α(H), 21β(H)-Homohopanes	(31H or 31S & 31R)*
23	C_{32} 17α(H), 21β(H)-Bishomohopanes	(32S & 32R)*
24	C_{33} 17α(H), 21β(H)-Trishomohopanes	(33S & 33R)*
25	C_{34} 17α(H), 21β(H)-Tetrakishomohopanes	(34S & 34R)*
26	C_{35} 17α(H), 21β(H)-Pentakishomohopanes	(35S & 35R)*

*Abbreviations used in the text, figures, and tables.

and distribution of 18α(H)-neohopanes and 17α(H)-diahopane series in the Morrow source rock. The 18α(H)-neohopanes exist in most source rock extracts and crude oils in the Anadarko basin, whereas the 17α(H)-diahopane series is absent (or in very low concentrations), in the Viola, Sylvan, Woodford, and Lower Mississippian source rocks and correlated oils. The relatively high concentration of diahopanes in the source rocks of Morrow, Chester, and Springer sequences may reflect the sub-oxic depositional environments of these formations and can be used as oil-source-rock correlation indicators.

Another pseudohomologue of C_{29} to C_{34} triterpanes that elutes much earlier than 17α(H)-diahopane series is also shown in Figure 18. Because of the limitation of identification method, the structure of this pseudohomologue was not revealed. It can be suggested that this pseudohomologue may be another series of rearranged hopanes.

Weathering in the Springer Formation

Biodegradation is a term generally used for crude oils that are attacked by bacteria in reservoir rocks. However, if a source rock is once exposed to (or near) the surface and contacted with air or oxygen-rich groundwater, the organic matter in the source rocks can also be attacked by bacteria (weathering) or washed by groundwater (water washing). As a result, the concentration and distribution of biomarkers in this source-rock extract will show features similar to those in a biodegraded oil (Philp and others, 1992).

Source-rock weathering appears to be a common phenomenon in the Springer Formation (samples Spr-13, 38, and 62). These weathered source rocks feature a high percentage of inert carbon over TOC, low absolute concentration of biomarkers contrasted to the non-weathered source rocks at approximately the same maturity levels, and

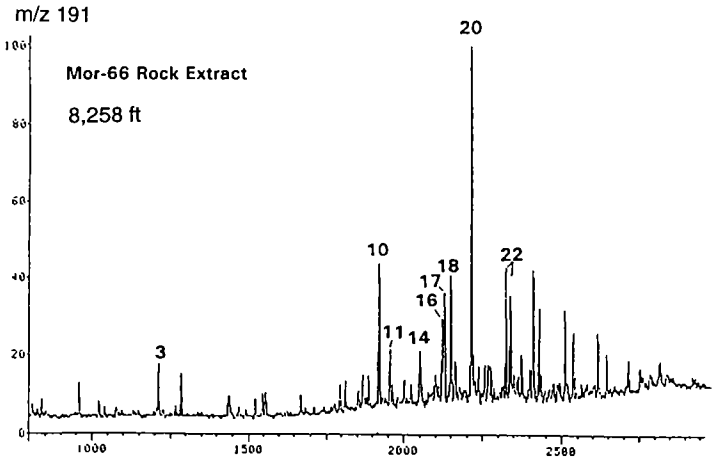

Figure 17. Typical distribution of terpanes in a Morrow source-rock extract (8,258 ft) as obtained by the gas chromatography and mass spectrometry (GCMS) and single ion monitoring analysis of the ion at m/z 191 of the saturate fraction. Peaks are identified in Table 3.

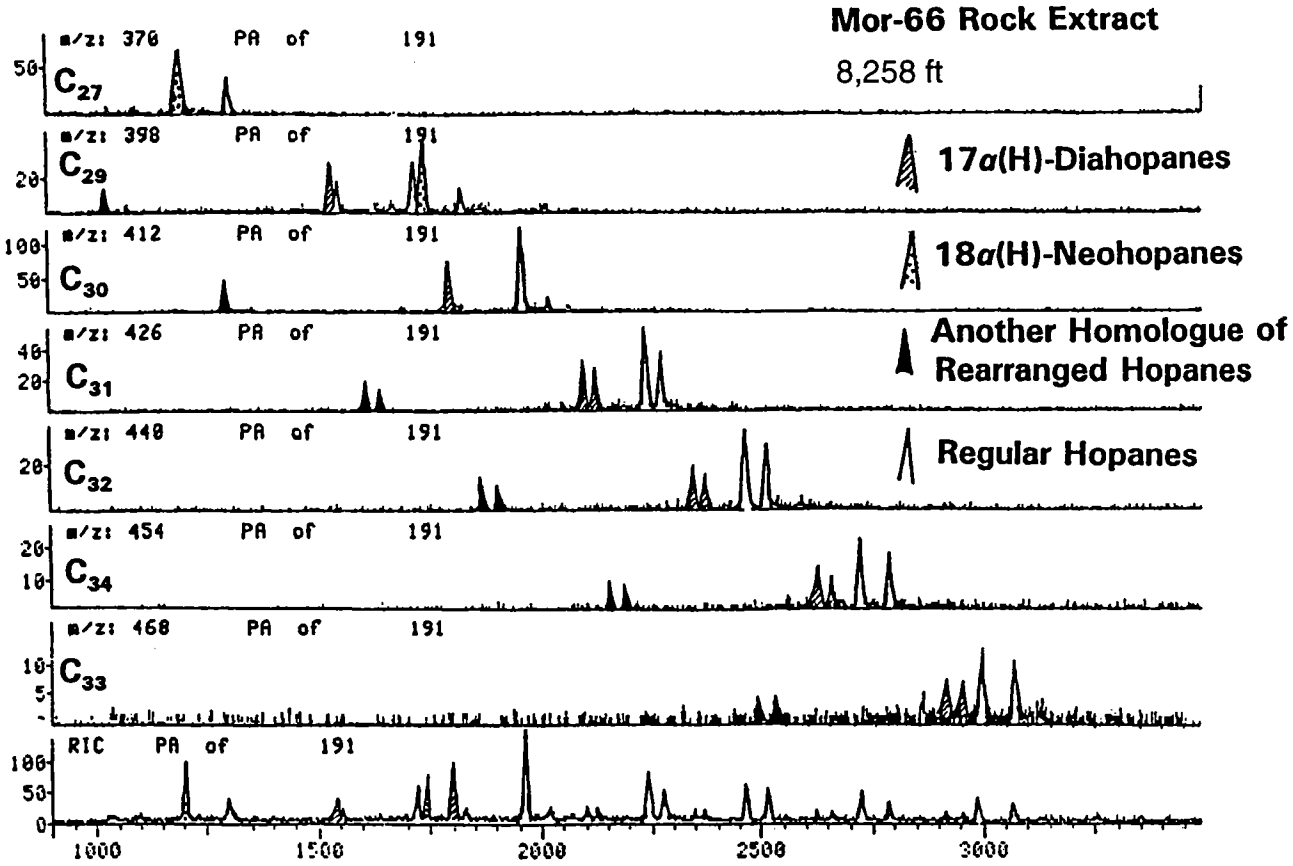

Figure 18. A composite chromatogram obtained by the GCMSMS analysis of the saturate fraction of the Morrow source-rock extract (8,258 ft) to determine the distribution of the C_{27} to C_{33} pentacyclic hopanes.

preferential removal of biomarkers less resistant to biodegradation.

A typical partial m/z 191 chromatogram of the weathered Springer source rock is shown in Figure 19, and tentative identification of the terpanes is given in Table 3. It can be seen in this chromatogram that pentacyclic hopanes have been removed preferentially, whereas the tricyclic terpanes are still present in relatively high concentrations. Quantitative analyses indicate that, although both pentacyclic hopanes and tricyclic terpanes have been partially removed, lesser amounts of tricyclic terpanes have been removed than the pentacyclic hopanes. This may suggest that tricyclic terpanes are more weathering resistant than pentacyclic hopanes.

The Springer source-rock sample contains a relatively high concentration of the C_{24} tetracyclic terpane, which is commonly associated with carbonate and evaporite depositional environments (Palacas and others, 1984). This compound can also be related to terrestrial organic matter and associated with levels of microbial activity (Philp and Gilbert, 1986). In the case of the Springer source rocks, the relatively high concentration of this compound may indicate that it is resistant to weathering (or biodegradation). The pentacyclic hopanes have been partially removed so that the C_{24} tetracyclic terpane appears in relatively high concentration.

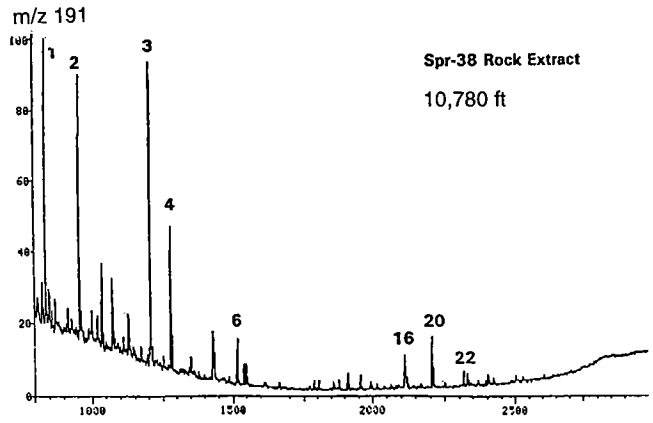

Figure 19. Typical distribution of terpanes in a weathered Springer source-rock extract (10,780 ft) as obtained by the GCMS and single ion monitoring analysis of the ion at m/z 191 of the saturate fraction. Peaks are identified in Table 3.

The m/z 217 chromatogram of the same Springer source rock is shown in Figure 20, and tentative identification of the steranes given in Table 2. It would appear that regular steranes—and to a lesser degree diasteranes—have been partially removed by weathering. In contrast, pregnanes appear to be unaltered.

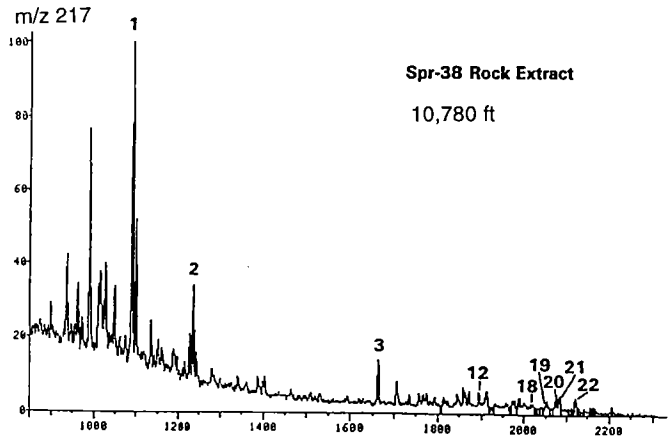

Figure 20. Typical distribution of steranes in a weathered Springer source-rock extract (10,780 ft) as obtained by the GCMS and single-ion monitoring analysis of the ion at m/z 217 of the saturate fraction. Peaks are identified in Table 2.

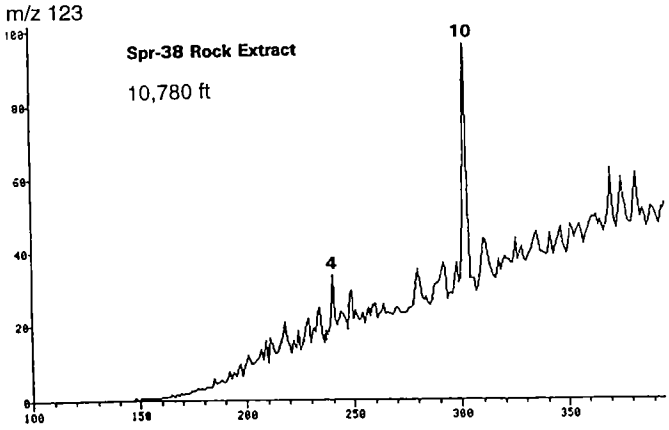

Figure 21. Typical distribution of terpanes in a weathered Springer source-rock extract (10,780 ft) as obtained by the gas chromatography and mass spectrometry (GCMS) and single-ion monitoring analysis of the ion at m/z 123 of the saturate fraction. Peaks are identified in Table 1.

This may suggest pregnanes are more resistant to weathering than dia- and regular steranes, and quantitative analysis confirms the suggestion that the absolute concentrations of pregnanes do not decrease very much with weathering.

Figure 21 illustrates a typical partial m/z 123 chromatogram showing the sesquiterpane distribution in the same Springer source rock, and Table 1 presents tentative identification of some C_{15} and C_{16} sesquiterpanes. Most of the C_{15} and C_{16} sesquiterpanes are either absent or present in very low concentrations, with the loss of sesquiterpanes being supported by quantitative analysis of biomarkers. The fate of sesquiterpanes with weathering (or biodegradation) has rarely been discussed in the literature but the results of this study show that the sesquiterpanes may be removed by heavy weathering.

The distributions of normal alkanes and isoprenoids of this weathered source rock are shown in the GC chromatogram in Figure 10 (sample Spr-38). It has been suggested that weathering (or biodegradation) would remove lower molecular-weight, normal alkanes first, resulting in high ratios of Pr/nC_{17} and Ph/nC_{18} and a large "hump," unresolved complex mixture of biodegraded products on the gas chromatogram (Peters and Moldowan, 1993). However, in the case of these weathered Springer source rocks, C_{20+} higher molecular-weight, normal alkanes were preferentially removed. The ratios of Pr/nC_{17} and Ph/nC_{18} are not very high compared with that of non-weathered samples, and usually only a small hump occurs in the GC chromatogram.

During the burial history of the Anadarko basin, the Springer Formation was covered with the thick Morrow Group and other Pennsylvanian and Permian formations throughout the basin. Most of the Springer source rocks are still buried very deeply today (as much as 12,000 ft) and nonetheless have weathered features. The only chance for the Springer Formation to have been exposed or near the surface would have been during the post-Mississippian and pre-Morrowan time. At that time, post-Mississippian erosion removed the Springer rock in northern Anadarko basin together with the Upper Chester Formation while the Springer Formation was immature.

This "pre-mature" weathering may be different from the ways of common "post-mature" weathering (or biodegradation in reservoirs) discussed in the literature, in which source rocks were buried deep enough to enter the oil window and then be uplifted by geologic or tectonic events prior to weathering, during which bacteria could attack the mature kerogen or generated oil. In the case of the immature Springer source rock, bacteria could have attacked immature kerogen precursors and/or the organic matter that was not incorporated into the structure of kerogen. After the weathering, the kerogen and organic matter were buried deeper and began to generate oil. Lower molecular-weight, normal alkanes are probably the products of bacteria-attacked kerogen or other organic matter that was not incorporated into kerogen. Alternatively, these lower molecular-weight, normal alkanes (Fig. 10) may be migrated hydrocarbons.

Maturation and facies variation, on the other hand, may (at least partially) be the reason for the biomarker distribution in Spr-38 (Figs. 19–21). Because a short section of core may represent thousands or even millions years of geologic time, facies variation could be significant in a short core sample, in which both absolute concentration and distribution of biomarkers could change considerably (Miranda and Walters, 1992). By normalizing the absolute concentration of biomarkers to TOC, the variation of absolute concentration caused by facies variation (richness) can be decreased to minimum but the variation of biomarker distribution caused by facies variation (different types of biota) will still exist. Therefore, care should be taken when interpreting the weathering features of source rocks.

The biomarker features of crude oils are variable, and the variation reflects the biomarker features of source rocks. Several oils can be correlated with their source rocks very well. Other oils cannot be correlated with particular source rocks because they are either mixtures of hydrocarbons generated by multi-sources or generated by source rocks that were not covered by this study.

Correlations

A ternary diagram for the steranes of the crude oils is given in Figure 22, and the areas occupied by the source rocks are marked for comparison. The oil samples are labeled with the names of the formations that are believed to be the source rocks of the oils (interpreted by other geochemical data). It can be seen that the Viola oils show a good correlation with the Viola source rocks. The other oils show less correlation with their suspected source rocks.

The distribution of the C_{31}-homohopanes has been utilized to interpret source environments and for correlations (Philp and Gilbert, 1986; Fu and others, 1986; Clark and Philp, 1989; Peters and Moldowan, 1991). In the present study, both the distribution and the absolute concentration of homohopanes were investigated. The absolute homohopane concentrations of source rocks and oils were calculated by normalization to the saturate fractions and the concentration and distribution of homohopanes are plotted in Figure 23. It can be seen from the diagram that oil P-20 correlates relatively closely with the Viola source rock by both distribution pattern and absolute concentration of homohopanes. The Woodford Shale has a very low concentration of homohopanes and a flat pattern of homohopane distribution. Oils E-7 and P-1 probably can be correlated with the Woodford source rock. The homohopane concentration of the Springer and Morrow are intermediate between the Viola and the Woodford, and oil E-3 may be correlated with the Springer and Morrow source rocks. Alternatively, this oil may be a mixture of contributions from several source rocks with the Morrow and Springer source rocks as the major contributors. The results of homohopane correlation basically agree with the results of sterane correlation. In order to utilize more biomarkers as correlation tools, the distribution and absolute concentration of several selected biomarkers are plotted in Figure 24. Biomarker abbreviations on the X-axis can be found in Tables 1–3. To compare between the source rock extracts and oils, the absolute biomarker concentrations were normalized to the saturate fractions.

A biomarker distribution plot (with the absolute biomarker concentration as the Y-axis) of Morrow and Springer source rocks extracts (these two formations are treated as one unit) and correlated oils is given in Figure 24. Three peaks are shown in Figure 24—the highest one at C_{30} hopane; the second one at Ts; and the third one between the C_{16} sesquiterpane and C_{23} tricyclic terpane. The height of the C_{29} norhopane in Morrow and Springer rocks is very low contrasted to that of the Viola Limestone. The distribution of correlated oils fits the envelope of the source rock well.

Source-Rock Evaluation

The black shales in the Springer Formation and Morrow Group are fairly good source rocks, which are both fairly rich in organic matter and occur in tremendous volumes in the Anadarko basin. These source rocks are mainly Type-III kerogens, so that they may not make a large contribution to the oil generated in the Anadarko basin. They may, however, make a significant contribution to the natural gas generated in

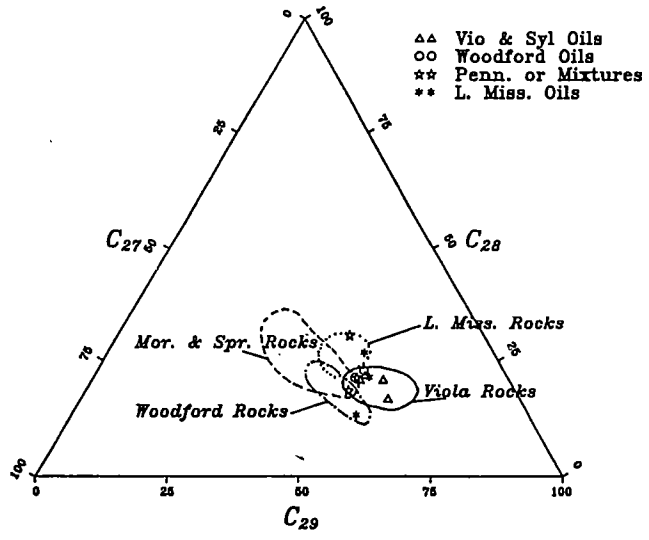

Figure 22. A ternary diagram showing the relative distribution of the C_{27} to C_{29} steranes in a number of oils and source rocks from the Anadarko basin. The distributions are determined from the relative proportions of the C_{27} to C_{29}14α(H),17α(H) 20R regular sterane isomers present in the m/z 217 chromatograms. Depth of samples in feet.

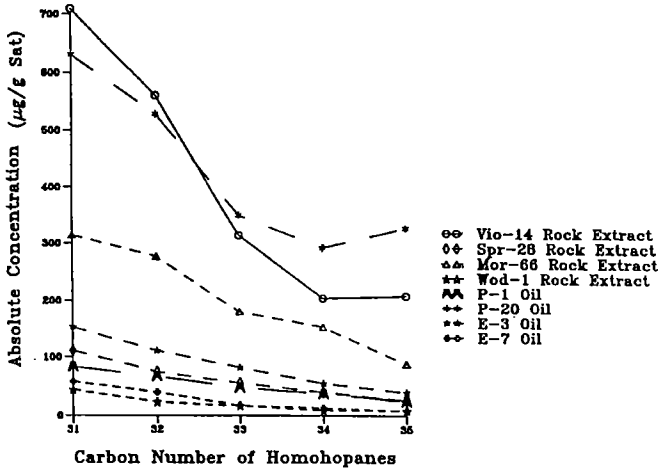

Figure 23. Homohopane pattern and absolute concentration normalized to the saturate fractions versus carbon number of the C_{31} to C_{35} homohopanes for selected oils and source-rock extracts from the Anadarko basin.

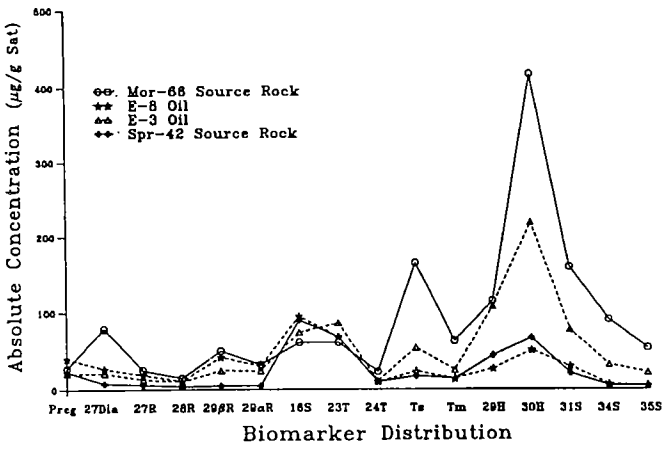

Figure 24. Absolute concentrations (in micrograms per gram—μg/g) of selected biomarkers in selected oils and source rocks from the Morrow Group and Springer Formation.

the Anadarko basin. From the limited data obtained, it can be proposed that the Chester Formation (either limestone or shale) is not a very good source rock. The formation is generally organic-lean and a Type-III kerogen.

Source-rock evaluation conducted by this study supports the proposal of multi-source oil and gas generation in the Anadarko basin. This conclusion is also supported by the data of biomarker characterization and quantification.

Biomarker Characterization of Source Rocks and Crude Oils

The common biomarker characteristics of these Paleozoic source rocks (all the formations under study) are as follows:

1. High relative concentration of diasteranes contrasted to that of regular sterane even in carbonate source rocks.
2. High relative concentration of C_{29} regular steranes—especially that of 14α(H), 17α(H)-isomers in most cases—contrasted to that of C_{27} and C_{28} regular steranes, even though all the formations under study are mainly of marine origin.
3. High relative concentrations of sesquiterpanes and tricyclic terpanes (for most formations) contrasted to those of other biomarker groups.

The Chester, Springer, and Morrow source rocks have very high relative concentrations of diasteranes contrasted to regular steranes and relatively high concentrations of neohopanes and diahopanes contrasted to those of the other formations. A few Springer rocks have very low relative and absolute concentrations of pentacyclic hopanes contrasted to that of tricyclic terpanes and very low relative and absolute concentrations of dia- and regular steranes contrasted to that of pregnanes. These rocks probably underwent heavy weathering during post-Mississippian erosion. The biomarker characteristics of the crude oils, which can be correlated with the Chester, Springer, or Morrow source rocks, are not very obvious. This is because these source rocks are mainly gas prone, and the oils are the mixed products of multi-sources.

Apparent correlations between source rocks and crude oils were conducted using biomarker distribution and the absolute biomarker concentration. The correlations are supported by carbon-isotope data and other geochemical properties of the source rocks and crude oils.

REFERENCES CITED

Alexander, R.; Kagi, R.; and Woodhouse, G.W., 1981, Geochemical correlation of Windalia oil and extracts of Winning Group (Cretaceous) potential source rocks, Barrow sub-basin, western Australia: American Association of Petroleum Geologists Bulletin, v. 65, p. 235–250.

Amsden, T. W., 1989, Depositional and post-depositional history of Middle Paleozoic (Late Ordovician through Early Devonian) strata in the ancestral Anadarko basin, *in* Johnson, K. S. (ed.), Anadarko basin symposium, 1988: Oklahoma Geological Survey Circular 90, p. 143–146.

Burruss, R. C.; and Hatch, J. R., 1989, Geochemistry of oils and hydrocarbon source rocks, greater Anadarko basin: evidence for multiple sources of oils and long-distance oil migration, *in* Johnson, K. S. (ed.), Anadarko basin symposium, 1988: Oklahoma Geological Survey Circular 90, p. 53–64.

Cardott, B. J., 1989, Thermal maturation of the Woodford Shale in the Anadarko basin, *in* Johnson, K. S. (ed.), Anadarko basin symposium, 1988: Oklahoma Geological Survey Circular 90, p. 32–46.

Cardott, B. J.; and Lambert, M. W., 1985, Thermal maturation by vitrinite reflectance of Woodford Shale, Anadarko basin, Oklahoma: American Association of Petroleum Geologists Bulletin, v. 69, p. 1982–1998.

Clark, J. P.; and Philp, R. P., 1989, Geochemical characterization and correlation of associated crude oils in the Black Creek Basin, Alberta: Bulletin of Canadian Petroleum Geology, v. 37, p. 401–416.

Davis, H. G.; and Northcutt, R. A., 1989, The greater Anadarko basin: an overview of petroleum exploration and development, *in* Johnson, K. S. (ed.), Anadarko basin symposium, 1988: Oklahoma Geological Survey Circular 90, p. 13–24.

Engel, M. H.; Imbus, S. W.; and Zumberge, J. E., 1988, Organic geochemical correlation of Oklahoma crude oils using R- and Q-mode factor analysis: Organic Geochemistry, v. 12, p. 157–170.

Fu, J. M.; Sheng, G. Y.; Peng P. G.; Brassell, S. C.; Eglinton, G.; and Jiang, J. G., 1986, Peculiarities of salt lake sediments as potential source rocks in China, *in* Leythaeuser, D.; and Rullkötter, J. (eds.), Advances in organic geochemistry, 1985: Pergamon Press, Oxford, p. 119–126.

Gilbert, M. C., 1992, Speculations on the origin of the Anadarko basin: International Basement Tectonics Association Publication 7, p. 195–208.

Hester, T. C.; Schmoker, J. W.; and Sahl, H. L., 1990, Log-derived regional source rock characteristics of the Woodford Shale, Anadarko basin, Oklahoma: U.S. Geological Survey Bulletin, 1886-D, 38 p.

Hussain, Mahbub; and Bloom, M. A., 1991 Pyrolysis and hydrocarbon source bed potential of the upper Devonian Woodford Shale, West Texas: American Association of Petroleum Geologists Bulletin, v. 75, p. 599.

Johnson, K. S., 1989, Geologic evolution of the Anadarko basin, *in* Johnson, K. S. (ed.), Anadarko basin symposium, 1988: Oklahoma Geological Survey Circular 90, p. 3–12.

Johnson, K. S. (ed.), Anadarko basin symposium, 1988: Oklahoma Geological Survey Circular 90, 289 p.

Johnson, K. S.; Denison, R. E.; Duton, S. P.; Goldstein, A. G.; Rascoe, Bailey, Jr.; Sutherland, P. K.; and Thompson, D. M., 1988, Sedimentary cover—North American craton; U.S.: Geological Society of America, The Geology of North America, v. D-2, p. 307–359.

Jones, P. J., 1986, The petroleum geochemistry of the Pauls Valley area, Anadarko basin, Oklahoma: University of Oklahoma unpublished M.S. thesis, 175 p.

Jones, P. J.; and Philp, R. P., 1990, Oils and source rocks from Pauls Valley, Anadarko basin, Oklahoma, U.S.A.: Applied Geochemistry, v. 5, p. 429–448.

Jorgensen, D. G., 1989, Paleohydrology of the Anadarko basin, central United States, *in* Johnson, K. S. (ed.), Anadarko basin symposium, 1988: Oklahoma Geological Survey Circular 90, p. 176–193.

Keighin, C. W.; and Flores, R. M., 1989, Depositional facies, petrofacies, and diagenesis of siliciclastics of Morrow and Springer rocks, Anadarko basin, Oklahoma, *in* Johnson, K. S. (ed.), Anadarko basin symposium, 1988: Oklahoma Geological Survey Circular 90, p. 147–161.

Kennedy, C. L.; Miller, J. A.; Kelso, J. B.; and Lago, O. K., 1982, The deep Anadarko basin: Petroleum Information Corporation, 359 p.

Langford, F. F.; and Blanc-Valleron, M. M., 1990, Interpreting Rock-Eval pyrolysis data by using S_2-TOC graph: American Association of Petroleum Geologists Bulletin, v. 74, p. 799–804.

Lewan, M. D., 1983, Effects of thermal maturation on stable organic isotopes as determined by hydrous pyrolysis of Woodford Shale: Geochimica et Cosmochimica Acta, v. 47, p. 1471–1479.

Lopatin, N. V., 1971, Temperature and geologic time as factors in coalification [in Russian]: Akademiya Nauk USSR Izvestiya, Seriya Geologicheskaya, v. 3, Moscow, p. 95–106.

McKirdy, D. M.; Aldridge, A. K.; and Ypma, P. J. M., 1983, A geochemical comparison of some crude oils from Pre-Ordovician carbonate rocks, *in* Bjøroy, M.; and others (eds.), Advances in organic geochemistry, 1981: J. Wiley and Sons, New York, p. 99–107.

Miranda, R. M.; and Walters, C. C., 1992, Geochemical variations in sedimentary organic matter within a "homogeneous" shale core (Tuscaloosa Formation, Upper Cretaceous, Mississippi, U.S.A.): Organic Geochemistry, v. 18, p. 899–911.

Moldowan, J. M.; Seifert, W. K.; and Gallegos, E. J., 1985, Relationship between petroleum composition and depositional environment of petroleum source rocks: American Association of Petroleum Geologists Bulletin, v. 69, p. 1255–1268.

Moldowan, J. M.; Fago, F. J.; Carlson, R. M. K.; Young, D. C.; Duyne, G. V.; Clardy, J.; Schoell, M.; Pillinger, C. T.; and Watt, D. S., 1991, Rearranged hopanes in sediments and petroleum: Geochimica et Cosmochimica Acta, v. 55, p. 3333–3353.

Noble, R. A., 1986, A geochemical study of bicyclic alkanes and diterpenoid hydrocarbons in crude oils, sediments, and coals: University of Western Australia Ph.D. thesis, 365 p.

Pawlewicz, M. J., 1989, Thermal maturation of the eastern Anadarko basin, Oklahoma: U.S. Geological Survey Bulletin 1866-C, 12 p.

Peters, K. E., 1986, Guidelines for evaluating petroleum source rock using programmed yrolysis: American Association of Petroleum Geologists Bulletin, v. 70, p. 318–329.

Peters, K. E.; and Moldowan, J. M., 1993, The biomarker guide: interpreting molecular fossils in petroleum and ancient sediments: Prentice Hall, Englewood Cliffs, New Jersey, 363 p.

Peters, K. E.; Moldowan, J. M.; Schoell, M.; and Hempkins, W. B., 1986, Petroleum isotopic and biomarker composition related to source rock organic matter and depositional environment: Organic Geochemistry, v . 10, p. 17–27.

Philp, R. P., 1985a, Fossil fuel biomarkers: application and spectra: Elsevier Science Publication Company, New York, 294 p.

_____ 1985b, Biological markers in fossil fuel production: Mass Spectrometry Reviews 1985, v. 4, p. 1–54.

Philp, R. P.; and Gilbert, T. D., 1986, Biomarker distributions in oils and predominantly derived from terrigenous source material, *in* Leythaeuser, D.; and Rullkötter, J. (eds.), Advances in organic geochemistry, 1985: Pergamon Press, Oxford, p. 73–84.

Philp, R. P.; Jones, P. J.; Lin, L. H.; Michael, G. E.; and Lewis, A. C., 1989, An organic geochemical study of oils, source rocks, and tar sands in the Ardmore and Anadarko basins, *in* Johnson, K. S. (ed.), Anadarko basin symposium, 1988: Oklahoma Geological Survey Circular 90, p. 65–76.

Philp, R. P.; Chen, J. H.; Galvez-Sinibaldi, A.; Wang, H. D.; and Allen, J. D., 1992, Effects of weathering and maturity on the geochemical characteristics of the Woodford Shale, *in* Johnson, K. S.; and Cardott, B. J. (eds.), Source rocks in the southern Midcontinent, 1990 symposium: Oklahoma Geological Survey Circular 93, p. 106–121.

Pitman, J. K.; and Burruss, R. C., 1989, Diagenesis of hydrocarbon-bearing rocks in the middle Ordovician Simpson Group, southeastern Anadarko basin, Oklahoma, *in* Johnson, K. S. (ed.), Anadarko basin symposium, 1988: Oklahoma Geological Survey Circular 90, p. 134–142.

Rascoe, Bailey, Jr.; and Hyne, N. J. (eds.), 1988, Petroleum geology of the Mid-Continent: Tulsa Geological Society Special Publication 3, 162 p.

Rice, D. D.; Threlkeld, C. N.; and Vuletich, A. K., 1989, Characterization and origin of natural gases of the Anadarko basin, *in* Johnson, K. S. (ed.), Anadarko basin symposium, 1988: Oklahoma Geological Survey Circular 90, p. 47–52.

Rubinstein, I.; Sieskind, O.; and Albrecht, P., 1975, Rearranged sterenes in a shale: Occurrence and simulated formation: Journal of the Chemical Society, Perkin Transaction I, p. 1833–1836.

Schmoker, J. W., 1986, Oil generation in the Anadarko basin, Oklahoma and Texas: modeling using Lopatin's method: Oklahoma Geological Survey Special Publication 86-3, 40 p.

_____ 1989, Thermal maturity of the Anadarko basin, *in* Johnson, K. S. (ed.), Anadarko basin symposium, 1988: Oklahoma Geological Survey Circular 90, p. 25–31.

Schoell, M., 1983, Recent advances in petroleum isotope geochemistry, *in* Schenck, P. A.; and others (eds.), Advances in organic geochemistry: Pergamon Press, Oxford, England.

Sieskind, O.; Joly, G.; and Albrecht, P., 1979, Simulation of the geochemical transformation of sterols: superacid effects of clay minerals: Geochimica et Cosmochimica Acta, v. 43, p. 1675–1679.

Sofer, Z., 1984, Stable carbon isotope composition of crude oils: application to source depositional environment and petroleum alteration: American Association of Petroleum Geologists Bulletin, v. 68, p. 31–49.

Summons, R. E.; Brassell, S. C.; Eglinton, G.; Evans, E.; Horodyski, R. J.; Robinson, N.; and Ward, D., 1988a, Distinctive hydrocarbon biomarkers from fossiliferous sediment of the Late Proterozoic Walcott Member, Chuar Group, Grand Canyon, Arizona: Geochimica et Cosmochimica Acta, v. 52, p. 2625–2637.

Summons, R. E.; Powell, T. G.; and Boreham, C. J., 1988b, Petroleum geology and geochemistry of the Middle Proterozoic McArthur basin, northern Australia: III. Composition of extractable hydrocarbons: Geochimica et Cosmochimica Acta, v. 52, p. 1747–1763.

Tissot, B. P.; and Welte, D. H., 1984, Petroleum formation and occurrence [2nd edition]: Springer-Verlag, New York, 699 p.

Tsiris, V. L., 1983, Organic geochemistry and thermal history of the uppermost Morrow Shale (Lower Pennsylvanian) in the Anadarko basin, Oklahoma: University of Oklahoma unpublished M.S. thesis, 163 p.

Walker, P. E. G., 1986, A regional study of the diagenetic and geochemical character of the Pennsylvanian Morrow Formation, Anadarko basin, Oklahoma: Oklahoma State University unpublished M.S. thesis, 156 p.

Integration of Lithofacies and Petrophysics in Marine and Estuarine Morrow Sandstone, Southwest Kansas: A Midcontinent Rock Catalog Example

Alan P. Byrnes, Luis A. Buatois, M. Gabriela Mángano, and Timothy R. Carr
Kansas Geological Survey
Lawrence, Kansas

ABSTRACT.—Fundamental for accurate assessment of reservoir potential, modeling of production characteristics, delineation of pay and non-pay zones, and basic reservoir management is the need for reliable models of the distribution of the reservoir properties of porosity, fluid saturations, and permeabilities. Because of the lithologic and architectural complexity of many reservoirs, it is generally not feasible to directly construct accurate numerical models of these reservoir properties. To construct accurate numerical storage and flow models it is generally necessary to first construct quantitative geologic models based on depositional, sequence stratigraphic, and lithofacies models of the reservoir and then "translate" or "map" these models into storage and flow models using correlations established between lithofacies and petrophysical properties.

As part of a program to sample and analyze a wide range of lithofacies present within Pennsylvanian and Permian reservoirs in the Midcontinent, a "rock catalog," integrating lithologic and petrophysical data of Morrow Sandstone marine and estuarine samples is being compiled. Integration of geology and core analysis for the Morrow Sandstone in southwest Kansas provides an understanding of lithologic controls on petrophysical properties, equations relating petrophysical variables, and guidelines for predicting hydrocarbon producibility in estuarine Morrow Sandstone reservoirs. Samples from three wells in two fields were studied. From these wells, the core was described, interpretations of lithofacies, ichnofacies, and depositional environments made, and a suite of petrophysical properties measured and analyzed.

Fifteen estuarine and marine lithofacies were identified in the study area. In general, petrophysical properties were closely tied to lithofacies. Routine porosity values range from 0% to 22% with *in situ* porosities averaging 92% of routine values. Fluvial and upper-estuarine channel facies exhibit maximum porosity and permeability. Capillary-pressure properties of Morrow Sandstone samples differ significantly between lithofacies. At 100 ft of oil-column height above free-water level, fluvial and upper-estuary channel deposits exhibit water saturations below 25% whereas estuary-mouth, restricted tidal-flat, and upper-shoreface deposits generally exhibit values greater than 50%. Lower-shoreface and deeper-water deposits generally display water saturations greater than 90%. Water saturations for all facies increase with decreasing permeability. *In situ* permeabilities range from 0.0001 to 150 millidarcies (md). Highest porosity and permeability values were measured in the fluvial and upper-estuary channel sandstones. Extensive clay drapes, bioturbation, and increasing silt content result in significant decrease in permeability in tidal-flat and marine facies. Permeability can be log-linearly correlated with porosity with each facies exhibiting a unique subparallel trend. The Archie cementation exponent averages m = 1.81 for fluvial and upper estuary channel facies and is approximately m = 2.00 for many of the other facies.

INTRODUCTION

The Lower Pennsylvanian Morrow Sandstone in southwest Kansas contains oil and gas reservoirs in a wide variety of shallow- and marginal-marine depositional environments, with delta-front, shoreface, and estuarine valley-fill reservoir sandstones encased in offshore and estuarine mudstones (Wheeler and others, 1990). Fundamental to accurate assessment of reservoir potential, modeling of production characteristics, delineation of pay and non-pay zones, and basic reservoir management is the need for reliable models of the

Byrnes, A. P.; Buatois, L. A.; Mángano, M. G.; and Carr, T. R., 2001, Integration of lithofacies and petrophysics in marine and estuarine Morrow Sandstone, southwest Kansas: a Midcontinent rock catalog example, *in* Johnson, K. S. (ed.), Pennsylvanian and Permian geology and petroleum in the southern Midcontinent, 1998 symposium: Oklahoma Geological Survey Circular 104, p. 59–64.

distribution of the basic reservoir storage and flow properties of porosity, saturation, and permeability (including oil and water relative permeability). Because of the lithologic and architectural complexity of many reservoirs, it is generally not feasible to directly construct accurate numerical models of these reservoir properties. To construct reliable numerical storage and flow models it is generally necessary to first construct quantitative geologic models based on depositional, sequence stratigraphic, and lithofacies models of the reservoir. These geologic models must then be "translated" or "mapped" into storage and flow models using correlations established between lithofacies and petrophysical properties.

This study presents results of the petrophysical characteristics of lithofacies in the marine and estuarine Morrow Sandstone. It represents a portion of a program to sample and analyze a wide range of lithofacies present within Pennsylvanian and Permian reservoirs in the Midcontinent and to develop a comprehensive database containing petrophysical properties of the lithofacies present. An efficient and highly useful format for such a database is a "rock catalog." The rock catalog is constructed from measurements performed on individual core plug samples representing "type" lithologies. Utilizing rock catalog information has provided an understanding of lithologic controls on petrophysical properties, equations relating petrophysical variables, and guidelines for predicting hydrocarbon producibility in shallow-marine and estuarine Morrow Sandstone reservoirs. This study is based on the analysis of samples from two cores from the Gentzler and one from the Arroyo oil and gas fields (Fig. 1) including (1) the Gentzler field cores Anadarko Petroleum Gaskill "A" 10-2 (C SE¼ sec. 10, T. 33 S., R. 38 W.; 5,952–6,085.5 ft) and Anadarko Nell "A" 19-1 (C W½NE¼ sec. 19, T. 33 S., R. 37 W.; 6,036–6,078 ft) and (2) the Arroyo field core J. M. Huber Kendrick 23-1 (C NW¼NE¼NW¼ sec. 23, T. 29 S., R. 41 W.; 5375–5,460 ft).

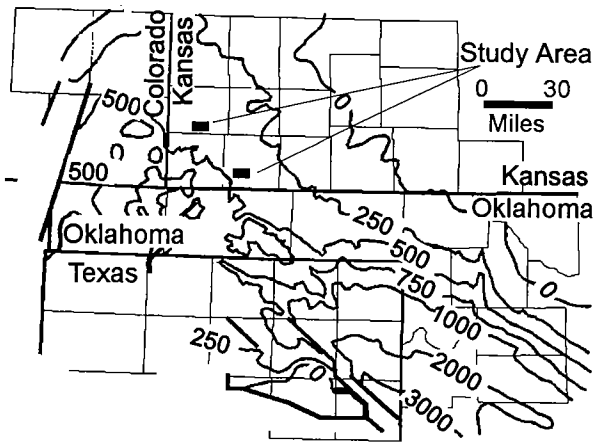

Figure 1. Isopach map of the Morrow Sandstone and location of Arroyo and Gentzler oil and gas fields investigated in study (modified after Swanson, 1979).

GEOLOGIC CHARACTERISTICS

The Morrow Sandstone (Kearny Formation) in the subsurface of southwest Kansas is informally divided into a lower and upper unit. The lower Morrow has been interpreted mainly as offshore shales and shoreface sandstones, whereas the upper Morrow has been interpreted as marine shales that encase transgressive valley-fill sequences. Marginal- and shallow-marine deposits of the Morrow Sandstone accumulated in the Hugoton embayment, which stretched into Kansas and Colorado from the deeper-water Anadarko basin in Oklahoma (Fig. 1). Wheeler and others (1990) recognized seven estuarine-valley sequences in the upper Morrow. Incision at the base of each sequence resulted from sea-level drop, with valley infill occurring during the subsequent sea level rise. During lowstands of sea level, valleys that are presently oriented northwest–southeast incised into older shelf deposits as the basin was drained to the shelf-slope break, located in Oklahoma north of the Anadarko basin. During highstands, valleys were backfilled, and a broad shelf covered the area.

Using integrated ichnologic, sedimentologic, and stratigraphic analysis, Buatois and others (1999) have provided an accurate characterization of the reservoir facies and geometry and distinction between assemblages of marine-shoreface and estuarine valley-fill facies evident in cores from the study area.

Estuarine deposits in the study area are consistent with the wave-dominated but partially tidally influenced estuarine model proposed by Dalrymple and others (1992) consisting of three zones: (1) an outer zone dominated by marine processes; (2) a central zone where marine energy is balanced by fluvial currents; and (3) an inner, river-dominated zone. The estuarine-facies assemblage includes both interfluve and valley-fill deposits, encompassing a variety of depositional environments, such as fluvial channels, paleosols, upper estuarine channels, estuary bay, restricted tidal flats, tidal channels, and estuary mouth (Fig. 2). The facies terminology used in this paper is indexed in Table 1.

The most proximal deposits within the valley consist of fluvial-channel massive to planar-bedded sandstones (*facies A*) with infrequent rooted siltstone paleosols (*facies B*). Fluvial facies are overlain by tidally influenced fine- (*facies C1*) to medium- and coarse-grained (*facies C2*) upper-estuarine–channel, planar cross-stratified, ripple cross-laminated, and wavy- to flaser-bedded sandstones. Sandstone packages deposited within estuarine channels are in turn overlain by central estuarine-bay, parallel-laminated shales (*facies D*) that locally exhibit isolated sand lenses and ripple laminae. Fine-grained deposits interfinger with coarse-grained, moderately fossiliferous, planar cross-bedded sandstones and pebble conglomerates (*facies H*) interpreted as having been deposited in the estuary mouth. Other peritidal facies include wavy-, flaser- and lenticular-bedded sandstones and siltstones with herringbone cross-stratification (*facies E*, restricted tidal flat) and

Table 1.—Index of Facies Noted in Text and the Corresponding Depositional Environment

Facies	Depositional environment
A	Fluvial
B	Nonmarine paleosol
C	Upper estuary channel
D	Estuary bay
E	Restricted tidal flat
F	Tidal channel
G	Lower estuary
H	Estuary mouth
I	Upper shoreface
J	Middle shoreface
K	Marine lower shoreface
L	Marine lower shoreface
M	Deeper water
N	Deeper water
O	Deeper water

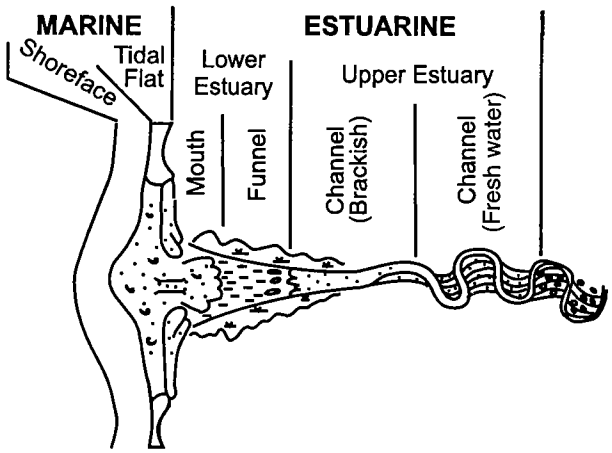

Figure 2. Generalized estuarine valley-fill model (modified after Dalrymple and others, 1992).

heterolithic stratification (*facies F*, tidal channel) and lower estuary laminated calcareous mudstones (*facies G*).

The open-marine facies assemblage consists of upper-, middle-, and lower-shoreface, offshore-transition, offshore, and shelf deposits. Morrow upper shoreface facies (*facies I*) consists of highly fossiliferous, planar cross-bedded sandstones succeeded by sparsely to moderately burrowed, planar cross-bedded, medium- to fine-grained sandstones representing proximal middle-shoreface (*facies J*) deposits. Distal middle-shoreface deposits (*facies K*) are moderately to thoroughly burrowed, rippled, fine-grained sandstones. The lower-shoreface (*facies L*), offshore-transition (*facies M*), offshore (*facies N*), and shelf deposits (*facies O*) represent a series progressing from thoroughly burrowed fine- to very fine grained silty sandstones with fading ripples through very fine grained silty sandstone and siltstone to the laminated black shales of the shelf deposits.

PETROPHYSICAL CHARACTERISTICS

The Morrow Sandstone exhibits petrophysical properties that can be tied to lithofacies and are generally correlative with more easily measured properties, such as porosity, that allow prediction of properties from log response. Properties exhibited by individual lithofacies are clearly illustrated in rock-catalog format but cannot be easily represented in publication format. The following discussion reviews general petrophysical properties.

Porosity and Compressibility

Routine helium porosity for the Morrow Sandstone studied ranges from 0% to 22%, Upper estuary-channel deposits (*facies A* and *C1*) exhibit maximum values of porosity, and estuary-funnel, estuary-mouth, lower-shoreface, transition, offshore, and shelf deposits exhibit minimum values. Upper-shoreface deposits (*facies I*) exhibit a wide range of porosities. Quartz overgrowth, pressure-solution suturing, and calcite cement are the dominant agents occluding intergranular porosity. Within estuary sandstones, porosity is primarily intergranular. In the marine sandstones, a significant portion of porosity can be secondary microporosity in glauconite and bioclasts. Porosity-log response, which measures *in situ* porosity, can be most accurately calibrated to routine core-analysis values if core porosity values reflect *in situ* values. At a net hydrostatic confining stress of approximately 3,000 pounds per square inch (psi), which approximates reservoir stress levels, *in situ* core porosity values average 92% of ambient or routine helium porosity values with the difference between routine and *in situ* values decreasing with decreasing porosity (Fig. 3).

Reservoir simulation and understanding of compaction drive requires an understanding of pore or bulk volume compressibility. Using the change in pore volume from 3,000 to 3,500 psi confining stress as a measure of the change a reservoir would undergo with production, and assuming that the matrix grains are incompressible, pore volume compressibilities (β_{pore}) decrease with increasing porosity (Fig. 4).

Capillary Pressure and Water Saturation

Capillary-pressure properties of Morrow Sandstone samples differ significantly between lithofacies. With structural closure in many Morrow fields in southwest Kansas of less than 100 ft, understanding the exact capillary-pressure–curve relationships becomes important. It is also important to note that 100 ft represents the maximum oil-column height and that much of the volume of a field may lie below these heights. Adopting 100 ft as the maximum oil-column height above free-water level, fluvial and upper-estuary channel deposits (*facies A* and *C*) exhibit water saturations at 100 ft above free-water level ($S_{w,\,100}$) below 25%, and near "irreducible" values. In contrast, estuary-mouth (*facies H*), restricted tidal-flat (*facies E*), and upper-shoreface deposits (*facies I*), with porosity near 12%, exhibit values of $S_{w,\,100}$ greater than 50%, primarily as the result

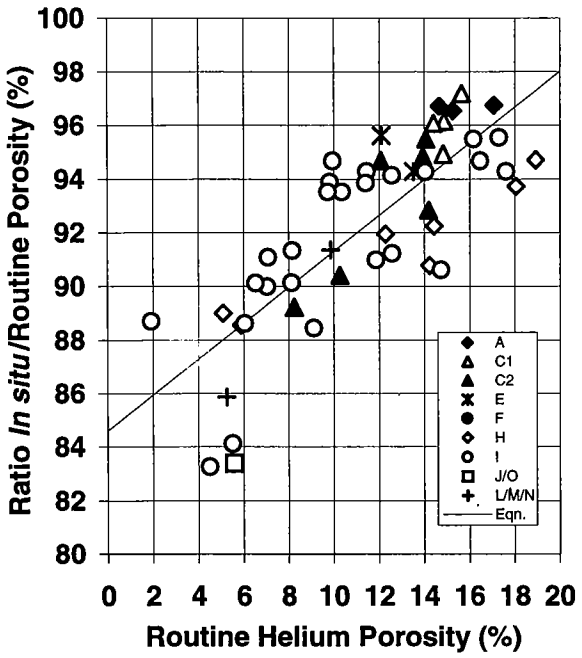

Figure 3. Cross-plot of relationship between ratio of *in situ*/routine porosity (%) and routine helium core porosity ($\phi_{routine}$, %). Linear regression provides the following predictive equation: Ratio $\phi_{in\ situ}/\phi_{routine}$ (%) = 0.67 * $\phi_{routine}$ + 84.6. See Table 1 for explanation of facies symbols, shown by uppercase letters. Eqn.—regression equation.

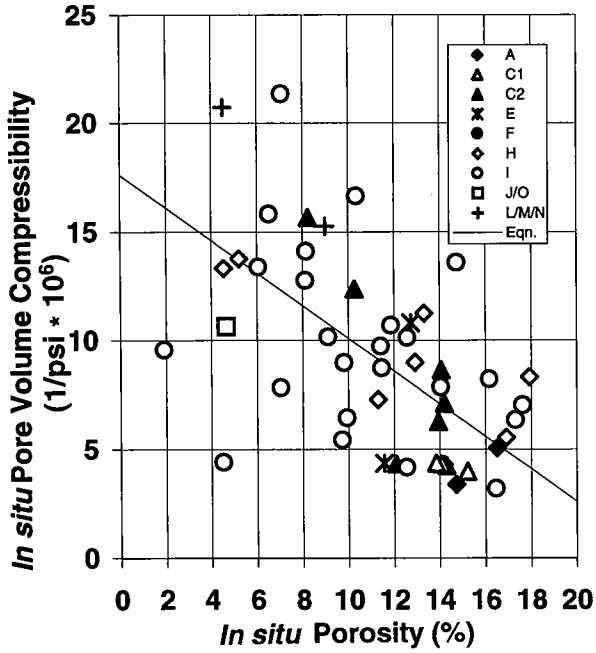

Figure 4. Cross-plot of pore volume compressibility (β_{pore}, psi^{-1} * 10^{-6}) versus *in situ* porosity ($\phi_{in\ situ}$, %) showing decrease in β_{pore} with increasing porosity as expressed by the equation: β_{pore} = –0.75 * $\phi_{in\ situ}$ + 17.6. See Table 1 for explanation of facies symbols, shown by uppercase letters.

of fine grain size, high clay content, and secondary porosity. Lower-shoreface and deeper-water deposits display water saturations greater than 90% (Fig. 5). Water saturations for all facies increase with decreasing permeability (Fig. 6).

Permeability

Routine air permeability values of the Morrow core studied range from 0.001 millidarcies (md) to 150 md. Highest porosity and permeability values were measured in the fluvial and upper-estuary channel sandstones (*facies A* and *C*). Coarse-grained sandstones (*facies C2*) exhibit higher permeability values at a given porosity than fine-grained cleaner sandstones (*facies A*). Extensive clay drapes, bioturbation, and increasing silt content result in significant decrease in permeability in tidal-flat and marine facies (e.g., *facies E* and *H*).

In situ Klinkenberg (high-pressure gas or liquid equivalent) permeability values are progressively lower than routine values with decreasing permeability (Fig. 7). *In situ* Klinkenberg permeability values are generally near 70% of routine air permeability values at permeabilities greater than 10 md. Below 1 md, *in situ* values decrease from 30% of routine values to <5% of routine values. Part of this difference is due to the effect of confining stress on pore throats and part is due to the Klinkenberg gas-slippage effect.

Generally, when pores are partially filled with water, the effective hydrocarbon permeability is also progressively less than *in situ* values with decreasing permeability resulting in a further reduction in the true *in situ* permeability of the lower permeability samples.

Permeability vs. Porosity

In many types of sandstone, permeability can be log-linearly correlated with porosity. Based on the available data, the general trend for all Morrow facies allows prediction of permeability (Fig. 8), although each facies exhibits a unique subparallel trend.

The wide variance evident in Figure 8 is attributable largely to the differences in permeability-porosity trends for the different lithofacies and to the wide variance introduced by bioturbated sandstones that exhibit no significant correlation between permeability and porosity. The permeability of *facies A* and *C1* is approximately an order of magnitude greater than other facies for a given porosity. Conversely, permeabilities of *facies F*, *J*, and *O* are approximately five to ten times less.

Electrical Resistivity

Capillary pressure-saturation relations can provide information on water saturation if the facies and height above free-water level are known or assumed; however, electric wireline logs allow the measurement of saturation using the Archie equation or modified Archie equations. Traditional saturation calculations use the Archie equation and cementation (m) and saturation

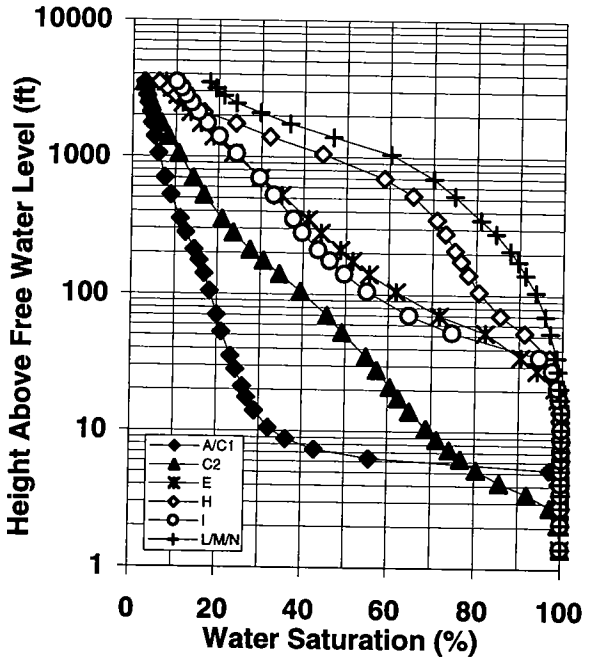

Figure 5. Generally representative water saturation versus hydrocarbon column height above free water level for major lower Morrow estuarine and shallow marine facies. Curves shift for each facies as a function of porosity and permeability. See Table 1 for explanation of facies symbols, shown by uppercase letters.

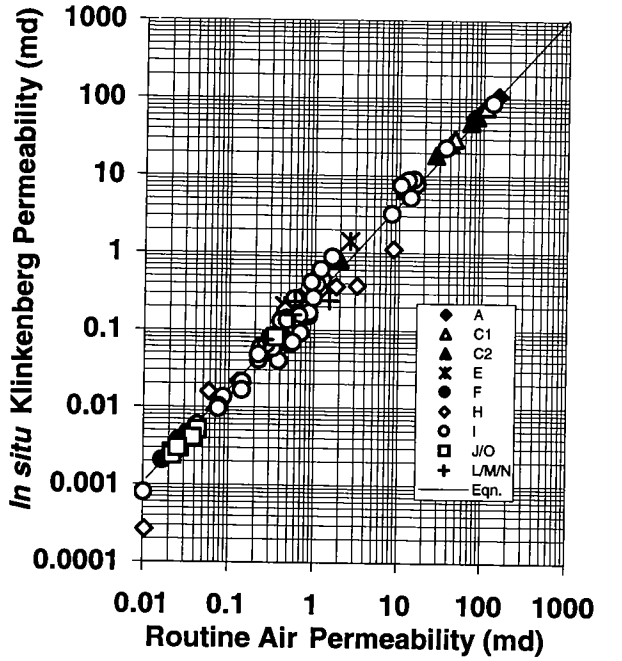

Figure 7. Cross-plot of *in situ* Klinkenberg (liquid equivalent) permeability versus routine air permeability showing progressively greater difference with decreasing permeability. *In situ* Klinkenberg permeability values can be predicted within a factor of 2.3 (2 standard deviations) from routine air permeability values using: $\log_{10}k_{in\ situ} = 1.2 * \log_{10}k_{routine} - 0.58$, where k is in millidarcies (md). See Table 1 for explanation of facies symbols, shown by uppercase letters.

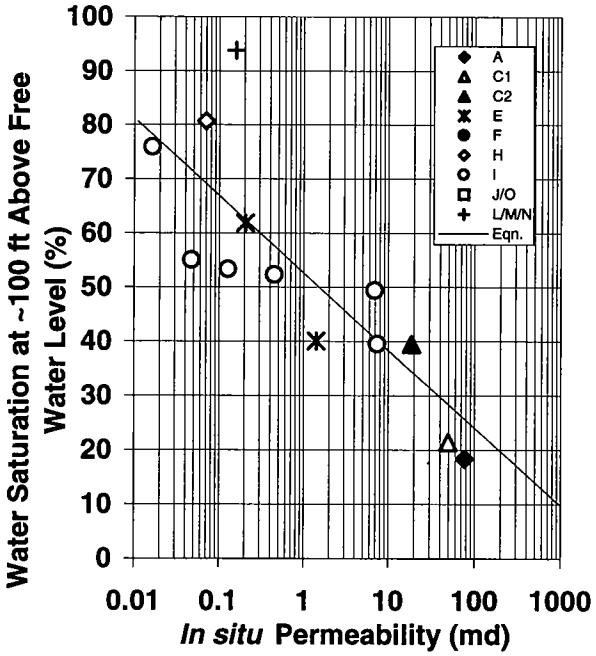

Figure 6. Cross-plot of water saturation at 100 ft of height above free water level ($S_{w,\ 100}$) illustrates the frequently observed trend that water saturation increases with decreasing permeability. $S_{w,100}$ can be predicted within ±13% (1 standard deviation) using: $S_{w,100}$ (%) = $-14.3 * \log_{10}k_{in\ situ} + 52.6$. See Table 1 for explanation of facies symbols, shown by uppercase letters. md—millidarcies.

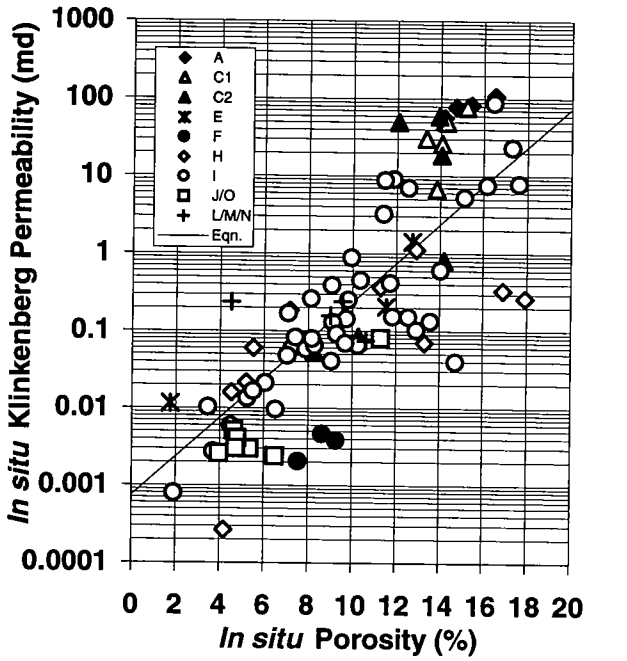

Figure 8. Cross-plot of *in situ* Klinkenberg permeability versus *in situ* porosity for all facies. Permeability can be predicted from porosity for all Morrow samples within a factor of ±8 (one standard deviation) using: $\log_{10}k_{in\ situ} = 0.25 * \phi_{in\ situ} - 3.13$. Note that permeability for facies A and C1 is ~10 times greater and for facies F/J/O is ~10 times less than general trend. See Table 1 for explanation of facies symbols, shown by uppercase letters.

exponent (n) values of 2. Formation resistivity factors (R_o/R_w) measured at R_w = 0.045 ohm-m (Fig. 9) indicate that the Archie cementation exponent (assuming an Archie intercept of 1.0) averages m = 1.81 for *facies A* and *C1* and m = 2.00 for many of the other facies.

CONCLUSIONS

Morrow Sandstone estuarine and marine lithofacies generally exhibit unique suites of petrophysical properties. In general, facies exhibiting good reservoir properties with high porosity and permeability and low $S_{w,100}$ include fluvial (*facies A*), upper-estuary channel (*facies C*), and upper-shoreface (*facies I*) sandstones. Facies exhibiting marginal reservoir properties with lower porosity and permeability, and $S_{w,100}$ greater than 50% include estuary-mouth (*facies H*), restricted tidal-flat (*facies E*), and middle-shoreface deposits (*facies J*). Non-reservoir facies, with low porosity and permeability and $S_{w,100}$ greater than 80% include nonmarine paleosols (*facies B*), central estuarine-bay shales (*facies D*), restricted-tidal-flat (*facies E*), tidal-channel (*facies F*) and lower-estuary mudstones (*facies G*), marine lower-shoreface (*facies K* and *L*), and deeper-water deposits (*facies M, N,* and *O*).

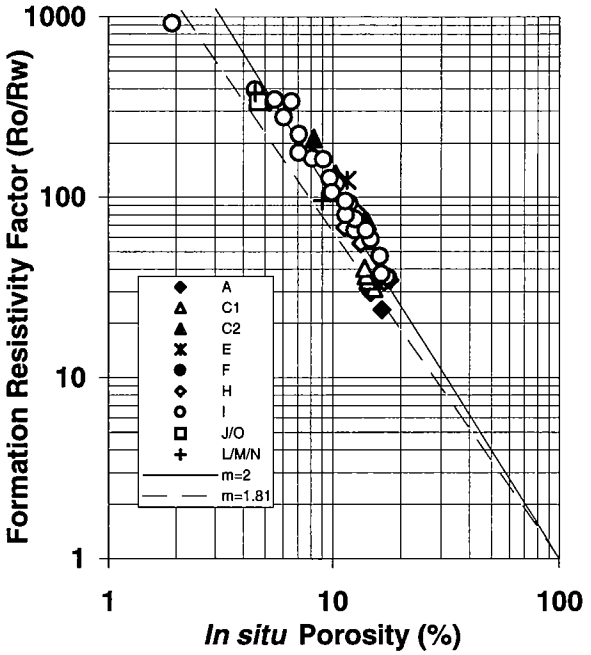

Figure 9. Cross-plot of formation resistivity factor (R_o/R_w) versus in situ porosity for all facies showing lower cementation exponent (m = 1.81) for better reservoir facies and standard value of m = 2 for remaining facies. See Table 1 for explanation of facies symbols, shown by uppercase letters.

REFERENCES CITED

Buatois, L. A.; Mángano, G.; and Carr, T. C., 1999, Sedimentology and ichnology of Paleozoic estuarine and shoreface reservoirs, Morrow Sandstone, Lower Pennsylvanian of southwest Kansas, USA: *in Current Research in Earth Sciences*, Kansas Geological Survey Bulletin 243, part 1. Available at <http://www.kgs.ukans.edu/Current/1999/buatois1.html>.

Dalrymple, R.W.; Zaitlin, B. A.; and Boyd, R., 1992, Estuarine facies models: conceptual basis and stratigraphic implications: Journal of Sedimentary Petrology, v. 62, p. 1130–1146.

Swanson, D. C., 1979, Deltaic deposits in the Pennsylvanian upper Morrow Formation of the Anadarko basin, *in* Hyne, N. J. (ed.), Pennsylvanian sandstones of the Mid-Continent: Tulsa Geological Society Special Publication 1, p. 115–168.

Wheeler, D. M.; Scott, A. J.; Coringrato, V. J.; and Devine, P. E., 1990, Stratigraphy and depositional history of the Morrow Formation, southeast Colorado and southwest Kansas, *in* Sonnenberg, S. A.; Shannon, L. T.; Rader, K.; von Drehle, W. F.; and Martin, G. W. (eds.), Morrow sandstones of southeast Colorado and adjacent areas: The Rocky Mountain Association of Geologists, Denver, p. 335.

Analysis of Completion/Stimulation Practices on Red Fork Recovery in the Anadarko Basin Using Artificial Neural System

Robert F. Shelley
Halliburton Energy Services
Oklahoma City, Oklahoma

Perry O. Scheuerman and Chris A. Talley
Halliburton Energy Services
Burns Flat, Oklahoma

Paul W. Smith
IHS Energy Group
Oklahoma City, Oklahoma

ABSTRACT.—The optimization of completion procedures is commonly difficult because of the variability in reservoir quality and lack of understanding about the complex interaction between well completion and stimulation and the reservoir. In this paper, we discuss the use of an Artificial Neural Network (ANN) as a new tool to enhance our ability to determine the effects of measurable and quantifiable variables on the productivity of completions in the Red Fork Formation. The ANN model has proven capable of predicting cumulative production from the Red Fork with an acceptable degree of accuracy (15% average absolute error). Sensitivity studies show that reservoir quality and completion methods both have significant effect on the production outcome of a Red Fork well. A case history will be presented in which an ANN sensitivity analysis was used to justify a change in stimulation fluid type. The production from this Red Fork completion exceeded the operator's expectations with nearly twice the rate compared to the standard completion used in the field.

ARTIFICIAL NEURAL NETWORKS

As early as 1943, it was thought that simplified artificial neurons could perform computational tasks (McCulloch, 1943). Today's artificial neural networks (ANNs) are based on the best understanding that we have of the basics of the human nervous system and how it operates. Many papers have been written that explain ANNs and their operation, so the details will not be discussed here. It is sufficient to say that an ANN can identify patterns in data and use these to predict future results. It is important to note, however, that the accuracy of an ANN is very dependant on the types and meaningfulness of the variables of each data set entered into it. The ANN does not care about the pertinence of the data it receives; it simply tries to create a predicting model with that data. In other words, ANNs can potentially identify patterns in variables that have no bearing on the desired outcome. However, ANNs have the potential to identify previously overlooked parameters that affect well production.

RED FORK FORMATION AND GEOLOGY BACKGROUND

The purpose of this ANN study is to evaluate the effects of a number of variables on the completion and consequent gas recovery of the Red Fork Formation in the Anadarko basin. The data sets used for the study originate from wells drilled in Custer and Roger Mills Counties in western Oklahoma (Fig. 1). The Red Fork in this area ranges in depth from 10,600 ft at the top to >14,600 ft at the bottom. It consists of mostly shales and siltstones with lenses of thinly interbedded sand-shale sequences. The Red Fork is typically a dry gas reservoir with a horizontal permeability generally ranging from 0.01 to 5 md (millidarcies) (Hentz, 1993). Bottom-hole pressures range from 0.54 to 0.63 psi/ft (pounds per square inch per foot). Because of its depth, detailed analysis of the formation through coring is sparse and three-dimensional seismic studies have only given a partial picture.

A large variety of completion and stimulation meth-

Shelley, R. F.; Scheuerman, P. O.; Talley, C. A.; and Smith, P. W., 2001, Analysis of completion/stimulation practices on Red Fork recovery in the Anadarko basin using artificial neural system, *in* Johnson, K. S. (ed.), Pennsylvanian and Permian geology and petroleum in the southern Midcontinent, 1998 symposium: Oklahoma Geological Survey Circular 104, p. 65–70.

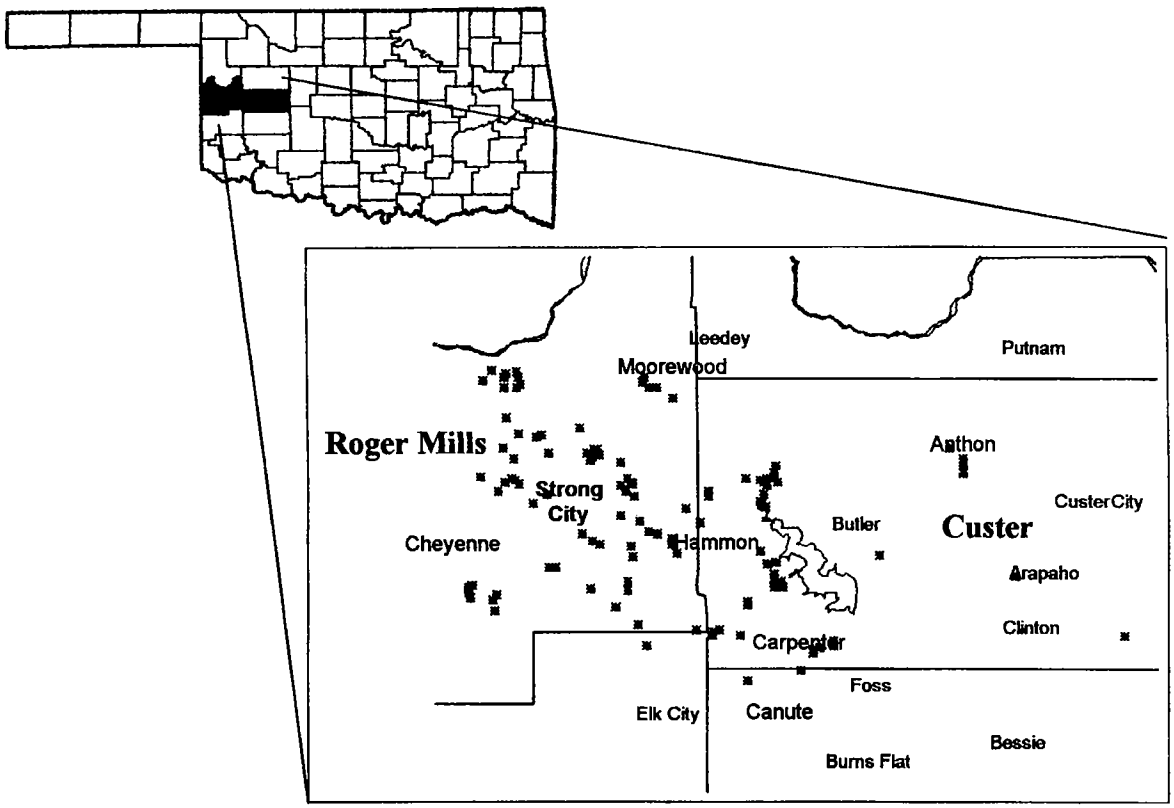

Figure 1. Red Fork study area.

ods have been performed on wells in the reservoir. In addition, there is a large number of wells with production data. With the availability of such a large number of data sets to work with, it was hoped that a determination of guidelines for completion and stimulation of new wells could be made on an individual well basis. Halliburton Energy Services merged completion and well information with a reservoir characteristics database built by IHS Energy Group. The reservoir-characteristics database consisted of more than 225 Red Fork completions. However, unavailable critical parameters resulted in the use of 107 records to develop the ANN model.

CREATING THE RED FORK ANN MODEL

The data set used to create an ANN trained for the Red Fork Formation consisted of parameters for each record. The parameters included stimulation fluid volume and type, proppant volume and type, number of stimulation stages, perforation location, perforated thickness and porosity, saturated thickness and porosity; water saturation, initial reservoir pressure, number of sand lobes, and other parameters. Most of the wells are located in the Strong City area with the rest from the fields of Carpenter, Hammon, Moorewood, Calumet, Cheyenne, Anthon, and Clinton (Fig. 1). The six-month cumulative production from these wells ranged from 21 MMscf to 1.7 Bcf (million cubic feet and billion cubic feet). About 20% of the 107 records were withheld for model-testing purposes.

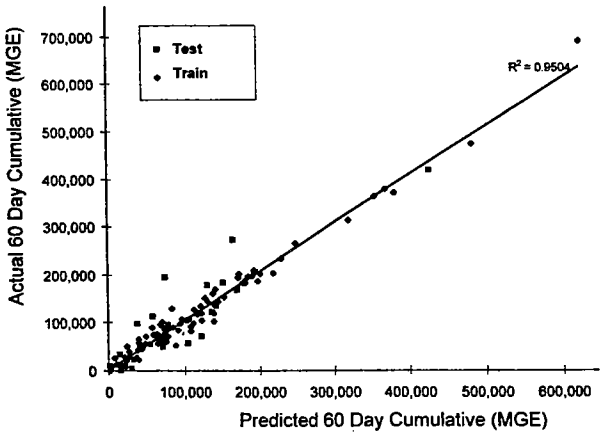

Figure 2. ANN predicted vs. actual hydrocarbon production over 60 Days. Excerpt from Shelley and others (1998).

The ANN type used for this study was a back-propagation neural network that uses one hidden layer with seven neurons. It was trained to the outputs of two-month cumulative gas-equivalent production values. Figure 2 compares the actual and predicted values for two-month cumulative gas-equivalent production for all of the data. The two-month cumulative gas-equivalent production values had an average absolute error of about 14% (Fig. 2) (Shelley, 1998).

SENSITIVITY ANALYSIS

Sensitivity analyses were performed after an acceptable absolute error was obtained in training the ANN. A sensitivity analysis tests the effect of a single variable on the overall result or outcome. Each of nine variables of the data sets entered into the Red Fork ANN model was varied, and the overall effect of gas and water production was studied. Quantitative data were varied by 10%, and other variables were changed individually (Table 1). The variables were grouped into four categories: (1) reservoir variables and treatment volumes, (2) number of sand units or separated lobes of sand seen on a log, (3) number of stages of stimulation performed, and (4) the type of fluid used for the stimulation treatments. Of the reservoir variables, reservoir pressure had the highest impact on the sensitivity analysis (Fig. 3), having a >10% increase in cumulative production. Changing the number of sand units also had a significant effect on production results, with one sand unit being the best (23% production increase) and three sand units being the worst (23% production decrease) (Fig. 4).

A surprising fact was that generally raising the treatment and proppant volumes 10% had little to no effect on production results. We interpreted this result as demonstrating little opportunity to increase production with larger stimulation volume. These are relative values based on the ANN-predicted model. The effect of multiple stages of stimulation was again surprising with only an 11% production difference between a one-stage stimulation and a three-stage stimulation (Fig. 5).

Table 1.—Summary of Sensitivity Analysis for All Wells in Red Fork Data Set

2-Month Cumulative Gas-Equivalent Production (Mscf)	
Actual production	13,192,550
ANN-predicted production	12,629,144
Prediction if all wells produce from one sand lobe	15,544,111
Prediction if all wells produce from two sand lobes	12,330,481
Prediction if BHP is increased by 10% in all wells	14,256,922
Prediction if porosity is increased by 10% in all wells	12,792,907
Prediction if shale index is increased by 10% in all wells	13,598,867
Prediction if all wells are treated with borate fluids	12,768,717
Prediction if all wells are treated with foam	18,055,757
Prediction if treatment volume is increased by 10% in all wells	12,631,406
Prediction if proppant weight is increased by 10% in all wells	12,618,308
Prediction if net perforated height is increased by 10% in all wells	12,573,909

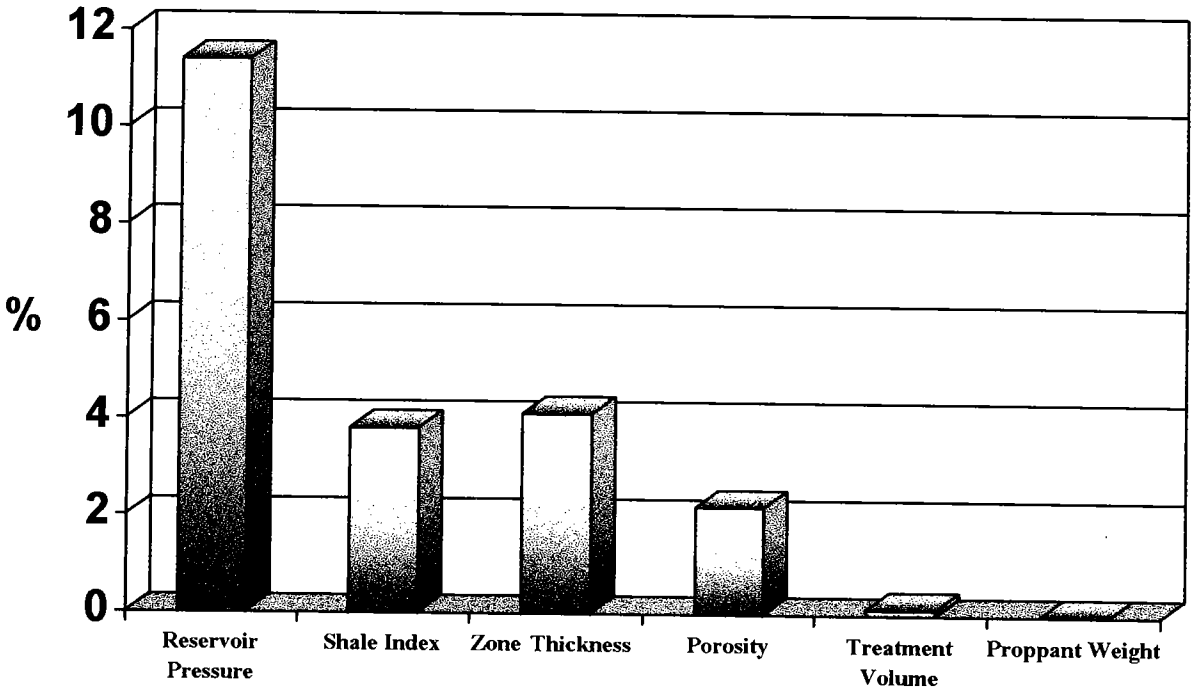

Figure 3. Sensitivity to a 10% increase to reservoir variables.

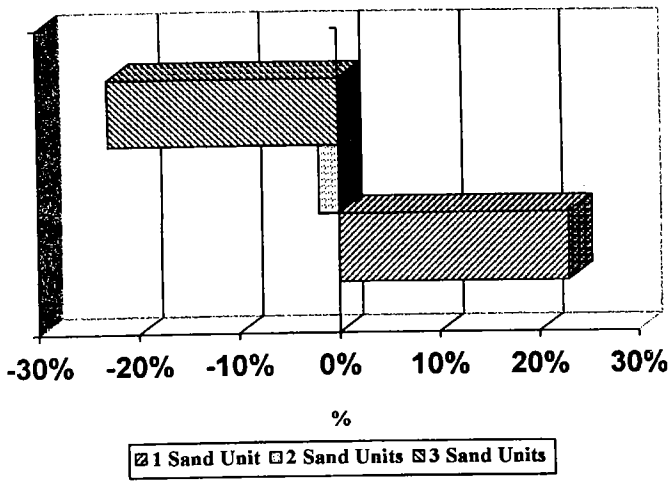

Figure 4. Sensitivity of 12-month cumulative production to changes in number of sand units.

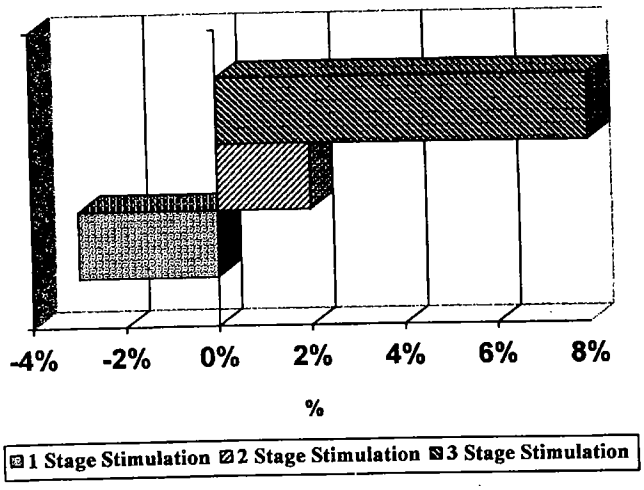

Figure 5. Sensitivity of 12-month cumulative production to changes in number of stimulation stages.

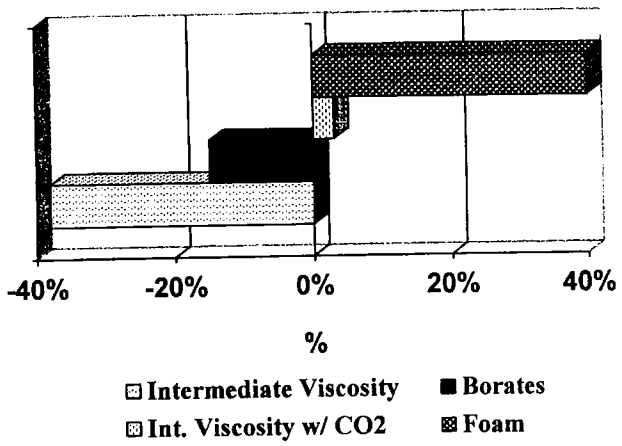

Figure 6. Sensitivity of 60-day cumulative production to changes in stimulation fluids.

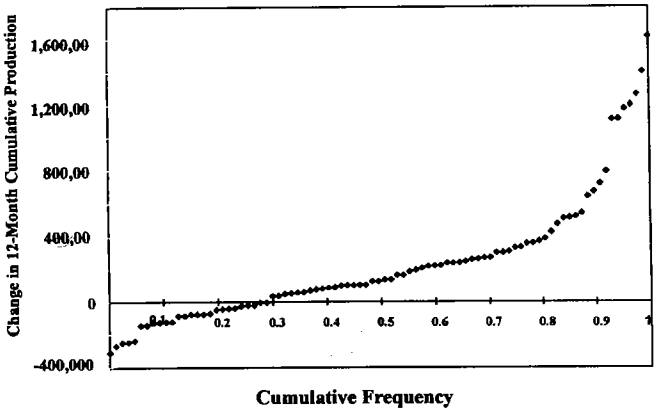

Figure 7. ANN-estimated effect of 65% CO_2-foam stimulation on production. Excerpt from Shelley and others (1998).

The highest impact observed by far was when stimulation fluid type was changed. This is very significant because it is one of the easiest things to modify when planning a well completion. Over the history of production in the Red Fork Formation, four main fluid types have been used: CO_2 foams, high viscosity borates, CO_2-assisted intermediate-viscosity fluids, and intermediate-viscosity fluids without CO_2. Results showed as much as a two-fold impact on cumulative production over a six-month period by varying fluid type alone. In general, moving from high-viscosity borates and intermediate-viscosity fluids to high-quality CO_2 foams increased production (Fig. 6). However, analysis of all of the wells in the data set indicated that use of high-quality foams is not always appropriate, and that this determination must be made on a well-by-well basis (Figs. 7, 8).

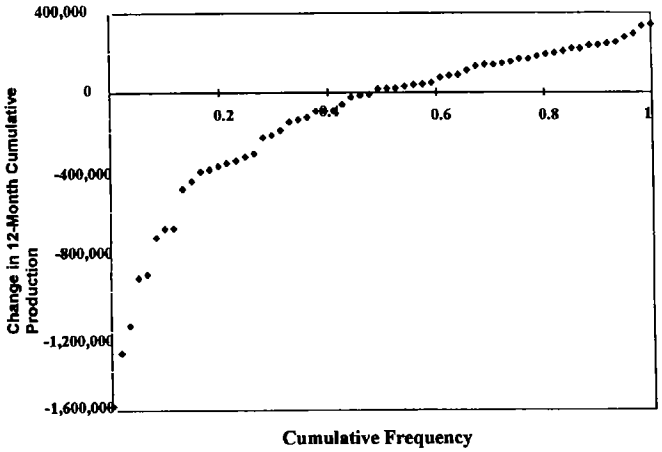

Figure 8. ANN-estimated effect of borate fluid stimulation on production. Excerpt from Shelley and others (1998).

CASE HISTORIES

Well A

Well A is located in Custer County and was to be completed in a single Red Fork interval. Analysis of open-hole logs showed that this well had a gross interval thickness of 98 ft with about 64 ft capable of producing gas. The average and maximum porosity were estimated at 8% and 12%, respectively. Bottom-hole pressure was estimated at 6,000 psi, indicating no significant depletion in the reservoir penetrated by the well bore. The well was treated with 101,000 lb of proppant placed with 40,000 gal of a borate–cross-linked fluid. Onsite diagnostic procedures confirmed the validity of the three-dimensional design assumptions. The ANN estimated an average production rate of about 1.83 MMscf/D for the first 60 days of production or a 60-day cumulative production of 110 MMscf. The ANN also indicated that a completion on this well with the use of foam stimulation fluids would have resulted in a 60-day cumulative production of 158 MMscf, a 44% increase in 60-day cumulative production (Fig. 9) (Shelley, 1998). However, the operator elected not to use the preferred stimulation technique. The actual 60-day cumulative production for this well is 111 MMscf. The ANN was within 1% of predicting the actual production for this well.

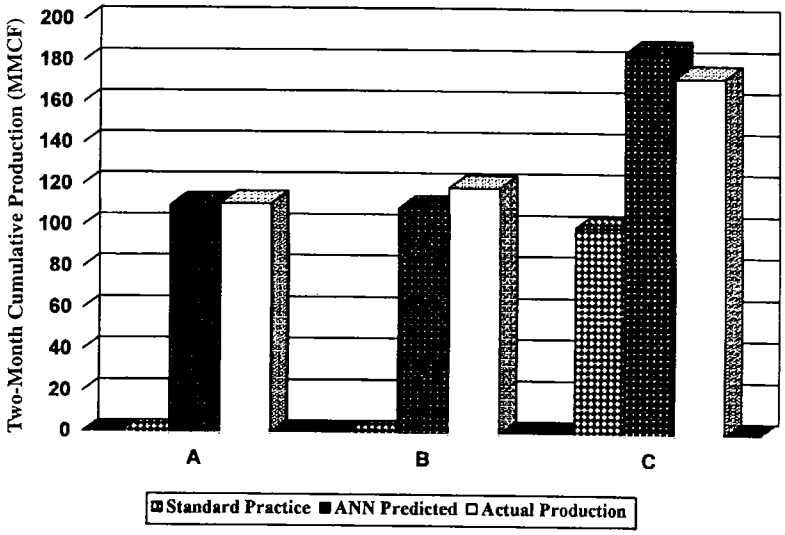

Figure 9. Comparison of case study ANN versus actual production.

Well B

Well B is also located in Custer County and was to be completed in multiple Red Fork intervals. Analysis of open-hole logs showed that this well had a gross interval thickness of 99 ft with about 96 ft capable of producing gas. The average porosity was estimated at 8.5%. Bottom-hole pressure was estimated at 7,000 psi, indicating no significant depletion in the reservoir. The ANN analysis showed that a completion with the use of a high-viscosity, borate–cross-linked fluid and an intermediate-strength proppant would provide the highest production values. The ANN estimated an average production rate of about 1.82 MMscf/D for the first 60 days or a 60-day cumulative production of 109 MMscf. The well was stimulated with approximately 122,000 lb of intermediate strength proppant placed with 47,000 gal of a borate–cross-linked fluid. Onsite diagnostic procedures confirmed the validity of the three-dimensional design assumptions. The actual 60-day cumulative production for this well was 119 MMscf, within 10% of the predicted ANN value (Fig. 9) (Shelley, 1998).

Well C

Well C, also located in Custer County, was to be completed in lower and upper Red Fork intervals. Analysis of open-hole logs showed that this well had a gross interval thickness of 60 ft with about 28 ft capable of producing gas. The average porosity was estimated at 11.4%. The sand development in this well correlated with offset producers, but there was no indication of significant depletion of bottom-hole pressure, which was estimated at 5,800 psi. On the basis of analysis and comparison with other wells in this field, the operator anticipated this well would be one of the better producers with a productive potential of about 2 MMscf/D for the first 60 days of production or a 60-day cumulative production of 120 MMscf.

The ANN analysis indicated significant additional potential from this well. The analysis indicated that the operator could achieve almost twice the productive potential in this well with the use of foam stimulation fluids—a completion technology not previously employed in this field. On the basis of this analysis, we proposed a completion that conformed to the optimum determined from the ANN. The fracturing procedure was designed with the use of a three-dimensional simulator. We then completed the well using a biased perforating scheme and stimulated the well with 96,500 lb of resin-coated sand placed with 40,000 gal of 65-quality CO_2 foamed, intermediate-viscosity fluid. On-site diagnostics confirmed the validity of the three-dimensional design assumptions. After the stimulation fluid was cleaned up, the well initially began producing 6.5 MMscf/D on a 23/64-in. choke. The actual two-month production was 173 MMscf, which was within 6.5% of the 185 MMscf predicted by the ANN (Fig. 9).

CONCLUSIONS

Red Fork completion analysis with ANNs produced the following conclusions:

- ANN analysis can predict well production with different completion scenarios using definable reservoir attributes. These production predictions facilitate quantification of the impact of various completion methods.
- A database containing detailed and consistent reservoir parameters allows for successful ANN predictive modeling.

- Stimulation-fluid selection can have a two-fold impact on production. Overall, high-quality CO_2-foam stimulation has the best chance of giving optimum production results in the Red Fork Formation.
- For best results, stimulation methods should be tailored for individual wells. Broad generalizations about the way to best stimulate a formation need to be replaced by an evaluation of each well.
- The low-cost completion/stimulation method may not be the optimal method. Using cost as a basis to make completion and stimulation decisions may hinder a well's producing potential. One should strive for an economic balance between the cost of completion and revenue from future production.
- It is likely that ANNs devised for other specific reservoirs could yield similar gains in improved completion techniques and provide operators with improved production.
- ANN analysis should augment well-completion optimization methods. The Red Fork-trained ANN is in no way a replacement for conventional engineering evaluation but should be used to test assumptions and help identify production enhancement opportunities.

ACKNOWLEDGMENTS

Appreciation is extended to Sonat, Enron, Marathon, and other operators who supplied well and treatment information used in this study.

REFERENCES CITED

Hentz, T. F., 1993, Geologic challenges and opportunities of the Cherokee Group play (Pennsylvanian), Anadarko basin Oklahoma: Gas Research Institute Topical Report, Contract No. 5082-211-0708.

McCulloch, W. S.; and Pitts, W., 1943, A logical calculus of the ideas immanent in nervous activity: Bulletin of Mathematical Biophysics, v. 5, p. 115–133.

Shelley, R.; and others, 1998, Red Fork completion analysis with the aid of artificial neural networks: Paper SPE 39963, presented at the 1998 Gas Technology Symposium, Calgary, Alberta, March 15–18.

Regional Correlation of Mountain-Front "Washes" and Relationship to Marine Sediments of Anadarko Basin and Shelf

Walter J. Hendrickson, Paul W. Smith, and Ronald J. Woods
IHS Energy Group
Oklahoma City, Oklahoma

ABSTRACT.—As part of a regional study, the logs from every producing well most of the Anadarko basin and shelf of Oklahoma and Texas were reviewed to verify the actual producing reservoirs and to assign consistent nomenclature. Both detail and regional cross sections were constructed and used to determine stratigraphic relationships and develop a stratigraphic-nomenclatural system that could be used across the area with accuracy, detail, and consistency. Correlation problems have long existed between the Pennsylvanian marine clastics of the northeastern half of the Anadarko basin and shelf and the Pennsylvanian terrigenous washes of the extreme southwestern portion of the Anadarko basin. These correlation problems have created nomenclatural problems resulting in thousands of feet of washes commonly referred to on completion reports and production records as "granite wash" or "Atoka Wash," where much greater accuracy and specificity is both needed and possible. Analysis indicated that the reservoir rocks were commonly neither granite wash (but rather chert or carbonate washes) nor Atokan (being either younger or older).

Because few detailed cross sections are available, regional and field-scale cross sections were constructed that have been correlated well-by-well and field-by-field using nearly every deep well drilled in the basin. These cross sections have been correlated from the Heebner Shale down to the deepest zones penetrated. This process has provided for a high degree of consistency. These cross sections have greatly diminished the correlation and nomenclature problems within the Anadarko basin and shelf.

It was possible to subdivide the washes and assign more accurate and definitive nomenclature with the regional correlations indicated by the cross sections. Certain markers proved to be regionally persistent from the marine clastics into the terrigenous washes making the subdivision of thousands of feet of washes possible. Those of greatest importance were the top of the Marmaton, the Cherokee Marker, the Pink "Limestone" Marker, the top of the Atoka, and the top of the Morrow. Once these and other subdivisions were made, production was allocated on a much more definitive basis.

PROJECTS AND METHODOLOGY

The original project that highlighted the need for regional correlations and cross sections involved reservoir-characterization studies of the major gas-producing reservoirs in the Anadarko basin. These studies utilized original work designed to provide up-to-date, high-quality, and highly consistent data. Detailed reservoir characterization was conducted to include geologic and engineering data such as depth, thicknesses, porosities, permeabilities, pressures, water saturations, field area, well spacings, and heterogeneities. Log analysis was conducted on the producing interval, saturated interval, and gross interval.

The first step in performing any reservoir characterization study is to properly correlate and identify the reservoir. Original reservoir nomenclature is generally only that provided by the operator. Due to a wide variety of factors, the resultant nomenclature is all too commonly vague and/or variable, too broad, or even altogether in error. As a result of this, the need for a regional framework of cross sections to standardize reservoir nomenclature was obvious. The construction of the regional cross sections first involved the construction of numerous field-scale cross sections in the major gas fields of the study area to properly identify and correlate the producing reservoirs within a given field. Then, adjacent fields were integrated into the previous

Hendrickson, W. J.; Smith, P. W.; and Woods, R. J., 2001, Regional correlation of mountain-front "washes" and relationship to marine sediments of Anadarko basin and shelf, *in* Johnson, K. S. (ed.), Pennsylvanian and Permian geology and petroleum in the southern Midcontinent, 1998 symposium: Oklahoma Geological Survey Circular 104, p. 71–80.

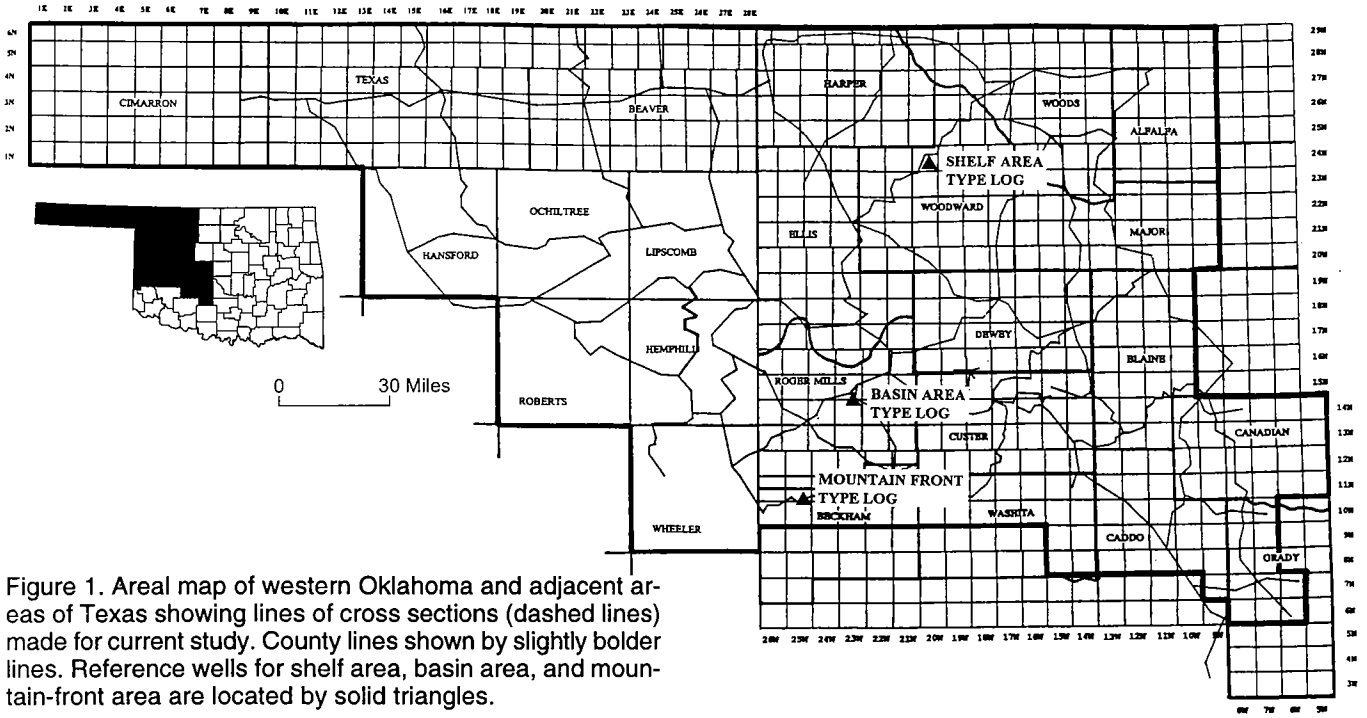

Figure 1. Areal map of western Oklahoma and adjacent areas of Texas showing lines of cross sections (dashed lines) made for current study. County lines shown by slightly bolder lines. Reference wells for shelf area, basin area, and mountain-front area are located by solid triangles.

framework. As work progressed, the most applicable and definitive reservoir nomenclature was developed, and the most persistent stratigraphic markers and intervals identified.

Near the end of the reservoir characterization studies for the Anadarko basin and shelf, the regionally persistent stratigraphic markers and intervals were used in the construction of the regional cross sections. Figure 1 indicates the approximate positioning and density of the 2,880 mi of contiguous regional cross sections drafted to date. Although many more logs were used in the construction of the cross sections, approximately one well every 3 mi was represented on the final presentation. Additionally, innumerable miles of cross sections from the field studies as well as detail cross sections from the more complex areas were used in the construction of the regional cross sections. Correlations were made from the Heebner Shale through the deepest zones penetrated. Due to constraints of reproduction, only 5,000 ft section could be represented on a single cross section. In the instances where zones of interest occurred over depth ranges in excess of 5,000 ft, additional cross sections were constructed covering the additional zones of interest. As a result, some of the cross sections have as many as three components—a shallow, a medium, and a deep component—that could ultimately cover 15,000 ft of stratigraphic interval.

Upon completion of the reservoir characterization project and the resultant cross sections, a second project was initiated which involved allocating all producing wells within the Oklahoma portion of the Anadarko basin and shelf. Going back to the original completion data, perforations for each productive well were plotted on its respective log with reservoir nomenclature then assigned to conform to the previously constructed regional cross sections. The result of this project has been the development of a database that has both a high degree of consistency of reservoir nomenclature on a regional basis as well as high definition in the reservoir nomenclature used.

LOG RESPONSES AND CROSS SECTIONS

Representative log responses for the stratigraphic markers and intervals identified through the course of the study are shown in Figures 2, 3, and 4. Figure 2 is indicative of the shelf area, Figure 3 the basin area, and Figure 4 the mountain-front deposits.

Additionally, contained herein is an example of a distinct stratigraphic horizon, the Pink Limestone Marker, being correlated from the shelf area, through the basin and into the washes. Figure 5 is a Pennsylvanian paleogeography map with the trace of a regional cross section indicated. This cross section is indicated schematically in Figure 6 and implies that correlations can be made from the shelf area to the north, through the basin and into the washes to the south. Figure 7 is the actual log cross section. The northernmost log (sec. 3, T. 24 N., R. 18 W.) is reproduced in its entirety and is typical of a shelf section. The Pink Limestone pick is indicated on this log. The southernmost log (sec. 32, T. 11 N., R. 25 W.) is reproduced in its entirety and is typical of a mountain-front section dominated by washes. The Pink "Limestone" interval is indicated on this log. For clarity, only the conductivity curves have been indicated for the intervening logs. As indicated, as one moves south, the Pink Limestone (a resistive marker easily correlated over a wide area) disappears.

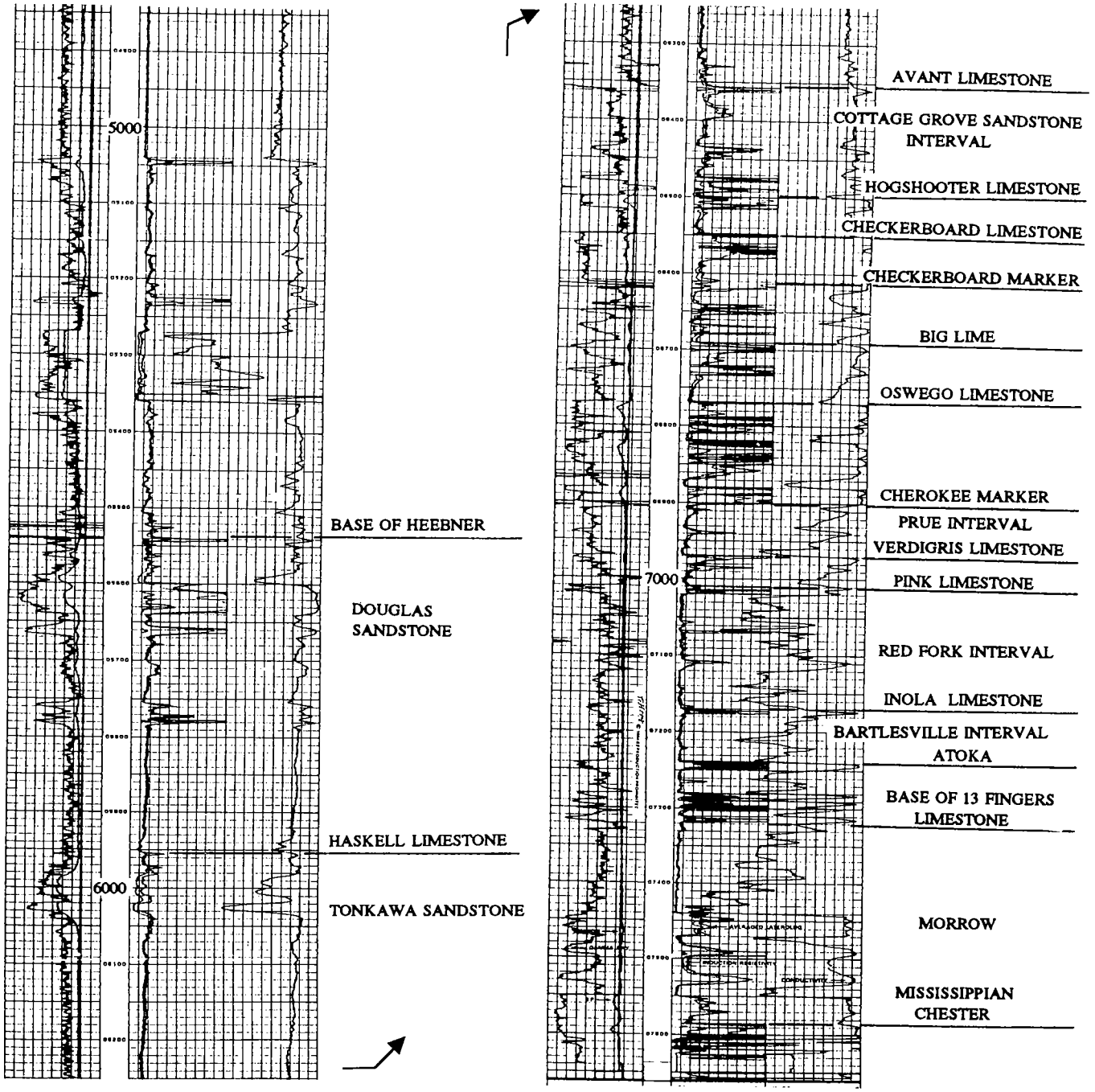

Figure 2. Type log for Oklahoma shelf area. Well is the Adena Exploration Harrison #1-22, located in N½S½ sec. 22, T. 24 N., R. 20 W., Woodward County, Oklahoma. Elevation of the Kelley bushing is 2,126 ft; log extends from depth of ~4,700 ft to ~7,670 ft. Formations and prominent marker beds are indicated on figure. Arrows show connections of log segments.

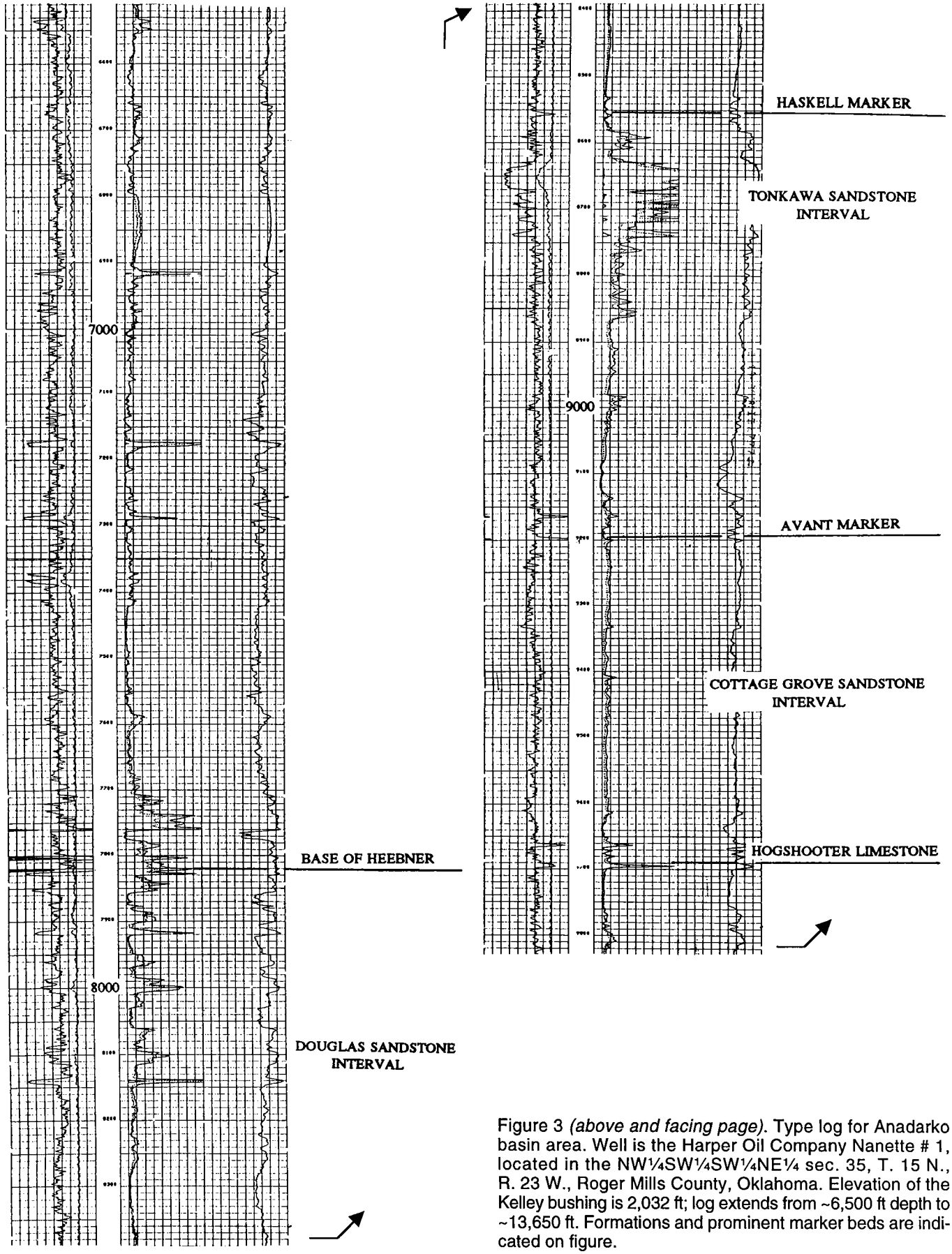

Figure 3 *(above and facing page)*. Type log for Anadarko basin area. Well is the Harper Oil Company Nanette # 1, located in the NW¼SW¼SW¼NE¼ sec. 35, T. 15 N., R. 23 W., Roger Mills County, Oklahoma. Elevation of the Kelley bushing is 2,032 ft; log extends from ~6,500 ft depth to ~13,650 ft. Formations and prominent marker beds are indicated on figure.

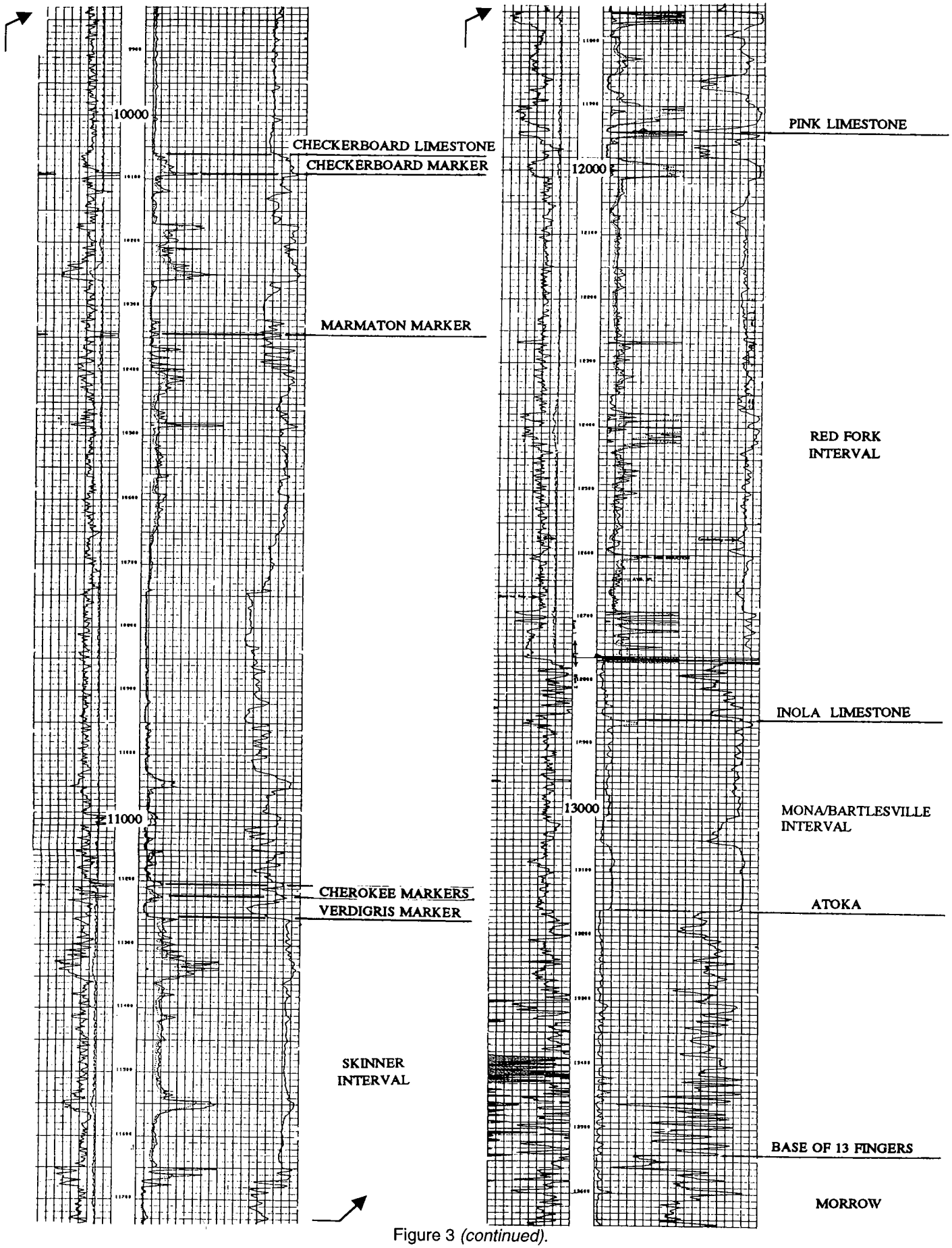

Figure 3 *(continued)*.

Generally, the Pink Limestone is present in the northeastern half of the Strong City District (centered in T. 14 N., T. 22 W.; see Fig. 7), and it is absent in the southwestern half. Prior to its disappearance, however, a distinctive shale unit develops on top of the Pink Limestone and persists toward the mountain front once the Pink Limestone is gone. It is this shale that can be carried into the mountain-front washes, as indicated by the cross section (Fig. 7).

The most important distinctions that were made were the top of the Marmaton, the Cherokee Marker, the Pink "Limestone" interval, the top of the Atoka and the top of the Morrow. As a result of the subdivisions that were made, production was allocated on a much more definitive basis, as indicated by Figure 8.

CONCLUSIONS

Detailed cross sections from the Heebner Shale down to the deepest zones penetrated were based on many hundreds of well logs constructed as part of the study. These cross sections covered the Anadarko basin and shelf area, from adjacent to the Wichita–Amarillo uplift, throughout the Anadarko basin, and across the shelf area. They have enabled nomenclatural standardization and a high degree of consistency in correlation that previously did not exist. It became possible to subdivide the "granite washes" or "Atoka washes" sourced in the Wichita Mountains and to assign more accurate and definitive nomenclature with the regional correlations indicated by the cross sections. Specific markers proved to be regionally persistent from the marine clastics of the shelf and basin into the terrigenous washes. These markers made the subdivision of thousands of feet of washes possible. The markers of greatest importance were the top of the Marmaton, the Cherokee Marker, the Pink "Limestone" Marker, the top of the Atoka, and the top of the Morrow. Once the subdivisions were constructed, production from the washes could be allocated on a much more definitive basis.

REFERENCES CITED

Lyday, J. R., 1985, Atoka (Pennsylvanian) Berlin field: genesis of recycled detrital dolomite reservoir, deep Anadarko basin, Oklahoma: American Association of Petroleum Geologists Bulletin, v. 69, p. 1931–1949.

Rascoe, Bailey, Jr., and Adler, F. J., 1983, Permo–Carboniferous hydrocarbona accumulations, Midcontinent U.S.A.: American Association of Petroleum Geologists Bulletin, v. 67, p. 979–1001.

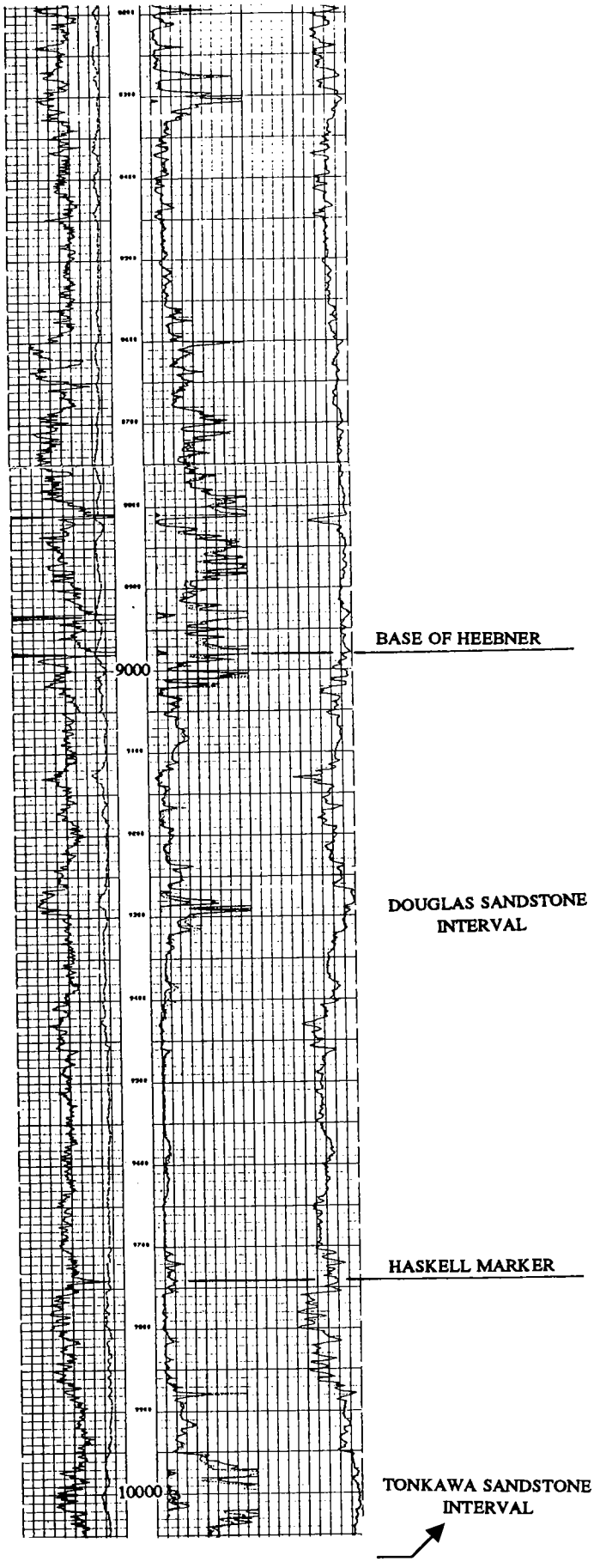

Figure 4 *(right and p. 77–78).* Type log for Wichita–Amarillo uplift, mountain-front area. Well is the Exxon Company U.S.A. Walne #1-34, located in the NE¼SW¼ sec. 34, T. 11 N., R. 25 W., Beckham County, Oklahoma. Elevation of the Kelley bushing is 2,069 ft; log extends from ~8,190 ft depth to ~17,510 ft. Final segments of log are shown on following pages; arrows show connection of log segments.

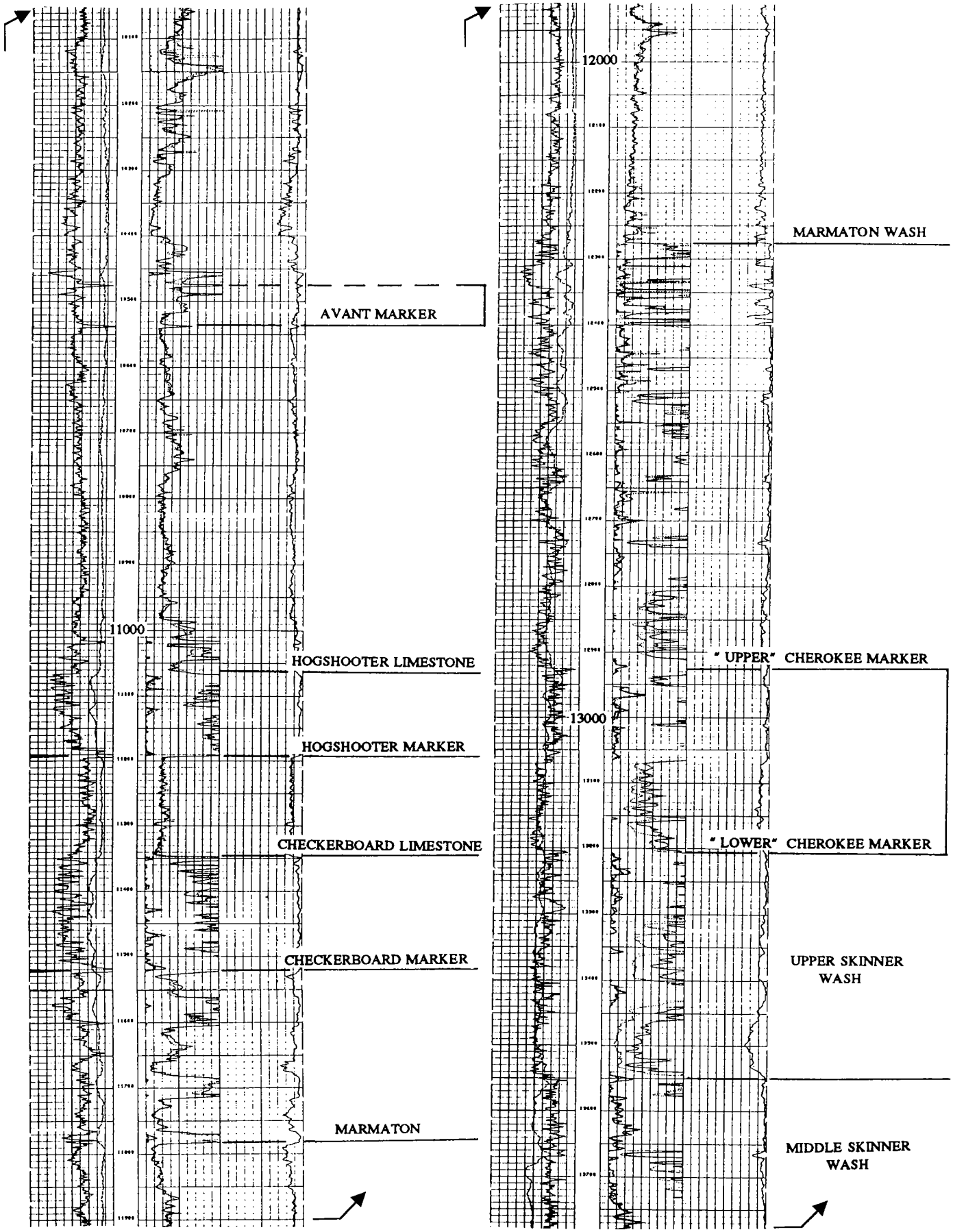

Figure 4 *(continued)*.

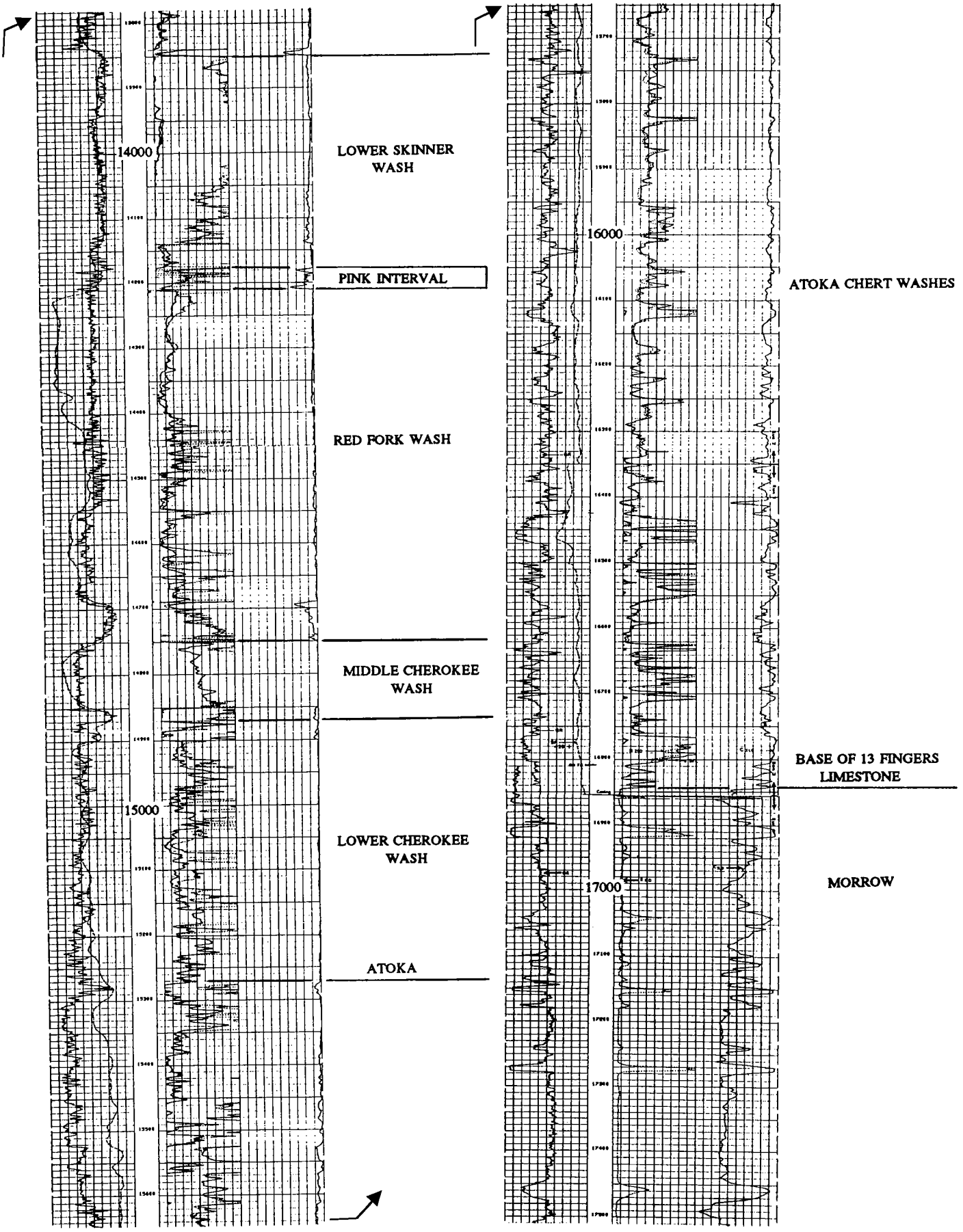

Figure 4 *(continued)*.

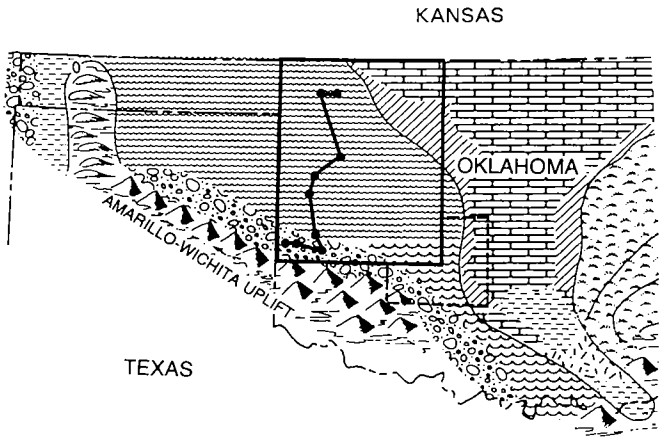

Figure 5. Paleogeographic map showing Amarillo–Wichita uplift with coarse-clastic apron to northeast (mountain-front area), Anadarko basin with wavy patterns (basin area), and Oklahoma shelf with predominantly limestone and shale patterns (shelf area). Line of cross section shown by bold, zig-zag line represents wells shown schematically on Figure 6. (Modified from Rascoe and Adler, 1983.)

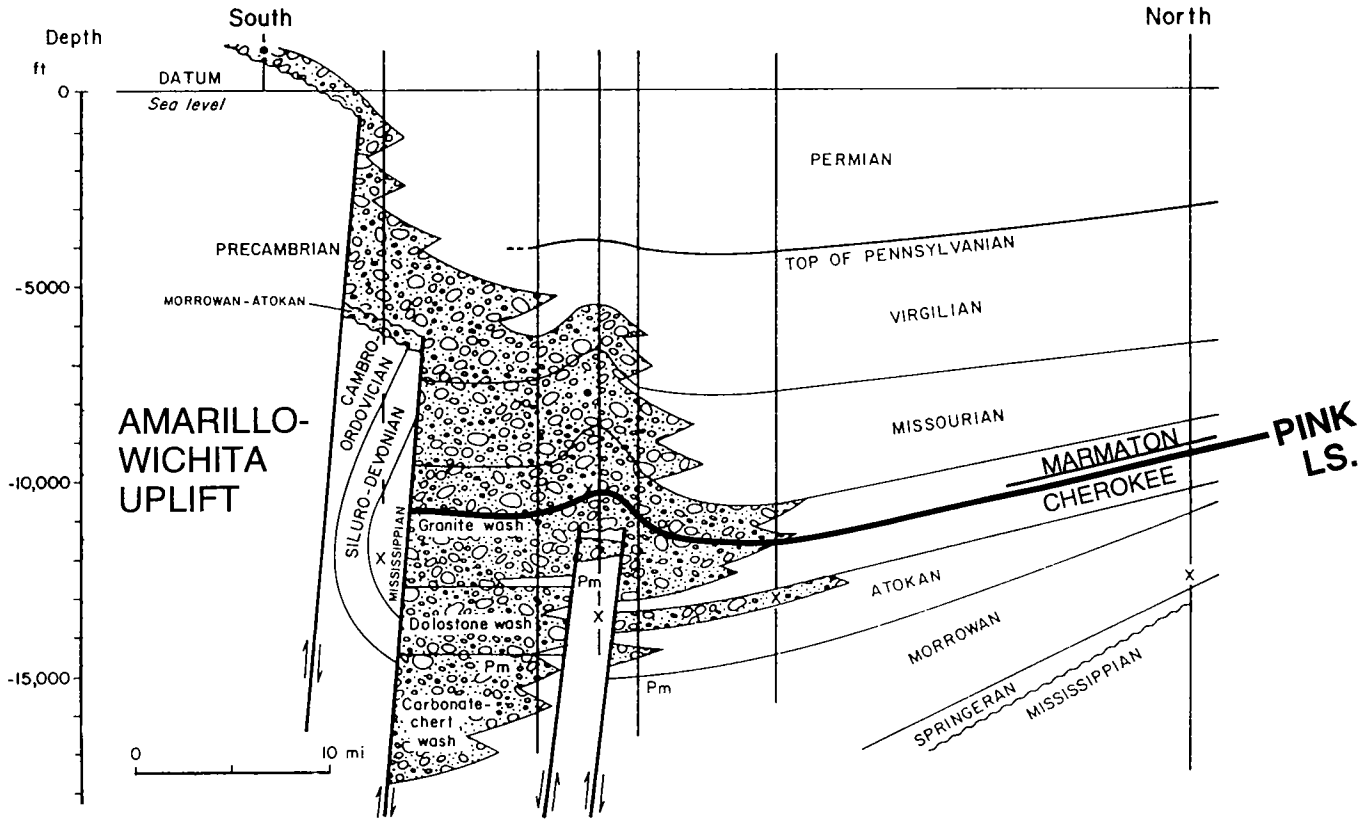

Figure 6. South–north schematic cross section showing correlations of major markers, coarse-grained clastic washes, and major structural blocks from Amarillo–Wichita uplift in south into Anadarko basin in north; line of cross sections located on Figure 5. (Modified from Lyday, 1985).

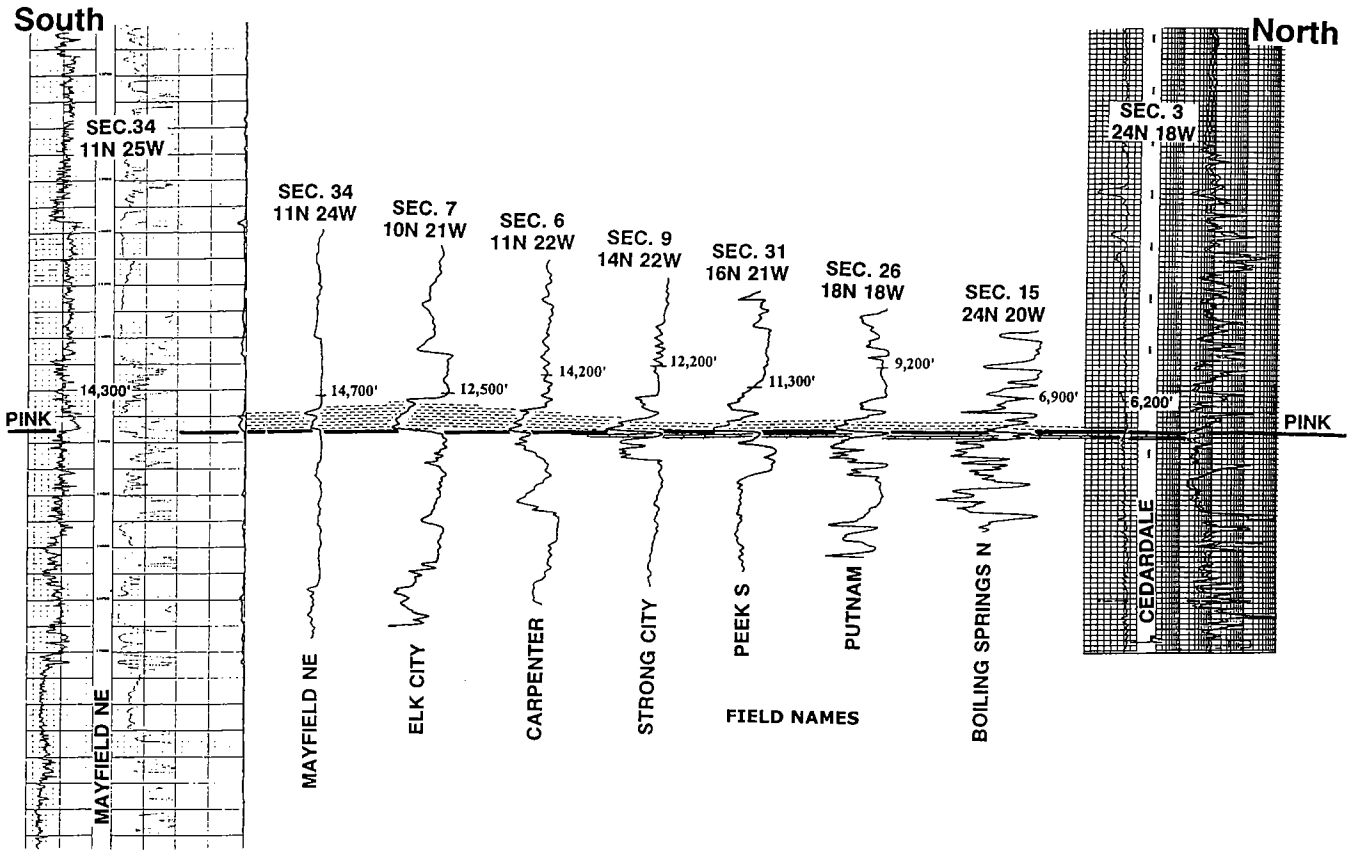

Figure 7. South–north correlation of sequence from Wichita–Amarillo uplift area (mountain-front sequence) generally northward into Anadarko basin, using Pink Limestone or southern equivalent section as datum. Well locations shown on Figure 5; names shown across bottom (Mayfield NE, Elk City, etc.) are 7½-minute quadrangles. None of the logs shown in the cross section are type logs for the three areas. The "Pink Lime" and shaly pattern above that bed form the key marker horizon in correlating these strata.

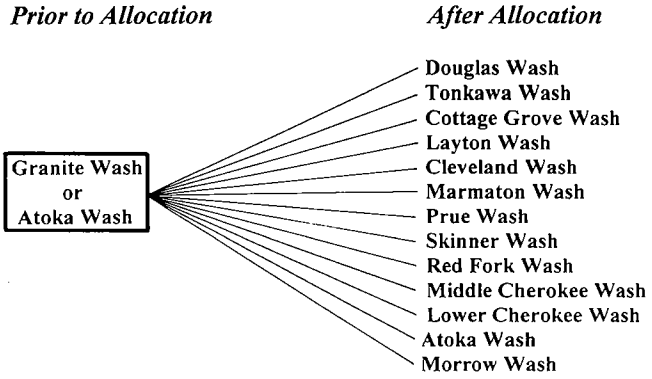

Figure 8. Diagram showing terminology of washes prior to current study and after study. This figure presents some idea of the magnitude of the nomenclatural problems and miscorrelation of these productive, coarse-clastic washes flanking the Wichita–Amarillo uplift.

Oklahoma Coalbed-Methane Completions, 1988 to 1996

Brian J. Cardott
Oklahoma Geological Survey
Norman, OK

ABSTRACT.—The coalbed-methane (CBM) industry in Oklahoma has developed rapidly since the first production of methane from the Hartshorne coal in 1988. The CBM play began in the Hartshorne coal beds (Hartshorne, Lower Hartshorne, and Upper Hartshorne; Middle Pennsylvanian) in the Arkoma basin. Completions in the Mulky and Rowe coal beds (Middle Pennsylvanian) on the northeast Oklahoma shelf began in 1994. Through 1996, 345 CBM completions were reported in Oklahoma, 214 in the basin, and 131 on the shelf. The CBM completions, separated into the Arkoma basin and the northeast Oklahoma shelf, are evaluated by coal bed, depth, initial-potential gas rate, and initial-produced water rate.

INTRODUCTION

Coalbed methane (CBM) was considered a hazard until the commercial production of CBM began in the San Juan basin of Colorado and New Mexico in 1977 and the Black Warrior basin of Alabama in 1980. Gas explosions in underground coal mines and safety studies of underground coal mines by the U.S. Bureau of Mines have demonstrated that Oklahoma coals contain large amounts of methane. Commercial production of CBM in Oklahoma began in 1988 with methane production from the Hartshorne coal (depth range of 611–716 ft; initial-potential gas rate of 41–45 MCFGPD (thousand cubic feet of gas per day) from seven wells in the Kinta anticline (sec. 27, T.8N., R.20E.) in Haskell County by Bear Productions. Until 1991, Bear Productions was the only CBM operator in Oklahoma.

The following discussion of Oklahoma CBM completions from 1988 to 1996 is based on information reported to the Oklahoma Corporation Commission. The names of coal beds are those reported by the operator and may not conform to usage accepted by the Oklahoma Geological Survey. Because not all of the wells are reported as CBM gas wells, some interpretation was necessary. Dual completions, including perforations of more than one coal bed, were made in some wells. Therefore, not all of the wells are exclusively CBM completions. This summary is incomplete because some wells may not have been known to be CBM wells or were not reported by the time of this compilation. This evaluation is based on reported CBM completions, which may or may not have been connected to a gas pipeline. Likewise, some completions may have produced gas but subsequently have been plugged. The data for this report were compiled in the coalbed-methane–completions table of the Oklahoma Coal Database and is available at the Oklahoma Geological Survey.

The coalfield in eastern Oklahoma is divided into the northeast Oklahoma shelf ("shelf") and the Arkoma basin ("basin") (Fig. 1). The commercial coal belt contains coal beds of minable thickness; coal beds in the noncommercial coal-bearing region are too thin or too deep for mining. CBM exploration has occurred in both areas.

Through 1996, 345 CBM completions were reported in Oklahoma, 214 in the basin and 131 on the shelf. Figure 2 summarizes the history of CBM completions by year and area. The CBM play began in the basin. There were five CBM completions on the shelf in 1994. In 1996, there were 28 CBM completions in the basin and 83 on the shelf, signaling increased activity on the shelf. The peak years for CBM completions in Oklahoma by area from 1988 to 1996 were 1992 in the basin (71 completions) and 1996 on the shelf (83 completions).

Figure 3 shows the main areas of CBM completions in 1988 to 1996. There are several areas in the basin and one large area on the shelf.

ARKOMA BASIN

Figure 4 shows the locations of 405 CBM completions in the basin through September 2000. CBM completions in the basin have been reported in Coal, Haskell, Hughes, Latimer, Le Flore, McIntosh, and Pittsburg Counties. In ascending order, the coal beds producing methane in the basin in 1988 to 1996 are the Lower Hartshorne (9 wells), Upper (and Lower) Hartshorne (10 wells), Hartshorne (undivided; 189 wells), McAlester (a CBM completion in Coal County

Cardott, B. J., 2001, Oklahoma coalbed-methane completions, 1988 to 1996, *in* Johnson, K. S. (ed.), Pennsylvanian and Permian geology and petroleum in the southern Midcontinent, 1998 symposium: Oklahoma Geological Survey Circular 104, p. 81–85.

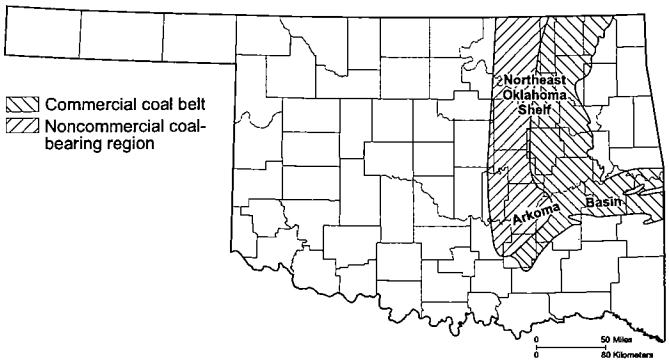

Figure 1. Map of Oklahoma coalfield.

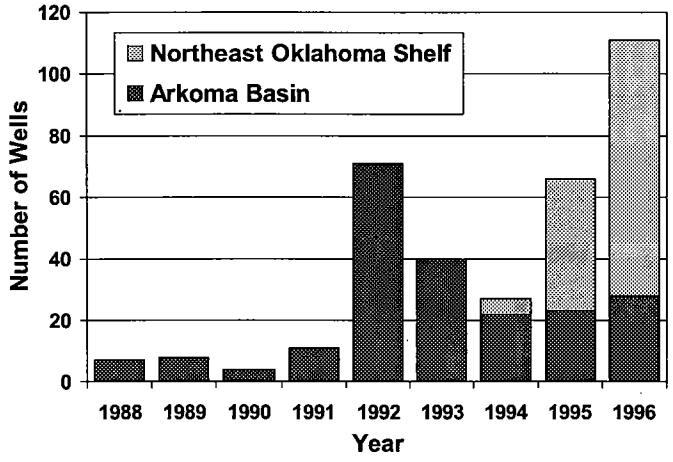

Figure 2. Histogram showing numbers of Oklahoma coalbed-methane completions, 1988 to 1996.

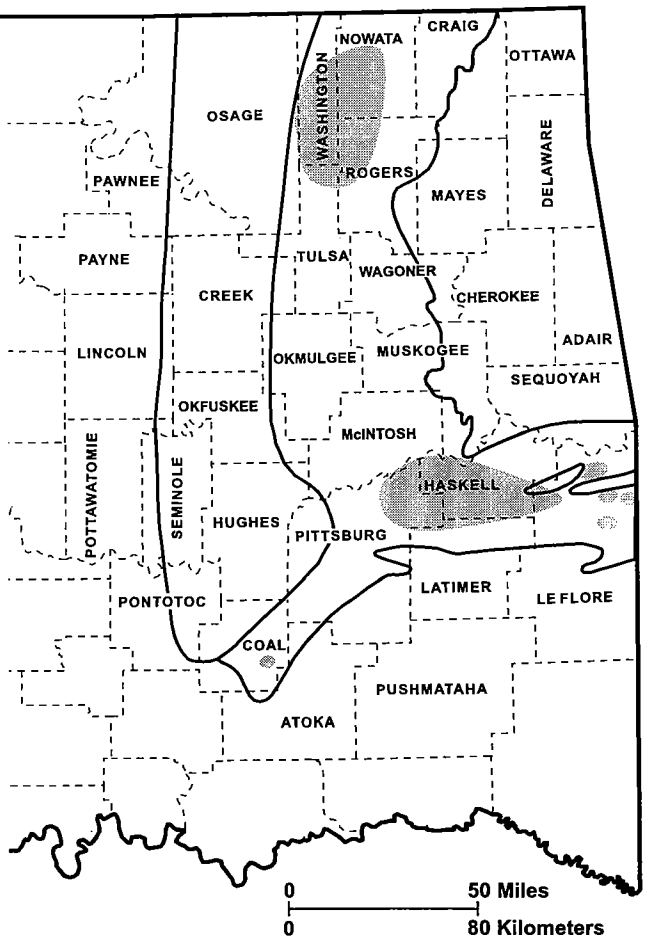

Figure 3. Map showing main areas of coalbed-methane completions, 1988 to 1996.

reported to be in the "Lehigh" coal is equivalent to the McAlester coal; 5 wells), and "Savanna" (McAlester coal?; 1 well) of Desmoinesian (Middle Pennsylvanian) age.

Figure 5 shows the depth range (in 200 ft increments) of CBM completions in the basin. Coal was perforated at depths-to-top of coal of 598–3,692 ft (average of 1,311 ft from 213 wells). Most of the wells produce methane from the Hartshorne coal beds at depths of 600–1,800 ft.

Initial-potential CBM rates range from a trace to 302 MCFGPD (average of 65 MCFGPD from 174 wells). Most of the wells produce 10–120 MCFGPD, with the mode at 30–49 MCFGPD (Fig. 6). The highest initial-potential gas rates are from the Hartshorne coal. Based on 174 completions with depth and initial potential pairs, Figure 7 shows no relationship between initial-potential gas rate and depth in the basin. Low gas rates (<50 MCFGPD) span the entire depth range.

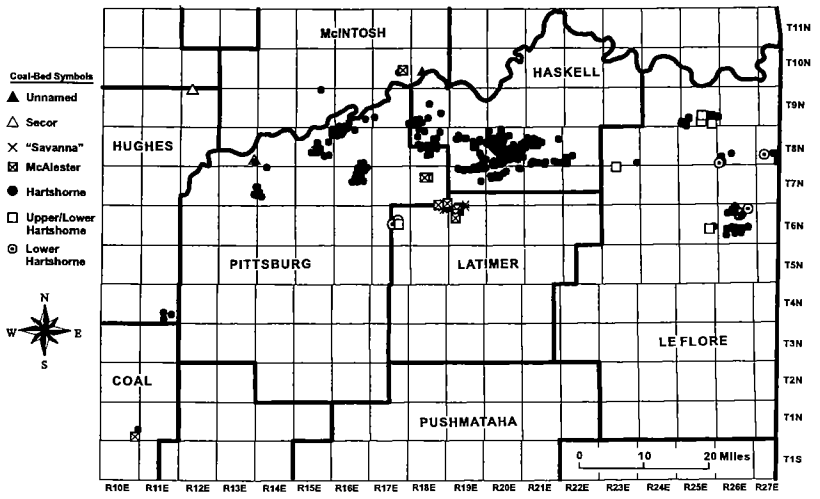

Figure 4. Map showing coalbed-methane completions in the Arkoma basin by coal bed, from 1988 to 1996 and including completions from 1997 to 2000.

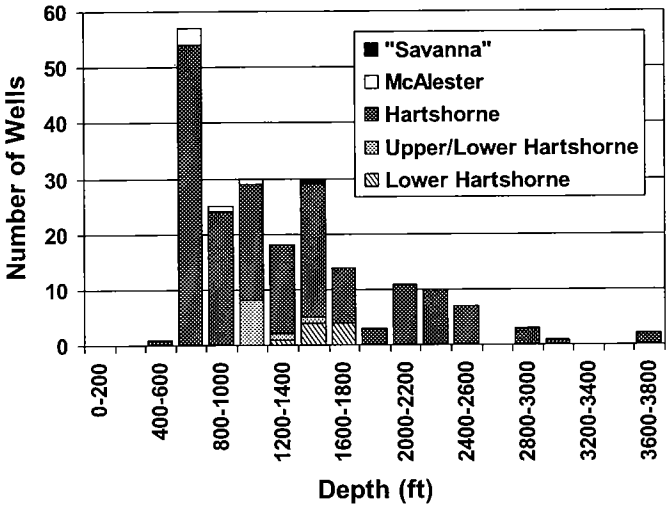

Figure 5. Histogram of numbers of coalbed-methane completions by depth (in feet) and coal bed in the Arkoma basin.

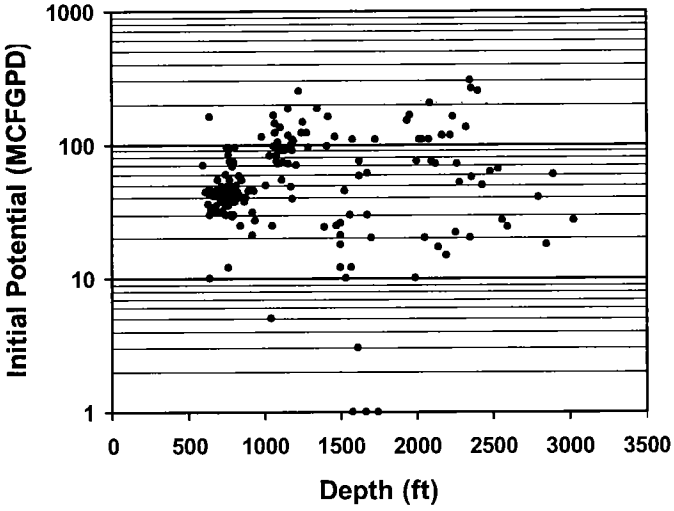

Figure 7. Scatter plot of initial-potential-gas rate (in thousand cubic ft of gas per day—MCFGPD) and depth (in feet) to top of coal in the Arkoma basin.

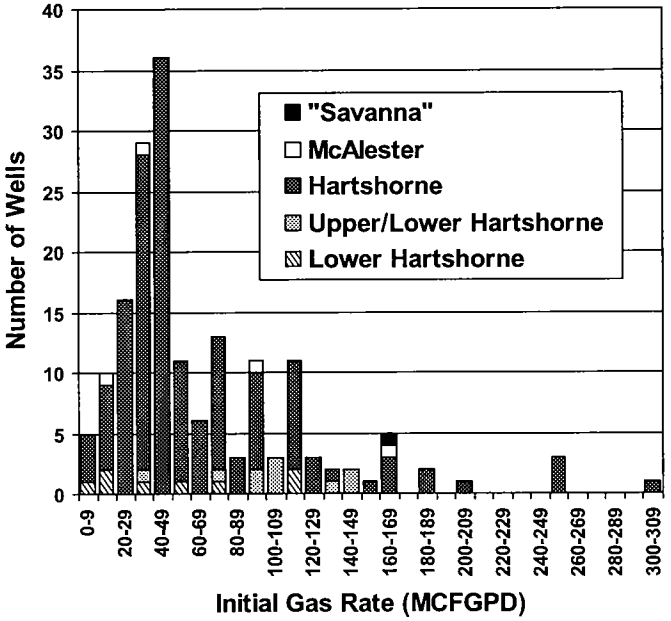

Figure 6. Histogram of numbers of coalbed-methane completions by initial-potential-gas rate (in thousand cubic feet of gas per day—MCFGPD) and coal bed in the Arkoma basin.

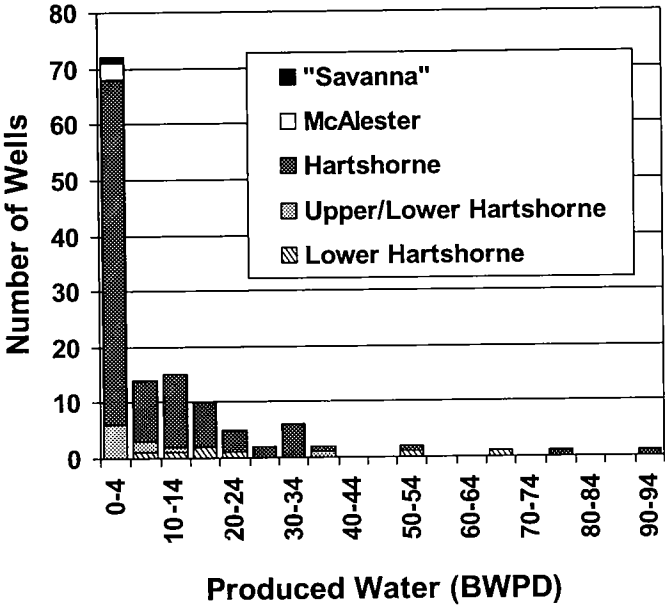

Figure 8. Histogram of numbers of coalbed-methane completions by produced water (in barrels of water per day—BWPD) and coal bed in the Arkoma basin.

The highest gas rates (>150 MCFGPD) are from depths of 600–2,500 ft, not associated with the deepest completions. Theoretically, gas content increases with increasing rank, depth, and reservoir pressure (Kim, 1977; Scott and others, 1995; Rice, 1996). However, gas production depends on many variables, including gas content, water volume, cleat mineralogy, permeability, porosity, and stimulation method.

Initial produced water ranged from 0–90 barrels of water per day (BWPD; average of 9 BWPD from 131 wells) in the basin. Most of the wells produced less than 20 BWPD (Fig. 8). Most Arkoma basin CBM completions are associated with anticlines and have relatively little produced water. An undisclosed amount of initial water production is frac water (introduced during fracture stimulation).

NORTHEAST OKLAHOMA SHELF

Figure 9 shows the locations of 641 CBM completions on the shelf through September 2000. CBM completions on the shelf have been reported in Craig, Nowata, Osage, Rogers, Tulsa, and Washington Counties. In ascending order, the coal beds producing meth-

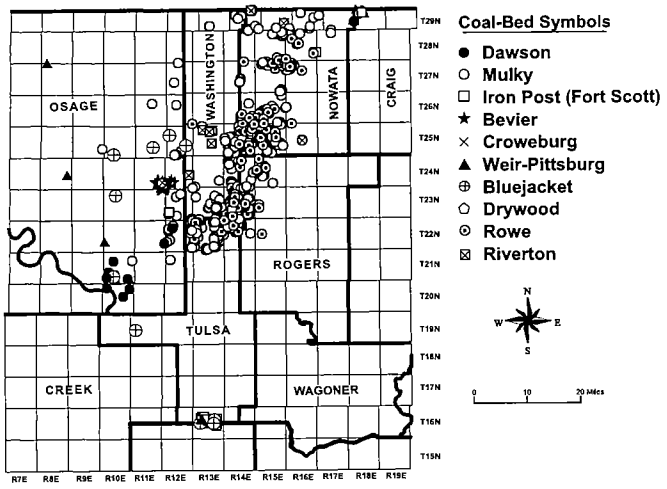

Figure 9. Map showing location of coalbed-methane completions in the northeast Oklahoma shelf by coal bed from 1988 to 1996 and including completions from 1997 to 2000.

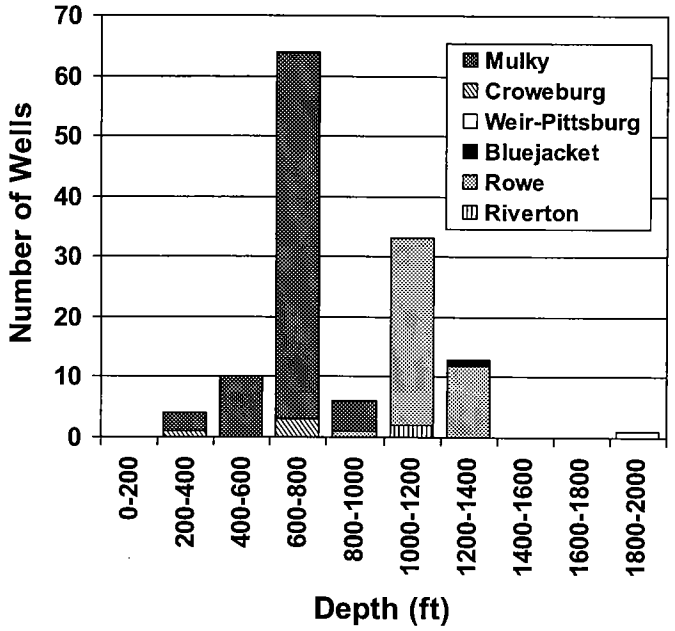

Figure 10. Histogram of number of coalbed-methane completions by depth (in feet) and coal bed in the northeast Oklahoma shelf.

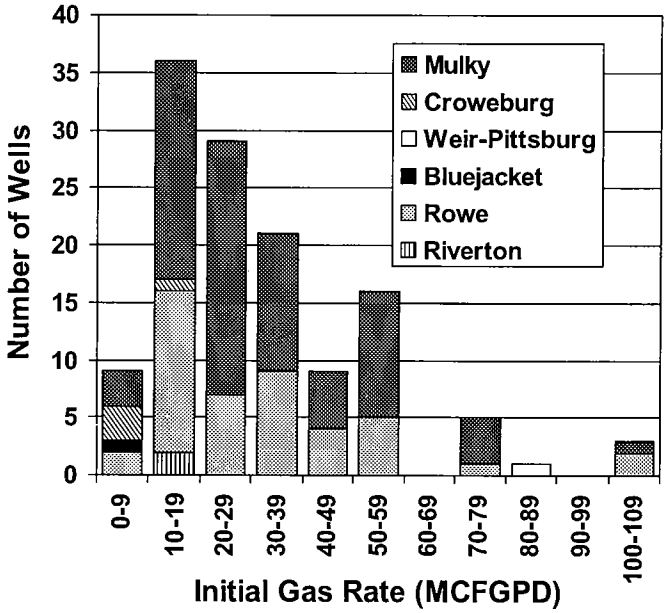

Figure 11. Histogram of number of coalbed-methane completions by initial-potential-gas rate (in thousand cubic feet of gas per day—MCFGPD) and coal bed in the northeast Oklahoma shelf.

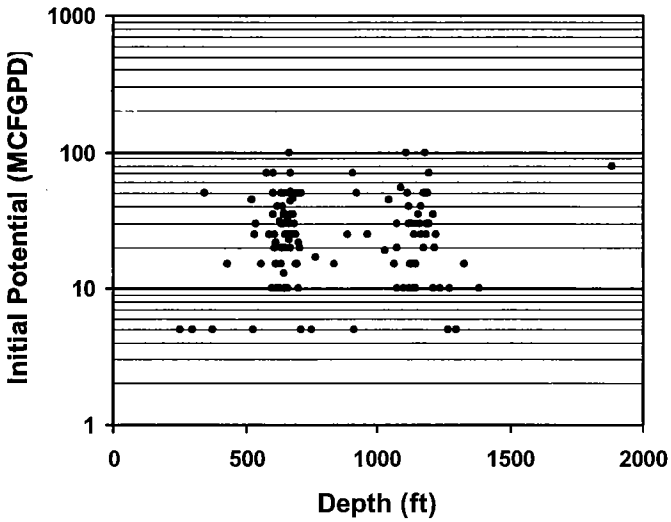

Figure 12. Scatter plot of initial-potential-gas rate (in thousand cubic feet of gas per day—MCFGPD) and depth (in ft) to top of coal in the northeast Oklahoma shelf.

ane on the shelf in 1988 to 1996 are the Riverton (2 wells), Rowe (44 wells), Bluejacket (1 well), Weir-Pittsburg (1 well), Croweburg (4 wells), and Mulky (79 wells) of Desmoinesian (Middle Pennsylvanian) age.

Figure 10 shows the depth range (in 200 ft increments) of CBM completions on the shelf. Coal was perforated at depths-to-top of coal of 256–1,884 ft (average of 840 ft from 131 wells). Most of the wells on the shelf are in the Mulky coal (depth range of 256–924 ft). The Mulky coal is the uppermost coal bed in the Senora Formation and occurs at the base of the Excello Shale Member (Hemish, 1987). The Mulky coal ranges from bituminous coal to carbonaceous shale, with increasing amounts of mineral matter (carbonaceous shale contains >50% mineral matter by weight or <30% carbonaceous matter by volume, Schopf, 1956; impure coal contains 25–50% mineral matter by weight, ASTM, 1994). The next most important CBM reservoir on the shelf is the Rowe coal (916–1,388 ft). The deepest CBM completion on the shelf (1,884 ft) is in the Weir-Pittsburg coal in Osage County.

Initial-potential CBM rates range from 5 to 100 MCFGPD (average of 29 MCFGPD from 129 wells; Fig. 11). Initial gas rates in both the Mulky and Rowe coal

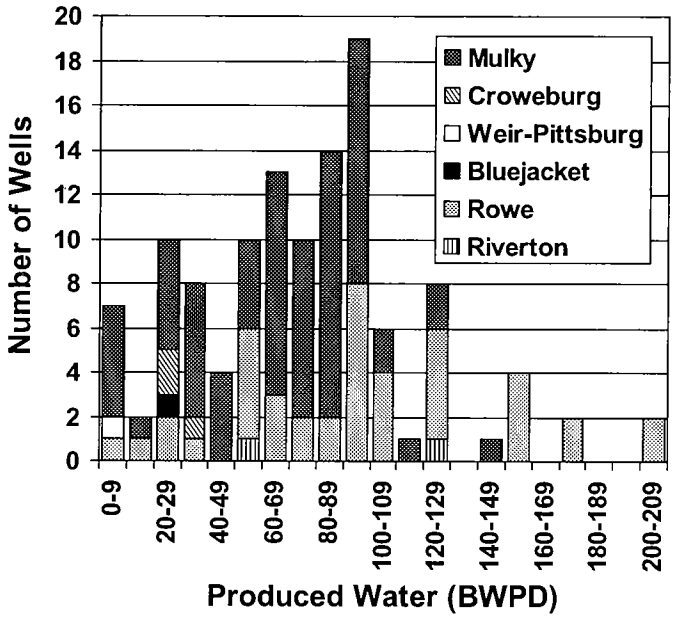

Figure 13. Histogram of number of coalbed-methane completions by produced water (in barrels of water per day—BWPD) and coal bed in the northeast Oklahoma shelf.

beds range from 5 to 100 MCFGPD. Figure 12 shows the relationship of depth and initial-potential gas rate for the shelf.

Initial-produced water ranged from 0 to 1,201 BWPD (barrels of water per day) with an average of 82 BWPD from 122 wells. Produced water follows a Gaussian distribution, with a mode at 80–99 BWPD, excluding one well with 1,201 BWPD (Fig. 13). Most of the water is suspected to be formation water and not frac water.

CONCLUSIONS

The Oklahoma CBM industry began in the basin in 1988. The play spread to the shelf in 1994. Through 1996, 345 CBM completions were reported in Oklahoma, 214 in the basin and 131 on the shelf. Nearly 60% more completions occurred in the basin than on the shelf. The primary CBM objectives were the Hartshorne coals (208 wells) in the basin and the Mulky (79 wells) and Rowe (44 wells) coals on the shelf. There were nearly twice as many completions in the Mulky coal as in the Rowe coal.

The range in depth of the CBM completions was 598–3,692 ft (average of 1,311 ft from 213 wells) in the basin, and 256–1,884 ft (average of 840 ft from 131 wells) on the shelf. Initial-potential gas rates range from a trace to 302 MCFGPD (average of 65 MCFGPD from 174 wells) in the basin, and from 5 to 100 MCFGPD (average of 29 MCFGPD from 129 wells) on the shelf. The average initial-potential gas rate in the basin is more than twice the average on the shelf.

Produced water ranged from 0 to 90 BWPD (average of 9 BWPD from 131 wells) in the basin, and from 0 to 1,201 BWPD (average of 82 BWPD from 122 wells) on the shelf. Clearly, produced water is a bigger problem on the shelf than in the basin.

REFERENCES CITED

ASTM, 1994, Standard terminology of coal and coke, *in* Annual book of ASTM standards: gaseous fuels; coal and coke: American Society for Testing and Materials, sec. 5, v. 5.05, Standard D 121-94, p. 137–148.

Hemish, L. A., 1987, Names of coal beds in the northeastern Oklahoma shelf area: Oklahoma Geology Notes, v. 47, p. 96–113.

Kim, A. G., 1977, Estimating methane content of bituminous coalbeds from adsorption data: U.S. Bureau of Mines Report of Investigations 8245, 22 p.

Rice, D. D., 1996, Geologic framework and description of coalbed gas plays, *in* Gautier, D. L.; and others (eds.), 1995 National assessment of United States oil and gas resources—results, methodology, and supporting data: U.S. Geological Survey Digital Data Series DDS-30, release 2, CD-ROM.

Schopf, J. M., 1956, A definition of coal: Economic Geology, v. 51, p. 521–527.

Scott, A. R.; Zhou, N.; and Levine, J .R., 1995, A modified approach to estimating coal and coal gas resources: example from the Sand Wash basin, Colorado: American Association of Petroleum Geologists Bulletin, v. 79, p. 1320–1336.

Geometry of the Triangle Zone and Duplex Structure in the Wilburton Gas Field Area of the Arkoma Basin, Southeastern Oklahoma

Ibrahim Çemen, Ata Sagnak, and Saleem Akthar
Oklahoma State University
Stillwater, Oklahoma

ABSTRACT.—The Arkoma basin, located in southeastern Oklahoma and western Arkansas, has long been recognized as the foreland basin of the Ouachita fold and thrust belt. The Wilburton gas field is located in the central part of the Arkoma basin and produces mostly from the lower Atokan Spiro sandstone. The Wilburton gas field area contains a well-developed triangle zone between the mildly compressed Arkoma basin and frontal Ouachitas fold-thrust belt. The triangle zone is floored by the lower Atokan detachment (LAD) and flanked by the Choctaw fault to the south and the Carbon fault to the north. The south-dipping Choctaw fault is the leading-edge thrust of the belt, and contains several south-dipping imbricate fan thrust faults in its hanging wall. Below the triangle zone, a duplex structure is formed by hinterland-dipping, imbricate thrust faults that splay in a break-forward sequence of thrusting from the Springer detachment (the floor thrust). The imbricate thrusts join to the LAD in the Atoka Formation. This geometry qualifies the LAD as the roof thrust of the duplex structure. The LAD continues in the Atoka Formation northward and displaces the Red Oak Sandstone before reaching a shallower depth and forming the Carbon fault as a north-dipping backthrust below the San Bois syncline, which involves the Desmoinesian rocks.

We present four balanced structural cross sections to illustrate the geometry of the triangle zone and duplex structure in the Wilburton gas field area. The cross sections are based on the updated surface geologic maps of the Oklahoma Geological Survey, wire-line well-log data, and our interpretations of seismic profiles donated by Exxon Oil Company. They are restored by using the "key-bed" method to find the percentage of shortening that was experienced in the area due to thrusting. When restored to their position at the time of the Spiro sandstone deposition, the cross sections suggest about 60% shortening in the Wilburton area.

INTRODUCTION

The Ouachita Mountains were formed during the compressional Pennsylvanian Ouachita orogeny and are elongate tectonic features extending in an east–west direction in eastern Oklahoma and western Arkansas (Fig. 1). Based on the structural style and stratigraphy, the Ouachita Mountains in Oklahoma are divided into three distinct assemblages: the frontal belt, the central belt, and the Broken Bow uplift. The Arkoma basin is a foreland basin formed during the Pennsylvanian Ouachita orogeny.

The Choctaw fault (CHF of Fig. 2) is generally considered the boundary between the frontal Ouachitas and the Arkoma foreland basin. The frontal Ouachitas contain typical imbricated thrust faults with tight to overturned folds of a fold-thrust belt. Broad to open folds and minor faults generally found in the foreland basins characterize the Arkoma basin. It contains up to 15,000-ft-thick Atokan sedimentary rocks that overlie the Morrowan strata throughout the frontal belt. The zone of gradation from the structures of the fold-thrust belt of the frontal Ouachitas to those of the Arkoma basin is usually referred as the transition zone.

Modern structural-geology studies of the Ouachita Mountains frontal belt and the Arkoma basin started in the mid- to late 1980s. Suneson (1995) summarized the results of these studies. Several of these studies proposed the presence of a triangle zone with a backthrust (Hardie, 1988; Camp and Ratliff, 1989; Reeves and others, 1990; Milliken, 1988; Perry and Suneson, 1990; Wilkerson and Wellman, 1993; Valderrama and others, 1994). The geometry and areal extent of the triangle zone, however, remains controversial. Some workers have suggested that all the thrust faults in the area are south-dipping (Bertagne and Leising,

Çemen, Ibrahim; Sagnak, Ata; and Akthar, Saleem, 2001, Geometry of the triangle zone and duplex structure in the Wilburton gas field area of the Arkoma basin, southeastern Oklahoma, *in* Johnson, K. S. (ed.), Pennsylvanian and Permian geology and petroleum in the southern Midcontinent, 1998 symposium: Oklahoma Geological Survey Circular 104, p. 87–98.

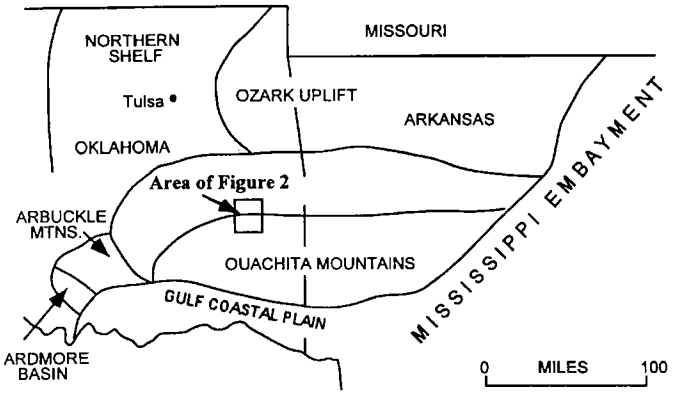

Figure 1. Map of major geologic provinces of eastern Oklahoma and western Arkansas (from Johnson, 1988).

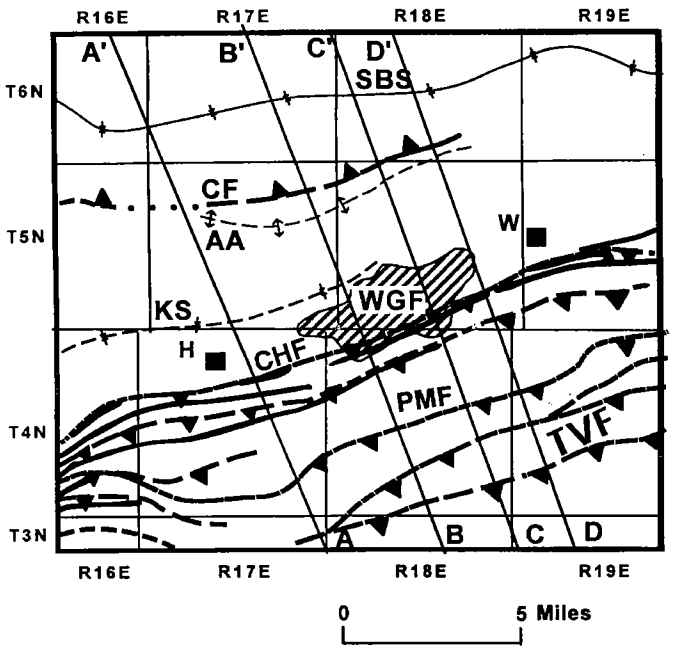

Figure 2. Simplified map of the Wilburton gas field (WGF—dark-gray area) and surrounding areas showing major structural features, outcrops of the Spiro sandstone (thick, light-gray lines), and lines of cross sections (see Figs. 6–9). Abbreviations: H—Hartshorne, W—Wilburton, AA—Adamson anticline, CF—Carbon fault, CHF—Choctaw fault, KS—Kiowa syncline, PMF—Pine Mountain fault, SBS—San Bois syncline, TVF—Ti Valley fault.

1989; Tilford, 1990), and, therefore, that a triangle zone is not needed. The presence of the duplex structure proposed by some studies (Roberts, 1992; Wilkerson and Wellman, 1993; Valderrama and others, 1994; Çemen and others, 1995, 1997; Al-Shaieb and others, 1995) is also controversial.

This paper is based on a subsurface structural study conducted as part of an Oklahoma Center for Advancement in Science and Technology (OCAST) project to examine overthrusted natural-gas reservoirs in the Wilburton gas-field area (WGF of Fig. 2) of the Arkoma basin. During the project, we constructed eight balanced structural cross sections to determine detailed configuration and geometry of the thrusting in the Wilburton gas-field area; four are used in this paper. The cross sections are based on updated surface geologic maps published by Oklahoma Geological Survey (Suneson and Ferguson, 1989; Hemish, 1992, 1995; Suneson, 1996), on wire-line well-log data, and on our interpretation of many seismic profiles provided by Exxon Oil Company.

The main purpose of this paper is to discuss the structural geometry of thrust faulting in the Wilburton gas-field area through the discussion of four out of eight balanced structural cross sections that were constructed during the OCAST project. We will first briefly outline the Pennsylvanian stratigraphy and then discuss the structural features of the area.

STRATIGRAPHY

Exposed in the Wilburton gas field and surrounding areas are mostly Pennsylvanian rocks of the Atokan and Desmoinesian Series. The pre-Pennsylvanian rock units of the Arkoma basin and Ouachita Mountains are shown, in a generalized form, in the columnar section (Fig. 3). Detailed descriptions of the pre-Pennsylvanian formations are contained in papers by Ham (1973), Johnson (1988), and Sutherland (1988). In this section, we will briefly describe the Pennsylvanian rocks of the Wilburton area.

The Atoka Formation is the Pennsylvanian rock unit that is most widely exposed in the area. It is generally divided into lower, middle, and upper Atokan. It is roughly 70% shale in the central and southern parts of the Arkoma basin and contains lenses and tongues of about 15 sandstone units mostly recognized only in the subsurface (Fig. 4). Atokan deposition in the basin was characterized by a series of meandering fluvial systems and deltas that had their origin in the north and northeast (Houseknect and Kacena, 1983; Sutherland, 1988). The thickness of the Atoka Formation ranges from several hundred feet to well over 15,000 ft in the basin (Johnson, 1988).

A regional unconformity is present between the Atokan and Morrowan sections in the northern margin of the basin. However, the pre-Atokan unconformity is absent in the southern section of the basin. The lowermost Atokan is represented by the Spiro sandstone and a persistent overlying shale. Sedimentation in this interval was initiated in Oklahoma with a source from the northeast by the development of fluvial systems and small deltas on the eroded surface of the underlying Wapanucka Formation (Sutherland, 1988).

The middle Atokan interval in Oklahoma consists predominantly of shale with a few thick sandstone units. The Red Oak Sandstone (Fig. 4) is a major sandstone in this interval and is readily observed in the well logs in the area. Vedros and Visher (1978) interpreted the Red Oak Sandstone as a submarine-fan deposit. The upper Atokan strata are composed predominantly of shallow-shelf and deltaic rocks (Sutherland, 1988).

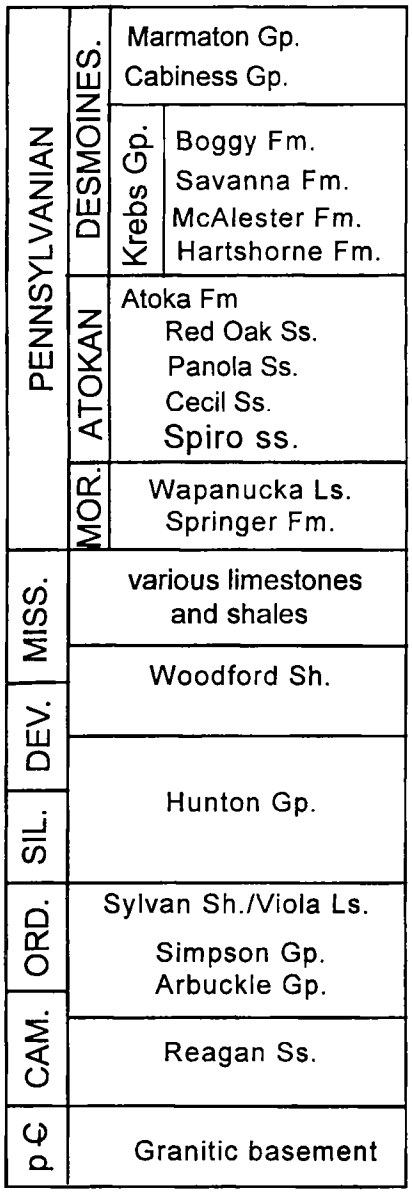

Figure 3. General stratigraphy of Oklahoma portion of the Arkoma basin (modified from Houseknecht and McGilvery, 1990). The Spiro sandstone of the Atoka Formation is the main gas reservoir in the Wilburton area. Abbreviations: MOR—Morrowan, CAM—Cambrian, ORD—Ordovician, SIL—Silurian, DEV—Devonian, MISS—Mississippian.

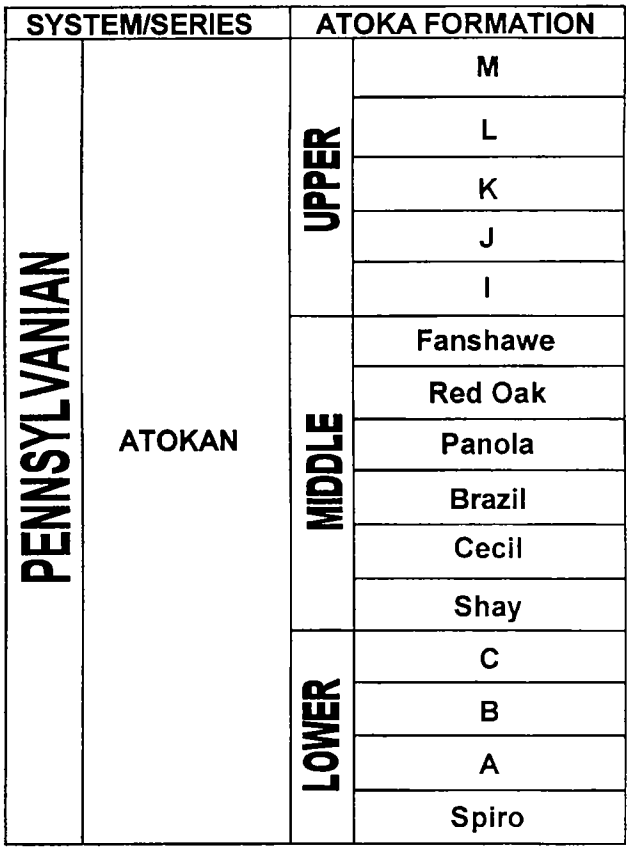

Figure 4. Chart showing general stratigraphy of the informally named sandstone units of the Atoka Formation. These 15 sandstone units are contained within about 15,000-ft-thick Atokan strata.

The Desmoinesian Series in the Arkoma basin and adjacent areas to the northwest consists of the Krebs, Cabaniss, and Marmation Groups (Fig. 3). In the Wilburton area, only the rocks of the Krebs Group (the Hartshorne, McAlester, Savanna, and Boggy Formations) crop out; however, strata assigned to the overlying Cabaniss and Marmation Groups are found along the northwest margin of the Arkoma basin. The Hartshorne Formation gradationally overlies the Atoka Formation. Sutherland (1988) interpreted the Hartshorne Formation as being deposited in high constructive, tidally influenced deltaic systems. He also concluded that the overlying McAlester through Savanna Formations were deposited during a series of transgressions and regressions and that the Boggy Formation was deposited in a deltaic complex.

STRUCTURAL GEOLOGY

In this section, we describe the structural features of the Wilburton area based on four updated versions of the eight balanced structural cross sections constructed during the OCAST project. We attempted to construct the cross sections using kink-band style of folding and the ramp-flat thrust model developed by Suppe (1983) and successfully used by Woodward (1985), Namson and Davis (1988), and Mitra (1986, 1988). However, we could not use this model because of the presence of competent sandstones scattered in about 15,000-ft-thick incompetent shale units of the Atoka Formation in the frontal Ouachitas and Arkoma basin (Fig. 4).

Kink folds are known to develop only in sedimentary successions either where the rocks are (1) very uniformly bedded, (2) possess regular bed thicknesses, *and* (3) exhibit periodic alternations of competent and incompetent layers, or where they exhibit a rather uniform anisotropy. A competent unit surrounded by incompetent rocks above and below develops a buckle fold by horizontal shortening (Ramsay, 1992), where upward and downward deflection of shortening of incom-

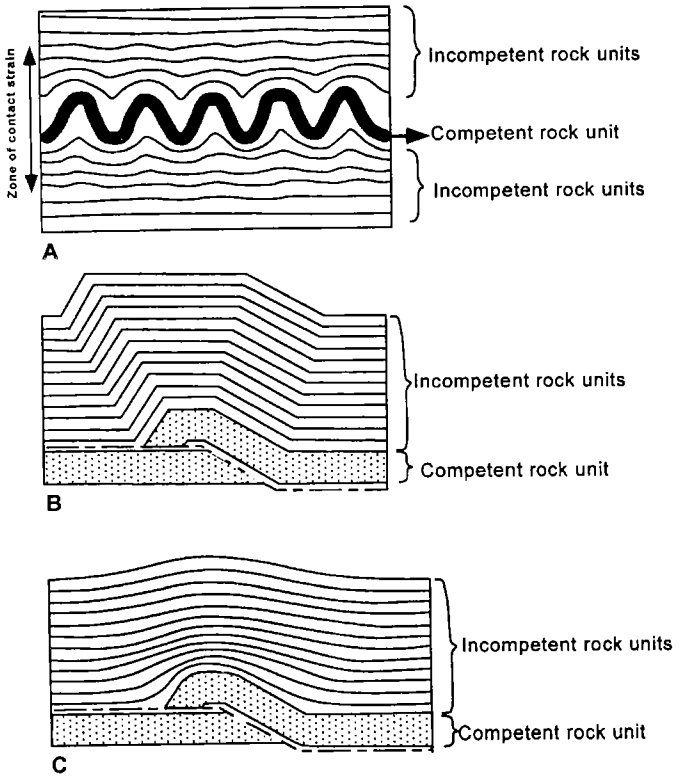

Figure 5. A geometric problem associated with using fault-bend–fold model of Suppe (1983) with kink folds and a modification to the model suggested by Ramsay (1992) with buckle folds. Modified from Ramsay (1992). (A) Typical active buckle folds developed by shortening of a competent rock unit surrounded by incompetent rock units. Buckle fold develops by shortening of the competent rock unit and causes the formation of progressively deamplifying folds in the zone of contact strain. (B) Classic fault-bend–fold model with kink fold above a competent rock unit overlain by incompetent rock units. (C) A possible modification to the fault-bend–fold geometry. The competent rock unit shows buckle fold geometry with deamplifying folds in the zone of contact strain.

petent rocks progressively decreases away from the surface of the buckled layer in the zone of contact strain (Fig. 5A). Ramsay (1992) suggested a possible modification to the fold-bend model where the competent layer shows buckle-fold geometry with deamplifying folds in the zone of contact strain (Fig. 5B,C).

We observe a similar situation in the Arkoma basin above the competent Spiro sandstone, which is surrounded by incompetent beds. Moreover, within the thick shale sequence of the Atoka Formation above the Spiro sandstone, a few competent beds are present, such as the Cecil, Red Oak, and Panola sandstones (Figs. 3, 4). Therefore, we used concentric folding in our cross sections (Figs. 6–9).

The series of cross sections A–A′ through D–D′ (Figs. 6–9) are constructed perpendicular to the tectonic-transport direction (from the south–southeast toward the north–northwest) (see Fig. 2). The control wells for these cross sections are given in the Appendix. Because the cross sections are constructed with this orientation, they show displacements along the thrust faults when appropriate piercing points are located in the hanging wall and footwall of the thrust faults. In all cross sections (Figs. 6–9), the Spiro sandstone is used as the key bed to determine the structural geometry. The Wapanucka Formation and the Spiro sandstone are not identified individually. The entire thickness is referred to as the Spiro and is assumed to have uniform thickness in the study area. Other units identified in the cross sections include the Red Oak sandstone, a marker bed called "marker X," the Hartshorne, McAlester, Savanna, and Boggy Formations. Like the Spiro sandstone, the Red Oak Sandstone and marker X are identified in the logs at their tops, and their thicknesses are considered to be constant throughout the study area.

The hanging wall block of the Choctaw fault in the cross sections contains many south-dipping listric thrust faults, splaying both from the Choctaw fault and from the main detachment surface within the Woodford Shale. The footwall block of the Choctaw fault displays two detachment surfaces, a duplex structure, and a triangle zone.

Choctaw Fault

The west–southwest to east–northeast trending Choctaw fault serves as a boundary between the Arkoma basin and the Ouachita Mountains (Fig. 2) and is the northernmost, south-dipping thrust fault in the Wilburton area. It extends more than 120 mi within Oklahoma. The hanging wall of the Choctaw fault contains south-dipping thrust faults exposed on the surface. Many asymmetrical to the north or overturned folds, formed by the thrust faults, are found in the hanging walls of the individual thrust faults. The Spiro sandstone is displaced by these faults (Figs. 6–9). Two of these thrusts are the Ti Valley and Pine Mountain faults, and several other unnamed thrust faults are also mapped (Fig. 2).

Ti Valley Fault

The Ti Valley fault is one of the major thrust faults in the Ouachita fold and thrust belt (Suneson, 1988), extending about 240 mi from near Atoka, Oklahoma, to near Jacksonville, Arkansas. In the Wilburton area, the Ti Valley fault trends west–southwest to east–northeast and has a steep dip of about 70–80°. As mapped on Oklahoma Geological Survey maps by Suneson and Ferguson (1989), Hemish (1992, 1995), and Suneson (1996), the Atoka Formation is the only unit present both on the north and the south of the Ti Valley fault.

The Ti Valley fault in the cross sections is interpreted as flattening at depth. The displacement along the Ti Valley fault could not be determined because of the lack of a piercing point to locate a bed on the hanging wall and footwall of the thrust fault.

Pine Mountain Fault

The Pine Mountain fault strikes west–southwest to east–northeast and is subparallel to the Ti Valley and

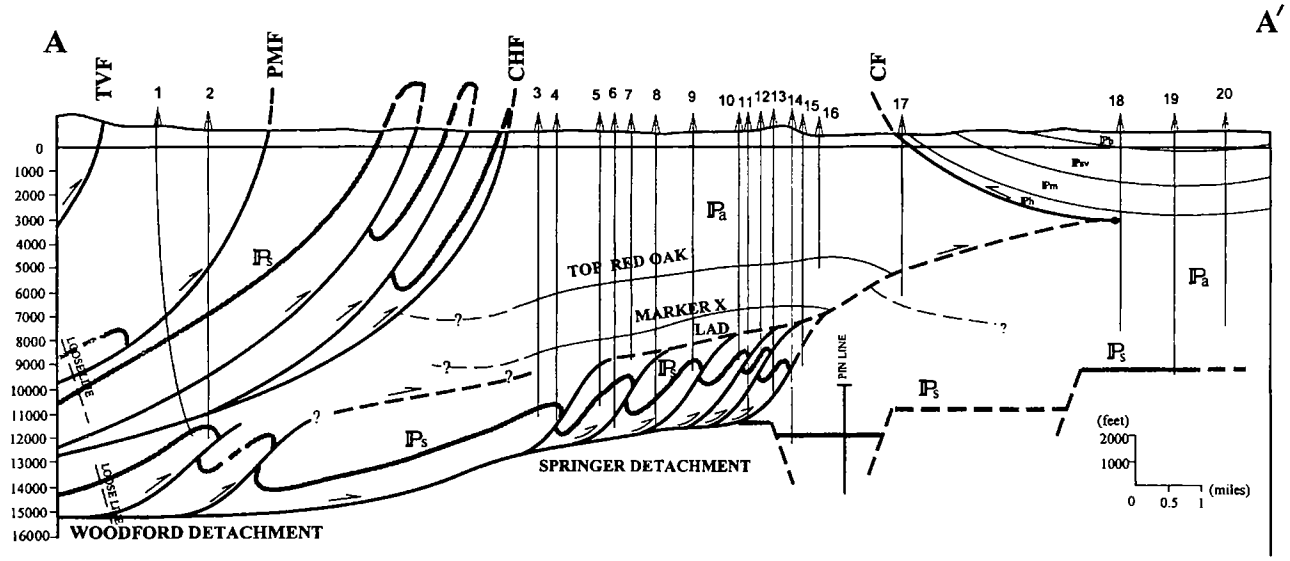

Figure 6. Cross section A–A′ showing the presence of the triangle zone, duplex structure, and other structural features in the Wilburton gas-field area. Line of cross section is located on Figure 2; well numbers are located and described in Appendix. Structural abbreviations: CF—Carbon fault, CHF—Choctaw fault, LAD—lower Atokan detachment, PMF—Pine Mountain fault, TVF—Ti Valley fault. Stratigraphic abbreviations: IPa—Atoka, IPb—Boggy, IPh—Hartshorne, IPm —McAlester, IPs—Spiro sandstone, IPsv—Savanna.

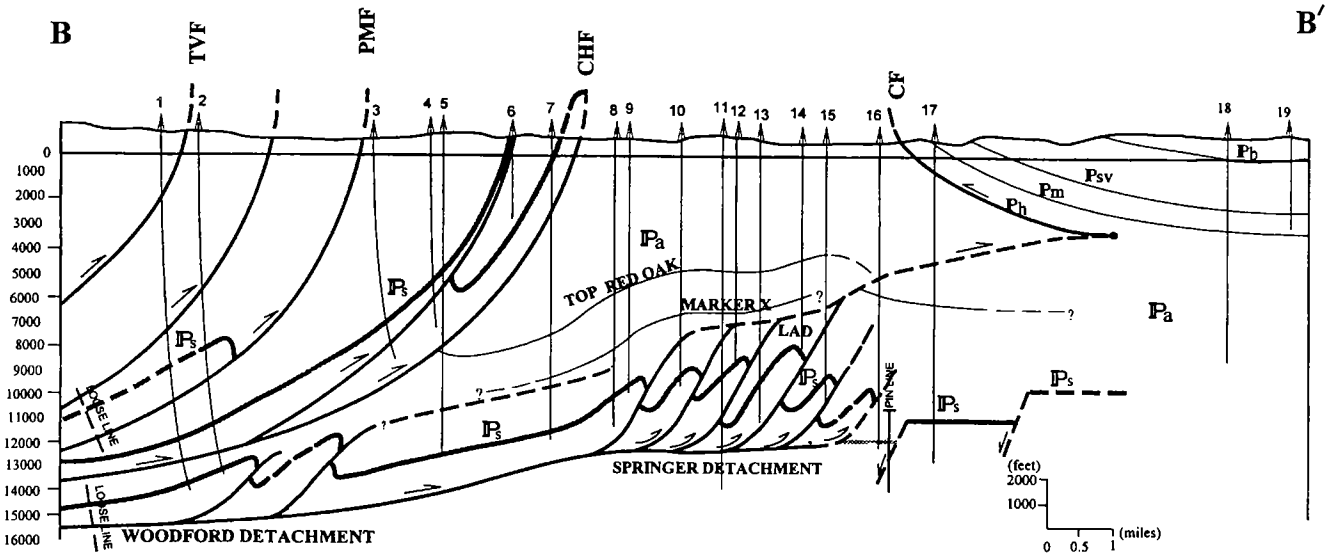

Figure 7. Cross section B–B′ showing the presence of the triangle zone, duplex structure, and other structural features in the Wilburton gas-field area. Line of cross section is located on Figure 2; well numbers are located and described in Appendix. Structural abbreviations: CF—Carbon fault, CHF—Choctaw fault, LAD—lower Atokan detachment, PMF—Pine Mountain fault, TVF—Ti Valley fault. Stratigraphic abbreviations: IPa—Atoka, IPb—Boggy, IPh—Hartshorne, IPm —McAlester, IPs—Spiro sandstone, IPsv—Savanna.

Choctaw faults. It dips roughly 70–80° to the south. Seismic profiles and wire-line–log data suggest that the fault loses its dip at depth and is a splay from either the Woodford detachment or the Choctaw fault. The displacement measured from the cross sections shows a minimum of 4,100 ft to a maximum of more than 7,500 ft of displacement (Figs. 7, 8).

Basal Detachment Surfaces

The Woodford and Springer detachments have long been recognized as the two basal detachment surfaces of the frontal Ouachitas fold-thrust belt. Locating these two detachment surfaces in the subsurface was primarily dependent on the availability of data. The seismic

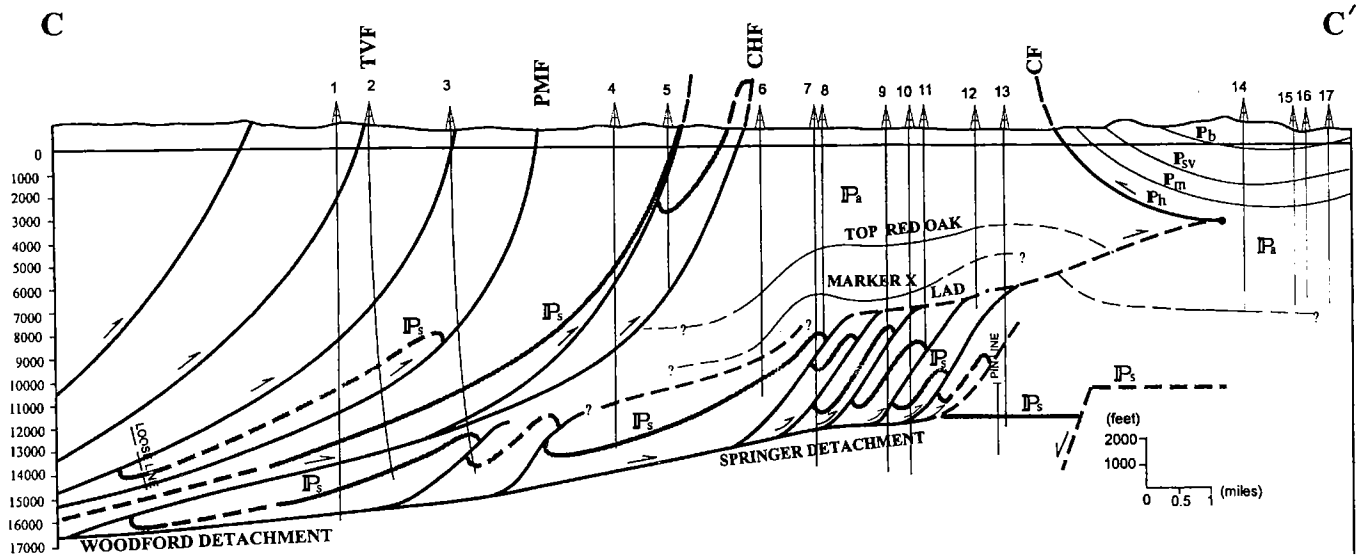

Figure 8. Cross section C–C′ showing the presence of the triangle zone, duplex structure, and other structural features in the Wilburton gas-field area. Line of cross section is located on Figure 2; well numbers are located and described in Appendix. Structural abbreviations: CF—Carbon fault, CHF—Choctaw fault, LAD—lower Atokan detachment, PMF—Pine Mountain fault, TVF—Ti Valley fault. Stratigraphic abbreviations: IPa—Atoka, IPb—Boggy, IPh—Hartshorne, IPm —McAlester, IPs—Spiro sandstone, IPsv—Savanna.

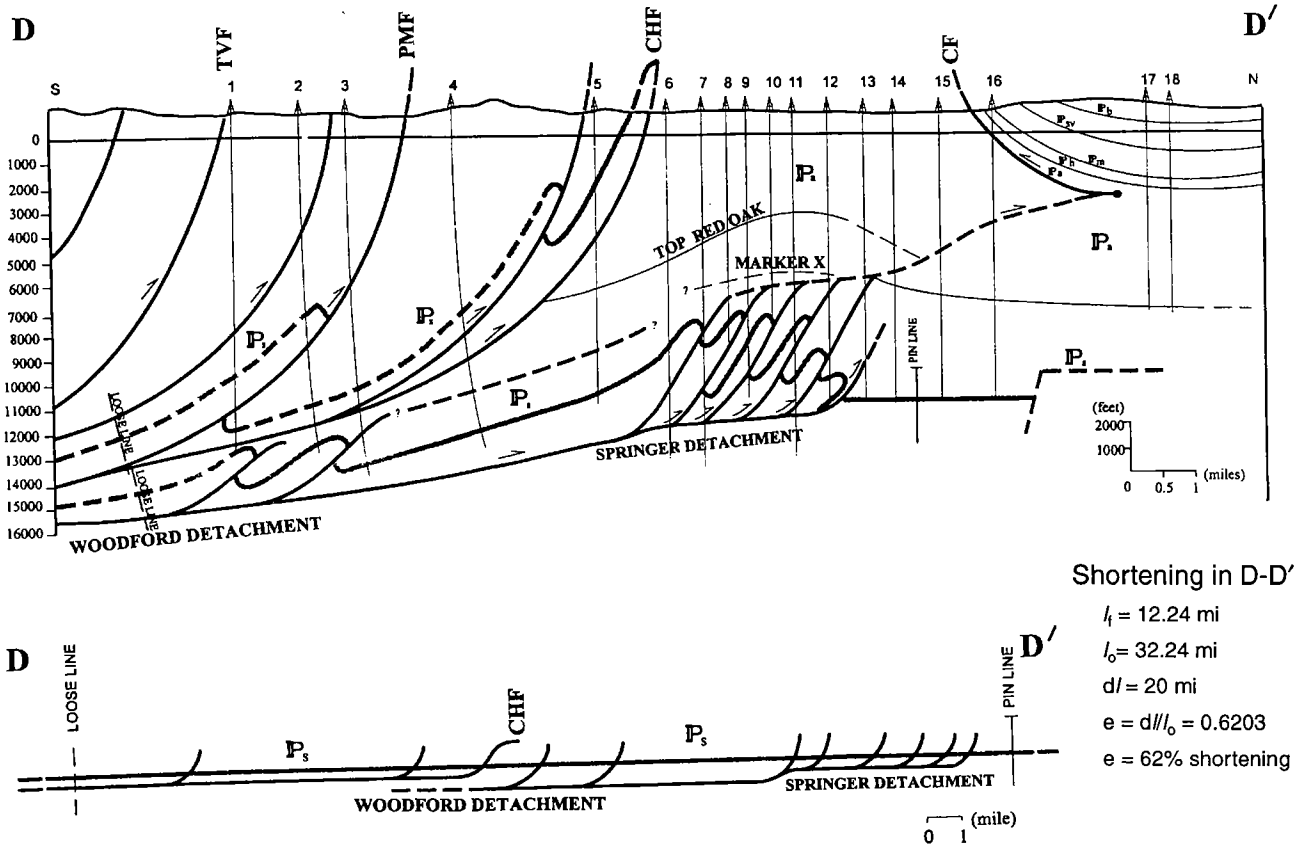

Figure 9. Cross section D–D′ showing the presence of the triangle zone, duplex structure, and other structural features in the Wilburton gas-field area (A) and structural restoration of the cross section (B). The restored cross section suggests 62.0% shortening along the original length of the Spiro sandstone due to Pennsylvanian thrusting in the area. See text for explanation. Line of cross section is located on Figure 2; well numbers are located and described in Appendix. Structural abbreviations: CF—Carbon fault, CHF—Choctaw fault, LAD—lower Atokan detachment, PMF—Pine Mountain fault, TVF—Ti Valley fault. Stratigraphic abbreviations: IPa—Atoka, IPb—Boggy, IPh—Hartshorne, IPm —McAlester, IPs—Spiro sandstone, IPsv—Savanna. Strain-formula abbreviations: l_f—length of deformed-state cross section, l_o—length of restored cross section, dl—difference between lengths of deformed-state cross section and restored cross section, e—shortening.

profiles examined during this study cover only the southern part of the study area where the Woodford detachment can be seen above the rocks of the Hunton Group. The Springer detachment was located primarily by using a limited number of deep-well logs.

The Woodford detachment propagates within the Woodford Shale and is named after the host formation (Hardie, 1988). It is a relatively flat detachment surface lying at about 15,000 ft below sea level in the Wilburton area. In the southern part of the study area, two imbricate thrust faults splay from the Woodford detachment (Figs. 6–9). These thrust faults probably form the Gale-Buckeye thrust system of Wilkerson and Wellman (1993). Farther north, the Woodford detachment makes a ramp and reaches a shallower depth in the Springer Formation (Figs. 6–9) where it is named the Springer detachment. This detachment is approximately 12,000–13,000 ft below sea level. It continues northward in the Springer Formation and forms the floor thrust of the duplex structures in the study area.

Duplex Structure and the Lower Atokan Detachment

In all cross sections (Figs. 6–9), a hinterland-dipping duplex structure is shown in the footwall block of the Choctaw fault. The duplex structure is floored by the Springer detachment and bounded on top by a roof thrust termed here the lower Atokan detachment (LAD). Horses found within the duplex structure are probably formed by the upward propagation of the imbricate thrust faults splaying from the basal detachment. These imbricate faults join the LAD.

The presence and location of a roof thrust are suggested by the great difference in geometry above and below the interval between the imbricately thrusted Spiro sandstone and a sand unit (marker X) in the Atoka Formation. In the wire-line well logs, marker X is identified by its higher gamma-ray and resistivity values. An attempt to correlate marker X with one of the other sand units within the Atoka Formation was unsuccessful because of the unavailability of type well-log signatures. Therefore, we have only informally named it. In some cross sections, marker X is not clearly distinguishable in the well logs. In all wells examined, marker X is found in exactly the same stratigraphic position. It displays a fold pattern similar to the geometry of the Red Oak Sandstone above it. On the other hand, the Spiro sandstone below marker X is imbricately thrusted. This geometry can be interpreted in two ways: (1) the part of the Atoka Formation below the marker X contains imbricate blind-thrust faults that die out in the shaley part of the section above the Spiro sandstone, or (2) a roof thrust below marker X separates the imbricately thrusted section below from the folded section above.

We prefer the second interpretation based on the following evidence. Several wells in the eastern part of the study area close to our line of cross section D–D′ (Fig. 9) penetrated the Red Oak Sandstone twice—one in the hanging wall of a thrust fault, another one in the footwall of a thrust fault. We interpret this thrust as a part of shallow-dipping LAD surface (the roof thrust). Therefore, in our cross sections, we depict the LAD as a south to north propagating detachment, located at 8,000–9,000 ft below sea level in the western part and 7,000–8,000 ft below sea level in the eastern part of the study area. The LAD makes a gradual ramp to the north of the leading imbricate thrust of the duplex structure and reaches a shallower depth. During its northward propagation, it displaces the Red Oak Sandstone (Fig. 9) and eventually reaches the Hartshorne Formation, where it forms the Carbon fault as a backthrust.

The location of the LAD is arbitrarily chosen to be in the middle of the interval separating two different structural geometries. It is not detected on the seismic profiles nor could it be inferred from the well-log signatures. The seismic profiles do not provide a well-developed velocity contrast, and the well logs do not suggest a characteristic log signature for the roof thrust. The absence of supporting evidence for the roof thrust most probably arises because the LAD is propagating within the shales of the Atoka Formation.

Up to five horses are depicted in the duplex structure shown in our cross sections (Figs. 6–9). The eastern cross sections C–C′ and D–D′ suggest that the leading imbricate thrust is actually a blind thrust that does not form a horse (Figs. 8, 9). Cross section B–B′ (Fig. 7) suggests two blind thrusts. The westernmost cross section A–A′ (Fig. 6) does not show blind thrusts but rather consists of up to five horses. The displacements along the hinterland-dipping thrust faults in the duplex structure are not constant. In addition to the differences along the thrust faults, the horses in the duplexes show slight changes in their dips. This change is most pronounced in the leading imbricate thrusts and associated horse structures.

The presence of a duplex structure in the Wilburton gas-field area was first proposed by Arbenz (1984). Other studies that proposed duplex structures in the frontal Ouachita Mountains include Hardie (1988), Perry and Suneson (1990), Wilkerson and Wellman (1993), Çemen and others (1995), Akthar (1995), Akthar and others (1995), Sagnak (1996), and Sagnak and others (1996).

Carbon Fault

To the north of Wilburton, an approximately east–west-trending fault has long been recognized as the Carbon fault (CF on Fig. 2). Its surface trace is prominent and is located at or adjacent to the boundary between the Atoka Formation and the Hartshorne Formation. The fault is shown as a north-dipping thrust fault on the Wilburton quadrangle geologic map by Hemish and others (1990). It follows the geometry of the Hartshorne sandstone and the overlying Desmoinesian units. The Desmoinesian sequence above the Carbon fault is gently folded and forms the southern limb of the San Bois syncline. These units show no evidence of displacement by thrust faulting.

This surface geometry and well-log data indicate

that the Carbon fault dips about 30–40° to the north and flattens at about 3,000–4,000 ft below sea level. Therefore, in all cross sections (Figs. 6–9), the Carbon fault is shown as a north-dipping thrust fault.

The surface trace of the Carbon fault in the western part of the study area is mostly inferred in alluvium or in water bodies. The cross sections coinciding with this area (Figs. 6, 7) show the Carbon fault as following the boundary between the Atoka Formation and Hartshorne Sandstone. To the east, where the fault is mapped within the Atoka Formation, the cross sections (Figs. 8, 9) suggest that the Carbon fault is propagating upward toward the Atoka–Hartshorne boundary within the Atoka Formation.

Using evidence from surface geologic maps and subsurface data, the Carbon fault is interpreted as formed by the continued upward and northward propagation of the roof thrust (LAD) within the shales of the Atoka Formation (Figs. 6–9). Within incompetent units like shales of the Atoka Formation, the LAD propagates with a low angle and forms a gentle ramp. Eventually, the detachment reaches a zero-displacement point where it encounters a hindrance to its forward (northward) movement. At this point, detachment is likely to form a backthrust. In the study area, surface and subsurface evidence suggest that the Carbon fault is a backthrust formed along the southern flank of the San Bois syncline (Figs. 6–9).

A foreland-verging thrust movement characterizes the Wilburton area. Duplexes and a roof thrust are at the frontal part of this thrust belt. As stated by Jones (1994), this kind of tectonic transport should be "accommodated by backthrusting with opposite vergence, in the section overlying the upper detachment." The Carbon fault formed to accommodate thrust movement in the study area.

Triangle Zone

The geometry formed by the south-dipping Choctaw fault, the LAD, and the north-dipping Carbon fault qualifies as a triangle zone (Figs. 6–9), similar to the ones that were found in the southern Cordilleran foreland in Canada (Dahlstorm, 1970; Jones, 1982, 1994; Price, 1986; Sanderson and Spratt, 1992) and in the Himalayan foreland in Pakistan (Jadoon and Frisch, 1997). The LAD floors the zone. The two opposing flanks of the triangle zone are formed by the south-dipping Choctaw fault and the north-dipping Carbon fault. All of the cross sections (Figs. 6–9) exhibit similar geometry throughout the study area and suggest that a triangle zone is present.

The Carbon fault disappears to the east adjacent to the eastern boundary of the study area. The seismic lines east of the Wilburton area suggest that the Carbon fault continues in the subsurface as a north-dipping blind thrust. In this area, Evans (1997) constructed cross sections and suggests that the triangle zone, which we have detected in the Wilburton area, continues to the east, although its northern flank in the subsurface is a blind backthrust. This condition results in the north–south size reduction of the triangle zone as the Choctaw and the Carbon faults get closer to each other in the subsurface east of the Wilburton area (Fig. 2).

Normal Faults

The Wilburton gas field and surrounding areas contain down-to-the-south normal faults present in the northern part of the cross sections to the north of the leading imbricate thrust of the duplex structure (Figs. 6–9). These faults are verified from the seismic and well-log data and have a general trend of east–west to east–northeast, paralleling the trend of the basin. The limited number of wells in this normal faulted area prevents any detailed interpretation. However, it has been suggested by Koinm and Dickey (1967) that an abrupt increase in the thickness of the middle and lower Atoka, along the normal faults, reveals that these faults were formed as growth faults. They also pointed out the presence of the turbidite-facies rocks present in the lower and middle Atoka as another line of evidence for active growth faults during Atokan sedimentation.

In all cross sections (Figs. 6–9), the normal faults are observed in the lower and middle Atoka in the northern part of the study area, but there is no evidence of displacement due to normal faulting in the upper Atoka. The Hartshorne sandstone is also observed unfaulted in the cross sections.

Cross sections A–A′ through D–D′ (Figs. 6–9) show that the normal faults displace the Spiro sandstone, but their extent into the pre-Atokan units could not be determined because of the absence of subsurface data below the Spiro. The seismic profiles suggest the presence of normal faulting below the detachment. In the absence of sufficient well control, the normal faults and the Spiro sandstone are mostly inferred from the adjacent cross sections. The cross sections suggest a maximum of 2,000 ft of dip separation along the normal faults. Ferguson and Suneson (1988) proposed that the normal faults in pre-Pennsylvanian rocks acted as barriers that forced the thrusts to ramp over basement rocks.

Amount of Shortening

The balanced structural cross sections (Figs. 6–9) are restored using the key-bed–restoration method to calculate the amount of shortening for the Spiro sandstone. In the Wilburton area, the Atoka shales dominate the rock units both at the surface and in the subsurface. Shales have characteristic responses to deformation. Because they are incompetent, they can be easily deformed, and selecting the bed boundaries within shales could be very difficult. While constructing the cross sections, this situation was encountered, and only the Spiro sandstone is used to define the subsurface structural geometry because of its recognizable well-log signature. Consequently, we could restore the cross sections only by using the Spiro sandstone as the key-bed.

The pin lines for the restored cross sections are located to the north of the leading thrust of the duplex

structure, where the Spiro sandstone is not affected by shortening in the frontal zone. The loose lines are located to the south where there is no piercing point for the thrusted Spiro sandstone. Calculations suggest about 60% shortening for the Spiro sandstone in the Wilburton area.

Figure 9 shows both our balanced structural cross section constructed along the line D–D′ (Fig. 2) and its restoration with a smaller scale. We found a 62.0% shortening along this cross section using the plain-strain formula of $e = dl/l_0$, where e is the extension (or shortening), dl is the difference between the lengths of the deformed-state cross section and the restored cross section, and l_0 is the length of the restored cross section. The other cross sections have provided a similar amount of shortening. The shortening is 61% along A–A′, 63% along B–B′, and 62% along C–C′.

CONCLUSIONS

In the Ouachitas, a basal detachment surface within the Morrowan Springer Formation separates the Cambrian to Mississippian platform rocks, consisting mostly of about 5,000-ft-thick sandstone and limestone, from the overlying more than 15,000-ft-thick, shale-dominated sequence of the Pennsylvanian Atoka Formation (Arbenz, 1989; Houseknecht, and McGilvery, 1990), which contains many 50–150-ft-thick sandstone units (Fig. 5). Within the thick shale sequence of the Atoka Formation above the Spiro sandstone, there are a few competent beds such as Cecil, Red Oak, and Panola sandstones. This sedimentary succession prevents using the fold-bend–fault model during balanced structural cross section constructions because kink folds develop only in the two types of regions: (1) where the sedimentary rocks are uniformly bedded, exhibit regular bed thicknesses, and have periodic alternations of competent and incompetent layers; or (2) where there is rather a uniform anisotropy (Ramsay, 1992). Therefore, we used concentric folding in our cross sections (Figs. 6–9).

Based on a detailed subsurface structural study, we suggest that a triangle zone is present in the Wilburton gas-field area (Figs. 6–9). The triangle zone is flanked by the Choctaw fault to the south and the Carbon fault to the north (Fig. 2). It is floored by a possible detachment surface in the Atoka Formation. We informally named this detachment surface the lower Atokan detachment or LAD (Figs. 6–9). Below the triangle zone, a duplex structure contains hinterland-dipping imbricate thrust faults splaying from a detachment surface within the Springer Formation (the floor thrust), which is usually recognized as the Springer detachment. The hinterland-dipping faults join to the LAD in the Atoka Formation (the roof thrust). The LAD continues in the Atoka Formation northward and displaces the Red Oak sandstone before reaching a shallower depth and forming the Carbon fault as a north-dipping backthrust below the San Bois syncline, which involves the Desmoinesian Series rocks (Figs. 6–9).

The surface trace of the Carbon fault disappears east of the Wilburton area. However, the triangle zone continues to the east in the subsurface because the Carbon fault becomes a blind backthrust to the east of the Wilburton area.

The hanging wall of the Choctaw fault—the leading edge thrust of the Ouachita fold and thrust belt—contains several south-dipping imbricate thrust faults. These faults, including the Ti Valley and Pine Mountain faults, probably join the Choctaw fault at depth. We interpret the duplex structure in the Wilburton area as being formed by a break-forward sequence of thrusting similar to the mechanism first proposed by Boyer and Elliot (1982). It remains in question, however, if any movement occurred along the Choctaw and other faults in its hanging wall (Figs. 2, 6–9) after the formation of the duplex structure. If such movement is documented, it will have important implications for determining the conditions that control movement along the thrust faults behind the leading-edge thrust, or along of the leading-edge thrust itself.

ACKNOWLEDGMENTS

We thank Neil Suneson, LeRoy Hemish, and Peter D'onfro for helpful discussions during the various stages of this investigation. This study was supported by the OCAST project, AR-25:4391, a multidisciplinary geologic study to investigate overthrusted natural-gas reservoirs in the Arkoma basin.

REFERENCES CITED

Akhtar, S., 1995, The geometry of thrust systems in Wilburton gas field and surrounding areas, Latimer County, Oklahoma: Oklahoma State University unpublished M.S. thesis, 97 p.

Akhtar, S.; Çemen, I.; and Al-Shaieb, Z., 1995, Geometry of thrust systems in Wilburton gas field and surrounding areas, Arkoma basin, Oklahoma [abstract]: Geological Society of America Abstracts with Programs, v. 27, no. 3, p. 33.

Al-Shaieb, Z.; Çemen I.; and Cleaves, A., 1995, Overthrusted natural gas reservoirs in the Arkoma basin: Final report, OCAST Project No. AR2-025:4391, 153 p.

Arbenz, J. K., 1984, A structural cross section through the Ouachita Mountains of western Arkansas: Arkansas Geological Commission Guidebook 84-2, p. 76–84.

Arbenz, J. K., 1989, The Ouachita system, *in* Bally, A. W., and Palmer, A. R. (eds.), The Geology of North America —an overview: Geological Society of America, The Geology of North America, v. A, p. 371–396.

Bertagne, A. J.; and Leising, T. C., 1989, Seismic exploration of Ouachita frontal fairway, southeastern Oklahoma: Oil and Gas Journal, v. 87, no. 4, p. 88–90.

Boyer, S. E.; and Elliot, D., 1982, Thrust systems: American Association of Petroleum Geologists Bulletin, v. 66, p. 1196–1230.

Camp, W. K.; and Ratliff, R. A., 1989, Balanced cross section through Wilburton gas field, Latimer County, Oklahoma: implications for Ouachita deformation and Arbuckle (Cambro–Ordovician) exploration in Arkoma basin [abstract]: American Association of Petroleum Geologists Bulletin, v. 73, p. 1044.

Çemen, I.; Al-Shaieb, Z.; Hess, F.; Akthar, S.; and Feller R., 1995, Geometry of thrusting in Wilburton gas field and

surrounding areas, Arkoma basin, Oklahoma: implications for gas exploration in the Spiro Sandstone reservoirs [abstract]: American Association of Petroleum Geologists Bulletin, v. 79, p. 1401.

Çemen, I.; Al-Shaieb, Z.; Sagnak, A.; Feller, R.; and Akthar, S., 1997, Triangle zone geometry of the frontal Ouachitas in the Wilburton area, Arkoma basin, Oklahoma: implications for fault sealing in the Wilburton gas field [abstract]: American Association of Petroleum Geologists 1997 Annual Convention Official Program, v. 6, p. A19.

Dahlstrom, C. D. A., 1970, Structural geology in the eastern margin of the Canadian Rocky Mountains: Bulletin of Canadian Petroleum Geology, v. 18, p. 332–406.

Evans, J., 1997, Structural geometry of thrust faulting in the Baker Mountain and Panola quadrangles, southeastern Oklahoma: Oklahoma State University unpublished M.S. thesis, 99 p.

Ferguson, C. A.; and Suneson, N. H., 1988, Tectonic implications of early Pennsylvanian paleocurrents from flysch in the Ouachita Mountains frontal belt, southeast Oklahoma, *in* Johnson, K. S. (ed.), Shelf-to-basin geology and resources of Pennsylvanian strata in the Arkoma basin and frontal Ouachita Mountains of Oklahoma: Oklahoma Geological Survey Guidebook 25, p. 49–61.

Ham, W. E., 1973, Regional geology of the Arbuckle Mountains, Oklahoma: Oklahoma Geological Survey Special Publication 73-3, 61 p.

Hardie, W. E., 1988, Structural style of the frontal thrust belt of the Ouachita Mountains, southern Pittsburg County, Oklahoma: Oklahoma Geology Notes, v. 48, p. 232–246.

Hemish, L. A., 1992, Geologic map of the Gowen quadrangle, Latimer County, Oklahoma: Oklahoma Geological Survey Open-File Report 1-92, scale 1:24,000.

_____ 1995, Geologic map of the Adamson quadrangle, Latimer and Pittsburg Counties, Oklahoma: Oklahoma Geological Survey Open-File Report 4-95, scale 1:24,000.

Hemish, L. A.; Suneson, N. H.; and Ferguson, C. A., 1990, Geologic map of the Wilburton quadrangle, Latimer County, Oklahoma: Oklahoma Geological Survey Open-File Report 2-90, scale 1:24,000.

Houseknecht, D. W.; and Kacena, J. A., 1983, Tectonic-sedimentary evolution of the Arkoma basin: Society of Economic Paleontologists and Mineralogists, Mid-Continent Section, v. 1, 119 p.

Houseknecht, D. W.; and McGilvery, T. A., 1990, Red Oak Field, *in* Beaumont, E. A.; and Foster, N. H. (eds.), Structural traps II, Traps Associated with Tectonics: American Association of Petroleum Geologists, Treatise of Petroleum Geology, Faulting Atlas of Oil and Gas Fields, p. 201–221.

Jadoon, I. A. K.; and Frisch, W., 1997, Hinterland-vergent tectonic wedge below the Riwat Thrust, Himalayan foreland, Pakistan: implications for hydrocarbon exploration: American Association of Petroleum Geologists Bulletin, v. 81, p. 438–448.

Johnson, K. S., 1988, General geologic framework of the field-trip area, *in* Johnson, K. S. (ed.), Shelf-to-basin geology and resources of Pennsylvanian strata in the Arkoma basin and frontal Ouachita Mountains of Oklahoma: Oklahoma Geological Survey Guidebook 25, p. 1–5.

Jones, P. B., 1982, Oil and gas beneath east dipping thrust faults in the Alberta foothills, *in* Powers, K. (ed.), Geologic studies of the Cordilleran thrust belt: Rocky Mountain Association of Geologists Guidebook, v. 1, p. 61–74.

_____ 1994, Triangle zone geometry and terminology [abstract]: Western Canadian and International Expertise, Exploration Update; a joint convention of CSEG and CSPG, Calgary, Alberta, 1994, p. 69–70.

Koinm, D. N.; and Dickey, P. A., 1967, Growth faulting in the McAlester basin of Oklahoma: American Association of Petroleum Geologists Bulletin, v. 51, p. 710–718.

Milliken, J. V., 1988, Late Paleozoic and early Mesozoic geologic evolution of the Arklatex area: Rice University, Houston, unpublished M.S. thesis, 259 p.

Mitra, S., 1986, Duplex structures and imbricate thrust systems: geometry, structural position and hydrocarbon potential: American Association of Petroleum Geologists Bulletin, v. 70, p. 1087–1112.

_____ 1988, Three dimensional geometry and kinematic evolution of the Pine Mountain thrust system, southern Appalachians: Geological Society of America Bulletin, v. 100, p. 72–95.

Namson, J. S.; and Davis, T. L., 1988, Structural transect of the western Transverse Ranges, California: implications for lithospheric kinematics and seismic risk evaluation: Geology, v. 16, p. 675–679.

Perry, W. J., Jr.; and Suneson, N. H., 1990, Preliminary interpretation of a seismic profile across the Ouachita frontal zone near Hartshorne, Oklahoma, *in* Suneson, N. H.; Campbell, J. A.; and Tilford, M. J. (eds.), Geology and resources of the frontal belt of the western Ouachita Mountains, Oklahoma: Oklahoma Geological Survey Special Publication 90-1, p. 145–148.

Price, R. A., 1986, The southeastern Canadian Cordillera: thrust faulting, tectonic wedging and delamination of the lithosphere: Journal of Structural Geology, v. 8, p. 239–254.

Ramsay, J. G., 1992, Some geometric problems of ramp-flat thrust models, *in* McClay, K. R. (ed.), Thrust tectonics: Chapman and Hall, London, U.K., p. 191–200.

Reeves, D. L.; Schreiner, W. P.; and Sheffield, T. M., 1990, Stop 6—New State Mountain (Amoco 1-5 Rosso Unit), *in* Suneson, N. H.; Campbell, J. A.; and Tilford, M. J. (eds.), Geology and resources of the frontal belt of the western Ouachita Mountains, Oklahoma: Oklahoma Geological Survey Special Publication 90-1, p. 37–40.

Roberts, M. T., 1992, Shelf to basin transect, eastern Oklahoma: Shreveport Geological Society Guidebook, May 27–29, 1992.

Sagnak, A., 1996, Geometry of the Late Paleozoic thrust system in the Wilburton area: Oklahoma State University unpublished M.S. thesis, 101 p.

Sagnak, A.; Çemen, I.; and Al-Shaieb, Z., 1996, Geometry of Late Paleozoic thrusting in the Wilburton–Hartshorne area, Arkoma basin, SE Oklahoma [abstract]: Geological Society of America Abstracts with Programs, v. 28, no. 1, p. 62.

Sanderson, D. A.; and Spratt, A. D., 1992, Triangle zone and displacement transfer structures in the eastern front ranges, southern Canadian Rocky Mountains; American Association of Petroleum Geologists Bulletin, v. 76, p. 828–839.

Suneson, N. H., 1988, The geology of the Ti Valley fault in the Oklahoma Ouachita Mountains, *in* Johnson, K. S.

(ed.), Shelf-to-basin geology and resources of Pennsylvanian strata in the Arkoma basin and frontal Ouachita Mountains of Oklahoma: Oklahoma Geological Survey Guidebook 25, p. 33–47.

_____ 1995, Structural interpretations of the Arkoma basin–Ouachita Mountains transition zone, southeastern Oklahoma: a review, *in* Johnson, K. S. (ed.), Structural styles in the southern Midcontinent, 1992 symposium: Oklahoma Geological Survey Circular 97, p. 259–263.

_____ 1996, Geologic map of the Hartshorne quadrangle, Latimer and Pittsburg Counties, Oklahoma: Oklahoma Geological Survey Open-File Report 1-96, scale 1:24,000.

Suneson, N. H.; and Ferguson C. A., 1989, Geologic map of the Higgins quadrangle, Latimer County, Oklahoma: Oklahoma Geological Survey Open-File Report 1-89, scale 1:24,000.

Suppe, J., 1983, Geometry and kinematics of fault-bend folding: American Journal of Science, v. 283, p. 648–721.

Sutherland, P. K., 1988, Late Mississippian and Pennsylvanian depositional history in the Arkoma basin area, Oklahoma and Arkansas: Geological Society of America Bulletin, v. 100, p. 1787–1802.

Tilford, M. J., 1990, Geological review of the Ouachita Mountains thrust belt play, western Arkoma basin, Oklahoma, *in* Suneson, N. H.; Campbell, J. A.; and Tilford, M. J. (eds.), Geology and resources of the frontal belt of the western Ouachita Mountains, Oklahoma: Oklahoma Geological Survey Special Publication 90-1, p. 169–196.

Valderrama, M. H.; Nielsen, K. C.; McMechan G. A.; and Hunter, H., 1994, Three-dimensional seismic interpretation of the triangle zone of the frontal Ouachita Mountains and Arkoma basin, Pittsburg County, Oklahoma, *in* Suneson, N. H.; and Hemish, L. A. (eds.), Geology and resources of the eastern Ouachita Mountains frontal belt and southeastern Arkoma basin, Oklahoma: Oklahoma Geological Survey Guidebook 29, p. 225–241.

Vedros, S. G.; and Visher, G. S., 1978, The Red Oak sandstone: A hydrocarbon-producing submarine fan deposit, *in* Stanley, D. J., and Kelling, G. (eds.), Sedimentation in submarine canyons, fans, and trenches: Dowden, Hutchinson, and Rose, Stroudsburg, Pennsylvania, p. 292–308.

Wilkerson, M. S.; and Wellman P. C., 1993, Three dimensional geometry and kinematics of the Gale–Buckeye thrust system, Ouachita fold and thrust belt, Latimer and Pittsburg Counties, Oklahoma: American Association of Petroleum Geologists Bulletin, v. 77, p. 1082–1100.

Woodward, N. B., 1985, Valley and ridge thrust belt: balanced cross sections, Pennsylvania to Alabama, Appalachian Basin Industrial Associates: University of Tennessee, Studies in Geology, v. 12, 64 p.

APPENDIX
Wells Used in Cross-Sections

Numbers to the right of the well names correspond to the numbers along the cross-sections.
Numbers to the left of the well locations indicate the distance of the well to line of the cross-section.

Cross-section A-A'

1) AMOCO
Mose Watts # 36-2
36-4N-17E (~1000E)

2) AMOCO
Retherford No. 1-A
25-4N-17E (~1500E)

3) ARKOMA
Sparks No. 1
3-4N-17E (~2300E)

4) KING RESOURCE
Layden No. 1-3
3-4N-17E

5) KING RESOURCE
Potichny No. 1-33
33- 5N- 17E (~300E)

6) ARKLA
Hare No. 1-33
33-5N-17E (~1300E)

7) TEXAS INT.
B.D. Jordan No.1
33-5N-17E (~600W)

8) ARCO
USA Sec. 28 # 2
28-5N-17E (~2000E)

9) SINCLAIR
USA Sec. 28 Unit # 1
28-5N-17E (~1500E)

10) ARCO
Pauline Bowman No. 3
20-5N-17E (~300E)

11) NICOR
Bowman No. 4
20-5N-17E (~1400W)

12) SINCLAIR
Pauline Bowman #1
20-5N-17E (~500E)

13) ARCO
P. Bowman no. 5
20-5N-17E (~700W)

14) DYCO
Bowman No. 1
17-5N-17E (~1400E)

15) SAMSON
Bowman Unit # 1
17-5N-17E (~600W)

16) TXO
Beatrice # 1
17-5N-17E (~200E)

17) GULFSTREAM
Adamson Townsite No. 1-7
7- 5N-17E (~200E)

18) SNEE & EBERLY
Oneth No. 1
25-6N-16E (~2300E)

19) HUTCHINSON & KING RES.
E.C. Mc. Kinzie No. 1
23-6N-16E (~1400W)

20) SNEE & EBERLY
No. 1 Baldwin A
14-6N-16E (~1700E)

Cross-section B-B'

1) ARCO
TNT No. 1-34
34-4N-18E (~ 1000E)

2) EXXON
Garret No. D-1
34-4N-18 (~1700E)

3) BTA
9001 JV-P Johnson #1
16-4N- 18E (~2100E)

4) BTA
9001 JV-P Glaser #1
16-4N-18E (~ 2200E)

5) SHELL
Mabry # 1-9
9-4N-18E (~2400E)

6) SHELL
R. Every # 1-5
5-4N-18E

7) TENECO
Mabry Trust No.1-5
5-4N-18E (~300W)

8) ARKOMA
Hunter Tucker No.2
31-5N-18E (~1000E)

9) TRIGGY
Hunter Tucker No.1-31
31-5N-18E (~1300W)

10) ARCO
Jessie Bennet #2
30-5N-18E (~900E)_

11) MARATHON
Fabbro Unit 3
24-5N- 17E (~1000W)

12) MARATHON
Fabbro Unit #1
24-5N-17E (~1300E)

13) MARATHON
Fabbro #2
24-5N-17E

14)SINCLAIR
Dunagan Unit # A-1
13-5N-17E (~1300W)

15) ARCO
Dunagan A#2
13-5N-17E (~400E)

16) GULFSTREAM
Vaughn No.1
12-5N-17E (~1900E)

17) ARCO
Sharp #1
2-5N17E (~2000E)

18) SNEE & EBERLY
Cllinton No.1-21
21-6N-17E (~600W)

19) OXLEY
Doly Hartshorne No.1
16-6N-17E

Cross-section C-C'

1) ARCO
Ulysses # 1
35-4N-18E (~1400E)

2) EXXON
Garret No. A-1
26-4N-18E (~4300E)

3) BTA
9001 JV-P Workman #1
22-4N-18E (~250E)

4) SHELL
Mabry # 1-9
9-4N-18E (~2100W)'

5) SHELL
Williams Mabry # 1-4
4-4N-18E (~700E)

6) ARKOMA
Kennedy # B-2
32-5N-18E (~1500W)

7) ARCO
Dobbs State # 2
29-5N-18E (~1000E)

8) AMBASSADOR
Dobbs State No. 1
29-5N-18E (~400E)

9) ARCO
Bennet State # 2
19-5N-18E (~100W)

10) ARCO
Bud Hampton # 2
18-5N-18E (~700E)

11) AMBASSADOR
Hampton Unit # 1
18-5N-18E (~1300W)

12) PETROLEUM INC.
Ferguson Unit No. 1
7-5N-18E (~100W)

13) SINCLAIR
Gardner Unit # 1
7-5N-18E

14) SKELLY
White N # 1-A
23-6N-17E (~3300W)

15) TEXAS
White "H" No.1
14-6N-17E (~600E)

16) OXLEY
Marine No.1
14-6N-17E (~100E)

17) SKELLY
White K # 1
14-6N-17E (~300E)

Cross-section D-D'

1) ANADARKO
Robe "A" # 1-25
25-4N-18E (~3000W)

2) BTA
BTA 9001 JV-P Amason #1
24-4N-18E (~1000W)

3) ARCO
Dollins No. 1-13
13-4N-18E (~2000E)

4) BTA
1-9001 JV-P Mabry
11-4N-18E (~1700W)

5) COQUINA
Watts No. 1
34-5N-18E (~200W)

6) ARCO
E.V. Enis No.2
27-5N-18E (~100W)

7) ARCO
R.F. Mc. Alester # 3
22-5N-18E (~2000E)

8) AMBASSADOR
Mc. Alester #2
22-5N-18E

9) ARCO
Paschall # 3
21-5N-18E (~3500W)

10) AMBASSADOR
Kilpatrick Unit # 1
16-5N-18E (~500W)

11) AMBASSADOR
Kilpatrick 2-16
16-5N-18E (~300W)

12) JMC EXP.
Toppins State # 2
9-5N-18E (~400E)

13) AMBASSADOR
Toppins State Unit # 1
9-5N-18E (~200E)

14) AMBSSADOR
Woods Unit No. 1
4-5N-18E (~2000E)

15) AMBASSADOR
Sawyer Unit # 1
5-5N-18E (~2000E)

16) SINCLAIR
Mitchell Unit # 1
32-6N-18E (~2000W)

17) HARPER OIL
Key # 1
20-6N-18E (~200E)

18) FERGUSON
Key No. 1
20-6N-18E

Interpretation of Red Fork Incised Valleys Using 3-D Seismic, Watonga-Chickasha Trend, Anadarko Basin, Oklahoma

Rich Bottjer
Coal Creek Resources, Inc.
Denver, Colorado

Lynn Peyton
Amoco Production Company[1]
Denver, Colorado

Greg Partyka
Amoco Exploration and Production Technology Group[1]
Tulsa, Oklahoma

Al Warner
Consulting Geologist
OklahomaCity, Oklahoma

ABSTRACT.—Extension of prolific Upper Red Fork incised valley gas production in the eastern Anadarko basin was one of the targets of three dimensional (3-D) seismic acquisition between 1993 and 1996. Integration of spectral decomposition, coherency, and geological data was critical in the mapping of the incised valley system and led to interpretation of a previuosly unrecognized stage of valley fill. This new stage is shale filled, and has erosionally removed the productive stage in the study area. Valley wall slump blocks were identified based on fault cuts in well logs and areas of low coherency on the seismic. We conclude that 3-D seismic is a powerful tool for mapping Upper Red Fork incised valleys.

INTRODUCTION

New three-dimensional (3-D) seismic interpretation techniques such as spectral decomposition and coherency have been shown to enhance recognition and interpretation of stratigraphic features in Tertiary and Quaternary poorly lithified rocks (Lopez and others, 1997). Coherency images seismic discontinuities by calculating localized seismic trace similarity (Bahorich and Farmer, 1995). Spectral decomposition uses the discrete Fourier transform to image time thickness variability. In the latter, the amplitude spectrum, computed from a short time window covering the geologic zone of interest, is tuned by the rock properties within the analysis window. When applied to 3-D seismic and presented in map form, these spectral responses image lateral variability within the zone of interest (Partyka and Gridley, 1997; Partyka and others, 1999).

In this paper, we present a case history where both spectral decomposition and coherency were used successfully to image deep (~10,000 ft) and old (Pennsylvanian) stratigraphic features in the U.S. Midcontinent.

The original objective of this study was to generate drilling prospects in the Middle Pennsylvanian (Desmoinesian) Red Fork Formation of the Anadarko basin, Oklahoma. The Red Fork is a prolific producer throughout the basin, producing from both marine and valley-fill sands (Bingham, 1993).

The study area is located in the eastern part of the Anadarko basin (Fig. 1). Pennsylvanian rocks throughout most of the Anadarko basin are dominated by shallow-shelf marine clastics. The Red Fork Formation in the study area is characterized by three coarsening-upward marine parasequences (Lower, Middle, and Upper Red Fork), herein referred to as Regional Red

Reprinted with minor modifications from Peyton, L.; Bottjer, R.; and Partyka, G., 1998, Interpretation of incised valleys using new 3-D seismic techniques: a case history using spectral decomposition and coherency: The Leading Edge, September, p. 1294–1298.

[1] Author's employer at time of original publication.

Bottjer, Rich; Peyton, Lynn; and Partyka, Greg, 2001, Interpretation of incised valleys using new 3-D seismic techniques: a case history using spectral decomposition and coherency, *in* Johnson, K. S. (ed.), Pennsylvanian and Permian geology and petroleum in the southern Midcontinent, 1998 symposium: Oklahoma Geological Survey Circular 104, p. 99–103.

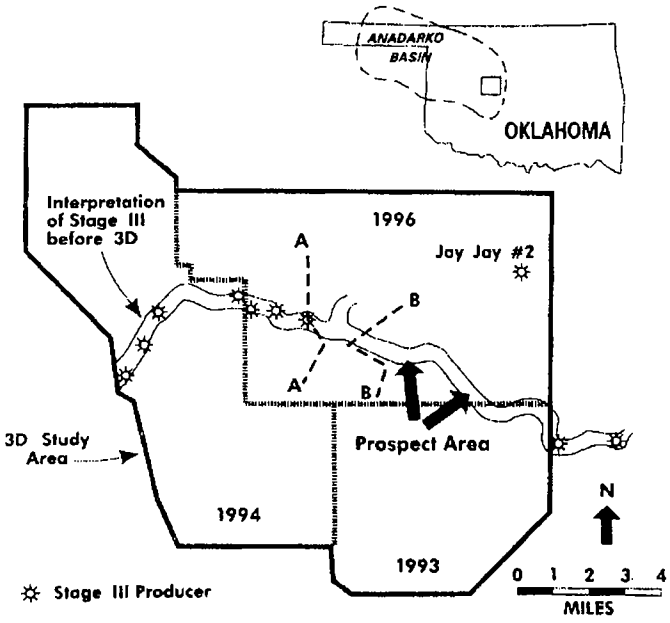

Figure 1. Location map showing 3-D survey outlines, lines of cross section, wells producing from Upper Red Fork Stage III valley fill, and interpreted outline of Stage III valley before acquisition of 3-D seismic data.

Fork, with regionally extensive limestones above (Pink Lime) and below (Inola Lime and Novi Lime). Incised valleys of the Lower, Middle, and Upper Red Fork have eroded into these regionally correlative parasequences. This paper will discuss only Upper Red Fork incised valleys, as they are the largest and most clearly imaged on the 3-D seismic and contain the best reservoir rocks in the area (Clement, 1991).

The Upper Red Fork incised-valley system consists of multiple stages of incision and fill, resulting in a stratigraphically complex internal architecture. Prior to acquiring 3-D seismic in the area, we followed the conventional belief that four main stages of valley fill exist, of which the third, Stage III, is the most abundant producer. Red Fork incised valleys are generally 0.5–1.0 mi wide and are, therefore, challenging exploration targets. Three-dimensional seismic technology was utilized in an attempt to decrease the risk associated with drilling for these narrow but prolific objectives.

ACQUISITION

Amoco acquired three 3-D seismic surveys over the study area. The first (27 mi^2) was shot in 1993. In 1994, 37 mi^2 were acquired. Both surveys had primary objectives below the Red Fork. In 1996, 67 mi^2 were acquired with the main objective of imaging the Upper Red Fork incised-valley system. The three surveys were merged to produce one 136-mi^2 survey (Fig. 1).

Data quality is excellent compared to typical land 3-D surveys, with a dominant frequency of about 50 Hz and up to 80 Hz present in the data.

Before acquisition of the 1996 survey, several wells in the area were interpreted as penetrating the edge of the Stage III valley fill. These wells do not produce, but they do indicate the presence of the Stage III valley. The distribution of wells that produce from Stage III sand (Fig. 1) shows a gap in production in the same part of the 1996 survey. We recognized that this area had good potential for unpenetrated, and therefore undrained, Stage III reservoir sand. This prospective area (Fig. 1) was a significant objective of the 1996 survey. It was necessary to image both the edges of the valley and the different stages of fill within the valley to map the Stage III valley fill and identify prospects.

INTERPRETATION

Geologically, the Red Fork is bounded above and below by regionally correlative marker beds (Pink Lime above and Inola and Novi Limes below), which have consistent character on electric logs. The same is true seismically, although the Lower Skinner Shale directly above the Pink Lime gives a more continuous reflection than the Pink itself. The Novi Lime provides the most continuous reflection below the Red Fork interval (Fig. 2a, page 101).

The seismic cross section in Figure 2a illustrates the difficulty of interpreting the Red Fork incised valley using traditional interpretation techniques (autopicking horizons, amplitude mapping, isochron mapping, etc.). The incised valleys are characterized by discontinuous reflections of varying amplitude that are difficult to interpret laterally. Individual stages of fill are almost impossible to identify. As we subsequently learned, the cross section in Figure 2a actually crosses from Regional Red Fork marine parasequences in the south through three different stages of valley fill and back into Regional Red Fork at the north end (Figure 2b, page 101). Due to the inadequacy of conventional interpretation techniques, we decided to use spectral decomposition and coherency. In the study area, the en-

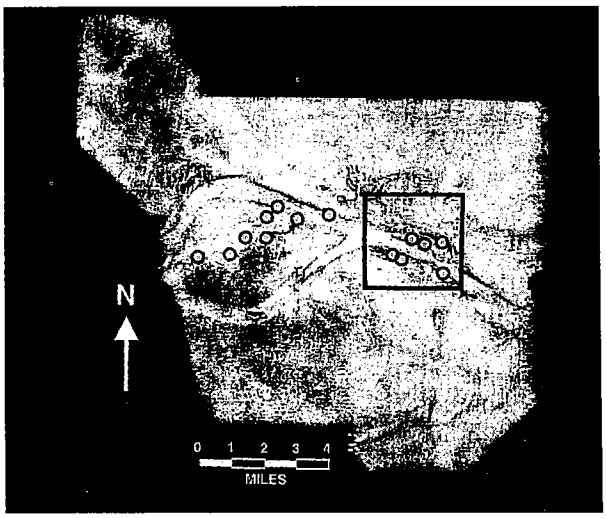

Figure 4. Coherency slice 36 ms below Lower Skinner horizon, showing wells with faults in the Red Fork and Inola intervals. Box shows location of Figure 5a.

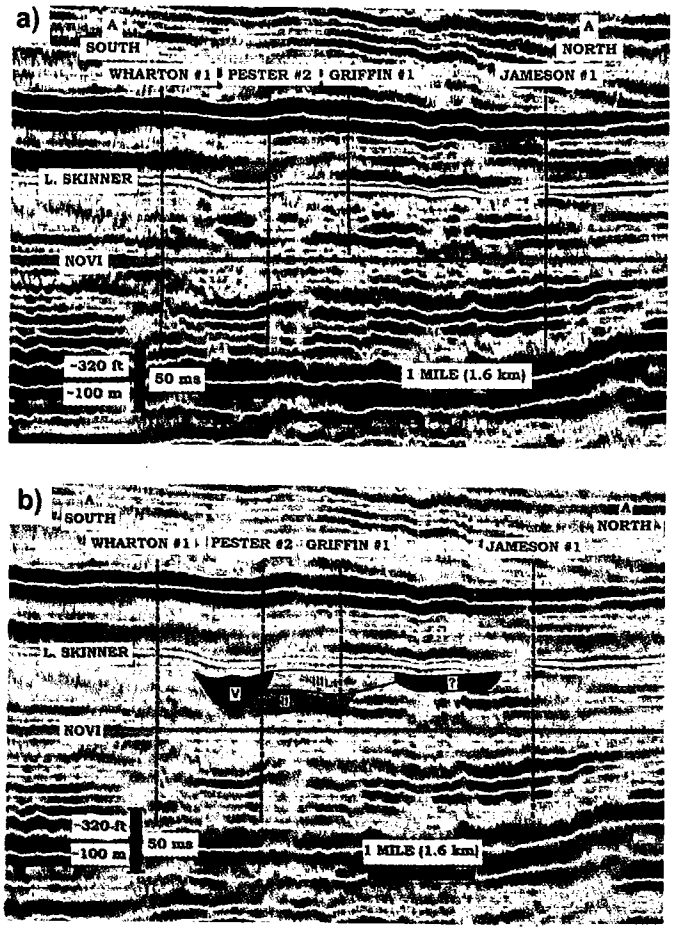

Figure 2. Seismic cross-section A flattened on Novi horizon; (a) without and (b) with current interpretation. Roman numerals correspond to valley-fill stages discussed in text.

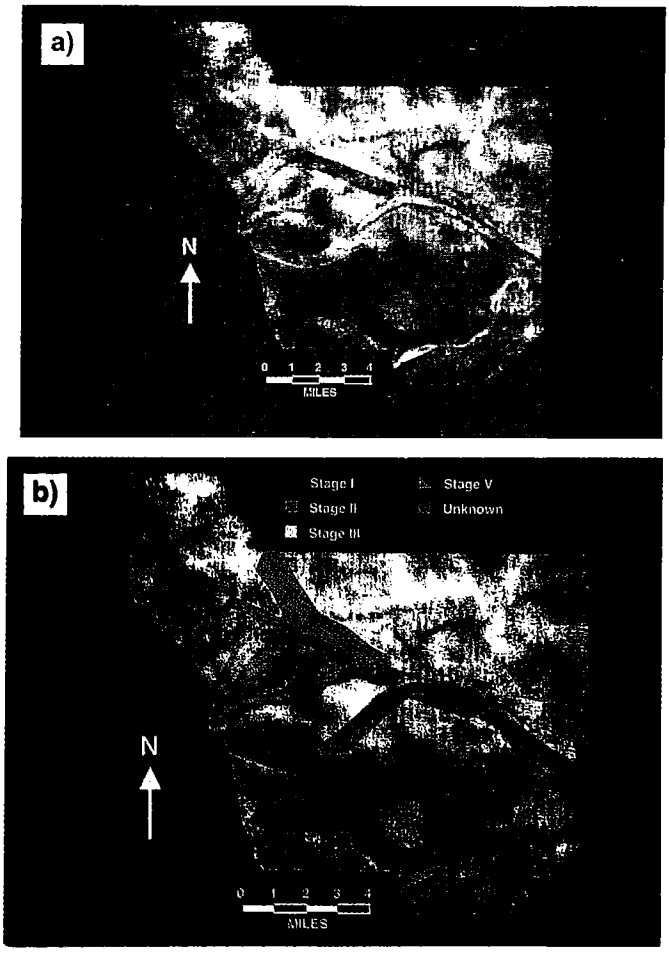

Figure 3. 36-Hz amplitude slice from Red Fork spectral decomposition; (a) without and (b) with current interpretation.

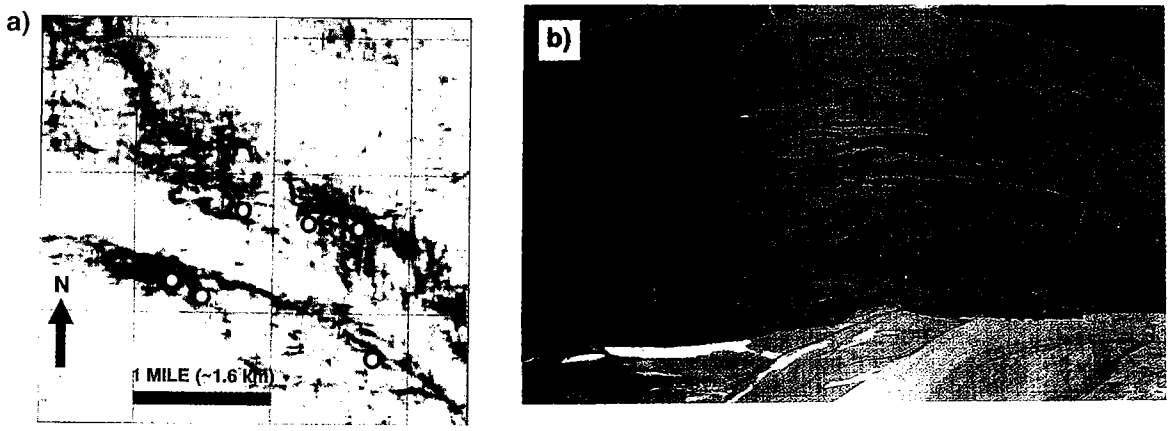

Figure 5. (a) Zoom from Figure 4 of coherency slice 40 ms below Lower Skinner horizon, showing wells with faults in the Red Fork and Inola intervals. Dark areas have low coherency. (b) Modern-day incised valley from the Canterbury Plains of New Zealand showing slump feature on valley edge. Slump is approximately 1 km long and 0.5 km wide (photo courtesy of Dale Leckie).

tire Red Fork interval is approximately 50 ms thick (~300 ft). Therefore, a 50-ms window below the Lower Skinner horizon, encompassing the Red Fork interval, was used as the input zone-of-interest volume into spectral decomposition.

Spectral decomposition imaged the Red Fork incised valley between about 20 Hz and 50 Hz. The 36-Hz amplitude slice was one of the best images of the valley throughout the survey area and was therefore chosen for display purposes (Fig. 3a, page 101). It is apparent from Figure 3a that spectral decomposition not only images the valley edges but also internal features which we have interpreted to be different stages of valley fill.

A coherency cube was computed for the entire 3-D volume. The cube was flattened on the Lower Skinner horizon, and time slices were taken through the flattened volume in the Red Fork interval. This is the same as taking horizon slices below the Lower Skinner horizon in the coherency volume. As expected, coherency slices imaged the edges of the valley and different stages of the valley-fill well (Fig. 4), although the level of internal detail present on the spectral decomposition image is not present on the coherency image.

Initial examination of the spectral decomposition and coherency images (Figs. 3a, 4) seems to show that the Stage III valley does indeed cross the 1996 survey and connect the producing wells in the west half of the study area with those to the east, as interpreted before the 3-D (Fig. 1). However, closer inspection of the spectral decomposition shows an apparently younger valley, which trends northwest in the east part of the 1996 survey and cuts out the Stage III, but then bends to the southwest and diverges from the Stage III valley. This interesting feature led us to reinterpret the well logs in the area, which resulted in the recognition of a new, younger stage of valley fill, Stage V. The current interpretation of the valley (Fig. 3b, page 101) is the result of integration of well-log interpretation with the shapes and patterns on the spectral decomposition and coherency results.

Unfortunately, geologic work shows that Stage V is a shale-filled valley with no potential for hydrocarbon production. Because most of the prospective Stage III has been erosionally removed by the Stage V valley, no drilling prospects were found in the Red Fork interval in the 3-D area.

The Stage III and Stage V valleys must diverge to the east of the survey area where Stage III production is encountered. It was disappointing that no valleys were imaged in the northeast part of the 3-D area, around the producing Jay-Jay 2 well (Fig. 1). This well produces from approximately 50 ft of Stage III sand. Time constraints on the project allowed only normal-incidence modeling to determine why the Stage III valley was not imaged in this area. Lack of good sonic-log data in the area made modeling difficult, but results showed very low impedance contrast between the Stage III valley and the Regional Lower Red Fork into which it cuts. This lack of impedance contrast may explain why the Stage III is not imaged around this well.

Interpretations of borehole, spectral decomposition, and coherency data were combined in the geologic interpretation of seismic cross sections (e.g., Fig. 2). Notice that the Red Fork interval (between the Lower Skinner and Novi Lime reflections) shows an isochron thin where Stage V fill is present. A corresponding isopach thin is apparent on the equivalent well cross section (Fig. 6). A 3-D visualization of the Red Fork interval isochron (Fig. 7) shows that the isochron thin coincides with the occurrence of Stage V. Indeed, the isochron map was used to identify the northeast-trending valley in the southeast part of the study area as Stage V. The isopach/isochron thin is probably due to differential compaction of the Stage V shale.

FAULTING AND SLUMPING

Significant faulting of the area occurred during Early Pennsylvanian (Atokan) time, and some movement persisted into the Desmoinesian. All faulting interpreted on the 3-D seismic is nearly vertical and generally basement-involved. Before acquisition of the seismic, several faults had been identified on well logs in the Red Fork and Inola intervals (Fig. 8); however, these faults could not be identified using 3-D seismic. This was unusual as faults are generally easy to interpret on 3-D seismic data in this area. The Ramsey 1 well (Fig. 8) is particularly interesting because the Inola Lime is missing, the Regional Red Fork marine parasequences sit directly on the Novi Lime, and the Stage II valley fill sits on top of the Regional Red Fork. We interpret a normal fault just above the Novi Lime that has downthrown the Regional Red Fork to a position immediately on top of the Novi in this well bore. This occurred before and/or during the deposition of the valley-fill sediments. When the wells with the Red Fork and Inola faults are plotted on the coherency map (Fig. 4), they all coincide with the edges of stages of the Upper Red Fork valley. More detailed inspection of a slightly deeper coherency slice (Fig. 5a, page 101) shows that the faulted wells coincide with dark areas of low coherency at the edge of the valley. This led to the conclusion that these faults are bounding faults of valley-edge slump blocks. These slump blocks seem to be of a similar scale to present-day examples from the Canterbury Plains of New Zealand (Fig. 5b, page 101).

CONCLUSIONS

Spectral decomposition and coherency displays of 3-D seismic data enabled interpretation of a complex incised valley-system that would have been difficult and time-consuming using standard interpretation techniques. We were able to map not only the limits of the Pennsylvanian Upper Red Fork valley system but also the distribution of different stages within the valley.

Integration of the 3-D seismic with the well data was absolutely essential for an accurate interpretation. Integration of the two disciplines led to the recognition of a new stage of valley fill, Stage V, in this part of the valley system. This had a significant impact on our exploitation program because the Stage V erosionally removed the productive Stage III in the area in which we were looking for prospects. The new interpretation prevented the drilling of dry holes.

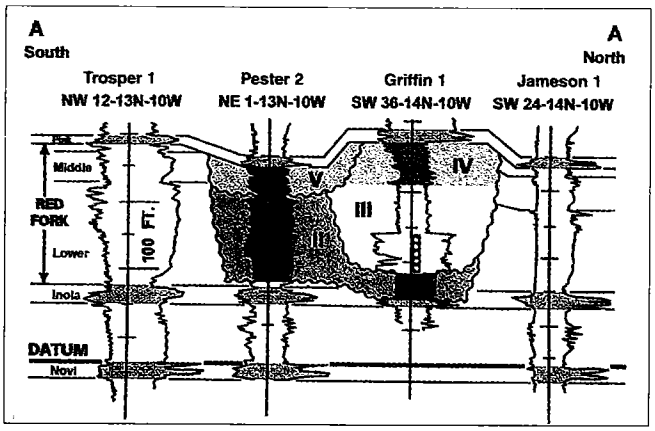

Figure 6. Stratigraphic well-log cross-section A showing stages II, III, IV, and V valley fill. Cross section datum is top of Novi Lime. Upper Red Fork valley stages and regionally correlative limestones are shaded. The Griffin 1 well (perforations shown) has produced 1.03 billion ft^3 of gas and 16.4 thousand bls oil from Red Fork Stage III Sand.

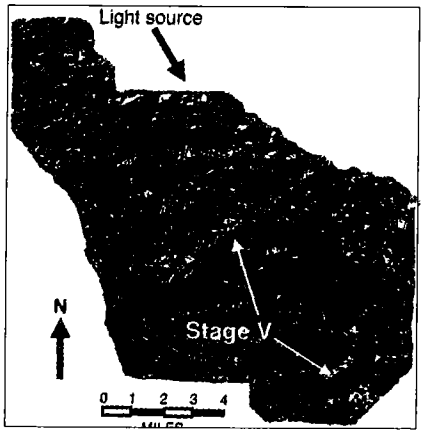

Figure 7. Three-dimensional visualization of Red Fork interval isochron (Novi Lime to Lower Skinner horizons).

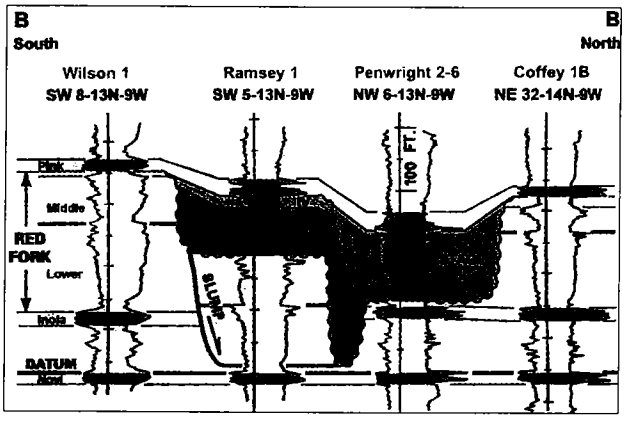

Figure 8. Stratigraphic well-log cross-section B showing stages II, IV, and V valley fill and slump fault in Ramsey 1 well. Cross-section datum is top of Novi Lime. Upper Red Fork valley stages and regionally correlative limestones are shaded.

Both spectral decomposition and coherency images show many valley-shaped features throughout the 3-D area in the Red Fork interval. Many of these features were previously unknown, and more work is needed to determine how they fit into the interpretation of the Red Fork. Coherency also led to the interpretation of valley-edge slump features and the recognition that not all faults in this area are basement involved.

ACKNOWLEDGMENTS

We thank Jim Gridley, who along with Greg Partyka developed and shared the spectral decomposition technology that was so instrumental in arriving at the final conclusions. Dale Leckie kindly provided his photograph of a modern incised valley and associated valley edge slumping in New Zealand. Many thanks to Allan Skorpen and Terri Olson for editing the original manuscript. Thanks to Amoco and Gothic Energy for allowing publication of these data and the results of this study.

SUGGESTIONS FOR FURTHER READING

Bahorich, M.; and Farmer, S., 1995, 3-D seismic discontinuity for faults and stratigraphic features: the coherence cube: The Leading Edge, v.14, p. 1053–1058.

Bingham, T. L., 1993, Desmoinesian fluvial-deltaic sandstone and shallow marine limestone—Anadarko basin, Oklahoma, *in* Bebout, D. G.; White, W. A.; Hentz, T. F.; and Grasmick, M. K. (eds.), Atlas of major Midcontinent gas reservoirs: Gas Research Institute, Bureau of Economic Geology, University of Texas at Austin, p. 33–35.

Clement, W. A., 1991, East Clinton field—USA, Anadarko basin, Oklahoma, *in* Foster, N. H.; and Beaumont, E. A. (eds.), Stratigraphic traps II: American Association of Petroleum Geologists Treatise of Petroleum Geology, Atlas of Oil and Gas Fields, p. 207–262.

Lopez, J. A.; Partyka, G.; Haskell, N. L.; Nissen, S. E., 1997, Identification of deltaic facies with 3-D seismic coherency and the spectral decomposition cube [abstract]: Society of Exploration Geophysicists 1997 International Meeting, Istanbul, Turkey, p. 191.

Partyka, Greg; and Gridley, J., 1997, Interpretation aspects of spectral decomposition [abstract]: Society of Exploration Geophysicists 1997 International Meeting, Istanbul, Turkey, p. 189–190.

Partyka, Greg; Gridley, J.; and Lopez, J., 1999, Interpretational applications of spectral decomposition in reservoir characterization: The Leading Edge, v. 18, p. 353–354, 356–357, 360.

Geochemical Study of Oils Produced from Four Pennsylvanian Reservoirs in Prairie Gem Field, Central Oklahoma

Elli Chouparova[1]
University of Oklahoma
Norman, Oklahoma

Kurt Rottmann
Independent Consultant
Oklahoma City, Oklahoma

R. Paul Philp
University of Oklahoma
Norman, Oklahoma

ABSTRACT.—The Prairie Gem field is located in Lincoln County, central Oklahoma (T. 16 N., R. 2 E.). It is geologically situated on the Cherokee platform, approximately 25 mi east of the Nemaha fault zone. Oils are produced in the field from four fluvial-deltaic reservoirs belonging to the Cherokee Group (Middle Pennsylvanian), namely the Skinner (Upper and Lower), Red Fork, and Bartlesville, the latter being a main producing formation. The most probable source-rock candidates for the oil accumulations are considered to be the Upper Devonian–Mississippian Woodford Shale and/or the Pennsylvanian black shales. Migration directions and pathways and the timing of oil accumulation in the field have not been well established.

The focus of the present study is on the geochemical characterization and evaluation of compositional similarities and differences of oils produced from the Bartlesville, Red Fork, and Lower and Upper Skinner reservoirs in Prairie Gem field. Geochemical parameters indicative of source, maturation, and migration characteristics of the oils are compared in an attempt to elucidate possible genetic relationships among the oils and to gain insight about the elements of petroleum system(s). Data were obtained from a set of experimental methods (high-performance liquid chromatography, gas chromatography, gas chromatography/mass spectrometry, high-temperature gas chromatography, and pyrolysis gas chromatography) directed to characterize C_{10+} bulk-oil fractions and molecular parameters, including the high-molecular–weight wax and asphaltene factions

The results suggest characteristics of common source-rock(s) for the oil accumulations in the Bartlesville, Red Fork, and Skinner reservoirs from the Prairie Gem field. Maturity of the oils, calculated from the aromatic hydrocarbon distributions, corresponds to a vitrinite reflectance range of 0.8–1%. Lower Skinner oil is distinguished from the other oils by a number of parameters indicating different maturation and/or migration history. To a lesser extent, some of these characteristics are also recognized for the Bartlesville oil. The most consistent explanation for the compositional differences of the Lower Skinner oil is based on the possibility of mixing an existing black-oil accumulation with a later migrated charge(s) of gas condensates. The origin of gas condensates could be thermogenic and/or resulting from migration/fractionation processes. A future regional geochemical-geologic study is suggested to further clarify these possibilities.

INTRODUCTION

The Paleozoic sequence within the sedimentary basins of Oklahoma represents one of the most prolific petroleum-producing regions in the continental United States. A wide distribution of high-quality source rocks and reservoirs coupled with favorable tectonic and maturation histories have contributed to intensive oil and gas generation and the formation of numerous hydrocarbon accumulations (e.g., Oakes, 1953; Huffman, 1959; Dogan, 1970; Pulling, 1979a,b; Mankin, 1986; Campbell and others, 1988; Johnson and others, 1988;

[1]Present address: Shell Oil Company, Houston, Texas.

Chouparova, Elli; Rottman, Kurt; and Philp, R. P., 2001, Geochemical study of oils produced from four Pennsylvanian reservoirs in the Prairie Gem field, central Oklahoma, *in* Johnson, K. S. (ed.), Pennsylvanian and Permian geology and petroleum in the southern Midcontinent, 1998 symposium: Oklahoma Geological Survey Circular 104, p. 105–113.

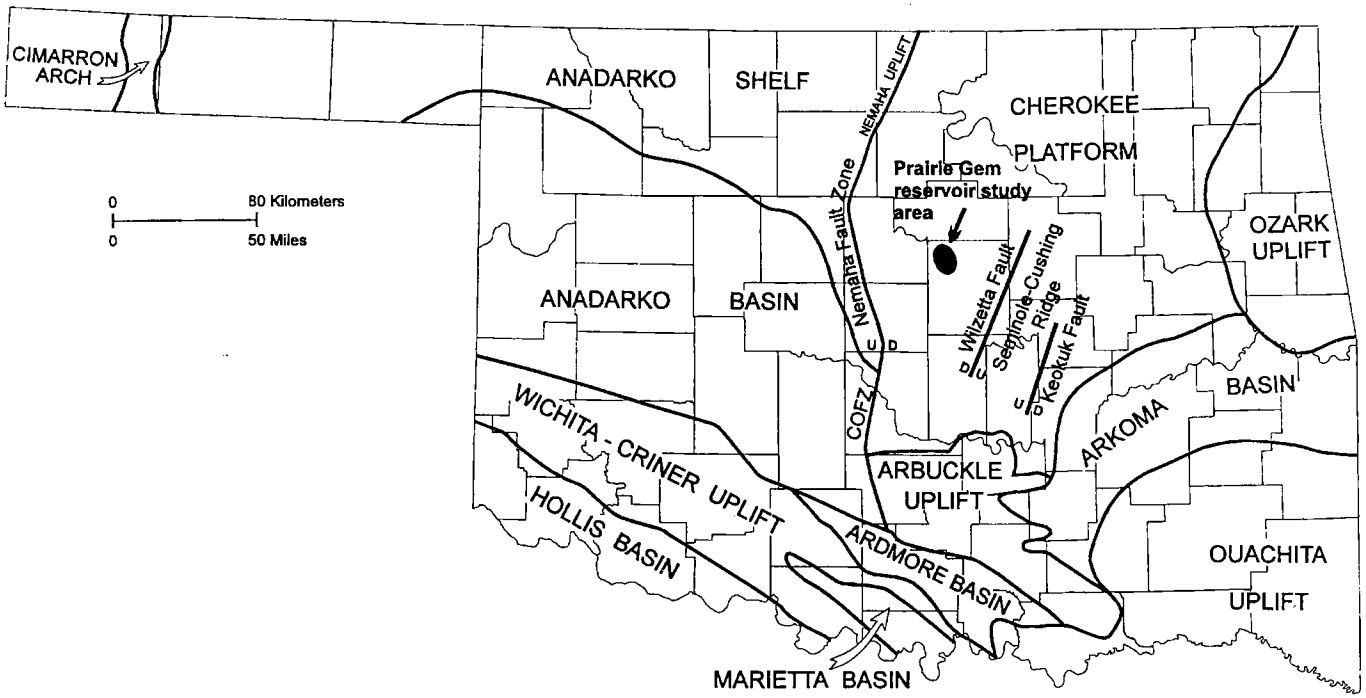

Figure 1. Tectonic map of Oklahoma showing the primary basins and major structural features in the vicinity of the Prairie Gem field study area. Abbreviation: COFZ—Central Oklahoma fault zone.

Johnson and Cardott, 1992; Northcutt and Johnson, 1996; Andrews and others, 1996, 1997a,b). A significant portion of the oil and gas production in Oklahoma comes from the Pennsylvanian fluvial-deltaic reservoirs (Northcutt and Johnson, 1996), which are also the primary producing horizons in the Prairie Gem field.

The focus of the present study is on the geochemical characterization of oils produced from four Pennsylvanian reservoirs, namely the Bartlesville, Red Fork, and the Lower and Upper Skinner sands, in the Prairie Gem field (T. 16 N., R. 2 E.), Lincoln County, Oklahoma (Fig. 1). Geochemical parameters indicative of source-rock, maturation, and migration characteristics for the oils are compared in order to establish possible genetic relationships and to gain insight about the elements of the petroleum system(s). The hydrocarbon accumulations in Prairie Gem field are largely in stratigraphic type traps. Late Devonian–Mississippian Woodford black shales are widely distributed in the region and are expected to be the most probable source rock for the oil accumulations in the Prairie Gem field, although a contribution from the Pennsylvanian black shales is also discussed (Comer and Hinch, 1987; Johnson and Cardott, 1992, and references therein). Migration directions and pathways as well as the timing of hydrocarbon accumulation in reservoirs of the studied field have not been well established.

GEOLOGIC SUMMARY

Prairie Gem is a small field located on the Cherokee platform approximately 25 mi east of the Nemaha fault zone (Figs. 1, 2). The oil production in the field is from the Upper and Lower Skinner, Red Fork, and Bartles-

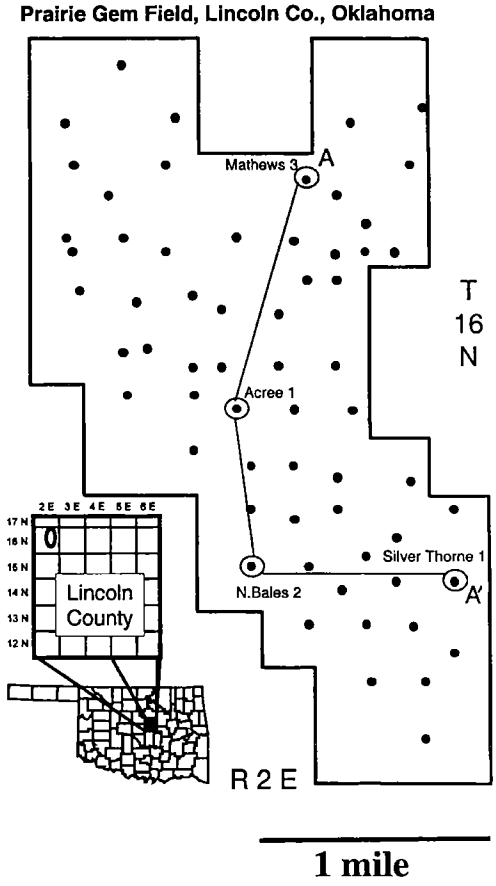

Figure 2. Generalized location map of Prairie Gem field in Lincoln County, Oklahoma. Line of cross section A–A′ (Fig. 3) is shown.

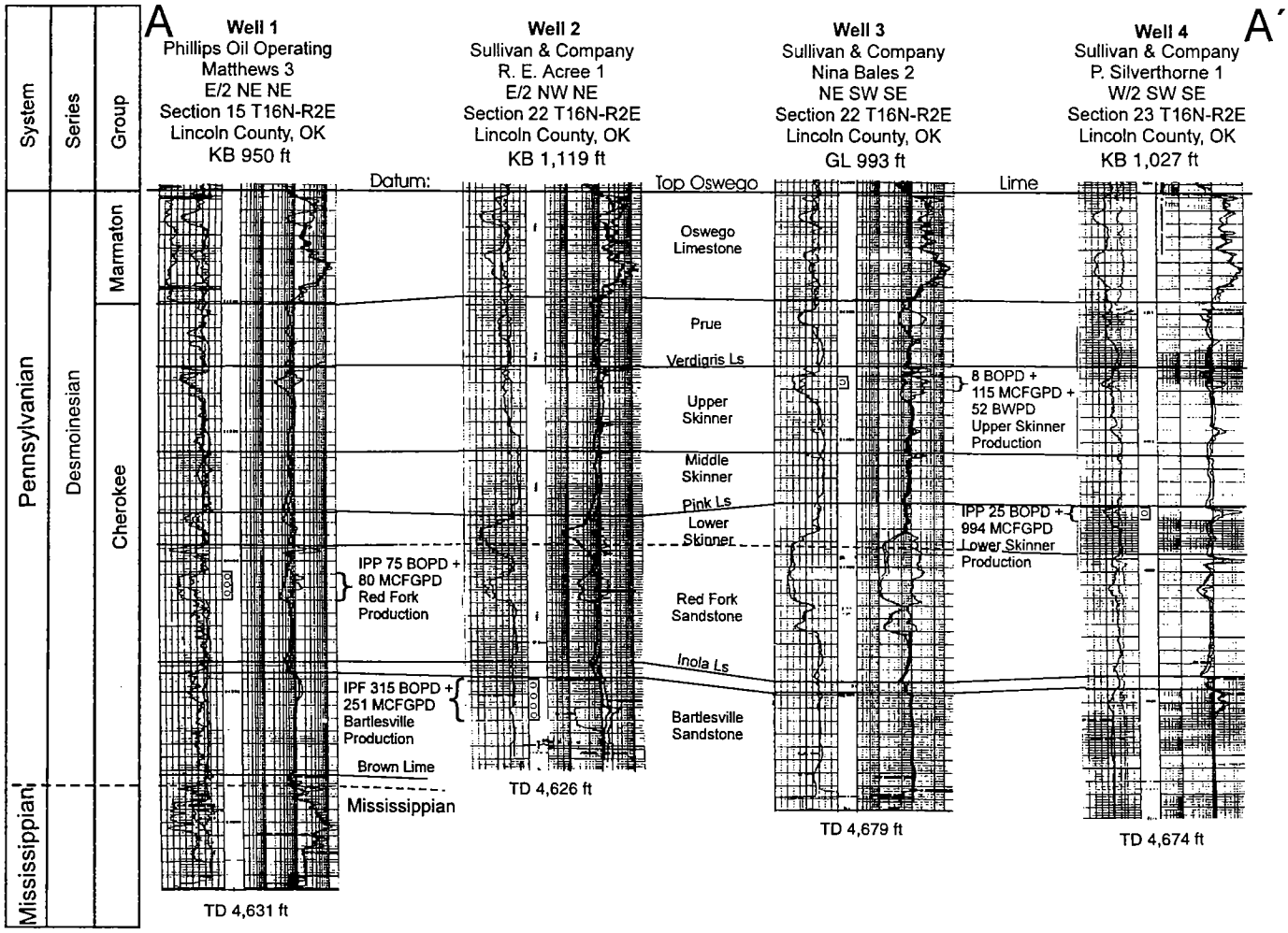

Figure 3. Stratigraphic cross section A–A′, illustrating the relationship of the Cherokee Group producing formations to each other. Line of section is shown on Figure 2. Abbreviations: KB—Kelley bushing (elevation); TD—total depth; BOPD—barrels of oil per day; MCFGPD—thousand cubic feet of gas per day; BWPD—barrels of water per day.

ville sands, the latter being the main producing formation. This report presents the result of the study of four reservoirs belonging to the Cherokee Group of the Middle Pennsylvanian Desmonesian Series (Fig. 3), which lies unconformably on the eroded Mississippian surface. A well-location map for the Prairie Gem field, situated in sec. 9, 10, 11, 14, 15, 16, 22, 23, 26, and 27, T. 16 N., R. 2 E., Lincoln County, Oklahoma, is presented in Figure 2.

The four studied wells and their respective producing zones identified on the location map (Fig. 2) constitute the stratigraphic cross section A–A′ (Fig. 3). The type log for the field is Phillips Oil Operating 3 Mathews (located in sec. 15), which is a Red Fork sand producer. The Sullivan & Company 1 R. E. Acree well (sec. 22) was chosen as representative for the Bartlesville sand producers. The Sullivan & Company 2 Nina Bales and 1 P. Silverthorne wells (secs. 22 and 23, respectively) are the only Upper and Lower Skinner sand producers in the field. The stratigraphic relationships for the four producing horizons in the field are shown in Figure 3.

SAMPLES AND METHODS

The Prairie Gem field was discovered in 1979 and was in primary production until December of 1993, when a waterflood program was initiated for the field. The oil samples used in the present study were collected from the wellheads of producing wells described above during the last year (November 1993) of primary production.

Data discussed in the present study were obtained from a set of experimental methods directed to characterize the C_{10+} oil fractions and high-molecular–weight waxes (HMW) and alphaltenes. The analytical procedures for high-performance liquid chromatography (HPLC), branched/cyclic fraction isolation, wax and asphaltene precipitation, gas-chromatography (GC) analysis of C_{10+} fractions, and high-temperature gas chromatography (HTGC) have been described previously (Tchouparova, 1999).

Gas-chromatography–mass-spectrometric (GC-MS) analysis of whole oils and oil fractions was performed using a Finnigan Triple Stage Quadropole (TSQ 70)

system equipped with 30 m × 0.32 mm inside-diameter DB-5 column with 0.25 μm film thickness. Temperature program was from 40°C to 300°C at 4°C/min. A deuterated C_{24} alkane was added as an internal standard. The majority of the analyses were performed in the selected-ion–monitoring mode (SIM), with a small number of samples run in full-scan mode. Peak heights were calculated from a baseline drawn on a cluster-by-cluster basis.

Flash Pyrolysis-GC (Py-GC) analysis was performed on asphaltene fractions. The asphaltenes (n-pentane insoluble fraction) were dissolved in methylene chloride and pyrolyzed using a CDS Pyroprobe coupled to a Varian 3300 gas chromatograph with a split injection system and flame ionization detector (FID). The setting for pyrolysis was 610°C for 20 s. The pyrolysates were rapidly removed from the heated interface (280°C) by a stream of helium onto a 15 m × 0.32 mm inside-diameter DB-1 HT column. The column temperature was held at –25°C for 4 min during the pyrolysis and then increased to 300°C at a rate of 4°C/min.

Stable–carbon-isotope analysis of oil fractions was performed in the laboratory of Professor M. Engel at the University of Oklahoma by Rick Maynard. The procedure is described in detail in Engel and Maynard (1989). The δ^{13} C (per mil) values for the samples analyzed are reported relative to the PDB Standard.

RESULTS AND DISCUSSION

A summary of bulk-compositional parameters and main results from geochemical characterization of the whole oils and oil fractions are presented in Tables 1, 2, 3, and 4 and Figure 4. The results suggest characteristics of common source rock(s) for the oil accumulations in the Bartlesville, Red Fork, and Skinner reservoirs of the Prairie Gem field, based on similarities in carbon-isotope composition of bulk oil fractions, carbon-preference index, sterane- and triterpane-based parameters (Tables 2–4). Maturity of the oils, calculated from the aromatic-hydrocarbon distributions, corresponds to a vitrinite-reflectance range of 0.8–1% (Table 4). The Lower Skinner oil is distinguished from the other oils by a number of parameters suggesting different maturation and/or migration history—high gas-oil ratio and API gravity (Table 1), "front-end" loading with $nC_{10} - C_{20}$ alkanes (Fig. 4), elevated ratios for pristane/phytane, C_{23} tricyclic terpane/C_{30} hopane, $C_{21}/(C_{21} + C_{28})$ triaromatic steranes, and low asphaltene and microcrystalline wax contents (Tables 2, 4). To a lesser extent, some of these characteristics are also recognized for the Bartlesville oil.

The most consistent explanation for the compositional differences of the Lower Skinner oil is based on the possibility of mixing an existing black-oil accumulation with a later-migrated charge(s) of gas condensates. The origin of gas condensates could be thermogenic and/or result from migration/fractionation processes. The possibility of mixing of migrated hydrocarbons with pre-existing accumulations on a regional scale could be supported by the abundance of prolific source rocks and the tectonic development of the region leading to oil and gas generation from several different source-rock formations during approximately the same geologic periods in different basins in Oklahoma (e.g., Engel and others, 1988; Burrus and Hatch, 1989; Jones and Philp, 1990; Wavrek, 1992). Geologic conditions for

Table 1.—Summary of Bulk Compositional Parameters from Initial Test Data (A) as Related to the Fluid-Type Classification (B) of McCain (1990)

(A) Producing well	Producing zone	Oil gravity (°API)	Gas–oil ratio (scf/STB) initial test data	Fluid-type classification (McCain, 1990)	Duration of production before sampling (years)
Acree 1	Bartlesville	36	796	Black oil	13
Mathews 3	Red Fork+	32	1,066	Black oil	9
Nina Bales 2	Upper Skinner	35	1,535	Black oil	12
Silver Thorne 1	Lower Skinner	45	39,760	Volatile oil or retrograde liquid	4

(B) Fluid type	Initial GOR (scf/STB)	Gravity (API)	Oil color	Amount C_{7+} (mole %)
Black oil (low shrinkage)	<2,000	<45	Dark, black, with or without greenish cast	>30
Volatile oil (high shrinkage)	2,000–3,000	>40	Brown, orange, green	12.5–30
Retrograde gas (gas condensate)	>3,300	40–60	Light-brown, orange, greenish, or water-white	<12.5

scf = standard cubic feet; STB = stock-tank barrels; GOR = gas–oil ratio.

Table 2.—Gross Composition of Oil Fractions (wt.% of oil) Based on HPLC, Asphaltene and Wax Precipitation, and Molecular Sieving Analyses

Well	Production zone	SAT	B/C*	ARO	NSO	ASPH	WAX	SAT+ARO / NSO+ASPH
Nina Bales 2	Upper Skinner	54.4	29.3	29.1	7.7	8.7	22.0	5.1
Silver Thorne 1	Lower Skinner	68.7	40.5	22.3	8.0	1.0	2.6	10.1
Mathews 3	Red Fork	55.2	31.2	27.3	7.1	10.5	10.4	4.7
Acree 1	Bartlesville	63.8	36.5	23.6	10.5	2.1	3.0	6.9

Notes: SAT, B/C, ARO, NSO, and ASPH refer to the saturate, branched/cyclic, aromatic, resin, and aphaltene fractions.
* % of saturate fraction.

Table 3.—Stable Carbon-Isotope Composition ($\delta^{13}C$, ‰) of Oil Fractions

Well	Production zone	SAT	B/C	ARO	NSO	ASPH
Nina Bales 2	Upper Skinner	–30.93	–30.76	–30.21	–29.83	–30.31
Silver Thorne 1	Lower Skinner	–30.87	–30.77	–29.83	–28.38	–28.56
Mathews 3	Red Fork	–30.94	–30.73	–30.43	–29.21	–30.57
Acree 1	Bartlesville	–30.90	–30.76	–30.11	–28.37	–29.83

burial of already-formed accumulations of oil and secondary cracking to gas condensates are readily available—e.g., in the Anadarko basin—as well as for gas-condensate generation from predominantly Type III kerogens in the Arkoma basin. Favorable geologic conditions for redistribution of hydrocarbons as a result of tertiary migration due to evaporative fractionation or migration/fractionation are also available, considering that the process involves: (1) migration of large amounts of allochtonous dry gas (methane) to an existing, shallower oil accumulation; (2) fractionation and migration of gas condensate from the oil accumulation due to pressure release (i.e., along an activated fault zone), leaving the residual oil accumulation rich in aromatics; and (3) formation of gas-condensate accumulation depleted in light aromatics and enriched in paraffins (Thompson, 1979, 1983, 1987). Gas-condensate accumulations formed by this process differ from the thermogenic gas condensates in the composition of their gasoline-range hydrocarbons as shown by Thompson (1987).

The present study demonstrated several characteristics of Lower Skinner oil that are indicative of the migration/fractionation processes, including "front-end" loading, elevated Pr/Ph, C_{23} tricyclic/C_{30} hopane, and C_{21}/C_{21} + 20R – C_{28} triaromatic steranes. These results are consistent with the observations of Curiale and Broomley (1996) and Dzou and Hughes (1993) for the compositional alteration of oils affected by migration/fractionation processes in the Gulf Coast and offshore Taiwan regions. We suggest, however, that a future regional geochemical study, including comparison of gasoline-range hydrocarbon composition, gas-isotope study, and possible identification of residual, aromatic-enriched oil accumulations, could provide more compelling evidence to support or reject such a possibility. It should also be noted that the classic compositional characteristics of residual oil accumulations could be masked under extensive and multiple-mixing processes.

Recent studies have presented strong evidence that fault activity has a major control on oil migration in faults (Losh, 1998; Losh and others, 1999). Considering this possibility, several local structures and features in the tectonic development of Cherokee platform appear relevant to a discussion on possible conduits for redistribution of hydrocarbons in different accumulations, including the Prairie Gem field, and timing of tertiary migration. Several major structures are in close geographic proximity to the Prairie Gem field—the Nemaha fault zone (~20 mi), the Seminole-Cushing ridge and Wilzetta fault (~20 mi), and the Ozark uplift (~90 mi), as illustrated in Figure 1. In addition, a number of other minor faults and fracturing of reservoirs are reported in the literature as discussed below.

The regional stratigraphic profiles and maps presented in previous studies (Dogan, 1970; Andrews and others, 1997a,b) suggest that Nemaha fault zone was a structurally and topographically positive feature during the time of deposition of Cherokee Group, even though local variations are present. For example, the zone had been completely buried by the end of Red Fork deposition in the northwestern part of Logan County (northwest of the Prairie Gem field), whereas in

Table 4.—Geochemical Indicators for Source, Maturity, and Migration Based on GC and GC-MS Analysis of Whole Oils (C_{10+} Components)

Parameter	Bartlesville	Red Fork	L. Skinner	U. Skinner
CPI[1]	0.94	0.94	0.97	0.81
Pr/Ph[2]	1.4	1.32	1.79	1.36
$(C_{17}–C_{19})/(C_{27}–C_{29})$[3]	2.87	4.43	6.38	4.08
% C_{27}:C_{28}:C_{29} steranes[4]	32:10:58	32:9:59	27:7:66	27:9:64
C_{29}/C_{30} ββ steranes	4.1	4.1	4.7	4.5
C_{29} ββ/αα steranes	1.09	0.95	1.06	1.18
20S/20S+20R[5]	0.45	0.48	0.50	0.50
C_{29}/C_{30}[6]	0.56	0.65	0.62	0.71
Tm/Ts[7]	1.57	2.55	1.67	2.78
22S/22S+22R[8]	0.62	0.61	0.54	0.60
C_{23}/C_{30}[9]	0.40	0.40	0.88	0.32
%TA/TA+MA[10]	74	84	62	86
TA(C_{21}/C_{21}+20R–C_{28})[11]	0.24	0.23	0.42	0.19
MPI3[12]	0.59	0.50	0.67	0.47
MPR[13]	0.91	0.68	0.83	0.71
MNR[14]	0.97	0.91	1.26	1.10
$\%R_{MPR}$[15]	0.91	0.77	0.86	0.79
$\%R_{MNR}$[16]	0.99	0.98	1.03	1.01

[1]Carbon Preference Index of n-alkanes = ½((C_{25}+C_{27}+C_{29}+C_{31}+C_{33})/(C_{24}+C_{26}+C_{28}+C_{30}+C_{32})+(C_{25}+C_{27}+C_{29}+C_{31}+C_{33})/(C_{26}+C_{28}+C_{30}+C_{32}+C_{34})).

[2]Pristane/Phytane.

[3](C_{17}+C_{18}+C_{19})/(C_{27}+C_{28}+C_{29}) n-alkanes.

[4]5α(H),14α(H),17α(H), 20R-cholestane, 5α(H),14α(H),17α(H), 20R-24-methylcholestane, and 5α(H),14α(H),17α(H), 20R-24-ethylcholestane as percentages of total αααR-C_{27-29} steranes.

[5]C_{29} ααα-steranes.

[6]C_{29} 17α(H),21β(H)-norhopane/C_{30} 17α(H),21β(H)-hopane.

[7]C_{27} 17α(H)-trisnorhopane/C_{27} 18α(H)-trisnorhopane.

[8]C_{32} 17α(H), 21β(H)-hopanes.

[9]C_{23} tricyclic terpane/C_{30} 17α(H), 21β(H)-hopane.

[10]C_{28} Triaromatic/(C_{28} Triaromatic+C_{29} Monoaromatics) steroid hydrocarbons.

[11]Triaromatic steroid hydrocarbons.

[12]Methylphenanthrene index MPI3=(2MP+2MP)/(1MP+9MP). Garrigues and others (1988).

[13]Methylphenanthrene ratio MPR = 2MP/1MP.

[14]Methylnaphthalene ratio MNR = 2MN/1MN.

[15]Mean vitrinite reflectance calculated as $\%R_{MPR}$ = 0.95+1.1$\log_{10}$MPR. Radke (1988).

[16]Mean vitrinite reflectance calculated as $\%R_{MNR}$ = 0.17MNR+0.82. Radke and others (1984).

the southern part of the same county, the zone has not been active during the Cherokee Group deposition. The central Oklahoma fault zone is interpreted as having been completely buried by the end of Red Fork and Lower–middle Skinner in the southern and northern parts of Oklahoma County, respectively (Andrews and others, 1996, 1997a,b). The McClain County fault zone, extending southward from the Oklahoma City uplift, represents a major zone of shearing between the Cherokee platform and the Anadarko basin. This fault zone is considered active during the Cherokee Group deposition (Pulling, 1979a). A number of local faults in the adjacent areas (Oklahoma, Logan, Payne, and Lincoln Counties) to the north, west, and south of Prairie Gem are apparent on the Mississippian isopach map of Rottmann (1997), and some of them had been active later, even though with a small displacements. Possible presence of a normal northwest–southeast-trending fault, <1 mi west–northwest of the Prairie Gem field, is suggested based on the structure map on top of the Pink lime by Shulman (1966).

The Seminole-Cushing ridge, with the associated Wilzetta and Keokuk faults to the west and east, respectively, is another structural element in close geographical proximity to the Prairie Gem field. The Keokuk fault is considered completely buried by the end of Red Fork interval deposition whereas the Wilzetta fault appears to be completely buried by the end of the Prue sand deposition (Andrews and others, 1997b). The difference in latest timing of activation between the eastern and western flanks of the Seminole-Cushing ridge could be related to the tectonic activity associated with the McClain fault and Pauls Valley uplift. The Wilzetta fault is evident on structure maps on top of the Viola, pre-Pennsylvanian unconformity map and top of the Verdigris in Pottawatomie County (Pulling, 1979a; Joseph, 1987). The initial uplift of the Seminole-Cushing ridge is believed to have occurred during the Middle Devonian associated with normal faulting along the Wilzetta fault representing the western flank of the Seminole-Cushing ridge. During the

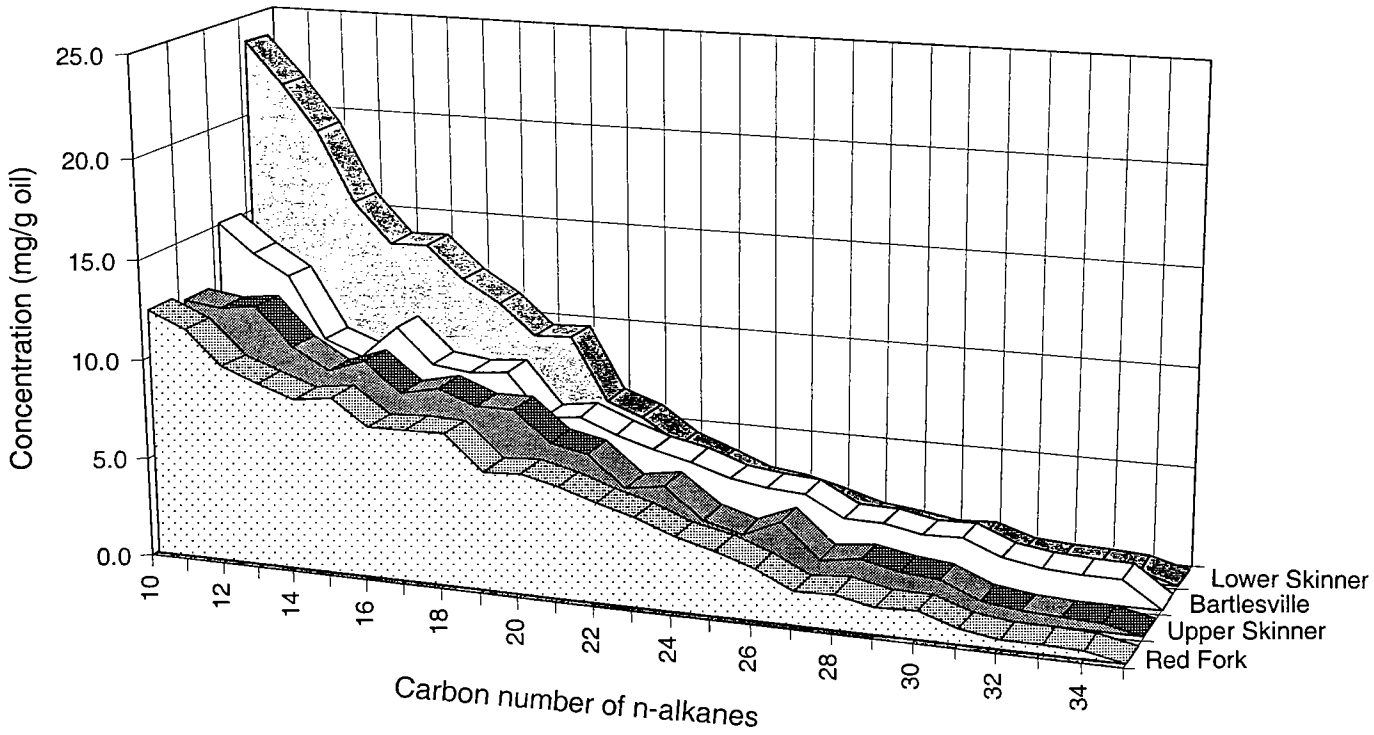

Figure 4. Plot of concentration of n-alkanes in milligrams per gram of oil versus carbon number of n-alkanes showing results of quantitative gas-chromatographic (GC) analysis of whole oils. Note the "front-end" loading with lower molecular weight $nC_{10} - C_{20}$ alkanes in Lower Skinner oil (for further discussion refer to text).

post-Mississippian to pre-Desmonesian time (late Morrowan), a major folding of the Seminole-Cushing ridge and rejuvenation of the Wilzetta and other northeast–southwest-trending faults took place that was related to the Pauls Valley uplift to the south. During this period of folding and faulting, the area was tilted toward the east, and eastward dips of Paleozoic strata below the pre-Pennsylvanian unconformity were established. During the Desmoinesian (Cherokee deposition), possible growth faulting, with recurrent movement, is suggested along the Seminole-Cushing ridge, resulting in the formation of thicker sequences on the downthrown side (Lozano, 1969; Pulling, 1979a; Joseph, 1987). During the late Desmoinesian, renewed movement of the Wilzetta fault is reflected on the Verdigris (top of Skinner) structure maps of Pulling (1979a) and Joseph (1987). Westward tilting of the area, reflected in westward dips of the Verdigris and pre-Pennsylvanian unconformity, is thought to have occurred during the post-Permian/pre-Cretaceous (Pulling, 1979a) or at the close of the Permian (Joseph, 1987). The change in the regional tilt from eastward to westward and the recurrent activation of major faults are two favorable conditions for initiation of hydrocarbons redistribution among pre-existing accumulations in the areas of Seminole-Cushing ridge and Pauls Valley uplift. Additional partial support comes from observations, such as the presence of tilted oil-water contacts in Red Fork sand accumulations (Creek County, T. 19 N., R. 8 E.; Hanke, 1967) and gradual changes in the type of Lower Skinner accumulations from black oil in the regions south–southwest of Prairie Gem (Kurt Rottmann, 1996, unpublished data) to greenish oil and gas in the areas northeast of the Prairie Gem field (Hanke, 1967).

CONCLUSIONS

The geochemical characteristics of oils in this study suggest common source rock(s) for the oil accumulations of the Bartlesville, Red Fork, and Lower and Upper Skinner reservoirs in the Prairie Gem field. The maturity level of the oils, calculated from the aromatic hydrocarbon distributions, corresponds to 0.8–1% vitrinite reflectance. Lower Skinner oil is distinguished by a number of parameters, suggesting different maturation and/or migration history—high GOR, "front-end loading" with $nC_{10} - C_{20}$ alkanes, elevated Pr/Ph, C_{23} tri/C_{30} hopane, $C_{21}/C_{21} + 20R$–C_{28} triaromatic steranes, low asphaltene, and micro-crystalline wax contents. To a lesser extent, some of these characteristics are recognized for Bartlesville oil as well. Based on analysis of the results, the possibility of mixing of original black-oil accumulation with later charge(s) of migrating gas condensates is proposed to account for the compositional differences of the Lower Skinner oil. The origin of gas-condensates could be thermogenic or result from migration/fractionation processes. A future regional geochemical and geologic study is suggested to further clarify these possibilities.

ACKNOWLEDGMENTS

We thank the production companies (Beard Co., Sensor, Ltd., and Phoenix PetroCorp, Inc.) of the Prairie Gem field for their help in collecting the samples, providing geologic and production information for the field, and permission to publish the results. A. Bishop is acknowledged for the establishment of initial contacts with Beard Co. and oil-sample collection. A number of participants at the "Pennsylvanian reservoirs" 1998 workshop are thanked for the useful discussions on the topic of this study.

REFERENCES CITED

Andrews, R. D.; Campbell, J. A.; Northcutt R. A.; Rottmann, K.; Bhatti, Z. N.; Knapp, R. M.; Yang, X. H.; and Simpson, R. P., 1996, Fluvial-dominated deltaic (FDD) oil reservoirs in Oklahoma: the Skinner and Prue plays: Oklahoma Geological Survey Special Publication 96-2, 106 p.

Andrews, R. D.; Northcutt R. A.; and Campbell, J. A., 1997a, Fluvial-dominated deltaic (FDD) oil reservoirs in Oklahoma: the Bartlesville play: Oklahoma Geological Survey Special Publication 97-6, 93 p.

Andrews, R. D.; Campbell, J. A.; Northcutt R. A.; and Rottmann, K., 1997b, Fluvial-dominated deltaic (FDD) oil reservoirs in Oklahoma: the Red Fork play: Oklahoma Geological Survey Special Publication 97-1, 90 p.

Burrus, R. C.; and Hatch, J. R., 1989, Geochemistry of oils and hydrocarbon source rocks, greater Anadarko basin: evidence for multiple sources of oils and long-distance oil migration, *in* Johnson, K. S. (ed.), Anadarko basin symposium, 1988: Oklahoma Geological Survey Circular 90, p. 53–64.

Campbell, J. A.; Mankin, C. J.; Schwarzkopf, A. B.; and Raymer, J. H., 1988, Habitat of petroleum in Permian rocks of the Mid-continent region: Midcontinent Society of Economic Paleontologists and Mineralogists Special Publication 1, p. 13–35.

Comer, J.; and Hinch, H., 1987, Recognizing and quantifying expulsion of oil from the Woodford Formation and age equivalent rocks in Oklahoma and Arkansas: American Association of Petroleum Geologists Bulletin, v. 71, p. 844–858.

Curiale, J. A.; and Broomley, B. W., 1996, Migration induced compositional changes in oils and condensates of a single field: Organic Geochemistry, v. 24, p. 1097–1113.

Dogan, N., 1970, Subsurface study of Pennsylvanian rocks in east-central Oklahoma (from the Brown Limestone to the Checkerboard Limestone): Shale Shaker, v. 20, p. 192–213.

Dzou, L. I. P.; and Hughes, W. B., 1993, Geochemistry of oils and condensates, K field, offshore Taiwan: a case study in migration fractionation: Organic Geochemistry, v. 20, p. 437–462.

Engel, M. H.; Imbus, S. W.; and Zumberge, J. E., 1988, Organic geochemical correlation of Oklahoma crude oils using R- and Q-mode factor analysis: Organic Geochemistry, v. 12, p. 157–170.

Engel, M.; and Maynard, R., 1989, Preparation of organic matter for stable carbon isotope analysis by sealed tube combustion: a cautionary note: Analytical Chemistry, v. 61, p. 1996–1998.

Garrigues, P.; de Sury, R.; Angelin, M. L.; Bellocq, J.; Oudin, J. L.; and Ewald, M., 1988, Relation of the methylated aromatic hydrocarbon distribution pattern to the maturity of organic matter in ancient sediments from the Mahakam delta: Geochimica et Cosmochimica Acta, v. 52, p. 375–384.

Hanke, H. W., 1967, Subsurface stratigraphic analysis of the Cherokee Group in north-central Creek County, Oklahoma: Shale Shaker, v. 17, p. 150–167.

Huffman, G. G., 1959, Pre-Desmoinesian isopachous and paleogeological studies in central Mid-Continent region: American Association of Petroleum Geologists Bulletin, v. 43, p. 2541–2574.

Johnson, K. S.; Amsden, T. W.; Denison, R. E.; Dutton, S. P.; Goldstein, A. G.; Rascoe, B.; Sutherland, P. K.; and Thompson, D. M., 1988, Southern Midcontinent region, *in* Sloss, L. L. (ed.), Sedimentary cover—North American craton; U.S.: Geological Society of America, The Geology of North America, v. D-2, p. 307–359. [Reprinted as Oklahoma Geological Survey Special Publication 89-2, 53 p.]

Johnson, K. S.; and Cardott, B. J., 1992, Geological framework and hydrocarbon source rocks of Oklahoma, *in* Johnson, K. S.; and Cardott, B. J. (eds.), Source rocks in the southern Midcontinent: Oklahoma Geological Survey Circular 93, p. 21–32.

Jones, P. J.; and Philp, R. P., 1990, Oils and source rocks from Pauls Valley, Anadarko basin, Oklahoma, U.S.A.: Applied Geochemistry, v. 5, p. 429–448.

Joseph, L., 1987, Subsurface analysis, "Cherokee" Group (Des Monesian), portions of Lincoln, Pottawatomie, Seminole, and Okfuskee Counties, Oklahoma: Shale Shaker, v. 37, p. 44–69.

Losh, S., 1998, Oil migration in a major growth fault: structural analysis of the Pathfinder core, South Eugene Island Block 330, offshore Louisiana: American Association of Petroleum Geologists Bulletin, v. 82, p. 1694–1710

Losh, S.; Eglinton, L.; Schoell, M.; and Wood, W., 1999, Vertical and lateral fluid flow related to a large growth fault, South Eugene Island Block 330 field, offshore Louisiana: American Association of Petroleum Geologists Bulletin, v. 83, p. 244–276.

Lozano, F., 1969, Subsurface geology of the Seminole area: Shale Shaker, v. 19, p. 118–130.

Mankin, C. J., 1986, Texas-Oklahoma tectonic region correlation chart, *in* Correlation of stratigraphic units in North America: American Association of Petroleum Geologists, Tulsa, Oklahoma.

McCain, W. D., 1990, The properties of petroleum fluids: PennWell Books, Tulsa, Oklahoma, 548 p.

Northcutt, R. A.; and Johnson, K. S., 1996, Pennsylvanian deltaic-channel reservoirs in Oklahoma, *in* Johnson, K. S. (ed.), Deltaic reservoirs in the southern Midcontinent, 1993 symposium: Oklahoma Geological Survey Circular 98, p. 32–45.

Oakes, M. C., 1953, Krebs and Cabaniss Groups of Pennsylvanian age in Oklahoma: American Association of Petroleum Geologists Bulletin, v. 37, p. 1523–1526.

Pulling, D. M., 1979a, Subsurface stratigraphic and structural analysis, Cherokee Group, Pottawatomie County, Oklahoma (part I): Shale Shaker, v. 29, p. 124–137.

_____ 1979b, Subsurface stratigraphic and structural analysis, Cherokee Group, Pottawatomie County, Oklahoma (part II): Shale Shaker, v. 29, p. 148–158.

Radke, M., 1988, Application of aromatic compounds as maturity indicators in source rocks and crude oils: Marine and Petroleum Geology, v. 5, p. 224–236.

Radke, M.; Leythaeuser, D.; and Teichmüller, M., 1984, Relationship between rank and composition of aromatic hydrocarbons for coals of different origins: Organic Geochemistry, v. 6, p. 423–430.

Rottmann, Kurt, 1997, Stratigraphy, paleogeomorphology, and structure of Simpson, Viola, and Mississippian strata, and their integral relationships to "Second Wilcox" production in Lincoln and Logan Counties, Oklahoma, *in* Johnson, K. S. (ed.), Simpson and Viola Groups in the southern Midcontinent, 1994 symposium: Oklahoma Geological Survey Circular 99, p. 137–154.

Shulman, C., 1966, Stratigraphic analysis of the Cherokee Group in adjacent portions of Lincoln, Logan, and Oklahoma Counties, Oklahoma: Shale Shaker, v. 16, p. 126–140.

Tchouparova, E., 1999, Petroleum wax deposition and production geochemistry: experimental results and field examples: University of Oklahoma unpublished Ph.D. dissertation, 321 p.

Thompson, K. F. M., 1979, Light hydrocarbons in subsurface sediments: Geochimica et Cosmochimica Acta, v. 43, p. 657–672.

_____ 1983, Classification and thermal history of petroleum based on light hydrocarbons: Geochimica et Cosmochimica Acta, v. 47, p. 303–316.

_____ 1987, Fractionated aromatic petroleums and the generation of gas-condensates: Organic Geochemistry, v. 11, p. 573–590.

Wavrek, D. A., 1992, Characterization of oil types in the Ardmore and Marietta basins, southern Oklahoma aulacogen, *in* Johnson, K. S.; and Cardott, B. J. (eds.), Source rocks in the southern Midcontinent: Oklahoma Geological Survey Circular 93, p. 185–195.

Principal Reference Section of Red Eagle Limestone

C. E. Keairns
Texas Tech University
Lubbock, Texas

D. R. Boardman II
Oklahoma State University
Stillwater, Oklahoma

ABSTRACT.—The Red Eagle Limestone currently is being considered for the placement of the Pennsylvanian–Permian Boundary. Such an important formation should have a well-documented type locality. Currently, all attempts to find K. C. Heald's 1916 measured section have failed. As a result, a designated principle reference section has been located and described. The new principal reference section allows easy access and offers complete measured sections of the Red Eagle Limestone. The section is measured and described; depositional events with respect to sea-level changes are interpreted; and conodont distribution is noted.

ORIGINAL TYPE LOCALITY

K. C. Heald described the original type locality for the Red Eagle Limestone in 1916. The locality was named for excellent exposures near the Red Eagle School southwest of Foraker. The only measured section given by Heald, however, is on a tributary of Hay Creek, a quarter of a mile east of the common corner of secs. 1, 2, 11, and 12, T. 26 N., R. 5 E. The section, according to Heald, is completely limestone, which is varied in color, fossil content, and lithology, and measures 16.5 ft (5.03 m) in thickness. Numerous attempts by the authors to locate and sample this locality have failed.

PRINCIPAL REFERENCE SECTION

Because Heald's original reference section cannot be located, a new principal reference section for the Red Eagle Limestone is proposed, located in a quarry adjacent to the town of Burbank, Osage County, Oklahoma. The new locality provides easily located and measured sections of the Red Eagle (Fig. 1; Table 1). The bounding paleosols of the Red Eagle sequence (Johnson Shale and Roca Shale) are exposed, allowing for a complete and accurate measurement of the Red Eagle Limestone to be made. In addition, two cores have been made available by the Oklahoma Geological Survey to serve as references.

DESCRIPTION

The Red Eagle Limestone along with the upper Johnson Shale constitutes a single, transgressive-regressive stratigraphic sequence complete with marine condensed sections. The rise and fall of sea level responsible for the deposition of these strata is a result of periodic glaciations.

The basal 17.3 ft (5.19 m) of the Johnson Shale is predominantly reddish to greenish, blocky mudstone. This is capped by a 4-in.-thick (0.10-m) chonetid lag deposit, and 15 in. (0.38 m) of gray shale. The basal 10 in. (0.25 m) of the Red Eagle Limestone consists of tightly interbedded gray shale and thin limestones topped by a 38-in.-thick (0.96 m) algal (phylloidal) limestone. Above is 25 in. (0.63 m) of predominantly limestone, with four thin, gray-shale partings. The upper 24.3 ft (7.33 m) is mostly medium-gray wackestone, although two small gray-shale partings exist. The Red Eagle is capped by the Roca Shale, which is a 16.3-ft-thick (5 m) red, blocky mudstone, to red fissile shale.

INTERPRETATION OF SEQUENCE

The stratigraphic column has been interpreted in the following manner (Fig. 1). (1) The Red Eagle sequence is bounded at the base by a blocky red mudstone, identified as a paleosol, evidenced by root traces and caliche nodules. (2) Following the formation of the paleosol, an initial marine transgression in the Johnson Shale deposited a thick, fossiliferous shale, thin lenticular limestones interbedded with shales, a carbonate lag deposit, and a fossiliferous shale capped by a thin chonetid lag deposit. (3) At this point, a thin, marine, condensed section with glauconite, phosphate, and an offshore-marine *Streptognathodus* conodont fauna (Fig. 2) was deposited, representing a maximum

Keairns, C. E.; and Boardman, D. R. II, 2001, Principal reference section of Red Eagle Limestone, *in* Johnson, K. S. (ed.), Pennsylvanian and Permian geology and petroleum in the southern Midcontinent, 1998 symposium: Oklahoma Geological Survey Circular 104, p. 115–118.

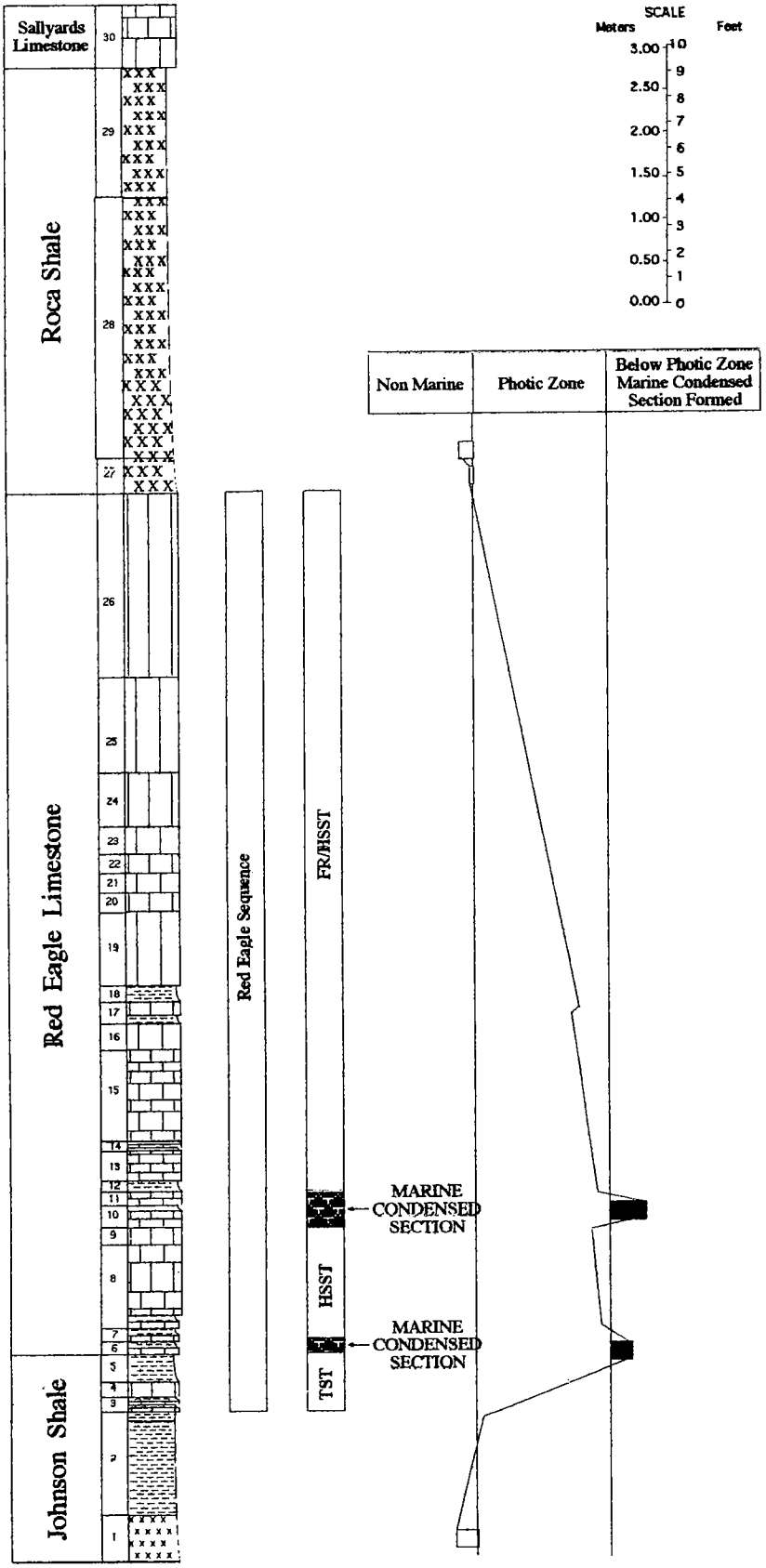

Figure 1. Measured stratigraphic section of Red Eagle Limestone (units 6–26) in quarry near Burbank, Osage County, Oklahoma. This section is recommended as new principal reference section of the Red Eagle Limestone. Abbreviations: TST—transgressive systems tract; HSST—high-stand systems tract.

Table 1.—Description of Stratigraphic Section at Burbank Quarry

Locality Description: Location is the Burbank Quarry in Burbank, Osage County, Oklahoma. The section measured is from the Johnson Shale through the Roca Shale. Burbank quadrangle, SE¼ sec. 25, T. 26 N., R. 5 E. Interval measured is the Johnson Shale, Red Eagle Limestone, and Roca Shale.

UNIT DESCRIPTIONS

1	162 in.	Johnson Shale: grayish-red to blackish-red shale; paleosol.
2	37 in.	Johnson Shale: grayish-yellow at the bottom to a yellowish-gray shale near the top.
3	1.5 in.	Johnson Shale: medium-gray lenticular limestone.
	2 in.	Johnson Shale: greenish-gray shale.
	1 in.	Johnson Shale: medium gray lenticular limestone.
	1 in.	Johnson Shale: greenish-tan shale.
4	4 in.	Johnson Shale: medium-gray lenticular limestone, abundant debris, lag deposit.
5	13 in.	Johnson Shale: greenish-gray shale.
	2 in.	Johnson Shale: medium-light-gray shale chonetid brachiopods, lag deposit.
6	2 in.	Red Eagle Limestone: medium-dark-gray limestone weathers very pale orange, crinoids, abundant brachiopods, marine condensed section, glauconite, phosphate, abundant *Streptognathodus* conodonts, wackestone.
7	1.5 in.	Red Eagle Limestone: green-gray shale.
	3 in.	Red Eagle Limestone: gray limestone, wackestone.
	1 in.	Red Eagle Limestone: greenish-gray shale.
	1.5 in.	Red Eagle Limestone: light-olive-gray to medium-light-gray limestone, wackestone, algae, large amounts of recrystallized calcite, brachiopods.
	2 in.	Red Eagle Limestone: light- to medium-gray shale.
8	34 in.	Red Eagle Limestone: medium-light to light-olive-gray limestone, algae, weathers irregular, brachiopods, crinoids, large amounts of recrystallized calcite, bryozoa, algal wackestone.
9	4 in.	Red Eagle Limestone: medium-light to light-olive gray limestone, phylloidal algae, calcite recrystallization, brachiopods, crinoid, bryozoa, ostracodes, hematite, *Adetognathus* conodonts, algal wackestone.
10	3.5 in.	Red Eagle Limestone: medium-gray limestone, weathers to a pale grayish orange, crinoids, brachiopods, bivalves, rare fusulinids, ostracodes, glauconite, phosphate, abundant *Streptognathodus* conodonts, packstone.
	2 in.	Red Eagle Limestone: medium-gray shale, marine condensed section.
11	4 in.	Red Eagle Limestone: medium-light-gray shale, fusulinids, brachiopods, bivalve, bryozoa, echinoderm, ostracodes, trilobite, glauconite, phosphate, abundant *Streptognathodus* conodonts, packstone.
12	1.5 in.	Red Eagle Limestone: medium-light-gray shale.
13	5 in.	Red Eagle Limestone: medium- to medium-light-gray limestone, weathers pale grayish orange, brachiopods, ostracodes, algae, foraminifera, bivalve, wackestone.
	5 in.	Red Eagle Limestone: medium-light-gray limy shale, crinoids, brachiopods, fusulinids, coral, ostracodes, algae, wackestone.
14	4 in.	Red Eagle Limestone: light-gray to medium-light-gray limy shale, weathers pale grayish orange, calcification evident, phylloidal algae, brachiopods, crinoids, bryozoa, *Diplognathodus* conodonts, wackestone.
15	11 in.	Red Eagle Limestone: medium-light-gray limestone, weathers grayish orange, crinoids, brachiopods bryozoa, algae, ostracodes, *Streptognathodus* conodonts, wackestone.
	12.5 in.	Red Eagle Limestone: medium-light-gray shale.
	18 in.	Red Eagle Limestone: medium- to medium-light-gray limestone, brachiopods, bryozoa, algae, *Diplognathodus* conodonts, wackestone.
16	20.5 in.	Red Eagle Limestone: medium-light-gray to medium-gray limestone, weathers very pale orange, brachiopods, corals, foraminifera, crinoids, trilobite, echinoderm, bryozoa, small amount hematite, wackestone.
17	3 in.	Red Eagle Limestone: medium-gray limy shale, crinoids, brachiopods.
	5 in.	Red Eagle Limestone: light- to medium-light-gray limestone, crinoids, brachiopods, bryozoa, ostracodes, echinoderm, wackestone.
18	6 in.	Red Eagle Limestone: medium-light-gray limy shale crinoids, brachiopods, coral, ostracodes, hematite, wackestone.
19	33.5 in.	Red Eagle Limestone: medium-light-gray limestone, brachiopods, ostracodes, echinoderms, bryozoa, crinoids, hematite, *Diplognathodus* conodonts, wackestone.
20	10.5 in.	Red Eagle Limestone: medium-light-gray limy shale, bryozoa, brachiopod, crinoid, hematite, wackestone.
21	6 in.	Red Eagle Limestone: medium-light-gray limestone, echinoderm, bryozoa, foraminifera, hematite, wackestone.
22	6 in.	Red Eagle Limestone: medium-light-gray limy shale.
23	14 in.	Red Eagle Limestone: medium- to medium-light-gray limestone, crinoids, wackestone.
24	22 in.	Red Eagle Limestone: light-gray limestone, bryozoa, ostracodes, brachiopods, crinoid, foraminifera, wackestone.
25	43.5 in.	Red Eagle Limestone: light- to medium-light-gray limestone, brachiopod, crinoid, bryozoa, ostracodes, hematite, wackestone.
26	83 in.	Red Eagle Limestone: light- to medium-light-gray limestone, massive, brachiopod, crinoid, echinoderm, bivalve, ostracodes, wackestone.
27	16 in.	Roca Shale: light grayish-green shale, blocky mudstone.
28	123 in.	Roca Shale: dusky-red to very dusky-red shale.
29	58 in.	Roca Shale: light brown to green shale.
30	26 in.	Sallyards Limestone: light grayish-green limestone.

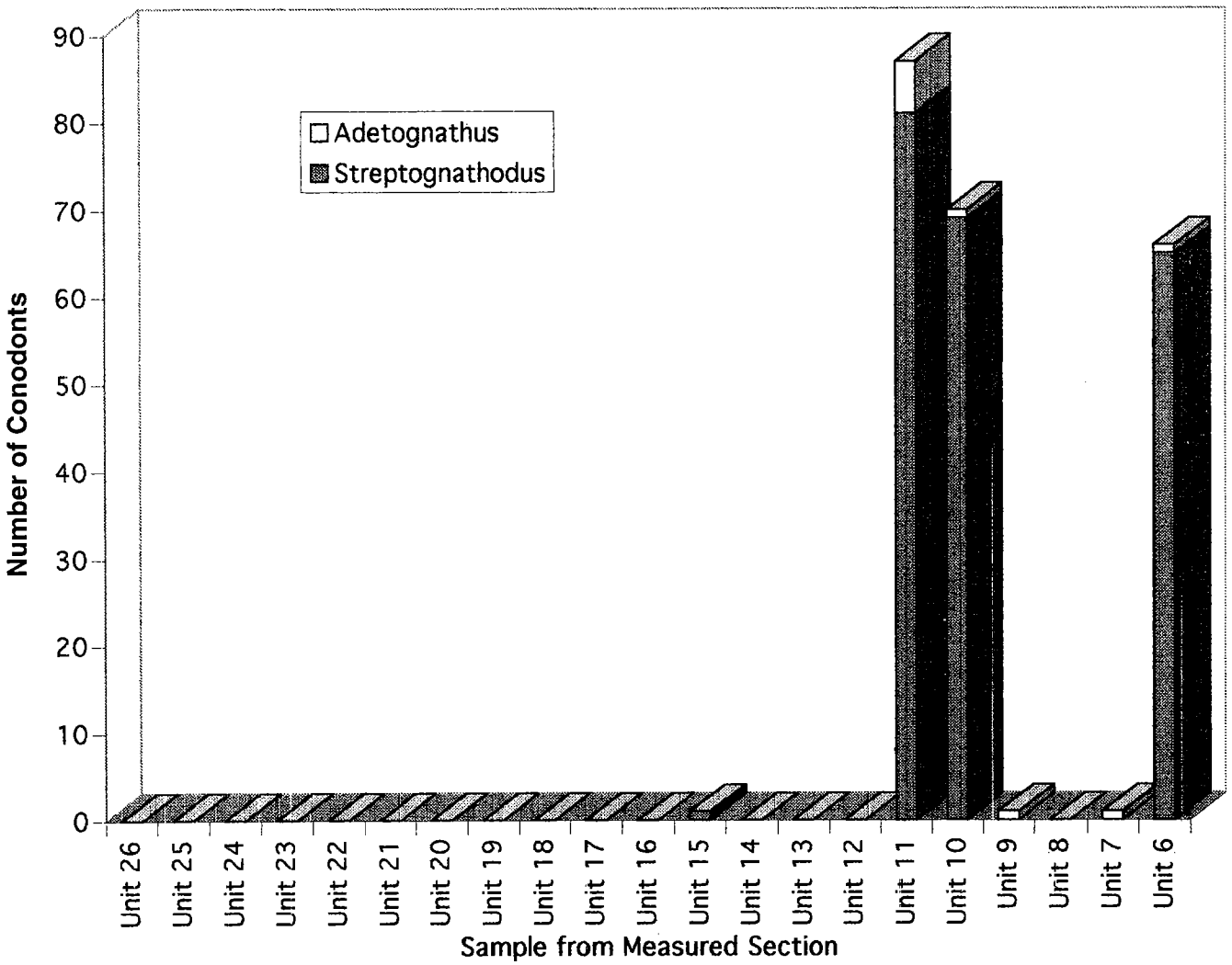

Figure 2. Conodont distribution in Red Eagle Limestone at Burbank Quarry. Units correspond to those of Figure 1 and Table 1.

transgression of sea level in the Red Eagle Limestone. The *Streptognathodus nodulinearis* and *flagulatus* (in Russian sense) identified in this condensed section correlates with the conodont fauna at the base of the Permian at the type Permian locality in Kazakhstan, Soviet Union. (4) Overlying this condensed section, a thick cabonate was deposited by a rapid regression in shallow-marine conditions, as indicated by the abundance of phylloid algae. (5) Next, a second, maximum transgression occurred, with the distinct marine condensed section characteristics—viz., glauconite, phosphate, and deep-marine *Streptognathodus* conodonts. (6) The rock above the upper marine condensed section consists entirely of fossiliferous, shallow-marine carbonates. In some sections, they appear as limy shales; however, they contain greater than two-thirds limestone. (7) Finally, the Roca Shale caps the sequence. The Roca is a blocky red-shale paleosol containing root traces and caliche nodules.

ACKNOWLEDGMENTS

The senior author would like to thank Darwin Boardman, Gary Stewart, and Zuhair Al-Shaieb for their help with my studies while at Oklahoma State University. Long stratigraphic sections of the Red Eagle were constructed, copies of which are available for the asking.

Redevelopment of Old Fields in the Upper Pennsylvanian and Lower Permian of Southeast New Mexico: Rejuvenation of Underdeveloped Fields Yields Major Reserves

Ronald F. Broadhead
New Mexico Bureau of Mines and Mineral Resources
Socorro, New Mexico

ABSTRACT.—Carbonate reservoirs in the Cisco and Canyon (Upper Pennsylvanian) and lower Wolfcamp (Permian) sections in the Permian basin of southeast New Mexico are significant reservoirs for oil and gas. The 400 fields that produce from the reservoirs have yielded a cumulative total of 490 million barrels oil (MMBO) and 3.2 trillion cubic feet of gas (TCFG), or 12% of the oil and 16% of the gas produced from southeast New Mexico. Sixteen of these fields have been identified that were underdeveloped at some stage in their history. These include Dagger Draw (40 MMBO cumulative production), Allison (24 MMBO cumulative production), and Baum (12 MMBO cumulative production).

Although initially underdeveloped, subsequent redevelopment added significantly to reserves and production. Statistical analysis of production-decline curves was used to estimate reserves developed during initial drilling of these fields and during subsequent phases of redevelopment. For the 16 fields studied, redevelopment accounted for a total of 72% of total field reserves. Redevelopment accounted for more than 95% of total reserves at Dagger Draw, 90% of reserves at Allison, and 99% of reserves at Baum.

Redevelopment in these fields was generally in undrilled portions of the fields, the potential of which was unrealized, and not in overlooked pay zones. Redevelopment resulted in a fivefold to tenfold increase in numbers of producing wells and productive acreage. Significant potential remains for other fields to remain underdeveloped.

WHAT IS AN UNDERDEVELOPED FIELD?

An *underdeveloped field* can be defined as an oil or gas field that was incompletely developed subsequent to initial field discovery. Underdeveloped fields typically produce minimal levels of oil and gas from only a few wells drilled in the period immediately following initial discovery (Fig. 1). One or more subsequent, discrete phases of development several years after field discovery reinvigorate production from these fields. These phases of redevelopment do not involve infill drilling nor do they involve secondary or tertiary recovery techniques. Rather, they are based upon drilling the same pay zone that was produced during initial development of the field but from proration units that remained undrilled during initial development (Fig. 2). As such, they represent new oil that was unrecognized at the time of field discovery and initial development.

THE UPPER PENNSYLVANIAN AND LOWER WOLFCAMPIAN CARBONATES OF SOUTHEAST NEW MEXICO

The Upper Pennsylvanian and Lower Wolfcampian strata of southeast New Mexico are primarily carbonates. These stratigraphic units have produced a cumulative 490 million barrels of oil (MMBO) and 3.2 trillion cubic feet (TCF) of gas from 400 fields (Fig. 3)—12% of the oil and 16% of the gas produced from southeast New Mexico. Depth to production varies from 5,900 ft to 11,500 ft. Most reservoirs are biohermal and were deposited either as patch reefs on the northwest shelf of the Permian basin or as shelf-margin barrier reefs on the margin between the northwest shelf and the deep Delaware basin to the south (Fig. 3; Broadhead, 1993; Cys, 1986; Cys and Mazzullo, 1985; Malek-Aslani, 1985; Speer, 1993). Porosity in most of these fields is secondary, occurring as systems of interconnected vugs within the biohermal complex.

Broadhead, R. F., 2001, Redevelopment of old fields in the Upper Pennsylvanian and Lower Permian of southeast New Mexico: rejuvenation of underdeveloped fields yields major reserves, *in* Johnson, K. S. (ed.), Pennsylvanian and Permian geology and petroleum in the southern Midcontinent, 1998 symposium: Oklahoma Geological Survey Circular 104, p. 119–122.

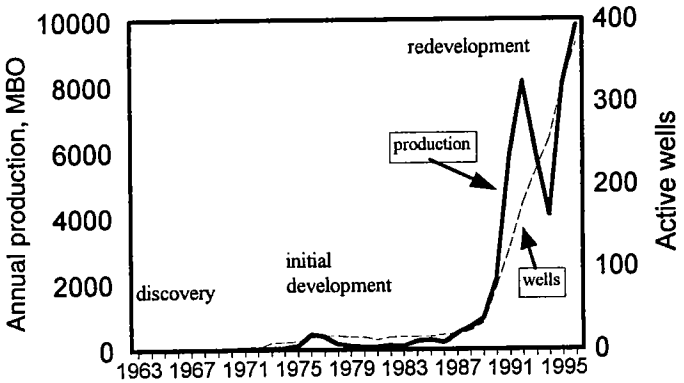

Figure 1. Annual production in thousand barrels of oil (MBO) and number of active producing wells for the Dagger Draw Upper Pennsylvanian oil pool, Eddy County, showing the effect of redevelopment on production. General field location shown on Figure 3.

Analysis of curves that show historical production and number of active producing wells (e.g., Fig. 1) indicates that 16 of the fields in the Upper Pennsylvanian and Lower Wolfcampian carbonates have been underdeveloped historically. All of these 16 fields had at least one stage of redevelopment and four of the fields had two stages of redevelopment (Table 1).

Reserves brought into production for each stage of development were calculated using a decline-curve technique for each of the 16 underdeveloped fields (Broadhead, 1999). The majority of reserves in these 16 fields were brought into production by redevelopment (Table 1). Discovery and initial development brought only 28% of reserves into production. After initial development, most of these fields were thought to be minor fields that would never yield significant amounts of oil.

A common theme underlies the reasons for underdevelopment of all 16 fields, except for the Four Lakes field. They are all stratigraphic traps, the areal extent of which is defined by the biohermal complex that forms the trap. However, the discovery wells for these fields were drilled on anticlinal structures (Fig. 2), and the initial phase of development took place under the premise of structural entrapment of the oil. The structures were defined either by reflection-seismic techniques or by subsurface geology. The initial development wells were confined to the anticlinal crests. Offset wells were not drilled in downdip locations. As a result, only the anticlines were drilled, and the larger parts of these fields were ignored. The majority of reserves in these fields remained unproduced until other operators came along years later and instituted new drilling programs.

The Four Lakes field is the exception. This field is a structural trap that is formed by an anticline. Redevelopment in this field had to wait until wells on the crest of the structure were depleted in a deeper pay zone (Devonian) and could be recompleted uphole in the Upper Pennsylvanian carbonates.

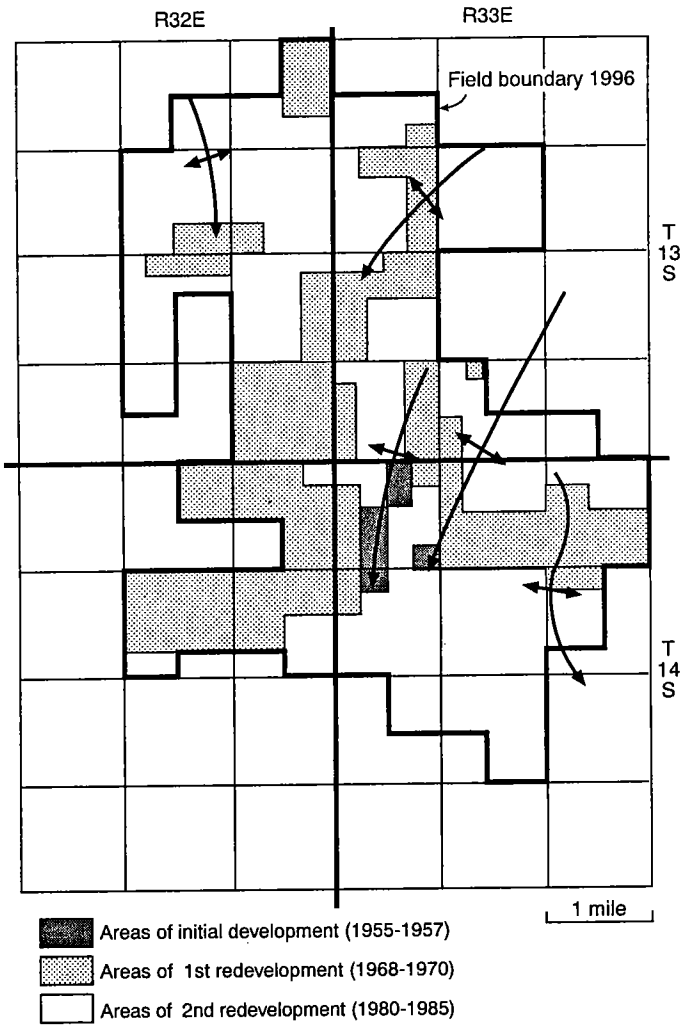

Figure 2. Map of the Baum Upper Pennsylvanian oil pool, Lea County, showing present-day (1996) outline of the field, areas of initial development (dark shading), the two phases of redevelopment (medium shading and white), and locations of major anticlinal noses in the field. General field location shown on Figure 3.

FUTURE POTENTIAL

The potential for additional underdeveloped oil reserves in the Upper Pennsylvanian and Lower Wolfcampian carbonates of southeast New Mexico is considerable. Of the 400 fields that produce from these reservoirs, 362 (91%) have less than ten producing wells and 299 (75%) had less than three producing wells. Of these small fields, 135 have no producing wells, having either been abandoned or not yet brought on line.

Whereas many of these small fields are undoubtedly small accumulations of oil and gas in small reservoirs, many are not delineated either wholly or partially by offsetting dry holes that have either tested or otherwise fully evaluated the Upper Pennsylvanian and Lower Wolfcampian carbonate reservoirs. Many

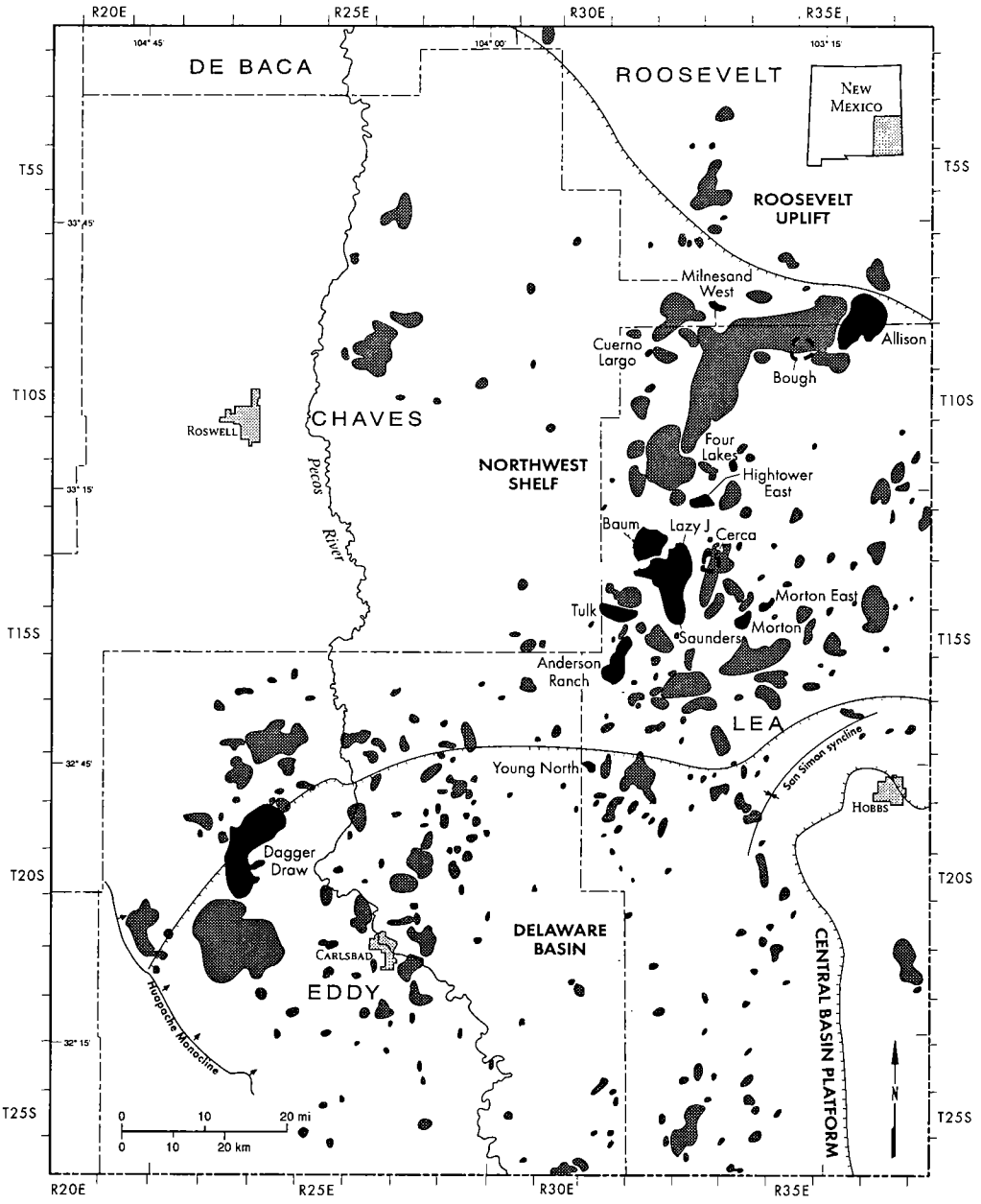

Figure 3. The geologic elements of the Permian basin in southeast New Mexico, fields productive from Upper Pennsylvanian and Lower Wolfcampian carbonates, and underdeveloped Upper Pennsylvanian and Lower Wolfcampian fields that have been redeveloped.

of these small fields were discovered by wells that were originally drilled to deeper zones, particularly the Morrow sands (Lower Pennsylvanian), in search of gas. They were recompleted in the Upper Pennsylvanian and Lower Wolfcampian carbonates only when the deeper zones proved unproductive or when those zones were abandoned after production declined to subeconomic levels. There is generally little attempt to fully develop the small fields found by these reworked wells. The full extent of many of these fields remains to be proved. They are reminiscent of the initial development of the 16 historically underdeveloped fields described above. How many more Dagger Draws, Allisons, and Baums have been discovered but remain unrecognized and underdeveloped?

REFERENCES CITED

Broadhead, R. F., 1993, PB-9 Wolfcamp carbonate, *in* Atlas of major Rocky Mountain gas reservoirs: New Mexico Bureau of Mines and Mineral Resources, p. 152.

Table 1.—Discovery and Redevelopment Dates and Reserve Data for the 16 Historically Underdeveloped Fields in the Upper Pennsylvanian–Lower Wolfcampian Carbonate Play of Southeast New Mexico

Field	Discovery year	Redevelopment year(s)	Cumulative production, 12/31/96 (MMBO)*	Percent of primary recovery from redevelopment
Allison	1954	1959	23.6	90%
Anderson Ranch	1953	1958, 1984	4.1	52%
Baum	1955	1968, 1980	12.7	99%
Bough	1949	1966	6.3	29%
Cerca	1968	1972, 1979	0.2	90%
Cuerno Largo	1971	1990	0.6	71%
Dagger Draw	1964	1990	40.4	95+%
Four Lakes	1956	1991	2.7	29%
Hightower East	1950	1980	1.0	92%
Lazy J	1952	1982	7.4	25%
Milnesand West	1968	1983	0.1	91%
Morton	1964	1980	2.5	40%
Morton East	1970	1986	1.7	16%
Saunders	1950	1980	38.1	32%
Tulk	1951	1969, 1983	2.3	35%
Young North	1989	1991	0.7	90%
Totals			**144.4**	**72%**

NOTE: Data modified from Broadhead (1999).
*Production in million barrels of oil (MMBO)

_____ 1999, Underdeveloped oil fields—Upper Pennsylvanian and Lower Wolfcampian of southeast New Mexico: Carbonates and Evaporites, v. 14, p. 84–105.

Cys, J. M., 1986, Lower Permian grainstone reservoirs, southern Tatum basin, southeastern New Mexico, *in* Ahlen, J. L.; and Hanson, M. E. (eds.), Southwest Section of American Association of Petroleum Geologists transactions and guidebook of 1986 convention, Ruidoso, New Mexico: New Mexico Bureau of Mines and Mineral Resources, p. 115–120.

Cys, J. M.; and Mazzullo, S. J., 1985, Depositional and diagenetic history of a Lower Permian (Wolfcamp) phylloid-algal reservoir, Hueco Formation, Morton field, southeastern New Mexico, *in* Roehl, P. O.; and Choquette, P. W. (eds.), Carbonate petroleum reservoirs: Springer-Verlag, New York, p. 277–288.

Malek-Aslani, M., 1985, Permian patch-reef reservoir, North Anderson Ranch field, southeastern New Mexico, *in* Roehl, P. O.; and Choquette, P. W. (eds.), Carbonate petroleum reservoirs: Springer-Verlag, New York, p. 265–276.

Reddy, G., 1995a, Dagger Draw North, *in* A symposium of oil and gas fields of southeastern New Mexico, 1995 supplement: Roswell Geological Society, p. 207–208.

_____ 1995b, Dagger Draw South, *in* A symposium of oil and gas fields of southeastern New Mexico, 1995 supplement: Roswell Geological Society, p. 209–213.

Speer, S. W., 1993, PP-1 Upper Pennsylvanian, *in* Atlas of major Rocky Mountain gas reservoirs: New Mexico Bureau of Mines and Mineral Resources, p. 154–156.

Subsurface Study of the Permian Ozona Canyon Sandstone, Val Verde Basin, Block MM, Southwest Crockett County, Texas

Melissa Kelly Harrell[1]
Texas Tech University
Lubbock, Texas

ABSTRACT.— The Lower Permian Ozona Canyon sandstone is a prolific tight-gas zone in the Val Verde basin of West Texas. The Ozona Canyon sandstone is classified as sublitharenite to litharenite with porosities averaging <3% and permeabilities <0.1 md (millidarcies). A study of the Ozona Canyon interval was conducted in the northern portion of Block MM, Crockett County, Texas. The study utilized net sand isopach maps and gamma ray log facies distribution maps to evaluate the depositional environment and determine potential infill drilling locations within the field.

The Ozona Canyon sandstone was divided into six distinct intervals, evaluated individually. The upper Ozona intervals, A and C, are defined as upper fan deposits based on their isopach trends and log facies and display both channel and lobe and levee characteristics. Middle fan deposits are represented by the Ozona E and F sands and are dominated by log facies and sand isopach trends characteristic of channel deposits. Ozona intervals G and H constitute the lower fan deposits and are distinguished from the upper and middle fan deposits by a hotter gamma ray response and the lack of strong, linear sand trends present in the other Ozona intervals. The G sand is composed almost entirely of channel log facies, whereas the H sand comprises lobe and levee log facies with virtually no channel log facies.

Mapping of the Ozona Canyon interval increased drilling potential in the Block MM field by defining the thick, channel quality sand zones. After completion of the initial maps in August 1996, more than 60 new wells have been drilled. Some of the wells drilled in 1997 yielded initial production (IP) values >1,000 thousand cubic feet per day (mcfd), higher than that of wells previously drilled in the Ozona Canyon sandstone. The increase in production is attributed to the correlation established between the sand isopach maps and the log facies distribution maps conducted in this study.

INTRODUCTION

The Pennsylvanian–Permian Canyon Sandstone is a prolific natural gas zone in the Midland and Val Verde basins of West Texas. The subsurface sands were correlated with the Pennsylvanian (Desmoinesian–Missourian) Canyon Group of north-central Texas (Hamlin and others, 1995). The work of Rall and Rall (1958) and Van Siclen (1958), however, earlier identified the West Texas Canyon sandstones as younger than the Desmoinesian and Missourian Canyon shelf deposits of central Texas. Further investigations concluded that deposition of the West Texas Canyon sandstones occurred in basin and slope settings, and are Virgilian, Wolfcampian, and Leonardian in age (Lehtonen, 1987; Neuberger, 1987). Despite the miscorrelation, the term "Canyon" is commonly used in the petroleum industry to identify the basin deposits of the Midland and Val Verde basins. This study focuses on the Ozona Canyon sandstone of Crockett County, Texas, in the Val Verde basin.

The area of study is a Union Pacific Resources (UPR), Pioneer (formerly known as Parker & Parsley) farmout. The field is located in the northeast portion of Block MM, ~20 mi southwest of Ozona, Texas (Fig. 1). The depth of the Ozona interval in this field is between approximately 5,500 ft and 7,400 ft subsurface.

The Ozona Canyon sandstone is Early Permian in

This paper is reprinted, with slight modifications, from Harrell, M. K., 1998, Subsurface study of the Permian Ozana Canyon sandstone in the Val Verde basin, Block MM, southwest Crockett County, Texas, *in* DeMis, W. D., and Nelis, M. K. (eds.), The search continues into the 21st century: West Texas Geological Society Publication 98-105, p. 107–117.

[1]Present address: Geological Consultant, Salt Lake City, Utah.

Harrell, M. K., 2001, Subsurface study of the Permian Ozana Canyon sandstone,Val Verde basin, Block MM, southwest Crockett County, Texas, *in* Johnson, K. S. (ed.), Pennsylvanian and Permian geology and petroleum in the southern Midcontinent, 1998 symposium: Oklahoma Geological Survey Circular 104, p. 123–141.

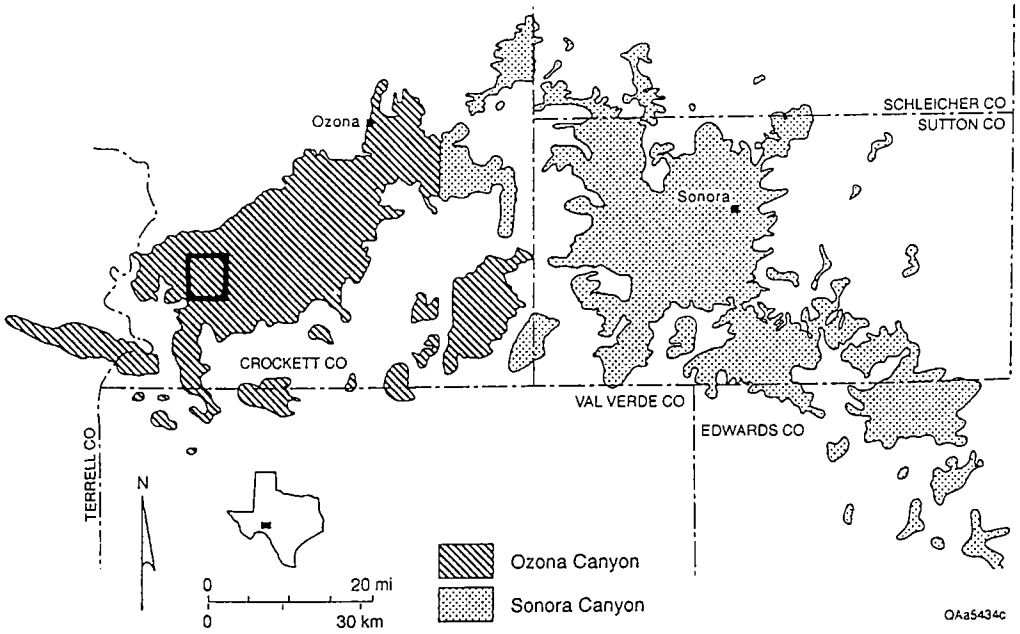

Figure 1. Block MM Ozona Canyon gas field (modified after Hamlin and others, 1995). The study area is outlined in black.

age and is believed to record the final clastic depositional episode filling the Val Verde basin (Hamlin and others, 1995). The sandstone lies directly above the Sonora Canyon interval and is overlain by Leonardian carbonates and mudstones. Core samples and sandstone distribution patterns of the Ozona Canyon sands indicate that deposition occurred in a basin margin turbidite system, or submarine fan (Mitchell, 1975; Berg, 1986; Lehtonen, 1987; Hamlin and others, 1992a). The Ozona interval occupied a basin floor position, but was at a much shallower depth than existed during deposition of older Canyon intervals (Hamlin and others, 1995).

The Ozona Canyon sand is dominated by interfingering sandstones and shales. Rall and Rall (1958) recognized a basinal facies including dark shale and fine-grained sandstone, constituting as much as 50% of the section. Regionally, the Ozona Canyon sand thickens gradually westward across Sutton and Crockett Counties, with abrupt thickening in southwest Crockett County (Hamlin and others, 1995). Although the Ozona Canyon sand is relatively continuous across the Val Verde basin, individual sand beds are discontinuous.

The Ozona Canyon Block MM field study was initiated through Union Pacific Resources in Fort Worth, Texas. The goal of the study was to evaluate infill potential within the sparsely drilled acreage. The field study began in the summer of 1996, and new well data were received through November 1997.

Core was not available from the Block MM study site; therefore, information regarding the depositional environment was derived from core data outside of the field and through the use of gamma ray logs. Logs and core data used in the study were obtained from Union Pacific Resources.

The Ozona Canyon sandstone was divided into a series of stratigraphic zones defined by characteristic gamma ray log facies. The stratigraphic framework was pre-established by Stan Lewis at Union Pacific Resources. It is important to note that the individual sand intervals do not represent single sands, but instead represent packages of stacked sands with a characteristic gamma ray response. The zones defined in the study are the Ozona A, C, E, F, G, and H, where A is the uppermost sand and H the lowermost sand (Fig. 2). The B sand is completely absent, and the D sand is present only in a few isolated wells within the study area. Neither the B nor the D sand will be discussed.

Once the sand zones were defined and correlated, net feet of clean sand was estimated from the gamma ray logs using a 40% sand-shale cut off (approximately midway between the maximum and minimum gamma-ray response). All gamma ray logs used in this study were modern API (American Petroleum Institute) calibrated gamma ray logs. Previous work conducted on the Canyon sands determined normalization to be unnecessary; therefore, the gamma ray logs were not normalized (Hamlin and others, 1995, and D. Jenkins, Union Pacific Resources, personal communication, 1996).

Independent of the sand isopach maps, log response distribution maps were created for the six Ozona intervals (A, C, E, F, G, and H). The log response pattern was annotated for each interval. The following log response classifications were used to describe the individual zones: CU—coarsening upward, SCU—serrate coarsening upward, S—serrate, SB—serrate blocky, CD—coarsening downward, and SCD—serrate coarsening downward (Fig. 3). A similar classification system is described by Galloway in a recent American

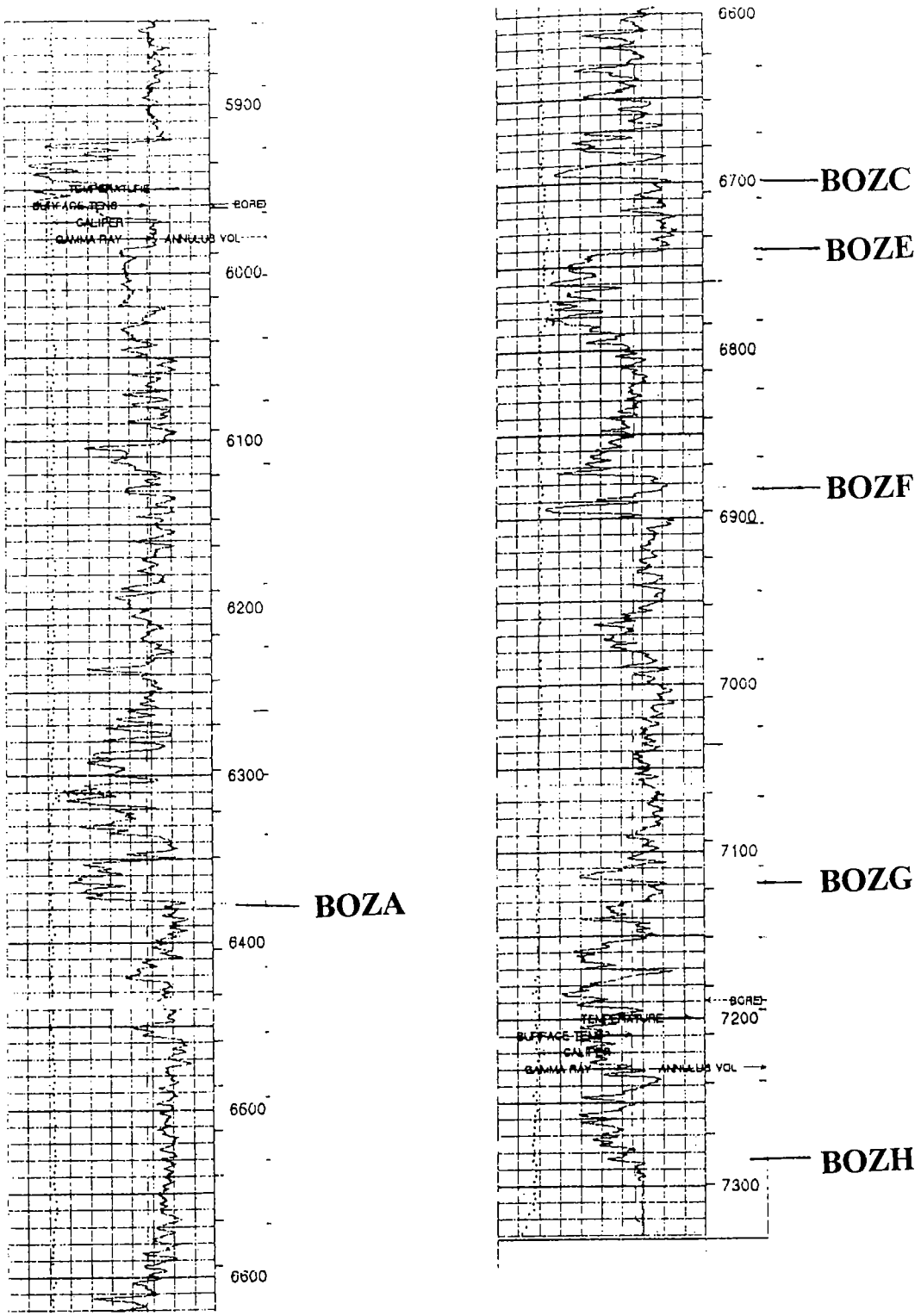

Figure 2. Ozona Canyon type log-UPR Zipp Ranch 34-14, API no. 42-105-37451. The Ozona Canyon intervals are marked according to the formation code. Depth are in feet.

Association of Petroleum Geologists Bulletin (Galloway, 1998).

The Canyon sands of the Val Verde basin have provided commercial gas production for more than 30 years. Canyon reservoirs have yielded more than 2 trillion cubic feet (Tcf) of gas and account for a large portion of the domestic low-permeability gas production, reserves, and new completions (Hamlin and others, 1995). Exploration for gas in the Val Verde basin began in 1952, with the successful discovery of the Puckett field (Hills, 1968; National Petroleum Council, 1980). In the early years, gas in the Val Verde basin was pro-

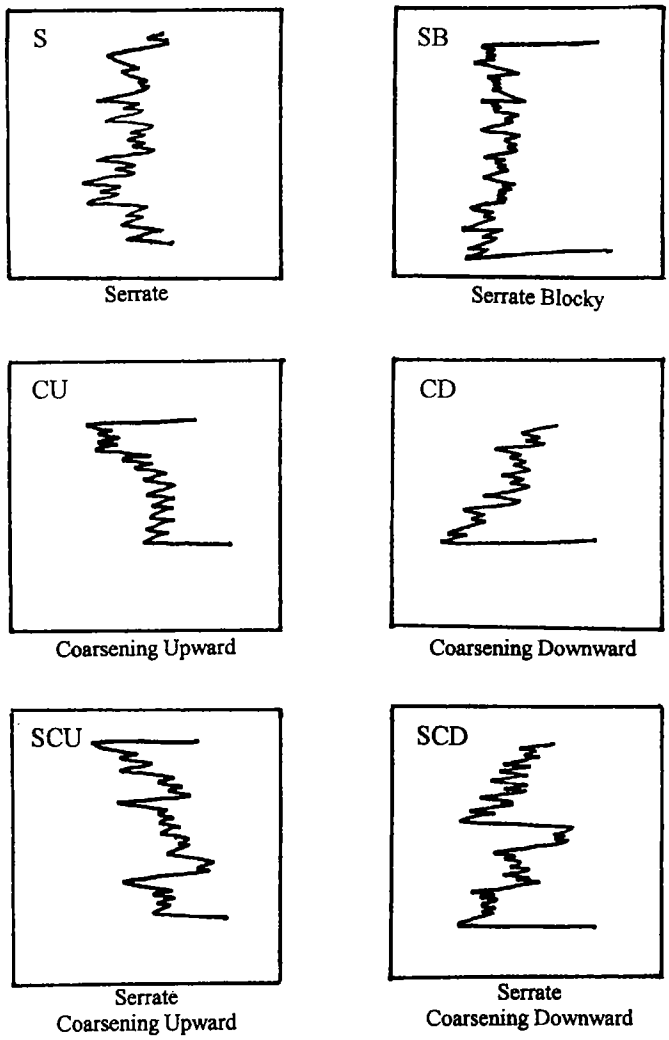

Figure 3. Ozona Canyon gamma ray log facies classification for the Block MM wells.

duced primarily from the Ellenburger and Strawn carbonates, with only minor amounts produced from the Canyon sands. Thick Pennsylvanian–Permian mudstones in the southern part of the Val Verde basin are believed to be the source rocks of gas in the Canyon sands (National Petroleum Council, 1980).

Unlike the Ellenburger and Strawn carbonates, Canyon sands are not conventional structural traps, with moderate permeabilities (1–100 millidarcies [md]) and distinct gas-water contacts. Instead, the Canyon sandstone reservoirs are subtle stratigraphic traps with low permeabilities (<0.1 md) (Hamlin and others, 1995). The inferred trapping mechanisms in the Canyon interval are updip and lateral facies changes between sandstones and shales (Huang, 1989). Sand quality is a key issue in the productivity of the Canyon sandstones, and acidizing and fracturing are essential for economic production.

DEPOSITIONAL ENVIRONMENT

Interpretation of the depositional environment of the Ozona Canyon sandstone was determined with the aid of core descriptions, well log response patterns, and net sand isopach maps. The Ozona Canyon sandstones were deposited in deep-water, turbidite systems (Hamlin and others, 1995). Reading and Richards's (1994) classification of turbidite systems delineated submarine fan systems based on their grain size and type of feeder system. The classification system defined by Reading and Richards (1994) effectively describes the depositional environment of the Ozona sands.

The problem with many submarine fan classification systems is that the contributing environmental factors cannot be directly measured. The classification system defined by Reading and Richards (1994), however, uses two fundamental and observable parameters—grain size and feeder system. The first component, grain size, is observable in the field, in core, and can be inferred from wireline logs. Second, the organization of turbidite deposits is dependent on how the sediment is delivered. The nature of the feeder system is defined by whether the sediment is concentrated and funneled through a single point source, transported by a multiple source, or by a linear source.

Core samples from the Ozona interval include sandstone and mudstone dominated facies (Hamlin and others, 1995). Distribution of the sandstone and sandstone geometries suggests that the depositional environment of the Ozona Canyon interval can be classified as a multiple-source mud/sand rich ramp using the turbidite system classification of Reading and Richards (1994) (Fig. 4). The system is generally fed by a mixed sand-mud delta that may either prograde across a gently sloping shelf or feed the basin through multiple source valleys. The presence of several feeders, active simultaneously, distinguishes the multiple-source mud/sand rich ramp from earlier fan systems (Reading and Richards, 1994).

SUBSURFACE MAPPING

Subsurface maps constructed from log data make up the bulk of the field study. The following section is a discussion of the results of the subsurface maps. The maps include sand isopach maps and log response distribution maps of the six Ozona intervals (A, C, E, F, G, and H). Structure maps of the field were deemed unnecessary due to the stratigraphic rather than structural nature of the reservoir.

The Block MM subsurface maps are divided into three categories based on their log and fan facies associations: the upper fan, middle fan, and lower fan. Fan divisions are based on sand isopach and log facies characteristics and do not necessarily represent a single fan progradational sequence. Sand packages within the Ozona Canyon interval are separated by thick basin plain shaly siltstones and shales (Fig. 2). Therefore, the individual Ozona Canyon intervals represent separate depositional lobes (Fig. 5). The lower fan facies associated with the middle and upper fan deposits (intervals A, C, E, and F) are represented by the shaly sandstones eliminated from the net sand map by the gamma ray cut-off.

The log facies S, CU, and SCU are classified as lobe

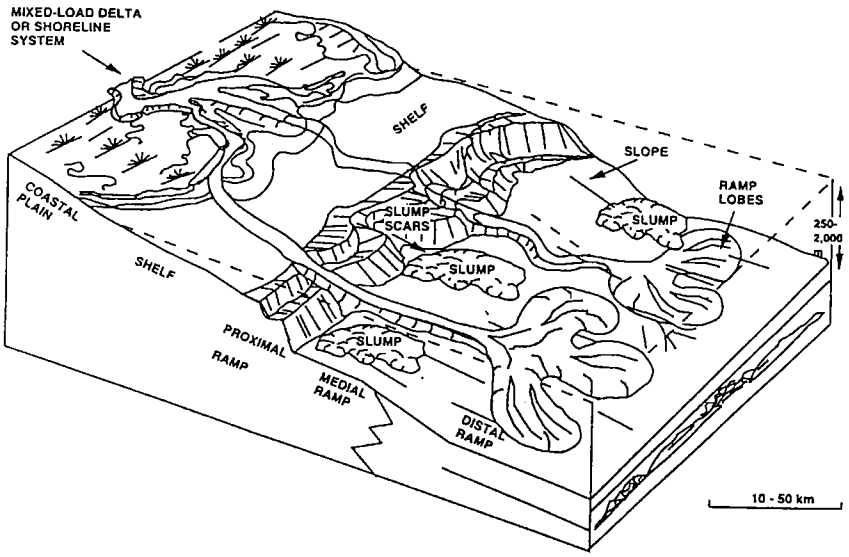

Figure 4. Depositional model for a multiple-source mud/sand rich ramp representing the Ozona Canyon sandstone (after Reading and Richards, 1994).

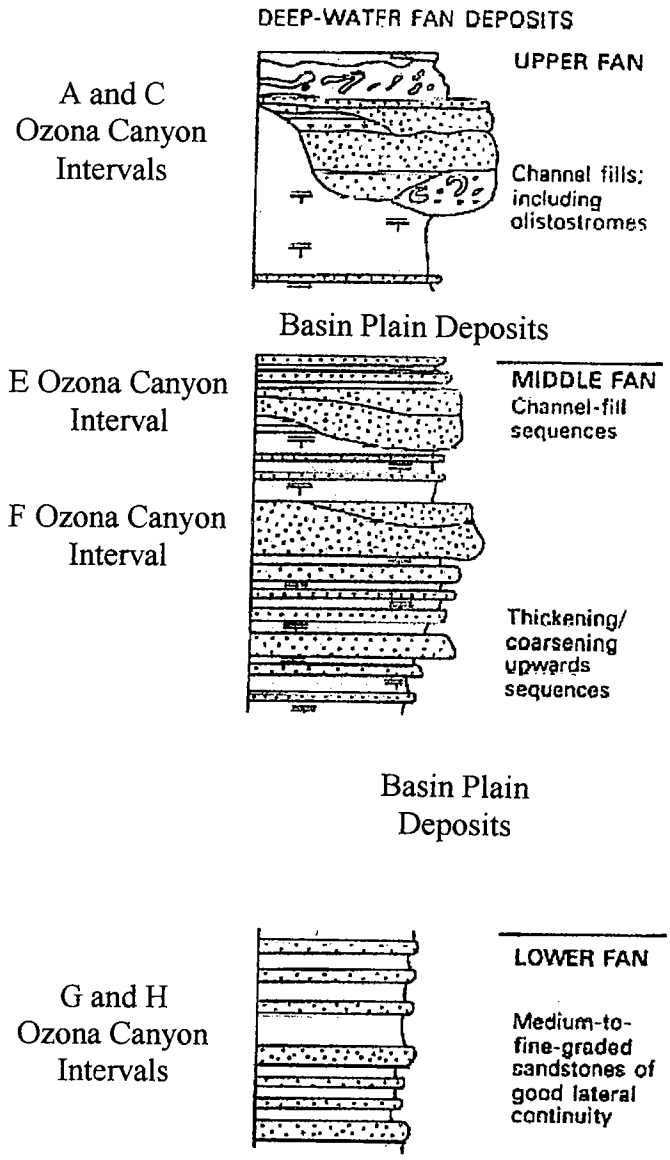

Figure 5 *(left)*. Facies and sequences making up the facies associations characteristic of deep-water fan environments (after Mutti and Ricci Lucchi, 1972). Each of the Ozona Canyon intervals represent different depositional lobes separated by basin plain shaly siltstones and shales.

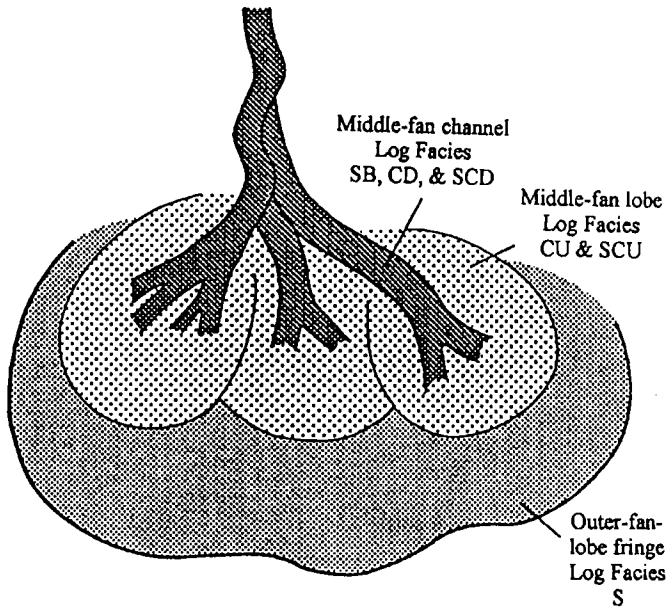

Figure 6 *(above)*. Simplified fan model showing gamma ray log facies characteristic within the fan (modified after Hamlin and others, 1995). See Figure 3 for explanation of log facies.

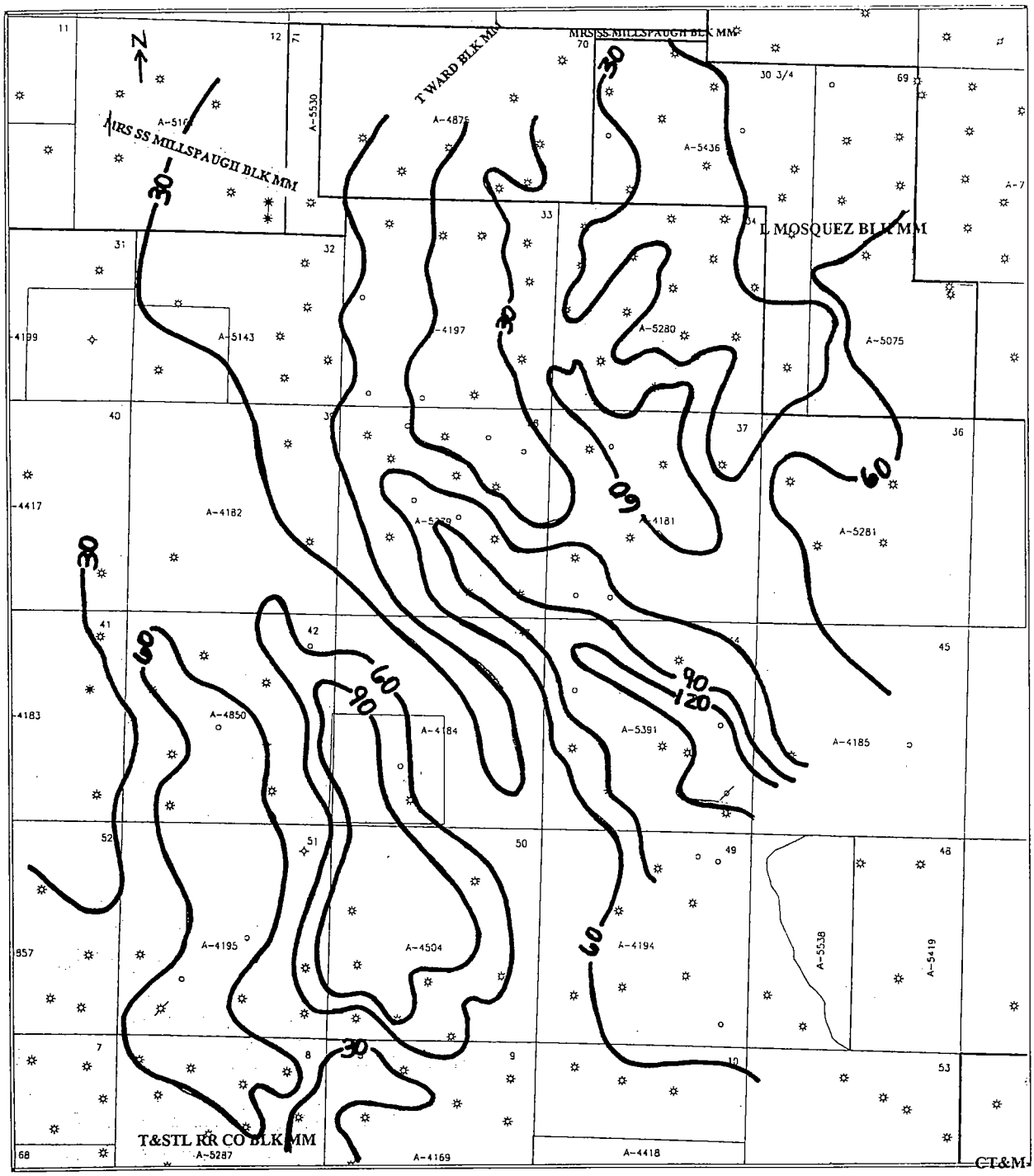

Figure 7. Sand isopach map of the Ozona Canyon A interval. Each section is one square mile, 30 ft contour interval.

and levee fringe deposits, and the log facies CD and SB represent channel deposits (Figs. 3, 6). The log facies denoted by SCD displays characteristics of both lobe and levee and channel deposits but is grouped with the channel deposits on the log facies distribution maps (Figs. 3, 6). Unlike the other channel log facies (CD and SB), the SCD notation represents thinner, probably finer grained channel deposits. Ozona intervals A and C represent the upper fan deposits, intervals E and F represent the middle fan deposits, and intervals G and H the lower fan deposits. The maps are discussed according to the fan facies association and in the order of well penetration, starting with the upper A sand and finishing with the lower H sand.

Upper Fan Deposits

Upper fan deposits are typically characterized by a thick-bedded, coarse-grained, lenticular sandstone-conglomerate facies and a laminated or bioturbated mudstone-marlstone facies representing channel and

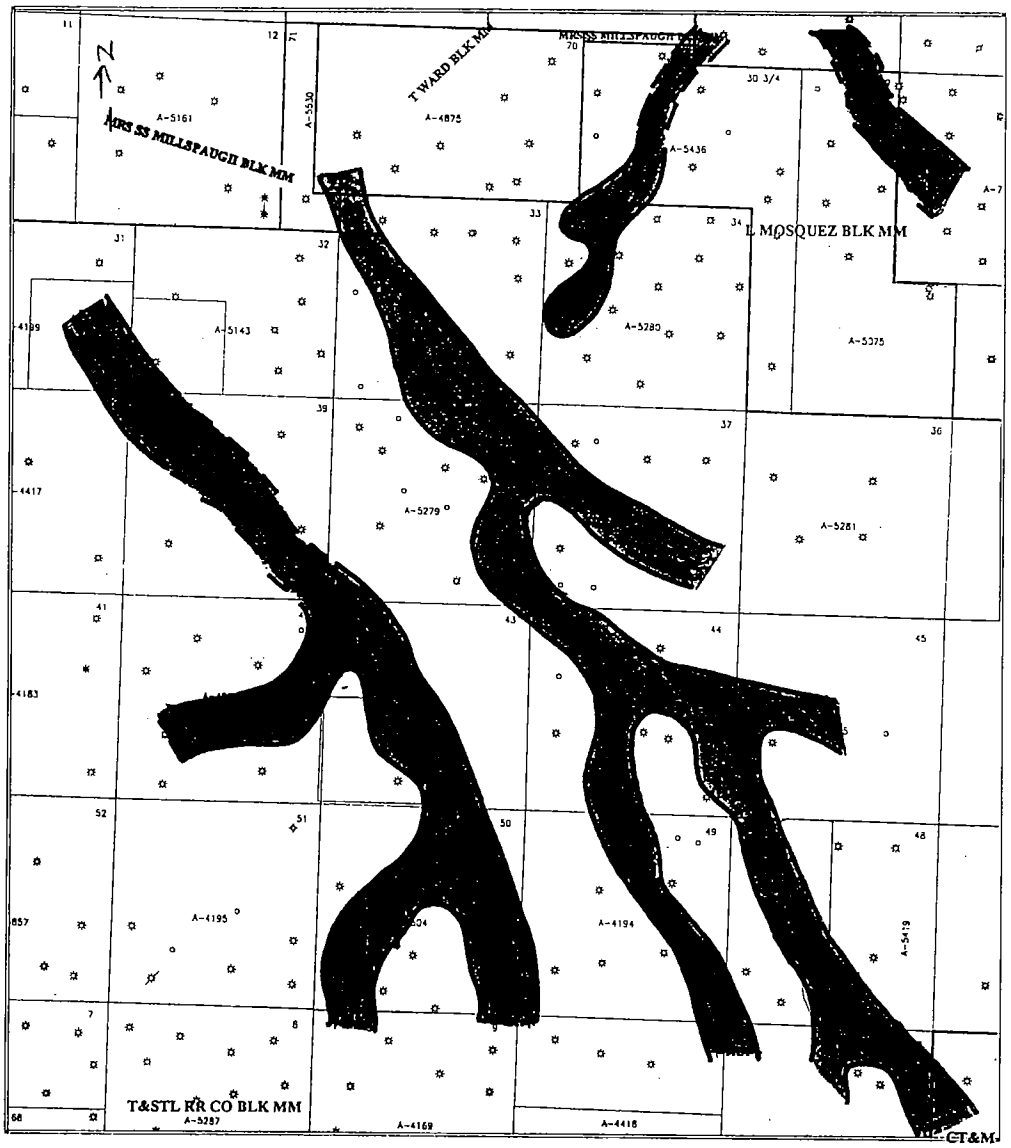

Figure 8. Log facies distribution map of the Ozona Canyon A interval. Shaded region includes the SB and SCD log facies, unshaded region includes the S log facies.

interchannel deposits (Fig. 5) (Reading, 1986). The upper fan deposits of the A and C sands are characterized predominantly by the S and SCD gamma ray log response patterns typical of channel (SCD) and lobe and levee deposits (S).

Ozona Canyon A Interval

The A zone is the youngest sand in the Ozona interval and is a thick package of stacked sands separated by alternating shale sequences (Fig. 7). Thickness ranges from <10 ft to >150 ft. Due to the variation in the thickness and the discontinuity of the individual sand beds within the A interval, no trends were expected from the sand isopach map. However, a distinct trend does appear in the data. The obvious sand isopach trend runs in a northwest–southeast direction, with strong indication of a northerly source. The linear thick zones are narrow in the northern portion of the field and bifurcate into two thick lobes toward the south, supporting the conclusion that sediment supply was from the north. The A sand is interpreted as a series of coalesced fans.

The gamma ray log response patterns in the A sand are dominated by the upper fan facies S and SCD comprising 80% and 17%, respectively (Fig. 8). True channel deposits (SB and CD) occupy only 3% of the map area and consist of only the SB log facies. The log response distribution map shows a strong correlation with the sand isopach map. In the northeast (sec. 30¾), there is an indication of a multiple feeder system noted in both the isopach and log response map. The trend in this section follows a northeast–southwest line, similar to that noted in the underlying E sand.

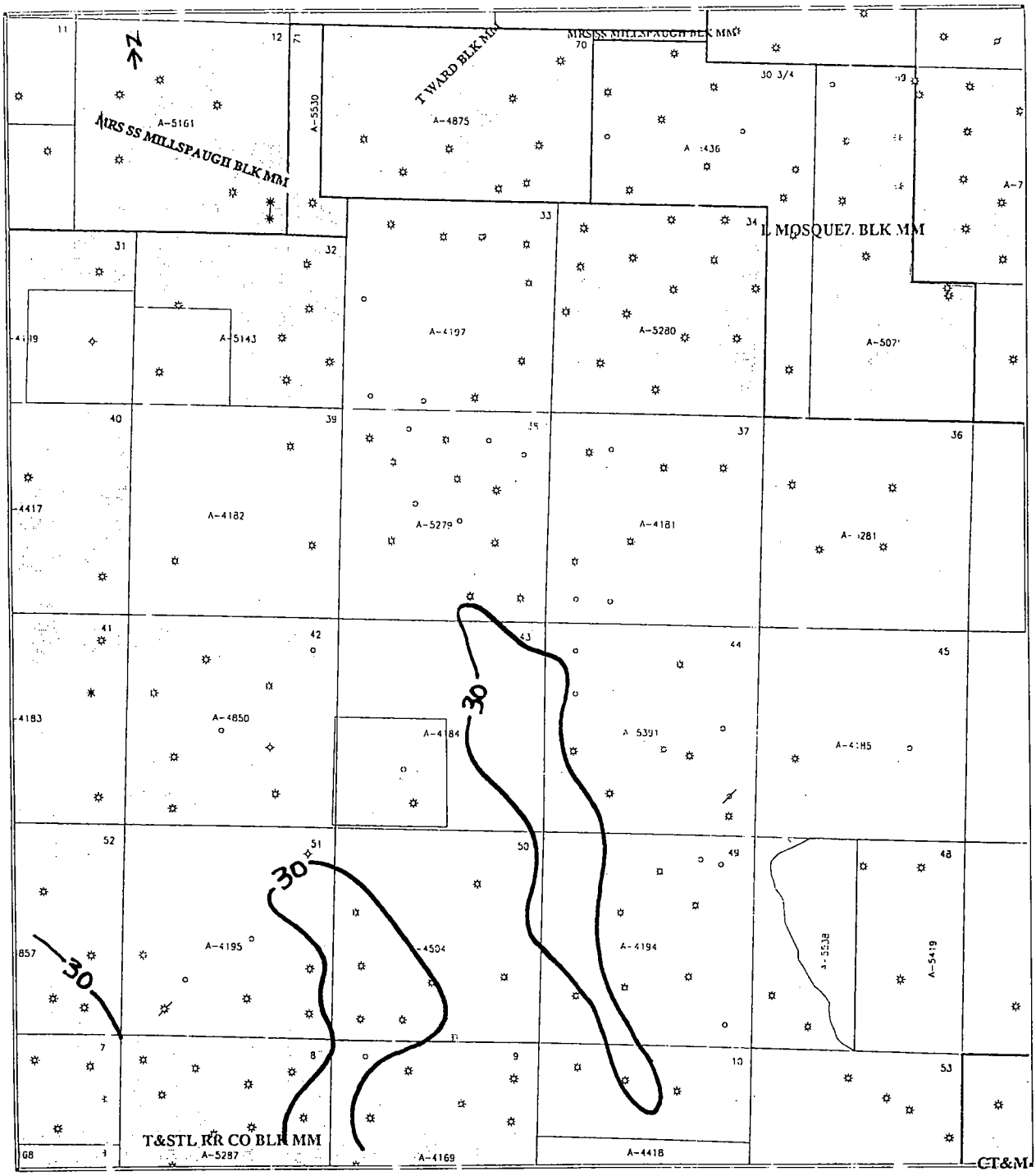

Figure 9. Sand isopach map of the Ozona Canyon C interval. Each section is one square mile, 30 ft contour interval. Closed contours are sand thicks.

Ozona Canyon C Interval

The Ozona Canyon C interval is not a dominant producer in the study area (Fig. 9). Although the sand follows the same northwest–southeast trend noted in the Ozona Canyon A interval, the sand is significantly thinner. Clean sand thickness in the northern half of the study area does not exceed 30 ft and is primarily less than 10 ft. The Ozona Canyon C sand does thicken toward the southwest edge of the map, with sand thickness greater than 50 ft. Productivity in the C zone begins to increase in these thicker sand trends.

The log response distribution map of the Ozona Canyon C interval exhibits a strong correlation with the sand isopach map (Fig. 10). Lobe and levee log response patterns constitute 70% of the field, and consist of only the S log facies. Log facies CD and SCD define the channel deposits, and make up 30% of the log facies.

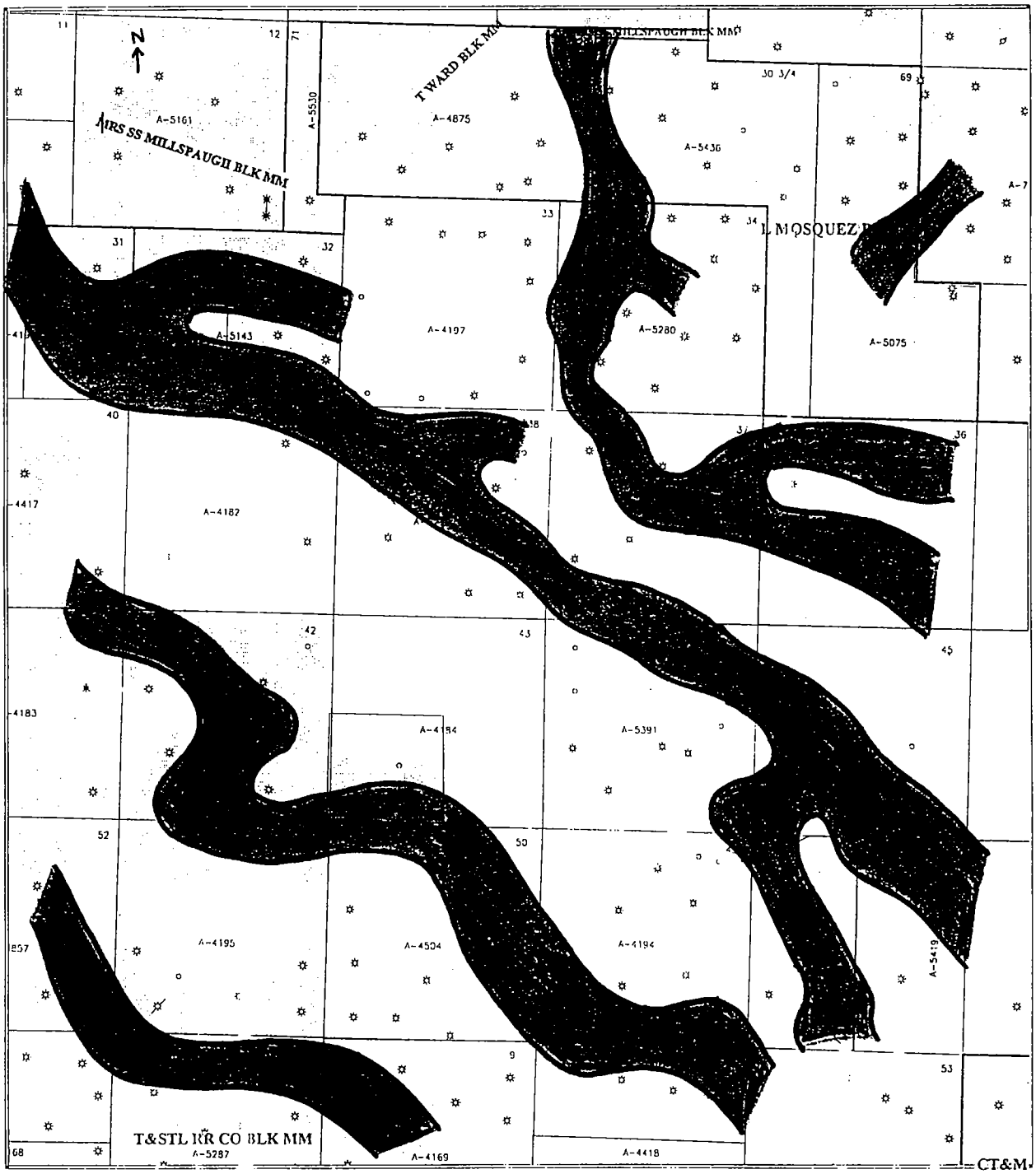

Figure 10. Log facies distribution map of the Ozona Canyon C interval. Shaded region includes the CD and SCD log facies, unshaded region includes the S log facies.

The gamma ray response of the Ozona Canyon C interval is hotter (higher API) than the other Ozona Canyon intervals, thus resulting in the thin, shaly, upper fan deposit.

Middle Fan

Middle fan deep-water deposits are characterized by thinning-upward sequences (distributary channels) overlying thickening-upward sequences (prograding lobes) (Fig. 5) (Reading, 1986). Ozona E and F intervals make up the middle fan deposits. These sands are dominated by the channel gamma ray response patterns consisting of the SB, CD, and SCD log facies. Lobe and levee responses (S, CU, and SCU) are also present in the E and F intervals, but are less abundant than in the upper and lower fan deposits.

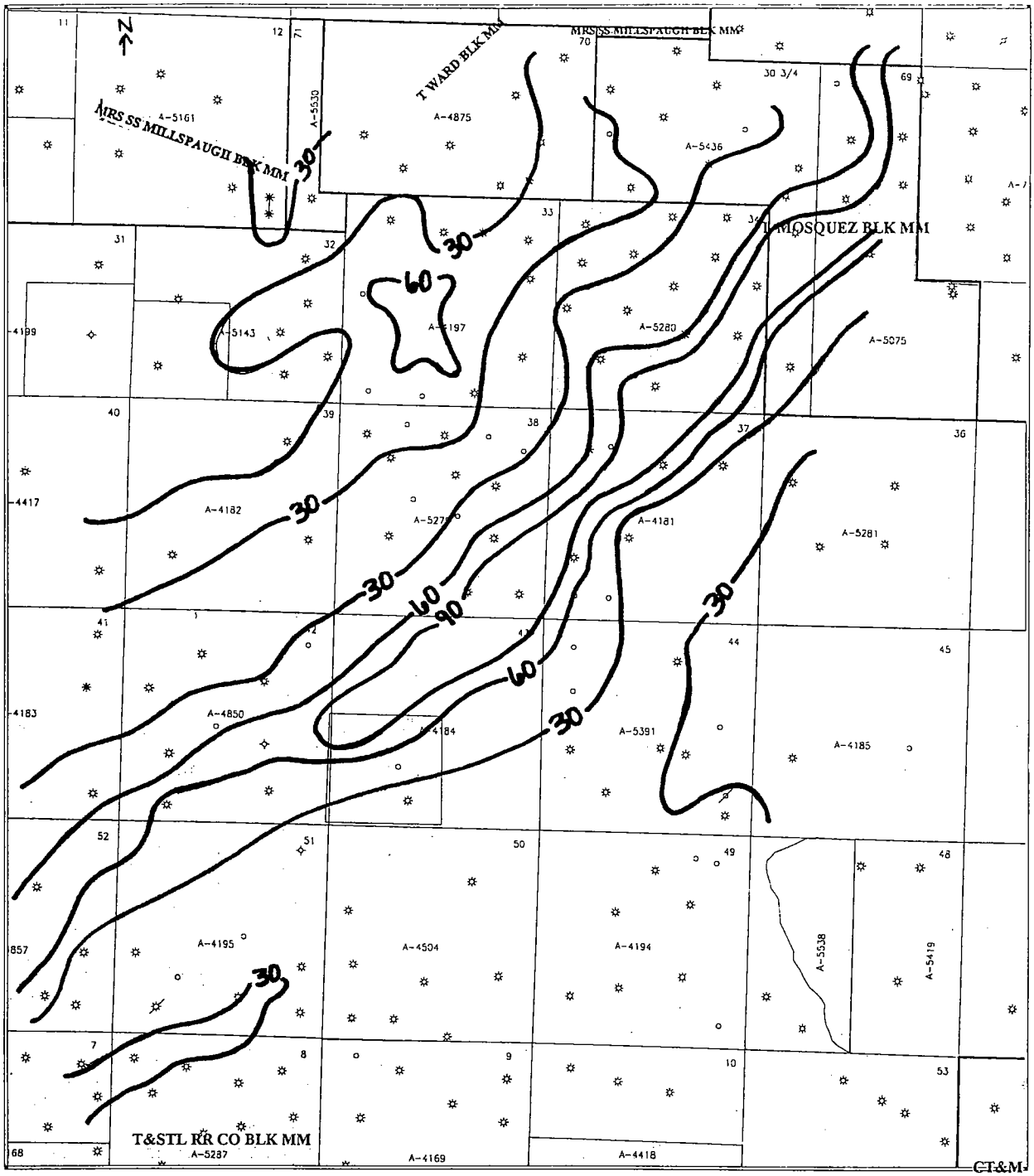

Figure 11. Sand isopach map of the Ozona Canyon E interval. Each section is one square mile, 30 ft contour interval.

Ozona Canyon E Interval

The most noticeable feature within the E sand is the distinctive linear thick, bisecting the study area. Maximum thickness exceeds 120 ft. The E interval displays an obvious southwest–northeast trend, perpendicular to the trend noted in the overlying Ozona intervals (Fig. 11). The reverse trend is supported by the sand isopach work completed in the northern portion of the field by Scott Hamlin with the Bureau of Economic Geology. Without core data from the field, the reason for the sand isopach trend change is unclear but is most likely due to a shift in the feeder system.

Log response patterns within the E zone are dominated by the channel responses, and a strong correlation exists between the log facies distribution map and the isopach map (Fig. 12). Channel deposits (SB, CD, and SCD) make up 47% of the field, with the SB log

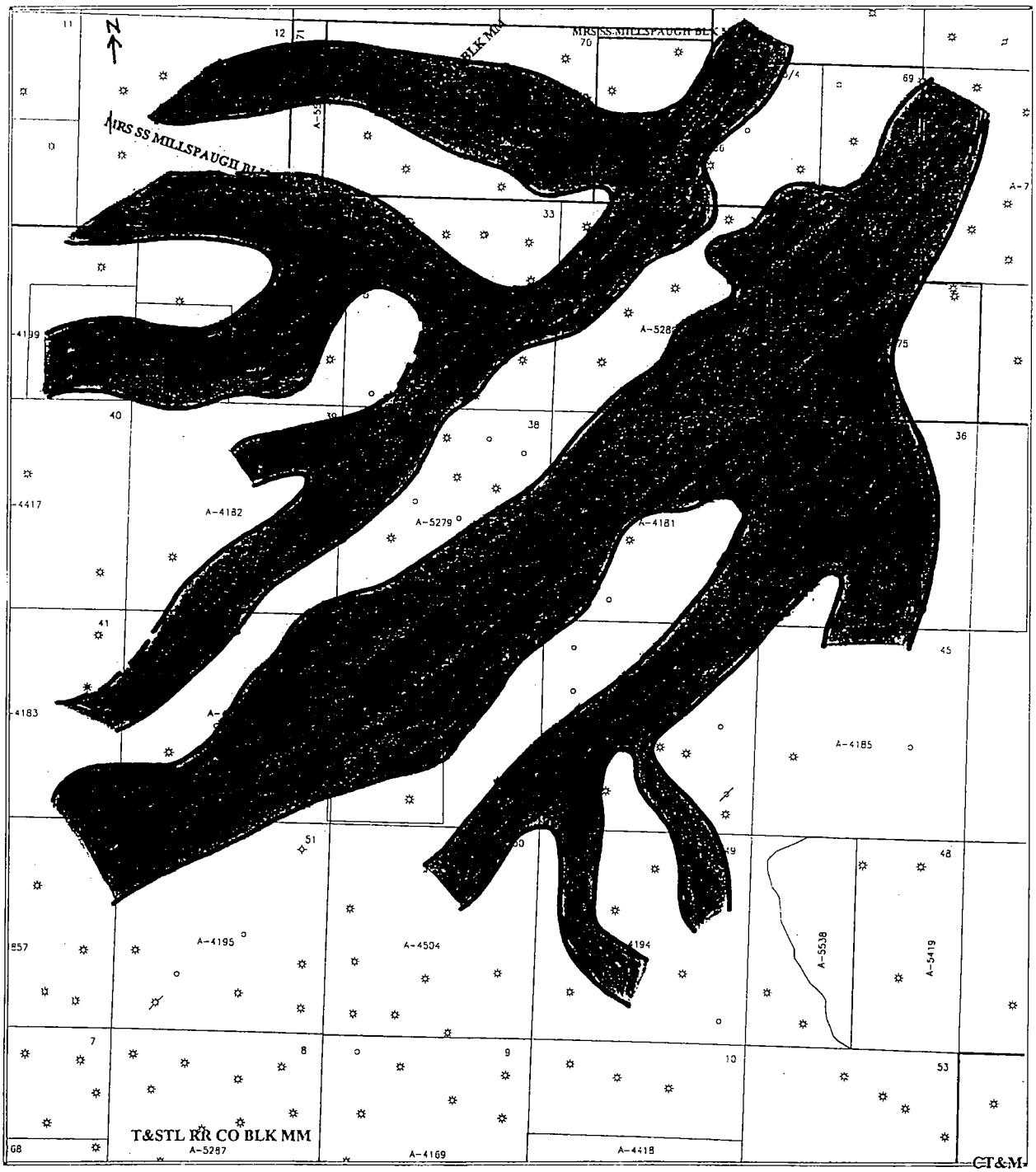

Figure 12. Log distribution map of the Ozona Canyon E interval. Shaded region includes the SB, CD, and SCD log facies, unshaded region includes the S, CU, and SCU log facies.

facies equaling 76% of the total channel facies. The channel log facies are heavily concentrated within the linear thick zone. The correlation between the log facies and the sand isopach trend supports the presence of a depositional channel within the E interval.

Ozona Canyon F Interval

The F sand reverses back to the characteristic northwest–southeast trend normally observed in the Ozona Canyon interval (Fig. 13). The F sand is made up of parallel, linear, thick pods with a maximum thickness of 60 ft. Sand isopach trends continue to support the idea of sediment supply from a northerly source. Evidence of the northerly source direction is inferred from the narrow feeder channels in the north part of the field, which open into broad, thick lobes toward the south. These linear thick zones parallel the zones of channel log facies on the log distribution map

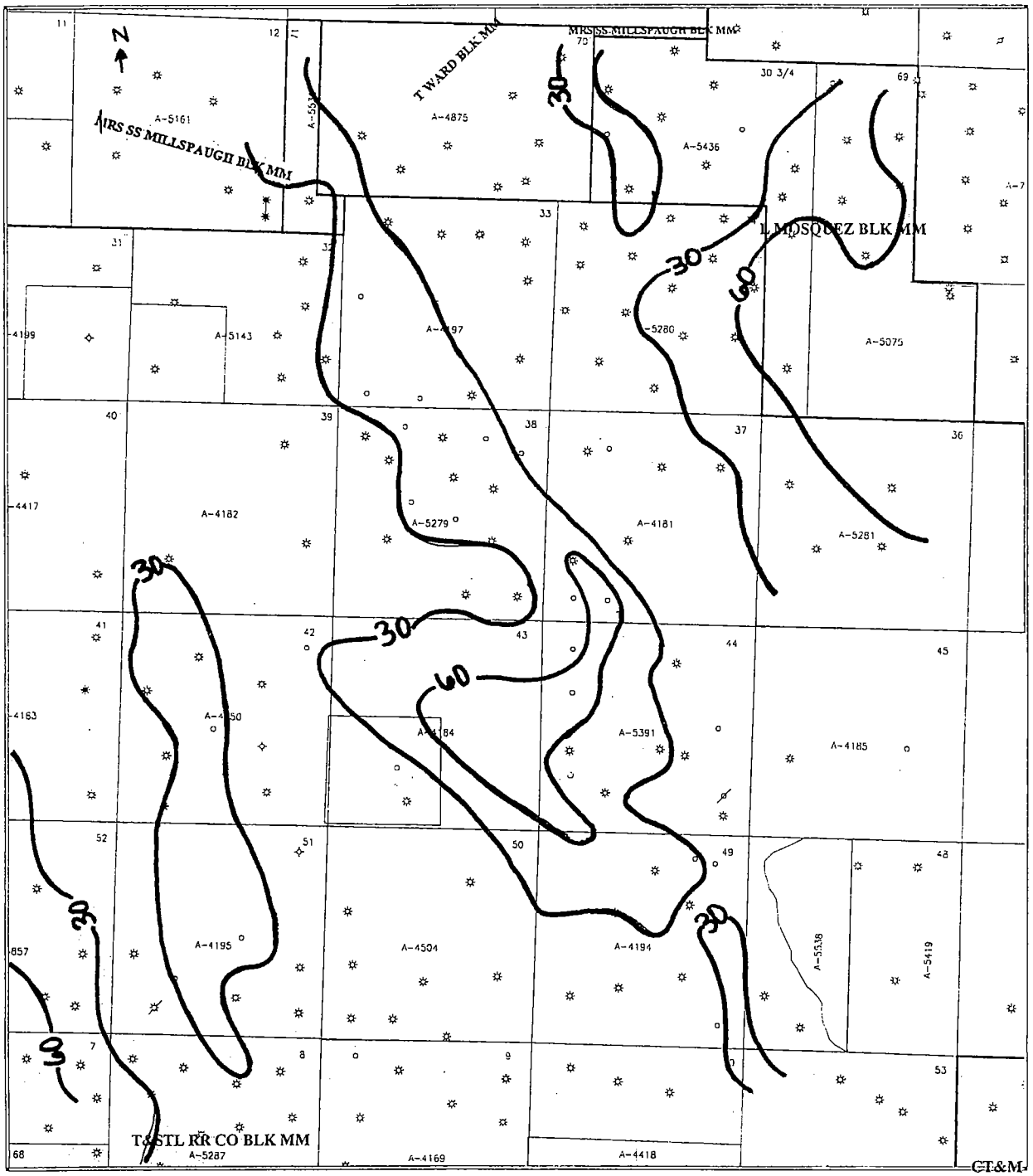

Figure 13. Sand isopach map of the Ozona Canyon F interval. Each section is one square mile, 30 ft contour interval.

(Fig. 14) showing a strong correlation between the two maps.

The linear thick zones on the sand isopach map are dominated by channel log facies (SB, CD, and SCD), and the thin zones are dominated by lobe and levee log facies (S, CU, and SCU). Channel log facies comprise 40% of the F sand, with 47% of the channel deposits made up of the SB log facies. The F sand also displays the same pattern in sec. 30¾ noted in the A sand. This section of the map appears to have a northeast–southwest trend similar to the trend in the overlying E sand.

Lower Fan

The lower fan deposits consist of medium- to fine-grained sandstones of good lateral continuity (Fig. 5) (Reading, 1986). The gamma ray log responses in the

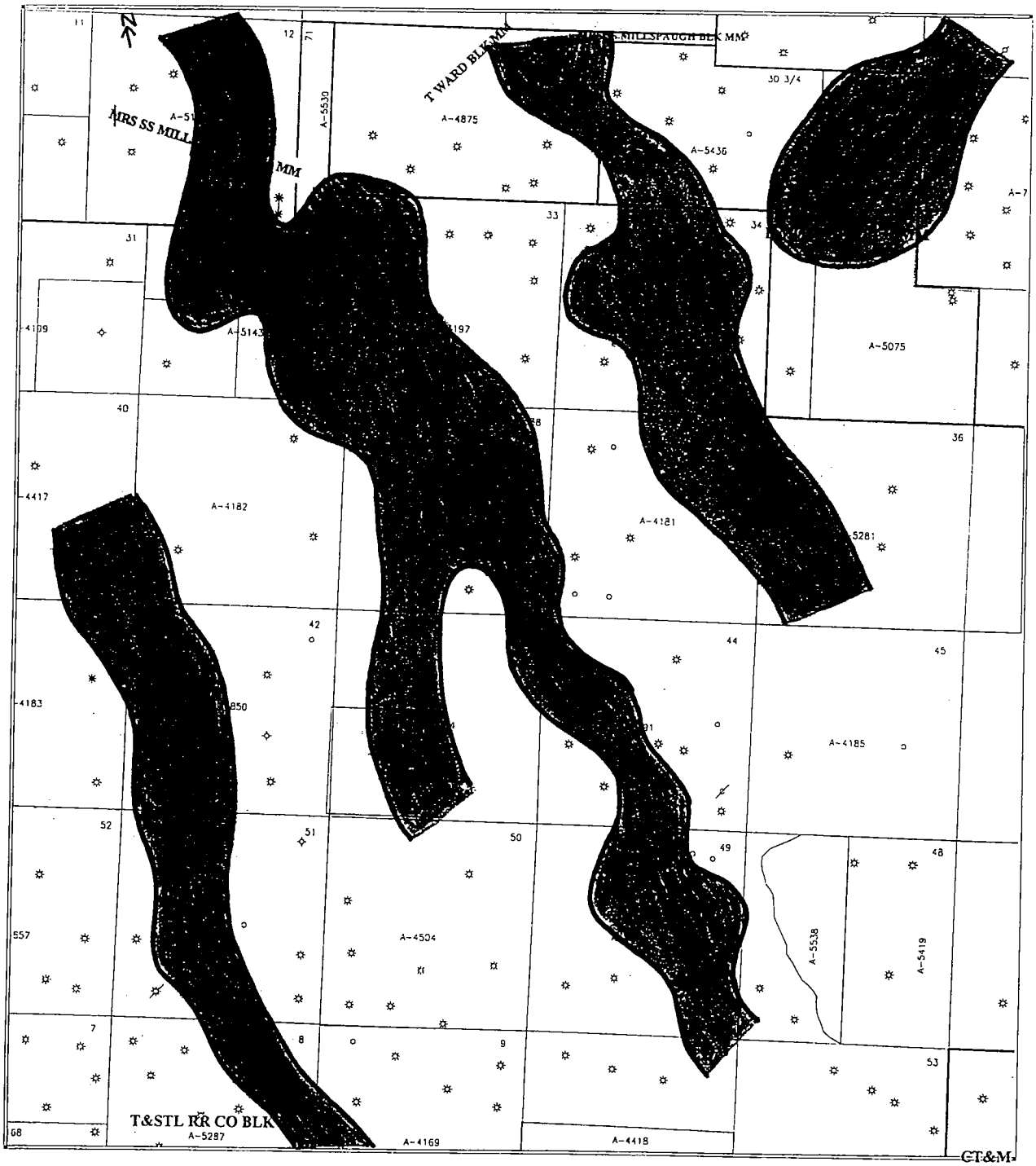

Figure 14. Log facies distribution map of the Ozona Canyon F interval. Shaded region includes the SB, CD, and SCD log facies, unshaded region includes the S, CU, and SCU log facies.

lowermost Ozona Canyon sands are more characteristic of lobe and levee deposits. Although the G and H sands are laterally continuous throughout the field, correlating the base of the G sand was difficult because the shale intervals (high gamma ray response) between the G and H sands can be discontinuous between wells. As a result of the correlation problems, mapping the sands proved difficult. These lower sands do not exhibit the same strong sand isopach trends and strong correlation to the log response maps as seen in the upper A through F sands.

Ozona Canyon G Interval

The G sand is the upper sand of the two lower fan deposits. Although subtle, the G interval appears to have the same northwest–southeast trend noted in the younger Ozona Canyon sands (Fig. 15). The log facies are dominated by the S, CD, and SCD patterns

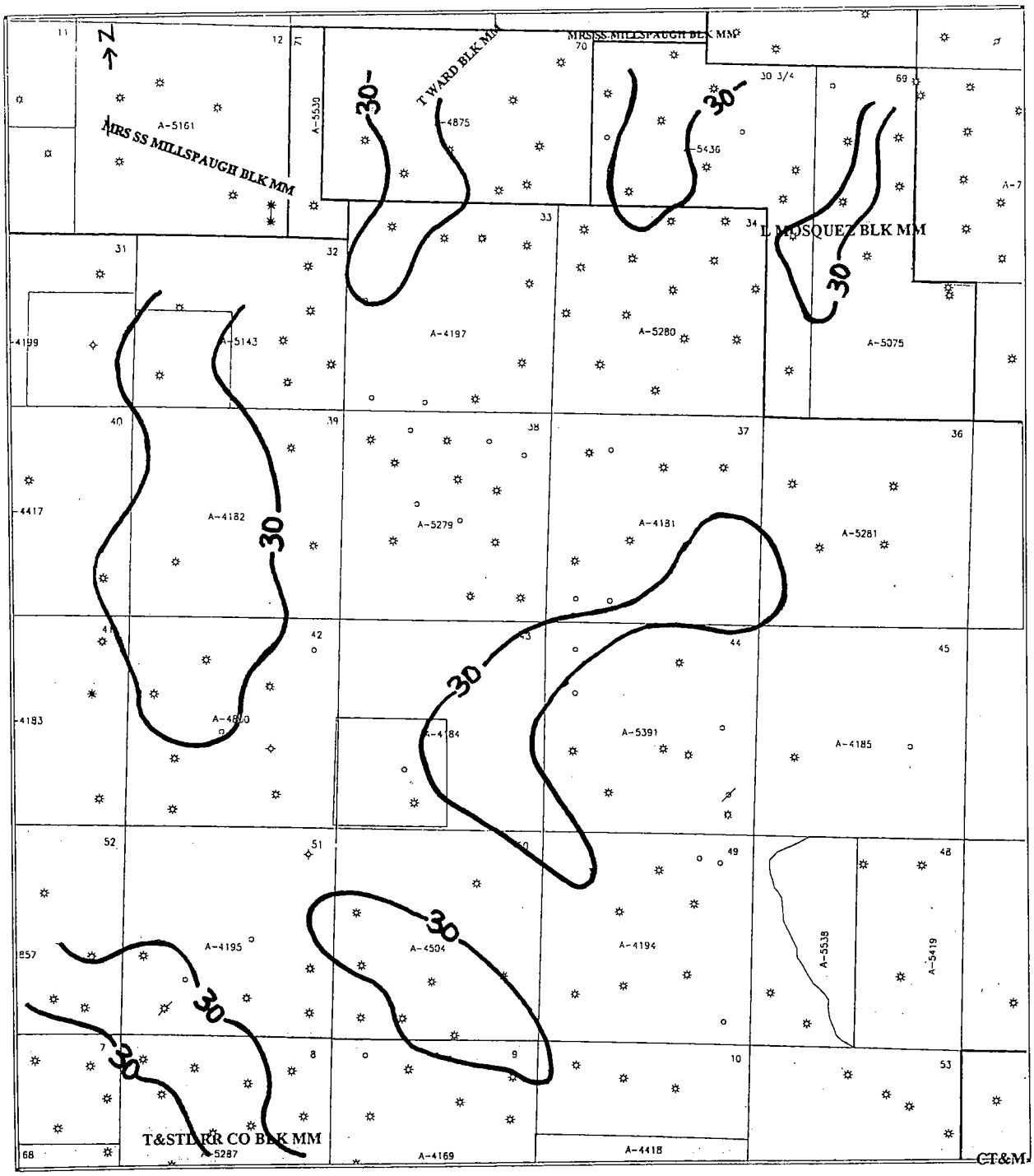

Figure 15. Sand isopach map of the Ozona Canyon G interval. Each section is one square mile, 30 ft contour interval.

(Fig. 16). Only three SB log facies are noted in the G interval. Although the CD and SCD log facies makes up 62% of the G interval, the CD and SCD log patterns differ from the channel responses observed in the A, E, and F sands. Gamma ray readings are typically hotter (higher API count) in the G sand than in the overlying sands; thus, the interval appears more shaly. In addition, individual sands within the G interval are significantly thinner than the overlying sands. Maximum thickness in the G is no greater than 50 ft net clean sand, significantly lower than the A sand with similar log response patterns.

Ozona Canyon H Interval

The oldest sand in the Ozona complex is the H sand (Fig. 17). As in the G sand, the trend in the H is subtle

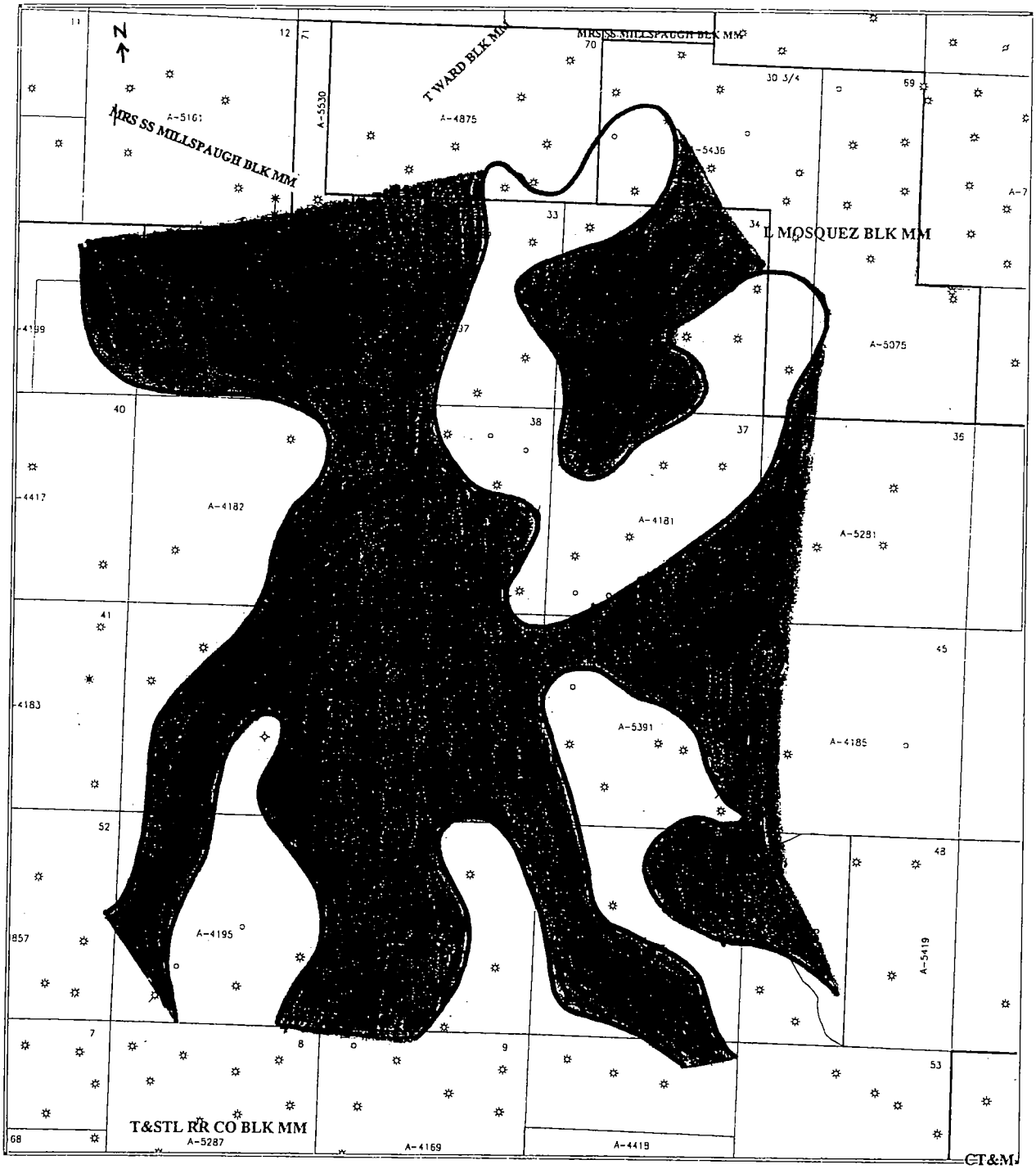

Figure 16. Log facies distribution map of the Ozona Canyon G interval. Shaded region includes the SB, CD, and SCD log facies, unshaded region includes the S log facies.

and difficult to distinguish. Log facies in the H interval are predominantly composed of lobe and levee fringe deposits (S, CU, and SCU) with only 16% represented by the channel log facies (SB, CD, and SCD) (Fig. 18). The SCD log facies, with characteristics of both channel and lobe and levee deposits, is concentrated in the southern part of the field, in what is interpreted as the distal fan fringe and makes up 89% of the total channel deposits.

The SCD and CD patterns in the H sand are similar to the log response noted in the G interval. Individual sands within the zone are thin and the overall package has a hotter gamma ray reading, indicating an increase in shale content. Correlation between the sand isopach map and the log facies distribution map is weak in the H interval. Net clean sand thickness within the zone is less than 75 ft in the majority of the wells and exceeds 100 ft in only a single well.

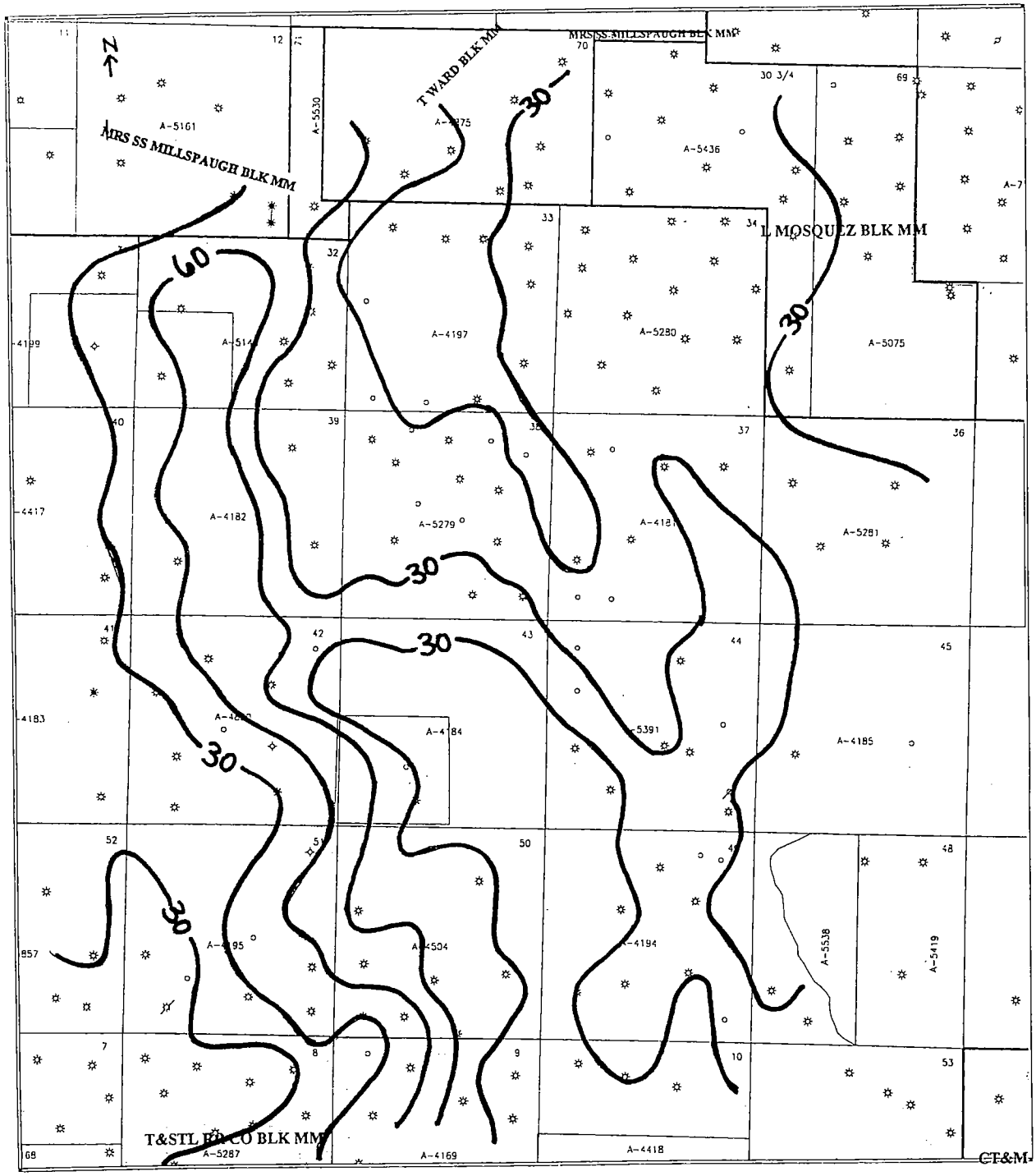

Figure 17. Sand isopach map of the Ozona Canyon H interval. Each section is one square mile, 30 ft contour interval.

OZONA CANYON PRODUCTION

Mapping of the Block MM study area was initiated in May 1996. Following completion of the first set of maps in August 1996, more than 60 new wells have been drilled in the field. The original maps were updated with new sand isopach data in both January 1996 and January 1997. In each case, only minor adjustments to the sand isopach maps were required, proving the accuracy of the original data set.

Production in the Ozona Canyon sandstone is generally correlated with sand thickness and sand quality. The average net pay within the Ozona interval is between 80 and 100 ft, thus making the primary drilling targets the thick sand zones. The sand isopach maps of the study area opened up new drilling potential by delineating thick sand trends. Several of the wells drilled

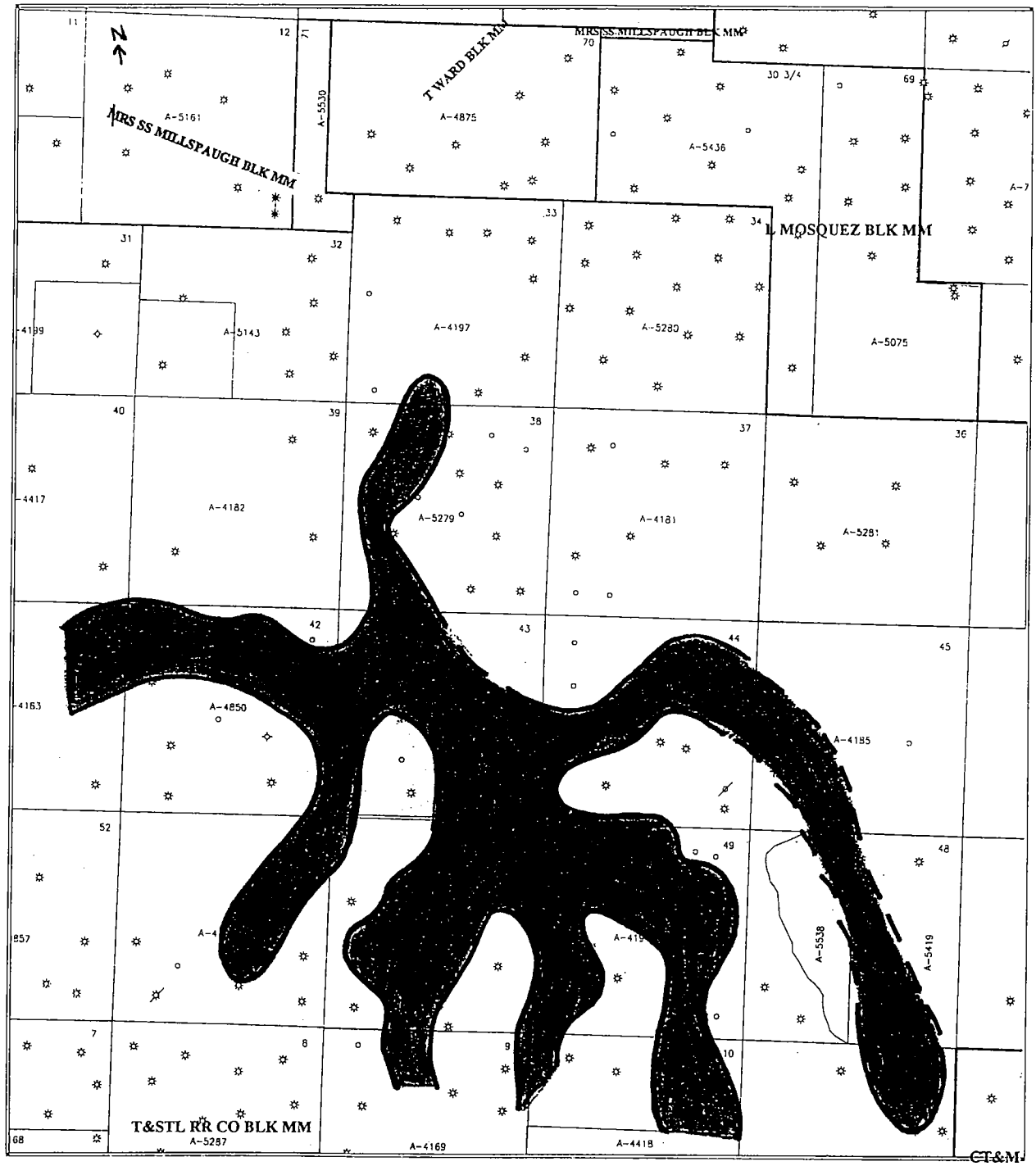

Figure 18. Log facies distribution map of the Ozona Canyon H interval. Shaded region includes the SB, CD, and SCD log facies, unshaded region includes the S, CU, and SCU log facies.

in late 1997 have yielded IP (initial potential) values >800 mcfd, exceeding that of any Ozona Canyon producing well in the area (Fig. 19) (J. Heinrich, Union Pacific Resources, personal commun., 1998). The increase in production is attributed to both an increase in drilling technology and the delineation of the sand trends depicted in the sand isopach maps, especially that noted in the Ozona Canyon E interval. In Figure 19 some of the wells drilled after 1996 do have low IPs, and it must be remembered that not all the new wells were drilled in the delineated "best" locations. Low drilling costs (approximately $230,000) in the Ozona Canyon sandstone make the lower IP wells economic producers.

SUMMARY

The Early Permian Ozona Canyon sandstone has been interpreted by Hamlin and others (1995) as a tur-

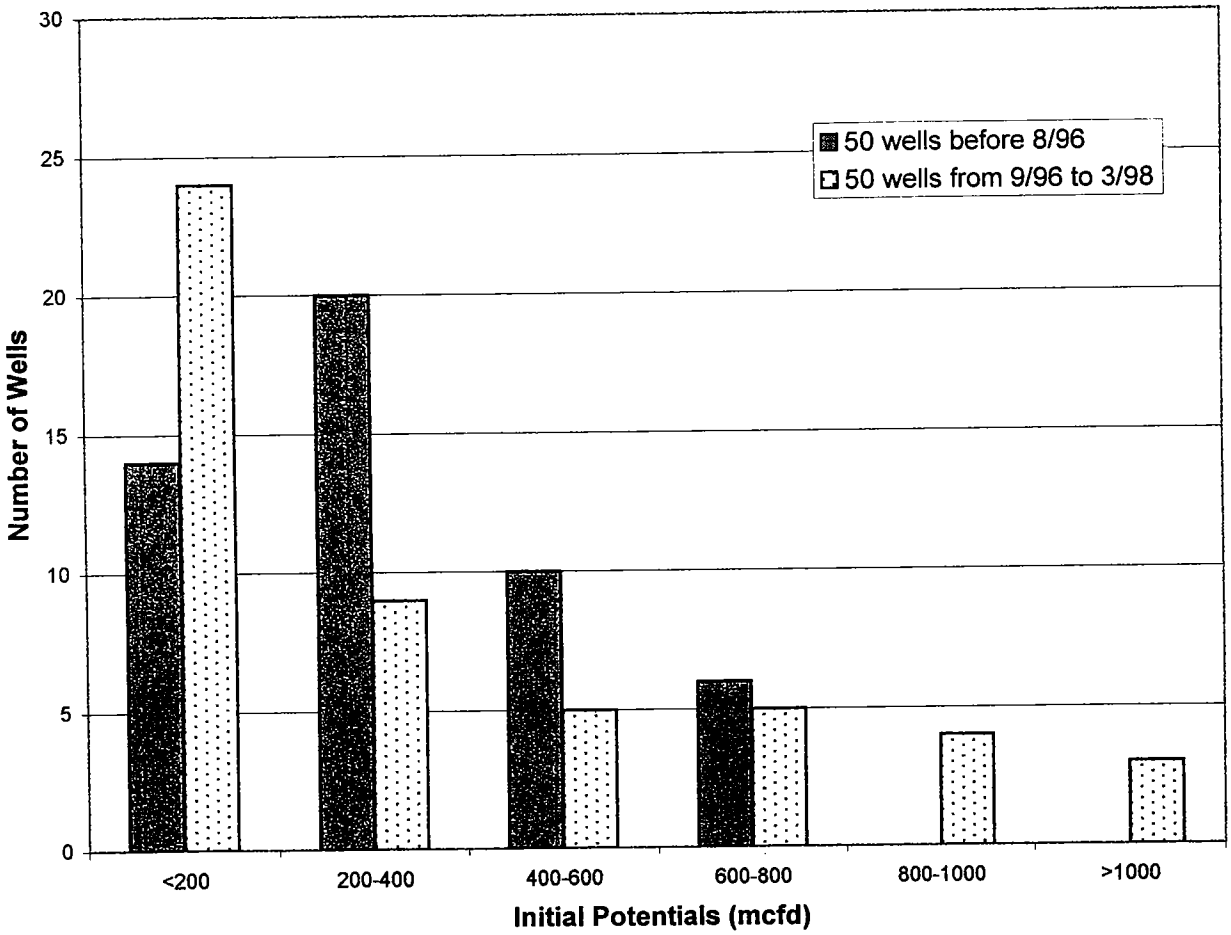

Figure 19. Production rates prior to the mapping project (pre-August 1996) and after the mapping project (post-August 1996).

bidite system deposited as a multiple source mud/sand rich ramp using the turbidite system classification of Reading and Richards (1994). The presence of multiple channel trends defined by log facies supports the multiple source turbidite system as defined by Reading and Richards (1994). Log facies within the Block MM study of the Ozona Canyon sandstone are divided into two groups; the channel log facies and the lobe and levee log facies. From the log facies and the sand isopach maps, the Ozona intervals were classified in terms of upper fan, middle fan, and lower fan deposits. The upper fan, made up of the Ozona A and C intervals, is dominated by the S and SCD log facies. The presence of both channel (SCD) and lobe and levee (S) log facies is characteristic of the upper fan. Ozona intervals E and F comprise the middle fan, and are dominated by the channel log facies (SB, CD, and SCD) characteristic of the middle fan. The lower fan sequence, composed of the Ozona G and H intervals, are dominated by the S log facies, representing lobe and levee deposits.

In addition to defining the depositional environment, the sand isopach maps and log facies distribution maps of the Ozona Canyon intervals are important tools in the determination of new drilling locations. The Block MM study proved that sand thickness as well as sand quality effect production in the Ozona Canyon reservoir. Identification of the thick sand zones with channel like log characteristics significantly increased the drilling potential in the Block MM field.

This study of the Ozona Canyon sandstone in Block MM resulted in the drilling of at least 60 new wells after August 1996, with additional well locations still being proposed. The study effectively established a correlation between the net sand isopach maps and the gamma ray log response maps that resulted in increased drilling potential and better production. This study may further aid in the development of hydrocarbons in the Ozona Canyon sands of Crockett County, Texas.

ACKNOWLEDGMENTS

The author expresses her gratitude to Union Pacific Resources, Fort Worth, for providing financial assistance and all subsurface data used in the study, and to Pioneer Natural Resources, Midland, and GeoQuest, Houston, for permission to publish and present the results of the study. A final thanks goes to George B. Asquith, Texas Tech University, for his guidance.

REFERENCES CITED

Berg, R. R., 1986, Reservoir sandstones: Prentice-Hall, Englewood Cliffs, New Jersey, 481 p.

Galloway, W. E., 1998, Siliciclastic slope and base-of-slope depositional systems: component facies, stratigraphic architecture, and classification: American Association of Petroleum Geologists Bulletin, v. 82, p. 569–595.

Hamlin, H. S.; Clift, S. J.; and Dutton, S. P., 1992a, Stratigraphy and diagenesis of Sonora Canyon deep-water sandstones, Val Verde basin, southwest Texas: American Association of Petroleum Geologists, Southwest Section Transactions, p. 209–220.

Hamlin, H. S.; Clift, S. J.; Dutton, S. P.; Hentz, T. F.; Laubach, S. E., 1995, Canyon sandstones—a geologically complex natural gas play in slope and basin facies, Val Verde basin, southwest Texas: University of Texas at Austin, Bureau of Economic Geology Report of Investigations 232.

Hills, J. M., 1968, Gas in Delaware and Val Verde basins, West Texas and southeastern New Mexico, *in* Beebe, B. W. (ed.), Natural gases of North America, part 3, Natural gases in rocks of Paleozoic age: American Association of Petroleum Geologists Memoir 9, v. 2, p. 1394–1432.

Huang, F. F., 1989, Depositional environments, diagenesis and porosity relationships of the Canyon sands, Edwards and Sutton Counties, Texas: Texas Tech University unpublished Ph.D. dissertation, 244 p.

Lehtonen, L. R., 1987, Late Paleozoic evolution of the Val Verde basin, West Texas: University of Texas at El Paso unpublished M.S. thesis, 164 p.

Mitchell, M. H., 1975, Depositional environment and facies relationships of the Canyon sandstone, Val Verde basin, Texas: Texas A&M University unpublished M.S. thesis, 210 p.

Mutti, Emiliano; and Ricci Lucchi, F., 1972, Le torbiditi dell'Apennino settentrionale: Introduzione all'analisi di facies: Memorie Societa Geologica Italiana, v. 11, p. 161–199. [English translation by T. H. Nilsen, 1978, International Geological Review, v. 20 p. 125–166.]

National Petroleum Council, 1980, Unconventional gas sources: Tight gas reservoirs, v. 5, part 1, p. 1–222; part 2, p. 10-1-19-24; and executive summary, 32 p.

Neuberger, D. J., 1987, Swastika (Upper Pennsylvanian) shelf-margin deltas and delta-fed turbidites, Flowers "Canyon sand field" area, Stonewall County, Texas: University of Texas at Austin unpublished M.S. thesis, 170 p.

Rall, R. W.; and Rall, E. P., 1958, Pennsylvanian subsurface geology of Sutton and Schleicher Counties, Texas: American Association of Petroleum Geologists Bulletin, v. 42, p. 839–870.

Reading, H. G., 1986, Sedimentary environments and facies [second edition]: Blackwell Scientific Publication, Oxford, London.

Reading, H. G.; and Richards, Marcus, 1994, Turbidite systems in deep-water basin margins classified by grain size and feeder system: American Association of Petroleum Geologists Bulletin, v. 78, p. 792–822.

Van Siclen, D. C., 1958, Depositional topography—examples and theory: American Association of Petroleum Geologists Bulletin, v. 42, p. 1897–1913.

Reservoir Characterization of the Giant Hugoton Gas Field, Kansas

Jack A. Babcock[1]
Amoco Production Co.[2]
Houston, Texas

Terrilyn M. Olson
Amoco Production Co.[2]
Denver, Colorado

K. V. K. Prasad
Amoco Production Co.[2]
Houston, Texas

Stephen D. Boughton
Amoco Production Co.[2]
Tulsa, Oklahoma

Paul D. Wagner
PGS Reservoir[2]
Houston, Texas

Mark H. Franklin
Rocky Mountain Petrophysics
Aurora, Colorado

Keith A. Thompson
Amoco Production Co.[2]
Tulsa, Oklahoma

ABSTRACT.—The Hugoton field in Kansas is the largest gas field in North America, with cumulative production over 23 trillion cubic feet (Tcf). Infill and deep drilling activity over the last 10 years have made it possible to build an extensive database of modern wireline log and core data. Such data formed the basis for a wide-ranging reservoir characterization done to obtain critical information for optimum reservoir management of the field. Reservoir heterogeneity and formation-evaluation problems made it difficult to characterize fluid distribution, estimate gas in place, and determine permeability from wireline log data, but few of the problems in this reservoir characterization study are unique to Hugoton. The techniques described here may be applicable to other reservoirs. Technologies employed to solve the formation-evaluation and lateral-variability problems included artificial neural networks, resistivity modeling, geostatistics, and three-dimensional grid manipulation.

The application of new technologies to problems in characterizing the Hugoton reservoir yielded both tools for evaluating specific areas of the field and a better understanding of field-wide pore volume gas in place (PVGIP) and its distribution. Geologic maps that include sealing faults, plus well plots from new applications of formation evaluation techniques, provide valuable tools to operations teams for increasing production and decreasing costs. PVGIP is estimated to be between 34.5 and 37.8 Tcf. The distribution of, and uncertainty in, the PVGIP values are important because they are also used to better manage the reservoir.

This paper is reprinted with modifications from the American Association of Petroleum Geologists Bulletin, v. 81, p. 1785–1803.

[1]Present address: Altura Energy Ltd., Houston, Texas.
[2]Author's employer at time of original publication.

Babcock, J. A.; Olson, T. M.; Prasad, K. V. K.; Boughton, S. D.; Wagner, P. D.; Franklin, M. H.; and Thompson, K. A., 2001, Reservoir characterization of the giant Hugoton gas field, Kansas, *in* Johnson, K. S. (ed.), Pennsylvanian and Permian geology and petroleum in the southern Midcontinent, 1998 symposium: Oklahoma Geological Survey Circular 104, p. 143–159.

INTRODUCTION

Kansas Hugoton is part of a continuous productive area that includes Guymon Hugoton in the Oklahoma Panhandle and Panhandle field in Texas. Although most hydrocarbon production within this extensive area is from Permian strata, the character of both the rocks and the fluids changes laterally. In this paper, we address only the reservoir characterization of Hugoton field in Kansas (Fig. 1).

Kansas Hugoton is the largest gas field in North America, has the highest cumulative production (Energy Information Administration, 1995), and is among the highest in annual production rates (Beene, 1996). The productive area includes about 10,620 km^2; average gross thickness of the Lower Permian Chase Group ranges from 75 to 105 m. Productive intervals lie between 640 and 885 m drilled depth.

Over 23 trillion cubic feet (Tcf) of natural gas have been produced from Hugoton field in the last 69 years, with years of productive life remaining. The most recent figures available (April 1997) show that production is occurring at a rate of 34.5 Gcf (billion cubic feet) per month (Kansas Corporation Commission, 1997). Companies with considerable Hugoton acreage include Amoco, Anadarko, Helmerich and Payne, Mesa, Mobil, Oxy, Plains, and Vastar.

Application of current concepts and technologies has greatly improved our ability to characterize and manage this multilayered gas reservoir. Discovered in 1927, Kansas Hugoton field has experienced waves of activity ever since. The most recent upswing in drilling activity started in 1987 after authorization of infill drilling by the Kansas Corporation Commission. The cores and modern logs acquired in recent deep (Pennsylvanian and Mississippian) wells and infill wells provided the database for this study (Fig. 1).

APPROACH

The key parameters for characterizing Hugoton field include the distribution of gas and water in the reservoir, the producibility of those fluids, and zonal permeabilities and their variation. To build a successful reservoir characterization, we analyzed the geologic framework of the reservoir (stratigraphy and diagenesis), and the gas-trapping components (structure and stratigraphy), and performed formation evaluation through core and wireline-log analysis. The resulting information was combined using three-dimensional (3-D) visualization software for examination of data relationships and calculation of volumetric gas in place. Although volumetric gas in place does not form the basis for reserve determinations in this reservoir, knowing the amount and distribution of the gas in situ provides an important benchmark for evaluating well performance.

PREVIOUS WORK

Most previous publications on Hugoton have suffered from access to small data sets compared to the size and complexity of the field (e.g., Parham and Campbell, 1993). One exception contains formation-evaluation work in Kansas Hugoton by a team from

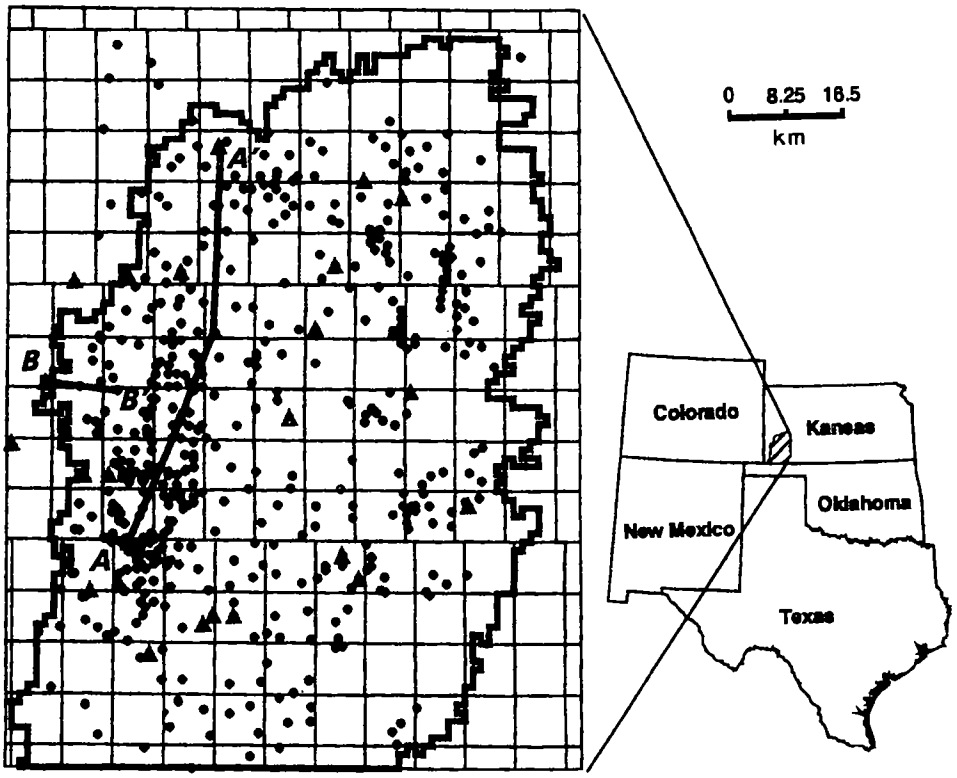

Figure 1. Location of Kansas Hugoton field with locations of cores (triangles) and modern log suites (dots) used in field study. The outline surrounds the productive area. Line of cross section A–A′ refers to Figure 4; line of cross section B–B′ refers to Figure 12.

Mobil (Gwiner and others, 1992). Transcripts of Kansas Corporation Commission hearings, notably those on Hugoton infill proceedings (Kansas Corporation Commission, 1986), provide additional sources of subsurface data and interpretations.

Graduate theses (e.g., Stever, 1987), core workshops (Caldwell, 1991), and some field-trip guidebooks (e.g., Toomey and Mitchell, 1986; Mazzullo and Teal, 1994) provided useful background for some aspects of the Chase Group but tend to be limited in scope. Mazzullo and others (1996) showed how Chase Group cycles fit with sequence stratigraphic terminology and concepts and described the component facies in outcrop in south-central Kansas. Miller and others (1996) described cycle patterns and interpreted climatic variations from Lower Permian paleosols of eastern Kansas. Geologic controls on the reservoir quality of Kansas Hugoton field are outlined in Olson and others (1996).

GEOLOGIC FRAMEWORK

Stratigraphy

The Hugoton field is productive from five main reservoir zones within the Permian Chase Group (Fig. 2). The terminology shown in the stratigraphic column corresponds to field usage (cf. Caldwell, 1991); the major productive units are the Herington, Krider, Winfield, Towanda, and Fort Riley Formations. Correlations with type sections in outcrops located approximately 320 km east are somewhat problematic, so outcrop terminology is not used.

The Chase Group consists of alternating marine and nonmarine units, with the reservoir-prone facies occurring largely within the marine layers. The main rock types are fossiliferous limestone or dolomite (marine), fine-grained quartzofeldspathic sandstone and siltstone (marginal marine), and mixed siltstones and claystones that are dominantly red in color (nonmarine). These rock types alternate repeatedly in distinctive vertical sequences (Fig. 2). Both symmetric and asymmetric sea-level cycles are represented within the Chase Group; there are three cycle variants (Fig. 3), which are important because the associated sequence pattern remains relatively constant for each time-correlative unit (e.g., Winfield Formation). Note the presence of marine sandstones and siltstones, which are not widely recognized as reservoir facies in Hugoton, and the absence of black shales.

The siltstones, sandstones, limestones, and dolomites that form the reservoir are laterally variable and mixed; one productive unit, such as the Herington or Winfield, con-

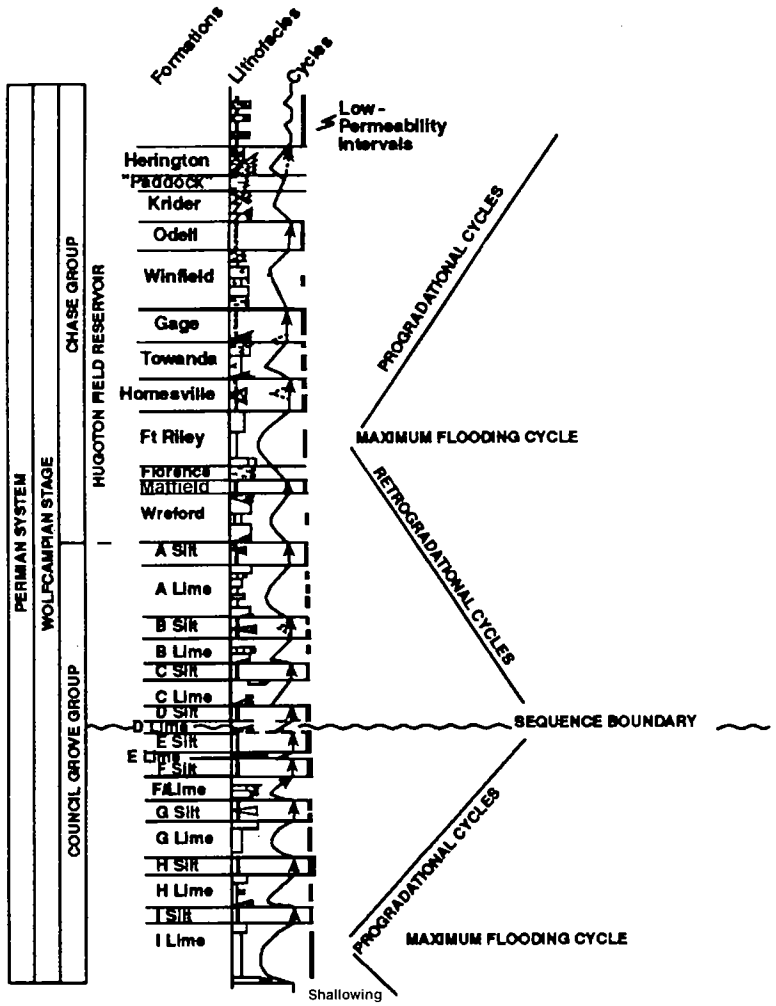

Figure 2. Schematic display showing stratigraphic nomenclature and depositional cycles, Hugoton field area. Vertical bars represent facies-dependent permeability barriers.

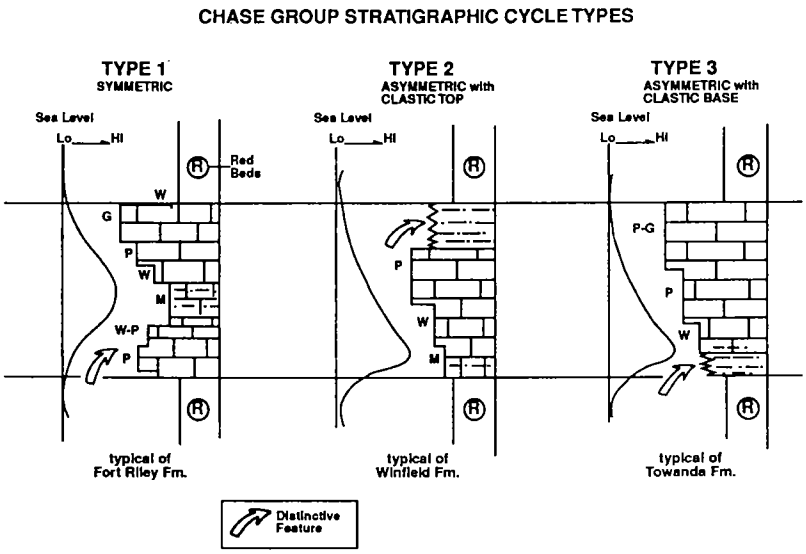

Figure 3. Schematic illustration of three distinct types of stratigraphic cycles found in the Chase Group formations. Dot-dash pattern represents siltstone; other lithofacies the same as in Figure 2.

sists of any or all of those rock types, depending on where it is in the field (Fig. 4). The cycle templates of Figure 3 allow us to categorize this variability and recognize patterns in the lithologic variation. These templates also give us three time-correlative reference points in each sequence—the top and basal boundaries and the maximum flooding surface or zone. The tops and bases of these sequences are indicated by abrupt vertical changes in facies between terrestrial red beds and marine carbonates or clastics. Maximum flooding events were identified on the basis of a combination of features in core: a distinctive fossil assemblage (thin-shelled brachiopods, crinoids, and fenestrate bryozoans), dark color, apparent organic-rich composition, and, commonly, argillaceous carbonate mudstone.

These reference points generally are recognizable on wireline logs—the sequence boundaries are indicated by distinctive gamma-ray, neutron porosity, and resistivity responses of terrestrial siltstone and claystone units; maximum flooding surfaces are recognizable on logs by high gamma-ray levels due to concentrations of fine-grained argillaceous carbonate, organic matter, and uranium at these surfaces. This log signature of the maximum flooding surface is particularly evident in the Fort Riley unit (see Fig. 4 for this log pattern in four wells).

Figure 5 is a conceptual diagram illustrating the relationships between depositional facies patterns and timelines along a dip section across Hugoton field for one sequence within the Chase Group. It shows that the various types of sediment that were deposited to form the rocks in the Chase Group cycles were not laid down as flat, continuous sheets, nor were they laid down at the same rate. Above the lower red beds, deposition was relatively slow, especially at the maximum flooding surface. Above the maximum flooding surface, the progradational (regressive) deposits were deposited faster. Three lines of evidence exist for this difference in sedimentation rate: (1) the asymmetry of the vertical facies sequences, suggesting more rapid deposition above the maximum flooding surface than below, (2) higher concentrations of terrigenous quartz silt (deposited from suspension at relatively constant rates), and (3) higher proportions of grain-rich rock and shallow-water fossils in the units above a maximum flooding surface that are related to higher energy, generally more rapid sedimentation.

Time lines cut across lithofacies boundaries (Fig. 5), indicating that different kinds of sediment accumulated at the same time. Our model shows (1) lateral heterogeneity due to depositional environment; (2) that shingling (onlapping and offlapping) exists within and between the cycles, suggesting appropriate layering schemes for building a numerical reservoir description; and (3) that the basal marine facies above the (sometimes reworked) red beds are flatter and more slowly deposited than the upper marine facies and form more laterally continuous flow units or barriers. The basal marine units have such continuity because they were formed as transgressive deposits across the basin as sea level rose and were deposited on the most planar surfaces that formed during the relative sea-level cycles, above topography-filling terrestrial red beds. Porosity and permeability data from routine core analysis of hundreds of samples indicate that the red beds are barriers and do not constitute flow units.

Diagenesis

Process controls on reservoir distribution extend beyond the depositional considerations discussed. The essential depositional control on reservoir quality was the 3-D distribution of clean grain-supported rocks of all types (carbonates, sandstones, and siltstones). See Figure 3 for positions in sequences occupied by grain-rich lithofacies (sandstone/siltstone, packstone, grainstone). Beyond deposition, diagenesis was critical in controlling reservoir quality through a combination of dolomitization, chemical compaction, leaching, and cementation.

Clean clastics (sandstones and siltstones) and dolomitized packstones/grainstones served as high-permeability pathways from early in the life of the reservoir. Most coarse-grained carbonate lithologies were dolomitized early on, and subsequent resistance to chemical compaction contributed significantly to permeability retention. Those limestone grainstones/packstones that did not undergo dolomitization (e.g., upper Fort Riley interval in most of the field) served as high-permeability pathways through shallow burial, but have since been degraded to varying degrees by burial-induced chemical compaction and associated calcite cementation. Natural susceptibility of limestones to chemical compaction contributed largely to permeability loss, especially where large admixtures of clastic materials were present.

Two major leaching events occurred that helped shape the present distribution of reservoir rocks. The first leaching event occurred at the surface or in the shallow subsurface (Fig. 6), either episodically punctuating deposition (i.e., from intermittent meteoric exposure) or generally invading the early plumbing system (i.e., expulsion of compaction fluids). Limestones were most affected; abundant moldic and secondary microporosity formed. The second leaching event occurred much later, after continual burial and significant chemical compaction (Fig. 7). The probable leaching fluid for this second event was an extremely calcic brine that formed by dissolution of overlying bedded anhydrite, and then moved downward and laterally through the late plumbing system. Dolomites and mixed dolomite-clastic intervals were most affected.

The difference in timing of leaching relative to chemical compaction is critical in defining reservoir quality. Many early-leached limestone reservoirs once had excellent porosity and permeability, but have since been degraded to "marginal" or "nonreservoir" rocks by compaction and associated burial cementation. Most late-leached dolomitic reservoirs have retained their good porosity-permeability characteristics both because of comparative resistance to compaction and because later degrading diagenetic processes had insufficient time or material to shut the permeability systems down.

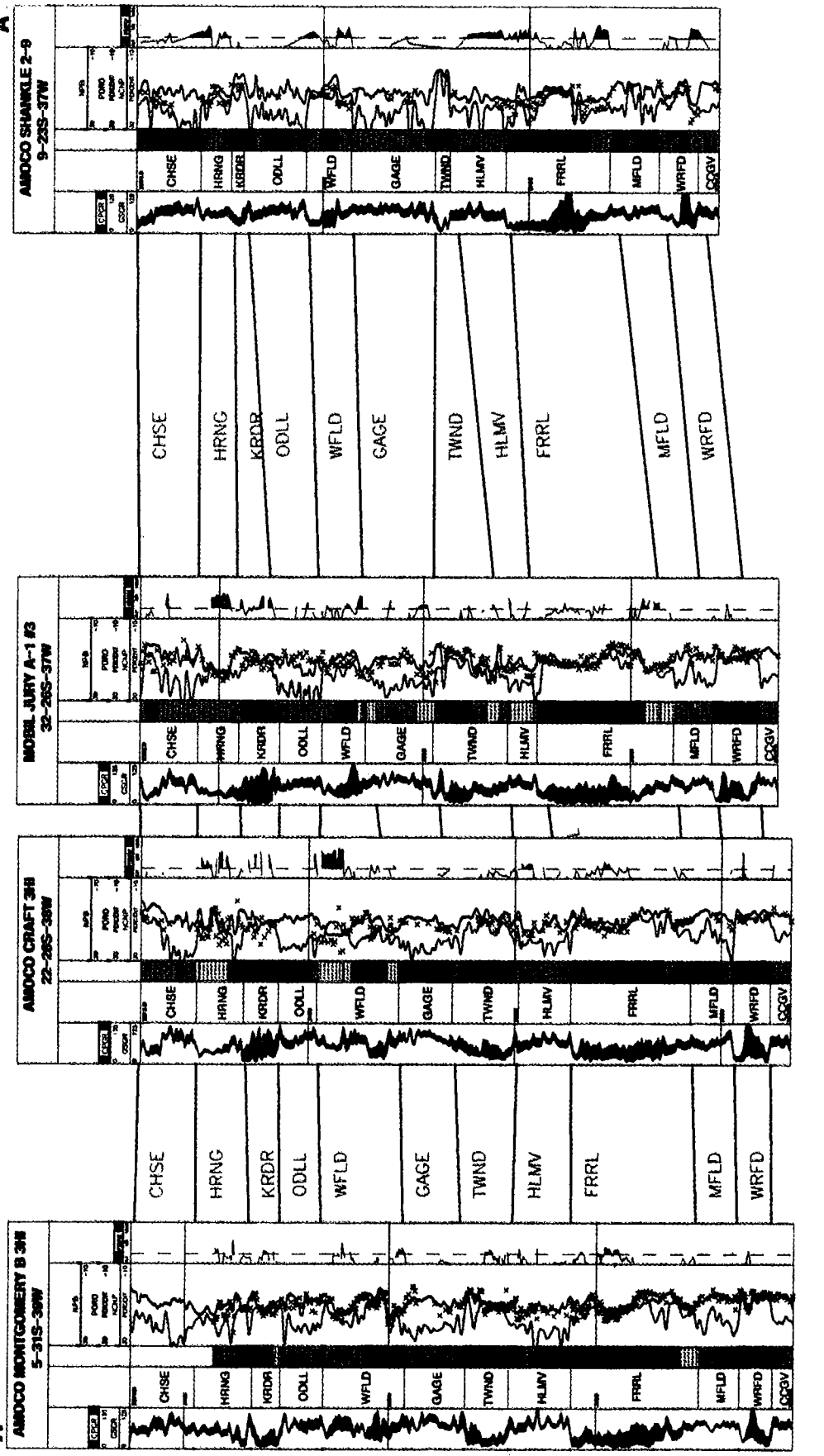

Figure 4. Stratigraphic cross section A–A' (cored wells). See Figure 1 for location. Core data include grain density (track 1), grain size/carbonate texture (track 2), lithology (track 3), porosity (track 4, "x"), and permeability (track 5). Wireline-log (and log-derived) curves shown are total and potassium-thorium gamma ray (track 1); density porosity, neutron porosity, neural-net porosity, and photoelectric factor (track 4). The two gamma-ray (GR) curves shown in this and subsequent figures indicate how much of the radioactivity is caused by uranium (the difference between the GR curves). This line of section lies roughly parallel to the paleoshoreline of the Hugoton embayment. The Shankle 2-9 well is in a position slightly more up depositional dip than the other wells, which is reflected by thinning of the marine units (notably Krider, Towanda, and Fort Riley Formations), the lithofacies change in the Towanda to anhydrite, and the amount of dolomite in the Fort Riley. Note the lateral and vertical variability of lithologies and permeability. Formation abbreviations: CGSE—Chase; HRNG—Herington; KRDR—Krider; ODLL—Odell; WFLD—Winfield; GAGE—Gage; TWND—Towanda; HLMV—Homesville; FRRL—Fort Riley; MFLD—Matfield ; WRFD—Wreford.

Cementation locally impaired porosity and permeability in some intervals. Some clastic intervals (e.g., Herington Formation in northern and western Hugoton field) contain abundant early-formed dolomite cement and clay replacements, and variable amounts of late-formed anhydrite and dolomite cements (Fig. 8). The most prevalent type of cements in dolomitic intervals is anhydrite (e.g., in Krider, Winfield, and Towanda dolomites and dolomitic sandstones). The chemical compaction of mud-supported limestone produced copious amounts of burial calcspars that helped seal some intervals in adjacent grain-supported limes (e.g., in the upper Fort Riley and lower Wreford Formations). Carbon isotopic data indicate that most of the carbonate cements were locally derived from this compaction mechanism (Fig. 9). Sulfur and strontium isotopic data indicate that most or all of the anhydritic cement was locally derived, with most of it probably sourced from the overlying bedded anhydrite (see Table 1).

Details on geologic controls on reservoir complexity can be found in Olson and others (1996). Interpretations of Chase Group subsurface diagenesis and porosity evolution farther south in Kansas and Oklahoma are included in Siemers and Ahr (1990), Caldwell (1991), and Stever (1987).

Trapping Mechanisms

The Hugoton field has long been considered an excellent analog for huge stratigraphic traps (e.g., Garlough and Taylor, 1941; Parham and Campbell, 1993). Hydrodynamic trap concepts also have been illustrated using Hugoton as an example (Hubbert, 1967; Mason, 1968). New data and a detailed look at fluid distribution near the field edges have shown that neither stratigraphic changes nor hydrodynamics fully explain the trap components of Hugoton field.

Table 1.—Strontium/Sulfur Isotope Results

Sample Number	$^{87}Sr/^{86}Sr$	$\delta^{34}S$
2420	0.70866 (4)	14.3
2478	0.70874 (3)	12.7
2518	0.70881 (4)	12.7
2542	0.70871 (2)	12.8
2579	0.70862 (3)	12.9
DUP	0.70865 (3)	12.9
2635	0.70854 (2)	12.9
2738	0.70861 (3)	12.9
DUP		12.8
2832	0.70851 (2)	14.2

Note: Strontium isotope results are shown with 95% confidence limit errors [SEM (standard error of mean)] in parentheses; National Bureau of Standards strontium isotopic standard number SRM 987 = 0.71030 (2) during the course of these analyses. Sulfur isotope results are relative to Canyon Diablo trailite standard (sulfide phase in meteorite).

Changes in water saturation with elevation in the Fort Riley Formation (Fig. 10) provided a key indication that something besides stratigraphic trapping is important in Hugoton. High water saturations in the updip area of the field, separated by a sharp boundary (sudden saturation change with elevation in Fig. 10) from low water saturations and Fort Riley gas production, indicated the presence of separate fluid compartments. A 3-D seismic survey in the area confirmed the presence of a significant fault (Fig. 11) that extends up into the lower Chase Group from deeper units (Fig. 12). Throw across this fault is variable; seismic and log-tops data indicate that throw increases (to >30 m) toward the south. This major fault acts as a barrier to flow and prevented gas charging of the updip fault block. Shallower Chase zones are not compartmentalized by this

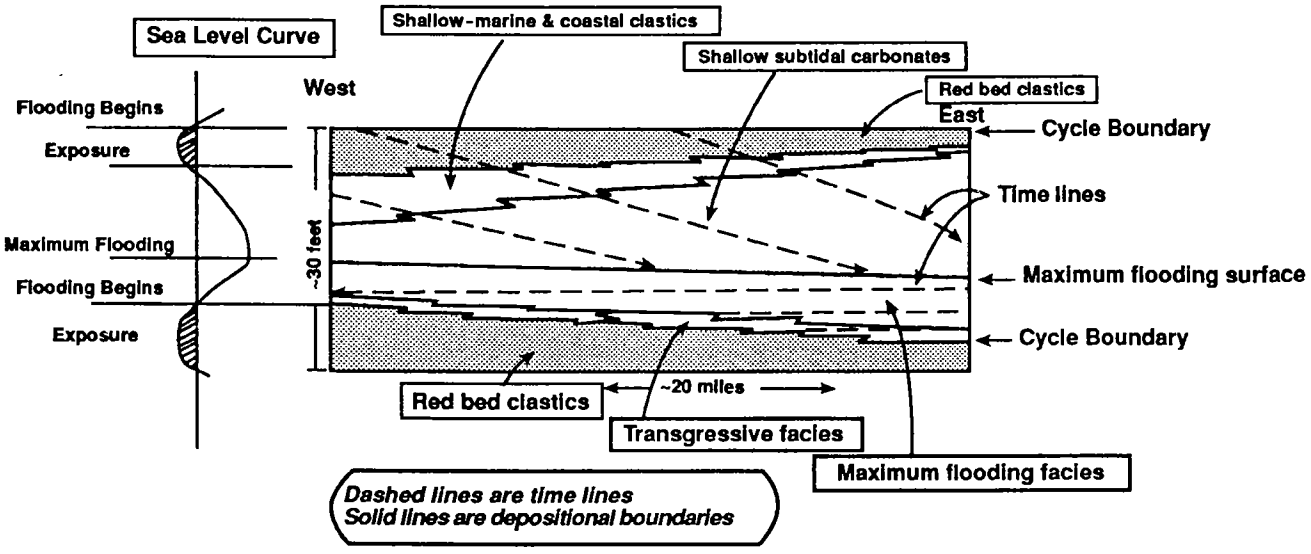

Figure 5. Chase Group conceptual two-dimensional cycle and depositional geometry. Solid lines represent lithofacies transitions, which are time transgressive. Approximate scale as shown.

fault and contain stratigraphically trapped gas farther west due to facies changes from carbonates to clastic red beds updip (Krider and Towanda Formations) or grain-size changes (Winfield Formation) (Fig. 12). Faults have also been recognized as a controlling factor in gas and water distribution in the Fort Riley Formation in the northwestern part of the field.

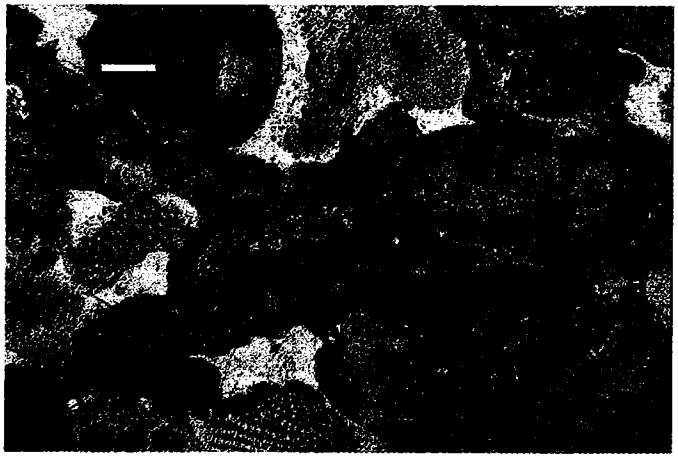

Figure 6. Photomicrograph of Towanda formation limestone from the Mobil Hayward 3-S well (sec. 16, T. 32 S., R. 37 W., Stevens County, Kansas). Porosity is shown with blue epoxy. Timing of early leaching is indicated by subsequent infilling of molds with calcite rim and blocky cements and by burial-induced mold crushing. Early leaching may have been caused by either meteoric or shallow-burial, marine-like fluids. Scale bar is 100 μm.

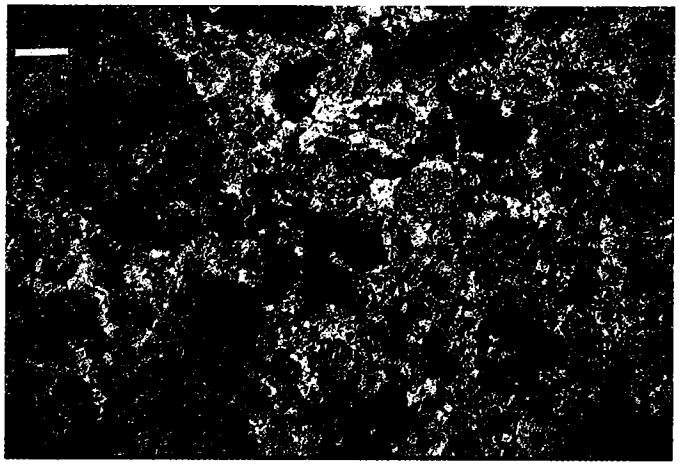

Figure 7. Photomicrograph of Krider Formation dolomite from the Mobil Hayward 3-5 well. Timing of late leaching is indicated by open fabric, comparative scarcity of carbonate pore-filling cements, and lack of subsequent compaction. Vug development that crosscuts burial-induced stylolites in this and other wells also indicates a late timing of leaching. Late leaching may have been caused by calcic brines that formed by dissolution of overlying bedded anhydrite and then gravity refluxed downward through the underlying Chase Group. Scale bar is 100 μm.

This new understanding of the role of faults in fluid distribution has greatly improved our ability to manage the reservoir by suggesting actions to minimize water production and associated operating costs and to maximize gas production through appropriate workovers and better drilling and completion planning. Four wells in the 1996 infill-drilling program that previously would have been drilled through the Fort Riley were drilled and completed only through the Towanda due to the wells' locations on fault blocks where the Fort Riley is wet. As a result, water production was avoided, and drilling and completion costs were lowered.

PROBLEMS IN RESERVOIR CHARACTERIZATION OF HUGOTON FIELD

Any field study will present problems peculiar to the particular combination of rocks, fluids, and the vintages and amount of data available. Some problems in characterizing the Hugoton reservoir relate to measurement or resolution of the data, whereas other problems pertain to logistics and techniques of data manipulation. Although some of these issues also affect the development of the geologic framework outlined, most of the issues pertain primarily to problems of more detailed formation evaluation.

Many of the following difficulties relate to wireline log data, which form the bulk of the data available for characterizing a field the size of Hugoton. There are numerous measurement- or resolution-related problems. One major problem is invasion of drilling fluids beyond the depth of investigation of conventional resistivity logging tools (resistivity measurements are a key component of fluid saturation calculations). This deep invasion stems from generally low reservoir pressures compared to the weight of a 670-m column of drilling

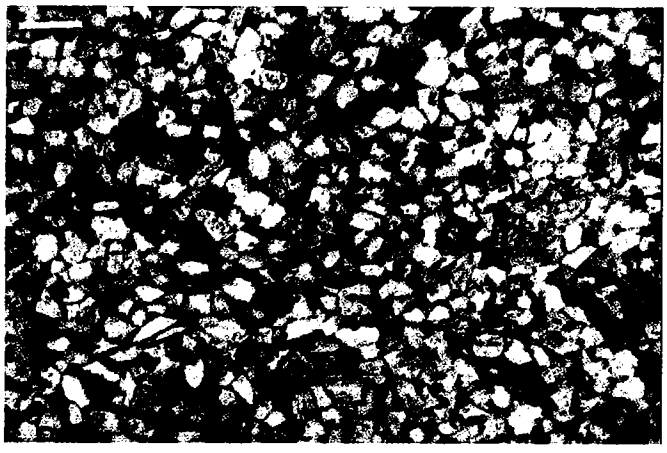

Figure 8. Photomicrograph of Winfield Formation fine-grained sandstone from the Amoco Shrimplin 2HI well. Cleaner sands such as this acted as distribution pathways for late-leaching fluids. Adjoining mixed clastic/dolomite intervals underwent significant leaching of dolomitic components. Minor dolomite cementation (small rhombic crystals) occurred between and after episodic, late leaching events. Note that no anhydrite cement is visible in this view. Scale bar is 100 μm.

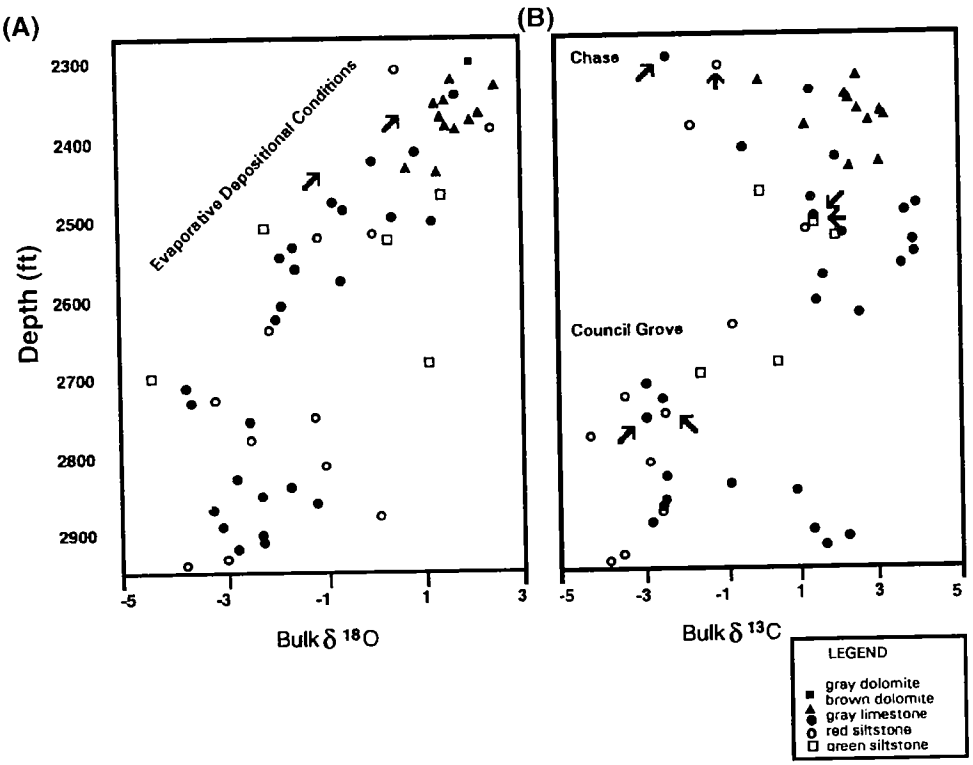

Figure 9. Stable isotope stratigraphy from the Amoco Craft 3HI (sec. 22, T. 28 S., R. 38 W., Grant County, Kansas). (A) Vertical variations in whole-rock oxygen isotopic compositions. Heavier (more positive) values with decreasing depths suggest increasingly evaporative depositional conditions toward the overlying bedded evaporites above the Chase Group. (B) Variations in whole-rock carbon isotopic compositions. Similarities in isotopic compositions (pairs of arrows) between carbonate cements in clastic samples (which make up the bulk of the carbonate material analyzed in the clastic whole-rock samples) and the surrounding chemically compacted depositional carbonates indicate local sourcing of these cements.

mud. Another resolution-related problem in characterization of Hugoton is the prevalence of thin beds of both reservoir and nonreservoir rocks. This is an especially important problem in resistivity logging. Standard resistivity tools have less vertical resolution than most other logging tools, because formation resistivity is typically not fully resolved in beds thinner than 30 m. Highly variable and complex rock types invalidate most assumptions for calculating porosity from logs (assumptions about matrix properties are oversimplified). Furthermore, a large number of minerals are needed to adequately characterize the rock system; typically, log analysis for lithology, porosity, and water saturation requires at least as many inputs as there are variables (cf. Doveton, 1991, 1994). The difference in volumes being measured, notably by core analyses and log measurements, makes it difficult to calibrate log analysis techniques with core data, especially in heterogeneous systems such as the Chase Group. Production-related engineering data, which would be valuable for validation of formation-evaluation techniques (especially permeability estimation), is typically a composite from multiple zones.

Characterization of Hugoton presents difficulties with data manipulation using standard techniques. The thick reservoir interval (91 m) over a large area (10,660 km^2) means there is a huge volume of reservoir to consider. Even the large data set comprising thousands of feet of core and 480 wells with modern logs is sparse in comparison with the heterogeneous volume being characterized. In such a thin-bedded reservoir, log data must be on depth with other logs from the same well and with core where available. Accurate depth-shifting to achieve adequate precision is difficult and time-consuming. The complexity of the geologic framework, in terms of the variation in rock types and pore systems, means that there is no single

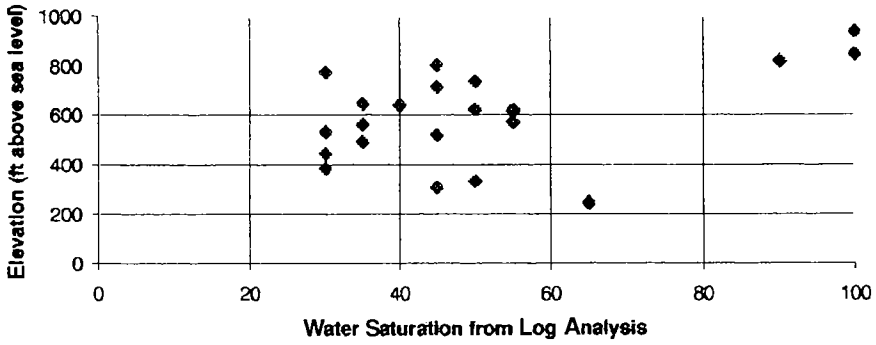

Figure 10. Crossplot of elevation above sea level versus log-derived water saturation for porous Fort Riley zone. Each point represents the equivalent zone in a different well. The scatter in the main group of points is mostly due to resistivity measurement inaccuracies due to invasion. Nonetheless, a general trend of decreasing water saturation with increasing elevation is observed up to 800 ft above sea level. Above that, a separate fluid compartment is observed; see Figure 11 for the location of that compartment.

relationship between porosity and permeability. The typical approach of estimating permeability from a linear regression with porosity (see Doveton, 1994, for Chase plot) produces several orders of magnitude of possible error and thus is useless.

Averaging problems in the standard approach to calculating volumetric gas in place (creating two-dimensional grids from three-dimensional data) can create large errors in the results. For Hugoton, Denver and Phillips (1992) showed that vertical averaging of porosity and water saturation values in the process of calculating gas in place can lead to underestimating the gas in place by >20%. This problem is most acute in vertically variable reservoirs, where much information is lost by averaging across many layers with different rock properties.

To produce a meaningful reservoir characterization of Hugoton field, we had to determine a number of key parameters. Standard log-based approaches to all of the following variables were problematic when applied to Hugoton for the following reasons:

1. Porosity at wells with modern logs (spectral gamma-ray, resistivity, density-neutron-photoelectric) depends on matrix assumptions and thus is difficult to calculate accurately.
2. Porosity distribution between control points (wells with modern logs) as a basis for calculating field-wide water saturation and gas volume is not reliable if merely interpolated, because of lateral variability and relatively sparse control in some areas.

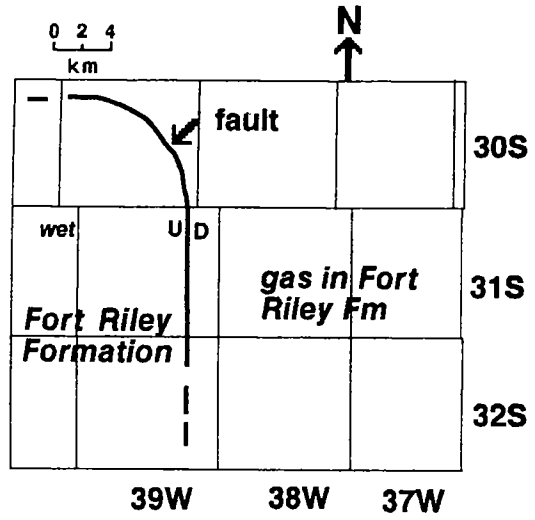

Figure 11. Map of sealing fault, southwest Kansas Hugoton field. The location of this fault is known from three-dimensional seismic data. The fault separates wet, porous Fort Riley Formation to the west from gas-bearing Fort Riley to the east, and apparently prevented hydrocarbon charging of the updip block.

3. Water saturation calculation at control points is complicated by invasion and vertical-resolution problems.
4. Permeability is difficult to predict accurately due to poor correlation with porosity.

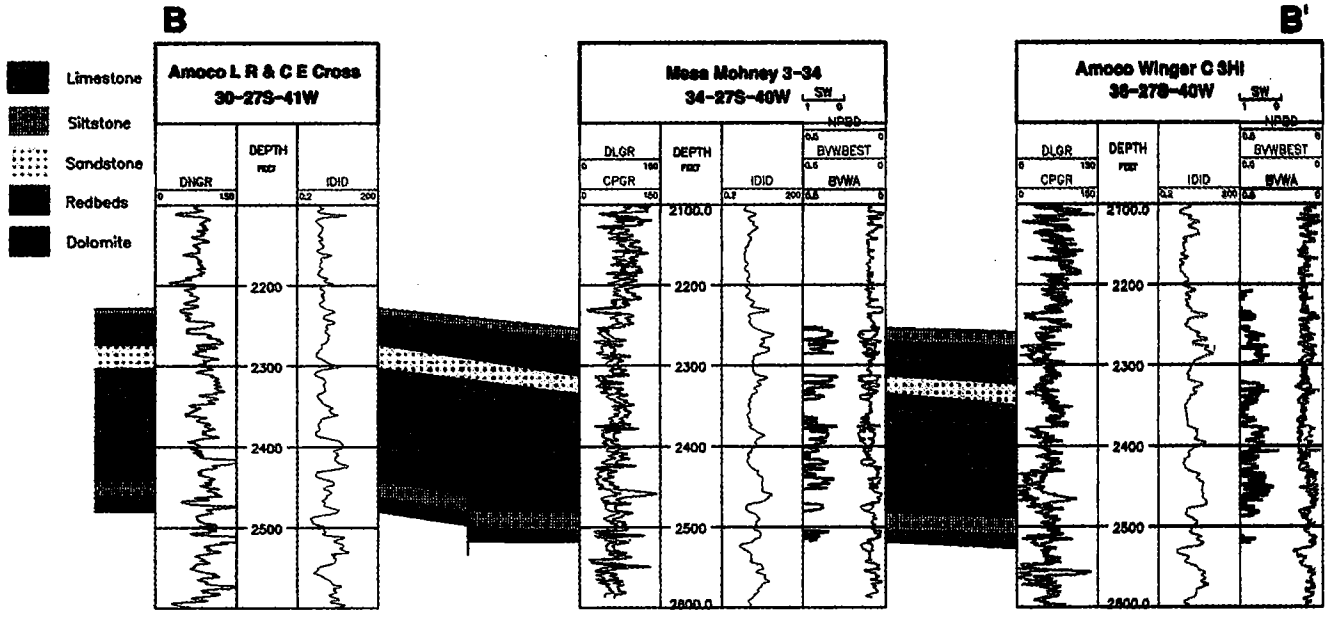

Figure 12. Structural cross section B–B′. See Figure 1 for line location. One of a system of faults that form the trap for the Fort Riley Formation is shown beneath the stratigraphic changes that form the trap for overlying units in Hugoton field. The track on the left shows producible fluids (gas between porosity [NPBD] and bulk volume water [BVW], BVWBEST; producible water between BVWBEST and irreducible bulk volume water [BVWA]). Lithic symbols: Limestone—brick pattern; dolomite—slanted-brick pattern; anhydritic dolomite—"v" pattern; siltstone—finely dotted pattern; sandstone—coarse-dotted pattern; redbed mudstone/siltstone units—finely dotted and dashed pattern.

There is no standard log-based approach to compute irreducible bulk volume water. The ability to determine irreducible bulk volume water is necessary for discriminating between bound water and producible water, which are both components of calculated water saturation.

SOLUTIONS TO HUGOTON RESERVOIR-CHARACTERIZATION PROBLEMS

In the preceding section, we described key problems faced in characterizing the Chase reservoir system in Hugoton field. In the following sections, we present the solutions we found to those problems. Undoubtedly, other solutions are available for most of the problems. Because none of these problems are unique to the reservoir considered here, our intent is to show some techniques that may be applicable for solving such problems in other places.

Porosity estimation from logs can be calibrated with quality core analyses. We attempted a variety of approaches to porosity from logs, including (1) concurrent estimation of lithology and porosity (using LINEAR™ software in the Western Atlas WDS); (2) matrix- and fluid-corrected density porosity; and (3) concurrent estimation of lithology, porosity, and water saturation (using WDS OPTIMA™). None of these approaches produced results with sufficiently small error, so we tried another method. The best results in terms of smallest mean absolute error were obtained using a backpropagation artificial neural network. (See Doveton, 1994, for an explanation of neural networks and their application to log analysis.) Log inputs consist of bulk density, potassium-thorium gamma ray, uranium gamma ray, and photoelectric curves (Prasad and others, 1996). The network was trained statistically with all the data from a number of cored wells (with measured porosities) and tested on cored wells not in the training set. Figure 13 shows neural-net-predicted porosity compared with core porosity for one cored well. One advantage of the type of neural-net software used was its ability to translate the network relationships into an equation that could easily be applied to all wells with the appropriate input curves.

Water saturation calculations have several inherent problems. These problems include erroneous readings due to deep invasion (most severe in deep wells and wells with high fluid loss in their drilling mud) and to poor vertical resolution. Our initial solutions depended on making various adjustments to standard deep resistivity data. The acquisition of resistivity logs measured with air or foam in the well bore from three wells gave us a basis for adjusting standard logs for invasion. There are more variables to the problem than we could really account for, so this adjustment tended to produce "corrected" resistivities that were too high (resulting in artificially low water saturation calculations). Another type of adjustment to compensate for vertical-resolution problems was more successful. Inverse modeling of resistivity data gave corrected curves that appeared to compensate for thin-bed effects, in comparison with available high-resolution resistivity data from different

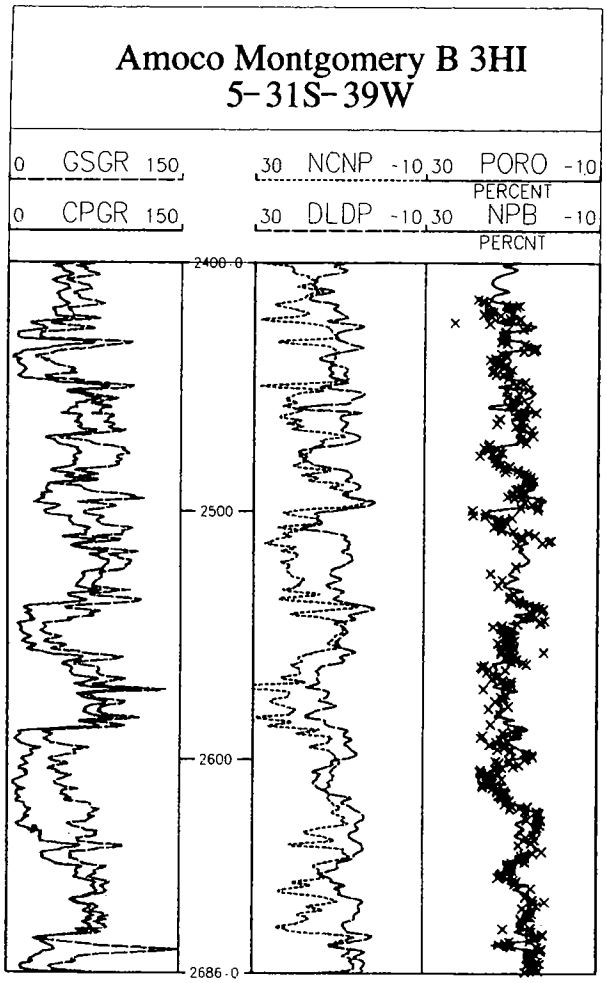

Figure 13. Wireline-log plot of a cored well over the entire Chase Group. Log porosity curves are shown in the center track: Neutron porosity (NCNP) is short dashed curve; density porosity (on limestone matrix, DLDP) is the long dashed curve. The right track shows neural-net (predicted) porosity (NPB) as a solid curve, and x = porosity from core analyses (PORO). Note that core porosity has better vertical resolution than neuralnet porosity, which is dependent on the vertical resolution of the input log curves. Total gamma ray (GSGR) is dashed curve on left, next to solid CPGR (potassium-thorium gamma ray).

logging companies (Halliburton's high-resolution induction log and MPI's magnetic pulsed induction log) that were acquired in low fluid loss (minimal invasion) situations. Where the invasion was low, the "thin-bed-corrected" modeled resistivity response was judged adequate for calculating accurate water saturation from logs.

The next iteration in calculating water saturation did not use resistivity measurements directly. The data set from wells drilled with air or foam provided a basis for developing a regression relationship that removed the necessity of using bad resistivity data. The regression between bulk volume water (water saturation × porosity) and potassium-thorium from the spectral gamma ray (Fig. 14) provided a method for estimating

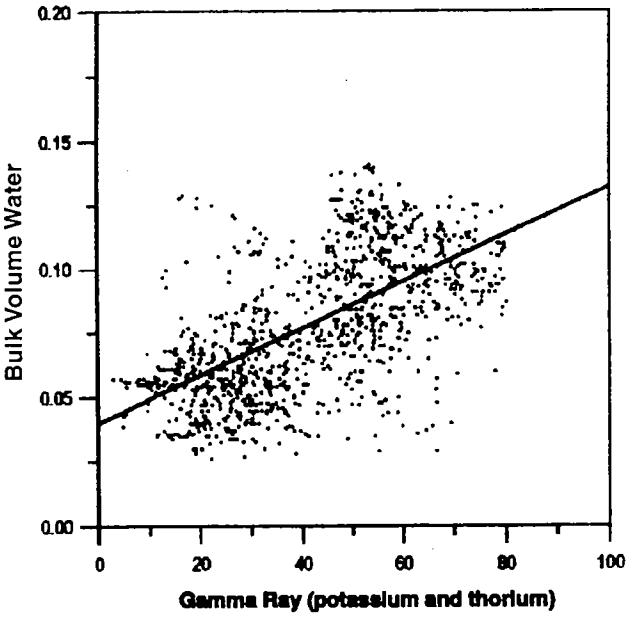

Figure 14. Bulk volume water versus potassium-thorium (K–Th) gamma ray from the Chase interval in three wells drilled and logged with air or foam in the well bore. The linear regression line shows the relationship between K–Th and irreducible bulk volume water, because the Chase formations in these wells are located high enough in the gas column to be at irreducible water saturation. Some of the scatter can be attributed to inadequate vertical resolution of the deep induction data that is one of the variables used in the calculation of bulk volume water. See Figure 17 for validation of this regression relationship.

water saturation without using resistivity data. Despite the fact that the resistivity curves (used in the calculation of bulk volume water for the air/foam data) that form the basis for this regression were not high-resolution data, the regression provided a very workable method for determining water saturation under certain conditions. The main condition that must be met for this method to be applicable is location high in the gas column, such that the reservoir is at irreducible water saturation. The wells with air or foam data all met this criteria; the regression is actually between irreducible bulk volume water and the nonuranium portion of the spectral gamma ray (potassium-thorium).

Although this set of solutions for water saturation calculation worked well in most zones in most wells, the combination of regression-based water saturation calculations and thin-bed–corrected water saturation calculations did not produce ideal results in all formations. Another method, based on capillary pressure data, was developed. This method related water saturation to permeability, height in gas column, and porosity, with different relationships (equations) between those parameters for each main reservoir unit. Clearly, this method can be used only if the input parameters exist. Height in gas column depends on recognizing and locating faults that control fluid distribution. Reliable permeability estimates are also needed (see following sections). When these parameters are available, it is possible to determine water saturation with more confidence than with the use of previous methods. See Figure 15 for comparison of the different types of water saturation calculations in one cored well.

Bulk volume water is a particularly useful parameter in reservoir characterization. Generated by multiplying water saturation times porosity, this number indicates what portion of the rock/fluid volume is water. An important related variable is irreducible bulk volume water, which indicates what portion of that water volume is bound water. The difference between bulk volume water and irreducible bulk volume water is producible water (Fig. 16). Plotting porosity, bulk volume water, and irreducible bulk volume water versus depth provides a graphical representation of fluid distribution in a well. So how do you get irreducible bulk volume water? In Hugoton, the regression, described above, of bulk volume water (actually irreducible bulk volume water in that data set, due to position of subject wells high in the gas column) on potassium-thorium gamma ray provides the answer. Because gamma ray (here with uranium removed) is assumed to reflect grain size (and, indirectly, pore size), the apparent correlation with irreducible bulk volume water must tie to pore sizes and the amounts of bound water different pore sizes would hold. Validation of the use of the gamma-ray regression to obtain irreducible bulk volume water is provided by a comparison between the irreducible bulk volume water so obtained and the irreducible water levels measured by the Numar nuclear magnetic resonance log (Fig. 17). Note also that total producible fluid is indicated by the difference between porosity and irreducible bulk volume water, and correlates well with core permeability (Fig. 16).

Permeability is a key component of flow capacity (permeability × thickness). This parameter is the one of most interest to reservoir engineers, and the hardest to obtain from logs. Our first approach was to attempt to categorize the reservoir into different flow units with rock-type and pore-system criteria and associated porosity/permeability relationships (after Kerans and others, 1994), based on extensive capillary pressure data, thin sections, and various log attributes. The vertical and lateral heterogeneity of the rock/pore system in Hugoton made this cumbersome and not very useful, because the flow units so defined varied meter to meter vertically.

We also tried another approach to permeability determination by running Numar nuclear magnetic resonance logs. Although Numar logs provided good information on irreducible fluid levels, they were not very useful for estimating permeability due to the variability in rock types and pore geometries, and relatively poor vertical resolution (~4 ft from the tool type then available).

An artificial neural network again provided the solution to determining a key parameter from logs. The network was trained from core "truth" permeability data, with input logs consisting of the same curves used for the porosity neural network (bulk density, photoelectric factor, potassium-thorium gamma ray, and uranium gamma ray), plus a neutron porosity. The choice of which log curves to use as inputs depends on

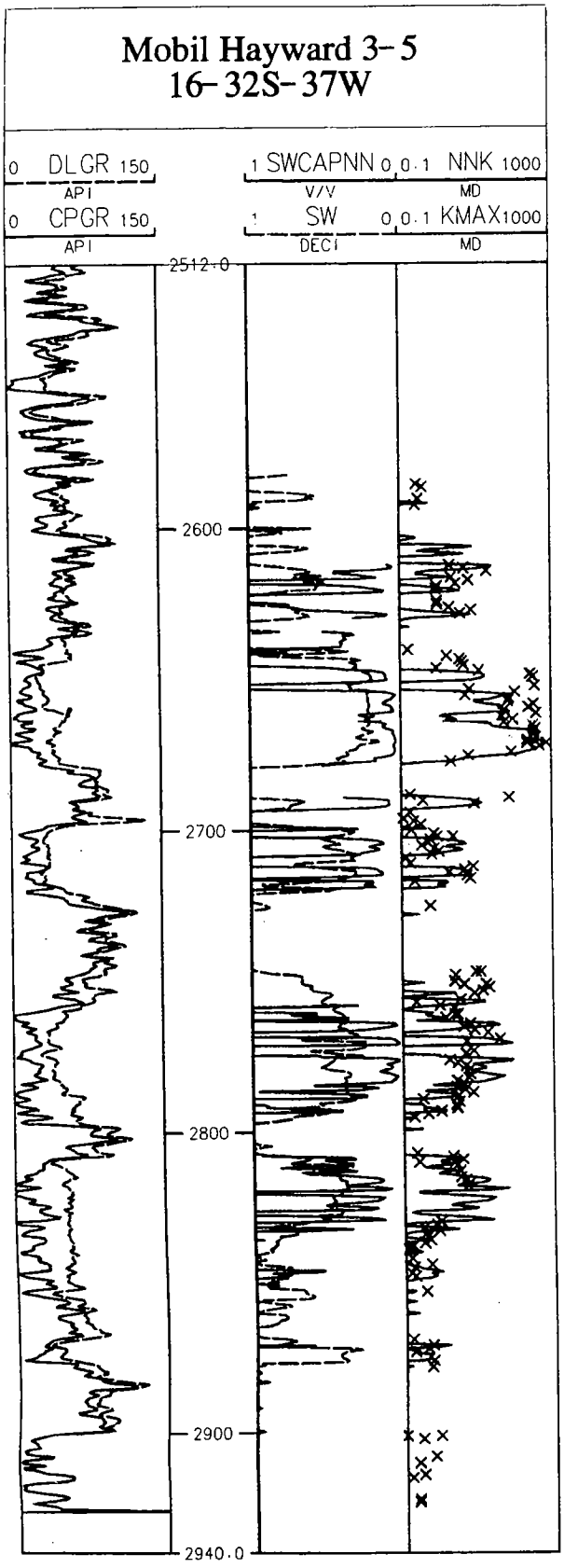

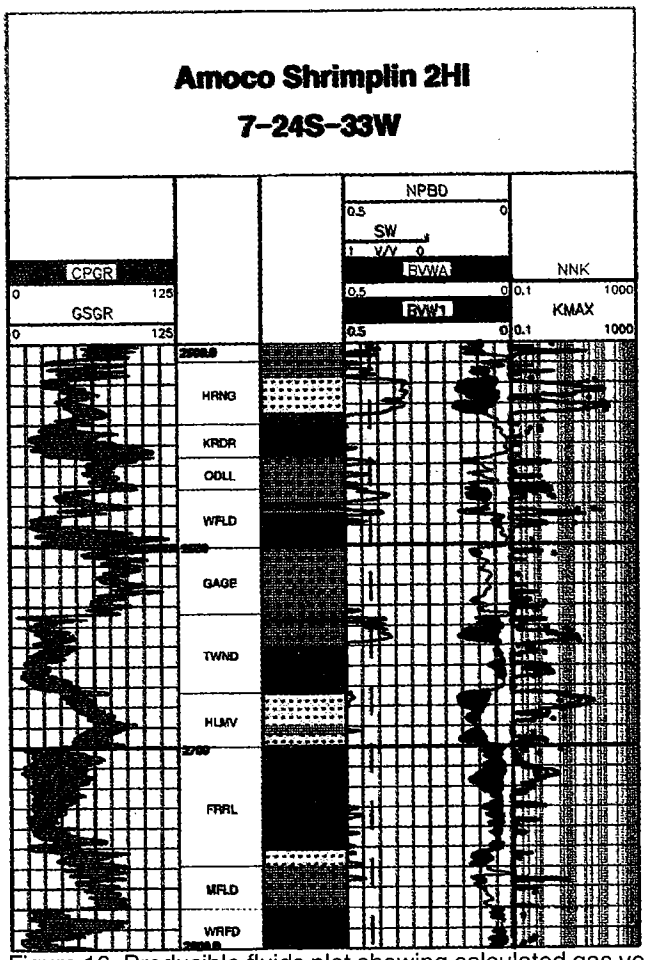

Figure 16. Producible fluids plot showing calculated gas volume and producible water. Irreducible water, indicated by BVWA (bulk volume water apparent), is not shaded area on far right of center track. Log-derived (neural-network) permeability (NNK) is shown by solid line on far right track, with core permeabilities (KMAX) shown by dots. Lithology from core is shown next to the depth track. Lithic symbols: Limestone—brick pattern; dolomite—slanted-brick pattern; anhydritic dolomite—"v" pattern; siltstone—finely dotted pattern; sandstone—coarse-dotted pattern; redbed mudstone/siltstone—finely dotted and dashed pattern. Formation abbreviations: CGSE—Chase; HRNG—Herington; KRDR—Krider; ODLL—Odell; WFLD—Winfield; GAGE—Gage; TWND—Towanda; HLMV—Homesville; FRRL—Fort Riley; MFLD—Matfield; WRFD—Wreford.

Figure 15 *(left)*. Wireline-log plot of a cored well over the entire Chase Group. Permeability curves are shown on far right: solid line is neural-network permeability (NNK); x = air permeability from core analyses (KMAX). The center track shows results from two types of water saturation (SW) calculation: SW is derived from a regression relationship (of bulk volume water on potassium-thorium gamma ray); SWCAPNN is from an equation based on capillary-pressure data that relates permeability, height above free water, and porosity to water saturation.

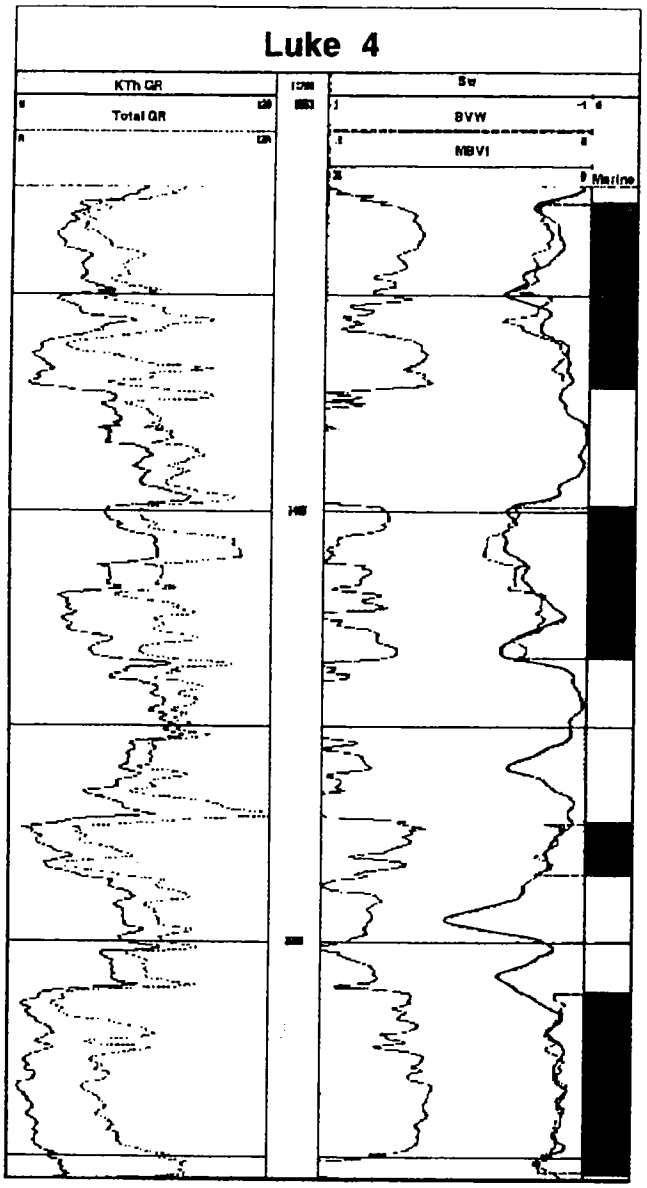

Figure 17. Comparison of irreducible bulk volume water. The dashed curve represents irreducible bulk volume water (BVW) generated by the regression relationship illustrated in Figure 14. The solid curve (MBVI) is the irreducible bulk volume water measured by the Numar nuclear magnetic resonance log. For reservoir intervals, shown by the vertical bars on the right, the two curves correspond very well. Much of the scatter in Figure 14 comes from the intervening nonreservoir, nonmarine units.

which curves appear to be related to the parameter to be estimated (permeability in this example), and on the vertical resolution as compared to the scale of variation of that parameter.

The type of neural-network software used for permeability estimation is different than that used for the porosity method. The software used to estimate permeability is more log oriented in that depth windows or intervals of data are considered in both the training and estimating processes. Another difference lies in the training method. The permeability network was trained selectively with data from specific points in the five cored wells of the training data set; this process required several iterations to optimize. Figures 15 and 16 illustrate the neural-net-predicted and measured (core) permeabilities. The predicted permeabilities match the core permeabilities over a wide range, and are especially good on a zonal flow-capacity basis. Although this is not the first time a neural network has been used to estimate permeability from logs (Osborne, 1992; Rogers and others, 1995; Wiener and others, 1995), this application is unique because of the input curves used and the complexity of the reservoir that the network characterizes due to multiple rock types, thinness of beds, etc. This application also differs from other published examples in the training and optimization methods used, because training was selective rather than statistical, intervals of data were used, and optimization involved changing the training data set rather than changing neural-network variables, such as the number of layers of neurons.

PORE-VOLUME GAS IN PLACE

The goal of determining volumetric gas in place dictated that we solve the problems inherent to characterizing the Hugoton reservoir and calculate porosity, permeability, and water saturation; however, the ability to calculate those parameters at the control points (480 wells with modern logs) did not mean we could generate realistic gas-in-place estimates or that we could capture any of the uncertainty in those estimates. The problems that remained to be solved included vertical averaging, lateral distribution of porosity and water saturation, and compensating for problems that still existed with the porosities determined from logs.

Performing water saturation calculations on 3-D grids rather than averaged 2-D (two-dimensional) grids (after Denver and Phillips, 1992) solved the averaging problem. Instead of generating 2-D porosity and water saturation grids (in ZMAP+™ software), we built 3-D models (in STRATAMODEL™ software) and performed the water saturation calculations there. The hydrocarbon pore volume information was then compressed into 2-D grids and exported (to ZMAP+ or ARCVIEW™ software) for volumetric calculations for specific areas.

Lateral distribution and uncertainty capture were approached using geostatistical distributions of porosity for each formation, in addition to the deterministic interpolation approach. The sequential Gaussian cosimulation (SGCOSIM) method was used, which incorporated both log-derived and core porosities. This use of geostatistics turned out to be a critical factor in generating realistic volumetric gas-in-place estimates; the deterministic method produced estimates of gas in place that were 20% less than has already been produced and thus woefully inadequate. Stochastic methods yielded a probable range of volumetric gas in place for Hugoton field of 34.5–37.8 Tcf. Geostatistics provided several process improvements: (1) geostatistics allowed us to compensate for problems in porosity determination from logs using the core porosity histo-

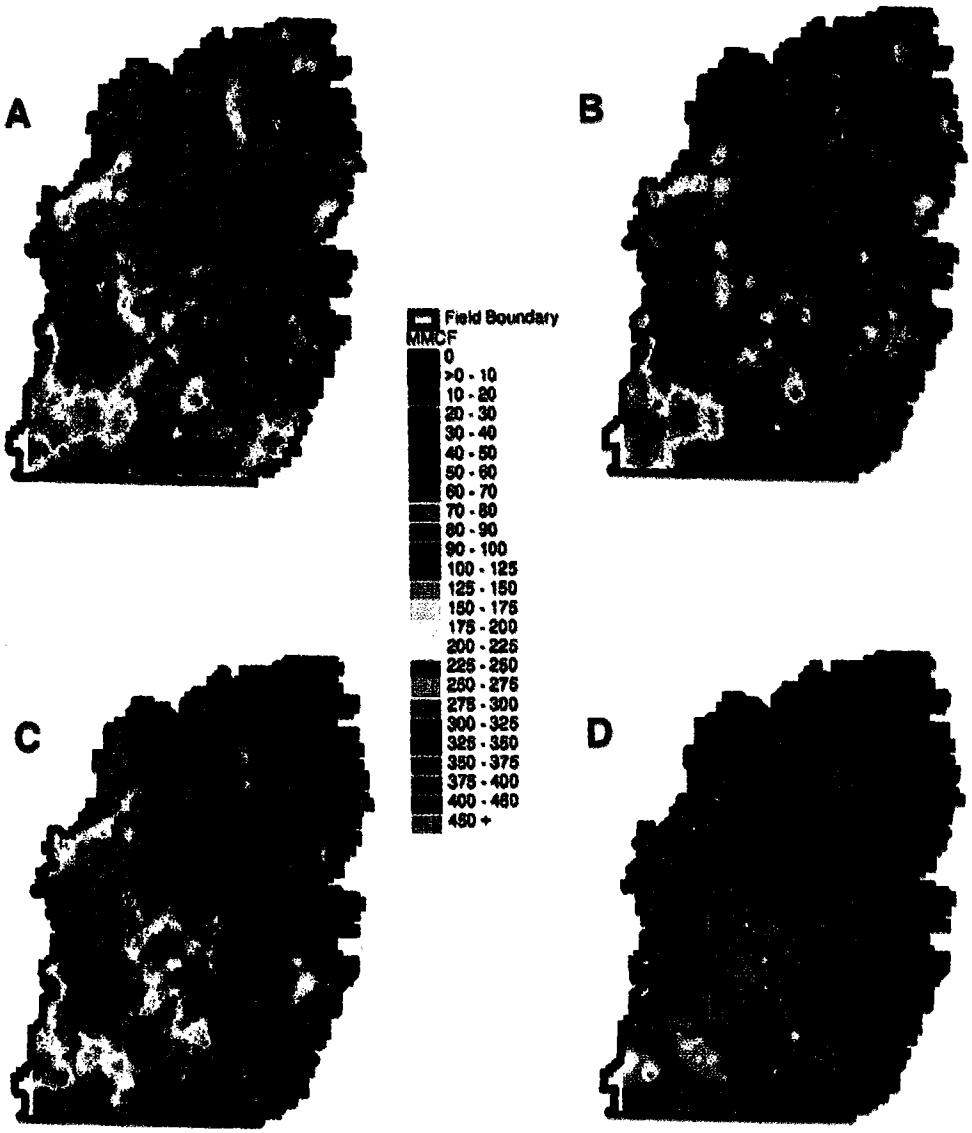

Figure 18. Four realizations of volumetric gas in place for the Winfield Formation. Scale is in millions of cubic feet of gas per grid cell (17.8 grid cells per square mile). The highest values are shown as dark shades of gray; the lowest are depicted as light shades. Maps A–C are based on geostatistical distributions of porosity and associated calculation of gas and water saturations. Map D is based on porosity values interpolated between wells rather than geostatistically distributed. The total amount of gas in the Winfield calculated from the data shown on (D) is significantly lower than the amounts calculated for the three geostatistical versions. Variations in maps A–C also show where there is significant uncertainty in the calculations (where they are different).

Figure 19. A "geobody," or connected grid cells with similar attributes, showing three-dimensional distribution of gas-bearing rock (water saturation <70%) with permeability over 0.5 md in the Towanda Formation. The cells are colored according to bulk volume gas levels (bulk volume gas = gas saturation times porosity, or the proportion of the rock/fluid system that consists of gas). Dark shades are high amounts of bulk volume gas (darkest = 17%) and light-gray shades are lower amounts of bulk volume gas. This figure graphically illustrates the connectivity of reservoir rocks in this formation.

grams (even the neural network tended to underestimate porosity at the high end, above 16% porosity); (2) geostatistics gave more realistic distributions of porosity in this highly heterogeneous reservoir; and (3) geostatistics allowed us to capture the uncertainty in the results by producing a suite of "equally probable" realizations of volumetric gas in place for each formation (Fig. 18). This process gave both a range of values and visual tools for seeing where the uncertainty was greatest (where the realizations were most different). The cosimulation approach provided more accurate estimates of volumetric gas in place than the deterministic approach because of the more realistic porosity distributions and the ability to compensate for problems with log-derived porosity values when using SGCOSIM.

In addition to showing the probable range of original gas in place and its distribution, the volumetric gas-in-place results provide another way of looking at well performance. Comparing volumetric gas-in-place results with performance-based gas-in-place results shows the difference between what wells in a given area are expected to produce and how much gas there was originally. Many potential reasons for such differences exist, some of which point to opportunities to increase production. Some differences can be attributed to compartmentalization of the reservoir; others to wells in need of repair.

TOOLS FOR RESERVOIR MANAGEMENT

The formation-evaluation results of the reservoir characterization study are useful for addressing operational issues, as well as calculating gas in place.

The plot of porosity, bulk volume water, and irreducible bulk volume water vs. depth (Fig. 16) is an excellent tool for planning completions or workovers in the plotted well or a well nearby, because it allows the operations engineer to predict which zones will produce gas, which zones will produce both gas and water, and which zones are wet and should be avoided. Maps of flow capacity, porosity and thickness, gas in place, and faults controlling fluid distribution are all useful in evaluating undrilled infill locations, evaluating workover candidates, planning drilling and completion of infill wells, and choosing test wells for new water disposal methods. A new way of combining some of the same information is shown in Figure 19. This "geobody" represents all the connected grid cells with low water saturation that meet a permeability cutoff. As such, it illustrates the connectivity of gas-bearing reservoir rock.

ECONOMIC IMPACT OF HUGOTON RESERVOIR CHARACTERIZATION

The economic impact of reservoir studies commonly is difficult to quantify. Effects on the "bottom line" provided by the Hugoton reservoir characterization project include incremental production and cost savings associated with optimization of drilling and completion of infill wells, and with repairs and recompletion of existing wells. The decreased costs and increased revenue that better understanding of the reservoir and better evaluation tools provide will continue to be reflected in the total cost of the project as long as these tools are used in management of the reservoir.

Some of the immediate monetary benefits that can be demonstrated at least in part as outcomes of this study include incremental production from infill wells and recompletions, reduced cost of infill wells, and improved property evaluations. Average production from new infill wells increased to approximately 350 kcf (thousand cubic feet) of gas per day in 1996 over 260 kcf of gas per day in 1995 infill wells. Thirty-one percent of the 1996 infill wells had initial rates over 500 kcf of gas per day, compared with 12% of 1995 infill wells. Operations engineers attribute the higher 1996 rates to more effective completions, which resulted from the use of bulk volume water log plots and fault maps to indicate probable sources of gas and water in the vicinity of each new well in the 1996 infill drilling program.

Recompletion of existing wells in 1995 and 1996 benefited from the results of the reservoir characterization study. Operations engineers successfully recompleted 26 wells through the use of the geoscience tools described above for identifying gas- and water-bearing intervals. The incremental production from these efforts totaled approximately 3.3 Mcf (million cubic feet) of gas per day.

Prior to the availability of tools from the reservoir characterization project, workovers had both a lower success rate and lower levels of incremental production.

The cost of drilling and completing infill wells was reduced by the results of the reservoir characterization study. The evaluation tools described provide a much better understanding of fluids distribution in the reservoir. This understanding has been applied to the planning of infill well drilling and completion to reduce costs. In 27% of the 1996 infill wells, the well was not drilled through formations now known to be wet, for an average saving of rig time and casing costs close to $3,000 per well. This same understanding of the location of water in the reservoir allowed for optimum fracture stimulation design; these smaller hydraulic fracture treatments also resulted in significant cost savings. Total well cost in 1996 were reduced by an average of $5,000 per well compared to 1995, mostly due to the optimized and smaller fracture stimulations.

Reservoir characterization results and tools also allow for more accurate property evaluations. Leases under consideration for acquisition, divestment, or trade were evaluated with the new methods, which provided a better estimation of value than was previously available using only production data.

CONCLUSIONS

New technologies can contribute significantly to our understanding of mature fields. In this study, artificial neural networks, new logging tools, resistivity modeling, and modern analysis techniques (including geostatistics and three-dimensional grid operations)

were used effectively to improve formation evaluation results and volumetric gas-in-place estimates. Determination of bulk volume water, producible water, and permeability from logs in this complex field were major technical breakthroughs. Such parameters are extremely useful in reservoir characterization studies geared toward improving reservoir management capabilities.

ACKNO'VLEDGMENTS

We thank the Hugoton JOMT of Amoco Production Company for permission to publish this study. We are grateful to Mobil Exploration and Production, U.S., especially W. H. Jamieson, Jr., for permission to use and publish additional core and log data. We also thank David Reese from Amoco (Denver) for his work on equations relating water saturation to permeability, porosity, and height in the gas column. 3-D seismic interpretation by Mike Bahorich (formerly with Amoco, currently with Apache) is appreciated. Thanks go to Amoco operations and reservoir engineers too numerous to mention for teamwork and testing of ideas herein. Ann Pettit and Stefan Nowina provided invaluable technical support. This paper benefited from constructive reviews by Robert Raynolds, Joyce Budai, N. C. Wardlaw, Salman Block, and Virginia Riggert.

REFERENCES CITED

Beene, D. L., 1996, 1994 total oil and gas production in Kansas: Kansas Geological Survey Home Page, http://www.kgs.ukans.edu/prs/petro/interactive.html, 1 p.

Caldwell, C. D., 1991, Cyclic deposition of the Lower Permian, Wolfcampian Chase Group, western Guymon–Hugoton field, Texas County, Oklahoma, *in* Watney, W. L.; Walton, A. W.; Caldwell, C. D.; and Dubois, M. K. (eds.), Midcontinent core workshop—integrated studies of petroleum reservoirs in the midcontinent: Kansas Geological Survey, Lawrence, p. 57–80.

Denver, L. E.; and Phillips, D. C., 1992, The impact of vertical averaging on hydrocarbon volumetric calculations—a case study, *in* Hamilton, D. E.; and Jones, T. A. (eds.), Computer modeling of geologic surfaces and volumes: American Association of Petroleum Geologists Computer Applications in Geology, no. 1, p. 219–234.

Doveton, J. H., 1991, Lithofacies and geochemical facies profiles from nuclear wire-line logs: new subsurface templates for sedimentary modeling, *in* Franseen, E. K.; Watney, W. L.; Kendall, C. G.; and Ross, W. (eds.), Sedimentary modeling: computer simulations and methods for improved parameter definition: Kansas Geological Survey Bulletin 233, p. 101–110.

_____ 1994, Geologic log analysis using computer methods: American Association of Petroleum Geologists Computer Applications in Geology, no. 2, 169 p.

Energy Information Administration, 1995, U.S. crude oil, natural gas, and natural gas liquids reserves 1994 annual report: U.S. Department of Energy, Office of Oil and Gas, 153 p.

Garlough, J. L.; and Taylor, G. L., 1941, Hugoton gas field—Grant, Haskell, Morton, Stevens, and Seward Counties, Kansas, and Texas County, Oklahoma, *in* Levorson, A. I. (ed.), Stratigraphic type oil fields: American Association of Petroleum Geologists, Tulsa, Oklahoma, p. 78–104.

Gwiner, D. M.; Laude, L. S.; Olmos, J. L.; Quirein, J. A.; and Reimer, L. J., 1992, Improved porosity/lithology estimates can locate productive zones: World Oil, v. 213, no. 5, p. 57–63.

Hubbert, M. K., 1967, Application of hydrodynamics to oil exploration: Proceedings of the Seventh World Petroleum Congress, Mexico City, Mexico, v. 18, p. 59–67.

Kansas Corporation Commission, 1986, Transcripts of Hugoton field infill hearings, Docket C-164.

_____ 1997, Hugoton gas report—May schedule of monthly allowables: Kansas Corporation Commission, Wichita, p. 105.

Kerans, C.; Lucia, F. J.; and Senger, R. K.; 1994, Integrated characterization of carbonate ramp reservoirs using Permian San Andres Formation outcrop analogs: American Association of Petroleum Geologists Bulletin, v. 78, p. 181–216.

Mason, J. W., 1968, Hugoton–Panhandle field, Kansas, Oklahoma, and Texas, *in* Beebe, B. W. (ed.), Natural gases of North America: American Association of Petroleum Geologists Memoir 9, v. 2, p. 1539–1547.

Mazzullo, S. J.; and Teal, C. S., 1994, A new look at old rocks: stratigraphy, sedimentology, and structure of the Chase Group (Permian, Wolfcampian), south-central Kansas, *in* Sanders, T.; Van Buskirk, C. C.; and Schnake, D. (compilers), Kansas Geological Society 1994 Field Trip Guidebook: Kansas Geological Society, p. 1–60.

Mazzullo, S. J.; Teal, C. S.; and Burnett, C. A., 1996, Facies and stratigraphic analysis of cyclothemic strata in the Chase Group (Permian, Wolfcampian), south-central Kansas, *in* Hyne, N. J. (ed.), Sequence stratigraphy of the Midcontinent: Tulsa Geological Society Special Publication 4, p. 217–248.

Miller, K. B.; McCahon, T. J.; and West, R. R.,1996, Lower Permian (Wolfcampian) paleosol-bearing cycles of the U.S. Midcontinent: evidence of climatic cyclicity: Journal of Sedimentary Research, v. 66, no. 1, p. 71–84.

Olson, T. M.; Babcock, J. A.; and Wagner, P. D., 1996, Geologic controls on reservoir complexity, Hugoton giant gas field, Kansas, *in* Swindler, D. L.; and Williams, C. P. (compilers), Transactions of 1995 American Association of Petroleum Geologists MidContinent Section Meeting: American Association of Petroleum Geologists Mid-Continent Section, p. 189–198.

Osborne, D. A., 1992, Permeability estimation using a neural network: a case study from the Roberts unit, Wasson field, Yoakum County, Texas: American Association of Petroleum Geologists Southwest Section Transactions, v. 92-90, p. 125–132.

Parham, K. D.; and Campbell, J. A., 1993, Wolfcampian shallow shelf carbonate—Hugoton embayment, Kansas and Oklahoma, *in* Bebout, D. G.; White, W. A.; and Hentz, T. F. (eds.), Atlas of major Midcontinent gas reservoirs: Bureau of Economic Geology, University of Texas at Austin, p. 9–12.

Prasad, K. V. K.; Olson, T. M.; and Boughton, S. D., 1996, Incorporating geologic and data uncertainties into Hugoton field pore volume estimates [abstract]: American Association of Petroleum Geologists 1996 Annual Convention Official Program, v. 5, p. A-114.

Rogers, S. J.; Chen, H. C.; Kopaska-Merkel, D. C.; and

Fang, J. H., 1995, Predicting permeability from porosity using artificial neural networks: American Association of Petroleum Geologists Bulletin, v. 79, p. 1786–1797.

Siemers, W. T.; and Ahr, W. M., 1990, Reservoir facies, pore characteristics, and flow units—Lower Permian Chase Group, Guymon–Hugoton field, Oklahoma: Society of Petroleum Engineers Paper 20757, p. 417–428.

Stever, R. C., 1987, Depositional and diagenetic framework of the Lower Permian Chase Group, southern Hugoton embayment: University of Oklahoma unpublished M.S. thesis, 198 p.

Toomey, D. F.; and Mitchell, R., 1986, Facies relationships and paleodepositional settings of the Herington-to-Winfield stratigraphic interval (Lower Permian), southern Kansas–northern Oklahoma: Field Guidebook, 4th Annual Meeting, Society of Economic Paleontologists and Mineralogists Midcontinent Section, Ponca City, Oklahoma, p. 1–158.

Wiener, J.; Rogers, J.; and Moll, B., 1995, Predict permeability from wireline logs using neural networks: Petroleum Engineer International, v. 68, no. 5, p. 18–24.

Low-Resistivity–Low-Contrast Permian Red Cave Sandstone Reservoirs, Spelunker Field, Baca County, Colorado

William T. Goff and Emily M. Hundley-Goff
Cholla Production, LLC
Denver, Colorado

ABSTRACT.— Recently, the Lower Permian Red Cave sandstone in Baca County in southeastern Colorado has become a primary drilling objective for low BTU gas and helium resources at drilling depths less than 2,000 ft. The discovery in December 1995 of the Spelunker field, located in T. 33 S., R. 43–44 W., kicked off an exploration play for the shallow gas sand in Colorado. The Red Cave sandstone is part of the Clear Fork Group, middle Leonardian Series of the Permian. The productive sandstone occurs directly below the base of the Stone Corral (Cimarron) anhydrite with the interval ranging in gross thickness from 30 to 45 ft.

The gas-productive Red Cave reservoir at Spelunker field is a red, very fine grained, dolomite-cemented sandstone with up to 7.0% mixed-layer illite-smectite clays. Density-log porosity values for the reservoir range up to 30.0%. Induction-resistivity values for a gas-bearing sandstone range from 1.5 to 6.0 ohms, whereas resistivity for surrounding shales and silts are 3.0–4.0 ohms, presenting a classic low-resistivity–low-contrast problem. The abundant well control from the deeper drilling in the region offers the ability to explore for a bypassed gas resource if the nuances of the zone's petrophysics are understood.

About half of the Spelunker field wells are completed naturally with initial potentials of up to 600 thousand cubic feet of gas per day (mcfg/d). The remaining wells are completed with (<15,000 lbs of sand) fracture treatments to overcome formation damage. Ultimate gas recovery projections for Spelunker wells range up to 1.2 billion cubic feet (BCF) of gas per 320-acre unit.

INTRODUCTION

The Lower Permian Red Cave sandstone has been known to be productive in the tri-state area of Colorado, Oklahoma, and Kansas since the discovery in 1965 of low-BTU gas at the Interstate field, Morton County, Kansas. The Red Cave reserves were developed at Interstate field for operations as well as to blend with the richer gas produced from the neighboring fields completed in the Pennsylvanian Topeka and Morrow Formations. Although the Red Cave completions at less than 1,400 ft came in at good producing rates, full-scale exploration for the zone never materialized due to the heating values less than 700 BTU and the high-nitrogen values of the gas coupled with difficult formation evaluation. Cities Service discovered oil in the Red Cave at Castenada NW field, Cimarron County, Oklahoma, in 1984 at drill depths of less than 2,000 ft. Cumulative production for the field will approach 2.0 million barrels of oil (MMBO), primarily from the Red Cave sandstone. Once again, an exploration play failed to develop because of low product values (oil prices). Recently, Energy Alliance Company, Denver, Colorado, began developing low-BTU–, high-helium–content Red Cave gas reserves in Baca County, Colorado. The company's development program at Spelunker field precipitated the building of the necessary pipeline and processing infrastructure for low-BTU gas and to perhaps finally provide the economic incentive for an exploration play targeting this truly bypassed pay zone.

GEOLOGIC OVERVIEW

Stratigraphy and Structure

The Red Cave sandstone of Baca County, Colorado, is part of the Clear Fork Group, Middle Leonardian Series of the Permian. It should be noted that the term Red Cave, as used in this paper, is equivalent to the Tubb Formation of the Panhandle field of Texas and the Bravo Dome CO_2-producing area of New Mexico rather than the stratigraphically older producing interval of the same name in the Panhandle field. The productive sandstone is capped by a rooted caliche-bearing zone of dolomite- and gypsum-cemented siltstone that

Goff, W. T.; and Hundley-Goff, E. M., 2001, Low-resistivity–low-contrast Permian Red Cave sandstone reservoirs, Spelunker field, Baca County, Colorado, *in* Johnson, K. S. (ed.), Pennsylvanian and Permian geology and petroleum in the southern Midcontinent, 1998 symposium: Oklahoma Geological Survey Circular 104, p. 161–166.

is unconformably(?) overlain by the Stone Corral (Cimarron) anhydrite.

The Middle and Late Permian in the western Midcontinent region of the United States was characterized by extremely arid conditions. A wadi-plain system extended from Colorado and Kansas south to Oklahoma, New Mexico, and Texas (Handford, 1980). These wadi-plain deposits consist of extensive redbed sequences and evaporites deposited in alluvial-fan systems that interfinger with sabkha or marginal-marine evaporite deposits. In general, the sandstones in these wadi plains are the products of ephemeral, braided streams that rapidly deposited their sediment loads during intermittent periods of high flow. Commonly, the individual episodes of flooding are marked by ripple-drift cross laminations capped by laminae of silt and mud with indications of desiccation (Glennie, 1972; Handford, 1980). The Red Cave sandstone at Spelunker field is a 30–45-ft thick interval of stacked sands that display all of the aforementioned attributes. The sands have ripple-drift cross-laminations, are commonly overlain by silt and mud laminae, and are cemented with dolomite and gypsum, indicating periods of desiccation. Occasional root marks and shallow burrows are present in the top of the Red Cave sandstone.

The geologic structure on the base of the Red Cave sandstone for the Spelunker Field is shown in Figure 1. The structure is a very simple, closed feature at the shallow depths of the Red Cave. As of June 2000, the Spelunker field covered roughly a 14-mi^2 area with its northwestern and southwestern limits as yet undetermined. Wet sands at a datum of +2,340 ft define the eastern limits.

Lithology

The productive reservoir of the Red Cave sandstone in Spelunker field is a red, very fine to fine-grained, dolomite-cemented, feldspathic sandstone deposited primarily as braided-stream deposits in a wadi plain. Core descriptions include ripple-drift cross-laminations with root marks and possible burrows indicative of rapid deposition followed by periods of exposure. Occasional rip-up clasts are also present at the base of individual sand laminae.

X-ray powder-diffraction analysis performed by BJ Services reveal the chief cements are dolomite and gypsum (Moore, 1996). Figure 2 is a high-magnification scanning-electron–microscope (SEM) photomicrograph of the non-reservoir sandstone located just below the rooted, caliche zone at the top of the Red Cave. The sandstone has 13.0% dolomite and 7.0% gypsum, resulting in 8.9% porosity and 0.034 millidarcies (md) permeability. The photomicrograph in Figure 2 is an enlargement of gypsum cement in this sample. Figure 3 is a high-magnification SEM photomicrograph of a core plug from the good reservoir rock. Note that the dominant pore type in the reservoir is intergranular porosity. Secondary porosity in the form of a leached potassium-feldspar grain is also illustrated in Figure 3. This view also demonstrates the presence of dolomite cement (8.0%) in this reservoir sample but the pore-plugging gypsum is absent.

X-ray powder-diffraction analysis indicates 6.0–7.0% of the productive reservoir samples consists of clay minerals composed of mixed-layer chlorite-smectite and illite-smectite. The mixed-layer clays with a slightly expandable structure and sensitivity to acids may be the most important minerals in the evaluation and treatment of the Red Cave sandstone. SEM analysis shows these clays to be primarily present as grain coatings. It is these grain-coating clays that tend to bind immovable water in the pores and contribute to the low formation resistivity.

ELECTRIC-LOG PROPERTIES

Electric-log properties for the Red Cave sandstone vary considerably with the amount of time the zone is exposed to the fluid within the wellbore. With virgin bottom-hole pressures of only 345 psi, resistivity profiles and gas effects on porosity logs in the Red Cave are commonly dramatically different in deeper wells than in shallower wells due to the effects of invasion. The type of fluid used to drill the Red Cave can have very dramatic effects on the resistivity readings. If the Red Cave is drilled with native fluids with no regard to water loss or building of mud cake, then the zone very likely will be totally flushed and give high deep-resistivity readings. If this deep invasion has occurred, then a quick look at the Permian section of rocks will show no resistivity or conductivity contrast on the log. If the driller has drilled the zone with good mud properties, however, then a strong resistivity or conductivity contrast between the Red Cave sandstone and the rest of the Permian section will be apparent on the log if the Red Cave sandstone contains hydrocarbons. Proper mud properties for drilling the Red Cave are: water loss <8 ml/L, weight of 8–9 ppg, pH of 6.9–7.4, and chlorides (cl) <5,000 ppm. The resistivity contrast occurs because the formation waters of the Permian, including the Red Cave, have extremely high salinity (up to 125,000 ppm cl). The high-salinity waters have a water resistivity (Rw) of 0.04 ohms at typical Red Cave depths of less than 2,000 ft and formation temperatures of about 95°F. Therefore, a sandstone filled only with this high-salinity brine will produce very low values of deep resistivity. Potentially hydrocarbon-productive resistivity values range from 1.5 to 6.0 ohms in the excellent reservoir sands. Unfortunately, the resistivity in the surrounding silts and shales is 3.0–4.0 ohms, thus presenting a classic low-resistivity–low-contrast problem (Fig. 4). Productive porosity ranges from 20.0% to 29.0% on the density log. As shown in Figure 4, the density-neutron log shows excellent gas effect when good drilling mud is used.

The combination of high porosity, grain-coating clays causing high irreducible-water saturations, and low Rw values due to high-salinity formation waters creates this low-resistivity play. Abundant well control exists to evaluate the play if an understanding of the invasion problems can be attained.

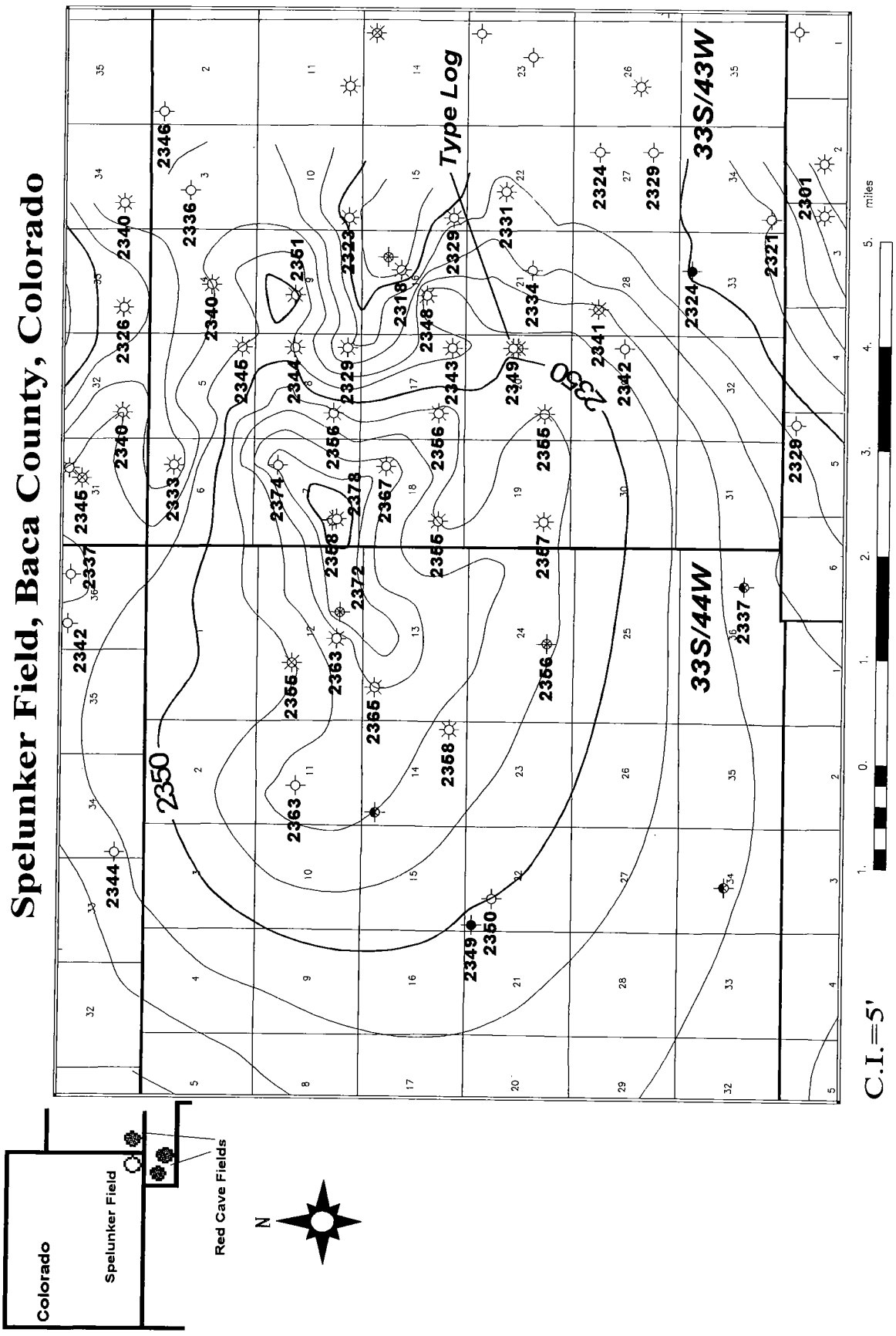

Figure 1. Base of Red Cave sandstone structure, Spelunker field, Baca County, Colorado. Contours in feet above mean sea level. General location of Spelunker field and nearby Red Cave sandstone fields in southwestern Kansas and the Oklahoma Panhandle are shown on small map in upper left corner.

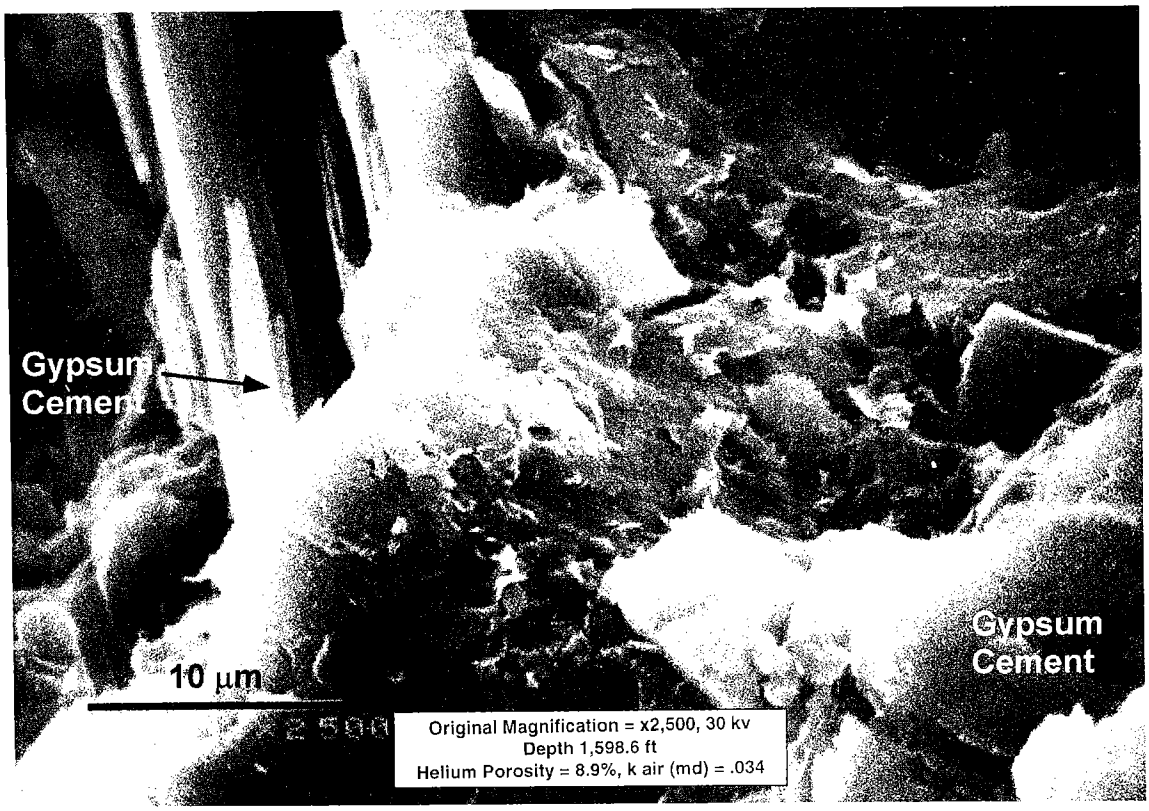

Figure 2. SEM photograph of tight, non-reservoir sandstone from the McKinley well. Photograph is of a very fine grained gypsum- and dolomite-cemented, feldspathic, quartzose sandstone. See Figure 1 for location of reference well.

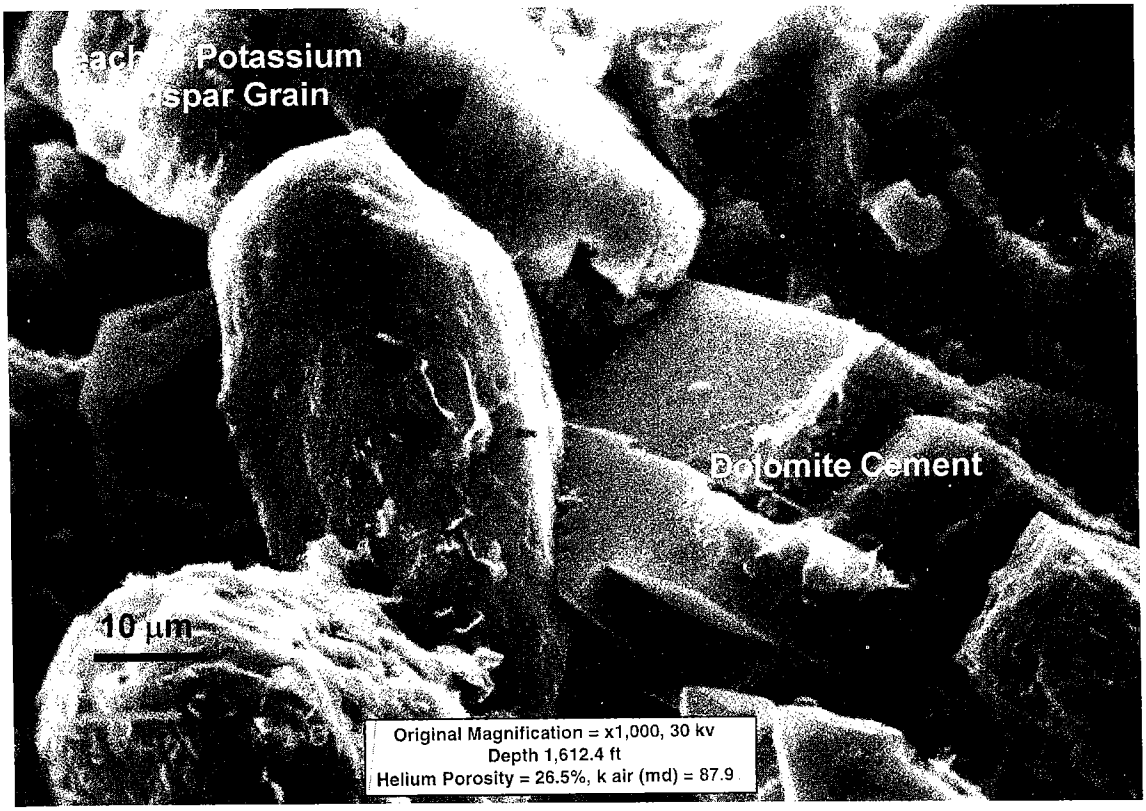

Figure 3. SEM photograph of reservoir-quality sandstone from the McKinley well. Photograph is of a very fine to fine-grained, dolomite-cemented, feldspathic, quartzose sandstone. See Figure 1 for location of reference well.

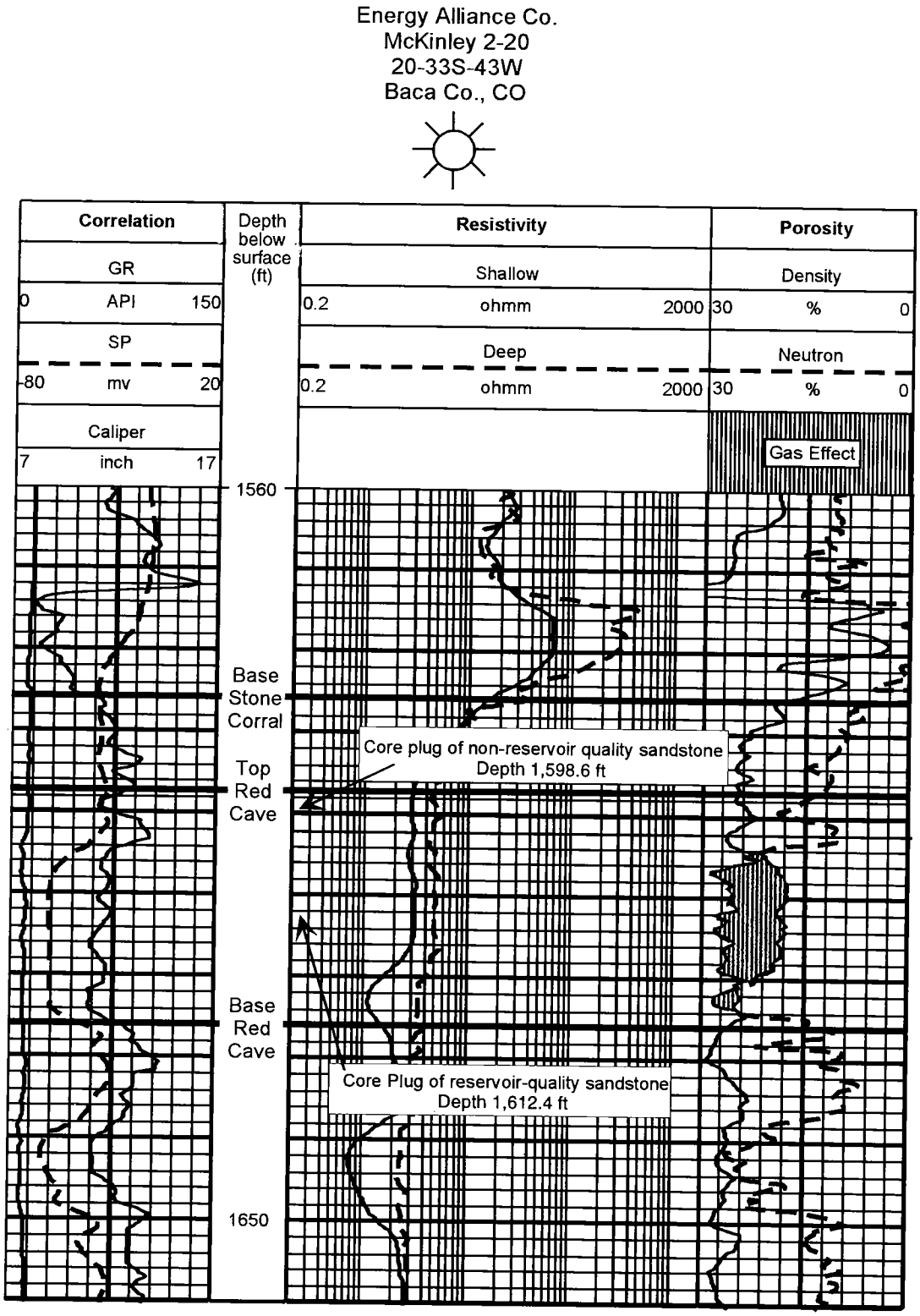

Figure 4. Type log of Red Cave sandstone from the Energy Alliance McKinley 2-20 well in sec. 20, T. 33 S., R. 43. W., Baca County, Colorado. See Figure 1 for location of reference well.

PRODUCTION

Spelunker wells located in the heart of the sand fairway have natural initial potentials of 300–600 mcfg/d. Wells located on the fringes of the sand deposit must be fracture treated to eliminate the effects of mud damage. The fractured wells will have initial potentials between 300 and 900 mcfg/d following stimulation. Unfortunately, the fracture treated wells also produce various levels of water, because, at the shallow depths

of the Red Cave, it is nearly impossible to keep the fracture in the zone. The potential gross reserves range up to 1.2 BCF of gas per 320 acres.

A typical gas analysis for the Spelunker field reveals a 440 BTU gas with 59.0% nitrogen and 1.6% helium. Fortunately, gas-processing technology has been developed to reject the nitrogen and capture the helium, thus making this low-quality resource economic.

CONCLUSIONS

The Red Cave sandstone of Baca County, Colorado, is a very fine grained hydrocarbon reservoir with a complex mineralogy that makes electric-log evaluation very difficult. Coupled with the fact that the sandstone is very susceptible to formation damage created by drilling and/or completion operations, a strong potential exists for a bypassed hydrocarbon reservoir.

The zone at Spelunker field has proven to be quite economic and justifies further exploration in the region. Any exploration for the Red Cave must acknowledge the following four factors. (1) If possible, become aware of the drilling-mud properties when the zone was drilled, not when the well was logged. This is essential in evaluating old logs. (2) Review the resistivity for the entire Permian section to look for resistivity contrasts between the Red Cave and the other deeper sands to determine the potential for bypassed hydrocarbons. (3) While drilling new wells, it is imperative to monitor the drilling-mud properties. Treat the Red Cave like the primary objective that it is. (4) Core the zone to determine the mineralogy before any completion operations can be performed.

The Red Cave has become a very viable exploration objective in the western Midcontinent region of the United States. The continued growth in demand for natural gas should bode well for this shallow, bypassed hydrocarbon zone.

ACKNOWLEDGMENTS

The authors thank Energy Alliance Company, Inc., for permission to publish the SEM photomicrographs and the results of the X-ray–diffraction study by BJ Services. In particular, we wish to acknowledge and thank Richard Wightman for all his efforts in making Spelunker field a reality.

REFERENCES CITED

Glennie, K. W., 1972, Permian Rotliegendes of northwest Europe interpreted in light of modern desert sedimentation studies: American Association of Petroleum Geologists Bulletin, v. 56, p. 1048–1071.

Handford, C. R.; and Fredricks, P. E., 1980, Facies patterns and depositional history of a Permian sabkha complex: Red Cave Formation, Texas Panhandle: Bureau of Economic Geology, University of Texas at Austin, Geological Circular 80-9, 38 p.

Moore, S., 1996, Energy Alliance McKinley #2-20 well: BJ Services Company, U.S.A., Research and Technology Center Report No. 96-03-0287, 8 p.

Clear Fork Group (Leonardian, Lower Permian) of North-Central Texas

W. John Nelson
Illinois State Geological Survey
Champaign, Illinois

Robert W. Hook
The University of Texas at Austin
Austin, Texas

Neil Tabor
The University of California at Davis
Davis, California

INTRODUCTION

The Clear Fork Group (Leonardian, Lower Permian) of North-Central Texas (Baylor, Foard, Knox, and Wilbarger Counties; Fig. 1) has long been known for its diverse record of early terrestrial vertebrates (e.g., Romer, 1928). Equally significant plant assemblages have been collected recently from these same rocks by field parties supported by the U.S. National Museum (Chaney and others, 1993). On the basis of over 500 outcrop observations and 197 subsurface records from an area of approximately 5,500 km^2, we outline stratigraphic and sedimentologic findings that provide a broader understanding of Clear Fork paleoenvironmental and paleoclimatic conditions.

STRATIGRAPHIC RELATIONSHIPS

The Clear Fork Group in our study area of North-Central Texas consists predominantly of continental redbeds that were deposited in alluvial-valley to coastal-plain settings on the eastern shelf of the Midland basin (Fig. 1). These rocks intertongue southward along the outcrop and westward into the subsurface with marine carbonates, mudstones, and evaporites. In North-Central Texas, the Clear Fork is approximately 380 m thick. It overlies interbedded red to gray mudstones and thin carbonates of the Albany Group and laterally equivalent red mudstones and sandstones of the Wichita Group (Fig. 2), and underlies the San Angelo Formation, a siliciclastic wedge that pinches out abruptly downdip to the west (Smith, 1974).

Beede and Waite (1918) divided the Clear Fork of Runnels County (200 km south of our study area) into the Arroyo (oldest), Vale, and Choza Formations. Vertebrate workers such as Romer (1928) and Olson (1958) extended use of this nomenclature into North-Central Texas. The Arroyo, Vale, and Choza Formations, however, are not mappable in our study area, because of facies changes and northward pinch-out of the carbonate beds that serve as formation boundaries in the type area. We informally divide the Clear Fork of North-Central Texas into lower, middle, and upper units and recognize several informal beds and members (Fig. 2).

Regional dip of the Clear Fork in the study area is 0.2°–0.3° toward the west–northwest. Subsurface mapping shows slight anticlinal folding of the Clear Fork across the Matador Uplift, an east-trending basement uplift active chiefly during the Pennsylvanian.

LITHOFACIES AND PALEOENVIRONMENTS

Lower Clear Fork

The lower Clear Fork in North-Central Texas (approximately equivalent to "Arroyo" of Romer and Olson) is 55–70 m of red claystone, siltstone, and sandstone with common carbonate nodules and no gypsum. Plant and vertebrate fossils are abundant at several stratigraphic levels.

The Craddock dolomite bed (informal; Fig. 2) is a zone of thin (<0.5 m) intertidal to supratidal dolomite layers and nodules about 12 m above the base of the Clear Fork. The Craddock persists at least 32 km along strike, and likely correlates with either the Lytle or Rainey Limestone Member to the south.

The Red Tank sandstone member (informal), 24–30 m above the base of the Clear Fork (Fig. 2), consists of one to three, upward-fining, multistory, suspended-load, high-sinuosity, meandering-channel deposits. Associated channel fills in the Red Tank have yielded the majority of lower Clear Fork vertebrate and plant remains.

The Brushy Creek sandstone member (informal) at the top of the lower Clear Fork is a ledge-forming unit 3–15 m thick. Its sheet-like and broad, shallow channel-form sandstone bodies probably represent braided-stream deposits. Large-scale crossbeds, upper-flow-regime planar beds, and conglomerates are indicative of high-energy–flow conditions. Northward coarsening

Nelson, W. J.; Hook, R. W.; and Tabor, Neil, 2001, Clear Fork Group (Leonardian, Lower Permian) of North-Central Texas, *in* Johnson, K. S. (ed.), Pennsylvanian and Permian geology and petroleum in the southern Midcontinent, 1998 symposium: Oklahoma Geological Survey Circular 104, p. 167–169.

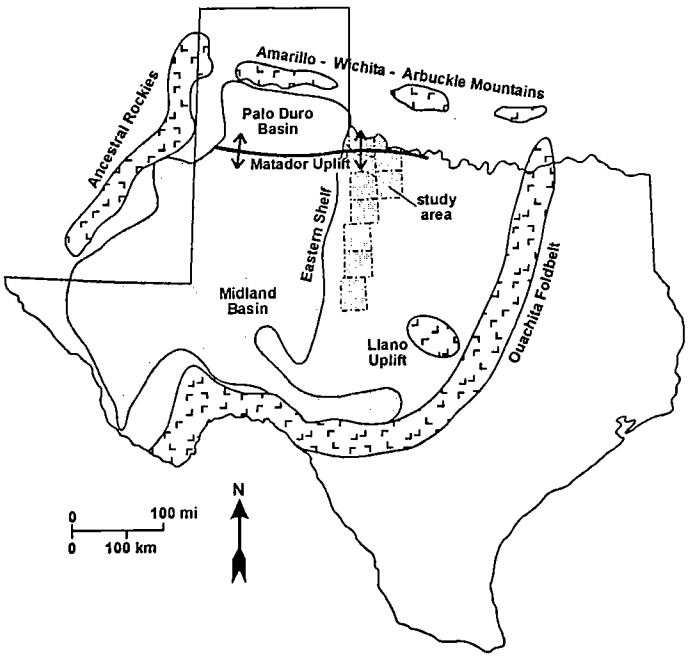

Figure 1. Study area location in North-Central Texas and major late Paleozoic paleogeographic and structural features in Texas and adjoining areas of Oklahoma and New Mexico.

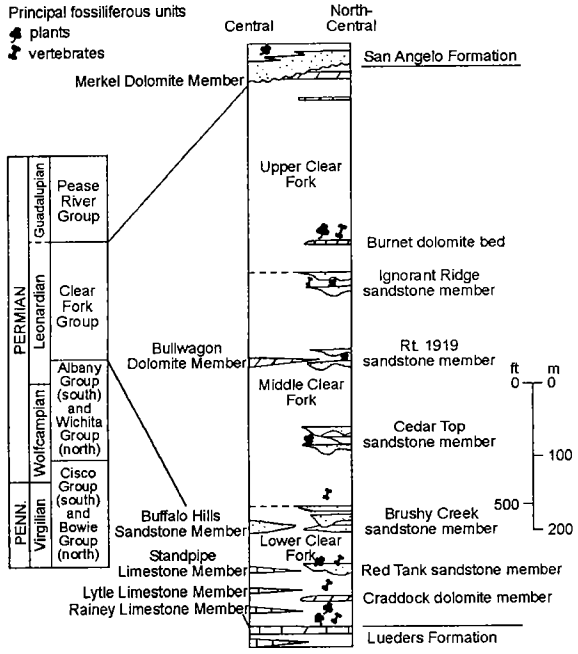

Figure 2. Left, uppermost Pennsylvanian and Lower Permian stratigraphic column, central and North-Central Texas. Right, schematic stratigraphic column, Clear Fork Group, central to North-Central Texas. Formally named members of the Abilene area are shown on the left, informally named members and beds of study area on the right. Scale applies only to north-central part of the column; the Clear Fork is about 150 m thinner in the Abilene area.

and increase in feldspar content implies a source in the Wichita Mountains. Fossils are sparse and poorly preserved in the Brushy Creek.

The remainder of the lower Clear Fork is dominantly reddish-brown, massive to blocky mudstones. These are largely floodplain deposits that contain multiple paleosols with abundant carbonate nodules and stringers. Fossils are sparse, except for vertebrate aestivation assemblages (Olson and Bolles, 1975). Small, silt-dominated, meandering channel deposits are associated with floodplain mudstones. Plant and vertebrate fossils are common in channels, particularly in local deposits of laminated bluish- to greenish-gray mudstones that represent channel abandonment. Limonite nodules, malachite and azurite masses, and fusain (mineralized charcoal) commonly accompany fossils in abandoned channel-fills (Chaney and others, 1993).

Middle Clear Fork

The middle Clear Fork, 125–160 m thick, is approximately correlative to the "Vale" of Romer (1928) and Olson (1958), and is composed largely of floodplain mudstones and high-sinuosity, suspended-load, channel deposits similar to those of the lower Clear Fork. Floodplain deposits exhibit multiple paleosols and lack fossils, except for sparse aestivation assemblages. Whereas pedogenic carbonate nodules gradually decrease in abundance upward, gypsum nodules, stringers, and veins increase. Several thin (0.3–0.9 m) ripple-laminated, mud-cracked, calcareous sandstones are mappable across many square kilometers. These sandstones grade laterally to silty or sandy carbonate beds. Possibly they are monsoonal tidal-flat deposits and updip equivalents of carbonate beds to the west and south. Silty channel-fills yield sparse plant remains.

Three sandy meander-belt units have been mapped in the middle Clear Fork. Informally called the Cedar Top, Rt. 1919, and Ignorant Ridge members, these meander-belt units resemble the Red Tank sandstone and (like the latter) commonly are fossiliferous. Edwards and others (1983) analyzed channel geometry and flow patterns of the Cedar Top member.

Upper Clear Fork

The upper 165–180 m of the Clear Fork Group is approximately equivalent to the "Choza" Formation of Romer (1928) and Olson (1958). This monotonous succession of reddish-brown, gypsum-rich, coastal-plain mudstones contains common nodules, irregular masses, stringers, veins, and thin (0.5 m) beds of gypsum. Several thin (5–10 cm) beds of microgranular dolomite are laterally traceable for kilometers; some may correlate with thicker carbonate beds interpreted on nearby geophysical logs. Gypsum and dolomite beds may represent either hypersaline lakes or coastal sabkhas (Smith, 1974). Siltstone and sandstone occur mainly as thin (0.3–0.9 m), planar, semi-tabular units and less commonly, in small, isolated meandering channels. Aside from plant fossils collected from channel-fills in the lowermost part of the upper Clear Fork, this interval is nonfossiliferous (Olson, 1958; Murry and Johnson, 1987).

PALEOSOLS

Clear Fork paleosols have features that suggest they were all hydromorphic soils: (1) sparse to dense rooting horizons 75–100 cm thick, (2) red to brownish-red colors with distinct gray to brown mottling, (3) pedogenic calcite nodules and cemented horizons, and (4) pedogenic slickensides. Both simple (noncumulative) and cumulative hydromorphic paleosols (sensu Kraus and Aslan, 1993; Alsan and Autin, 1998) have been identified. Simple paleosols typically are thin red mudstones with weak horizonation and weak secondary enrichment of calcite and iron minerals. Cumulative paleosols are thick (to 7 m) and exhibit large slickensides, common to abundant calcite nodules, rhizoliths, and cemented horizons. Rooted and calcic horizons recur throughout cumulative paleosol sequences.

Simple paleosols, classified as entisols or inceptisols, developed in areas of rapid sedimentation (such as alluvial meander belts and natural levees) where rapid burial halted weathering and pedogenesis in their early stages. Cumulative paleosols, all of which are classified as vertisols, reflect slow, continuous sedimentation and several generations of uninterrupted pedogenesis in settings such as back-swamps. Thus, position on the paleo-landscape rather than climatic change probably was the key control on soil formation in the Clear Fork Group.

Several inferences about paleoclimate can be made. Pedogenic slickensides indicate a seasonal climate under which clays swelled and shrank with changing moisture. Calcite nodules and cemented horizons attest to an extended dry season. The transition from abundantly rooted lower and middle Clear Fork soils to sparsely rooted upper Clear Fork soils attests to increasingly arid climate and decrease in vegetation cover through time.

SUMMARY

The lower half of the Clear Fork Group in North-Central Texas records an Early Permian landscape of coastal to alluvial-valley environments. Fluvial deposits, paleosols, and diverse floral and faunal records indicate a range of habitable environments that were far less xeric than previously portrayed. The absence of fossils in the upper Clear Fork is attributed mainly to a paleoenvironmental shift to evaporite-dominated, coastal-plain (sabkha) settings that lacked fluvial conditions suitable for the preservation of terrestrial plants and animals. Paleoclimate was seasonal with extended dry seasons and became more arid through time.

ACKNOWLEDGMENTS

The Walcott Fund of the U.S. National Museum (Smithsonian Institution) provided partial financial support for this study. We are grateful to D. S. Chaney, W. A. DiMichele, the late N. Hotton III, S. H. Mamay, I. P. Montanez, and J. T. Thomas for their collaboration, to W. A. DiMichele, L. R. Follmer, and T. F. Hentz for critical review of this paper, and to landowners of North-Central Texas for property access.

REFERENCES CITED

Aslan, A.; and Autin, W. J., 1998, Holocene flood-plain soil formation in the southern lower Mississippi Valley: implication for interpreting alluvial paleosols: Geological Society of America Bulletin, v. 110, p. 433–449.

Beede, J. W.; and Waite, V. V., 1918, The geology of Runnels County: University of Texas Bulletin 1816, p. 1–64.

Chaney, D. S.; DiMichele, W. A.; Hook, R. W.; and Mamay, S. H., 1993, Paleoecological implications of plant assemblages from red beds of the Arroyo Formation (Leonardian, Permian) of North-Central Texas [abstract]: Journal of Vertebrate Paleontology, v. 14, p. 20A.

Edwards, M. B.; Erickson, K. A.; and Kier, R. S., 1983, Paleochannel geometry and flow patterns determined from exhumed Permian point bars in North-Central Texas: Journal of Sedimentary Petrology, v. 53, p. 1261–1270.

Kraus, M. J.; and Aslan, A., 1993, Eocene hydromorphic paleosols: Significance for interpreting ancient floodplain processes: Journal of Sedimentary Petrology, v. 63, p. 453–463.

Murry, P. A.; and Johnson, G. D., 1987, Clear Fork vertebrates and environments from the Lower Permian of North-Central Texas: The Texas Journal of Science, v. 39, p. 253–266.

Olson, E. C., 1958, Fauna of the Vale and Choza: 14. Summary, review and integration of the geology and the faunas: Fieldiana, Geology 10, p. 397–448.

Olson, E. C.; and Bolles, K., 1975, Permo-Carboniferous fresh water burrows: Fieldiana, Geology 33, p. 271–290.

Romer, A. S., 1928, Vertebrate faunal horizons in the Texas Permo–Carboniferous red beds: The University of Texas Bulletin 2801, p. 67–108.

Smith, G. E., 1974, Depositional systems, San Angelo Formation (Permian), North Texas—facies control of redbed copper mineralization: The University of Texas at Austin, Bureau of Economic Geology, Report of Investigations 80, p. 1–74.

Permian Sedimentation and Diagenesis on the Northern Margin of the Wichita Uplift

R. Nowell Donovan, Kathy Collins, and Steve Bridges
Texas Christian University
Fort Worth, Texas

ABSTRACT.—Early Permian sedimentation on the northern margin of the Wichita uplift took place in the interior of a large continent—Pangaea. The area was located in an arid to semi-arid climatic belt developed in low latitudes in the Northern Hemisphere. As the tectonic definition of the southern Oklahoma area drew to an end in the latest Pennsylvanian, creation of the Wichita uplift ceased and the topographic relief of the area was reduced gradually. Various distinctive continental facies record the destruction of this relief: (1) fault-scarp–recession breccias; (2) talus deposits; (3) alluvial-fan deposits; (4) small, constantly avulsing, braided-river–system deposits; and (5) calcrete accumulations.

Variation in conglomerate clasts can be used to establish paleo-drainage patterns. The calcretes, which can be used as chronostratigraphic and lithostratigraphic markers in subsurface correlation, record periods of geomorphic and hence tectonic stability. The increased frequency of calcretes in sections adjacent to the mountains suggests that they are condensed by comparison to sections farther to the north in the Anadarko basin.

Rocks available for destruction in the area were dominantly either carbonates or igneous (mostly acidic, but including some basic and ultrabasic units). The carbonates were subject to intense karst weathering, as attested by numerous small caves. The igneous rocks underwent considerable hydrolysis, leading to the formation of tors and the production of large amounts of clay minerals. Increasing aridity in the Permian led to the gradual cessation of weathering and eventual entombment of the landscape.

INTRODUCTION

For the last 550 million years, the dominant tectonic control in southern Oklahoma has been a zone of crustal weakness that begins in the neighborhood of Durant, Oklahoma, and trends N. 60° W. into the Texas Panhandle. This zone is recognized in a general sense as the southern Oklahoma aulacogen (Shatski, 1946). The first (Cambrian) stage of aulacogen evolution involved the intrusion and extrusion of a bimodal suite of igneous rocks within an extensional-rift setting. Following a cessation of thermal activity and a period of crustal subsidence, the aulacogen redefined as a linear depocenter during the Late Cambrian and Early Ordovician. This second stage, which lasted from the Cambrian until the Mississippian, was a period of cratonic sedimentation. Quantitatively, most of the rocks deposited during this period were carbonates. Sediment-entrapment rates within the aulacogen were approximately 2–4 times those on the adjacent craton; the overall rate of sediment entrapment declined with time (Donovan, 1986).

The southern Oklahoma aulacogen differentiated into a series of linear uplifts and basins under a generally transpressive-stress regime associated with assembly of the Pangaean supercontinent during the late Paleozoic. As a result of this partial inversion, erosion of the entire lower Paleozoic sedimentary sequence, as well as substantial parts of the igneous basement, took place in various linear uplifts such as the Wichita, Criner, and Arbuckle uplifts. Sediment shed from these uplifts was deposited in adjacent linear basins, such as the Ardmore, Anadarko, Hardeman, and Marietta basins. The aulacogen terrane has, by and large, functioned subsequently as an undefined and inert component of the Laurentian (i.e., North American) craton.

This paper examines the sedimentary record of a period of time in the Early Permian when the tectonic definition of the uplifts and basins was drawing to a close. The particular focus of the paper is the area known as the Slick Hills, a hilly terrain situated between the Wichita Mountains and the Anadarko basin (Fig. 1).

Donovan, R. N.; Collins, Kathy; and Bridges, Steve, 2001, Permian sedimentation and diagenesis on the northern margin of the Wichita uplift, *in* Johnson, K. S. (ed.), Pennsylvanian and Permian geology and petroleum in the southern Midcontinent, 1998 symposium: Oklahoma Geological Survey Circular 104, p. 171–184.

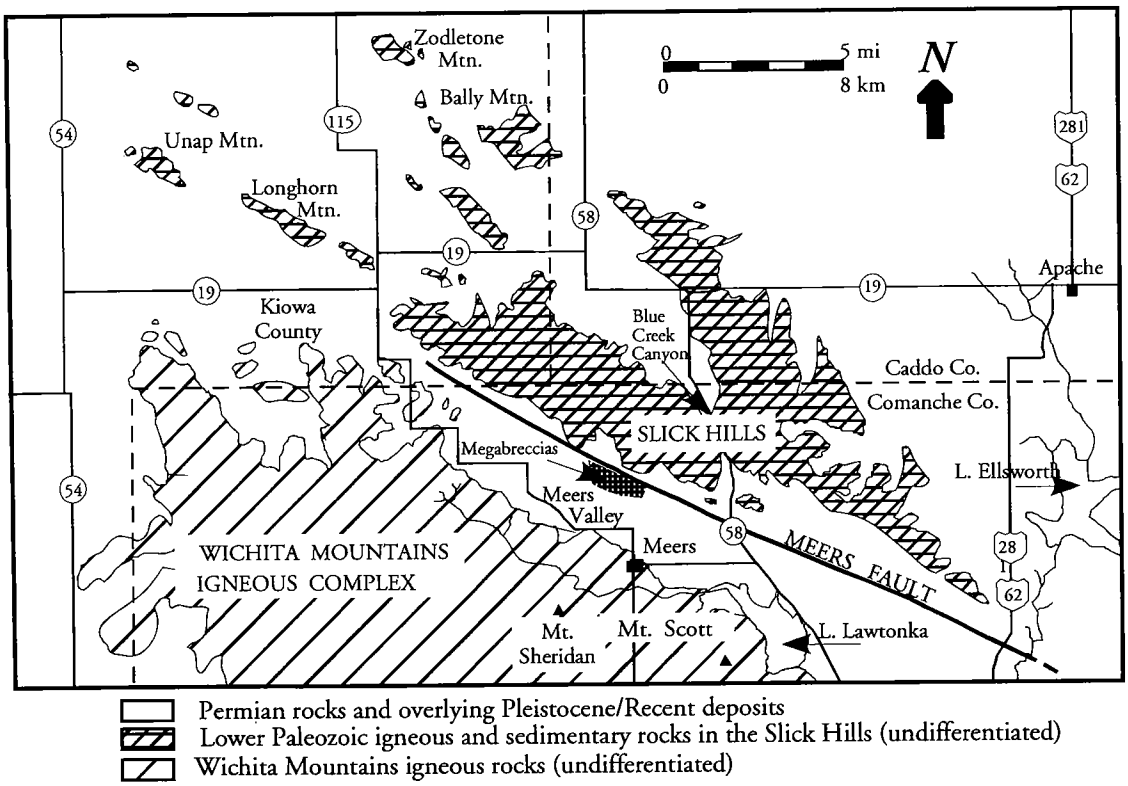

Figure 1. Map showing location of Slick Hills, southern Oklahoma, and related features.

THE SLICK HILLS AREA

The Slick Hills of southwestern Oklahoma constitutes the exposed portion of the frontal fault zone, an area of great tectonic complexity lying between the Wichita uplift and the Anadarko basin. Deformation during the Pennsylvanian and earliest Permian resulted in a maximum stratigraphic displacement of the Cambrian igneous basement of ~13,720 m across the zone. This displacement is the sum of two distinct architectural elements. During the Pennsylvanian, the lower Paleozoic sedimentary basin was partly inverted. The Wichita uplift is the area of greatest inversion. Up to ~3,300 m of lower Paleozoic strata, plus perhaps ~1,650 m of igneous basement, have been eroded from the uplift (Donovan and Butaud, 1993). The Anadarko basin developed as a complex syntectonic depocenter, in which up to ~10,000 m of Late Mississippian, Pennsylvanian, and Permian rocks were deposited atop the lower Paleozoic sequence. Movements on very large, oblique (left-lateral) reverse faults produced most of the displacement within the frontal fault zone.

The Slick Hills are built of Cambro–Ordovician sedimentary rocks that unconformably overlie the Cambrian igneous basement (Fig. 2). The great bulk of the outcrop is formed by carbonates (mostly limestones, but with some dolomites) assigned to the Arbuckle Group.

Exhumed Topography

Both the Wichita Mountains and the Slick Hills are impressive examples of exhumed topography that formed during the Early Permian and were then buried beneath a blanket of later Permian alluvium, eolian sandstones, and evaporites (Donovan, 1986). Previous work has analyzed the Permian geomorphology of the area. Gilbert (1982) described a tor topography in the granitic terrains of the Wichitas. Such topography forms as a result of feldspar hydrolysis, i.e., spheroidal weathering. Tor topography is also developed in the ultrabasic rocks of the Meers Valley. In the limestones of the Slick Hills, pediment surfaces, ancient cliff lines, and megabreccia deposits of two types have been documented. They are breccias formed by gravity-driven cliff collapse and fault-scarp recession (Collins, 1985; Donovan, 1986; Donovan and others, 2001). In addition, karst is widespread, mostly in the form of solution-enlarged fissures (Simpson, 1979; Donovan, 1982; Donovan and Busbey, 1991; Donovan and others, 1992). These caves are securely dated as Lower Permian on the basis of their vertebrate-fossil content.

LOWER PERMIAN DEPOSITIONAL PATTERNS

Quality of Outcrops

Outcrop quality of the enveloping Permian rocks is moderately good to nonexistent in contrast to the Wichita Mountains and Slick Hills. Conglomerates, consisting of various sizes of limestone pebbles, are generally well exposed, especially where they have been incised by recent drainage patterns, as on the northern flank of the Meers Valley. In this area, cliffs up to ~9.1 m yield valuable information. Throughout the Slick Hills, conglomerate outcrops mantle the sub-Permian unconformity and, in some cases, form large

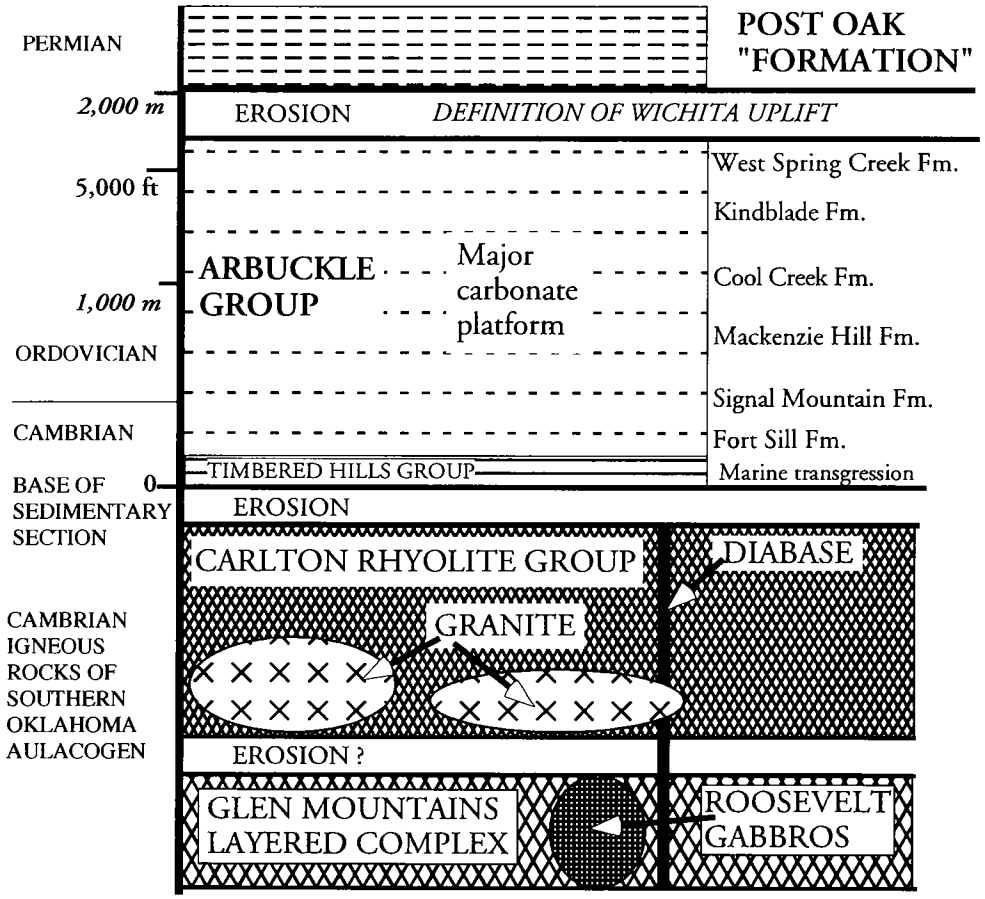

Figure 2. General stratigraphic relationships in the Slick Hills and surrounding areas

outliers. The disposition of these basal conglomerates clearly suggests that the present profile of the Slick Hills is close to that which had developed during the Permian.

Finer-grain-size deposits are generally poorly exposed, again being seen as small cliffs associated with recent incision. Other significant exposures occur on the eastern shore of Lake Lawtonka and on some road cuts. Elsewhere, particularly to the north, exposures are essentially nonexistent.

Permian Stratigraphy

The formal Lower Permian stratigraphy of the Wichita is complex and has been the subject of considerable debate (e.g., Chase, 1954; Miser, 1954; Havens, 1977; Al-Shaieb and others, 1980). For the current study, the classification of Bridges (1985) is preferred (Fig. 3). The problem has three dimensions. First, in an area of poor exposures, it is difficult to correlate facies that are tied to the Wichita–Slick Hills topography to those of the adjoining basins (i.e., the Anadarko and Hardeman basins to north and south, respectively). Second, the uplift-tied facies traditionally has been divided into a subsurface unit—the "Granite Wash," so-called regardless of its petrographic composition—and a surface unit, the "Post Oak," also known as the "Post Oak Conglomerate" or "Post Oak Formation." Logically, it is improbable that the present land surface bears any relationship to the Permian correlation problem. Therefore, we use the two terms in an informal sense, as descriptive of a homotaxial facies, without any suggestion of chronostratigraphic equivalence. Third, the uplift-tied facies consist of alluvium that shows rapid facies variation and is internally very difficult to correlate.

A further dimension of the correlation problem relates to the differential rates of subsidence between the uplift and basin. The net result of this differential movement is that the facies in the uplift area are "condensed" with respect to those in the adjacent basin (Fig. 4).

Facies and Provenance in the Post Oak Formation

General Controls

Both Granite Wash and the Post Oak consist of alluvium of various types that in part mantles the Permian topography. In consequence, it is highly varied in character and thus difficult to correlate. In general, clast composition is an inverted record of the lower Paleozoic stratigraphy. Thus, carbonate-derived detritus is overlain by siliciclastic detritus derived from the adjacent inverted basement (Donovan and Butaud, 1993). Contemporary tectonism, however, locally has obscured

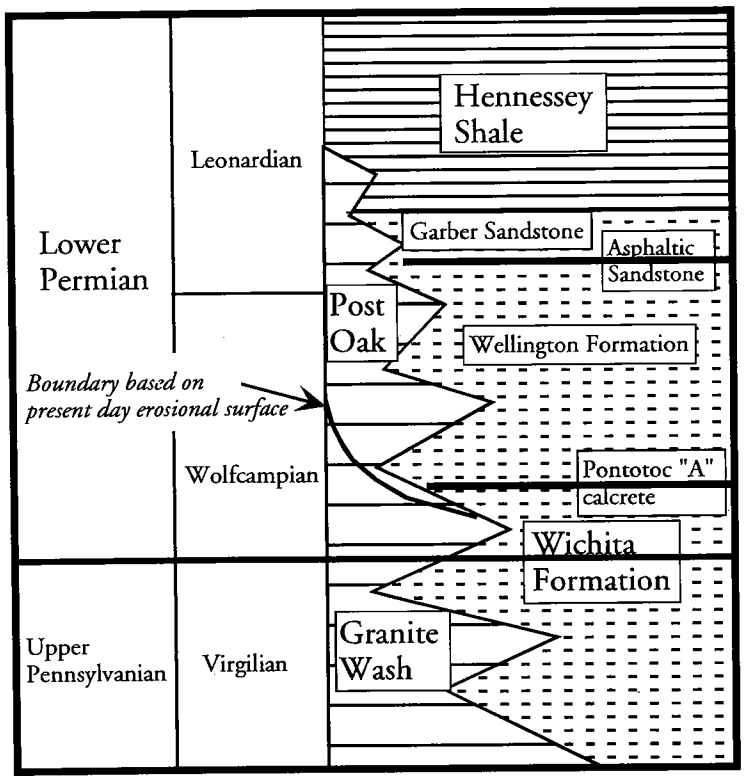

Figure 3. Stratigraphic relationships of uppermost Pennsylvanian and Lower Permian strata in the Wichita Mountain area, illustrating the ambiguous relationships between the Granite Wash and Post Oak. (Modified from Bridges, 1985.)

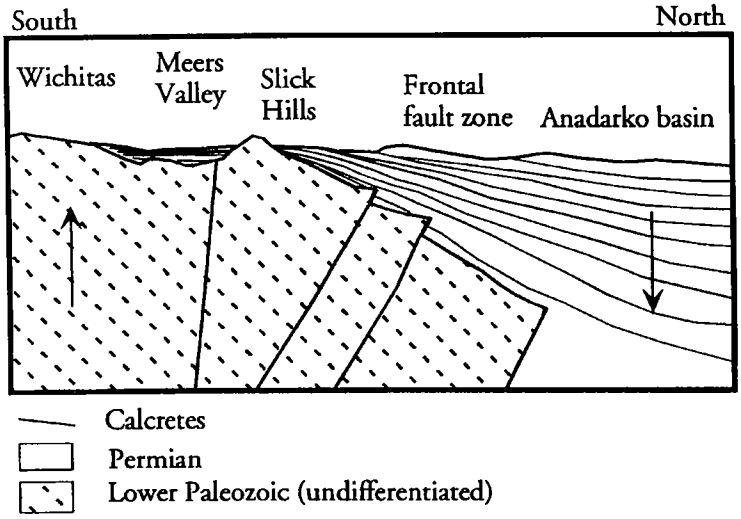

Figure 4. Schematic cross profile illustrating the condensation of section that occurs in the Permian above the Wichita uplift. Calcrete formation is dependent upon geomorphic stability; more calcretes occur in any given section in the Wichita area than in the actively subsiding Anadarko area. Note the numerous hiatuses (marked by calcretes) near Wichita uplift and the thinning of the stratigraphic sequence beneath these time lines. (Based on Collins, 1985; Bridges, 1985; Donovan, unpublished data.)

and even reversed this trend and additionally has led to considerable variation in thickness (Donovan and others, 2001).

The intensity of tectonism in the area decreased from the Pennsylvanian into the Lower Permian, as basin definition slowly ceased. One result of this is that the younger (Permian) conglomerates are simply the result of topographic planation, whereas the older conglomerates record a topographically more unstable setting.

The tectonic assembly of Pangaea accompanied a gradual drift northward of the area into the desert latitudes of the Northern Hemisphere. As a result, "Oklahoma" became increasingly isolated from maritime influences, and an increasingly arid climate developed in the area. This aridity is recorded both by "fossilization" of the topography (as recorded above) and by climatic indicators in the lower Permian sedimentary rocks (Donovan and Butaud, 1993).

Specific Facies

Conglomerates, sandstones, and shales each exhibit different geometries and sedimentary structures in and around the Slick Hills. Types of conglomerate deposits, all of which are dominated by limestone clasts, are: (1) complex, multistoried deposits, up to 5 m thick and 8 m wide, that may be deeply incised into the underlying beds (Figs. 5, 6); (2) lenticular deposits that are not incised into the underlying beds; (3) multistoried, flat-based sheets up to 1.5 m thick and 15 m wide (Fig. 7); and (4) megabreccia horizons.

Most of the megabreccia horizons, which are composed of colossal limestone blocks (some as large as a small house), are restricted to the southern margin of the western Slick Hills on the northern edge of the Meers Valley. At this location they have been interpreted as cliff-collapse deposits following tectonic activity on the Meers fault (Collins, 1985; Donovan and others, 2001). Two other megabreccias in Blue Creek Canyon have been interpreted as fault-scarp–retreat deposits (Donovan and others, 1988).

The other types of conglomerate are found at various sites around the entire Slick Hills. In general, pebble size in these deposits decreases away from the nearest Permian topography, and clast composition is similarly parochial. This is perhaps best demonstrated in Blue Creek Canyon, where conglomerates from either side of the canyon closely reflect the basement lithologies that have been juxtaposed by the Blue Creek Canyon fault (Donovan, 1986). Most limestone clasts are angular to subangular to subround; it is difficult to determine the relative roles of abrasion and dissolution in determining pebble shape.

Only in the finer conglomerates are bed forms such as parallel laminations and trough cross-bedding preserved (Fig. 7). Orientations of the

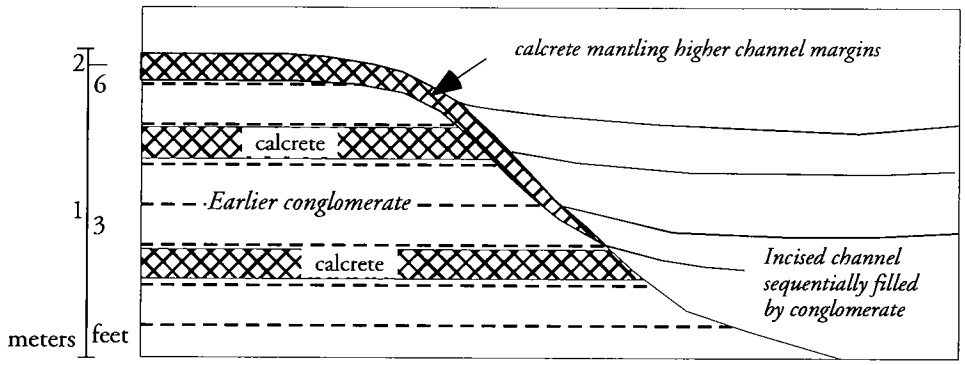

Figure 5. Schematic section showing complex channeling in conglomerates on the southern flank of the Slick Hills. Multiple calcrete formation suggests slow rates of sediment accumulation; the channel probably records a major avulsion event. (Redrawn from Donovan, 1988.)

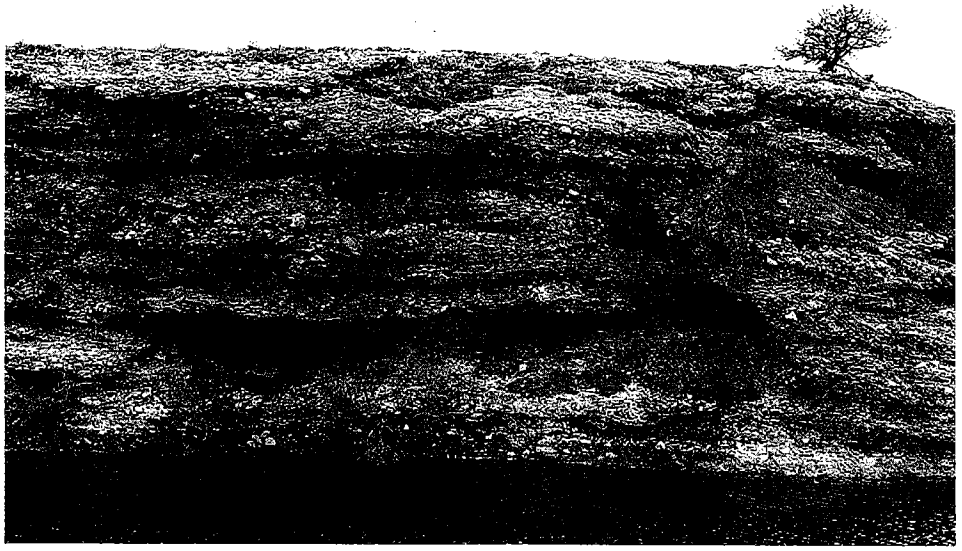

Figure 6. Outcrop photograph of multistoried limestone-pebble conglomerate section on the southern flank of the Slick Hills. The section is built of lenticular beds, some of which have erosive bases (e.g., bottom right and top left). Cliff is approximately 6.1 m high.

Figure 7. Outcrop photograph of flat-based limestone-pebble conglomerate resting on a calcrete developed in red shale. Planar cross bedding, which is developed only in the finer part of the conglomerate, suggests transport to the south (to the right), in the direction of the Meers Valley.

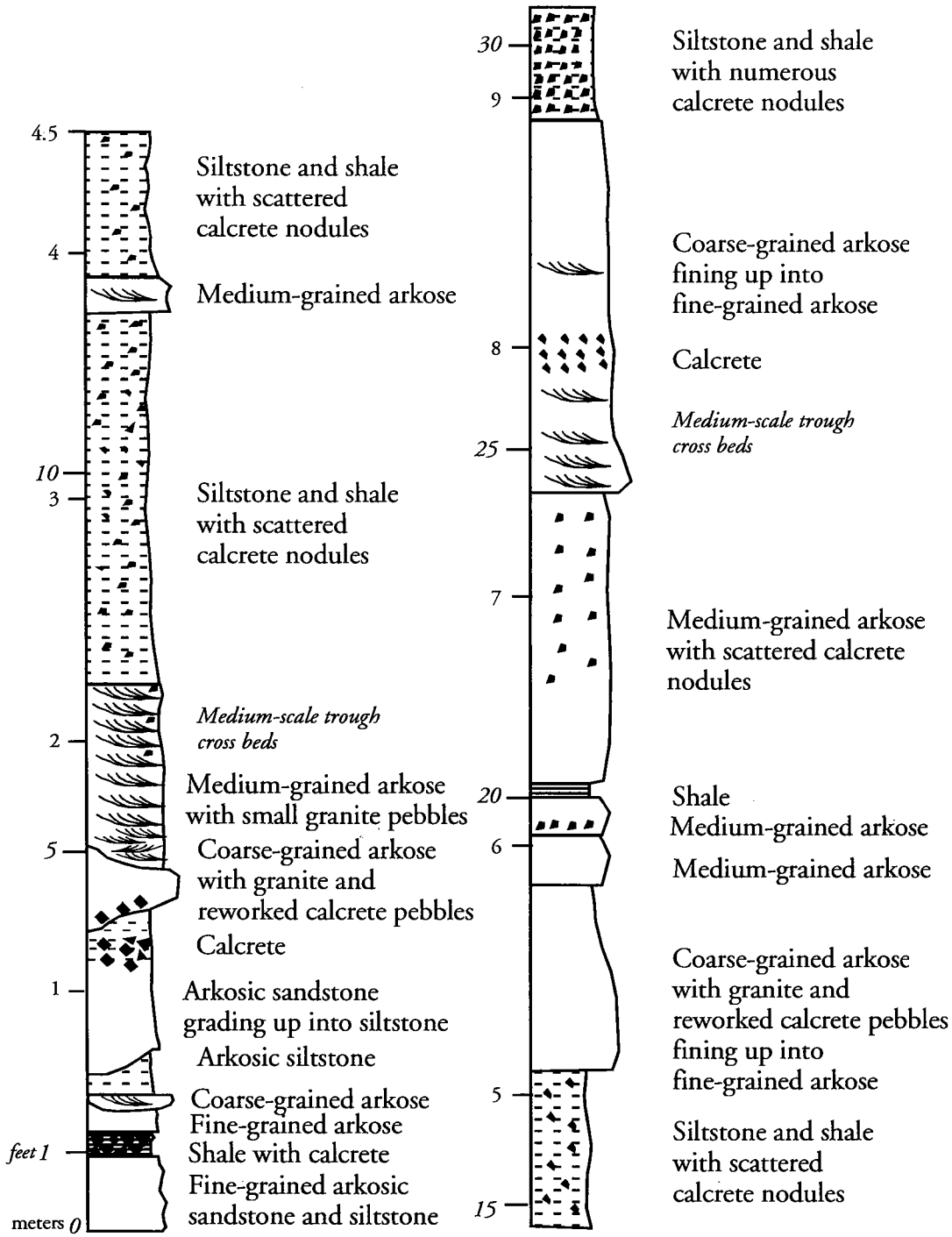

Figure 8. Measured section of sequence exposed on stream bank in southeastern part of the Meers Valley (NW¼, sec. 2, T. 3 N., R. 12 W.). Section is interpreted as braided alluvium distal to fans lying to the west. Note numerous calcrete horizons.

latter, admittedly few in number, are consistent with transport away from the Permian topography.

Sandstone deposits are less common than might be expected. This is largely because the limestones of the Slick Hills did not weather to form abundant sand-sized particles. Most of the sandstones are found in areas where there is a siliciclastic source, most notably the Mount Scott granite, which outcrops to the south of the Meers Valley (Collins, 1985; Donovan and others, 2001). Thus, in the southeastern part of Meers Valley, reddish-brown arkosic sandstones form erosive-based, lenticular sandstones up to 2 m thick and 20 m wide. They are generally interbedded with sequences of shale and siltstones (Fig. 8). Some sandstones exhibit basal lags of granite, limestone, and calcrete fragments, most of which display parallel lamination and medium-scale trough cross bedding. In some cases, opaque heavy minerals, chiefly magnetite presumably derived from

the gabbros and ultrabasic rocks of the Wichita uplift, accent individual laminations (Fig. 8). Some of the sandstones grade upward into siltstones and shales, whereas others are discretely, non-upward grading beds, defined by sharp top surfaces.

Most shale deposits are reddish-brown, less commonly green and gray. They are generally poorly exposed. Some show silt-mud laminations, others consist entirely of mud. Subaerial mud is occasionally present.

Calcretes

Calcretes are ancient accumulations of authigenic carbonates that formed in soil horizons; caliche is the most commonly used name for recent equivalents. Although calcretes are strictly a diagenetic product, they are presented in this section because they yield important clues as to the nature of the depositional history of the Permian. In addition, it is clear that some have been reworked into the base of channel-filling sandstones and conglomerates, where they are seen as angular limestone pebbles.

Factors that play a role in calcrete development include carbonate supply, temperature, rainfall, geomorphic stability, and sedimentation rate. In general, the interplay of these factors results in optimum calcrete/caliche formation in tectonically, and hence geomorphically stable settings, characterized by hot semiarid conditions in which annual precipitation ranges from 10 to 60 cm (Reeves, 1970; Steel, 1974; Leeder, 1975). Sedimentation rates must be minimal if thick calcretes are to form. Ideal locations for calcrete development include the stable portions of alluvial fans and, more commonly, floodplains and braided-stream channels adjacent to alluvial fans.

Calcrete formation begins when calcium carbonate is reprecipitated from rainwater about 50 cm below the ground surface. The carbonate initially fills pore spaces, and, as drainage is plugged, intense carbonate impregnation takes place. This impregnation may be both displacive and replacive. Watts (1978) noted that some calcretes contain 2.5 times the amount of calcium carbonate needed to fill the void space of normally packed sediment. The excess of carbonate must either expand the original volume of the host rock (displacive impregnation) or destroy the host material (replacive impregnation). With time, this plugged horizon extends upward toward the surface and is seen as massive and laminar horizons. As the calcrete plugs the soil horizon, the underlying sediments may be reduced, and herein lies the origin of the green shales that are found beneath some calcretes.

Successive stages in calcrete and caliche formation have been identified by various authors (Gile, 1970; Steel, 1974; Leeder, 1975). These stages develop within a temporal framework, measured in terms of thousands of years, the most "mature" profiles taking a minimum of 10,000 years to develop (Leeder, 1975). In addition, they are seen in sections as spatially superimposed—i.e., in any given example, "mature" profiles overlie less mature ones (Figs. 9–11). In nongravelly sediments, the initial calcrete deposits are seen as small (about 1–2 cm) nodules that are widely scattered throughout the host rock. In gravelly sediments, the original pebbles act as nuclei for carbonate precipitation. Although many of these nodules are more or less circular, others are elongate and apparently form as rough approximations of root casts, the roots themselves having functioned as permeability pathways. With time, the nodules enlarge in size, occupying more and more of the soil profile, replacing and displacing the host clastic sediment. Individual nodules may record periods of wetting and drying in the form of sparite-filled, circum-granular cracks. The profile eventually becomes completely plugged by carbonate. The zones above the plugged horizon are typified by laminated, brecciated, and pisolitic textures. In such "mature" or "old-age" profiles, non-organic chert may precipitate along with the carbonate, presumably recording fluctuations in alkalinity in the upper part of the profile.

Calcrete horizons are abundant in all lithologies and at all stages of development in the Permian rocks under discussion, (Figs. 5, 7, 11). In general, "old-age" calcretes commonly are found in the conglomerates (e.g., Donovan, 1982), whereas calcretes in the finer-grained rocks are generally less mature. This suggests either that the sedimentation rate in the areas of conglomerate was less than that in the areas of finer deposition and/or that reworking of previously deposited material was more common in the latter areas. The latter explanation is perhaps more likely, because, once cemented, the conglomerate would be very difficult to rework.

Facies Interpretation

Previous authors have interpreted the Permian deposits that mantle the Wichita uplift as a complex of talus, alluvial-fan and braided–river-channel, and floodplain deposits (Al-Shaieb and others, 1980; Bridges, 1985; Collins, 1985; Donovan, 1986). This model is reaffirmed in this study both with respect to the Wichita uplift as a whole and the Slick Hills in particular (Fig. 12).

In the context of the Slick Hills, the limestone-clast conglomerates are interpreted as alluvial talus that has been partly reworked by small flashy streams and deposited around the Slick Hills as alluvial fans. Little fine-grained matrix is present in the conglomerates. Consequently, they effectively functioned as sieve deposits. Such deposits are generally described as poorly imbricated, mostly angular, and well sorted (Collinson, 1996); such is the case here. The high initial porosity of these deposits was infilled by calcrete, sparry cement, or limited amounts of hematite "dust," probably of aeolian origin. In places, calcrete deposits are developed directly on the unconformity, and most sections show one or more calcrete horizons. These horizons are commonly plugged, although they are generally no more than 50 cm or so thick. The great concentration of calcretes suggests that sedimentation rates were extremely slow, a suggestion that is supported by the fact that avulsion channels are common.

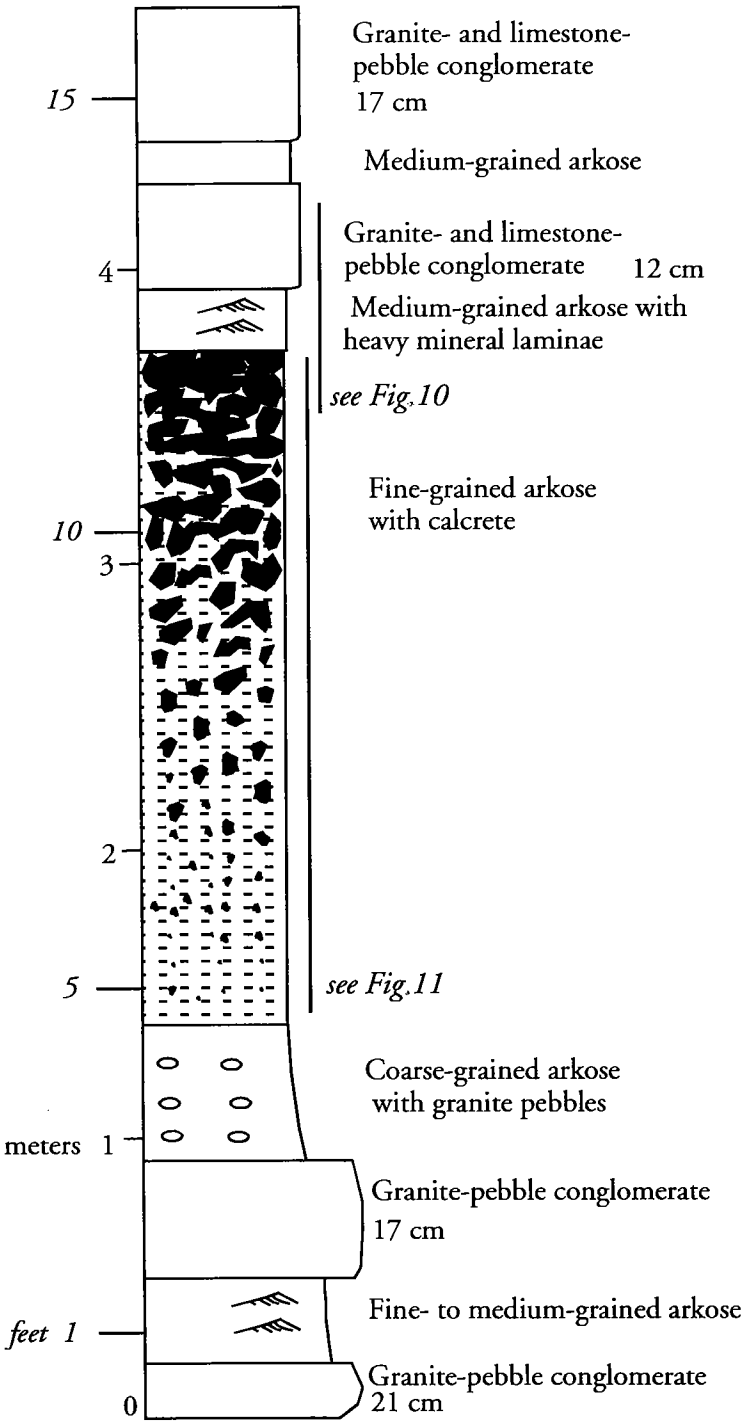

Figure 9. Measured section of sequence exposed in the SE¼, sec. 5, T. 3 N., R. 12 W., on the eastern shoreline of Lake Lawtonka in Meers Valley. The calcrete records a period of geomorphic stability, following which a braided fluvial system inundated the area. Clast composition in the conglomerates above and below the calcrete varies, suggesting an adjustment to drainage patterns. Average size of the 10 largest pebbles in conglomerates is given in centimeters. Figures 10 and 11 are keyed to the log.

This picture of environmental torpor is consistent with the notion that the rate of weathering was slowing dramatically in the increasingly arid environment and eventually led to the preservation of the Permian topography beneath a veneer of slowly accumulating detritus. The major *caveat* to this interpretation is that, although tectonic activity in the area was gradually ceasing, movement was still taking place on the Meers fault and, less certainly, on the Blue Creek Canyon fault. This movement led to the formation of several "megabreccia" horizons with clasts up to 30 m in diameter (Collins, 1985; Bridges, 1985; Donovan and others, 2001). The megabreccias apparently record catastrophic cliff collapse, probably involving rock falls, landslips, and perhaps air cushion transport.

The finer deposits in the area generally occur distally to the Slick Hills. They are generally less well exposed than the conglomerates, and the best sequences are found in the Meers Valley. It is suggested that the sandstones were deposited in the channels of braided-stream complexes and that the siltstones were deposited as floodplain overbank deposits. Avulsion was common, as suggested both by channel geometries and by the abundance of reworked calcrete fragments in the bases of channel deposits. Details of the local paleogeography are difficult to determine; there is good evidence that drainage in the Meers Valley was axial to the southeast (Donovan and others, 2001). Less certainly, drainage was axial and to the northwest in the valley of the Blue Creek Canyon fault between the eastern and western Slick Hills. Elsewhere, paleocurrent evidence is lacking.

DIAGENESIS

Major post-depositional events affecting the Permian rocks around the Slick Hills include several phases of cementation and hydrocarbon migration. Various forms of calcium carbonate cement most rocks. Textures observed include the spectrum of types associated with calcrete formation, plus anhedral, fibrous, pendant, and poikilitic sparite. Clay cements are virtually absent in the limestone-derived detritus, although authigenic kaolinite is widespread in the granite-derived detritus around the Wichita Mountains (Al-Shaieb and others, 1980).

Calcrete textures are "classic," involving original dense micritic fabrics that are cut by several generations of spar-filled shrinkage veins (Fig. 13). These veins, which commonly curve around the circumference of micritic nodules, probably record periods of desiccation of the soil profile. Evidence of replacement is seen as corroded quartz grains, and evidence of displacement is seen in a general lack of grain-to-

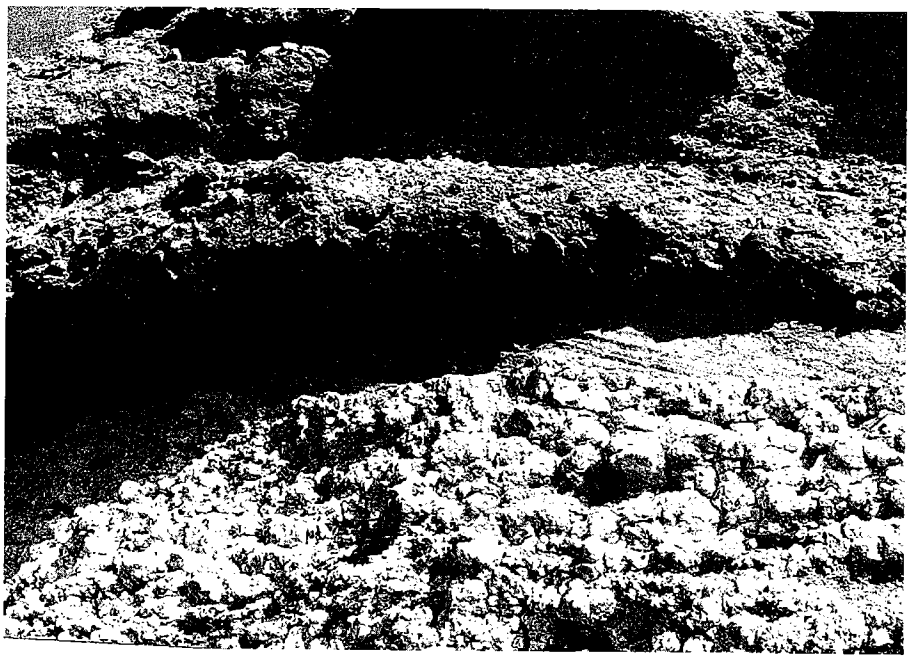

Figure 10. Portion of the section depicted in Figure 9, showing a dense layer of calcrete abruptly overlain by cross-bedded arkose with heavy-mineral bands, which is, in turn, overlain erosively by conglomerates. About 0.8 m of section is shown in photograph.

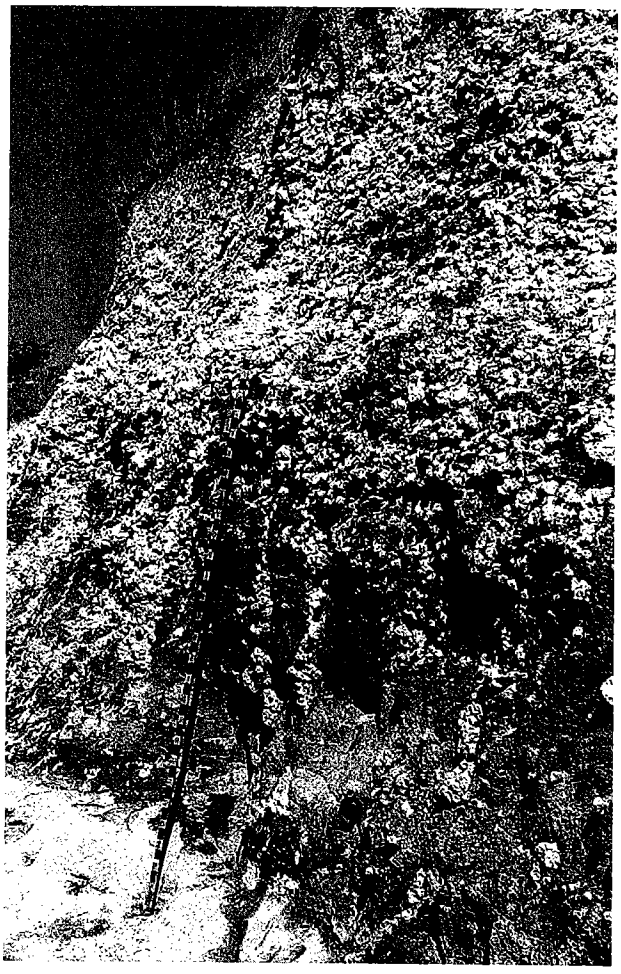

Figure 11 *(left)*. Portion of the section depicted in Figure 9, showing a calcrete profile with increasing upward displacement of the host sediment by calcrete nodules. Scale marked in inches.

grain contacts and the splitting of detrital grains, such as biotite, along cleavage. More mature textures are seen as micritic laminae and poorly shaped pisolites.

The open, matrix-free framework of the limestone conglomerates, in many places and especially close to the basal unconformity, was coated by fibrous calcite precipitated from saturated vadose water (Fig. 14). Such crystals are up to 10 cm in length, showing crystallographic continuity across growth bands that are marked by the inclusion of hematite "dust" into the crystal structure. Pendant or dripstone calcite cements associated with the limestone conglomerates provide further evidence of vadose precipitation. Because fibrous calcite and calcretes both occur as the earliest cements in different parts of the same rock units, it is possible that they formed simultaneously. In other words, subsurface fibrous calcite cementation occurred within the fan at the same time that calcrete formed at the surface of the fan.

Anhedral drusy sparite occurs as the latest calcium-carbonate cement in both the sandstones and conglomerates. In general, this sparite records competitive crystal growth from numerous pore-margin nucleation sites under phreatic conditions. In this case, most of the spar is nonferroan, indicating oxidizing conditions and suggesting that burial depths may not have been too great when this cement formed.

The least-common calcite cement is poikilitic calcite in

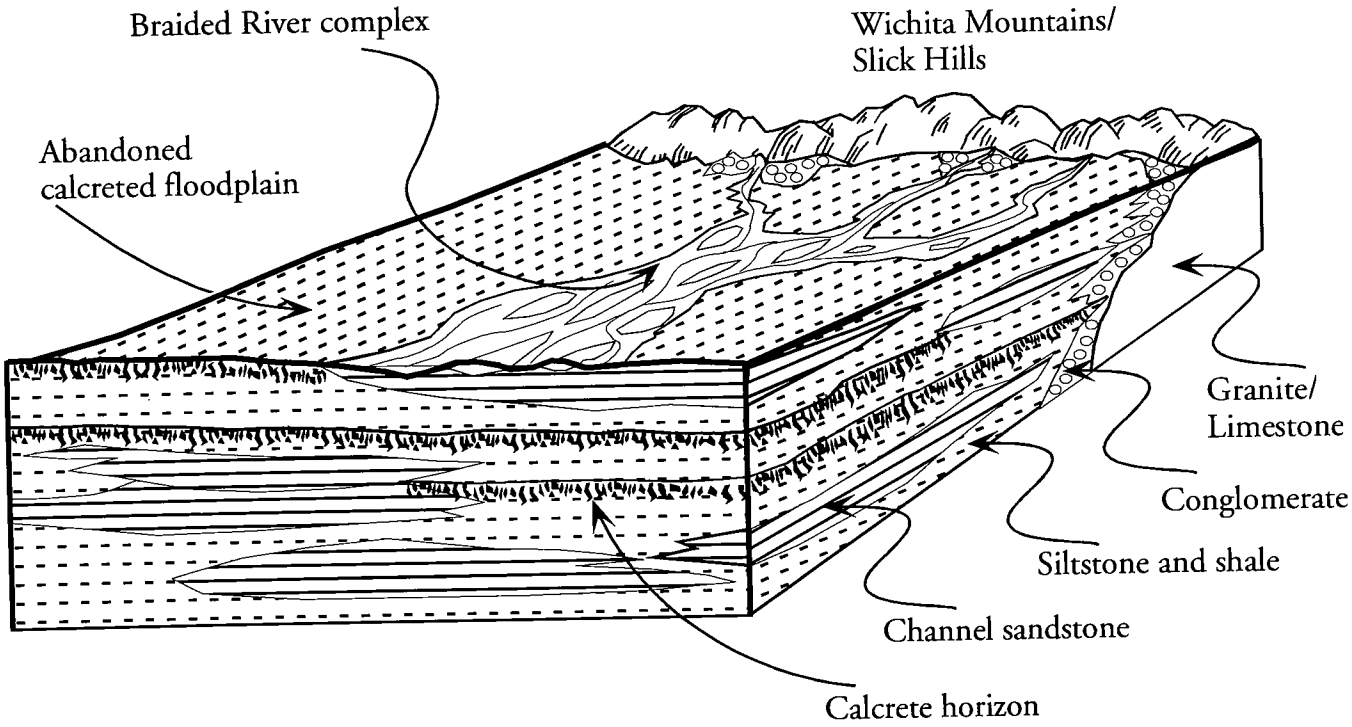

Figure 12. Depositional model for the Post Oak facies developed around the exposed portion of the Wichita uplift as a whole.

the form of large equant crystals up to 2 cm in diameter (Fig. 15). Cement of this type has been encountered in only a few of the sandstones in the Meers Valley. This texture forms in clastic sediments when pore waters are saturated and ponded and there are few nucleation sites for precipitation.

Euhedral-dolosparite cement occurs locally in conglomerates that consist of predominantly dolomite clasts. For example, dolosparite cement occurs in the deposits that mantle the Maukeen dolomite (Kindblade Formation) in the Saddle Mountain area of the western Slick Hills.

Other cements include hematite, which occurs as particulate coats around clastic grains (including some carbonate clasts) and generally appears to be an early event. It is responsible for the red coloration of shales and siltstones. The origin of the mineral is uncertain, but some could have been derived from weathering of the igneous basement rocks of the Wichita uplift.

Barite and pyrite cements are uncommon late cements that generally exhibit euhedral crystals (Fig. 16). Younger and others (1986) documented an active barite-precipitating spring at Zodletone Mountain in the northwestern Slick Hills. They suggested that the spring waters are modified oil field brines that have migrated upward from the Anadarko basin along faults and fissures. Such migration may have led to the formation of both pyrite and

Figure 13 *(right)*. Photomicrograph of a calcrete developed in limestone conglomerate in Blue Creek Canyon, showing original dense micritic fabrics that are cut by several generations of spar-filled shrinkage cracks that probably formed during periods of desiccation. Long axis of photograph is ~3.2 cm.

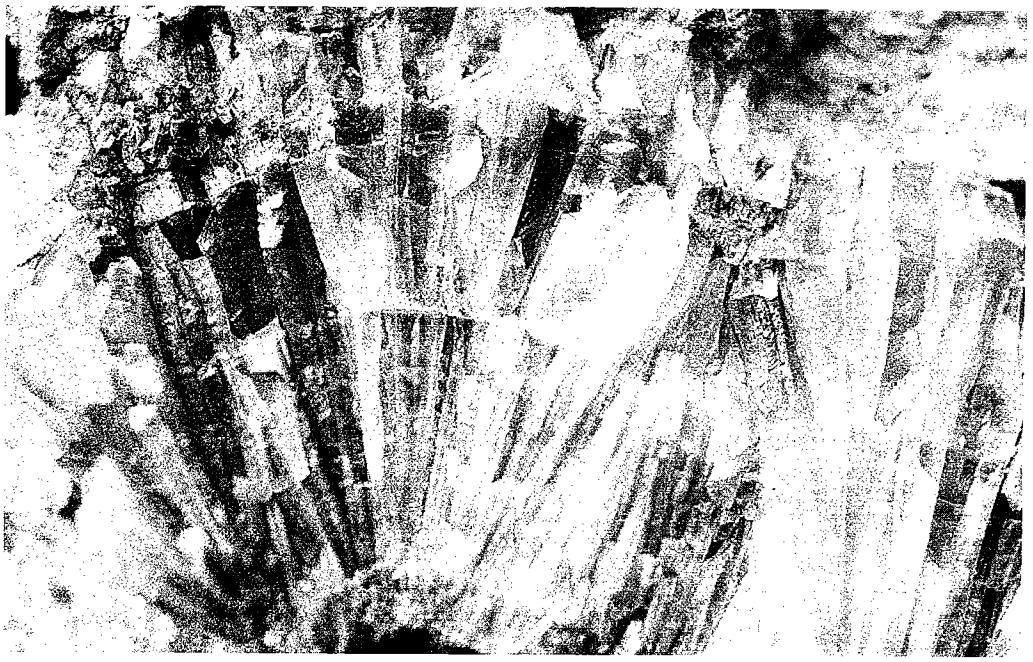

Figure 14. Outcrop photograph of fibrous calcite developed in limestone-pebble conglomerate above the sub-Permian unconformity in Blue Creek Canyon. Growth bands in the crystals are defined by hematite inclusions. Individual crystals are up to 5 cm long.

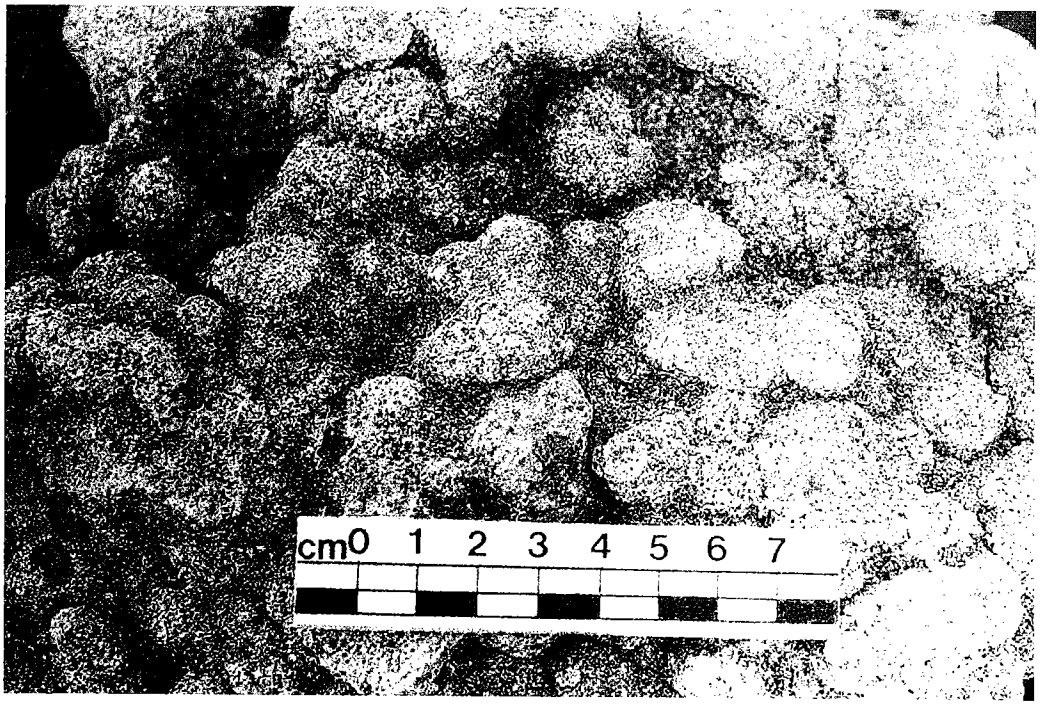

Figure 15. Outcrop photograph showing poikilitic calcite cementing a medium-grained arkose in the southeastern part of the Meers Valley.

barite. Certainly numerous traces of hydrocarbons are present in the Permian strata, including datable Permian speleothems and fracture-fills in calcrete nodules (Donovan, 1986). Hydrocarbon traces tend to be more common in the vicinity of the Meers fault, suggesting that the latter was a conduit for migration. In a similar vein, traces of copper mineralization in the form of chalcopyrite, chalcocite, and malachite are associated with basal Permian conglomerates that lie atop the major fault trace in Blue Creek Canyon.

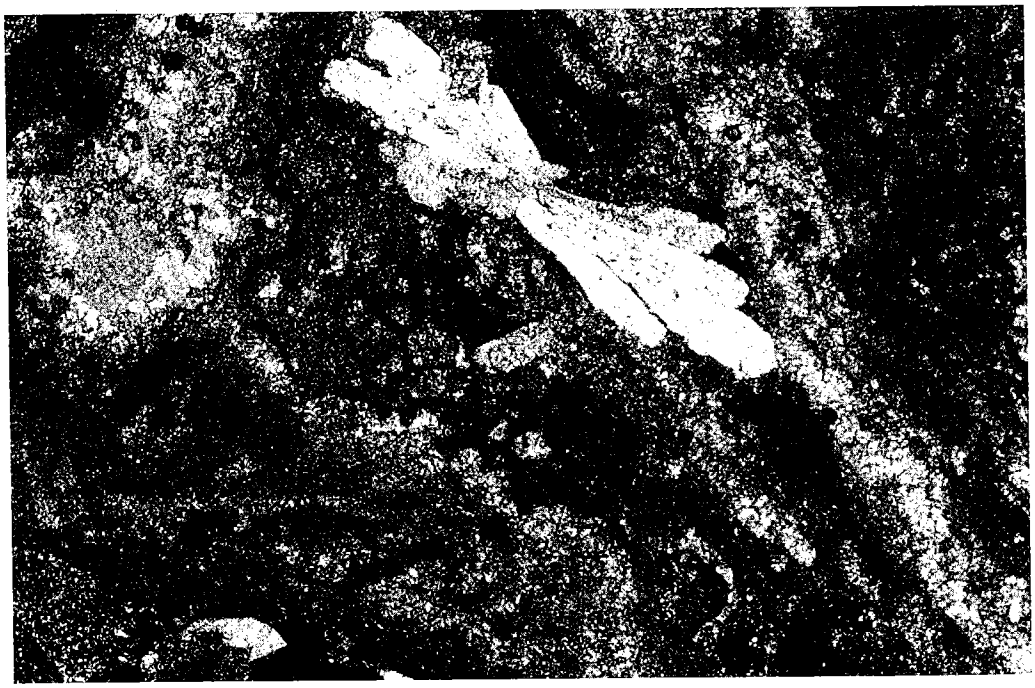

Figure 16. Outcrop photograph of a "bow tie" of euhedral barite crystals in a dense laminated calcrete developed on the western edge of the Slick Hills. Long axis of photograph is ~3.5 cm.

Diagenetic Sequence

The timing of the various diagenetic phases is straightforward. The earliest cements were essentially penecontemporaneous including: (1) widespread calcrete formation on fan and floodplain surfaces; (2) speleothem formation in karst-enhanced tectonic fissures related to the sub-Permian unconformity; (3) fibrous-calcite precipitation from vadose waters (most likely to be located at or close to the sub-Permian unconformity); and (4) hematite precipitation in the form of particulate grain coatings and as a minor constituent in speleothems where it defines growth lines.

Poikilitic calcite and drusy spar are somewhat later cements, precipitated from phreatic groundwater. The latter constitutes the youngest cementation event and is by far the most common in most of the limestone conglomerates. Nonetheless, much primary porosity still remains in the conglomerates.

All the cements noted in the preceding paragraph owe their origin to surface-tied hydrology. This is consistent with burial-curve analysis, which indicates that the area has never been deeply buried (Donovan, 1986). It is clear, however, that deep-basin brines and hydrocarbons have migrated through the sequence, resulting in the precipitation of barite and pyrite and very small amounts of copper minerals. This migration was due to structural overpressuring of basin brines in the Anadarko basin, which lies to the north and partially beneath the Slick Hills (Donovan, 1986). The extraordinary depth of the Anadarko basin resulted in the maturation of source rocks in the Paleozoic section (particularly the Upper Devonian–lowermost Mississippian? Woodford Formation. Although the sulfates and sulfides appear to have formed later than most of the carbonate cements, evidence from speleothems indicates that hydrocarbons were migrating to the surface prior to and at the time of Permian deposition (Donovan and others, 1992).

CONCLUSIONS

The dismemberment of the southern Oklahoma aulacogen during the Pennsylvanian and earliest Permian resulted in the partial inversion of the lower Paleozoic basin to form the Wichita uplift. To the north of the uplift the Slick Hills is the exposed portion of the frontal fault zone, a region of intense tectonism that defines the southern margin of the immensely deep Anadarko basin. Detritus shed from the uplift into the basin falls into two categories: (1) earlier syntectonic deposits, that formed rapidly and is seen as immensely thick deposits of alluvium (referred to informally as the "Granite Wash"); and (2) relief-related detritus, that formed more slowly and is seen as much thinner, condensed alluvium (referred to informally as the "Post Oak").

The Post Oak around the Slick Hills generally consists of a few to several tens of meters of limestone-clast conglomerates, sandstones of various grain sizes, siltstones, shales, and nodular carbonates, interpreted as calcretes. The following deposits, representing discrete paleoenvironments, are recognized. (1) Fault-scarp–recession breccias record the last events in the late Paleozoic tectonism. (2) Talus deposits are present. (3) Alluvial-fan deposits formed. Individual fans were small and subject to flashy discharge. In the absence of fines, many of the fan conglomerates had very high

initial porosities. (4) Braided-river flood-plains deposits are characterized by small streams and frequent avulsion. In addition, nodular limestones, interpreted as calcretes (calcareous soil profiles) are common in both the fan and braided-river deposits and may mantle the sub-Permian unconformity surface.

The character of the Post Oak is controlled by an interplay of (1) the amount of associated tectonism, (2) variation in the rate of sediment entrapment, and (3) an overall change in environment from humid to arid. The general pattern is one of decreasing rates of subsidence so that the final detritus is a relatively thin veneer associated with the reduction of available relief. This relief was essentially fossilized as active weathering ceased. The result is that the sub-Permian unconformity is extremely irregular—in essence, a buried range of hills.

Most diagenetic imprint on the sequences discussed took place early in the history of the deposit and involved the precipitation of several varieties of calcite, including both vadose and phreatic textures, and hematite. In addition, hydrocarbons migrated through the sequence, sourced from the adjacent Anadarko basin; brines from the same source precipitated pyrite and barite.

ACKNOWLEDGMENTS

We are very grateful to the landowners in the Slick Hills for their continuing support. In particular, we would like to thank Charlie Bob and Dixie Oliver, Tom Cavanagh, the Kimbell family, and Doyle Leatherbury. Financial support from Oklahoma State University and the Moncrief fund of Texas Christian University is gratefully acknowledged.

REFERENCES CITED

Al-Shaieb, Zuhair; Hanson, R. E.; Donovan, R. N.; and Shelton, J. W., 1980, Petrology and diagenesis of sandstones in the Post Oak Formation (Permian), southwestern Oklahoma: Journal of Sedimentary Petrology, v. 50, p. 43–50.

Bridges, S. D., 1985, Mapping, stratigraphy, and tectonic implications of Lower Permian strata, eastern Wichita Mountains, Oklahoma: Oklahoma State University unpublished M.S. thesis, 125 p.

Chase, G. W., 1954, Permian conglomerate around the Wichita Mountains, Oklahoma: American Association of Petroleum Geologists Bulletin, v. 38, p. 2028–2035.

Collins, K. H., 1985 Depositional and diagenetic history of the Permian rocks in the Meers Valley, southwestern Oklahoma: Oklahoma State University unpublished M.S. thesis,, 110 p.

Collinson, J. D., 1996, Alluvial sediments, *in* Reading, H. G. (ed.), Sedimentary environments: processes, facies and stratigraphy: Blackwell Science, Oxford, p. 37–82.

Donovan, R. N., 1982, Permian paleokarst features, *in* Gilbert, M. C.; and Donovan, R. N. (eds.), Geology of the eastern Wichita Mountains, southwestern Oklahoma: Oklahoma Geological Guidebook 21, p. 65–77.

_____ 1986, The geology of the Slick Hills, *in* Donovan, R. N. (ed.), The Slick Hills of southwestern Oklahoma—fragments of an aulacogen?: Oklahoma Geological Survey Guidebook 24, p. 1–12.

_____ 1988, The Meers fault scarp, southwestern Oklahoma, *in* Hayward, O. T. (ed.), Geological Society of America Centennial Field Guide, South-Central Section: Geological Society of America, Decade of North American Geology, v. 4, p. 79–82.

_____ 1995, The Slick Hills of Oklahoma and their regional tectonic setting, *in* Johnson, K. S. (ed.), Structural styles in the southern Midcontinent, 1992 symposium: Oklahoma Geological Survey Circular 97, p. 178–186.

Donovan, R. N.; and Busbey, A. B., 1991, Leatherbury's Quarry—The world's smallest oil field, *in* Johnson, K. S. (ed.), Arbuckle Group core workshop and field trip: Oklahoma Geological Survey Special Publication 91-3, p. 255–258.

Donovan, R. N.; and Butaud, T., 1993, The Vanoss Conglomerate—a record of late Pennsylvanian basin inversion on the northern flank of the Arbuckle Mountains, southern Oklahoma, *in* Johnson, K. S.; and Campbell, J. A. (eds.). Petroleum-reservoir geology in the southern Midcontinent, 1991 symposium: Oklahoma Geological Survey Circular 95, p. 10–24.

Donovan, R. N.; Collins, Kathy; and Bridges, S. D., 2001 [this volume], Evolution of the Meers Valley, southwestern Oklahoma, *in* Johnson, K. S. (ed.), Pennsylvanian and Permian geology and petroleum in the southern Midcontinent, 1998 symposium: Oklahoma Geological Survey Circular 104, p. 213–223.

Donovan, R. N.; Ragland, D. A.; Rafalowski, M. B.; McConnell, D.; Beauchamp, W.; Marcini, D.; and Sanderson, D. J., 1988, Pennsylvanian deformation and Cambro–Ordovician sedimentation in the Blue Creek Canyon area, Slick Hills, southwestern Oklahoma, *in* Hayward, O. T. (ed.), Geological Society of America Centennial Field Guide: South-Central Section: Geological Society of America, Decade of North American Geology, v. 4, p. 127–145.

Donovan, R. N.; Busbey, A. B.; Elmore, R. D.; and Engels, M. H., 1992, Oil in Permian karst in the Slick Hills of southwestern Oklahoma, *in* Johnson, K. S.; and Cardott, B. J. (eds.), Source rocks in the southern Midcontinent, 1990 symposium: Oklahoma Geological Circular 93, p. 198–209.

Gilbert, M. C., 1982, Geological setting of the eastern Wichita Mountains with a brief discussion of unresolved problems, *in* Gilbert, M. C.; and Donovan, R. N. (eds.), Geology of the eastern Wichita Mountains, southwestern Oklahoma: Oklahoma Geological Survey Guidebook 21, p. 1–30.

Gile, L. H., 1970, Soils of the Rio Grande border in southern New Mexico: Soil Science Society of America Proceedings, v. 34, p. 465–472.

Havens, J. S., 1977, Reconnaissance of the water resources of the Lawton quadrangle, southwestern Oklahoma: Oklahoma Geological Survey Hydrologic Atlas 6, scale 1:250,000.

Leeder, M. R., 1975, Pedogenic carbonates and flood plain accretion rates—a quantitative model for alluvial arid-zone lithofacies: Geological Magazine, v. 112, p. 257–270.

Miser, H. D., 1954, Geologic map of Oklahoma: Oklahoma Geological Survey, scale 1:500,000.

Reeves, C. C., 1970, Origin, classification, and geologic his-

tory of caliche on the southern High Plains, Texas and eastern New Mexico: Journal of Geology, v. 78, p. 353–362

Shatski, N. S., 1946 , The Great Donets basin and the Wichita system: Comparative tectonics of ancient platforms: Akademiia Nauk SSSR Doklady, Geology Series No. 6, p. 57–90.

Simpson, L. C., 1979, Upper Gearyan and Lower Leonardian terrestrial vertebrate faunas of Oklahoma: Oklahoma Geology Notes, v. 39, p. 3–21.

Steel, R. J., 1974, Cornstone (fossil caliche)—its origin, stratigraphic and sedimentological importance in the New Red sandstone, western Scotland: Journal of Geology, v. 82, p. 351–369.

Watts, N. L., 1978, Displacive calcite: evidence from Recent and ancient calcretes: Geology, v. 6, p. 699–703.

Younger, P.; Donovan, R. N.; and Hounslow, A., 1986, Barite travertine at Zodletone Mountain in the Slick Hills, southwestern Oklahoma, *in* Donovan, R. N. (ed.), The Slick Hills of southwestern Oklahoma—fragments of an aulacogen?: Oklahoma Geological Survey Guidebook 24, p. 75–81.

Enhancement of "Limited" Log Suites Using Neural Networks

Jeff S. Arbogast
Applied Neural Networks, LLC
Denver Colorado

Mark L. Butler
Trueblood Resources, Inc.
Denver Colorado

Mark H. Franklin
Rocky Mountain Petrophysics
Aurora, Colorado

Keith A. Thompson
Amoco Exploration and Production Co.
Denver, Colorado

ABSTRACT.—The Artificial Neural Network (ANN) is a general-purpose exploration and development tool that allows an easy transformation of log data into any desired output parameter. Specific mathematical relationships between predictors (logs) and target values (rocks) need not be known. Even the relative importance of the predictors need not be known.

The authors believe that ANNs offer significant advantages over traditional regression-analysis methods. ANNs, for example, do not force predicted values to lie near mean values and better preserve original data variability. In addition, ANN software uses a feature called depth-interval sampling (DIS), which allows the ANN to incorporate and apply peripherally related data to the specific "training" points chosen by the investigator.

In this paper, ANN software is demonstrated to successfully enhance limited log suites in the Morrow channel-sandstone play in Beaver County, Oklahoma. ANNs are trained to recognize patterns using a complete, accurate, modern log suite in a control well. Using back-propagation network architecture and input data from adjacent wells with limited log suites (i.e., spontaneous potential and deep resistivity), the ANN successfully predicts log responses that would have occurred if modern logs had been run (i.e., gamma ray, density porosity, and acoustic travel time) and creates reliable synthetic logs.

In the example developed herein, stratigraphic correlation and petrophysical calculations were modified significantly by incorporating the ANN-synthesized control. The viability and accuracy of the ANN predictions were confirmed by known initial-potential and cumulative-production data.

INTRODUCTION

What Are Neural Networks?

The human brain is a biological neural network comprised of approximately 10 billion interconnected neurons. Artificial Neural Networks (ANNs) are relatively new data-processing mechanisms that transform input data into desired output data. This is accomplished by use of an internal architecture that is patterned after engineering maps and resultant descriptive equations describing the inner workings of the human nervous system. They have been shown to be effective in providing sophisticated data-processing solutions to complex and dynamic problems (i.e., problem diagnosis, decision making, prediction, and other classifying problems where both empirical pattern recognition is critical and precise algorithm-derived answers are either not required or are not easily obtained).

Because the ANN mimics the problem-solving process of the human brain, the network can apply knowl-

Arbogast, J. S.; Butler, M. L.; Franklin, M. H.; and Thompson, K. A., 2001, Enhancement of "limited" log suites using neural networks, *in* Johnson, K. S. (ed.), Pennsylvanian and Permian geology and petroleum in the southern Midcontinent, 1998 symposium: Oklahoma Geological Survey Circular 104, p. 185–195.

edge gained from past experience to new problems and situations. The ANN, in effect, uses a "training" experience to build a system of neurons and weight links that allow it to make new decisions, classifications, and predictions.

One of the most popular architectures of ANNs is the back-propagation neural network (BPNN), a supervised learning algorithm which is flexible, easy to use, and suitable to predicting problems where non-linear associations between input/output functions need to be learned from experience (i.e., no model is required). The BPNN "learns" by adjusting the interconnection weights between layers of neurons when the weight changes are back-propagated (sent backward) through the network after the output layer is evaluated (Fig. 1). Like the human brain, repeated training using good data will improve these associations. Accordingly, training using bad data will yield poor results.

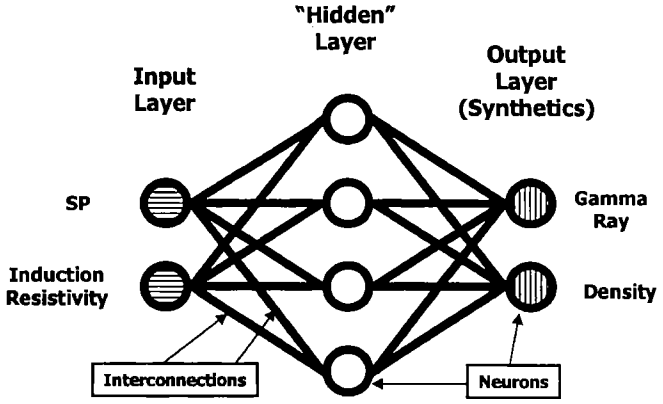

Figure 1. Diagram showing back-propagation neural-network architecture for generating synthetic gamma-ray and density-porosity logs from spontaneous-potential and deep-induction–resistivity logs.

Why Use Neural Networks to Tie Rocks to Logs?

The effective use of neural networks allows a relatively easy transformation of log data into any desired output parameter, as long as truthful relationships between input log curves and output log curves are used in the training and learning process. The specific mathematical relationships between predictors (logs) and target values (rocks or pseudo-logs) need not be known. Even the relative importance of the predictors need not be known. Complex, non-linear predictions are easily solved, and the ANN offers some advantages over traditional regression analysis. For example, the ANN does not require known algorithmic ties between input and output parameters (i.e., model equations). In addition, the ANN does not force predicted values to lie near mean values and thereby preserves raw-data variability.

Historical Use of Neural Networks in Petrophysical Problem Solving

The theory behind ANNs and their application in mineral identification from well logs was introduced by Halliburton Logging Services, Inc., and is discussed in some detail in Baldwin and others (1990). Specific applications relating to permeability prediction (especially in difficult-to-predict, mixed carbonate/clastic lithologies) are well presented in Thompson and others (1996) and in Rogers and others (1995). ANN applications to support log-derived, bulk-volume water calculations used to prospect for producible hydrocarbons are discussed in Franklin (2001).

METHODOLOGY

General

The ANN learns from good data as well as from bad data. Thus, it is important to train it on the best data available. Choosing appropriate predictors and values for training points is critical to the efficient and accurate use of ANNs in petrophysical evaluations and predictions. Prior to applying ANN software, all digital data must be cleaned up by using a high-quality, digital log-analysis program. Specifically, the investigator must be able to depth-shift, normalize, patch, and baseline-shift curves. In addition, "bad hole" areas must be identified (caliper and bulk density correction curves work well) and avoided when choosing ANN training points. The data clean-up and the choice of training examples requires experience with digital log data and a knowledge of the relationships between lithology and log response in the study area.

What to Use as Predictors

The investigator should use predictors (input curves) that are generally available in the vast majority of wells in the study area and that are known to relate to the observed output in the control (training) well. The investigator should never use a predictor that is believed to be irrelevant to the relationship.

Selecting Training Examples

The ANN will yield accurate results only if it learns from logical, accurate data relationships. The following tips will help make the best use of the predictive abilities of the ANNs:

- Provide examples only where you have good ties between predictors and target values.
- Select examples where you can "see" the relationship.
- Select examples over the range of values that you want predicted.
- Select examples only at points where logs are fully resolved.
- Do not select training examples where the predictors are very close to each other and the predicted output values are widely different.
- Include new examples only that contain new information.
- Do not include any training data that you have not examined in detail.

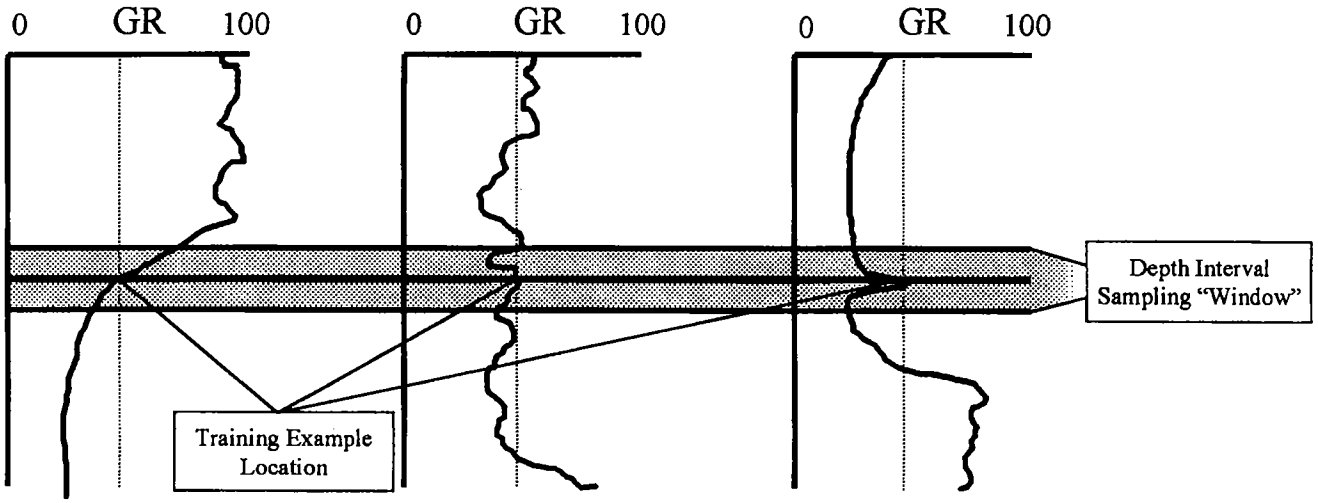

Figure 2. Depth interval sampling (shaded area) helps the ANN accommodate the fact that well logs are not perfectly resolved vertically (i.e., thin-bed effects, etc.). By incorporating data above and below the specific training example chosen, the ANN can be trained to learn the differences in the curve patterns in the three logs shown, even though the specific training examples chosen yield identical gamma-ray (GR) values (45 API Units).

Depth Interval Sampling

The authors recommend the use of ANN software that uses depth-interval sampling (DIS) on the input data. DIS allows the neural network to incorporate and apply peripherally related data to the selected training examples. In effect, this enhancement allows the ANN to compensate for the well-known fact that logs are not perfectly resolved vertically. An example of DIS structure and a potential application are shown in Figure 2.

Testing and Applying ANN Results

To evaluate the practical application limits of any given ANN in a study area the synthetic results should be compared to those recorded in modern logs in offset wells. If the ANN results match those shown by logs in an offset well, the investigator can be reasonably confident that the ANN can be applied to all wells located between the training well and the offset well. If the ANN results do not match those shown in an offset well, the investigator can simply retrain another ANN on the log data from the offset well and subsequently test its practical application limits.

BALKO (SOUTHEAST) AREA, BEAVER COUNTY, OKLAHOMA

The example used for this paper is the Balko Southeast area of Beaver County, Oklahoma, which is a mature oil and gas province that produces prolifically from Lower Pennsylvanian (upper Morrowan) point-bar sandstones (Fig. 3). Isopach and structure maps of the upper Morrow "A" and "B" sands show a southeast regional dip superimposed on discontinuous point-bar–sandstone deposits (Fig. 4) that are difficult to correlate.

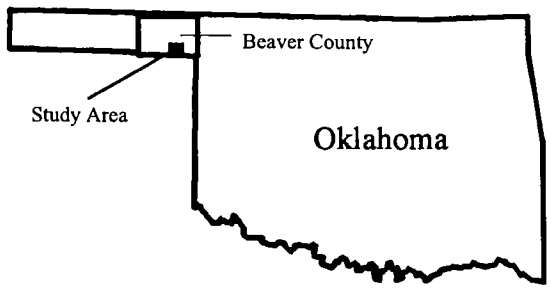

Figure 3. Index map of the study area.

The Problem

The investigator was tasked with correlating discontinuous point-bar sandstones and evaluating hydrocarbon prospects using data from both recent and older wells. Data constraints (old electric-log suites) in this and many other mature provinces severely limit accurate formation evaluation. ANNs were used successfully to evaluate hydrocarbon production potential in the upper Morrow "A" and "B" sandstones in four wells by generating synthetic bulk-density (porosity), gamma-ray, and acoustic (porosity) logs from the limited, older log data that were available. The addition of these synthetic data resulted in a more accurate evaluation of the older wells and facilitated prospect generation capabilities in the study area.

This paper shows the results derived from four wells in the study area to illustrate the application of ANN technology. (1) The Pounds #2-34 well had a relatively complete suite of modern logs, including gamma-ray (GR), spontaneous-potential (SP), deep-induction–resistivity (DIR), and density-porosity (DPL) logs. (2) The

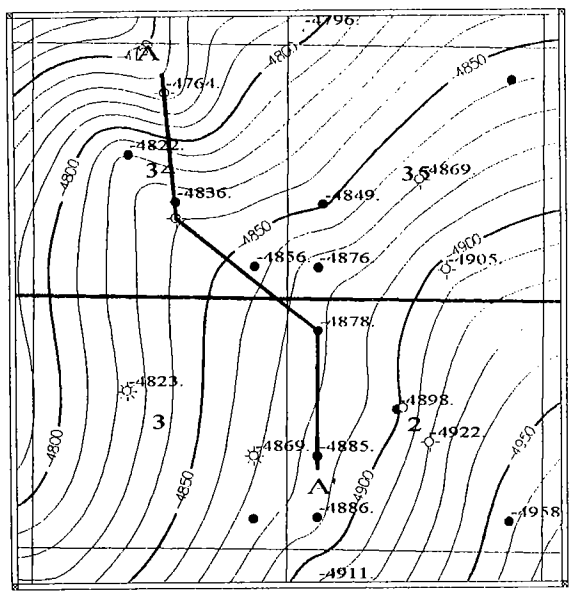

Structure Top Upper Morrow "A" Sand

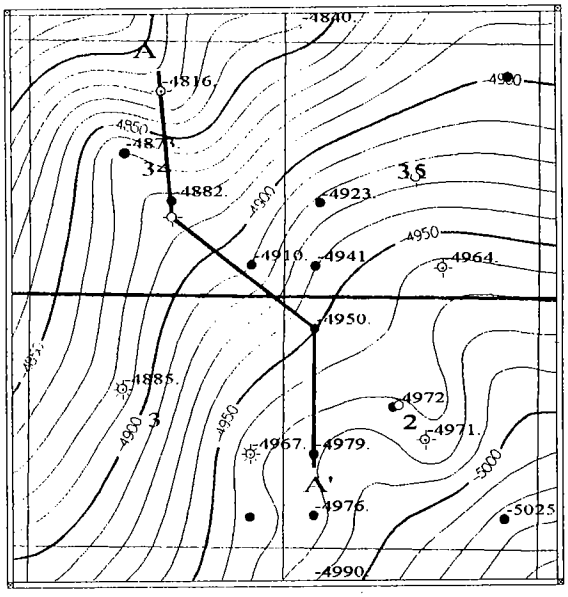

Structure Top Upper Morrow "B" Sand

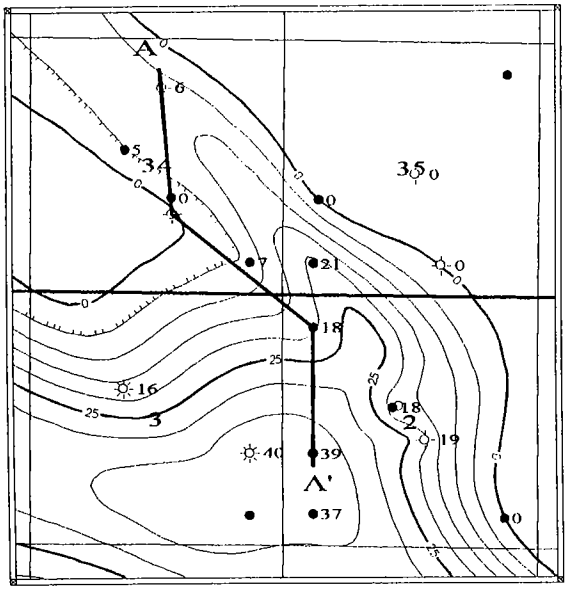

Isopach Gross Upper Morrow "A" Sand

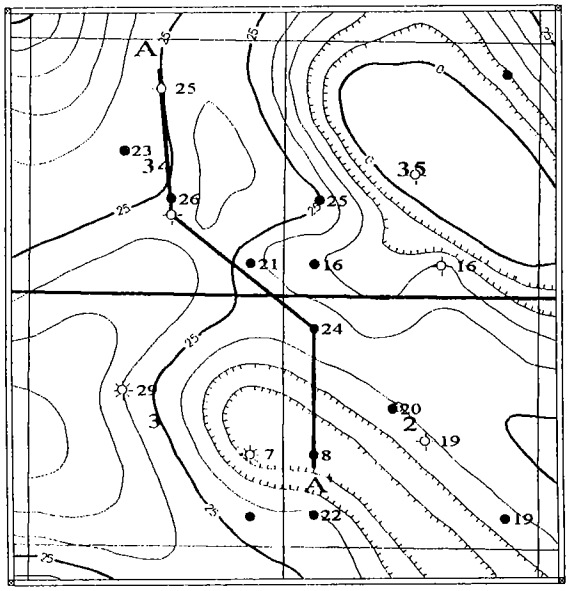

Isopach Gross Upper Morrow "B" Sand

Figure 4. Structure and isopach maps of the upper Morrow "A" and "B" sandstones (lithologic correlations strongly influenced by synthetic logs generated with ANN software). Contour lines in feet; structure contour lines in feet below mean sea level.

Schlehofer #1 well had only GR, SP, and DIR logs. (3) The #1 Elnora Schlehofer had only SP, DIR, and PSL (acoustic-porosity) logs. (4) The #1 Helen Bradley had only the SP and DIR logs.

Training the ANN "Brain"

The Pounds #2-34 well had a complete, high-quality log suite. Therefore, it was the clear choice for the training well. Four neural-net training examples (Fig. 5) were selected (three in the point-bar sandstone and one in the underlying shale). These four training examples allowed the DIS-supported ANN to learn the interrelationships among all four actual log curves.

After the ANN was trained, its predictions were tested or ground-truthed. The ANN predictions were checked by comparing its *synthetic* gamma-ray and density-porosity logs (derived by using only the SP and DIR logs) with the pre-existing, *recorded* gamma-ray and density-porosity logs (Fig. 5). A second ANN was applied (using only the DIR curve) to generate a synthetic acoustic-porosity log. The successful match

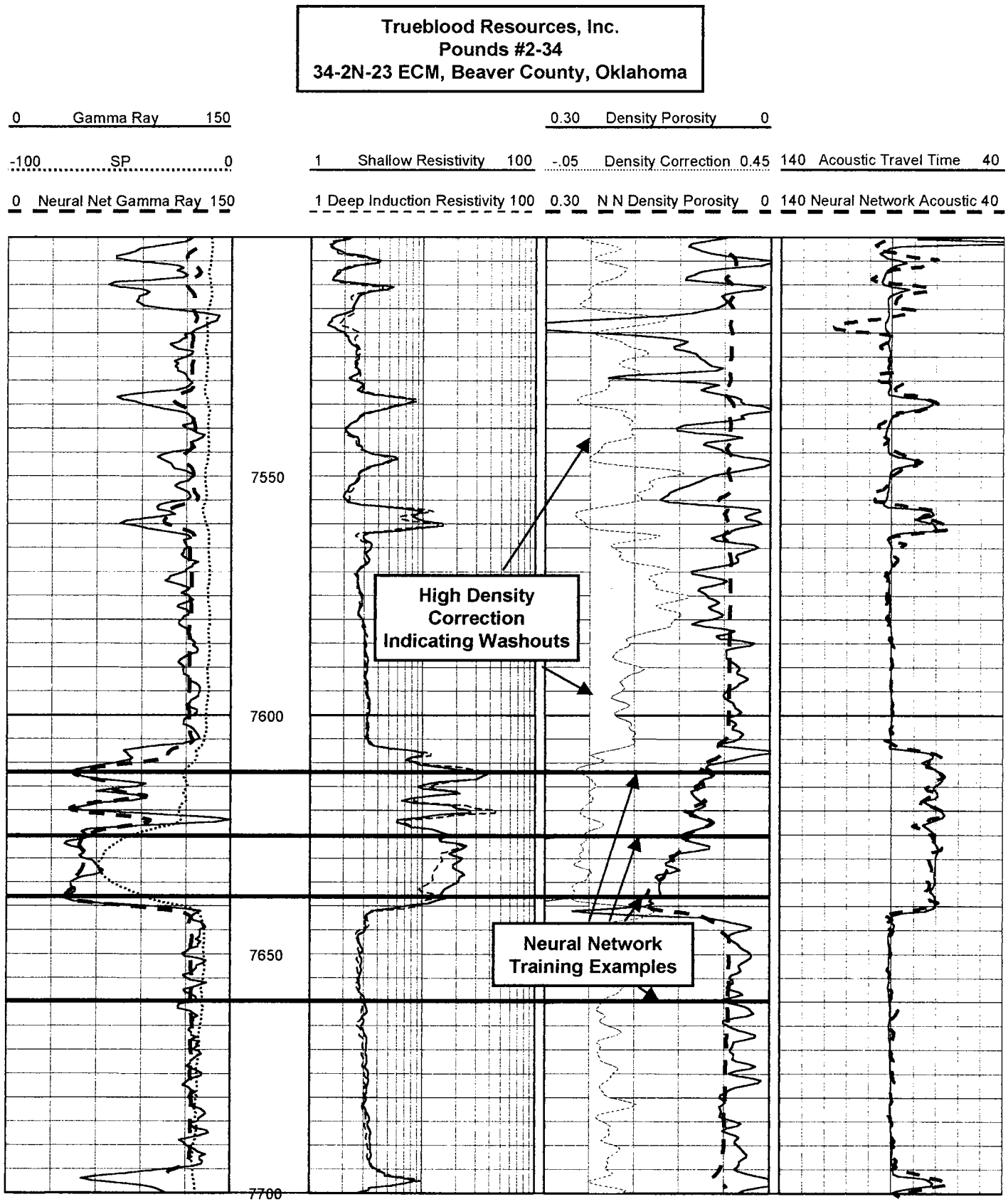

Figure 5. Comparison of recorded logs and neural-network–derived synthetic logs (bold, dashed curves) in the Trueblood Resources, Inc., Pounds #2-34 well used to train the ANN. Depth in feet below mean sea level.

between the ANN-generated synthetic logs and the actual logs in the training well justified applying the ANN to other wells in the study area.

Applying the ANN "Brain" to Other Wells

The neural-net software applied the ANN that was generated in the training well to the Schlehofer #1 well (Fig. 6) and produced a synthetic gamma-ray curve (bold) that was tested against an actual gamma-ray curve run in the well. The two curves overlaid nearly perfectly. The ANN-generated, synthetic, neural-net density-porosity log yielded values ranging from 10% to 14% in the "A" sandstone. Before applying ANN technology to this well there was no porosity control in this well bore and no data from which to calculate water saturation (Sw) or bulk-volume water (BVW).

Next, the ANN was applied to the #1 Elnora Schlehofer well to yield a synthetic gamma-ray curve and a synthetic density-porosity curve (Fig. 7). The synthetic gamma-ray curve better defines both the "A" and "B" point-bar sandstones (especially the upper lobe of the "B" sandstone). In the point-bar sandstones, the synthetic density-porosity curve nearly overlays the recorded acoustic-log–derived porosity curve (density-porosity and acoustic-porosity values are expected to diverge widely in the shales).

Finally, the ANN was applied to the #1 Helen Bradley well to yield a synthetic gamma-ray log and a synthetic density-porosity log that enhanced thin-bed resolution in the "B" sandstone and indicated up to 20% porosity in the massive "A" sandstone.

Cross-section A–A′ (Fig. 8) was correlated initially using only the logs that were actually run on the four wells. The "A" sandstone appeared to be relatively continuous in all four wells, and the "B" sandstone appeared to be absent in the Pounds #2-34 and the #1 Schlehofer wells. After the ANN was applied to all four wells and synthetic gamma-ray and density-porosity logs were generated, cross-section A–A′ yielded a significantly different interpretation (Fig. 9).

With accurate gamma-ray and density-porosity logs in all four wells, hydrocarbon producibility was evaluated. The Archie equation (with parameters appropriate for the rocks in the study area), was used to calculate water saturation (Sw). Bulk-volume water (BVW), the amount of water in the reservoir expressed as a fraction of total reservoir volume, was then calculated. When used with porosity, BVW is commonly a better indicator of producibility than is Sw, especially in tighter reservoirs.

The "A" sandstone in the Helen Bradley #1 well (average BVW value of 2.5) initially produced 1,278 barrels of oil per day (BOPD) with a cumulative production of 215 thousand barrels of oil (MBO) (Fig. 10). The "A" sandstone in the E. Schlehofer #1 well (average BVW of 4.0) initially produced 276 BOPD plus 3.7 million cubic feet of gas per day (MMCFD) and cumulatively produced 139 MBO. The "B" sandstone in the Schlehofer #1 well (average BVW value of 5.0) initially produced 120 BOPD but quickly watered out with a cumulative production of only 7,317 BO. The "B" sandstone in the Pounds #2-34 well (average BVW value of 6.0) was drill-stem tested and shown to be water productive, recovering 110 ft of muddy water.

A new, qualitative BVW "quick-look" technique is discussed in detail in Franklin (2000). He observed that the "shape" of the BVW curve generally conforms to the shape of the gamma-ray curve in hydrocarbon-productive clastic reservoirs. Conversely, in water-productive reservoirs, the shape of the BVW curve varies significantly from that of the gamma-ray curve. This relationship is based on the theory that the gamma-ray curve indicates clay content and "fines" that account for "bound" (irreducible) water in the reservoir. The BVW curve matches the shape of the gamma-ray curve where the only water in the reservoir is irreducible. Where movable water is present, these curves do not appear to track.

A comparison between the BVW/gamma-ray relationship in the water-productive "B" sandstone of the Pounds #2-34 well and the BVW/gamma-ray relationship (based on neural-net–derived synthetic-density porosity and gamma-ray curves) in the hydrocarbon-productive "A" sandstone of the Elnora Schlehofer #1 well supports Franklin's conclusions (Fig. 10).

The additional information provided by the ANN will have a significant impact on future prospect evaluation in the study area.

OTHER APPLICATIONS

The ANN is a general-purpose tool that can be applied to solving any complex, non-linear, dynamic petrophysical problem. A few of the more obvious applications include:

- Producing synthetic logs (i.e., acoustic logs to tie two- and three-dimensional seismic data).
- Interpreting old E-logs (after using inversion software).
- Synthesizing special log measurements (NMR, porosity, bulk-volume irreducible fluids).
- Synthesizing properties measured from cores or cuttings.
- Total organic carbon.
- Shear-wave acoustic velocity.
- Capillary-pressure properties.
- Total fluid-flow capacity.
- Lithology or rock-type classification.
- Expected production rates.

CONCLUSIONS

The ANN is a general-purpose data-processing tool that can be applied to solving any complex, non-linear, dynamic petrophysical problem provided that the ANN is trained on accurate digital data that reflect "truthful" input/output relationships. The ANN allows an easy transformation of log data into any desired output parameter. Specific mathematical relationships between predictors (logs) and target values (rocks) need not be known. Even the relative importance of the predictors need not be known.

The specific applications discussed in this paper rep-

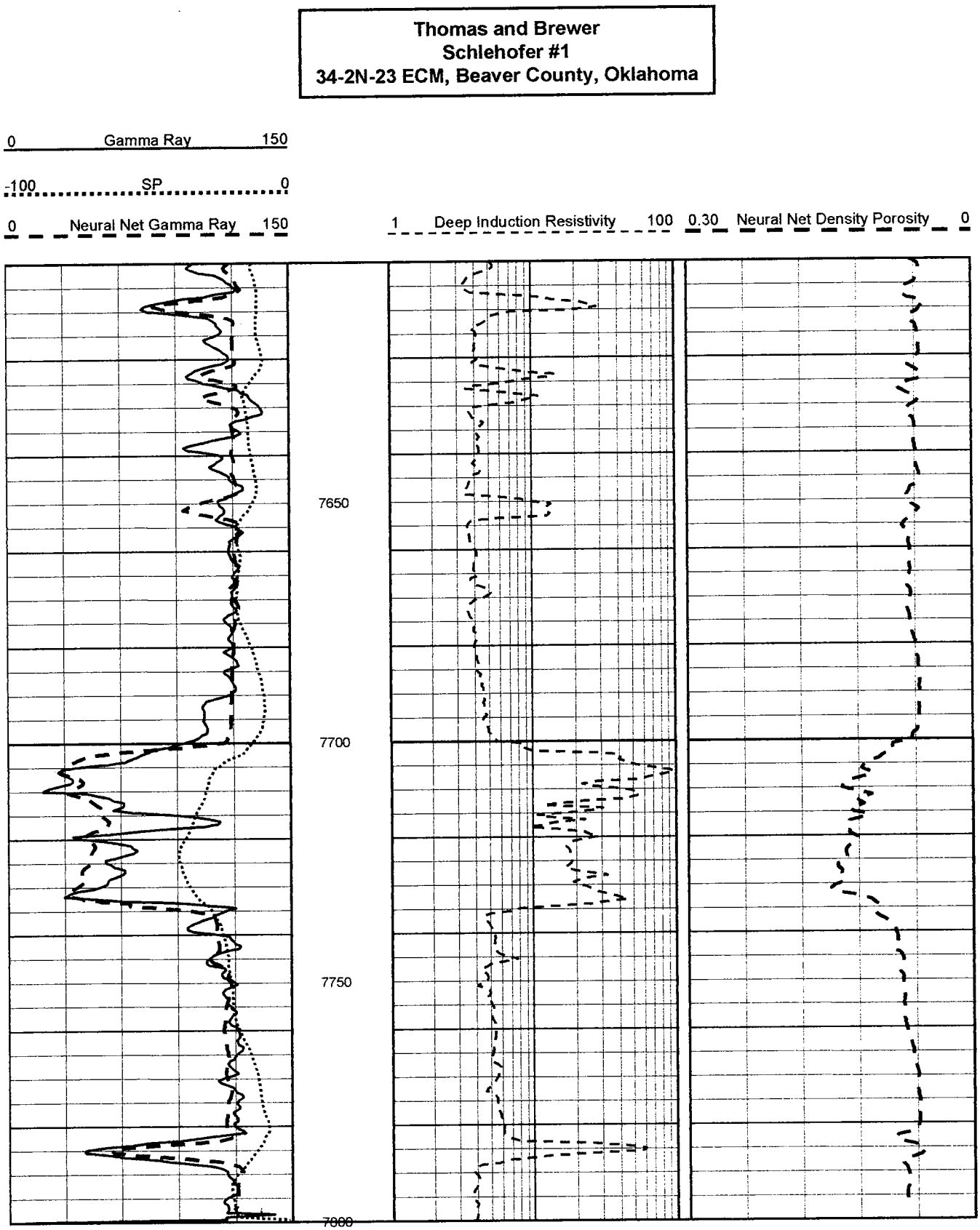

Figure 6. Neural-network–derived density-porosity log (bold, dashed curves in Track 3) for Thomas and Brewer, Schlehofer #1 well, based only on input data from spontaneous-potential and deep-induction–resistivity logs. Neural-network–derived gamma-ray log (bold, dashed curve in Track 1) is also based on data from spontaneous-potential and deep-induction–resistivity logs and is compared with an actual recorded gamma-ray log in the well as a check on ANN reliability. Depth in feet below mean sea level.

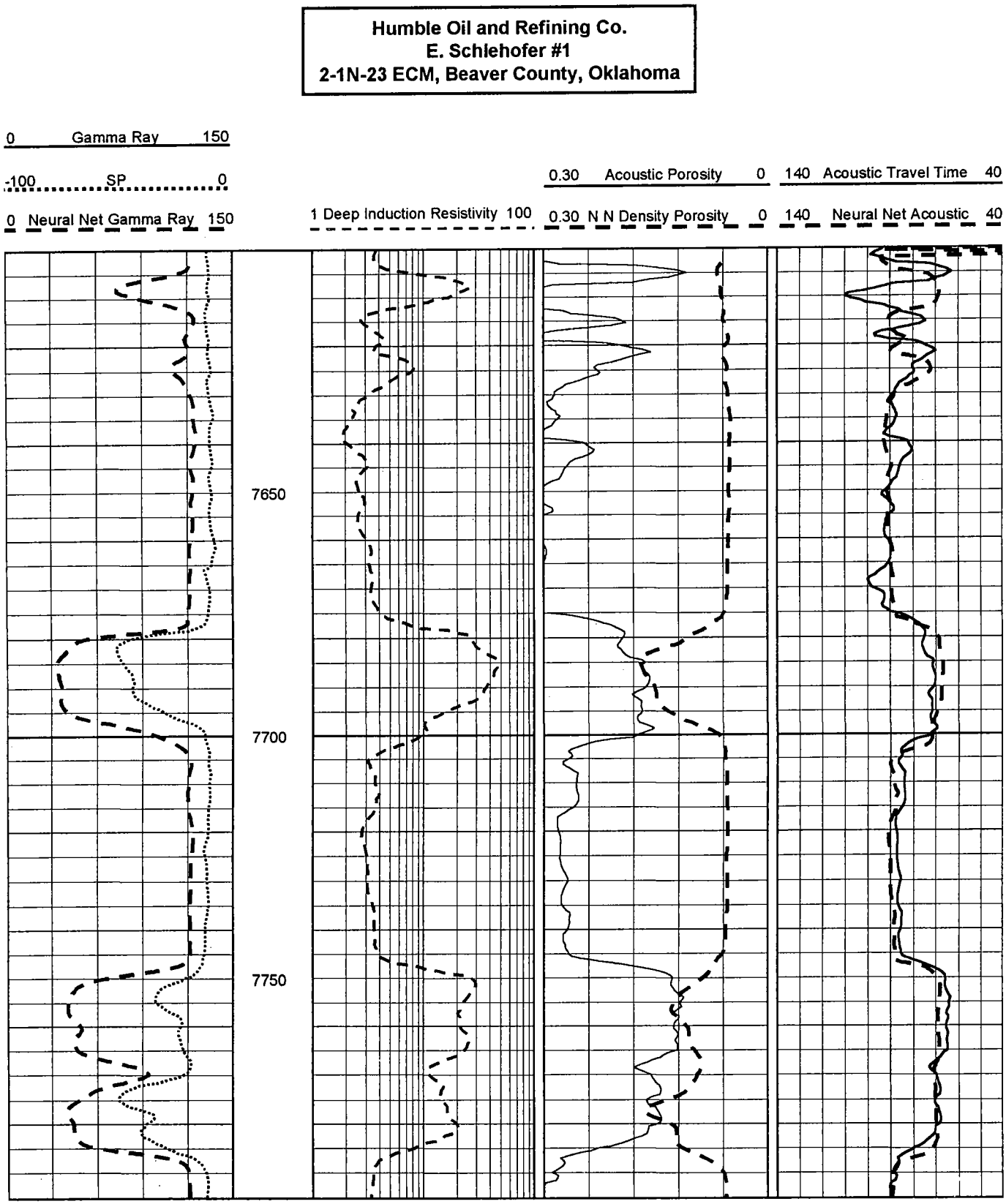

Figure 7. Neural-network–derived gamma-ray, density-porosity, and acoustic logs (bold, dashed curves in Tracks 1, 3, and 4, respectively) based only on input data from spontaneous-potential and deep-induction–resistivity logs for Humble Oil and Refining Co., E. Schlehofer #1 well. A recorded acoustic log in Track 4 is used to check the ANN synthetic acoustic log. Depth in feet below mean sea level. Note how well the ANN-derived synthetic-density–porosity log and the recorded acoustic-porosity log agree in the clean sandstones in Track 3 (acoustic-porosity and density-porosity logs are expected to differ widely in the shale sections).

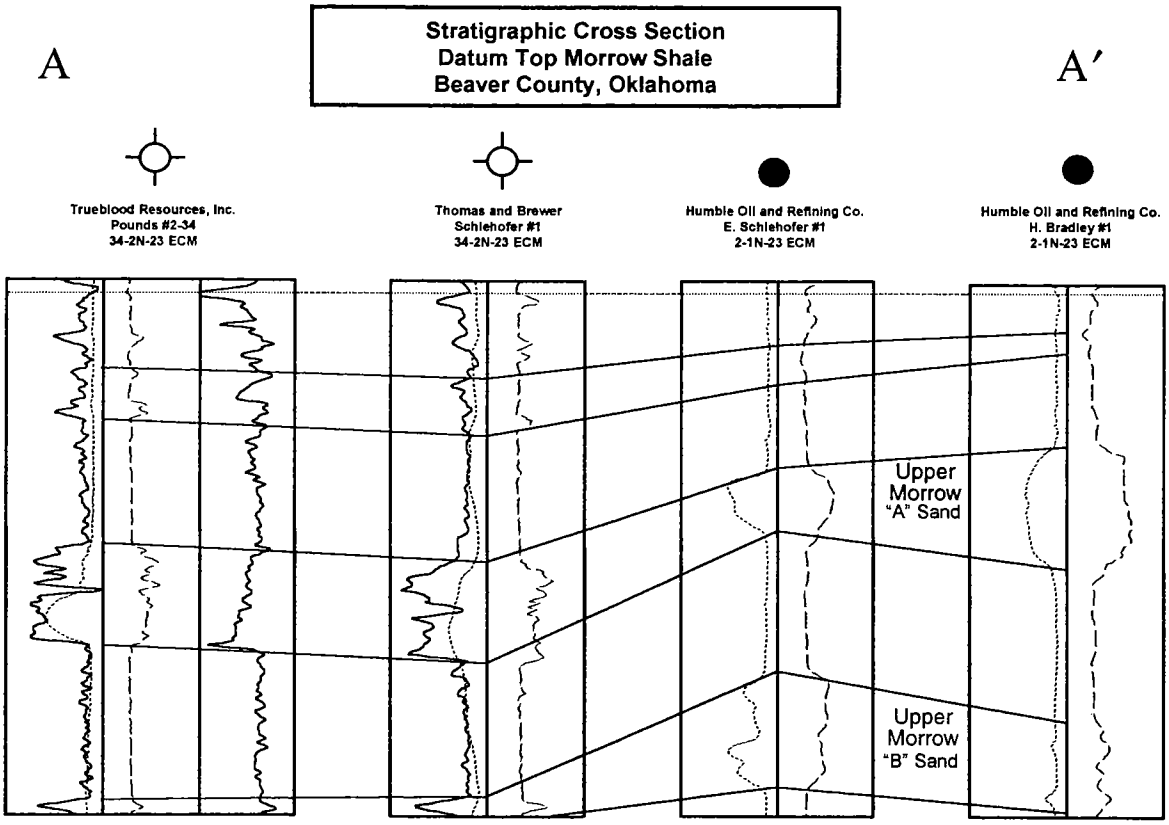

Figure 8. Cross section A–A′ using only the original, recorded logs on the four wells. Locations of wells and cross section shown in Figure 4.

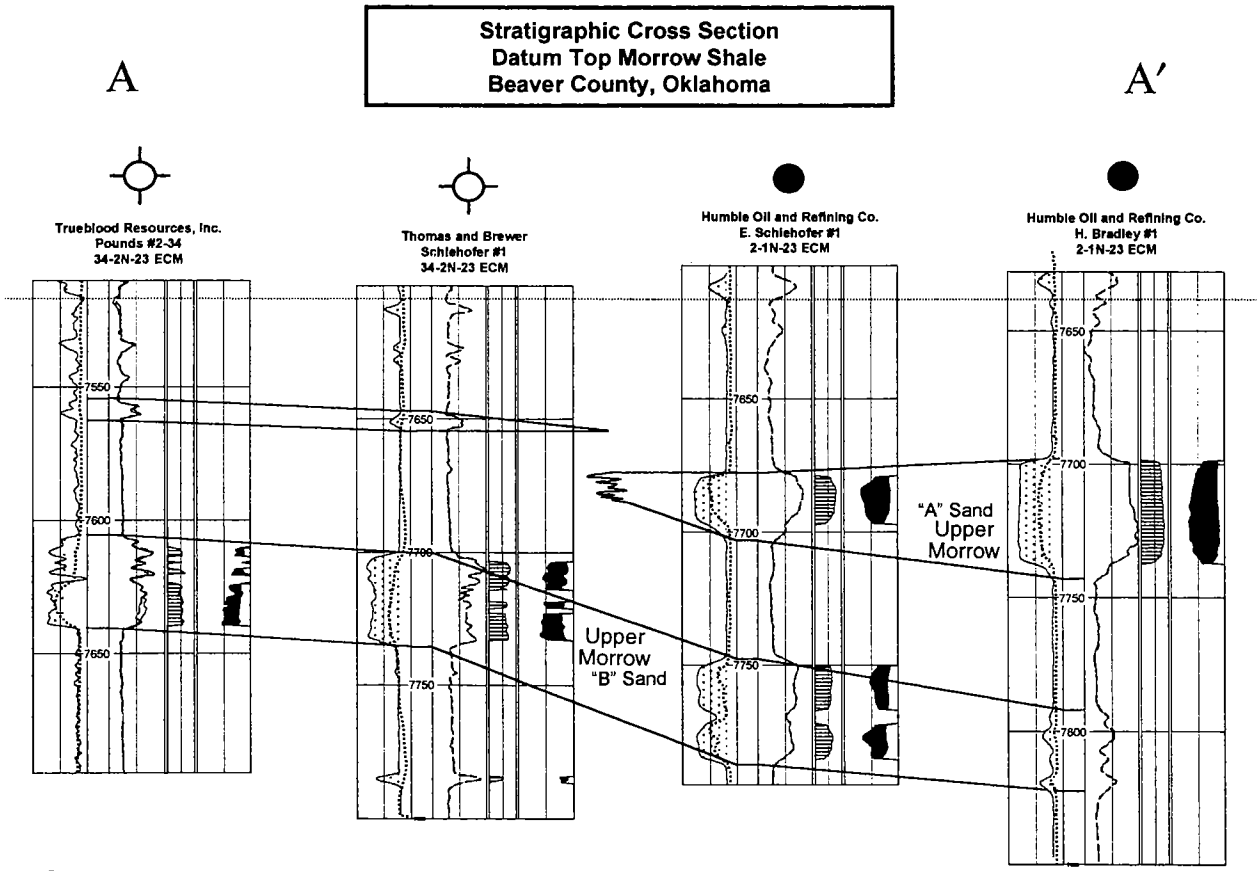

Figure 9. Cross section A–A′ as interpreted using neural-network–derived logs and resultant petrophysical calculations in the four wells. Locations of wells and cross section shown in Figure 4.

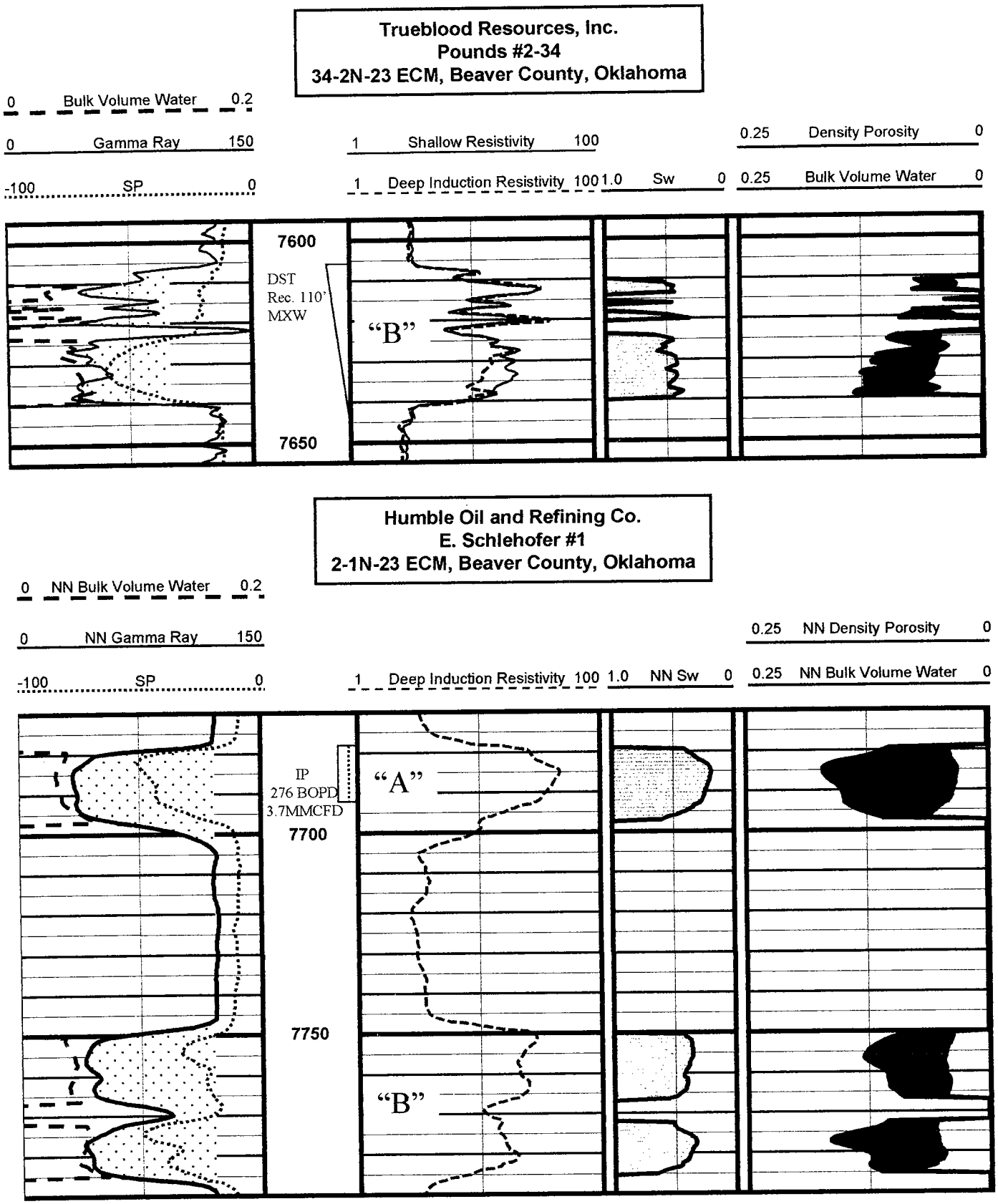

Figure 10. Water-saturation (Sw) and bulk-volume water (BVW) representations using recorded logs on the ANN training well (upper) and neural-network–derived synthetic logs (lower). Note that Sw and BVW could not have been calculated without the values provided by the ANN-derived synthetic logs. Upper Morrow "A" and "B" sands shown only by "A" and "B". Depths in feet below mean sea level. DST—drill stem test; MXW—mud cut water; IP—initial production; BOPD—barrels of oil per day; MMCFD—million cubic feet of gas per day.

resent only the tip of the iceberg regarding the potential use of this very powerful formation evaluation and exploration tool. The effective use of neural-network technology need not be confined to major oil companies and large service companies. User-friendly, modestly priced software has recently become available, which allows virtually anyone with a modern personal computer (and the skills to work with digital log-analysis software) to effectively apply ANN technology to petrophysical-problem solving, and petrophysical consulting companies specializing in neural-network applications are available to the industry.

REFERENCES CITED

Baldwin, J. L.; Bateman, R. M.; and Wheatley, C. L., 1990, Application of a neural network to the problem of mineral identification from well logs: The Log Analyst, September–October, p. 279–293.

Franklin, M. H., 2001 [this volume], Hydrocarbon prospecting using "quick-look" bulk-volume water, *in* Johnson, K. S. (ed.), Pennsylvania and Permian geology and petroleum in the southern Midcontinent, 1998 symposium: Oklahoma Geological Survey Circular 104, p. 197–205.

Rogers, S. J.; Chen, H. C.; Kopaska-Merkel, D. C.; and Fang, J. H., 1995, Predicting permeability from porosity using artificial neural networks: American Association of Petroleum Geologists Bulletin, v. 79, p. 1786–1797.

Thompson, K. A.; Franklin, M. H.; and Olson, T. M., 1996, Use of artificial neural networks to predict permeability in Hugoton field [abstract]: American Association of Petroleum Geologists 1996 Annual Convention Official Program, v. 5, p. A-139.

Hydrocarbon Prospecting Using "Quick-Look" Bulk-Volume Water

Mark H. Franklin
Rocky Mountain Petrophysics, LLC
Denver, Colorado

ABSTRACT.—Bulk-volume water (BVW) is the amount of water in a formation expressed as a fraction of the total volume. BVW-analysis techniques provide a convenient method for identifying producible water and hydrocarbons using wireline logs. Traditional applications are reviewed briefly and a new, "quick-look" bulk-volume water (QLBVW) technique is introduced.

Previous BVW analysis required the generation of cross-plots of porosity and water saturation. Its usefulness was limited in complex and inconsistent lithologies. Preferable techniques, including QLBVW, use depth plots of measured and calculated logs to quickly predict whether a formation will produce water, hydrocarbons, both, or neither.

The QLBVW technique accommodates complex and changing lithologies and provides higher resolution in "simple" and consistent lithologies. The QLBVW technique plots gamma-ray (GR) and BVW curves together (versus depth) and compares the relative shapes of these curves. A similarity in the respective shapes of GR and BVW curves implies no movable water. QLBVW analyses provide quick assessments of movable water, even when porosity logs are not available. By synthesizing GR curves using neural networks, this technique can be extended to older wells with "limited" log suites.

METHODOLOGY

What is Bulk-Volume Water?

Bulk-volume water (BVW) is a log-derived value representing the amount of water in a formation. Quantitatively, BVW is the product of porosity and water saturation:

$$BVW = \Phi \times Sw$$

Where:
Φ = Log-derived porosity
Sw = Log-derived water saturation

For example:

If $\Phi = 10\%$ and $Sw = 45\%$,
Then, $BVW = (0.10) \times (0.45) = 0.045$ or 4.5%.

How Is BVW Used?

Geoscientists commonly use log-derived–BVW techniques to determine movable fluids in rocks and to classify petrophysical rock types. Morris and Biggs (1967) noted that, in a homogeneous rock with no movable water, BVW is constant. Conversely, BVW varies with porosity in formations with movable water. Therefore, in many homogeneous reservoir rocks, the "activity" (the change in shapes and values) of the BVW curve alone may be an indication of the type of movable fluid present.

For illustration purposes, consider a porous, permeable, water-wet reservoir that contains both movable oil and water (Fig. 1). The buoyancy of hydrocarbon in water produces a zone of irreducible water at the top of the formation in which the only movable fluid is hydrocarbon. Beneath the hydrocarbon-only productive zone is a transition zone, where both hydrocarbon and water are producible in varying amounts. Below the transition zone only water will be produced.

In a reservoir above the transition zone, water saturation (Sw) is equal to irreducible-water saturation (Sw_{irr}). Irreducible-water saturation, however, is not constant; it changes with porosity. Water-cut can be difficult to interpret from Sw. For example, Sw_{irr} can be a large number (i.e., 70%) for a reservoir with high clay content (or microporosity) that produces water-free hydrocarbons. Sw can also be misleading because Sw also changes with porosity (even in zones with no movable water). The application of BVW techniques helps distinguish movable from nonmovable water.

Franklin, M. H., 2001, Hydrocarbon prospecting using "quick-look" bulk-volume water, *in* Johnson, K. S. (ed.), Pennsylvanian and Permian geology and petroleum in the southern Midcontinent, 1998 symposium: Oklahoma Geological Survey Circular 104, p. 197–205.

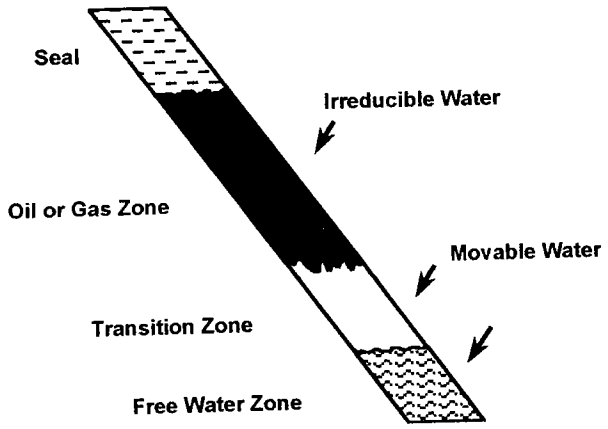

Figure 1. Schematic diagram of an oil/water reservoir.

Example: Oil Creek Sandstone, Garvin County, Oklahoma

Wireline logs from an Oil Creek Sandstone well in West Whitebead Field in Garvin County, Oklahoma, are shown in Figure 2. The Oil Creek sandstone is a relatively homogeneous, clean, quartzarenite encased in nonporous shales. The display format of this log *vs.* depth plot is important in the application of this technique. Most of the "raw," recorded logs are displayed on the first three tracks (gamma-ray, SP, caliper, resistivity, and porosity curves). Calculated curves, such as Archie Sw, effective porosity, and BVW are shown on the two right-hand tracks. This format is beneficial because the raw curves provide quality control for the calculated results and allow a visual comparison of many different measurements. This format offers significant advantages over two-dimensional cross-plots (which allow less than five different quantities to be viewed simultaneously) and facilitates the visualization of hydrocarbon/water systems, especially when looking at multiple wells in a structural cross section.

The Archie equation is adequate, in most cases, to calculate Sw and BVW. Barring conductive minerals, the total water component reflected in Sw and BVW analyses can be used to differentiate the movable from nonmovable fractions of water in a reservoir. The power of this technique is based on the ability of the analyst to quickly "get on paper" the simple curves needed for BVW interpretation.

In Figure 2, this interpretation of "classic" BVW analysis shows irreducible water at depths between 6,010 and 6,034 ft. In this interval, BVW calculated from logs has a "flat" shape and is equal to irreducible bulk-volume water (BVW_{irr}), which is approximately 0.05 for this rock type. The flat shape of the BVW curve at the top of the sandstone means that water content is at an irreducible level, compared to varying amounts of water in the reservoir below 6,034 ft.

Water-free hydrocarbon (oil) would be produced from the interval above 6,034 ft. From 6,034 to 6,050 ft the shape of BVW "curve" begins to follow that of the porosity curve, indicating the transition zone. Both oil and water would be produced from this interval. From 6,050 ft to the base of the zone at 6,114 ft, BVW is approximately equal to porosity and is much higher than BVW_{irr}, indicating producible water. In this example, BVW analysis discouraged completion attempts in the transition zone.

How Does BVW Handle Heterogeneous Lithology?

Most reservoir-characterization problems are difficult because they involve heterogeneous lithologies (especially clay content variability). BVW analysis is critical in predicting movable fluids in changing rock types where:

$$BVW_{irr} = \Phi \times Sw_{irr}.$$

The irreducible bulk-volume water (BVW_{irr}) is a property of the rock that is related to the permeability of the rock (Fertl and Vercellino, 1978). It may differ from BVW, which is a log-derived quantity indicating the total amount of water in a reservoir including both movable and nonmovable water.

If a reservoir is water-wet and has a homogeneous pore structure throughout, BVW_{irr} is fixed, because it is related to the pore structure of the rock and the ability of the rock to hold water by capillary force against the buoyancy force of hydrocarbons—hence, the correlation with permeability. Under these conditions (homogeneous pore structure and water-wet), BVW_{irr} remains constant even as porosity increases because the larger pore spaces will be occupied by either movable water or movable hydrocarbons.

Commonly, BVW_{irr} is constant even in adjacent formations and even when lithologies change because BVW_{irr} occupies the small spaces in the rocks and these spaces commonly result from shared diagenetic phenomena. Historically, investigators experienced only limited success in using these "traditional" BVW methods in inconsistent lithologies.

A New, Qualitative "Quick Look" Technique

A new, qualitative BVW technique can help evaluate difficult and complex lithologies. For example, the general "shape" of the BVW curve conforms to the shape of the GR curve in hydrocarbon-productive reservoirs with no movable water. Conversely, in water productive reservoirs, the shape of the BVW curve varies significantly from that of the GR curve. The theory that the GR curve is indicating clay content and the "fines" that account for "bound" water in the reservoir explain this empirically derived relationship. The BVW curve "tracks" the shape of the GR curve when the only water present in the reservoir is irreducible. In other words, these curves track where all water in the formation is tied to the lithology.

Where movable water is present, these curves do not appear to track. In a water-producing formation, BVW will commonly increase in value as GR decreases. To view this effect, display the gamma-ray and BVW curves together on the strip log, scaling them so that they track each other in productive zones. In Figure 2,

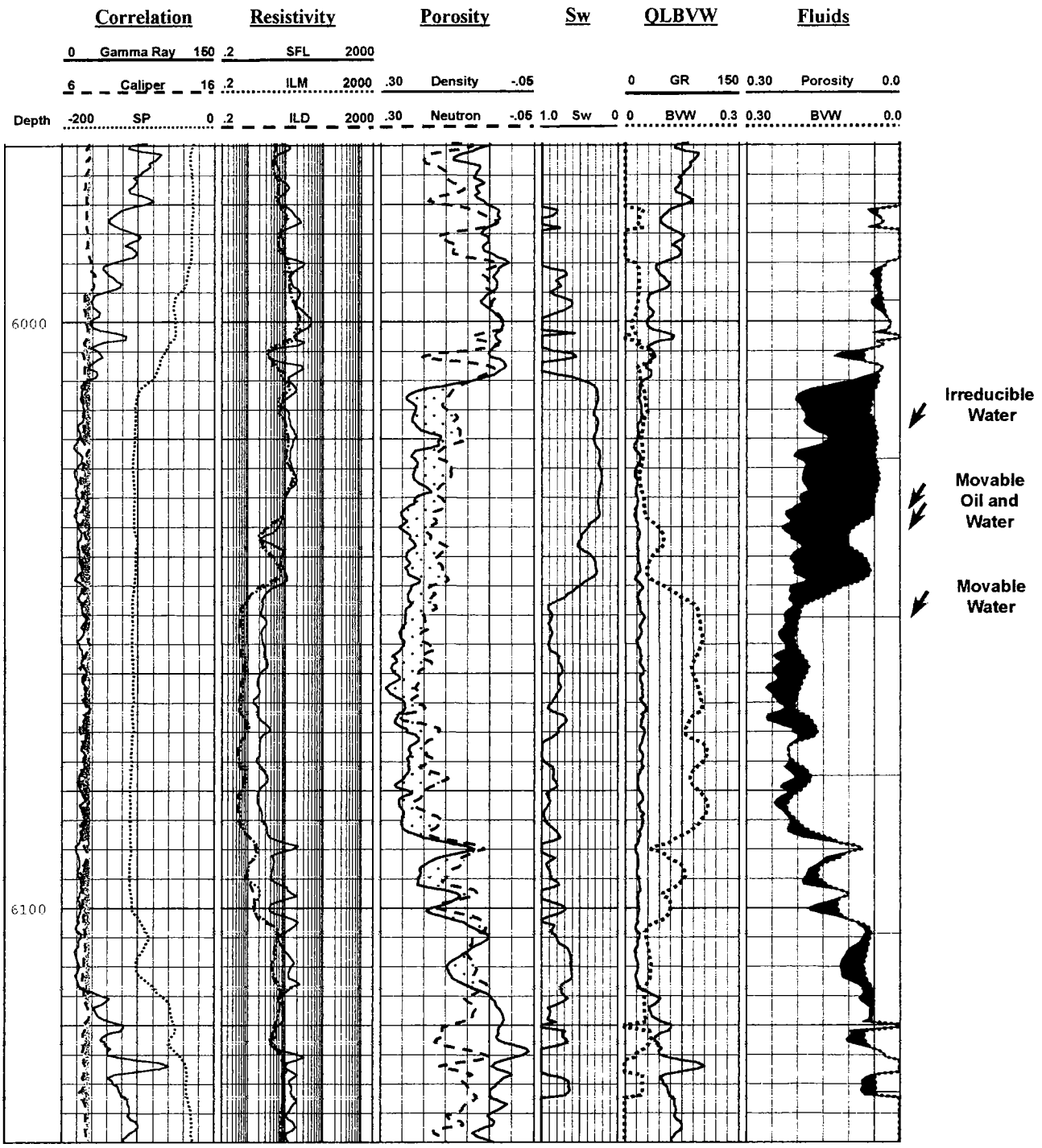

Figure 2. Example of bulk-volume water calculated in a homogeneous sandstone oil/water reservoir in the Lario Oil and Gas West Whitehead #2-2 (sidetrack) in Garvin County, Oklahoma. Depth in feet. Abbreviations: QLBVW—"quick-look" bulk-volume water, BVW—bulk-volume water, GR—gamma ray.

these curves are displayed in the fifth track, called "QLBVW." The scales used in Figure 2 work well for most sandstones. Notice the similar curve shapes (GR to BVW) in the irreducible-water zone above 6,030 ft. Below 6,030 ft, these curves no longer track. This curve separation indicates movable water.

This technique may be used even when porosity information is unavailable, because BVW is dependent primarily on Rt (the resistivity of the uninvaded formation). The Archie equation for water saturation illustrates this dependency. The Archie equation is commonly expressed as:

$$Sw = \sqrt[n]{\frac{a \cdot Rw}{\Phi^m \cdot Rt}}$$

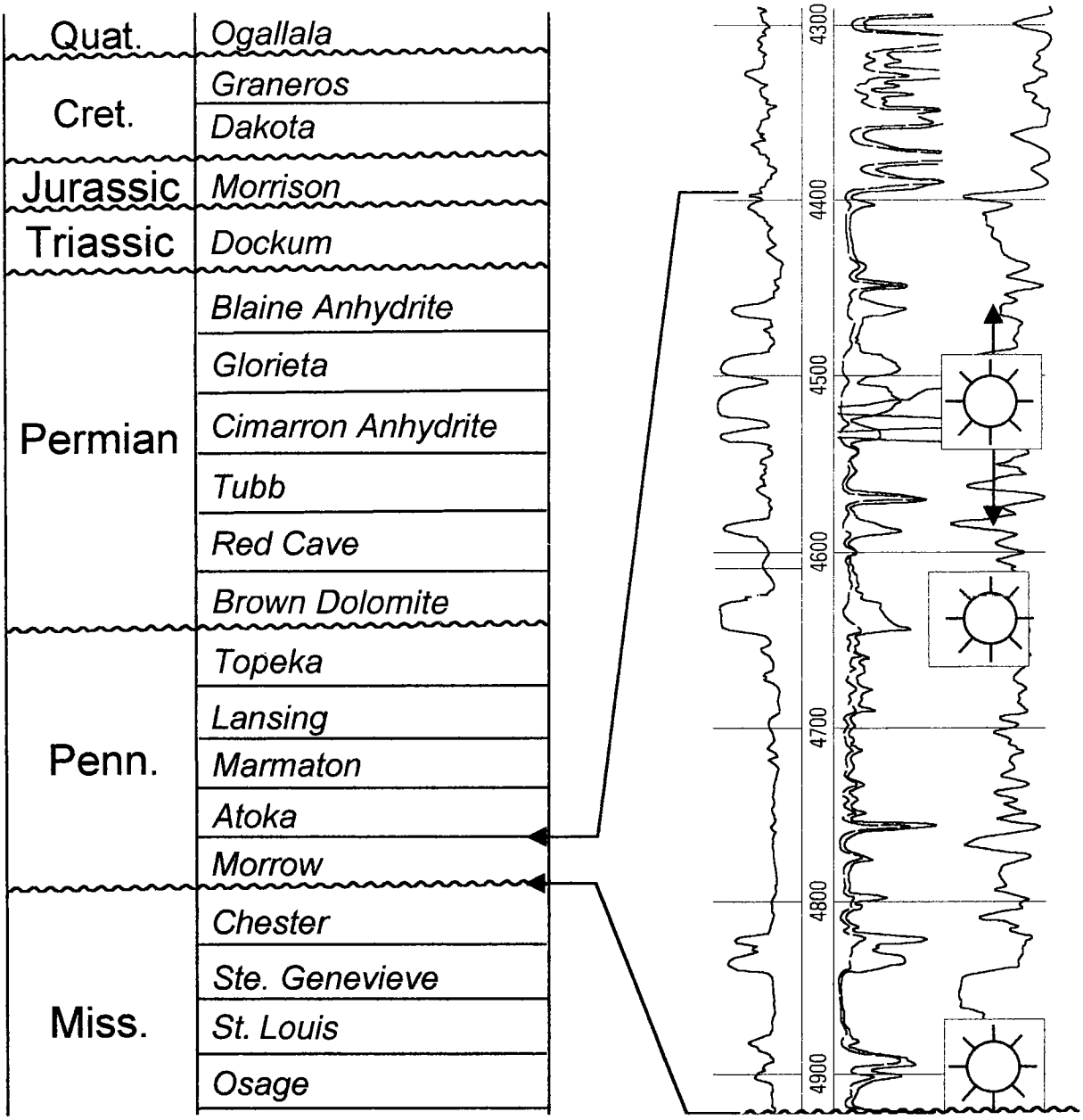

Figure 3. Stratigraphic section and type log for Morrowan interval, southwestern Kansas. Depth in feet.

where Φ is porosity. For this demonstration, assume that Archie parameters "a", "m", "n", and "Rw" are constant and "m" is equal to "n." This equation reduces to:

$$Sw = f\left(\frac{1}{\Phi \cdot \sqrt[n]{Rt}}\right)$$

By multiplying Sw by porosity to obtain BVW, the equation reduces again to show that—under these assumptions—BVW is dependent only on resisitivity.

$$Sw \cdot \Phi = BVW = f\left(\frac{1}{\sqrt[n]{Rt}}\right)$$

USING QLBVW TO INDICATE PRODUCIBILITY

An example from the Morrow Sandstone in southwest Kansas documents the successful application of this new, QLBVW technique. Morrowan rocks of the far western Midcontinent region produce hydrocarbons from incised-valley networks that trend southeastward toward the Anadarko basin in Oklahoma (Figs. 3, 4). During the Morrowan, the network drained the surrounding highlands including the Amarillo-Wichita uplift to the south, the Sierra Grande uplift to the southwest, the Ancestral Rockies to the northwest, the Transcontinental arch to the north, and the central Kansas uplift to the northeast.

The study area is located on the south plunge of the

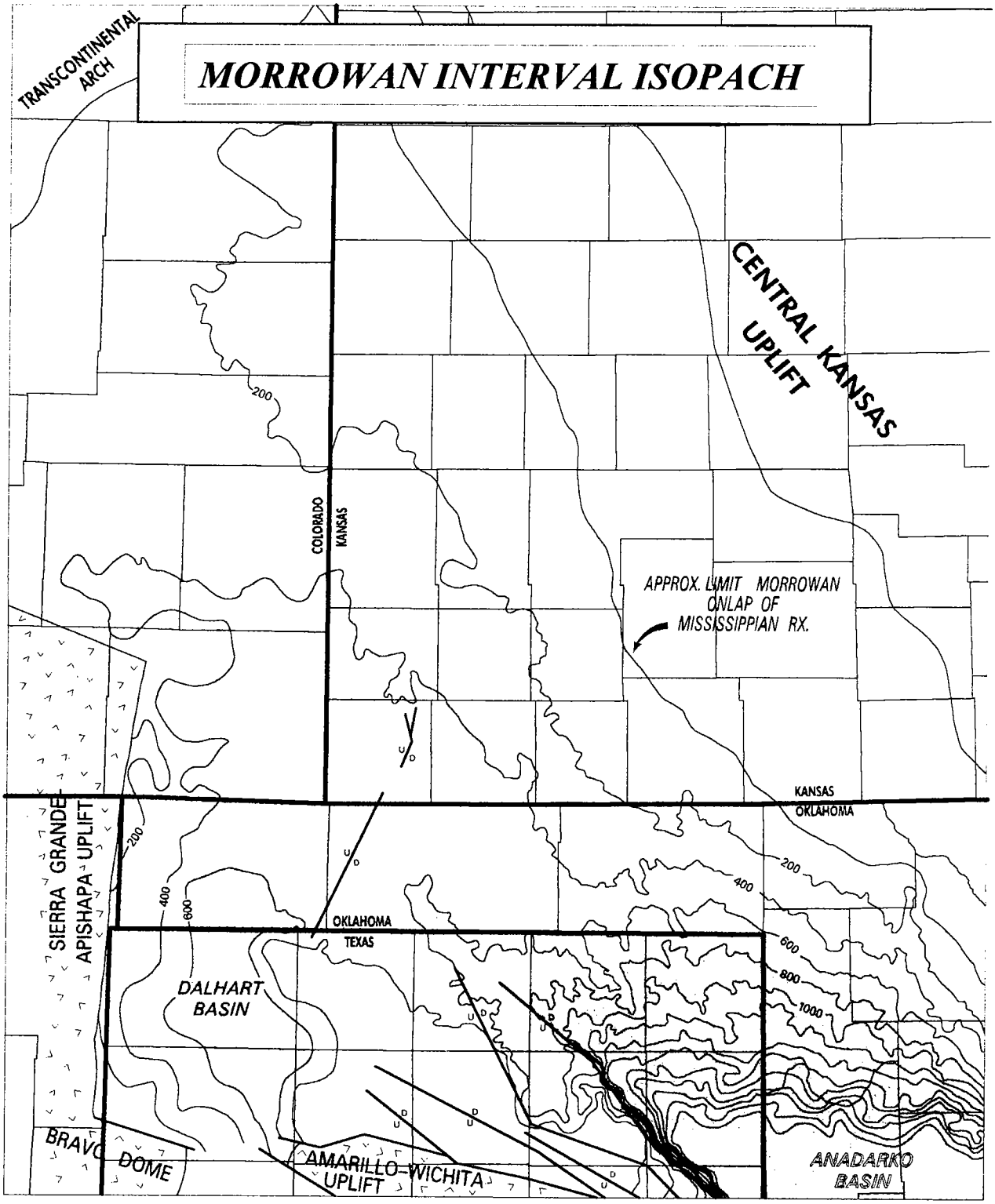

Figure 4. Isopach map (in feet) of Morrowan interval, southwestern Kansas and surrounding area.

Keyes dome in eastern Cimarron County, Oklahoma. Three distinct packages are productive from the Morrowan interval, including the basal Keyes interval (the main productive interval at Keyes dome), a mid-Morrowan incised valley that trends generally east–west, and the upper Morrowan stacked-channel sequence that is the subject of this study. Individual fluvial channels of the upper Morrowan interval are typically 5–30 ft thick, yielding 20–70 ft of clean sandstone in the sequence.

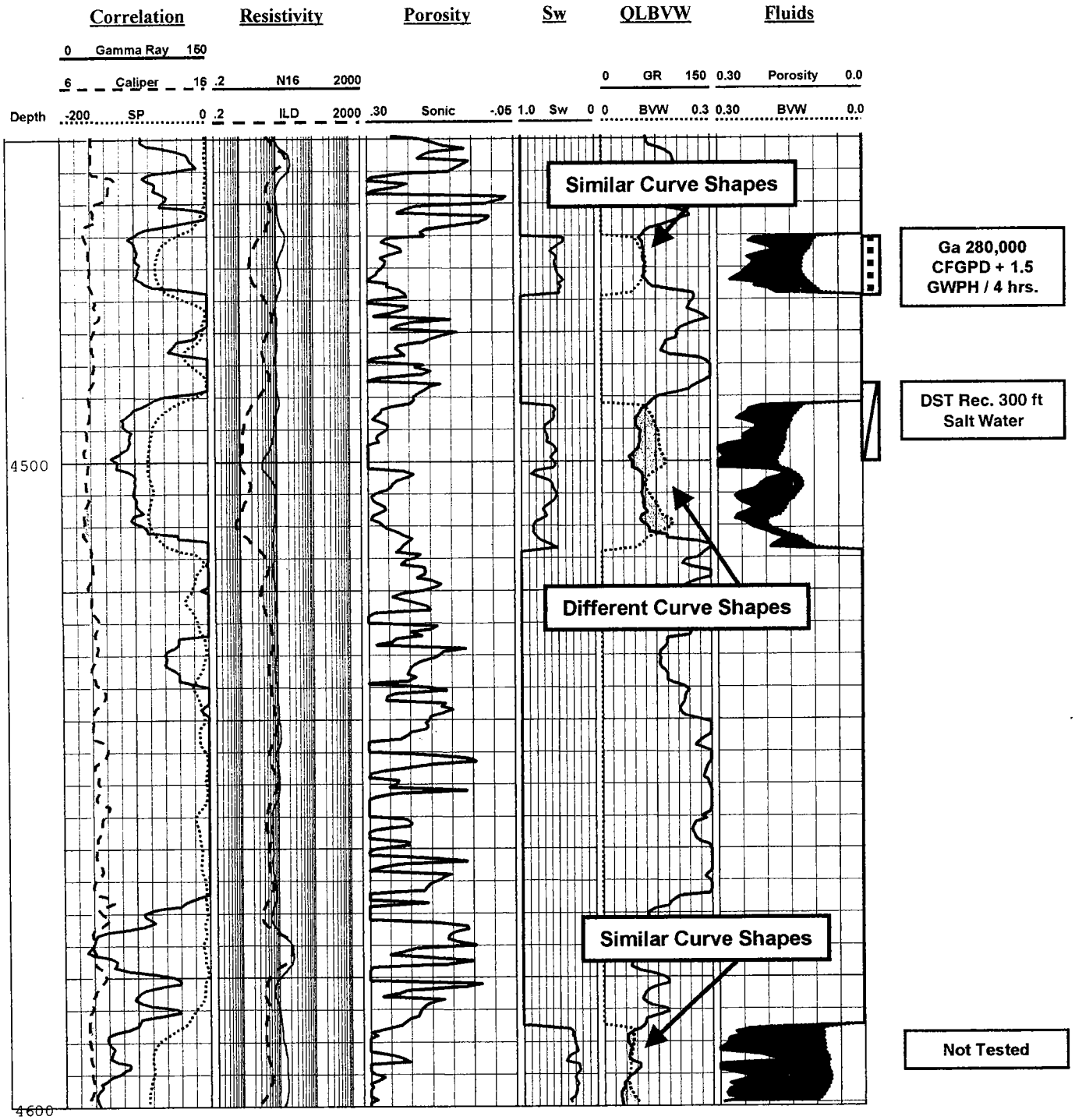

Figure 5. Example of quick-look bulk-volume water (QLBVW) "curve-shape" interpretation using gamma-ray (GR) and bulk-volume water (BVW) curves in the Cities Service Oil Company #1 Warren "B", in sec. 27, T. 2 N., R. 8 E. CM, Cimarron County, Oklahoma. Similar curve shapes indicate irreducible water. Depth in feet. Abbreviations: CFGPD—cubic feet of gas per day, DST—drill-stem test, GWPH—gallons of water per hour.

Discriminating pay from nonpay in these sandstones has been difficult. Water saturation in productive zones can be as high as 70%, and BVW can be as high as 12%. Lithologic effects on resistivity measurements (due to deep invasion and conductive clays) partly explain these unusually high numbers. Traditional log interpretation (using Sw and porosity cutoffs) fails and commonly causes operators to test wet zones unnecessarily.

Figure 5 is a log from the Cities Service Oil Co. #1 Warren "B" well in sec. 27, T. 2 N., R. 8 E. CM, Cimarron County, Oklahoma. The upper two sandstones were tested in this well with widely different results. The drill-stem test (DST) of the top part of the lower zone (4,488–4,500 ft) recovered 300 ft of salt water.

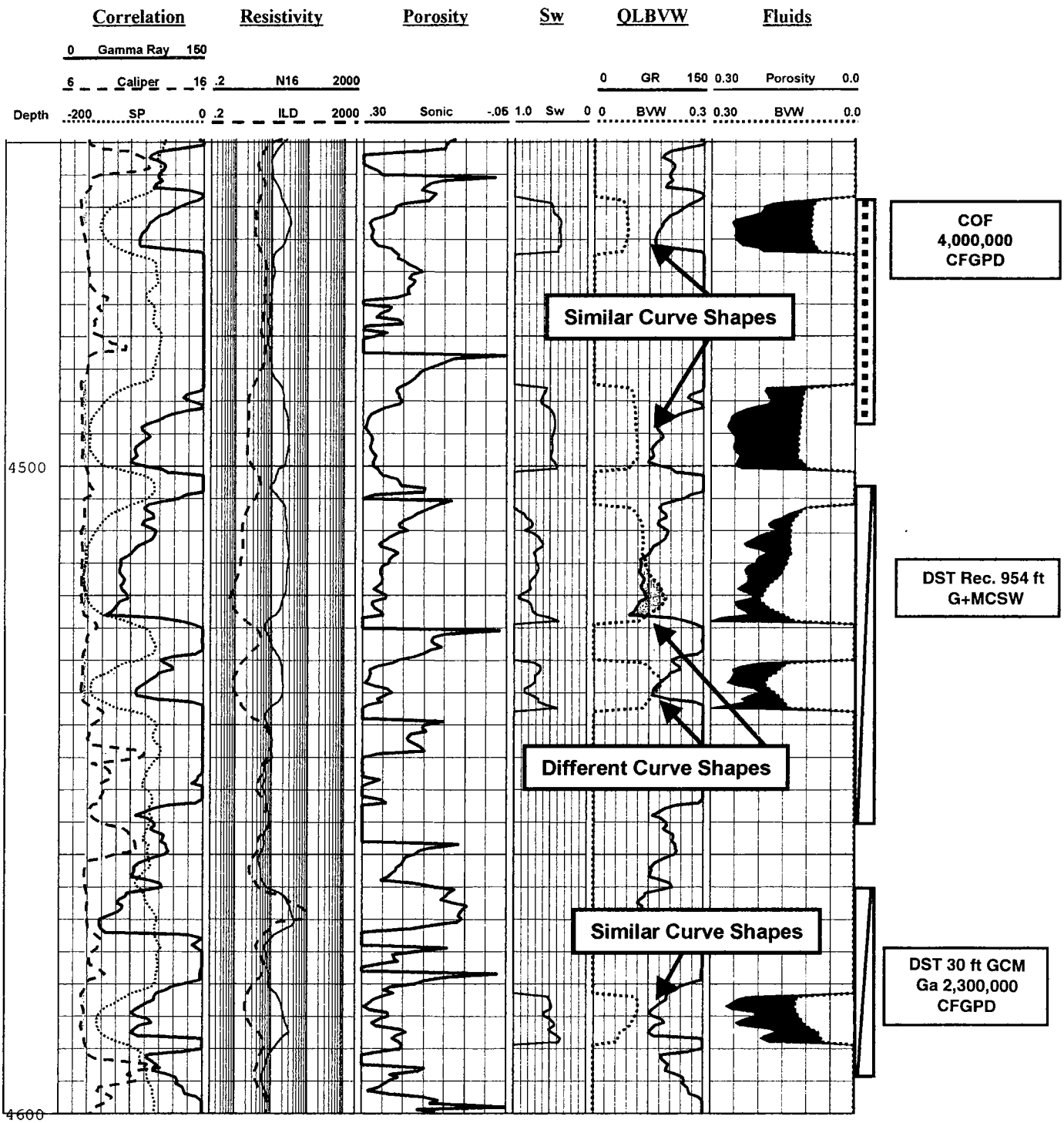

Figure 6. Example of quick-look bulk-volume water (QLBVW) "curve shape" interpretation using gamma-ray (GR) and bulk-volume water (BVW) curves in the Cities Service Oil Company Dungan "A"–1 in sec. 21, T. 2 N., R. 8 E. CM, Cimarron County, Oklahoma. Similar curve shapes indicate irreducible water. Depth in feet. Abbreviations: COF—calculated open flow, CFGPD—cubic feet of gas per day, DST—drill-stem test, G+MCSW—gas plus mud-cut salt water.

Using the QLBVW technique, this could have been predicted from the dissimilar GR- and BVW-curve shapes. Compare this top portion of the lower zone to the top zone (4,465–4,475 ft), in which the GR and BVW curves have similar shapes. The top zone tested an initial potential of 280 thousand cubic feet of gas per day (MCFGPD). The lower zone (4,590–4,600 ft) was not tested, but should be hydrocarbon productive according to the QLBVW plot.

Figure 6 shows a nearby well, where tests of the uppermost and lowermost members resulted in a combined potential of 6,300 MCFGPD. Sandwiched be-

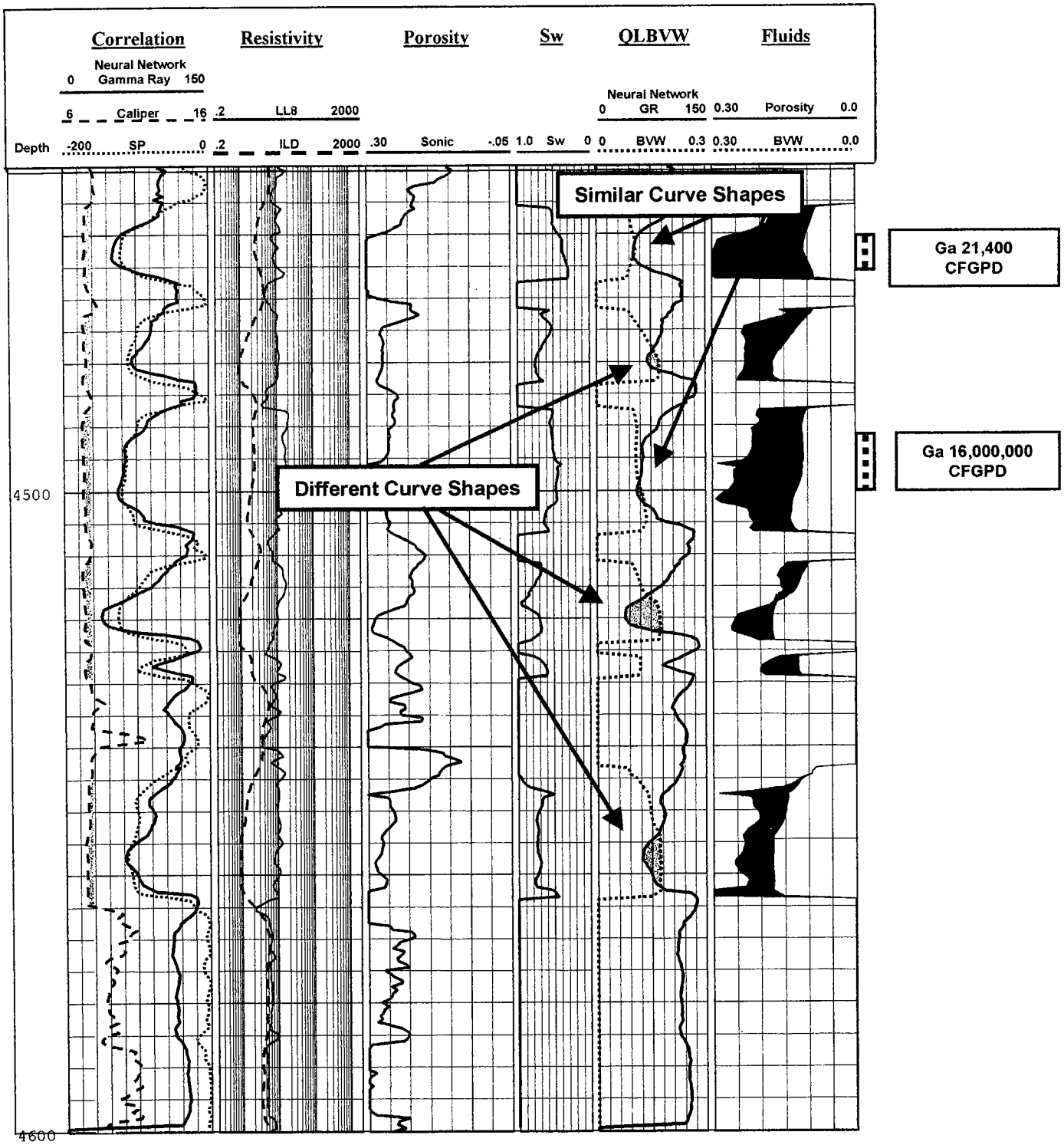

Figure 7. Example of quick-look bulk-volume water (QLBVW) "curve shape" interpretation using bulk-volume water (BVW) curves and synthetic gamma-ray (GR) curves generated using neural networks. No GR was run on this older (1964) log (Texaco Rod Taylor Unit #1 in sec. 9. T. 2 N., R. 8 E. CM, Cimarron County, Oklahoma). Similar curve shapes indicate irreducible water. Depth in feet. Abbreviations: CFGPD—cubic feet of gas per day.

tween these two producing formations are two sandstone formations that together tested 954 ft of salt water on a drill-stem test. Again, these results (gas versus water) could have been predicted using the curve shapes in the QLBVW track, and expensive testing could have been eliminated.

Figure 7 shows a nearby well that was drilled and logged in 1964. No gamma-ray was run on this well. To apply the QLBVW technique, a synthetic GR curve was created using neural-network methods (Arbogast and others, 2001). For this neural-network application, the spontaneous potential (SP), and deep-induction logs

were used as predictors of GR response. This relationship was "trained" on examples from nearby modern wells. The QLBVW technique works just as well using the neural-network–derived synthetic-GR log, and identifies the productive intervals by similar curve shapes (4,455–4,465 ft and 4,488–4,507 ft). The remaining intervals with different curve shapes are likely to be water bearing. The powerful combination of neural-network and QLBVW methods greatly reduces risk when looking for bypassed pay in older wells where only SP and resistivity logs are available.

CONCLUSIONS

This QLBVW technique is easy to use, requiring only a strip-log display of simple "Archie" calculations. The relative shapes of the GR and BVW curves indicate water *vs.* hydrocarbon producibility. The author has applied the technique with success in many geographic settings in both sandstone and carbonate lithologies; however, carbonate reservoirs on occasion require additional measurements to determine lithology (such as photoelectric effect) in combination with or in place of the GR. QLBVW techniques can be applied in areas with inconsistent or limited logging suites by using neural networks to generate required synthetic-curve data.

REFERENCES CITED

Arbogast, J. S.; Butler, M. L.; Franklin, M. H.; and Thompson, K. A., 2001 [this volume], Enhancement of "limited" log suites using neural networks, *in* Johnson, K. S. (ed.), Pennsylvanian and Permian geology and petroleum in the southern Midcontinent, 1998 symposium: Oklahoma Geological Survey Circular 104, p. 185–195.

Fertl, W. H.; and Vercellino, W. C., 1978, Predict water cut from well logs, *in* Practical log analysis—4: Oil and Gas Journal, vol. 76 (June 19, 1978), p.111–116.

Morris, R. L.; and Biggs, W. P., 1967, Using log-derived values of water saturation and porosity: Society of Professional Well Log Analysts, 8th Annual Logging Symposium Transactions, paper X, p. X1–X26.

Progress Report on Geologic Mapping of Pennsylvanian–Permian Strata in Oklahoma: The STATEMAP Project

Neil H. Suneson, LeRoy A. Hemish, Thomas M. Stanley, and T. Wayne Furr
Oklahoma Geological Survey
Norman, Oklahoma

Mark S. Gregory
Oklahoma State University
Stillwater, Oklahoma

INTRODUCTION

The Oklahoma Geological Survey (OGS) has participated in the U.S. Geological Survey's (USGS) COGEOMAP (Cooperative Geologic Mapping) and STATEMAP (State Mapping) programs every year since 1984 (fiscal year 1985). To date, the OGS has released 30 detailed 7.5′ geologic maps (scale 1:24,000) as open-file reports and five 1:100,000-scale digital geologic maps (Fig. 1). Most of the earlier COGEOMAP 1:24,000-scale mapping was resource-oriented and focused on the Ouachita tectonic belt–Arkoma basin transition zone (Fig. 2), an area undergoing significant natural-gas exploration, discovery, and development (Johnson and Suneson, 1996). In 1992, President George Bush signed the National Geologic Mapping Act (NGMA) into law. One component of NGMA is STATEMAP, which is designed to provide federal assistance to state geological surveys in support of new geologic mapping and digital compilation. Beginning in FY93, STATEMAP replaced COGEOMAP.

GEOLOGIC MAPPING

The Oklahoma Geologic Mapping Advisory Committee (OGMAC) recommended in late 1994 that, beginning in FY96, the OGS map the geology of the growing McAlester, Oklahoma, area, which is adjacent to previously mapped areas of the Arkoma basin. Therefore, part of the FY96 STATEMAP proposal emphasized land-use issues as well as resource concerns and stratigraphic problems. In addition, OGMAC recommended that the OGS prepare a series of 1:100,000-scale digital geologic maps that would serve as the basis for a new 1:500,000 Geologic Map of Oklahoma (Furr, 1999). The Watonga and Foss Reservoir quadrangles (Fig. 1) were proposed (FY96) to test OGS compilation efforts and digital capabilities. These quadrangles were chosen because the bedrock geology, which consists mostly of very gently dipping Permian redbeds, is relatively simple and well known. The highly dissected terrain, however, results in complex cartographic patterns.

In September 1996, OGMAC recommended that new detailed geologic mapping of the Oklahoma City (OKC) metropolitan area be started in FY97. The OGS identified twelve 7.5′ quadrangles that included most of the metropolitan area and developed a three-year, four-quadrangles/year mapping program of OKC and major suburbs to the west, north, and east (Fig. 3; FY97, FY98, FY99). The purpose of the OGS FY97 STATEMAP program (year one) was to provide a basis for addressing environmental and engineering concerns as well as Permian stratigraphic problems in the northern tier of quadrangles (Piedmont, Bethany NE, Edmond, and Arcadia). Similar concerns in the next tier of four quadrangles to the south (Bethany, Britton, Spencer, and Jones) were the focus of the FY98 mapping program. The geologic maps of these eight quadrangles have been completed and are available. New 1:24,000-scale geologic mapping of the Mustang, Oklahoma City, Midwest City, and Choctaw 7.5′ quadrangles (Fig. 3) is under way, and the maps are available as of June 2000.

Also in 1996, OGMAC recommended that the OGS prepare 1:100,000-scale digital geologic maps of the Oklahoma Panhandle, because of increasing transportation-infrastructure needs, numbers of stockyards and meat-processing plants, and to complement ongoing studies of the area by the Oklahoma Water Resources Board and Water Resources Division of the USGS. In November, the OGS proposed (FY97) to the USGS that the geology of the Boise City 1:100,000-scale map in the Panhandle (Fig. 1) be compiled and digitized. New 1:100,000-scale digital geologic maps of the remainder of the Oklahoma Panhandle (Guymon and Beaver quadrangles) (Fig. 1) are part of the OGS FY98 STATEMAP project. The five 1:100,000-scale digital geologic maps in northwest Oklahoma proposed as parts of the FY96, FY97, and FY98 STATEMAP programs have been completed and are available to the

Suneson, N. H.; Hemish, L. A.; Stanley, T. M.; Furr, T. W.; and Gregory, M. S., 2001, Progress report on geologic mapping of Pennsylvanian–Permian strata in Oklahoma: the STATEMAP project, *in* Johnson, K. S. (ed.), Pennsylvanian and Permian geology and petroleum in the southern Midcontinent, 1998 symposium: Oklahoma Geological Survey Circular 104, p. 207–211.

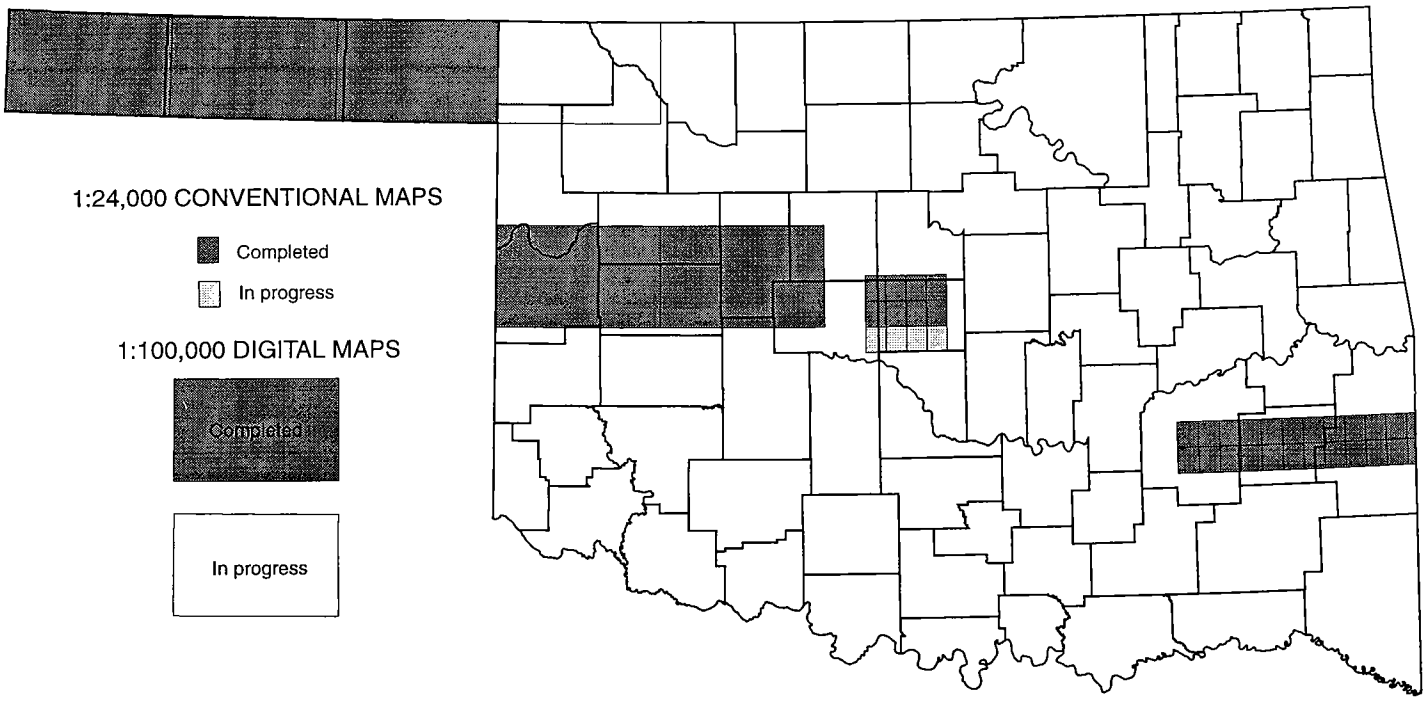

Figure 1. Map showing geologic maps produced as part of COGEOMAP and STATEMAP projects. Areas shown as "in progress" are part of FY99.

public. Field work in the Buffalo 1:100,000-map area (Fig. 1), proposed for FY99, is in progress.

In September 1999, the OGS recommended and OGMAC agreed that detailed 1:24,000 geologic mapping of the Oklahoma City metropolitan area continue and should include major suburbs to the south and to the east, where an "outer-loop" interstate bypass had been proposed by the Oklahoma Department of Transportation. The OGS submitted a proposal to map the first tier of southern quadrangles (Oklahoma City SW, Oklahoma City SE, Moore, and Franklin) (Fig. 3) to the USGS in November 1999. The proposal was accepted in March 2000, and mapping is to begin in the 2000–2001 winter field season.

MAPPING AND PRODUCTION PROCEDURES

Current Procedures

The OGS procedure for producing the 1:24,000-scale geologic maps and supporting information is:

1. Review existing maps and literature and/or interpret aerial photographs;
2. Map in the field on 1:24,000-scale topographic base maps;
3. Hand-transfer field data to stable-base mylar, greenline base maps, including oil- and gas-well locations. Well locations are determined from scout tickets, Oklahoma Corporation Commission 1002A well-completion forms, and Herndon Map Service maps;
4. Construct geologic cross-section(s) based on surface geology and interpretation of electric logs;
5. Prepare description and correlation of units, list of wells, symbols, title block, etc.;
6. Lay out map components (mockup);
7. Enlarge or reduce items in number 5 as appropriate;
8. Register base-map negatives to geologic data;
9. Prepare and composite film negatives;
10. Prepare single-film positive of entire map sheet;
11. Reproduce (in black and white) for customers, as needed, on a large-format engineering copier.

OGS geologists currently perform procedures 1 through 5; OGS cartographic staff completes procedures 6 through 10; and the OGS print shop does procedure 11.

Past Procedures

Past OGS procedure for producing the 1:100,000-scale digital geologic maps was (Furr, 1999):

I. OGS geologist does the following:

1. Conducts library research and compiles all existing modern geologic maps on 1:24,000-scale base maps;
2. Supplements compilation and resolves different geologic interpretations with aerial-photographic interpretation and/or reconnaissance field checking;
3. Drafts by traditional "pen and ink" methods the geologic data on to a stable 1:100,000-scale mylar greenline base map;
4. Colors the formations on a paper print of the 1:100,000-scale map, checking for gaps or open formation contacts;
5. Prepares description and correlation of units, symbols, area of investigation map, title block, etc.;

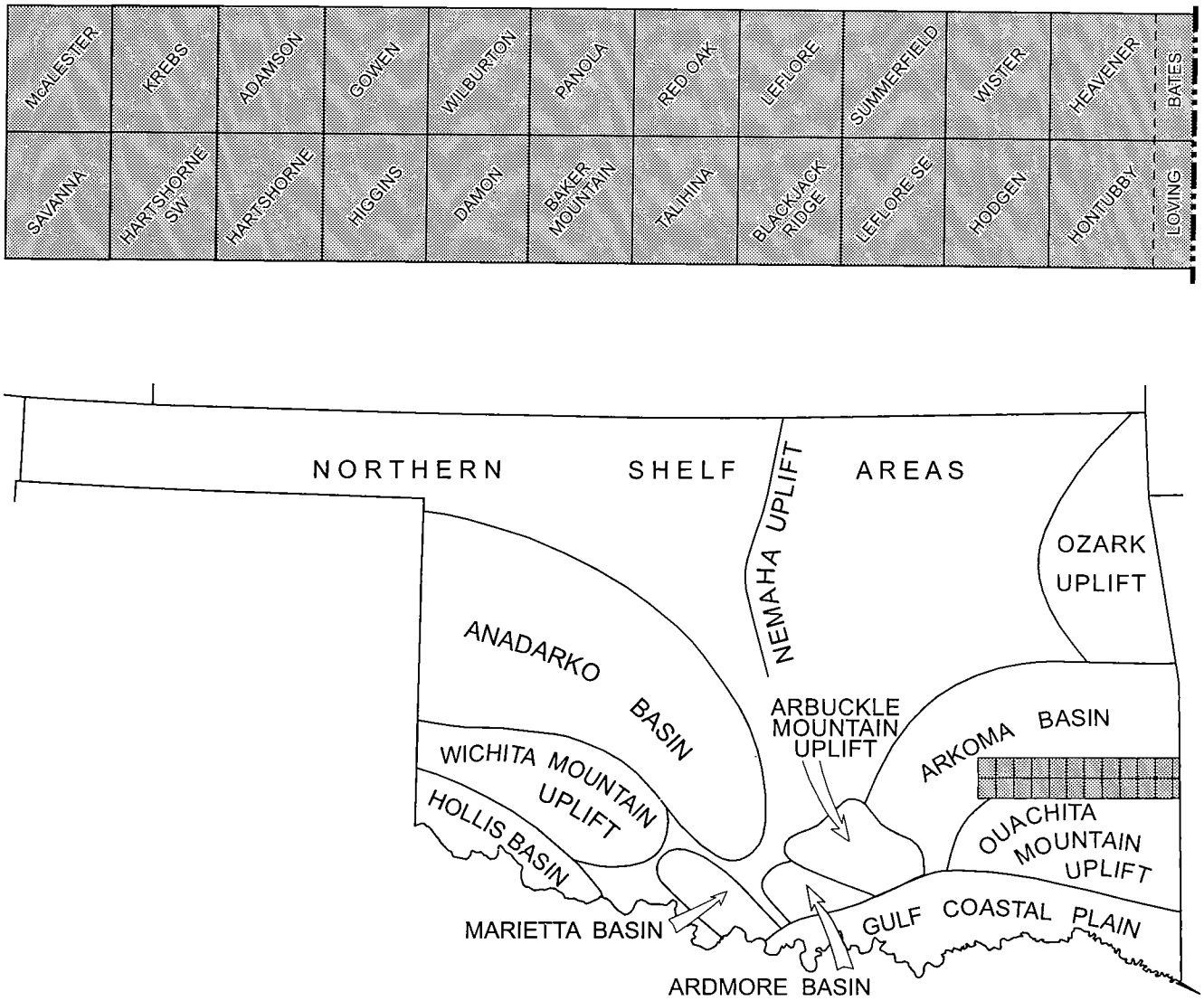

Figure 2. Map showing 1:24,000 detailed geologic maps of northern Ouachita Mountains and southern Arkoma basin. Geologic maps were produced as part of U.S. Geological Survey–sponsored COGEOMAP and STATEMAP programs.

6. Turns this information over to the OGS cartographic staff for processing.

II. OGS cartographic staff does the following:

7. Using scribing, makes a line-work separation of the geologic contacts from the base map;
8. Prepares a geologic color-selection guide;
9. Prepares a map layout guide;
10. Makes a clear film or paper photo print of the geologic line work;
11. Turns over to the GIS specialist the photo print, color selection guide, and map layout guide.

III. The GIS specialist does the following:

12. Scans 100:000-scale photopositive of geologic map sheet at 400 dots per inch on an ANAtech 3640 Eagle optical scanner;
13. Converts scanned (raster) image to vector polygons utilizing LtPlus raster-to-vector conversion software on a SUN SPARC workstation;
14. Plots digital vector data at 1:100,000-scale on an HP650C plotter and visually compares results with original map compilation to ensure completeness and precision of scanning and data conversion;
15. Within LtPlus, creates polygon topology, attributes each polygon twice, and performs a series of quality-control checks with software macros (programs);
16. Exports digital base-map data from LtPlus in standard USGS DLG-3 format and imports digital data into Arc/Info version 7.0.3;
17. Writes and executes Arc Macro Language program to utilize the digital geology polygons as part of the 1:100,000-scale geologic map;
18. Places geologic-polygon and base-map image file layers on OSU (Department of Plant and Soil Sciences) file server in ArcView shapefile

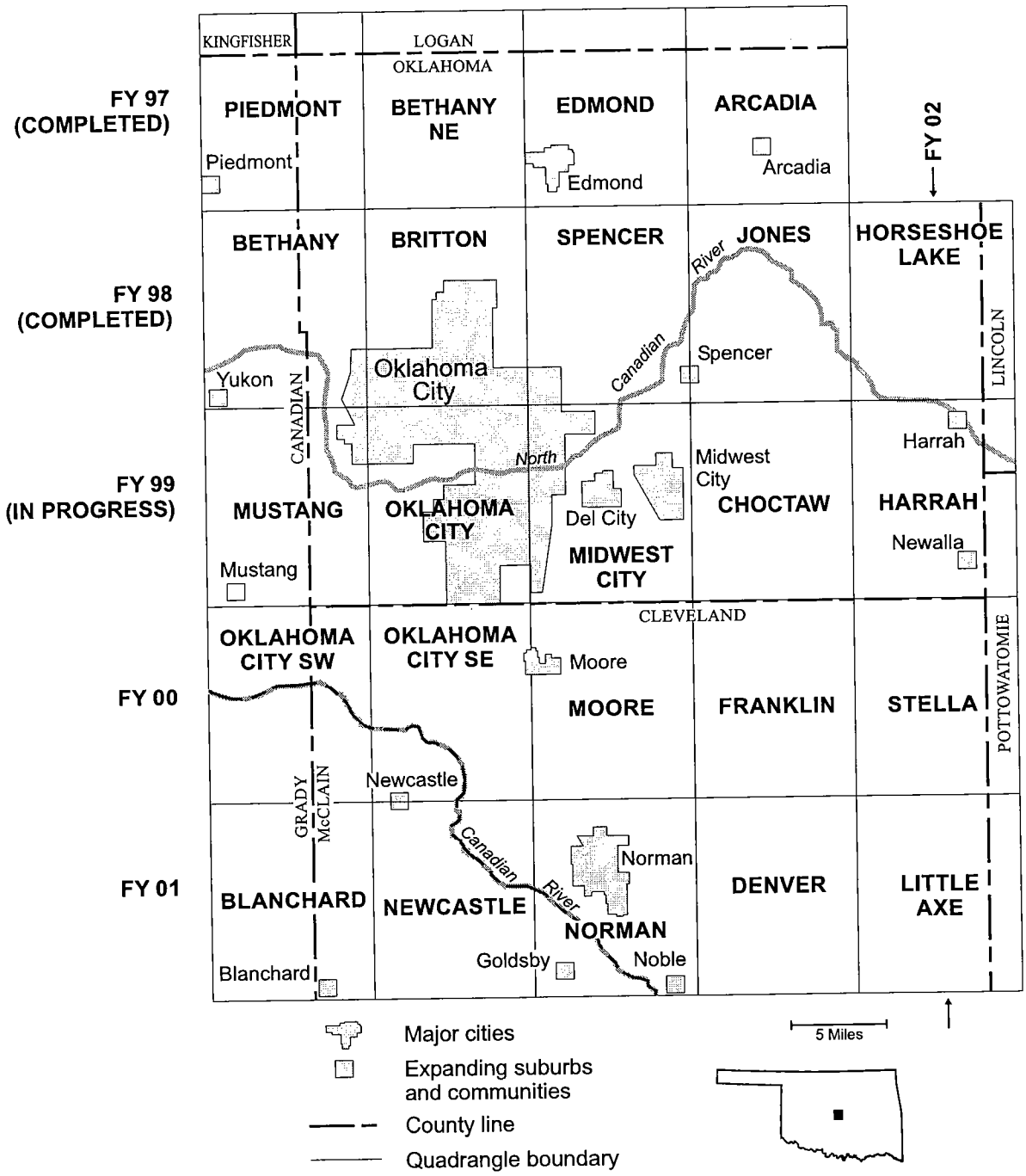

Figure 3. Map of the Oklahoma City metropolitan area showing completed (FY97, FY98), in progress (FY99), funded (FY00), and to-be-proposed (FY01, FY02) 1:24,000-scale geologic maps.

format. These data are used by the OGS cartographic staff.

IV. The OGS cartographic staff does the following:

19. Transfers file to OGS computer network using standard file transfer protocol (ftp);
20. Moves ArcView shapefiles into Adobe Illustrator using MAPublisher's import filter;
21. Using Illustrator, performs necessary cartographic work to bring map to OGS standards by adding title, explanation, index map(s), geologic letter symbols, and colors;
22. Creates file formats for printing maps and sends formats to printer;
23. Exports geologic map database in ArcView shapefile format for use in GIS applications;
24. On request, makes available to the public the completed map data sets in one of the following formats: (a) Arc/Info export format (.e00), (b) ArcView shapefiles, or (c) USGS DLG-3 format

for access throughout the World Wide Web via a Web browser or by ftp.

Future Procedures

The OGS currently is reevaluating its procedures for producing the 1:100,000-scale digital geologic maps. In an effort to streamline the process and increase production speed, many of the steps outlined above will be dropped, and others will be handled by OGS personnel. We probably will digitize the field-checked and/or remapped 1:24,000 geologic maps directly into ArcView or by using a digitizing tablet. These detailed map data sets will then be compiled at a scale of 1:100,000. In the future, the OGS also will digitize the detailed 1:24,000 geologic maps; this may enable colored maps to be printed on demand at an economical cost. In addition, the maps may be made available in a geographic information system (GIS).

SUMMARY

The OGS STATEMAP program and preceding COGEOMAP program have been unqualified successes. In addition to the 35 1:24,000- and 1:100,000-scale maps released to the public, the geologists associated with the mapping have published more than 60 abstracts and papers in scientific journals. Five guidebooks on the geology of southeastern Oklahoma are available, and two of them contain numerous papers by non-OGS geologists. Much of the information published in the OGS guidebooks by industry and university geologists would not be available to the public if the new mapping completed under the STATEMAP and COGEOMAP programs had not been undertaken. More than 200 geologists attended field trips held in conjunction with publication of the guidebooks. In addition, OGS geologists conducted numerous field trips for industry geologists, university groups, and organizations such as Elderhostel. The maps and field experience also provided the basis for several theses by university graduate students.

The OGS will continue to support geologic mapping in Oklahoma, the NGMA, and the USGS STATEMAP program. At the time this paper was rewritten (Spring 2000), the OGS was planning to apply for STATEMAP funds to complete mapping the OKC metropolitan area. Completion of the southernmost four-quadrangle tier south of OKC in FY01 will accomplish the goal of providing city planners and engineers as well as homeowners with new, detailed geologic maps of this rapidly growing part of Oklahoma. For FY02, the OGS will propose detailed geologic mapping of a north–south strip of quadrangles directly east of the OKC metropolitan area because this area is the site of a possible future "outer loop" or interstate bypass around OKC. If the outer loop is built, it will be the focus of new business and residential development. The OGS will also continue and potentially accelerate its program of 100,000-scale digital geologic-map compilation, with the ultimate goal being a new geologic map of Oklahoma.

REFERENCES CITED

Furr, T. W., 1999, Geologic mapping at the Oklahoma Geological Survey: the move from traditional to digital cartography, *in* Soller, D. R. (ed.), Digital mapping techniques '99—workshop proceedings: U.S. Geological Survey Open-File Report 99-386, p. 7–10.

Johnson, K. S.; and Suneson, N. H., 1996, COGEOMAP: Cooperative Geologic Mapping program in Oklahoma, 1984–1993: Oklahoma Geology Notes, v. 56, p. 36–48.

Evolution of the Meers Valley, Southwestern Oklahoma

R. Nowell Donovan, Kathy Collins, and Steve D. Bridges
Texas Christian University
Fort Worth, Texas

ABSTRACT.—The modern Meers Valley trends east-southeast–west-northwest and lies between the eastern Wichita Mountains and the Slick Hills in southwestern Oklahoma. These two ranges are the exposed part of the Wichita uplift, a major Pennsylvanian terrain. The valley is about 15 mi long and opens to the east-southeast. The valley is floored by Recent and Pleistocene soil, alluvium, and regolith, Permian continental facies (talus, fan, braided alluvium, and calcretes), and a variety of Cambrian igneous rocks (mostly basic and ultrabasic rocks plus some rhyolite).

The form of the valley is intimately linked to the east-southeast–west-northwest–trending Meers fault. This structure has a long and complicated history. During the Cambrian, the fault probably helped to define the early igneous development of the southern Oklahoma aulacogen. Specifically, the fault may have formed to locus for intrusion of basic dike-like intrusions, while, during a later phase, the petrography of basal Cambrian sediments is compatible with the presence of a substantial fault that was downthrown to the east-northeast.

The fault was reactivated in the Pennsylvanian as a major member of the frontal fault zone, a linear zone of intense transpressive tectonic deformation that separates the Wichita uplift from the Anadarko basin. At this time, the fault facilitated a stratigraphic separation of at least 4,000 ft (~1,220 m) between the Slick Hills and Wichita Mountains. Structural styles in the Slick Hills suggest a major component of left-lateral displacement at this time.

Differential erosion across the Meers fault scarp during the Early Permian led to the first period of formation of Meers Valley. Initial Permian drainage and erosion off the rising Wichita Mountains to the north-northeast (into the Anadarko basin) removed a thick, lower Paleozoic sedimentary section plus a substantial thickness of Cambrian acidic igneous rocks (the Carlton Rhyolite and Mount Scott Granite).

Definition of the Meers Valley as a subsequent drainage system controlled by the fault trace began when ultrabasic rocks beneath the Mount Scott Granite were rapidly eroded. The northern front of the Wichita Mountains evolved as a fault-line scarp retreating to the south-southwest. Permian facies in the Valley are compatible with drainage to the east-southeast by fans and braided rivers in a semiarid environment.

Permian rejuvenation of the Meers fault with a modest throw down to the south-southwest is recorded by megaclast breccias on the northern edge of the Valley. Blocks of limestone as much as 60 ft (~18 m) across in this area apparently fell from an active fault scarp. Subsequently, the Permian landforms in the area were preserved in the extreme aridity of the area before entombment by later Permian rocks.

EXHUMED PERMIAN TOPOGRAPHY

The Wichita uplift in southern Oklahoma formed during late Paleozoic inversion of the southern Oklahoma aulacogen. During the Pennsylvanian and Early Permian, erosion removed much of the lower Paleozoic sedimentary cover to expose a complex igneous basement. This erosion was particularly severe in the Meers Valley, a linear declivity that lies between the Slick Hills and Wichita Mountains (Fig. 1). As the tectonic inversion ceased, the resulting land surface was gradually buried beneath Lower Permian sediments, collectively referred to the Post Oak Formation (Chase, 1954; Donovan and others, 1982; Donovan, 1986a). Preservation of significant topography was possible because the climate in the area became increasingly arid, probably because of a combination of two factors. (1) The Laurentian craton was drifting into the northern hot-desert belt during this time. (2) Concurrently, the area of what is now Oklahoma was becoming in-

Donovan, R. N.; Collins, Kathy; and Bridges, S. D., 2001, Evolution of the Meers Valley, southwestern Oklahoma, *in* Johnson, K. S. (ed.), Pennsylvanian and Permian geology and petroleum in the southern Midcontinent, 1998 symposium: Oklahoma Geological Survey Circular 104, p. 213–223.

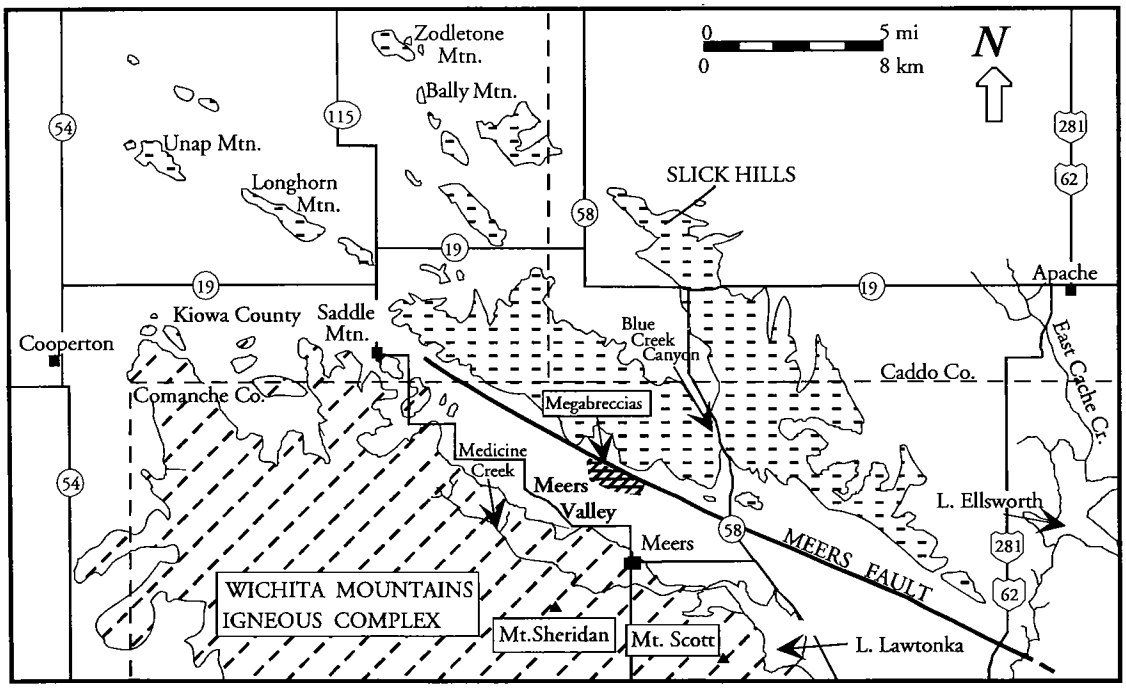

Figure 1. Map showing location of Meers Valley and some specific sites and features.

creasingly isolated from moisture sources during the tectonic assembly of Pangaea (Donovan and others, 1992). Thus, in a sense, the topography of the Wichita Mountains area is a Permian inheritance, exhumed from its cover and only slightly altered during the present erosion cycle. Permian topography is preserved in surprising detail, from ancient granite and gabbro tors and scarps (Gilbert, 1982) to extensive fissure-karst and pediment surfaces (Donovan, 1992). This paper examines some details of the geomorphic evolution of the Meers Valley.

THE PRESENT GEOGRAPHY OF MEERS VALLEY

Structural Control

The Meers Valley in southwestern Oklahoma lies between the Wichita Mountains to the south and the Slick (or "Limestone") Hills to the north. The valley trends east-southeast–west-northwest, parallel to the trace of the Meers fault, a major structure that has been the dominant control on the geomorphic evolution of the Valley (Fig. 1). Pennsylvanian movement on this fault resulted in several thousand meters of stratigraphic displacement down to the north and east. This movement ultimately determined the character of Meers Valley.

The axis of the Valley can be traced presently for approximately 15 mi (~24 km) from a gentle divide at 1,725 ft (~540 m) in the west-northwest near the Saddle Mountain Indian Mission to the line of Cache Creek north of Lawton, where the Valley opens into the plains of southern Oklahoma at around 1,200 ft (~375 m). The topographic fall from west-northwest to east-southeast is thus about 35 ft per mi (~7 m per km).

The northeastern divide of Meers Valley is located in the Slick Hills (Fig. 1), an area of intensely folded and faulted Lower Paleozoic rocks—mostly carbonates assigned to the Cambro-Ordovician Arbuckle Group (Fig. 2). The Hills are built of slopes with angles of up to 25° and are heavily dissected by a number of small, mostly ephemeral streams. Summits on the divide rise from approximately 1,500 ft (~470 m) in the southeast to almost 2,100 ft (~660 m) near the Indian Mission. This means that the orthogonal fall from this divide to the valley axis ranges from 300 to 400 ft (about 95 to 125 m) in a distance of about 2 mi (~3.2 km).

The southwestern divide of the valley is a dissected, cliff scarp formed by the Mount Scott Granite, a sill-like intrusion that lies atop basic and ultrabasic intrusives and is itself overlain by the Carlton Rhyolite. This scarp is the most dramatic topographic element in the Wichita Mountains and effectively defines almost the entire southwestern side of the Valley. Relief on the scarp is steepest in the vicinity of Meers, where Mount Scott and Mount Sheridan both rise to over 2,400 ft (~750 m). The orthogonal fall from the top of Mount Scott to the valley axis is around 1,100 ft (~340 m) in a distance of about 2 mi (~3.2 km). Clearly, the valley has a highly asymmetric cross profile (Fig. 3).

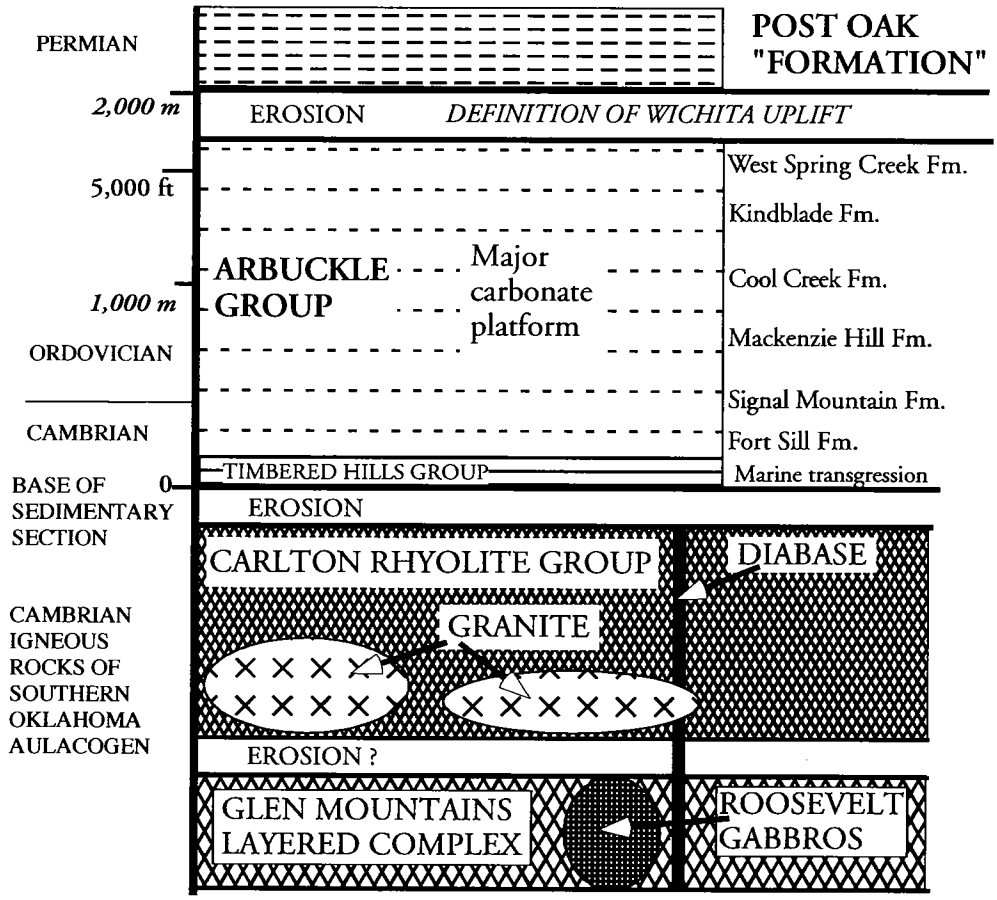

Figure 2. Geologic relationships of rocks exposed in the watershed of the Meers Valley.

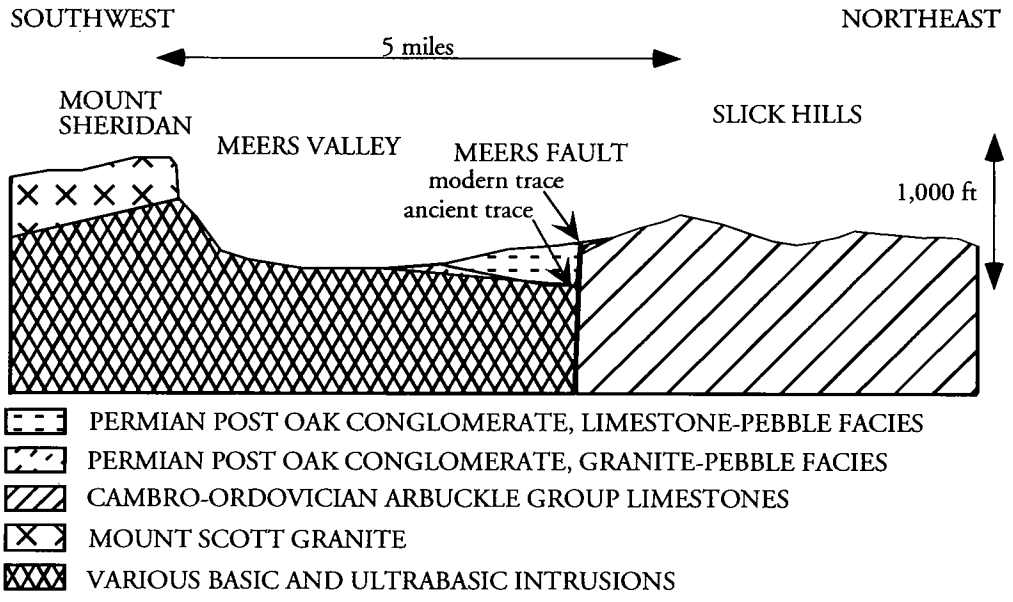

Figure 3. Simplified cross section showing main geomorphic and geological features in the Meers Valley area. Vertical exaggeration 25x.

Modern Drainage Patterns

Modern drainage patterns are superimposed on the Meers Valley, principally in the form of a number of south-southeast–draining streams that flow into Medicine Creek, which itself is deeply incised into the igneous core of the Wichita Mountains (Fig. 1). Few of the streams show any clear systematic control by inversion tectonics. The principal examples of this are (1) linear segments of Medicine Creek in the neighborhood of the Meers Township, which seemingly relate to large fractures in the ultrabasic core (Crawford and others, 1991), and (2) the course of Blue Creek Canyon Creek, which partly follows the trace of the fault of the same name (Donovan and others, 1982).

In places, the modern drainage is partly incised into the exhumed Permian land surface, although most of the ancient contours are still clear. No modern drainage follows the axis of Meers Valley.

GEOLOGICAL FRAMEWORK OF MEERS VALLEY

Pre-Permian Rocks and Structure

As noted, lower Paleozoic rocks of dissimilar character form the flanks of the Meers Valley. Thus, the Slick Hills contain principally carbonate rocks that are underlain locally by the Carlton Rhyolite, whereas the Wichita Mountains in the Meers area consist of granite that overlies both basic and ultrabasic intrusives. These two suites of rocks are juxtaposed by the Meers fault, a major structure with a history of movement that dates back to at least the Cambrian (Cecil-Jones and others, 1995). The principal phase of movement on the fault took place during Pennsylvanian inversion of the southern Oklahoma aulacogen. It was at this time that the geologic framework that would determine the form of the Meers Valley was set; subsequent movements on the fault have but slightly modified the Pennsylvanian setting (Donovan and others, 1983; Gilbert, 1983).

The Meers fault trace approximately demarcates the northern edge of the Valley (i.e., the southern edge of the Slick Hills). To the southwest of this fault, the floor of the Valley is mostly composed of ultrabasic rocks. The latter are well exposed at the northwestern end of the valley and are increasingly covered by a veneer of Permian sediments to the southeast.

Permian Sediments in Meers Valley

None of the sedimentary rocks in the Meers Valley has yielded diagnostic fossils; they are assumed to be of Early Permian age on the basis of their similarity in general facies to more securely dated strata in the area surrounding the Wichitas. In addition, karst fissures at a number of sites in the Slick Hills appear to be part of the same erosional cycle as the Permian deposits that overly them. This karst contains an abundant and varied Lower Permian vertebrate-fossil assemblage (Donovan and Busbey, 1991; Donovan and others, 1992).

Permian sediments in Meers Valley rest with a profound unconformity on all underlying rocks. The surface of unconformity is highly irregular in many places, and it is clear that the Permian deposits entombed a landscape that was remarkably similar to that of today. The general pattern of sedimentation is clear throughout the valley—coarse conglomerates pass upward and laterally (from positive topography) into poorly sorted sandstones and shales. The finer-grained rocks are found principally in the southeast part of the valley, where they are generally poorly exposed. Few units of any kind are laterally persistent. There is one noteworthy exception; fossil calcareous soils (calcretes) are abundant throughout the Valley and can be found in all lithologies (Donovan, 1978; Bridges, 1985; Collins, 1985). Most of these calcretes are thin, about 12 in. (~30 cm) thick; one or two are much thicker, as much as 6 ft (~2 m).

The assemblage and distribution of facies in the valley is compatible with a gradual infill of the topography by the coalescence of small alluvial fans in a semiarid environment (Fig. 4). The few reliable paleocurrent indicators found indicate axial drainage to the southeast. This interpretation is supported by sediment-provenance studies, discussed subsequently in this paper. Similar alluvial facies mantle the entire Wichita uplift.

Permian Sediment Provenance

Within Meers Valley, local patterns of sediment provenance are of great importance in interpreting the history of the valley. The following four trends are noteworthy.

Basal Conglomerates

The basal conglomerates contain no clasts of basic or ultrabasic igneous source rocks, nor are any mafic minerals preserved in the sandstones, with the exception of magnetite grains that form discrete laminae associated with some cross-bedded sequences. Some heavily weathered feldspars encountered in arkosic sandstones in the area of Lake Lawtonka may have been sourced by mafic rocks. The near absence of mafic-sourced materials indicates that these rocks were subject to intense chemical weathering. Such weathering implies a hot and moist environment. In places in the Meers Valley, heavily weathered tors of ultrabasic rocks, preserved beneath a covering of Permian sediment, further attest to this mode of weathering.

Sediment Contribution by Mount Scott Granite

The biggest contributor of clastic sediment to the Permian sediments was the Mount Scott Granite. As noted, this intrusion forms an escarpment along the entire southern edge of the Valley (Fig. 3). Detritus from this scarp can be found over much of the southern part of the Valley, extending northward almost to the line of the modern Meers fault scarp. This detritus takes the form of conglomerates consisting of well-rounded pebbles and cobbles and a spectrum of gener-

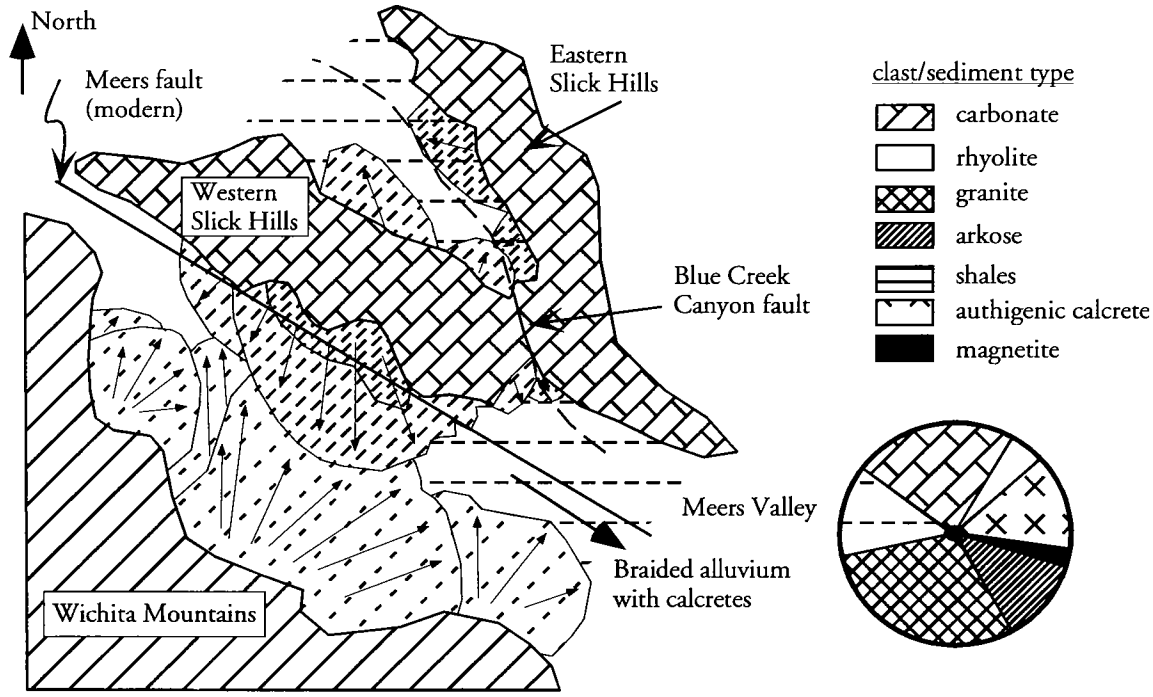

Figure 4. Geologic map showing Permian sediment dispositions. The Meers Valley drained to the southeast, slowly being filled by pebbly sandstones and shales deriving from both sides of the Valley. Calcretes developed in the semiarid environments. Only magnetite grains record the basic and ultrabasic rocks that underlie the Valley. The proportions of clasts and sediment types is an amalgam determined from sections to the east of Lake Lawtonka in the southeastern part of the Valley.

ally poorly sorted arkosic sandstones. Mineralogically similar sand forms the matrix of the conglomerates. Doubtless some of the rounding of the conglomerate pebbles is due to abrasion, but most is due to in situ rounding of granitic outcrops due to hydrolysis (i.e., spheroidal weathering). Such weathering is a characteristic feature of tor formation (Gilbert, 1982) and can be observed occurring today at many places in the Wichitas.

Contrast in Alluvial Fans on Sides of Meers Valley

The northern edge of the valley is more complex than the southern. In the Blue Creek Canyon area, rhyolite clasts are a conspicuous feature in some conglomerate lenses, reflecting the underlying basement (Donovan and others, 1982, 1986). In general, rhyolite clasts are subrounded and are associated with some arkosic sandstones. Most of the alluvial fans on the northern edge of the valley are composed of conglomerates built of varieties of carbonate rocks derived from the Arbuckle Group. For several reasons, the geometry of these fans is both complex and unusual. First, given the nature of the parent material, fines are limited to small amounts of hematitic clays that are probably infiltrates of eolian origin. Second, instead of being held together by a detrital matrix, the conglomerates are generally cemented by drusy calcsparite or, more comprehensively, by calcretes. The result of this cementation is that the "carbonate" fans form an area of positive topographic relief on the northern side of the Valley. Third, calcretes are remarkably abundant and show cross-cutting relationships that suggest reworking of fan surfaces, an interpretation supported by the common occurrence of avulsion channels (Donovan, 1986a, 1988).

Megabreccias

The fourth and most spectacular feature of the northern fans is the occurrence of megabreccias, bedded deposits of immense, angular limestone boulders (Fig. 5). Clasts are up to the size of a small house and can be mapped as individual exposures. In fact, it is not always possible to demonstrate that the largest fragments are independent clasts (i.e., that they are detached from their parent outcrop). However, in other cases megabreccia deposits are clearly interbedded with pebble conglomerates of "normal" character (Fig. 6). The megabreccias are restricted in area (see Fig. 1), being exposed only in sec. 19, T. 4 N., R. 13 W., where they extend about half a mile from the nearest outcrop of the Arbuckle Group.

The preferred explanation for their existence is that they formed as the result of the collapse of one or more limestone cliffs either as individual rock falls and/or by more comprehensive collapse, perhaps associated with "air cushion" flow. The most likely cause of cliff formation is by rejuvenation of the Meers fault. In this context, it is noteworthy that no outcrops of megabreccia occur to the north of the line of the modern fault scarp. Following this line of argument, the fault reversed its

Figure 5. Photo showing megabreccia deposit overlying more typical carbonate fan conglomerates in sec. 19, T. 4 N., R. 13 W. Height of cliff is ~20 ft (6 m).

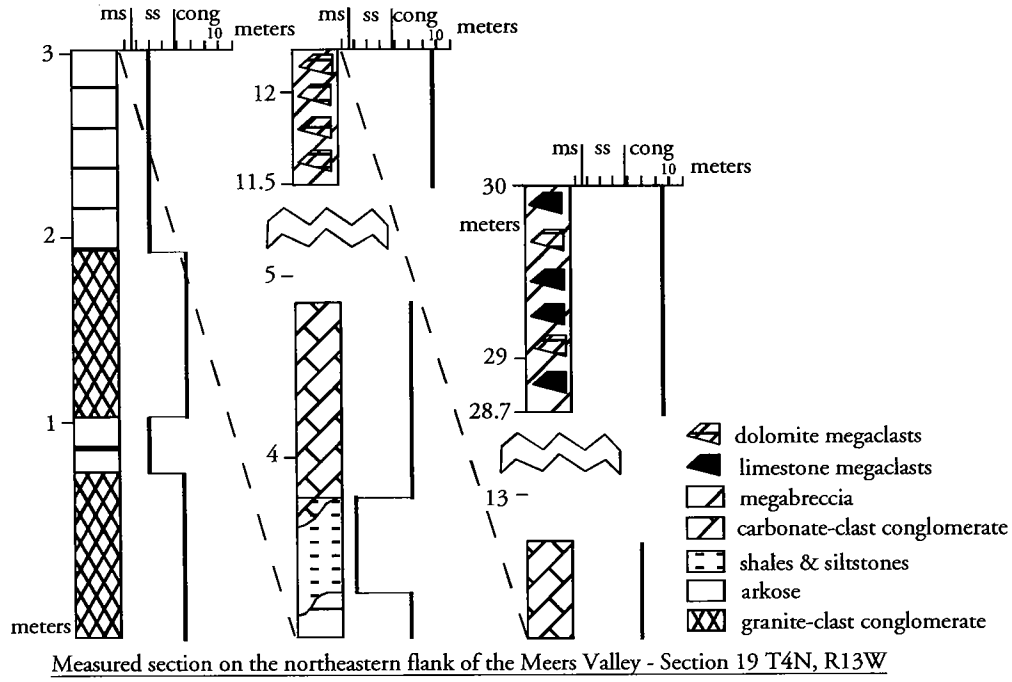

Figure 6. Measured section on the northeastern flank of the Meers Valley, sec. 19, T. 4 N., R. 13 W. Carbonate detritus overlies granitic detritus, illustrating the increasing importance of relief in the Slick Hills. The megabreccias are most likely tied to reactivation of the Meers fault and collapse of the resulting fault scarp. Two periods of fault movement may be recorded by the variation in megaclast type.

sense of throw in the Early Permian, with a small movement of uncertain magnitude down to the south and west. This sense of downthrow is the same as that of the most recent movements on the fault.

This interpretation probably simplifies a potentially more complex scenario. For example, the megabreccia deposits are spatially restricted, suggesting that any cliff-forming displacements were similarly restricted. Further, some of the megaclasts are from lithologies from formations of the Arbuckle Group that are not

present in the immediately adjacent Slick Hills. This observation suggests that strike-slip movement may have taken place. On the present emplacement of formations in the Slick Hills, the most likely strike-slip displacement would be a left-lateral movement of 2–3 mi (about 3.5–5 km). Such a movement would also be one possible way of explaining the large numbers of dolomite clasts in the megabreccias—considerably more than are found in the adjacent sequences in the Slick Hills (Donovan and Ross, 1991). One final point needs to be made; the trace of the modern Meers fault is a compellingly straight, yet geologically modest feature. The nature of the late Paleozoic fault trace is unknown in detail (being covered by Permian conglomerates). It is possible that the megabreccias record a deviation in the older fault trace, perhaps an en echelon splay or restraining bend. Such a scenario might explain their localized occurrence.

Fan Overlap

One feature of the various alluvial-fan deposits is the degree of overlap that can be demonstrated or inferred. In this context, a critical section in sec. 19, T. 4 N., R. 13 W., shows a "normal" sequence of granite-pebble conglomerates and cross-bedded arkoses, the latter grading upward into reddish-brown siltstones that are sharply overlain by limestone-pebble conglomerates (Fig. 6). Within these limestone conglomerates are two megabreccia horizons, the lower of which contains boulders of both limestone and dolomite, and the upper of which is dominated by dolomite boulders. This section and a similar one nearby suggest strongly that recession of the Mount Scott escarpment predated the emergence of the Slick Hills as a positive topographic feature. This suggestion adds support to the notion that the megabreccias were a response to down-to-the-south faulting along the line of the Meers fault. On the other hand, the Slick Hills originally may have been defined as a range in response to climatic change. The carbonates would have been increasingly resistant to dissolution in an increasingly arid climate.

As noted, the Valley opens to the south and east. Conglomeratic exposures in the general area of Lake Lawtonka show a more heterogeneous suite of pebbles, including granite, rhyolite, Arbuckle Group carbonates, and fragments of reworked calcrete (Collins, 1985). These facts suggest both reworking of fan surfaces and mixing of detrital-grain populations along the opening axis of the Valley.

INFERRED SEQUENCE OF EVENTS IN THE EVOLUTION OF MEERS VALLEY

The linear Wichita uplift formed in the Pennsylvanian as a result of the partial inversion of the southern Oklahoma aulacogen. Concurrently, the Anadarko basin developed to the northeast of the uplift; the net structural relief between basin and uplift is enormous—between 40,000 and 50,000 ft (12,500–15,500 m). The trend of the uplift, east-southeast to west-northwest, is parallel to the Meers fault and other related fractures in the frontal fault zone, a region of intense tectonic deformation between uplift and basin. The Slick Hills are the surface expression of these features.

The initial drainage off the uplift was presumably consequent (i.e., orthogonal to the axis of the uplift) (Figs. 7, 8) and directed generally toward the north-northeast. Detrital products of this drainage, in the form of fan deltas, are encountered in the subsurface on the southern flank of the Anadarko basin. Conglomerates in these sequences generally record an "inverted stratigraphy," as increasingly older rocks were stripped off the uplift (Donovan and Butaud, 1993). Much of the lower Paleozoic sequence that was removed during this time consisted of carbonates (Fig. 2). Given the moist equatorial climate of the Pennsylvanian in the area that is now Oklahoma, Donovan and others (1992) estimated that karst-dissolution processes could have removed much of the section.

Eventually, tectonic definition of the area drew to a close in the Late Pennsylvanian and Early Permian. At the same time, the climate became increasingly arid. This Early Permian aridity is indicated by intensive calcrete development, and, subsequently, major eolian-dune formation and evaporite precipitation took place.

Definition of the Meers Valley began when erosion removed the Mount Scott Granite (and perhaps other acidic rocks) from the top of the basic and ultrabasic intrusives beneath (Fig. 9). As the Meers fault formed the northeastern edge of the granite/basic terrain, subsequent drainage developed parallel to the fault. The northern edge of the resulting valley was formed by carbonate terrain. The evolution of the latter into topographic relief was probably a consequence of a combination of: (1) the more rapid weathering and erosion of the ultrabasic/basic terrain; (2) decreasing dissolution of the carbonates in an increasingly arid environment; and (3) tectonic enhancement of the Slick Hills terrain by rejuvenation of the Meers fault with a net south-southwest downward displacement. Details of this process are given in Figures 10–12.

RETROSPECTIVE

The scenario outlined above is just a small part of the story of the topographic evolution of the Wichita uplift. The interpretation presented is based on evidence contained within the Meers Valley. Two additional lines of evidence offer support.

In the first case, a core cut in Lower Permian rocks north of the Slick Hills shows fine limestone conglomerates overlying granitic conglomerates and arkoses (Donovan, unpublished data). Such a reversal of provenance may record the emergence of the Slick Hills as a topographic barrier between the Anadarko basin and the Wichita Mountains.

The second line of evidence is more whimsical and concerns the topographic evolution of a part of the fault trace of the modern Meers fault. One small segment of the fault, described by Donovan (1986b, 1988), displays a cameo copy of the Permian Meers Valley. In this segment, the southwest-facing fault scarp has interrupted a northeast-draining stream system; at the present

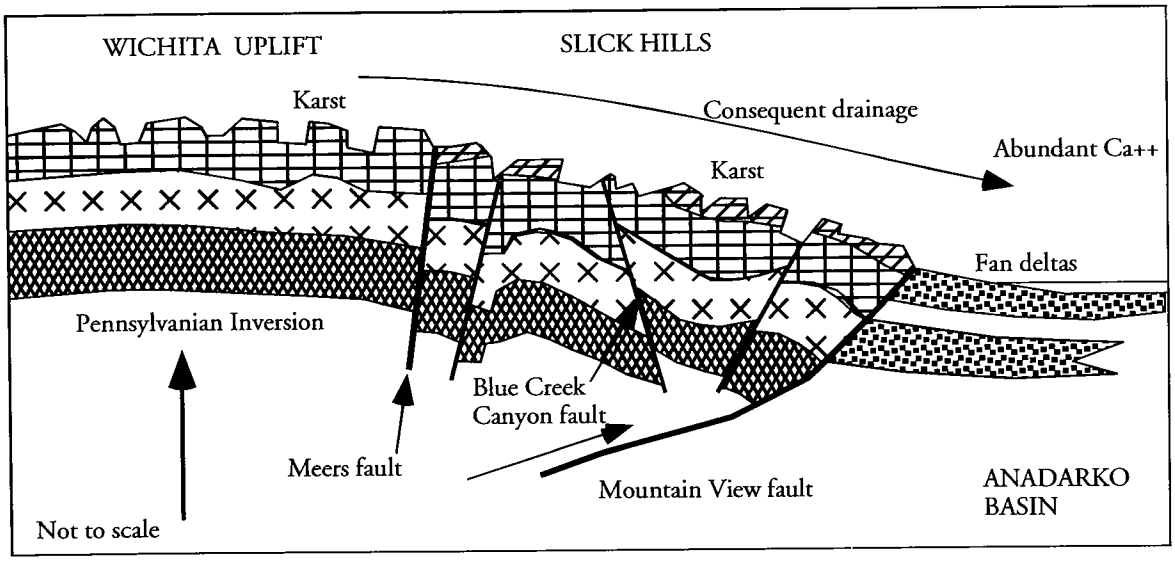

Late Mississippian - Pennsylvanian detritus, including chert-pebble conglomerates

Ordovician - Mississippian rocks (mostly carbonates)

Cambrian - Ordovician Timbered Hills and Arbuckle Groups

Cambrian acidic intrusives and extrusives

Cambrian basic and ultrabasic intrusives

Figure 7. Schematic interpretation of general patterns of denudation at an early stage in the evolution of the Wichita uplift and Anadarko basin.

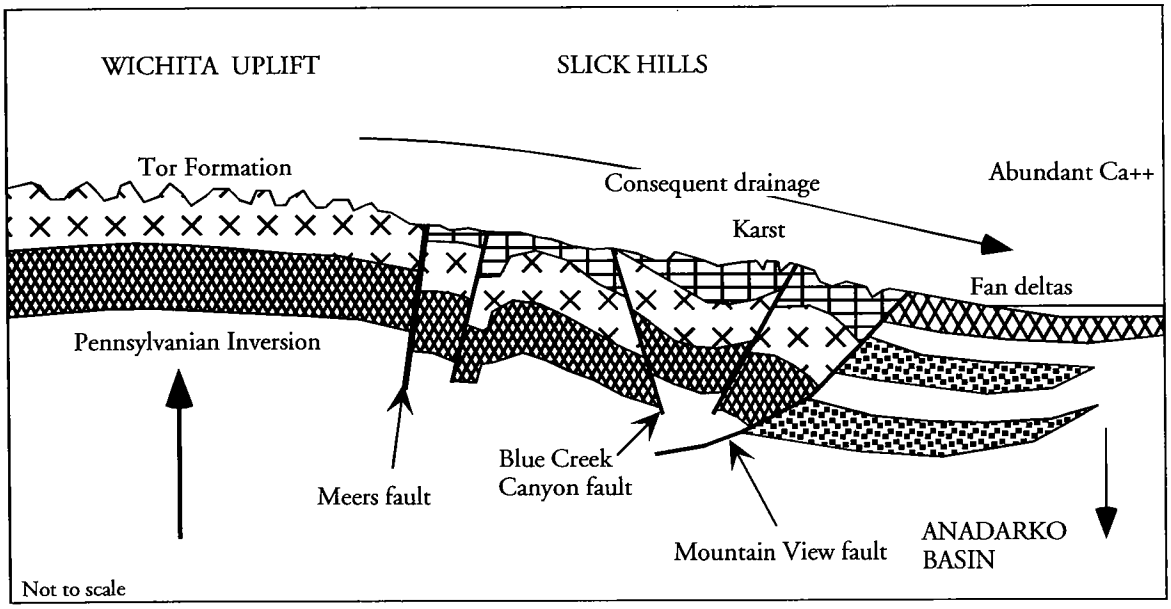

Late Pennsylvanian deposits, including granitic detritus.

Late Mississippian - Pennsylvanian detritus, including chert-pebble conglomerates

Cambrian - Ordovician Timbered Hills and Arbuckle Groups

Cambrian acidic intrusives and extrusives

Cambrian basic and ultrabasic intrusives

Figure 8. Schematic interpretation of general patterns of denudation at a later stage in the evolution of the Wichita uplift and Anadarko basin.

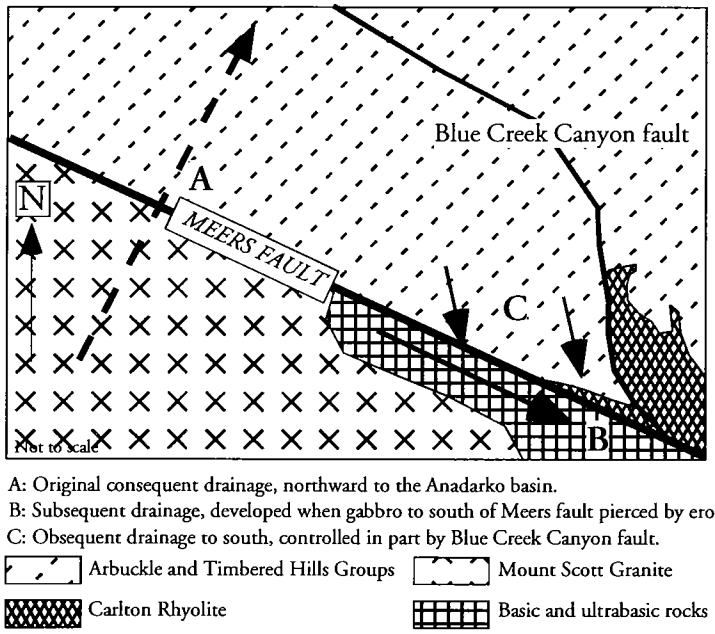

Figure 9. Schematic map showing the reorientation of drainage patterns as a result of the definition of the Meers Valley.

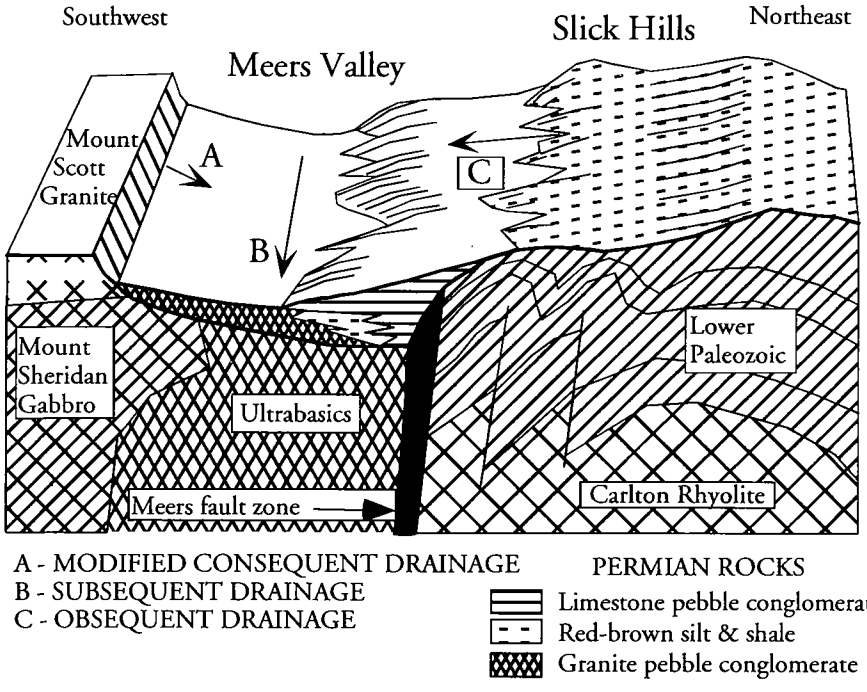

Figure 10. First stage of definition of the Meers Valley. Preserved infill of the Meers Valley was from the retreating granite fault-line scarp and consists of granite-pebble conglomerates, arkoses, and red-brown shales. As relief-nversion progressed small limestone fans debouched from the Slick Hills atop the earlier arkoses.

time, a subsequent drainage is evolving along the line of the fault. In essence, this is a near perfect mimic of the processes that molded the Meers Valley in the Early Permian.

ACKNOWLEDGMENTS

It is a pleasure to acknowledge the cooperation and interest of landowners in the Meers Valley area, notably Charlie Bob and Dixie Oliver, Tommy Cavanagh, and the Kimbell family. In addition, the intellectual companionship of M. Charles Gilbert was a constant stimulation.

REFERENCES CITED

Bridges, S. D., 1985, Mapping, stratigraphy and tectonic implications of Lower Permian strata, eastern Wichita Mountains, Oklahoma: Oklahoma State University unpublished M.S. thesis, 125 p.

Chase, G. W., 1954, Permian conglomerate around the Wichita Mountains, Oklahoma: American Association of Petroleum Geologists Bulletin, v. 38, p. 2028–2035.

Collins, K. H., 1985 Depositional and diagenetic history of the Permian Rocks in the Meers Valley, southwestern Oklahoma: Oklahoma State University unpublished M.S. thesis, 110 p.

Crawford, M. F.; Morgan, K. M.; Donovan, R. N.; and Brown, W. G., 1990, Remote sensing techniques applied to structural geology and oil exploration in south-central Oklahoma: Geological Society of America Field Trip Guide No. 4, Dallas, 105 p.

Donovan, R. N., 1978, Late Pennsylvanian and Permian cornstones (caliche) in Oklahoma [abstract]: Geological Society of America Abstracts with Programs, v. 10, no. 1, p. 4.

_____ 1986a, Geology of the Slick Hills *in* Donovan, R. N. (ed.), The Slick Hills of southwestern Oklahoma—fragments of an aulacogen?: Oklahoma Geological Survey Guidebook 24, p. 1–12.

_____ 1986b, Stop 5—The Meers fault: modest finale for a hoary giant?, *in* Donovan, R. N. (ed.), The Slick Hills of southwestern Oklahoma—fragments of an aulacogen?: Oklahoma Geological Survey Guidebook 24, p. 106–108.

_____ 1988, The Meers fault scarp, southwestern Oklahoma, *in* Hayward, O. T. (ed.), Geological Society of America Centennial Field Guide,

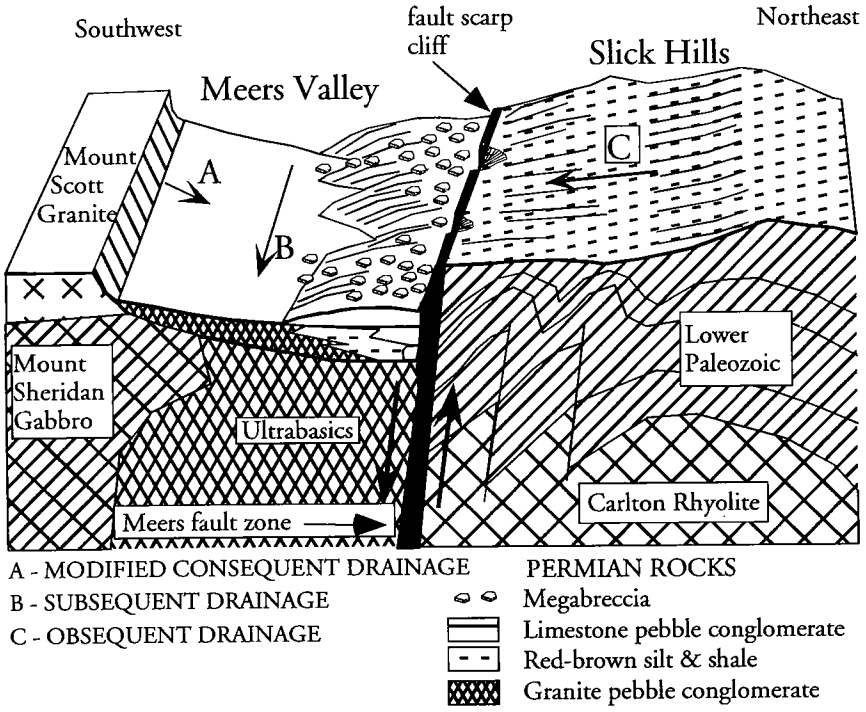

Figure 11. Second stage of definition of the Meers Valley. Subsequently, the Meers fault rejuvenated with a downthrow to the southwest, followed by fault scarp recession to the northeast at which time the megabreccias formed. Some dolomitizing fluids ascended the fault zone, playing a limited role in cementation.

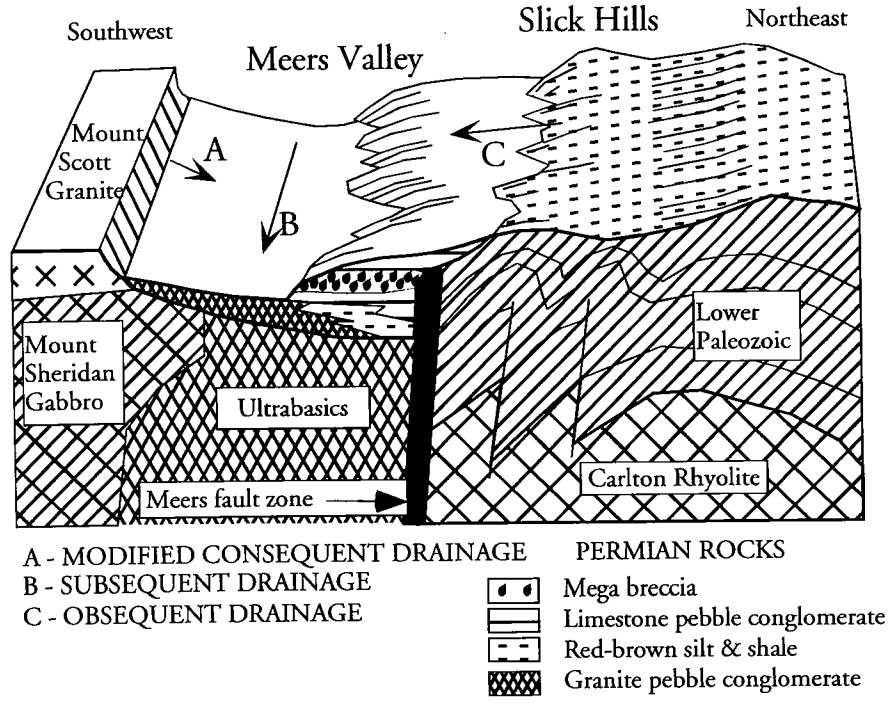

Figure 12. Third stage of definition of the Meers Valley. In the final phase, relief-related breccias were shed from the Slick Hills atop the megabreccias as the Mount Scott fault-line scarp continued to retreat slowly to the southwest.

South-Central Section: Geological Society of America, Decade of North American Geology, v. 4, p. 79–82.

Donovan, R. N.; and Busbey, A. B., 1991, Stop 13—Leatherbury's Quarry—the world's smallest oil field, *in* Johnson, K. S. (ed.), Arbuckle Group core workshop and field trip: Oklahoma Geological Survey Special Publication 91-3, p. 255–258.

Donovan, R. N.; and Butaud, Todd, 1993, The Vanoss conglomerate—a record of Late Pennsylvanian basin inversion on the northern flank of the Arbuckle Mountains, southern Oklahoma, *in* Johnson, K. S.; and Campbell, J. A. (eds.), Petroleum-reservoir geology in the southern Midcontinent, 1991 symposium: Oklahoma Geological Survey Circular 95, p. 10–24.

Donovan, R. N.; and Ross, D. L., 1991, Stop 14—The Saddle Mountain dolomite on Maukeen Hill, *in* Johnson, K. S. (ed.), Arbuckle Group core workshop and field trip: Oklahoma Geological Survey Special Publication 91-3, p. 259–262.

Donovan, R. N.; Babaei, A.; and Sanderson, D. J., 1982, Stop 10—Blue Creek Canyon, *in* Gilbert, M. C.; and Donovan R. N. (eds.), Geology of the eastern Wichita Mountains, southwestern Oklahoma: Oklahoma Geological Survey Guidebook 21, p. 148–153.

Donovan, R. N.; Gilbert, M. C.; Luza, K. V.; Marchini, David; and Sanderson; David, 1983, Possible Quaternary movement on the Meers fault, southwestern Oklahoma: Oklahoma Geology Notes, v. 43, p. 124–133.

Donovan, R. N.; Ragland, D. A.; Rafalowski, M. B.; Collins, K.; Tsegay, T.; McConnell, D.; Marchini, D.; Beauchamp, W.; and Sanderson, D. J., 1986, Stop 1—Geological highlights of the Blue Creek Canyon area, *in* Donovan, R. N. (ed.), The Slick Hills of southwestern Oklahoma—fragments of an aulacogen?: Oklahoma Geological Survey Guidebook 24, p. 84–91.

Donovan, R. N.; Busbey, A. B.; Elmore, R. D.; and Engels, M. H., 1992, Oil in Permian karst in the Slick Hills of southwestern Oklahoma, *in* Johnson, K. S.; and Cardott, B. J. (eds.), Source rocks in the southern Midcontinent, 1990 symposium: Oklahoma Geological Survey Circular 93, p. 198–209.

Gilbert, M. C., 1982, Geologic setting of the eastern Wichita Mountains with a brief discussion of unresolved problems, *in* Gilbert, M. C.; and Donovan,

R. N. (eds.), Geology of the eastern Wichita Mountains, southwestern Oklahoma: Oklahoma Geological Survey Guidebook 21, p. 1–30.

_____ 1983, The Meers fault: Unusual aspects and possible tectonic consequences [abstract]: Geological Society of America Abstracts with Programs, v. 15, no. 1, p. 1.

Jones-Cecil, Meridee; Donovan, R. N.; and Bradley, Lee-Ann, 1995, Structural framework of the Meers fault and Slick Hills area, southwestern Oklahoma, based on magnetic data, *in* Johnson, K. S. (ed.), Structural styles in the southern Midcontinent, 1992 symposium: Oklahoma Geological Survey Circular 97, p. 187–207.

Sequence Stratigraphy and Stratigraphic Framework of the Upper Morrow, Anadarko Basin

Zuhair Al-Shaieb and Jim Puckette
Oklahoma State University
Stillwater, Oklahoma

ABSTRACT.—Oil and gas production from the Upper Morrow interval in the Anadarko basin is primarily from channel-fill reservoirs. On the northwestern shelf of the basin, these are mainly incised valley-fill deposits that formed during marine transgressions that followed regional drops in sea level. A series of southeast-trending valleys were eroded as a result of decreased accommodation space during these sea-level lowstands. During the subsequent transgressions, the valleys filled with a variety of fluvial, floodplain, estuarine, and marine sediments. Marine muds blanketed the valley-fill deposits during the major highstands. The complex depositional pattern and resultant diverse lithofacies contributed to reservoir heterogeneity and affected reservoir quality. The primary reservoirs are typically coarser-grained fluvial sandstones. Marine-influenced sandstones with abundant skeletal grains commonly exhibit low porosity as the result of extensive calcite cement. Tidal-influenced, estuarine, fine-grained sandstones are poor-quality reservoirs due to burrowing that destroyed primary porosity.

Along the Wichita–Amarillo uplift, the upper Morrow reservoirs were deposited by a system of northward-prograding fan-delta complexes that are separated by highstand marine muds. There, depositional style was strongly influenced by uplift and basin subsidence rates. Distribution patterns and internal characteristics of specific reservoirs reflect the changes in sediment supply and accommodation space. Increased uplift (abundant sediment supply) formed the Puryear deltaic complex in the W. Cheyenne and Reydon fields. Diminished accommodation space during tectonically or eustatically induced lowstands forced stream incision that resulted in the valley-fill reservoirs of the Hollis interval. The influx of granitic rock fragments from the core of the Wichita uplift during lowstands was critical to the development of porosity and evolution of quality reservoirs.

Al-Shaieb, Zuhair; and Puckette, Jim, 2001, Sequence stratigraphy and stratigraphic framework of the Upper Morrow, Anadarko basin, *in* Johnson, K. S. (ed.), Pennsylvanian and Permian geology and petroleum in the southern Midcontinent, 1998 symposium: Oklahoma Geological Survey Circular 104, p. 225.

Red Fork Sandstone of Oklahoma: Depositional History, Sequence Stratigraphy, and Reservoir Distribution

Richard D. Fritz[1]
Masera Corporation
Tulsa, Oklahoma

ABSTRACT.—The Middle Pennsylvanian Red Fork Sandstone formed as a result of progradation across eastern Kansas and most of Oklahoma. It is one of several transgressive-regressive sequences (cyclothems) developed within the Desmoinesian "Cherokee" Group. Sea-level changes together with varying subsidence were dominant factors controlling the general stratigraphic (correlative) characteristics of the Red Fork interval. Progradation was episodic with sand deposition in the more active part of the basin during lower sea-level stands and valley-fill deposition in the more stable areas during sea-level rises.

The Red Fork was correlated, subdivided, and mapped using data from more than 27,000 wells. Maps of Red Fork sand trends reveal a fluvial-deltaic complex covering most of Oklahoma. The Red Fork consists primarily of undifferentiated alluvial-valley and alluvial-plain (fluvial) bodies in the northernmost part of Oklahoma; fluvial-deltaic bodies in most of the remaining parts of shelf area; and off-shelf, submarine-fan and slope–basinal-floor complexes within the deeper part of the Anadarko basin. The basinal facies can also be interpreted as lowstand deltaic deposits.

The Red Fork appears to represent a single, Vail-type third-order sequence. It can be divided into at least three parasequences, which, for the purpose of this study, are called upper, middle, and lower. Each parasequence represents a transgressive-regressive episode commonly separated by thin regional limestones or shale markers. Correlation of these parasequences is relatively easy from the lower shelf to the basin but more difficult on the upper shelf.

The provenance for the Red Fork was most likely an extensive drainage system to the north and northeast of Oklahoma. This drainage system probably extended as far as the Canadian Shield or even Greenland and appears to be subparallel to the Midcontinent rift. A secondary source for the Red Fork was the Wichita-Amarillo Mountains in the south.

[1] Current address: American Association of Petroleum Geologists, Tulsa, Oklahoma.

Fritz, R. D., 2001, Red Fork Sandstone of Oklahoma: depositional history, sequence stratigraphy, and reservoir distribution, *in* Johnson, K. S. (ed.), Pennsylvanian and Permian geology and petroleum in the southern Midcontinent, 1998 symposium: Oklahoma Geological Survey Circular 104, p. 226.

Trace and Rare-Earth Elemental Variation in a Midcontinent Carbonate Sequence—A Key to Understanding Reservoir Development

Peer Hoth
GeoForschungsZentrum
Potsdam, Germany

Timothy R. Carr
Kansas Geological Survey
Lawrence, Kansas

Michael Bau and Peter Dulski
GeoForschungsZentrum
Potsdam, Germany

ABSTRACT.—Subaerial exposure surfaces and associated features are common components of shallow-marine Paleozoic sequences in the Midcontinent. Recognition of such surfaces is of economic importance because the distribution of reservoir facies is closely associated with subaerial exposure. Problems in lithostratigraphic correlation at both the reservoir and regional scales are caused by the absence of unambiguous lithologic and petrographic evidence of subaerial exposures in these sequences.

Selected Upper Pennsylvanian carbonate sequences of the Kansas City Group (Bronson Subgroup) in southeast Kansas and northwest Missouri have been investigated to understand the style of alteration associated with subaerial exposure, to derive criteria to recognize distinctive signatures in both the surface and subsurface, and to better understand the genesis of the carbonate sequences. Detailed field descriptions, petrographic examination, spectral gamma-ray logs, and analysis of trace elements and rare-earth elements (REE) were the bases of our study. Geochemical investigations included Inductively Coupled Plasma Mass Spectrometry (ICP-MS), using two methods for sample decomposition (decomposition with 8 M HNO_3 in open beakers and bulk decomposition with HF + $HClO_4$ in pressure vessels). The different methods provide independent information about trace and rare-earth element concentrations of carbonate and detrital phases (alumino-silicates and heavy minerals). Investigated rocks include different types of oolitic grainstones, skeletal packstones, wackestones, and different shale types. Signs of subaerial exposure such as root traces, root tubes filled with micritic internal sediment, rhizolite crusts, and *in situ* brecciation were recognized through fieldwork and microscopic analysis.

Geochemical investigation shows that detrital influx during carbonate sedimentation of the Bronson Subgroup generally increased toward the exposure surfaces. Zr, Rb, Th, and total REE content are the most useful geochemical indicators of this trend. Shale normalized REE-patterns of the limestones (normalized against PAAS) have very characteristic features. Important differences between upper and lower parts of the limestone members are shown by differences in Ce and Y signatures of the shale-normalized REE-patterns. Other than these distinctive signatures, typical trends of the Y/Ho ratios were detected through the limestone sequences.

The lower part of the Benthany Falls Limestone (mainly wackestones and skeletal packstones/grainstones) is characterized by negative Ce anomalies, positive Y anomalies and Y/Ho-ratios between 55 and 40. Both of the REE-anomalies are typical for carbonates and other minerals precipitated in equilibrium with seawater. Magnitude of the Ce and Y anomalies generally decreases upward to the top of the limestone member. Flat REE-patterns are typical for the oolitic-grainstone facies and for the *in situ* brecciated and mottled wackestones of the upper part of the Benthany Falls Limestone. Y/Ho ratios of these limestones are lower than 35. Although a general correlation between the decreasing size of the Ce and Y anomalies and the increase of detrital phases is obvious, several exceptions exist (e.g., laminar calcretes).

In addition to IGP-MS analysis, relative uranium enrichment was detected by measurement of gamma radiation using a hand-held spectral scintillometer in outcrops, and by the analysis of existing spectral gamma-ray well logs in the subsurface. In several sequences, distinctive change in uranium concentration is observed at the contact of the vadose and marine-phreatic zones. Based on detailed examination, the uranium anomalies cut across primary sedimentary

Hoth, Peer; Carr, T. R.; Bau, Michael; and Dulski, Peter, 2001, Trace and rare-earth elemental variation in a Midcontinent carbonate sequence—a key to understanding reservoir development, *in* Johnson, K. S. (ed.), Pennsylvanian and Permian geology and petroleum in the southern Midcontinent, 1998 symposium: Oklahoma Geological Survey Circular 104, p. 227–228.

structures, and are caused by selective inclusion of uranium in micrite cements and associated clays concentrated at the contact between vadose and marine-phreatic environments.

Porosity development and preservation in the Benthany Falls Limestone oolitic-grainstone facies, a major oil-producing interval in Kansas, appear related to the position of the overlying exposure surface. Recognition of previously undetected vadose-phreatic contacts can provide insight into porosity trends in other units. The study of trace and rare-earth elemental variations can improve our understanding of genetic mechanisms influencing reservoir development in similar shallow-marine Midcontinent reservoirs.

Facies and Sequence Stratigraphy of the Upper Permian Yates Formation on the Western Margin of the Central Basin Platform of the Permian Basin

Ron Johnson and Jim Mazzullo
Texas A&M University
College Station, Texas

ABSTRACT.—This abstract examines the facies, stratigraphy, and reservoir properties of the Upper Permian Yates Formation in North Ward Estes field, Ward and Winkler Counties, Texas. The study is based upon the descriptions and petrographic analyses of 11 Yates cores and 38 well logs from North Ward–Estes field, part of the "River of Sand" that stretches along the western shelf margin of the central basin platform.

The Yates of North Ward–Estes field consists of subarkosic sandstones and siltstones and dolomitic mudstones and wackestones that were deposited in fluvial, deltaic, eolian, sabkha, and shallow-subtidal settings during two successive cycles of relative sea-level fall and rise. Six facies are distinguished in the formation:

1. Massive, well-sorted sandstones with occasional planar laminae, root casts, and paleosols—interpreted as eolian sand-sheet deposits;
2. Laminated silty to very fine grained sandstones with mud drapes, ripples, load structures, fluid escape structures, and bioturbation traces—interpreted as desert braided-stream and fan-delta deposits;
3. Graded beds of gravelly to fine sandstones with dolomicrite clasts—interpreted as channel and distributary deposits of braided streams and deltas;
4. Poorly stratified reddish-brown fine sandstones and siltstones with evaporite nodules, clay drapes, and haloturbation structures—interpreted as clastic-dominated sabkha deposits;
5. Massive dolomitic mudstones and wackestones with cryptalgal laminae, stylolites, and collapse breccias—interpreted as shelf-interior deposits; and
6. Nodular-mosaic anhydrites and anhydrite-rich, gray sandy siltstones— interpreted as evaporite-dominated sabkha deposits.

Two sequences and 12 stacked "upward-drying" high-frequency cycles (HFCs) are recognized in the Yates. Each sequence consists of a basal transgressive systems tract (TST) overlain by an upper highstand systems tract (HST) and is thought to record a single cycle of relative sea-level rise and fall. Each HST consists of stacked HFCs, which become thicker and more clastic-rich upward, whereas each TST consists of stacked HFCs, which become thinner and more carbonate-rich upward.

The eolian sandstones of the Yates, with porosities of up to 20% and permeabilities of several hundred millidarcies, are the major reservoirs in North Ward–Estes field, and the gravelly channel sandstones form minor reservoirs. The porosities in these two sandstones are largely secondary in origin and are the product of the dissolution of evaporite and carbonate cements and labile grains during burial diagenesis. The seal for the reservoirs is the contact between the Yates and updip and overlying evaporites of the Yates and Tansill Formations. The thickest and most extensive reservoirs are in the upper of the two Yates sequences, which contains abundant eolian sandstone beds.

Johnson, Ron; and Mazzullo, Jim, 2001, Facies and sequence stratigraphy of the Upper Permian Yates Formation on the western margin of the central basin platform of the Permian basin, *in* Johnson, K. S. (ed.), Pennsylvanian and Permian geology and petroleum in the southern Midcontinent, 1998 symposium: Oklahoma Geological Survey Circular 104, p. 229.

Depositional Facies of the Lower Permian Section, Northeastern New Mexico: Preliminary Observations and Interpretations

Jennifer L. P. Kessler and Gerilyn S. Soreghan
University of Oklahoma
Norman, Oklahoma

ABSTRACT.—The Lower Permian section (Abo and Tubb Formations) in northeastern-most New Mexico consists of complexly interbedded mudstone, siltstone, sandstone, and conglomerate that was deposited southeast of the Sierra Grande uplift and buried the Bravo dome uplift. In this region, the study section lies directly on Precambrian basement and is overlain by the Cimarron Anhydrite. The depositional facies of the section are poorly known but are important for constraining Early Permian paleogeography and paleoclimate in this region. Preliminary observations from subsurface data suggest that deposition occurred in a variety of continental to possibly marginal-marine (sabkha) environments.

This preliminary analysis is based on facies studies of core from three wells (Amoco #1 Pittard, Amoco State 11N, and Amoco Heimann #2) that form an east-west dip transect through the Bravo dome high in northeastern New Mexico.

In these wells, we distinguish four distinct facies. The first facies consists of alternating matrix- and clast-supported conglomerate. It ranges in thickness from 10 cm to 10 m and is typically sharply to erosively based. The conglomerate commonly grades upward into the second facies, a medium- to coarse-grained, planar- to cross-bedded sandstone ranging up to 2 m thick. Based on sedimentary fabrics, structures, and bedding relationships, we interpret this two facies to record deposition in ephemeral, fluvial (wadi-type) streams. The third facies consists of red mudstone ranging up to 4 m thick and occurring as two subfacies: (1) gypsiferous mudstone (with displacive evaporite nodules) associated with root traces, and (2) rubbly mudstone displaying apparent pedogenic features such as conchoidal fractures and slickensided fracture surfaces. We interpret both mudstones as paleosols—specifically, gypsisols (subfacies 1) and vertisols (subfacies 2). Gypsisols reflect formation in regions that receive less than 25 cm mean annual precipitation, whereas vertisol formation is promoted by semiarid conditions with seasonal precipitation (Mack, 1997). Further, gypsisols suggest the influence of a marginal-marine (sabkha) environment. The fourth facies is a locally bioturbated, massive to parallel-laminated siltstone. The siltstone is commonly associated with paleosols, suggesting a dominance of continental depositional processes. The siltstone is very well sorted and commonly massive, which may reflect eolian transport processes. The local presence of planar and ripple laminations, however, suggests the influence of water reworking. Local association with sharp-based conglomeratic sandstone (of suspected fluvial origin) also suggests probable fluvial reworking.

The four facies described above reflect deposition in continental (fluvial and possible eolian-influenced) environments to probable marginal-marine (sabkha) environments in a generally arid system. Within the study interval, older strata are fluvial-dominated, coarse-grained, poorly sorted, and immature (possibly reflecting proximity to source), whereas younger strata are finer, better-sorted, more mature, and influenced by possible eolian deposition. Continental deposits predominate in the western wells and yield eastward to increasingly gypsiferous, marginal-marine strata. Presence of gypsisols and vertisols suggest an arid to seasonally wet paleoclimate.

Additional data collection is needed to refine facies associations and paleoclimatic and paleogeographic interpretations.

REFERENCE CITED

Mack, G. H., 1997, Paleosols for sedimentologists: Geological Society of America Short Course Notes [2nd edition], Boulder, Colorado, 114 p.

Kessler, J. L. P.; and Soreghan, G. S., 2001, Depositional facies of the Lower Permian section, northeastern New Mexico: preliminary observations and interpretations, *in* Johnson, K. S. (ed.), Pennsylvanian and Permian geology and petroleum in the southern Midcontinent, 1998 symposium: Oklahoma Geological Survey Circular 104, p. 230.

Overpressure and Hydrocarbon Generation in the Anadarko Basin, Southwestern Oklahoma

Youngmin Lee and David Deming
University of Oklahoma
Norman, Oklahoma

ABSTRACT.—The Anadarko basin is the deepest sedimentary basin on the North American craton; total sediment thickness is greater than 11 km. Although it has been tectonically quiescent for more than 100 million years, the Anadarko is known to have extensive areas of overpressuring. Static hypotheses explain the existence of high fluid pressures in the Anadarko basin by invoking pressure seals—rock units that are essentially impermeable over geologic time. Dynamic hypotheses explain the existence of overpressures in the Anadarko basin as a transient imbalance caused by a geologic process (e.g., hydrocarbon generation) creating overpressures faster than they may be dissipated from low-permeability rocks.

We have constructed single-phase models of overpressuring in the Anadarko basin due to oil and gas generation from kerogen. These models are constrained by the geologic history, paleothermal indicators, present-day estimates of the thermal gradient and heat flow, and geochemical analyses of source rocks. Our preliminary results indicate that recent gas generation may be one of the most important causes of present-day overpressuring in the Anadarko basin. Modeling indicates that excess pressure due to gas generation from kerogen dissipates completely within a relatively short period of time (ca. 10 Ma). Also, our results show that low average permeability ($\sim 10^{-19}$ m^2 = 10^{-4} mD) and an almost constant thermal gradient (>23°C/km) over geologic time are required if present-day overpressures in the Anadarko basin are to be explained through hydrocarbon generation in the basin.

At the present time, we are refining models that will incorporate geologic constraints of the Anadarko basin.

Lee, Youngmin; and Deming, David, 2001, Overpressure and hydrocarbon generation in the Anadarko basin, southwestern Oklahoma, *in* Johnson, K. S. (ed.), Pennsylvanian and Permian geology and petroleum in the southern Midcontinent, 1998 symposium: Oklahoma Geological Survey Circular 104, p. 231.

Depositional and Diagenetic Origins of Sandstone Reservoirs in the Queen Formation, Permian Basin of Texas

Jim Mazzullo
Texas A&M University
College Station, Texas

ABSTRACT.—The Queen Formation is a sequence of interbedded and interfingering carbonates, clastics, and evaporites that was deposited on the back-reef shelves of the Permian basin during the Late Permian (Guadalupian). The origins of the carbonates and evaporites in the formation are fairly well understood, but considerable disagreement has existed about the origins of the clastics, and, specifically, whether they represent deposition during sea-level low stands or high stands.

This abstract presents data from a decade-long series of core, log, and petrographic studies of the Queen Formation in oil fields on the central basin platform and northwest shelf. The results of these studies show that the clastics of the formation were largely deposited in continental and coastal environments that were established on the back-reef shelves during periods of lowered sea level. Five clastic facies are recognized in the Queen Formation. They are:

1. Braided-stream facies—characterized by shoestring bodies of massive, cross-laminated, gravelly channel and channel-bar sandstones;
2. Desert, fluvial-sand-flat facies—characterized by shoestring bodies of massive- and cross-bedded channel sandstones encased in sheets of rippled and laminated silty sandstones and siltstones;
3. Fan-delta facies—characterized by lenticular (lobate) bodies of rippled, laminated, bioturbated, and slumped sandstones, siltstones, and mudstones;
4. Eolian sand-sheet facies—characterized by sheets of massive and laminated well-sorted fine sandstones; and
5. Clastic-dominated sabkha facies—characterized by sheet bodies of poorly laminated and haloturbated silty sandstones and siltstones with thin beds and displacive nodules of halite and anhydrite.

The results of these studies also determined the depositional and diagenetic origins of the sandstone reservoirs in the Queen. Generally, the most productive reservoirs are the well-sorted sandstones of the eolian sand-sheet facies, which have average porosities in excess of 15% and permeabilities of hundreds to thousands of millidarcies, and, to a lesser extent, the moderately sorted channel sandstones of the braided-stream and fluvial-sand-flat facies, which have porosities in excess of 8% and permeabilities on the order of tens to hundreds of millidarcies. The pores in these reservoir facies are generally secondary in origin and appear to be largely formed by the dissolution of early evaporite or carbonate cements and labile detrital grains.

Mazzullo, Jim, 2001, Depositional and diagenetic origins of sandstone reservoirs in the Queen Formation, Permian basin of Texas, *in* Johnson, K. S. (ed.), Pennsylvanian and Permian geology and petroleum in the southern Midcontinent, 1998 symposium: Oklahoma Geological Survey Circular 104, p. 232.

Tectonic Overview of the U.S. Southern Midcontinent during the Pennsylvanian and Permian

Thomas L. Thompson and James R. Howe
Consulting Geologists
Boulder, Colorado

ABSTRACT.—Ye and others (1996) provide new insight to Pennsylvanian–Permian tectonics of the U.S. southern Midcontinent with their recognition that deformation associated with the greater Ancestral Rocky Mountains (including the Wichita-Arbuckle trend) reasonably reflects flat-plate subduction of Paleozoic oceanic crust beneath southwestern North America, thereby transmitting stress far inland beneath the continent. This mechanism readily explains the synchronism and similarity of late Paleozoic deformation between the Rocky Mountain and the southern Midcontinent geographic regions. In this view, the Ancestral Rocky Mountains are a direct analog of the later Rocky Mountain Laramide orogeny, for which the prevailing tectonic model is one of low-angle subduction of the oceanic crust of the Farallon Plate. Emplacement of the Marathon, Ouachita, and Appalachian Mountains terranes along the southeast margin of late Paleozoic North America most likely did not strongly deform the continental interior because subduction was away from North America when Gondwana (combined Africa and South America) collided with North America during the assembly of Pangaea.

Late Paleozoic transpression across rifted and subsided Precambrian basement blocks in southern Oklahoma accounts for dominant structural styles along the Wichita-Arbuckle trend. The various structures and their mechanical linkages find common explanation in context of east-northeast–west-southwest compression and reactivation of west-northwest–trending basement faults. This fault reactivation and associated basin inversion resulted in structural relief of at least 6 mi (10 km) and accumulation of a 3-mi (5-km) thickness of synorogenic sediment, dominant oblique-slip faulting, extensive thrusting, and left-slip faulting. Dip-slip shortening of the preorogenic rocks amounts to about 9 mi (15 km), whereas net left-slip displacement exceeds 18 mi (30 km).

Dynamic interplay among basement blocks under transpression inverted igneous-filled grabens and formed several types of mechanically linked structures in the overlying sedimentary sequences. First, northwesterly trending, left-reverse, oblique-slip faults vary in attitude, depending on the attitude of basement-block interfaces, with greater structural relief and imbricate faulting at confining bends in the basement block pattern (e.g., the Wichita uplift–Cyril basin pair and the Criner Hills–Ardmore deep pair). Second, northeasterly trending basement fractures apparently provided antithetic adjustment to the dominant northwest-trending en echelon folds and faults. Third, flower structures formed at several scales, including the complex Cumberland anticline and faulting above the Criner, Tishomingo, and Wichita-Marietta basement blocks.

REFERENCE CITED

Ye, H.; Royden, L.; Burchfiel, C.; and Schuepbach, M., 1996, Late Paleozoic deformation of interior North America: the greater Ancestral Rocky Mountains: American Association of Petroleum Geologists Bulletin, v. 80, p. 1397–1432.

Thompson, T. L.; and Howe, J. R., 2001, Tectonic overview of the U.S. southern Midcontinent during the Pennsylvanian and Permian, *in* Johnson, K. S. (ed.), Pennsylvanian and Permian geology and petroleum in the southern Midcontinent, 1998 symposium: Oklahoma Geological Survey Circular 104, p. 233.